# Acceptor-Substituted Cyclopentadienyl Compounds

Inaugrural-Dissertation

to obtain the academic degree

**Doctor rerum naturalium (Dr. rer. nat.)**

submitted to the department of
Biology, Chemistry, Pharmacy of Freie Universität Berlin

by

**Susanne Margot Rupf**

Berlin, 2023

# Declaration of independence

The work for this dissertation was done in the group of Dr. Moritz Malischewski from May 2019 until March 2023 at the Institute of Chemistry and Biochemistry at Freie Universität Berlin. I declare that this dissertation is my own work except where stated contrary. This dissertation has not been submitted to obtain any other degree.

Susanne Margot Rupf

| | |
|---|---|
| First referee: | Dr. Moritz Malischewski |
| Second referee: | Prof. Dr. Sebastian Hasenstab-Riedel |
| Date of disputation: | June 2, 2023 |

# Acknowledgments

First, I would like to thank Dr. Moritz Malischewski not only for the opportunity to write my PhD thesis in his group, but also for the excellent and supportive supervision and guidance as well as all those great chemistry talks during this work. I benefited of lot from his advice and inspiring ideas scientifically and also personally. In addition, I thank Prof. Dr. Sebastian Hasenstab-Riedel for being the second examiner of this work and for his input during this thesis.

Furthermore, I'd like to thank my collaboration partners Dr. Marc Reimann, Prof. Dr. Martin Kaupp, Yannick Schulte, Prof. Dr. Stephan Schulz, Dr. Carlo Fasting and Dr. Patrick Pröhm for their contributions to this work. I also want to thank the students who I supervised during their internships or bachelor theses, Amina L. Moshtaha, Irina S. Dimitrova, Paulin Riemann, Sofiia Zuieva, Robin Sievers, Cafer C. Kaplan and Gabriel Schröder for their motivation and reliable work. Our teamwork as well as discussions beyond chemistry were always a pleasure for me.

Moreover, I thank Prof. Dr. Dieter Lentz, Dr. Günther Thiele and Dr. Adelheid Hagenbach for introducing me to the theoretical backgrounds in crystallography as well as for further scientific advices and supportive feedback. Thanks to Dr. Simon Steinhauer for his advice and helpful discussion regarding NMR related questions. Many thanks to Dr. Patrick Pröhm, Dr. Alex J. Plajer and Sonja Utsch for proofreading of this work.

I would like to thank all former and current members of AG Malischewski for the continuously pleasant and enjoyable time at work, and for the great group activities outside the university. Moreover, I am deeply grateful for all the friendships I was able to gain. In addition, I want to thank all current and former members of AG Riedel for creating a kind and helpful atmosphere, and for providing various chemicals. In this context, I thank all other colleges in the chemistry department, especially the employees at the technical department, the material store, the BioSupraMol and ZEDAT facilities as well as the secretaries and the glass-blowers for ensuring smooth operations in the department. Furthermore, I want to thank Dr. Carsten Müller and Marie Nickel and all other speakers and members of the CRC 1349 for the coordination of scientific projects, the broad insights I gained about fluorine chemistry, for the financial support as well as the related opportunities to participate in scientific workshops and conferences.

Last but not least, I would like to thank my friends, my family and my lovely husband for supporting me ever since. I have no words to describe how important you are to me.

# Abstract

Efficient methodologies for the synthesis of acceptor-substituted perfunctionalized cyclopentadienyl (Cp) compounds were investigated. A facile multigram, one-pot synthesis of $[FeC_{10}(HgO_2CC_3H_7)_{10}]$ from ferrocene and $Hg(O_2CC_3H_7)_2$ is reported. In the corresponding compound, the Hg-C bonds are inert towards oxygen, moisture and even strong Brønsted acids like trifluoroacetic acid and $[C_5F_5NH][SbF_6]$. Instead, protonation of the carboxylic groups is observed yielding $[FeC_{10}(HgO_2CCF_3)_{10}]$ and $[FeC_{10}Hg_{10}(C_5F_5N)_n][SbF_6]_{10}$. In the compound $[FeC_{10}Hg_{10}(C_5F_5N)_n][SbF_6]_{10}$, the labile $C_5F_5N$ ligands are readily displaced by MeCN or tetrahydrothiophene (THT) to afford rare examples of organometallic decacations $[FeC_{10}(HgL)_{10}][SbF_6]_{10}$ (L = MeCN, THT). Electrochemical investigations on the (soluble) permercurated compounds reveal increasing redox potentials of the corresponding Fe(II)/Fe(III) redox couples with increasing Lewis acidity of the Hg-sites. The isolation of the oxidized forms was realized by reaction with $[NO]^+$ or $[NO_2]^+$ salts or $MoF_6$. Furthermore, the first crystallographic characterization of permetalated aromatic compounds $[FeC_{10}(HgX)_{10}]$ (X = Cl, $O_2CCF_3$, $O_2CCCl_3$), $[FeC_{10}(HgTHT)_{10}][SbF_6]_{10}$ and $[FeC_{10}(HgMeCN)_{10}][SbF_6]_{10}[MoF_6]$ is presented.

Complete halodemercuration is observed in the reaction of $[FeC_{10}(HgO_2CC_3H_7)_{10}]$ with $K[Br_3]$ followed by halogenation with $FeBr_3$ and elemental $Br_2$. An oxidation potential of $E_{1/2}$ = 1.1 V renders the corresponding ferrocenium cation as potent oxidizing agent. The isolation is realized by reaction of $[FeC_{10}Br_{10}]$ with $AsF_5$. Further functionalization of $[FeC_{10}Br_{10}]$ is achieved by metalation with elemental Mg or by lithium-halogen-exchange with $^t$BuLi. Quenching experiments with dimethylsilylchloride (DMSCl) yielded polysilylated compounds. Full functionalization was achieved after multiple metalation-silylation sequences. The resulting product $[FeC_{10}DMS_{10}]$ displays the first example of a persilylated metallocene. A series of polysilylated derivatives $[FeC_{10}DMS_nH_{10-n}]$ ($n$ = 7, 8, 9, 10) is analyzed by CV, single-crystal XRD, NMR and UV/VIS spectroscopy to evaluate the effect of silylation on the electronic properties of metallocenes. The obtained data are supported by quantum-chemical calculations.

In the context of perhalogenated Cp compounds, the reaction of $C_5X_6$ (X = Cl, Br) with $AsF_5$ and $SbF_5$ is investigated. Here, the formation of unprecedented [2+2]-cycloaddition products of two Cp cations $[C_5X_5]^+$ is observed. The obtained dications $[C_{10}X_{10}]^{2+}$ are analyzed by XRD and NMR spectroscopy. DFT calculations reveal that the dimerzation to [2+2]- instead of [2+4]-products is thermodynamically preferred due to the formation of two allylic $\pi$-electron systems. Furthermore, in cooperation with the group of Prof. Dr. Schulz the electrochemical properties of $[C_5(C_6F_5)_5]^+$ are presented.

# Kurzzusammenfassung

Im Rahmen dieser Arbeit wurden effiziente Strategien zur Synthese von perfunktionalisierten Cp-Verbindungen untersucht. Es wird eine Eintopfreaktion im Multigramm-Maßstab zur Synthese von $[FeC_{10}(HgO_2CC_3H_7)_{10}]$ ausgehend von Ferrocen und Quecksilber(II)butyrat beschrieben. In der resultierenden Verbindung sind die Hg-C-Bindungen inert gegenüber Oxidation und Hydrolyse durch Wasser oder starken Brønsted-Säuren, wie Trifluoressigsäure oder $[C_5F_5NH][SbF_6]$. Die Reaktion mit den jeweiligen Brønsted-Säuren führt zur vollständigen Protonierung der Carboxylateinheiten, wohingegen $[FeC_{10}(HgO_2CCF_3)_{10}]$ und $[FeC_{10}Hg_{10}(C_5F_5N)_n][SbF_6]_{10}$ gebildet werden. Im Pentafluoropyridinkomplex werden die Liganden durch Solvolyse in stärker koordinierenden Lösemitteln substituiert, wobei die seltene Beispiele für organometallische Decakationen $[FeC_{10}(HgL)_{10}][SbF_6]_{10}$ (L = MeCN, THT) entstehen. Die Bestimmung der jeweiligen Oxidationspotentiale zeigt eine steigende Redoxkraft der jeweiligen (löslichen) Ferrocenderivate in Abhängigkeit zur Lewis-Acidität der Hg-Positionen. Die chemische Oxidation mittels $[NO]^+$- und $[NO_2]^+$-Salzen sowie mit $MoF_6$ erlaubt die Isolation der jeweiligen Undecakationen. Auf der Basis von Einkristall-Röntgenbeugung der Verbindungen $[FeC_{10}(HgX)_{10}]$ (X = Cl, $O_2CCF_3$, $O_2CCCl_3$), $[FeC_{10}(HgTHT)_{10}][SbF_6]_{10}$ und $[FeC_{10}(HgMeCN)_{10}][SbF_6]_{10}[MoF_6]$ werden erstmalig kristallographische Daten über permetalierte aromatische Verbindungen präsentiert.

Eine vollständige Halodemercurierung der Verbindung $[FeC_{10}(HgO_2CC_3H_7)_{10}]$ wird durch Reaktion mit $K[Br_3]$ gefolgt von Halogenierung mit $FeBr_3$ und elementarem Brom erzielt. Die Oxidation zum entsprechenden Ferroceniumkation erfolgt durch Umsetzung mit $AsF_5$. Mit einem Oxidationspotential von $E_{1/2}$ = 1.1 V vs. Ferrocen stellt $[FeC_{10}Br_{10}]^+$ eines der potentesten Ferrocen-basierten Oxidationsmittel dar. Die Funktionalisierung der C-Br-Bindungen in $[FeC_{10}Br_{10}]$ wird durch Metallierung mit elementarem Magnesium oder Lithium-Halogen-Austausch erzielt. Anschließende Reaktion mit DMSCl führt zur Entstehung von Gemischen aus polysilylierten Ferrocenen. Ein vollständig silyliertes Derivat $[FeC_{10}DMS_{10}]$ wird durch wiederholte Metallierungs-Silylierungs-Sequenzen erhalten. Die Serie an Polysilylferrocenen $[FeC_{10}DMS_nH_{10-n}]$ ($n$ = 7, 8, 9, 10) wurde mittels XRD, NMR- und UV/VIS-Spektroskopie hinsichtlich Änderungen der elektronischen Struktur untersucht. Der Ergebnisse wurden durch quantenchemische Berechnungen unterstützt.

Mit dem Ziel, kationische Cp-Verbindungen zu isolieren, wurden die Reaktionen von $C_5X_6$ (X = Cl, Br) mit den Lewis-Säuren $AsF_5$ und $SbF_5$ untersucht. Dabei wird die Entstehung der formalen Produkte einer [2+2]-Cycloaddition ausgehend von zwei

$[C_5X_5]^+$-Einheiten beobachtet. Die entstandenen Dikationen $[C_{10}X_{10}]^{2+}$ wurden mittels XRD und NMR-Spektroskopie untersucht. Quantenchemische Berechnungen zeigen, dass die Dimerisierung zu [2+2]- anstelle von [2+4]-Produkten aufgrund der Bildung von zwei allylischen $\pi$-Elektronsystemen thermodynamisch bevorzugt ist. Des Weiteren werden in Kooperation mit der Gruppe um Prof. Dr. Schulz die elektrochemischen Eigenschaften der Verbindung $[C_5(C_6F_5)_5]^+$ präsentiert.

# List of Abbreviations

| Abbreviation | Definition |
|---|---|
| Ac | acetyl, COMe |
| AO | atomic orbital |
| Bu | butyl, $C_4H_9$ |
| Cp | cyclopentadienyl, $C_5H_5$ |
| $\Delta E_{\text{elstat}}$ | electrostatic interaction energy |
| $\Delta E_{\text{int}}$ | interaction energy |
| $\Delta E_{\text{orb}}$ | orbital interaction energy |
| $\Delta E_{\text{Pauli}}$ | Pauli interaction energy |
| $\Delta G^{\ddagger}$ | rotational barrier |
| DFT | density-functional theory |
| DMS | dimethylsilyl, $SiMe_2H$ |
| *et al.* | *et alii* |
| $E_{1/2}$ | half-wave potential |
| $E$ | electrostatic potential |
| EDA | energy decomposition analysis |
| EN | electronegativity |
| EPR | electron paramagnetic resonance |
| EWG | electron withdrawing group |
| HOMO | highest occupied molecular orbital |
| IR | infrared |

| Abbreviation | Definition |
|---|---|
| LCAO | linear combination of atomic orbitals |
| LDA | lithium diisopropylamide |
| LUMO | lowest unoccupied molecular orbital |
| Me | methyl, $CH_3$ |
| MO | molecular orbital |
| *peri*-naph | *peri*-naphtyl, $C_{10}H_6$ |
| NBO | natural bond orbital |
| NFSI | N-fluorobenzenesulfonimide |
| NHE | normal hydrogen electrode |
| NMR | nuclear magnetic resonance |
| NQR | nuclear quadrupole resonance |
| py | pyridine, $C_5H_5N$ |
| $q$ | natural charge |
| SALC | symmetry adapted linear combination |
| SCE | standard calomel electrode |
| TFA | trifluoroacetate, $O_2CCF_3$ |
| THT | tetrahydrothiophene |
| TIPS | tri-*iso*-propylsilyl, Si(*iso*-$C_3H_7$) |
| TMP | 2,2,6,6-Tetramethylpiperidinyl, $C_9H_{18}N$ |
| TMS | trimethylsilyl, $SiMe_3$ |
| tos | tosyl, $CH_3C_6H_4SO_2$ |
| UV | ultraviolet |
| VE | valence electron |
| VIS | visible |
| XRD | X-ray diffraction |

# Table of Contents

# 1 Introduction

Since the serendipitous discovery of ferrocene by the thermal cracking of dicyclopentadiene in iron tubes as a “yellow sludge" in the late 1940s,[1] it was unforeseeable that cyclopentadienyl (Cp) chemistry was going to overwhelm organometallic chemistry and reveal the tremendously versatile field of metallocenes. From the moment of its discovery, ferrocene has fascinated chemists due to basically unprecedented thermally and chemically inert metal-carbon bonds, its high solubility in organic solvents and its tolerance for water. At the time, its composition was unclear, however, the attention was attracted when Kealey and Pauson in 1951[2] as well as Miller *et al.* in the following year[3] independently reported the isolation of a compound with the overall formula $FeC_{10}H_{10}$. The authors suggested $\sigma$-bonded cyclopentadienyl ligands to a central iron atom as the molecular structure. However, this structural suggestion was contradicted by the experimental observations of the absence of a dipole moment, its infrared (IR) spectrum as well as the diamagnetism observed by Wilkinson and co-workers.[4] In the same year, the structure was unambiguously determined by Fischer using X-ray diffraction data (XRD), revealing a doubly $\eta^5$-coordinated iron center.[5,6] The correct structural description of ferrocene, in combination with the understanding of its electronic structure represents a milestone for general chemistry from the last decades. In 1973 Fischer and Wilkinson were awarded the Nobel prize for their contributions in the field of organometallic chemistry.

Since then, numerous applications were found for ferrocene and its derivatives from electrochemistry[7] to catalysis.[8–10] They are known as building blocks in particular for polymers,[11–13] dendrimers[14–17] as well as micelles[18] and supramolecular structures.[19–21] Apart from that, ferrocene derivatives have found pharmaceutical applications in a number of drugs,[22–24] for instance the well-known anti malaria agent ferroquin.[25,26] The extraordinary stability of ferrocene, as well as its heavier congeners ruthenocene and osmocene, can be rationalized with the 18-valence electron (VE) rule[27,28] in contrast to the neighboring manganocene derivatives in the low-spin state (17 VE) and cobaltocene (19 VE, a powerful reductant). Nevertheless, it can be easily oxidized at $E_{1/2}$ = 0.31 V vs. saturated calomel electrode (SCE) yielding deep blue ferrocenium salts $[FeC_{10}H_{10}]^+$ which are isoelectronic to manganocene.[29] As expected those ferrocenium compounds reveal sensitivity towards oxygen, moisture and nucleophiles,[30] but to a considerable less extent in comparison to manganocene. Functional groups have a significant influence on the electrochemical properties of ferrocene (Figure 1). For instance, while the permethylation of the cyclopentadienyl ligands lowers

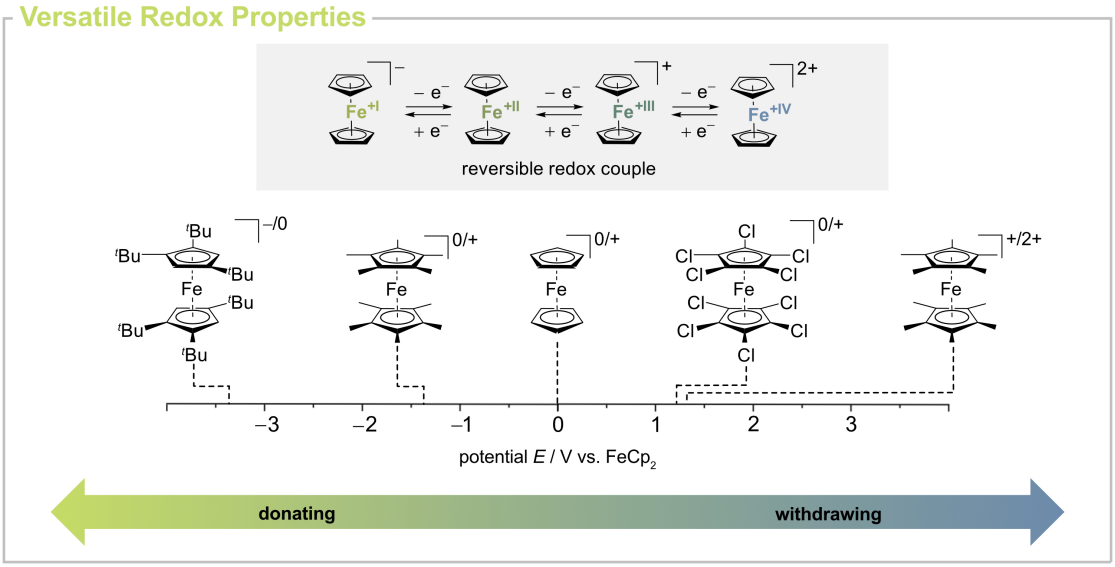


**Figure 1.** Representation of possible redox states in ferrocene derivatives and redox potentials of selected metallocenes.

the first oxidation to $E_{1/2} = -0.096$ V vs. SCE,[31] electron-withdrawing groups, e.g. carboxylic or halogenated groups, increase the oxidation potentials drastically.[32] Moreover, the fine-tuning of the redox properties enables the isolation of reactive (redox)species, which was illustrated recently by the structural characterization of an iron(I)[33] and an iron(IV)[34] species. Functionalization of cyclopentadienyl ligands is therefore an active research field in organometallic chemistry resulting in an ever-growing family of substituted cyclopentadienyl compounds.[35]

Acceptor-substituted cyclopentadienyl anions are promising materials to access extreme electron poor metallocenes as well as other Cp complexes or to stabilize reactive cations, e.g. silyl cations,[36] due to the expected increased stability towards strong oxidizers and Lewis acids. However, the preparation of acceptor-substituted cyclopentadienyl ligands presents a synthetic challenge due to changed intrinsic physicochemical properties of the ligand itself, especially regarding its stability and basicity. Additionally, side reactions induced by electron withdrawing groups (EWGs) can be problematic. Generally, substituted ferrocenes are available by either reaction of a prefunctionalized Cp ligand with iron(II) sources or by postfunctionalization of ferrocene itself, typically by electrophilic aromatic substitutions or deprotonations. The latter approach has proven to be especially useful in terms of diastereo- and enantioselective synthesis of chirally disubstituted metallocenes *via* directed metalation followed by functionalization with an electrophile.[37] However, the reactivity towards electrophilic attacks becomes drastically decreased when acceptor-substituents are taken into account. For instance, fluorination of 1,1′,2,3,4,5-hexafluoroferrocene with *n*-BuLi and N-fluorobenzenesulfonimide (NFSI) was unsuccessful as the nucleophilicity of the metalated cyclopentadienyl ligand was too low.[38] Further on, cyclopentadienyl anions with multiple withdrawing groups show

in many cases drastically reduced Lewis basicity as demonstrated by the $[C_5(CF_3)_5]^-$ anion which displays a weakly coordinating behavior instead of forming metal-carbon bonds in several metal complexes.[39] Especially, when halogenated groups are taken into account, the coordination of an acceptor substituted cyclopentadienyl anion to a Lewis acidic metal center often results in thermally unstable compounds due to possible metal halide elimination which is emphasized by decomposition of $[Li(C_5(CF_3)H_4)]$ to the corresponding fulvene.[40] If the withdrawing groups exhibit Lewis basic sites a possible coordination *via* the aromatic $\pi$-electron system might be prevented as demonstrated by $[C_5(CN)_5]^-$ which forms $\sigma$-bonded metal complexes *via* the nitrile groups.[41,42] Due to these difficulties acceptor-substituted cyclopentadienyl compounds are less represented in the literature in contrast to their donor-substituted counterparts. Here, the most popular derivatives are polyalkylated or -arylated cyclopentadienyl ligands. In the following chapters synthetic pathways to highly acceptor-substituted cyclopentadienyl compounds as well as the changes in the chemical and electronic behavior of the corresponding compounds will be discussed.

## 1.1 Electronic Properties

The Cp anion is a prototypical aromatic compound as it features a planar, conjugated $6\pi$-electron system in agreement with Hückel's rule and undergoes electrophilic aromatic substitution reactions similar to benzene but is resistant towards catalytic hydrogenation and Diels-Alder type reactions. Hence, Woodward and co-workers concluded that also ferrocene has aromatic character.[43] Depending on the substituents on the cyclopentadienide the properties as a ligand in metal-organic complexes vary. The conjugated $\pi$-electron system comprises five $p_z$ atomic orbitals (AOs) which can be combined in a MO-LCAO-ansatz to five molecular orbitals (MOs). The highest occupied molecular orbital (HOMO-$e_1$) and lowest unoccupied molecular orbital (LUMO-$e_2$) are both degenerated twice, while the lowest orbital has an $a_1$-symmetry (Figure 2). The latter is responsible for the $\sigma$-donor properties of the ligand, while $\pi$-donor and $\delta$-acceptor properties are governed by the HOMO and LUMO, respectively. The donor and acceptor properties depend on the energies of the orbitals, and therefore ultimately depending on the substituents as they are influencing the orbital energies. Generally, acceptor substituents lower the energies of all orbitals and consequently the Cp's $\sigma$- and $\pi$-donor ability but increase its $\delta$-acceptor properties. However, the extent of these effects depends on many factors, such as the electron-pulling behavior of the groups and their elements, making it difficult to predict it *a priori*. For example, the perfluorinated Cp anion $[C_5F_5]^-$ exhibits only slightly decreased frontier orbital energies in comparison the unsubstituted analogue. Here, the withdrawing $-$I-effect of fluorine is compensated by the competing +M-effect. In contrast, in $[C_5(CF_3)_5]^-$ those energies are significantly lowered due to a missing +M-effect of the $(CF_3)$-groups, resulting in weaker donor abilities and consequently decreased overall bonding interactions in metal complexes.[44]

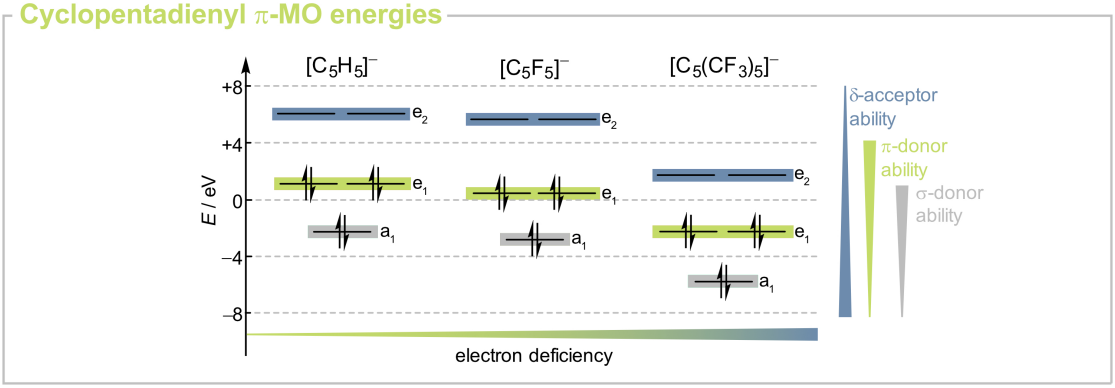


**Figure 2.** Simplified $\pi$-MO (BP86-D3(BJ)/def2-TZVP) energies of HOMO-$e_1$ (green), sub-HOMO-$a_1$ (grey) and LUMO-$e_2$ (blue) of selected cyclopentadienyl anions and the corresponding influence on donor and acceptor properties.[44]

Further insight into the bonding situation of metal complexes can be generated from MO considerations. In case of ferrocene, a physical realistic interpretation of the chemical bond could use neutral radical fragments. However, a neutral Cp fragment with $D_{5h}$ symmetry is subject to Jahn-Teller distortion due to occupation of the $e_1$ orbital by three electrons. Hence, the use of ionic fragments, $Cp^-$ and $Fe^{2+}$, results in a simplified qualitative model.[46] Here, the previously mentioned five $\pi$-MOs, $a_1$, $e_1$ and $e_2$, for two Cp anions can be combined to a total of ten pairwise symmetry adapted linear combinations (SALC, Figure 3, top). Linear combination of the corresponding ligand SALC-MOs and the valence AOs of the metal results in the MO diagram depicted in Figure 3 (bottom).[45] The frontier orbitals in ferrocene are mainly metal-centered and are separated into three sets $e_{2g}$ ($d_{x^2-y^2}$, $d_{xy}$), $a'_{1g}$ ($d_{z^2}$) and $e^*_{1g}$ ($d_{xz}$, $d_{yz}$) whereas the first one describes a bonding, the second one a non-bonding and the latter an anti-bonding contribution.[47] The main contribution to the bonding, according to quantum chemical calculations, is an interaction between the occupied $e_{1g}$- and $e_{1u}$-SALC-MOs (which are derived by combination of two $e_1$-orbitals - $HOMO^{Cp}$) of the ligands and empty Fe-AOs ($d_{xz}$, $d_{yz}$).[46] This interaction is strongly depending on the relative energies of the SALC-MOs, $e_{1g}$ and $e_{1u}$, hence, on the $\pi$-donor ability of the ligand. $\delta$-backdonation is best described by interactions of empty $e_{2g}$ and $e_{2u}$ ligand orbitals and the occupied $e_{2g}$ metal orbitals *via* the $d_{xy}$ and $d_{x^2-y^2}$ orbitals of iron. The $a_{1g}$-SALC MO interactions with the $d_z$ orbitals contribute to the bonding by integration of empty s and $p_z$ orbitals.[46] The trend observed in the MO energies of acceptor substituted cyclopentadienyl ligands may lead to the assumption, that electron withdrawing groups will also lead to an overall energetic decrease of the metallocene $\pi$-orbital energies. However, theoretical and experimental results show that the orbital energy trend cannot be directly transferred to the corresponding coordinated ligand in a metal complex, i.e. a metallocene. For instance, in haloferocenes the substituents mainly stabilize the HOMO while weakly destabilizing the LUMO explaining e.g. hypsochromic shifts of observed bands associated with d-d

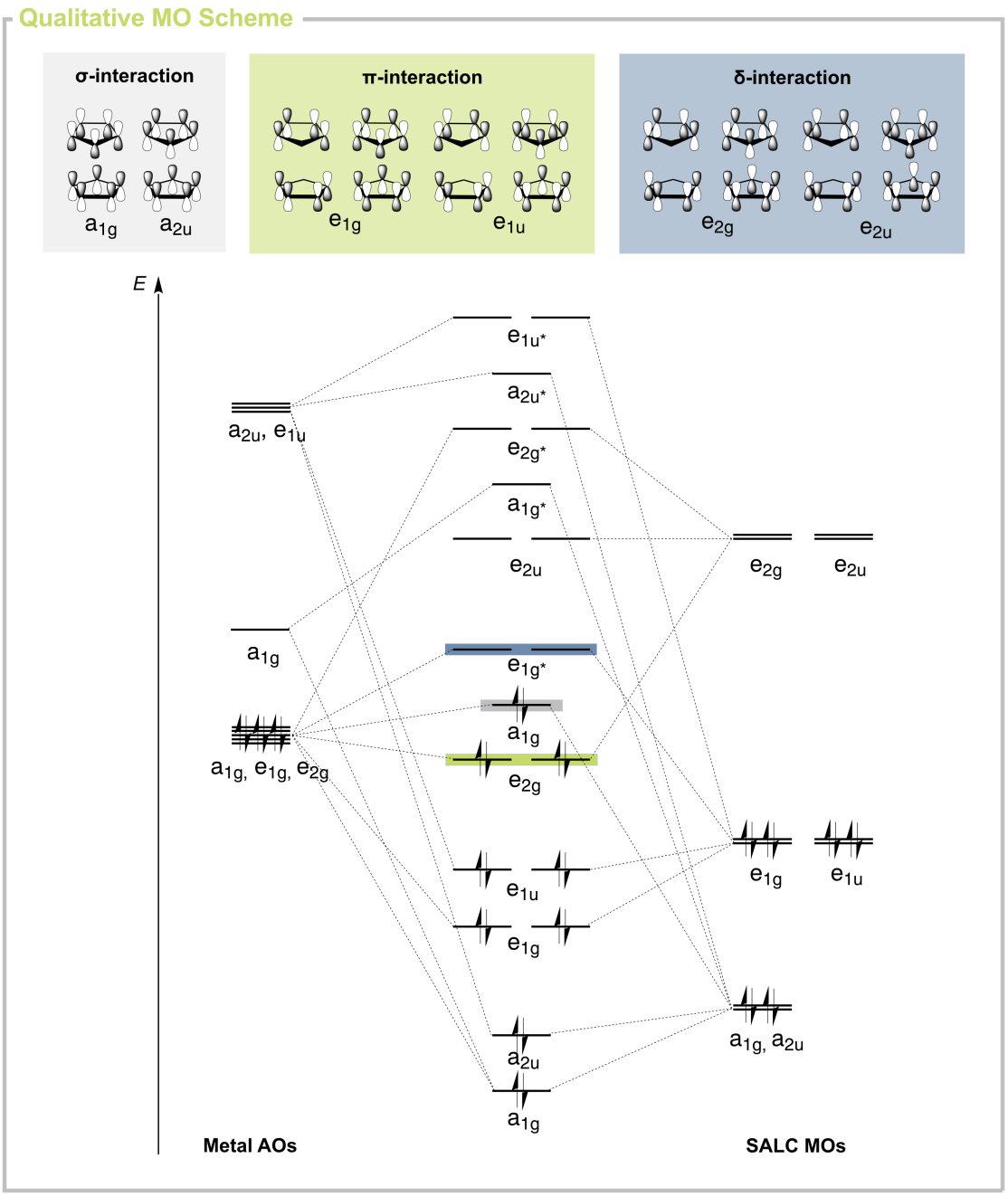


**Figure 3.** Simplified $\pi$-MO diagram of ferrocenes (bottom) as well as illustration of SALC-MOs of HOMO ($e_1$-SALC), HOMO-1 ($a_1$-SALC) and LUMO ($e_2$-SALC) the cyclopentadienyl ligand.[45]

transitions in their UV/VIS spectra.[48] In contrast to this, trimethylsilyl groups (weak acceptors) only marginally influence the HOMO energies but predominantly lower the LUMO energy as demonstrated by bathochromic shifts of these bands in the UV/VIS spectra of polysilylated ferrocenes.[49,50]

To analyze the overall bonding regarding its different contributions, i.e. constructive and repulsive orbital as well as electrostatic interactions, energy decomposition analysis (EDA) is used.[51,52] The interaction energy ($\Delta E_{int}$) between two fragments, i.e. metal and ligand, can be partitioned in three major contributions ($\Delta E_{elstat}$, $\Delta E_{Pauli}$ and $\Delta E_{orb}$) according to Equation 1.1. Here, $\Delta E_{elstat}$ is the electrostatic contribution, $\Delta E_{Pauli}$ describes repulsion of filled orbitals and $\Delta E_{orb}$ stabilizing orbital interactions. The ratio $\Delta E_{elstat}/\Delta E_{orb}$ can be used to interpret the bond character. In ferrocene covalent (48.9 to 55 %) and electrostatic interactions (45 to 51.1 %) are roughly similar. Orbital interactions are mainly a result of $\pi$-donation from the HOMO ($e_1$) to the metal center (64.7 % of $\Delta E_{orb}$).[53]

$$\Delta E_{int} = \Delta E_{elstat} + \Delta E_{Pauli} + \Delta E_{orb} \tag{1.1}$$

Considering electron withdrawing groups (e.g. halogens, nitriles, silyl groups) the $\pi$-donor ability of the cyclopentadienyl ligand decreases with every acceptor substituent affecting the overall interaction energies. This was analyzed by Kudinov *et al.* by EDA on monosubstituted ruthenocene derivatives in particular.[54] Considering the $[RuCp]^+$ and the $[C_5H_4X]^-$ fragment the introduction of one electron withdrawing group (e.g., X = OAc) the interaction energies $\Delta E_{int}$ decrease mainly due to strongly reduced elec-

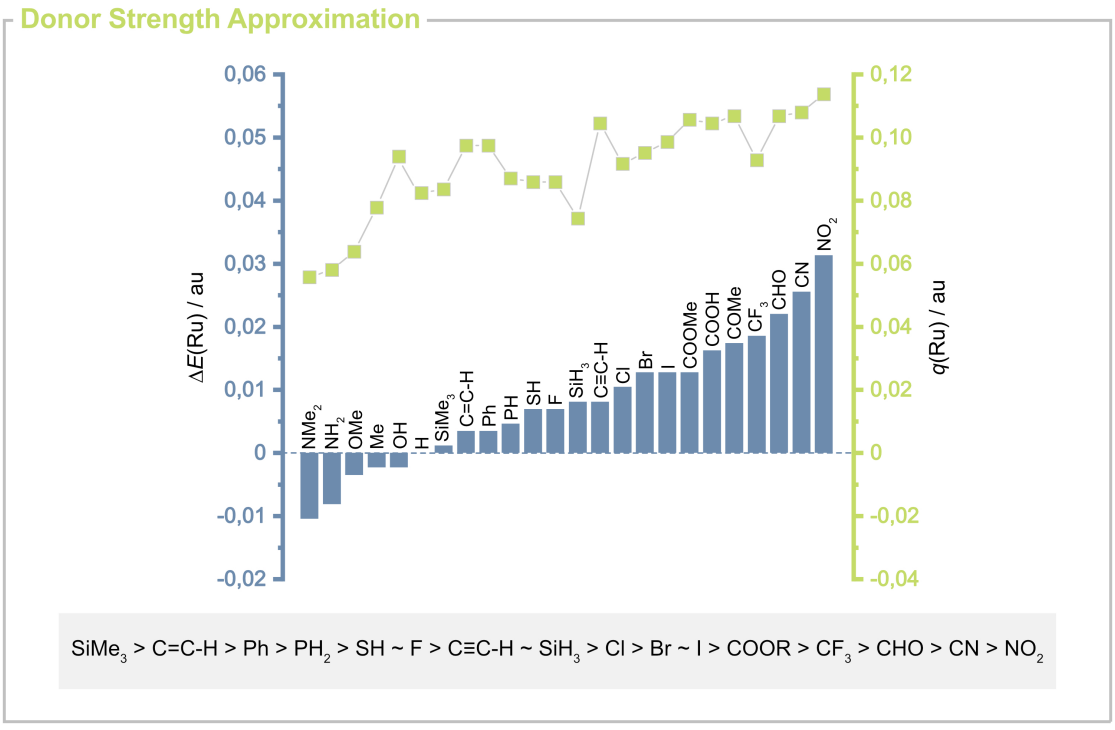


**Figure 4.** Illustration of the difference in the electrostatic potentials at Ru ($\Delta E$(Ru), blue) in $[RuCp(C_5H_4R)]$ and natural charges at the Ru atom ($q$(Ru), green) depending on different Cp substitutents (BP86/def2-TZVPP//BP86/TZ2P). Gray box: derived donor strength approximation of EWGs by evaluation of $\Delta E$(Ru) and $q$(Ru) values.[54]

trostatic interaction $\Delta E_{\text{elstat}}$. The contributions $\Delta E_{\text{orb}}$ and $\Delta E_{\text{Pauli}}$ decrease as well but to a considerable less extent. In addition to the considerations above, the Cp donor properties were analyzed depending on the metallocene's electrostatic potential. Here, the change in the potentials at the corresponding bonding partners in [RuCp($C_5H_4R$)] with respect to unsubstituted ruthenocene were discussed. As a result, a correlation regarding the Cp donor strength was found (Figure 4, blue axis) allowing a qualitative ranking of the donor abilities of the corresponding functional groups (X). Further on, NBO analysis reveals increased natural charges at the ruthenium center $q$(Ru) (Figure 4, green axis) which is roughly consistent with the donor ability of the substituents further demonstrating the withdrawing character of the functional groups. Although these calculations reveal general trends in monosubstituted metallocene derivatives generalization towards poly- or perfunctionalized compounds is difficult due to synergistic effects of several functional groups.

## 1.2 Cyclopentadienyl Ions with Acceptor-Substituents

Electrochemical investigations on cyclopentadienyl anions reveal two one-electron oxidations indicating the possible formation of a radical species as well as a cyclopentadienyl cation (Figure 5). Herein, alkyl substituted anions are readily oxidized as the oxidation processes already take place at low potentials exemplarily shown for $[C_5{}^{i}Pr_5]^-$ with a first oxidation at $E_{1/2} = -1.91$ V and the second at $E_{1/2} = 0.58$ V vs. ferrocene.[55] Substitution of the $^{i}$Pr substituents by electron-withdrawing groups increases the oxidation potentials up to $E_{1/2} = 0.38$ V for radical formation and up to $E_{1/2} = 0.89$ V for cation formation as shown in $[C_5(CN)_4NH_2]^-$.[56] As the observed oxidation potentials should be still accessible by common oxidizing agents[57] the isolation of such redox species is reasonable. However, in view of the number of spectroscopically detected cyclopentadienyl radicals and cations only a few of them were structurally characterized so far due to the high reactivity of the corresponding species due to disrupted aromaticity. Those are summarized as a series of alkylated and arylated cyclopentadienyl radicals stabilized by sterically demanding substituents[58–61] and one donor-acceptor stabilized compound $[C_5(CN)_4NH_2]^{\cdot}$[56] (Figure 5). A structurally characterized cyclopentadienyl cation was never reported in the literature.

To explain the instability of the cyclopentadienyl cation $[C_5H_5]^+$ the electronic structure has to be considered. The Cp cation is one of the most prominent examples for antiaromatic compounds, due to its cyclic $4n$ $\pi$-electron system which leads to a strong destabilization of the molecule, according to Breslow.[62] Generally, the concept of (anti)aromaticity classifies a compound regarding its thermodynamic (de)stabilization originating from a delocalized $\pi$-electron system, relative to its non-delocalized analogue. However, the simplified definition using purely the electron count of the $\pi$-electron system has to be treated with care as it lacks of a well-founded physical basis. The indirect evaluation of (anti)aromaticity by physicochemical properties, like bond length

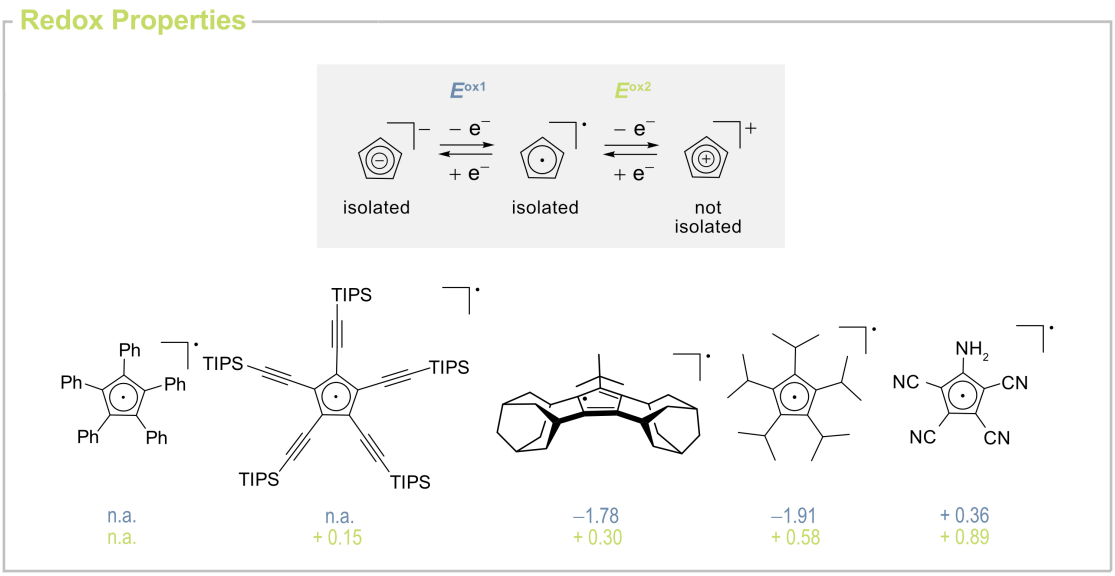


**Figure 5.** Selected known structurally characterized cyclopentadienyl radicals and the corresponding redox potentials of $E(Cp^{-}/Cp^{\cdot})$ (blue) and $E(Cp^{\cdot}/Cp^{+})$ (green) vs. ferrocene.[56]

equalization, energetic stabilization of magnetic properties, allows an improved understanding of the $\pi$-electron system.[63] For instance, based on these properties Baird and Karadakov concluded reverse $\pi$-electron count ($4n$ – aromatic, $4n$+2 – antiaromatic) in the first exited triplet states of benzene and cyclobutadiene.[64,65]

Considering the cyclopentadienyl cation $[C_5H_5]^+$ and its derivatives $[C_5R_5]^+$ calculations reveal two possible electronic ground states on various levels of theory which are summarized as a degenerate Jahn-Teller distorted (antiaromatic) singlet state ($^1A_1$) with (partially) localized $\pi$-bonds and an (aromatic) triplet state ($^3A_2'$).[66–73] Triplet-singlet energy gaps are found to be small which is consistent for all reported cyclopentadienyl cations (R = H, Cl, $^i$Pr, Ph).[55,74–76] The diradical character, induced by the triplet $^3A_2'$ state, allows several side reactions which prevented the isolation so far. For instance, the unsubstituted cyclopentadienyl cation typically undergoes dimerization *via* formation of diamagnetic [2+4] cycloaddition species.[77] Dimerization can be suppressed by sterically demanding substituents, which is an efficient strategy for the stabilization of cyclopentadienyl radicals but insufficient for cations since those cations are strongly oxidizing and Lewis acidic themselves. Therefore, the $[C_5Ph_5]^+$ decomposes *via* C-H cleavage and formation of additional C-C bonds[78] while for $[C_5{}^iPr_5]^+$ hydrogen abstraction from the organic solvent as well as the alkyl groups is observed.[55,79] In 2002, the structural characterization of the stable permethylated cation $[C_5Me_5]^+$ was reported,[80] but this result turned out to be incorrect a few months later and the isolated cation was identified as $[C_5Me_5H_2]^+$, instead.[81–83]

Theoretical studies (B3LYP/6-311+G(d, p) closed-shell, UB3LYP/6-311+G(d,p) open-shell) reveal that the electronic structure of the cyclopentadienyl cation $(C_5H_4R)^+$ is

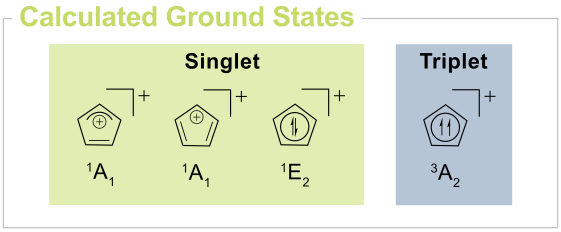


**Figure 6.** Representations of possible ground states in the cyclopentadienyl cation with a $4\pi$-electron system.[67]

significantly affected by substitutional effects. The triplet state is favored when the antiaromatic character is decreased according to Baird's rule. The antiaromaticity is influenced by $\pi$-electron substitutional effects. Here, electron-donating groups (e.g., R = $NH_2$, OH, F, $CH_3$, NO) strongly interact with the $\pi$-system. As a consequence, the extent of antiaromaticity is increased with increasing density of delocalized electrons while electron withdrawing groups are found to promote electron delocalization and therefore triplet aromaticity.[73] The sensitivity towards substitutional effects demonstrate that the stabilization of a cyclopentadienyl cation by suitable functional groups is reasonable. Based on the experimentally observed decomposition pathways of previously observed cyclopentadienyl cations perfunctionalization of cyclopentadienyl compounds is crucial in order to block decomposition *via* C-H bonds. Another requirement to potential substituents is stability towards strong Lewis acids and oxidizing agents, inferring that perhalogenated groups might be able to stabilize a Cp cation by effectively inhibiting possible decomposition pathways. Based on these results the Dutton group was able to identify perfunctionalized cyclopentadienyl cations with fluorinated groups (-$CF_3$, -$C_6F_5$) which should display a sufficient stability as they offer a large singlet-triplet energy gap with a singlet ground state. Furthermore, those cations exhibit similar electronic and magnetic properties as the isolobal boroles which are known to be stable. Additionally, the tendency to undergo side reactions, such as Diels-Alder reaction, halide abstraction, etc., is expected to be low as these reactions are calculated to be endothermic under ambient conditions.[66] However, these specific substitutional patterns were never synthetically realized until today which prevents the experimental proof.

## 1.3 Perfunctionalization with Withdrawing Groups

Functionalization of nonreactive C-H bonds is one of the most fundamental concepts in organometalic chemistry and has been the focus of considerable investigation. However, in cyclopentadienyl chemistry, there is a strong discrepancy between the number of monofunctionalized cyclopentadienyl compounds compared to persubstituted ones. Perfunctionalization, especially with electron withdrawing groups, often proceeds in a two-step process, first metalation and secondly transformation of the carbon-metal moiety to the carbon-EWG function. Conceptually, this can be accomplished in an iterative

fashion by multiple consecutive metalation/functionalization steps or by activating all C-H bonds in a single step.

There are three conceptual pathways to obtain perfunctionalized Cp motifs $C_5R_5$ (Figure 7): firstly, by reaction of suitable functionalized building blocks to generate a Cp framework (e.g., *via* cyclization of prefunctionalized olefins or alkynes). Secondly, the fivefold functionalization of unsubstituted $C_5H_6$ and thirdly the postfunctionalization of existing Cp-containing compounds, such as metallocenes. The first two routes are advantageous because they offer access to the isolated ligand which can then be converted into the corresponding metal complexes. The postfunctionalization approach is in that regard inferior since optimization for different metal complexes appears likely. Nevertheless, also the first path has, often practical, barriers. It is widely used for the synthesis of the donor-substituted pentamethylcyclopentadiene from 3,4,5-trimethyl-2,5-heptadien-4-ol and *p*-toluenesulfonic acid.[84] However, the corresponding acceptor-substituted olefins are not readily available and cyclization conditions can be harsh (high temperatures, autoclave conditions).[39,85,86]

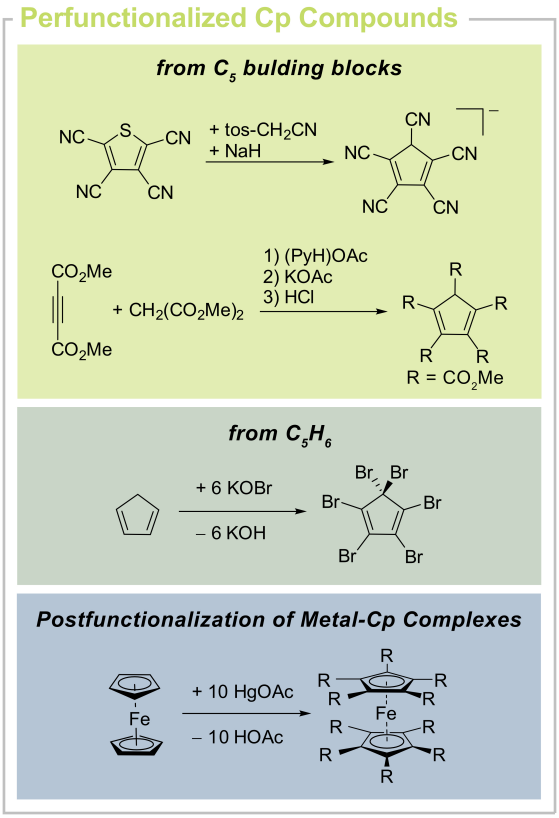


**Figure 7.** Selected reactions to obtain perfunctionalized Cp compounds starting from $C_5$ building blocks (top), $C_5H_6$ (middle) and Cp complexes (bottom).

The usage of unfunctionalized cyclopentadiene is challenging because the compound itself is not stable at room temperature and readily undergoes Diels-Alder reaction[87–89] with itself.[90,91] Although the dimerization is kinetically favored at room temperature, the corresponding *retro*-Diels-Alder reaction is thermodynamically preferred above 150 °C allowing the isolation of monocyclopentadiene. Generally, the tendency to undergo dimerization depends on the substitutional pattern as more electron-withdrawing substituents favor monomerization. In sterically demanding cyclopentadienyl compounds, $C_5R_5H$ (e.g., R = Me)[92] and in metal complexes[93] this type of reaction is sufficiently suppressed as well.

On the general Brønsted acidity scale cyclopentadiene is a weak acid. However, for a hydrocarbon its p$K_a$ of 16.0[94] is surprisingly low, especially when compared to other $sp^2$- or $sp^3$-hybridized hydrocarbons such as benzene (p$K_a$ = 43[95]) or methane (p$K_a$ > 48[96,97]). This can be explained by the extraordinary stabilization of the corre-

sponding anion $[C_5H_5]^-$, due to its aromatic character. The acidity is further increased when electron withdrawing groups are applied, exemplarily shown for $C_5(CF_3)_5H$ with a p$K_a$ value similar to sulfuric acid.[98] Hence, cyclopentadiene derivatives are easily transformed into the corresponding alkali metal compounds by appropriate Brønsted bases, such as organolithium reagents[99,100] or alkali metals[101] as well as alkali hydrides[102–106] or alkali amides.[107,108] Despite their high sensitivities against moisture and oxygen, those alkali metal salts have been established as typical cyclopentadienyl transfer reagents to convert different metal chlorides into the corresponding Cp-containing compounds, driven by the thermodynamically favored precipitation of alkali metal chlorides.[109] Thus, not only ferrocene was synthesized by metathesis of anhydrous $FeCl_2$ and NaCp[110] but also a large variety of other element cyclopentadienyl complexes, including main group compounds,[111,112] lanthanide[113] and some actinide complexes,[114] as well as transition metal derivatives.[115] Herein, especially 3d-transition metal complexes are strongly represented due to the great stability of the corresponding compounds including unsubstituted cyclopentadienyl ligands which can be easily handled. Second and third row complexes tend to be more reactive than their lighter counterparts and are therefore difficult to isolate. The kinetic stability of those complexes is increased by sterically demanding cyclopentadienyl ligands, such as polyalkylated or -silylated cyclopentadienyl anions.[116] Nevertheless, the different sensitivities of the corresponding metal compounds limit a possible postfunctionalization.

Postfunctionalization of preformed metal complexes can be accomplished by electrophilic aromatic substitution, metalation, cross-coupling reactions, by derivatization of substituents or by thermolysis of $\eta^6$-arene complexes.[117] For metallocenes, the electrophilic aromatic substitution pathway is of significant importance due to the surprisingly high reactivity of metallocenes.[118] Ferrocene undergoes $10^6$ to $10^9$ times faster electrophilic substitutions than benzene[119–121] and is therefore designated as “superaromat". Mechanistically, the reaction involves the addition of an electrophile ($E^+$) *via* formation of a $\sigma$-bonded cationic intermediate which is transformed into the substitution product after elimination of a proton attached to the attacked carbon atom.[122] Herein, the cation formation displays the rate determining step as the aromaticity of the compound is temporarily disrupted.[123] For metallocenes different possible intermediates have been discussed as the electrophilic attack could occur either at the cyclopentadienyl ring (*exo*-attack) or at the metal center (*endo*-attack). Protonated ferrocene, $[FeCp_2H]^+$, as the first identification of a metal-electrophile interaction[124] in this context displays a prototypical $\sigma$-complex. The absence of agostic interactions in the solid state structure (Figure 8)[125] confirms the existence of an *endo*-attack-pathway. However, in sterically demanding cyclopentadienyl compounds the electrophilic attack is found to occur at the ligand rather than at the metal center indicating the existence of an additional *exo*-pathway.[126] Until today, several types of electrophilic aromatic substitutions have been established including the famous Friedel-Crafts[122,127] and Vilsmeier-Haack reaction.[128,129] However, reactions introducing strongly withdrawing

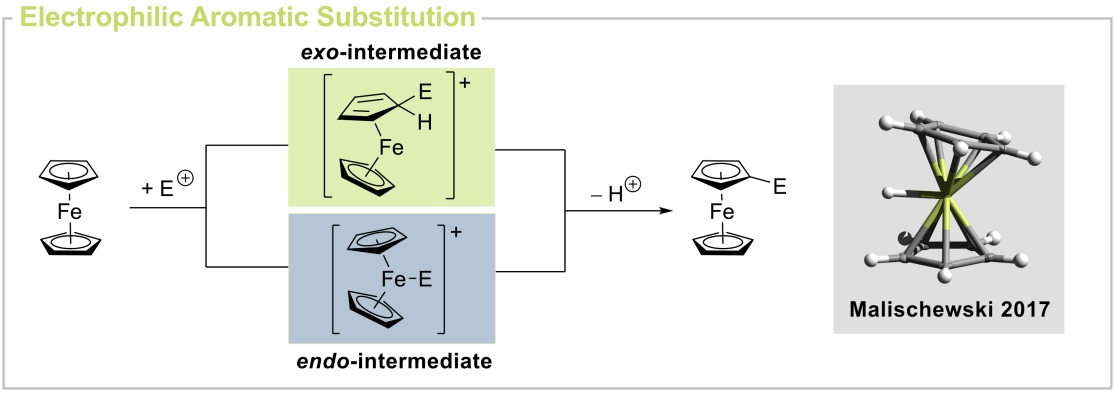


**Figure 8.** Possible electrophilic substitution pathways of ferrocene (left) and molecular structure of the $[FeCp_2H]^+$ (right).[125] Ellipsoids drawn with 75 % probability level. Color code: green - iron, grey - carbon, white - hydrogen.

groups such as sulfonation and Friedel-Crafts acylation usually stop after a single substitution per cyclopentadienyl ligand.[118,130,131] Moreover, direct substitution by oxidizing electrophiles (e.g. nitration or halogenation) is inhibited, as the ferrocenium cation is incapable to undergo electrophilic substitution.[132] Consequently, the introduction of multiple acceptor-substituents is difficult to achieve. In the following chapter synthetic pathways to perfunctionalized acceptor-substituted cyclopentadienyl compounds will be discussed.

### 1.3.1 Mercuration

Since the beginning of the $20^{th}$ century aromatic organomercury compounds are known for their bacteriostatic and fungicidic effect and have played an increasingly important role in medicine[133–135] and agriculture,[136] during the first half of the century. Hence, seed dressings based on phenylmercury chloride (Agronal) or acetate (Falisan) in particular have been developed and widely used.[137] However, possible hazards became apparent foremost in the 1950's after an organomercury poisoning in Minamata, Japan caused by biological methylation of mercury in the environment forming more toxic alkylmercury compounds.[138–140] Nowadays, the usage of organomercury compounds for industrial purposes is strictly regulated to reduce environmental pollution.[137] Consequently, these compounds are only rarely employed but are still used in particular as antiseptic,[141,142] for the modulation of surfaces[143–147] or in (metal)organic synthesis.[148]

The great toxicity of alkyl mercury compounds, $HgR_2$, is explained by their volatility and lipophilicity allowing rapid penetration through the skin and respiratory tract as well as its ability to pass the blood-brain barrier.[149,150] Furthermore, the stability of mercury carbon bonds prevent a simple degradation in organisms.[151] However, the toxicity and hazard of organomercury compounds differ between $R_2Hg$ (R = alkyl > aryl) and ionic RHgX salts due to their decreased volatility reducing the risk of exposure and can be therefore handled more safely. Organomercury compounds of the type RHgX (X =

halides, carboxylates, nitrates, etc.) are therefore mostly used for synthetic purposes.[148] The demand of mercury(II) compounds in (metal)organic synthesis can be explained by their superior reactivity towards nonreactive C-H bonds as sources of $Hg^{2+}$ which easily undergoes mono- or polymetalation of aromatics,[152–156] olefines[157] and even alkanes, such as methane.[158,159] The resulting metalated compounds are valuable precursors for further functionalizations, such as transmetalation[160–164] halogenation[165–167] or reductive demercuration reactions.[168–170]

A general feature of organomercury compounds is the formation of mercurophilic interactions. Metallophilicity is a non-covalent interaction which is typically observed for heavy late transition metal compounds, like $Pt^0$, $Hg^{2+}$ and $Au^+$, or main group compounds, like $Tl^+$, $Pb^{2+}$ and $Bi^{3+}$, with low coordination numbers.[172,173] Here, the nature of the phenomenon is attributed to relativistic and dispersion effects.[174–176] There is only limited experimental data available regarding the strength of this interaction,[177–181] however, the strongest $Au^+\cdots Au^+$ interactions were found to exceed even very strong hydrogen bonds, like in the anion $[HF_2]^-$.[174] Mercury involving $d^{10}\cdots d^{10}$ interactions are usually weaker and typically observed in solid state.[172,182] As a general rule of thumb, the strength of a mercurophilic interaction can be roughly estimated by the distances of the mercury atoms. This implies that Hg···Hg distances above 3.50 Å should only be associated with interaction energies in the order of magnitude of van-der-Waals interactions, especially considering the van-der-Waals radius of mercury (1.75 Å[183]).[172] There are only few examples of strong mercurophilic $d^{10}\cdots d^{10}$ contacts close to or below the distance of crystalline mercury (3.00 Å[184]). Here, the interaction is mainly enforced by the geometry of the ligand at the mercury center.[171,185] The shortest $Hg^{2+}\cdots Hg^{2+}$ distances of 2.80 Å are found in the *peri*-mercurated naphtalene dimer, *peri*-$[Hgnaph]_2$ (Figure 9). In the crystal structure the C-Hg-C angles clearly deviate from linearity to minimize the Hg···Hg repulsion. Evidence for mercurophilic interactions in solution or in the gas-phase is scarce.[186–190] However, mercurophilic interactions can have tremendous influence on the spectroscopic properties of certain compounds in solution or in solid state.[191,192] For instance, aggregates in solid state of $[Hg(C_6F_4)]_3$ are highly luminescent while the emission is quenched due to breakup of the aggregates by solvolysis.[193] In addition to that, investigations on mercurated aromatic acetylene compounds reveal that the heavy atoms have a positive impact on the phosphorescence properties due to increased intersystem crossing rates.[186–188]

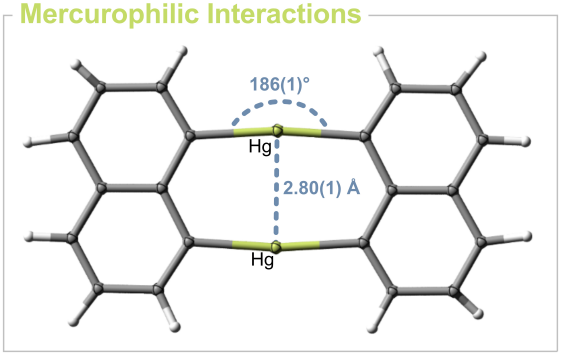


**Figure 9.** Molecular structure of *peri*-$[Hgnaph]_2$[171] in solid state as well as selected bond distances and angles. Ellipsoids drawn with 50 % probability level. Color code: green - mercury, grey - carbon, white - hydrogen.

The first evidence of a mercurated aromatic compound dates back to the end of the $19^{th}$ century by Dimroth who investigated the reaction of benzene with mercury(II) carboxylates (Eq. 1.2).[194–196] The reaction was later found to proceed *via* an electrophilic substitution pathway.[197,198] The success of the reaction depends on the electronic situation of the aromatic compounds as the presence of electron-donating groups facilitates the substitution emphasized by the reaction of phenol with mercury acetate which proceeds already at room temperature in contrast to benzene. However, in substituted aromatic compounds, $C_6H_5R$ (observed for R = $NO_2$, Me, $HgClO_4$), isomerization in *ortho-*, *meta-* and *para*-position is possible due to reversibility of the mercuration process.[199]

$$C_6H_6 + HgOAc_2 \longrightarrow C_6H_5HgOAc + HOAc \tag{1.2}$$

In addition to monomercuration, the usage of mercury(II) carboxylates is an excellent approach to obtain poly- and even permercurated derivatives as well.[200] Examples range from benzene[166,201] and naphthalene[167] compounds over five membered heterocycles like pyrrole,[202,203] furan[203,204] and thiophene[205,206] to cyclopentadiene.[207] Metal complexes were less investigated but examples are known for permercurated cymantrene and the corresponding rhenium analogue[208,209] as well as metallocenes[210–215] (Figure 10). Herein, the sandwich compounds exhibit a surprisingly high reactivity towards permercuration as shown by reaction of pentamethylruthenocene with one equivalent of mercury(II) acetate yielding a 4:1 mixture of unsubstituted and pentamercurated pentamethylruthenocene indicating autocatalytic reactivity.[154] This activity increases from iron to osmium within the group 8 metallocenes, although osmocene exhibits the lowest reactivity towards electrophilic aromatic substitution.[216,217] This contradicting trend is probably explained by increasing solubility of highly mercurated metallocenes in the order M = Os > Ru > Fe.[218] While mercuration of ruthenocene[213] and osmocene[214] affords pure mercurated products, the analogous ferrocene derivatives, $FeC_{10}(HgOAc)_{10}$[215] and $FeC_{10}Me_2(HgOAc)_8$,[218] suffer from insolubility and are therefore only poorly characterized by infrared spectroscopy and elemental analysis. Instead, the success of the reaction was determined indirectly by further transformation into the soluble perhalogenated analogues (see section 1.3.2). Here, the complete mercuration is seemingly hindered due to low solubility of the polymercurated intermediates yielding a mixture of polymercurated compounds containing low yields of the permercurated derivatives.[215,218]

The permetalated metallocene and cyclopentadiene derivatives should be ideal precursors for the synthesis of other perfunctionalized cyclopentadienyl compounds as the mercury-carbon bonds typically exhibit relatively low bonding energies.[219] However, linear organomercury compounds are typically stable towards air and moisture or other electrophiles explained by the low polarity of the Hg-C bonds as well as the low

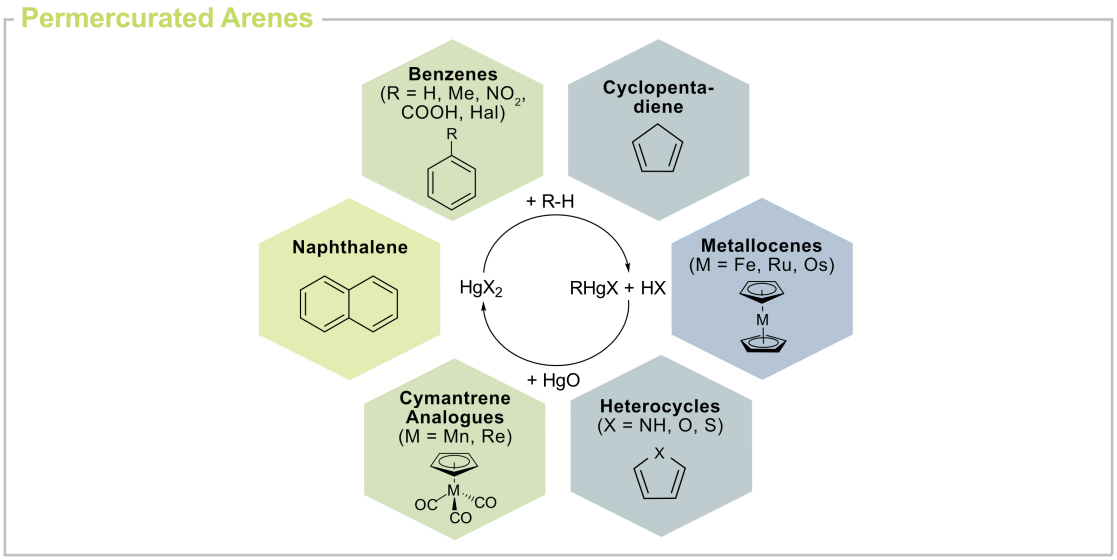


**Figure 10.** Overview of isolated permercurated arenes.

tendency to form adducts while increasing the coordination number.[220] Consequently, these derivatives are less reactive towards electrophiles than other analogous permetalated species (e.g., organomagnesium, organolithium). Electrophilic substitutions are limited to halogenation reactions. Transmetalations to effort more reactive metallocenes are realized with alkyllithium, RLi (R = Me, Bu),[221] or by Grignard reagents, like MeMgCl *via* formation of alkylmercury compounds, $HgR_2$.[222] This derivatization was successful for the mercurated analogues of ruthenocene and pentamethylruthenocene. Due to the high reactivity and poor solubility of the resulting compounds the success of the reaction was again estimated by analysis of the reaction products after treatment with electrophiles like methyl iodide, water or bromine. Similar reactions with a permercurated cyclopentadiene derivative were never reported.

### 1.3.2 Halogenation

Halogenation is an important tool in synthetic chemistry for the derivatization of compounds. Several postfunctionalization approaches were established so far including metal-halide exchange or cross-coupling reactions.[223] Furthermore, there is an increasing demand of halogenated groups for pharmaceutical[224,225] and agricultural[226] applications since halogen atoms or halogenated groups can act as bioisosters. Consequently, a large variety of mono- and polyhalogenated compounds have been reported, so far.

However, halogenation of single C-H bonds can lead to significant changes of the physical and chemical properties of (metal)organic compounds, due to steric and electronic effects. Halogens are electronegative elements. Replacement of C-H to C-X bonds results therefore in more polarized bonds and an increased overall dipole moment.[227] Hence, the overall polarity of the molecule is increased. Further on, the induced asym-

metry of the bonding electron density decreases the electronic richness of a molecule. In organic compounds, this negative inductive effect is reflected by decreased p$K_a$ values which is exemplarily shown for the deprotonation of a series of acidic acid compounds, $CR_3COOH$, with increasing halogen content.[228] Moreover, an increased oxidative stability of (per)halogenated groups is observed as a consequence of this effect. The extent of this withdrawing character correlates with the electronegativity of the introduced halogen atoms and should be therefore the highest for C-F bonds. However, due to competing $\pi$-donor ability *via* the lone pairs the inductive effect is compensated in the order F > Cl > Br > I according to nuclear magnetic resonance (NMR) experiments by the Olah group.[229] However, this conclusion is still under debate.[230] The $\pi$-donation of the halogens typically results in shortening of the C–X bond which was observed in several carbocations before.[231–237] This resonance effect is beneficial if the halogen is attached in $\alpha$-position to the cationic site ($\alpha$-halogen effect) but destabilizing if the cation is located in $\beta$-position to the R-X bond.[238] Both effects allow a charge delocalization in ionic compounds. For the isolation of the highly electrophilic and oxidizing cations, perfluorinated anions such as $[Al(OC(CF_3)_3)]^-$ or $[B(C_6F_5)_4]^-$ have found broad applications due to minimized coulomb interactions, oxidative sensitivity and polarizability of the anion surface.[239,240] Moreover, element-fluorine bonds typically exhibit relatively high bond energies causing a high thermal stability of the corresponding anions.[241]

Considering electrostatic potential calculations on R-X bonds, an anisotropic charge distribution is observed around the halogen atom due to polarization towards the R-X bond region. As a result, the halogen atoms are negatively polarized perpendicular to the R-X bond but become more positive at the outer-sphere.[242,243] The so-called $\sigma$-hole is more pronounced for the heavier halogen atoms (F < Cl < Br < I) due increased polarizability and decreased electronegativity (Figure 11). Additionally, halogenated compounds are able to form complexes with Lewis bases[244,245] *via* $\sigma$-hole interactions, the so-called halogen bonding.[246] The strength of this type of interaction is in range of 10 to 200 kJ mol$^{-1}$ and is the highest in iodinated compounds and the lowest in fluorinated compounds due to less pronounced $\sigma$-holes.[247,248] Halogen bonding *via* C-F bonds is therefore rarely

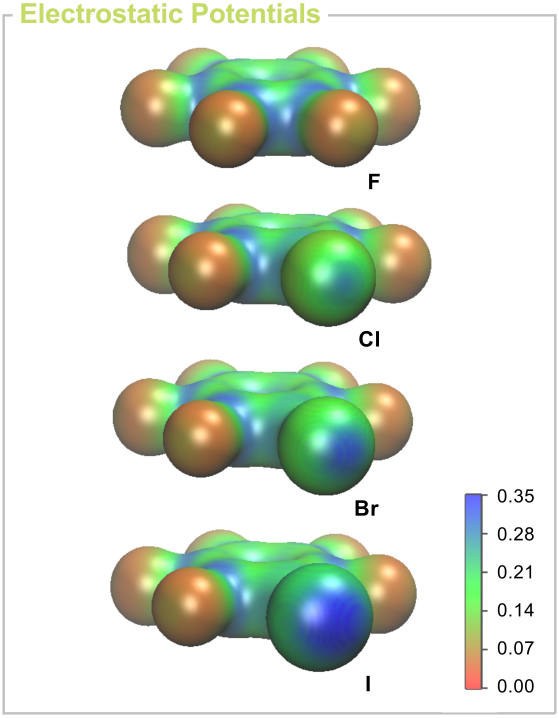


**Figure 11.** Plots of electrostatic potentials of perhalogenated benzenes (B3LYP/def2-TZVPP), $C_6F_5X$ (X = F, Cl, Br, I).

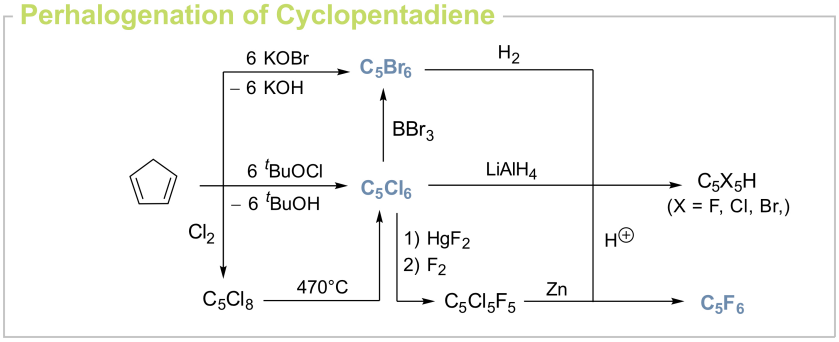


**Figure 12.** Selected reactions towards penta- and hexahalogenated cyclopentadiene compounds starting from $C_5H_6$.

observed.[249] However, the extent of the $\sigma$-hole is increased by electron withdrawing groups.[250,251] Further on, the introduction of halogens into a molecule could offer therefore additional hydrogen bonding sites as the halogen atom in the R-X bond can serve as a hydrogen bond acceptor (X = F, Cl, Br, I).[248]

Considering cyclopentadienyl compounds, all perhalogenated derivatives of the type $C_5X_6$ (X = F,[252] Cl,[253,254] Br[255,256]) are reported in literature except $C_5I_6$. In all cases, a synthetic protocol *via* direct halogenation of cyclopentadiene is difficult to achieve due to possible side reactions including the oxidation of the double bonds.[257–259] Nevertheless, this approach can be used if the resulting mixture of perhalogenated cyclopentenes and cyclopentanes are transformed into the cyclopentadiene derivatives at high temperatures[253] or by mild reducing agents like zinc or sodium amalgam, subsequently.[252] A direct conversion to the perhalogenated compounds is achieved by milder halogenation agents which is demonstrated by the reaction of $C_5H_6$ with an excess of potassium hypobromite or *tert*-butyl hypochlorite yielding $C_5X_6$ (X = Br,[255] Cl[260]). The corresponding perhalogenated derivatives are sources of electrophilic halogens themselves[261–263] and can be therefore easily converted into the $C_5X_5H$ derivatives by e.g. hydrogenation.[264–267] However, the pentahalogenated derivatives are prone to undergo *homo*-Diels-Alder reaction.

The perhalogenated derivatives were used in several investigations on the generation of a cyclopentadienyl cation by Lewis acids. Here, the choice of an appropriate Lewis acid is crucial to avoid possible side reactions, like halogen exchange[268] or oligomerization.[256,269–271] Promising results were obtained by Breslow *et al.* after treatment of $C_5Cl_6$ with neat $SbF_5$.[272] The electron paramagnetic resonance (EPR) spectrum of the mixture revealed signals which were assigned to a triplet state cyclopentadienyl cation (*vide supra*). However, the generated cation rapidly decomposed in the $SbF_5$ matrix above the freezing point of $SbF_5$. Quenching experiments with methanol revealed only 5 % monomeric $C_5Cl_5OMe$ but 90 % dimeric perchlorinated ketones. Similar reactions with $C_5F_6$ and $SbF_5$ (and $AsF_5$) resulted in fluorination of the double bonds.[266]

Attempts to generate a perhalogenated anion turned out to be surprisingly difficult with respect to the expected stability of the aromatic $\pi$-electron systems. A first report about a cyclopentadienyl anion dates back to 1955. Herein, the anion was generated by reaction of $C_5Cl_6$ with $LiAlH_4$.[267] The obtained anion distinguishes itself by extraordinary thermal instability probably due to possible alkali halide elimination. Although the use of thallium and tetraalkylammonium precursors is expected to stabilize cyclopentadienyl anions, $[Tl(C_5Cl_5)]$ and $R_4N[C_5Cl_5]$ were not structurally characterized due to remaining thermal instability:

> *"[Tl(C$_5$Cl$_5$)] ignites spontaneously at* $-15\,°C$ *in air or in a nitrogen atmosphere with emission of orange light but without violence, yielding a deep blue ash."*[273]

Based on EPR experiments, a postulated decomposition pathway involves the formation of cyclopentadienyl radicals, $[C_5Cl_5]^{\cdot}$, followed by dimerization. Despite the problems associated with the perchlorinated compounds described above, the perfluorinated derivatives $Q[C_5F_5]$ (Q = Li, Tl, Cs, Na[18-crown-6]) were synthesized by reaction of $C_5F_5H$ with $Q[N(SiR_3)_2]$ but not structurally characterized, again due to their instability. However, the ionic nature of the anions was identified by NMR and nuclear quadrupole resonance (NQR) techniques.[252,273] Both, $[C_5F_5]^-$ and $[C_5Cl_5]^-$ are extraordinarily weak bases. Coordination attempts of $[C_5Cl_5]^-$ with $[CpFe(CO)_2I]$, [CpHgCl] and $^nBu_3PCuI$ yielded thermally unstable mixtures while reaction of metal halides, $MX_2$ (M = Fe, Ni), is assumed to result in the corresponding solvent adducts, $[M(THF)_n][C_5Cl_5]_2$.[273] Analogous coordination attempts of $[C_5F_5]^-$ with transition metal halides, amides, alcoholates or carbonyl precursors yielded no conversion.[266] Instead, the introduction of perhalogenated cyclopentadienyl ligands was realized by reaction of metal halides, $[Cp^*RuX_2]_n$ ($n$ = 2, 4) or $[(COD)Rh\mu\text{-}X]_2$ (X = Cl, Br) or $[MnCl(CO)_5]$ with the corresponding diazo compounds, $C_5X_4N_2$. The necessary diazo derivatives are accessible by treatment of $C_5X_6$ (X = Cl, Br) with organic azides under basic conditions but cannot be isolated due to their explosive nature.[274–276]

Starting from complexes containing unsubstituted cyclopentadienyl ligands a direct halogenation using elemental halogens is difficult to achieve due to competing oxidation reaction or total decomposition.[132,277] Synthetically useful approaches involve multi-step metalation followed by reaction with an electrophilic halogenation agent. Considering metallocenes, $[MC_{10}X_nH_{10-n}]$, polyhalogenation ($n$ = 2-8) lead to a large number of possible isomers.[278] Isomerically pure perfuctionalization of cyclopentadienyl ligands were achieved by iterative *ortho*-lithiation with, e.g., LiTMP or lithium diisopropylamide (LDA) followed by halogenation. *Via* this approach 1,2,3,4,5-pentafluoro-,[38] -pentachloro-[279] and -pentabromoferrocene[280,281] were successfully generated but also two fully perchlorinated metallocenes were reported: $[MC_{10}Cl_{10}]$ (M = Fe,[282,283] Ru[283]). However, perhalogenated cyclopentadienyl complexes and metallocenes are more efficiently obtained by permercuration followed by perhalogenation in two steps (Figure 13). Here, the halogenation is typically achieved by electrophilic

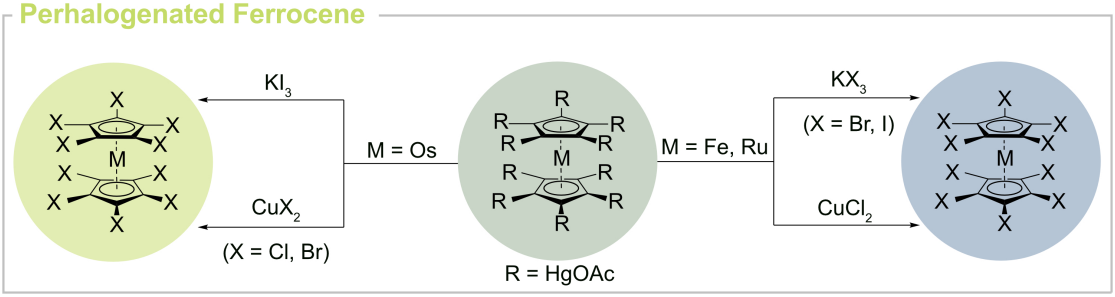


**Figure 13.** Perhalogenation of $[MC_{10}(HgOAc)_{10}]$ (M = Fe, Ru, Os) with trihalogenides and copper(II)halides.

substitution with trihalogenides, $Q[X_3]$ (Q = Na, K; X = Br, I) or with copper(II) salts, $CuX_2$ (X = Br, Cl). Perhalogenated cymantrene derivatives, $[Mn(CO)_3(C_5X_5)]$ (X = I), as well as all combinations of the type $[MC_{10}X_{10}]$ (M = Fe, Ru, Os; X = Cl, Br, I)[213–215] were successfully isolated so far. However, the incompleteness of the mercuration of ferrocene (*vide supra*) raises serious doubts about the subsequent perhalogenation. Regarding the lightest halogen, fluorine, the permercurated compounds are too unreactive towards mild fluorinating agents like N-fluoropyridinium triflate but decomposes in presence of $F_2$ or $CH_3CO_2F$.[154]

The electrochemical potentials of the perhalogenated metallocenes are a useful experimental probe to gain deeper understanding of the electronic situation, especially in the Cp ligand. Unfortunately, they are relatively poorly studied. It is known, however, that the reversibility of the first one-electron oxidation is typically not effected by halogenation. Here, the potentials systematically increase with the degree of halogenation, indicating a rising electron depletion on the metal center: the oxidation potentials of the neutral compounds $[FeC_{10}H_{10-n}Cl_n]$ ($n$ = 1, 2, 5, 10) increase gradually by $\Delta E$ = 0.12-0.16 V per Cl[282] and of $[FeC_{10}H_{10-n}F_n]$ ($n$ = 1, 2, 3, 4, 5) by $\Delta E$ = 0.16 V per fluorine atom.[284] The systematic increase of the oxidation potential was correlated with empirically determined Hammett substituent constants[285] resulting in a linear behavior (Figure 14) that should, in principle, allow for the prediction of other (poly)substituted ferrocenes.[31,48,286–288] As a result, the increase of redox potentials were determined to be the highest for decachloro- and decabromoferrocene

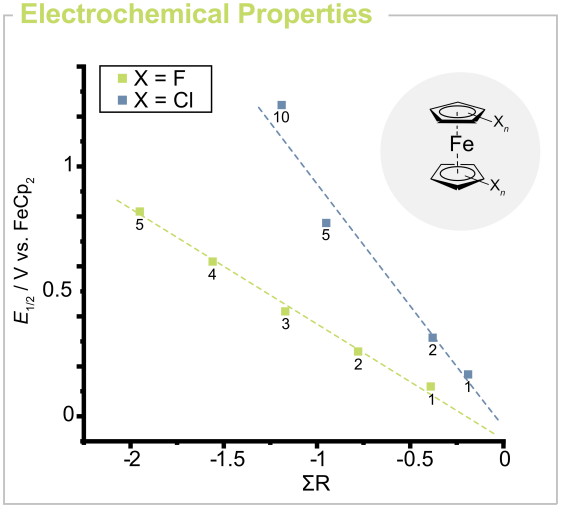


**Figure 14.** Plot of $E_{1/2}$ of polychlorinated $[FeC_{10}Cl_nH_{10-n}]$[282] (blue, $n$ = 1, 2, 5, 10) and -fluorinated $[FeC_{10}F_nH_{10-n}]$[284] (green, $n$ = 1, 2, 3, 4, 5) vs. sum over all resonance factors (R).[153]

according to the following trend: Cl ∼ Br > I > F. However, those correlations should be treated carefully since competing effects like electrostatic repulsion of the ligand and the metal center, resonance effects, covalent stabilization and through-space interactions between the iron center and the halogen atoms may cause a discrepancy in linearity.[48]

### 1.3.3 Introduction of Pentafluorophenyl Groups

Given the outstanding variety of possible halogenated cyclopentadienyl complexes reported so far, cyclopentadienyl ligands bearing pentafluoroaryl groups clearly stand out for their induced oxidative stability. Perfluorination of benzene increases its oxidation potentials significantly. Considering the ionization potentials of benzene and perfluorobenzene,[289] an oxidation of $C_6F_6$ is expected to proceed at $E > 2.86\,V$ vs. normal hydrogen electrode (NHE).[290] The corresponding cations are stable enough to be even isolated above room temperature without loss of halides or reductive C-C bond formation.[236] Hence, an enhanced stability of pentafluoroaryl groups towards electrophilic metal cations is expected in contrast to -$CX_3$ groups or the pure halides themselves allowing the isolation of pentafluoroarylated cyclopentadienyl anions. Further on, the weak basicity of the pentafluorophenyl groups is beneficial in the development of electron deficient catalysts due to avoided $\sigma$-coordination of the functional groups to catalytically active species. So far, applications were found in the olefin polymerization with group four cyclopentadienyl complexes.[291,292] On the other hand, the highly withdrawing group is prone towards nucleophilic attacks (Figure 15).

Early reports on the transfer of pentafluorophenyl groups to cyclopentadiene compounds describe the reaction of [CuCp($PBu_3$)] with $C_6F_5I$ *via* postulated oxidative addition of the corresponding aryl iodide.[293] In another approach [$TiCp_2(C_6F_5)_2$] is photolytically decomposed under formation of $C_5H_5(C_6F_5)$.[294,295] In both reactions the resulting pentafluoroarylated cyclopentadiene is obtained in low yields disqualifying those reactions for further rational syntheses. A more reliable reaction is achieved by nucleophilic substitution of $C_6F_6$ with NaCp in presence of NaH which yields purely monoarylated cyclopentadiene below room temperature. Herein, the addition of NaH is necessary to prevent the diene to dimerize or to transfer its acidic proton to unreacted cyclopentadienyl anions.[296] The use of an excess of $C_6F_6$ affords polyarylated cyclopentadienes, $C_5(C_6F_5)_nH_{6-n}$ ($n$ = 2, 3, 4) which have to be separated.[103,297] Reaction with NaH allows the isolation of the corresponding cyclopentadienyl anions, Na[$C_5(C_6F_5)_nH_{5-n}$] ($n$ = 1, 2, 3, 4), which are suitable precursors for the generation of metal complexes by metal halide metathesis.[117] A pentaarylated derivative is obtained by reaction of the cyclopentadienone, $C_5(C_6F_5)_4O$, with $LiC_6F_5$ yielding the corresponding alcoholate which is transformed into the cyclopentadiene compound by reduction with elemental zinc.[298] However, no further reports were made, neither on the generation of a cyclopentadienyl anion or cation nor on metal complex syntheses.

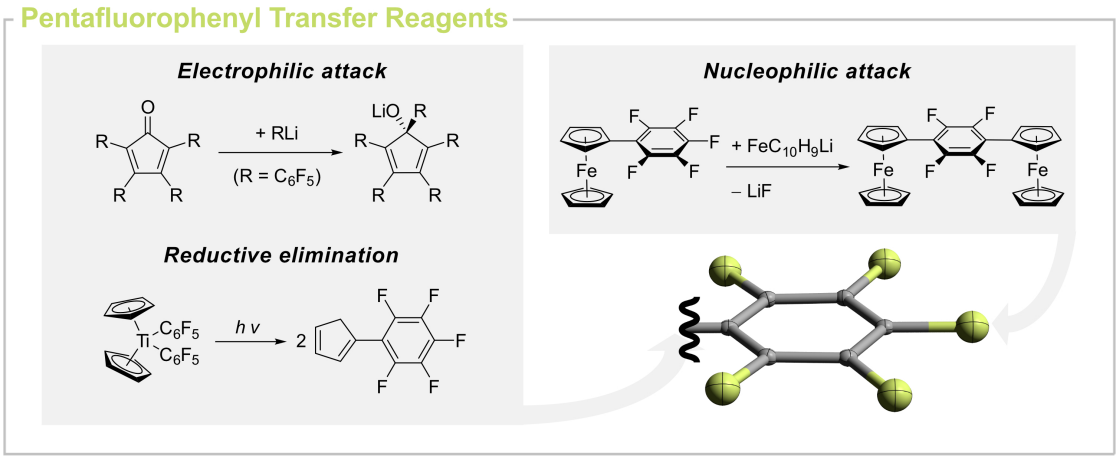


**Figure 15.** Overview of suitable precursors towards pentafluoroarylated cyclopentadienes.

Considering metallocenes, multiple arylations were achieved by reaction of mono- and dilithioferrocene with $C_6F_6$ yielding the corresponding mono- and diarylated compounds. However, the introduced aryl groups are prone to undergo nucleophilic attack in *para*-position causing oligomerized byproducts.[299] More efficient is the reaction of the corresponding cyclopentadienyl anions with $MBr_2$ salts (M = Fe, Co) yielding the homoleptic metal complexes containing up to six pentafluorophenyl groups.[103] Another pathway involves the protonation of cobalt(I) cyclopentadienone complexes to afford $[CoCp(C_5(C_6F_5)_4OH)]^+$.[300]

In metal complexes, changes of the electronic properties are indicated by cyclic voltammertry, as mentioned above. Another powerful tool to study the electronic structure is infrared spectroscopy, especially when CO co-ligands are present in the complex. Investigations of $\nu$(CO) stretching frequencies of arylated cymantrene compounds indicate a strong withdrawing character by blue-shifted bands of $\Delta\tilde{\nu} = 4\,\mathrm{cm}^{-1}$ per $C_6F_5$ group. In $C_6H_5$ substituted cymantrenes an opposite effect is observed.[292,301] Similar trends are observed by cyclic voltammetry experiments of phenylated ferrocene derivatives revealing a linear increase of the redox potentials. However, the induced withdrawing character is seemingly superior in comparison to other halogenated groups as [1,2,3-$((C_6F_5)_3C_5H_2)_2$Fe] ($E_{1/2}$ = 0.951 V vs. ferrocene[103]) and [1,2,4-$((C_6F_5)_3C_5H_2)_2$Fe] ($E_{1/2}$ = 0.940 V vs. ferrocene[103]) exhibit oxidation potentials in the same order of magnitude as the perfunctionalized $[FeC_{10}Cl_{10}]$ ($E_{1/2}$ = 1.246 V vs. ferrocene[282]).[117]

### 1.3.4 Silylation

Tetraorganosilanes offer great structural features and reactivity compared to alkanes and are used in cyclopentadienyl chemistry in order to generate sterically demanding ligands. Although Si-C (314 kJ/mol[302]) and Si-H (377 kJ/mol[303]) bonds are significantly weaker than C-C (334 kJ/mol[304]) and C-H (435 kJ/mol[304]) bonds, thermally and chemically

stable organosilicon moieties are quite feasible. Herein, cyclopentadienyl ligands with dimethylsilyl (DMS) or trimethylsilyl (TMS) groups have found synthetic applications in the isolation of reactive f-block[305–309] as well as main group complexes[310–314] since they promote the formation of monomeric compounds and increase the solubility in nonpolar solvents.[315]

As silicon (EN = 1.74) exhibits a lower electronegativity compared to carbon (EN = 2.50) treating silyl groups as EWGs seems to be counterintuitive.[316] Actually, silicon offers several hyperconjugation effects allowing a charge delocalization of a $\pi$-electron system *via* $\sigma$(Si-C$^{Me}$) and $\sigma$*(Si-C$^{Me}$) orbital controlled interactions. Herein, DFT calculations of aromatic silyl compounds reveal weak destabilization of the HOMO by $\sigma$-$\pi$ conjugation of the Si-C$^{Me}$ orbitals while the LUMO is significantly stabilized due to $\sigma$*-$\pi$* interaction.[317,318] As a result, incorporation of dimethyl- and trimethylsilyl groups causes bathochromic shifts in the UV/VIS spectra due to decreased HOMO-LUMO energy gaps.[49,50,319] Moreover, the combination of sterically demanding substituents and increased acceptor properties are used in the stabilization of low-valent metal complexes, which was demonstrated by the isolation and structural characterization of a series of low valent actinide and lanthanide compounds, $[M(C_5H_{5-n}TMS_n)_3]^-$ ($n$ = 1, 2), containing metal centers with a formal oxidation state of +II.[320–325]

Although an increased number of silyl groups is expected to result in an increased kinetic stability of reactive species, the persilylated ligand is only poorly investigated in coordination chemistry. The steric overcrowding and the further changed electronic properties of the cyclopentadienyl ligands due to the silyl groups cause a synthetic challenge in generating high degrees of silylation or even persilylated cyclopentadienyl complexes. Hence, the persilylated ligand is only rarely reported in the literature. Sekiguchi *et al.* obtained a persilylated compound, $C_5DMS_6$, by metalation of $C_5Br_6$ with elemental magnesium in presence of DMSCl. Subsequent treatment with *n*-butyl lithium yield the corresponding cyclopentadienyl anion, $[C_5DMS_5]^-$ as a lithium salt.[326] Analogous TMS compounds cannot be derived by this approach due to the increased steric demand and reduced electrophilicity of the TMS group. Hence, only the corresponding lithium,[327] sodium,[328] potassium,[312] as well as thallium compounds[329] of $[C_5TMS_3H_2]^-$ were isolated, so far. Although those cyclopentadienyl metal compounds are ideal precursors for the generation of metal complexes by treatment with the corresponding metal halides, no follow-up reactions of $Li[C_5DMS_5]$ are reported probably due to a missing reliable synthetic protocol. Instead, Sünkel and Hofmann reported the first metal complex with a persilylated cyclopentadienyl ligand by iterative lithiation and silylation to yield $[Mn(CO)_3(C_5DMS_5)]$.[330] The DMS groups were transformed into TMS substitutents by halogenation of the Si-H bonds with $PdCl_2$ followed by alkylation with MeMgCl, subsequently.[331,332]

Considering metallocenes, the existence of a persilylated compound was only confirmed by mass spectrometry, so far.[334] However, high degrees of silylation were achieved by reaction of metal halides with the tris(trimethylsilyl)cyclopentadienyl

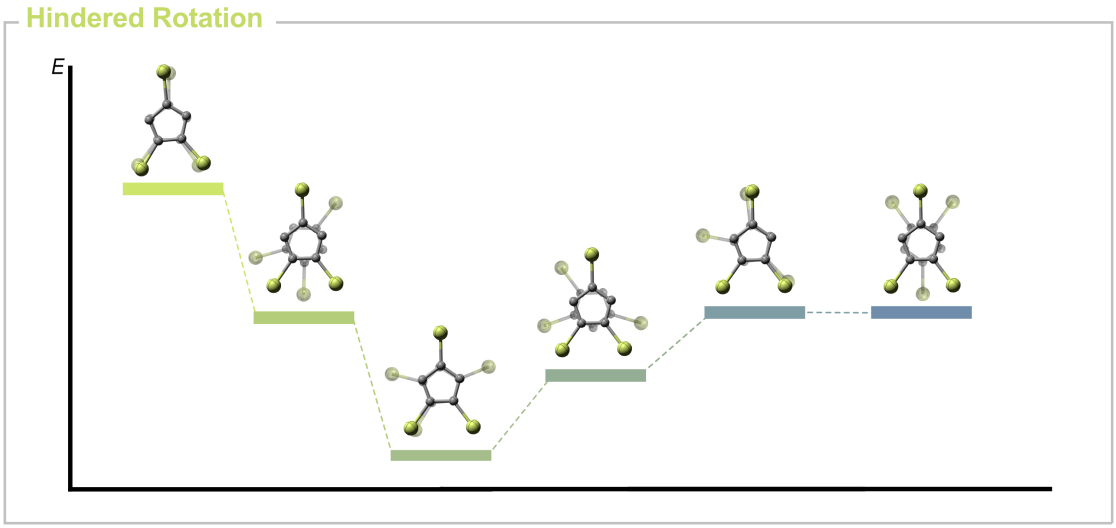


**Figure 16.** Qualitative energy profile[333] of the rotation in $[Fe(C_5TMS_3H_2)_2]$ along the metal-carbon axis.

anion[313,328,329,333,335–337] or by deprotonation of $C_5TMS_3H_3$.[338] Another approach involves the silylation of polylithiated metallocenes with TMSCl[334,339] yielding the corresponding hexakis(trimethylsilyl)metallocene. In those sandwich-like structures, crystal structure determination reveal predominantly eclipsed conformers in the solid state. However, the highly silylated ligands are found to exhibit a non-planar geometry. Herein, the steric demand is compensated by distortion of the Si-$C^{Cp}$ bonds. The angles between the Si-Cp bond and the Cp plane vary (e.g. $[Mg(C_5TMS_3H_2)_2]$[338] - 8°, $[Fe(C_5TMS_3H_2)]$[333] - 13°) within the series of metal complexes. Similar to the chemistry of *tert*-butyl cyclopentadienyl derivatives,[340] this phenomenon has consequences for the behavior in solution.[333,341] However, a comparison of TMS and *tert*-butyl substituted ferrocenes shows that the TMS group is superior in steric demand. Here, Okuda and Herdtweck conducted extensive NMR studies on $[Fe(C_5TMS_3H_2)_2]$, revealing a hindered rotation of the cyclopentadienyl ligands with a energy barrier of $\Delta G^{\ddagger}$ = 11 kcal/mol (Figure 16).[333] Substitution of TMS to *tert*-butyl reduces this barrier to $\Delta G^{\ddagger}$ = 9.7 kcal/mol.[50,342]

# 2 Objective

As presented above, cyclopentadienyl compounds are omnipresent in organic and organometallic chemistry resulting in a large family of functionalized derivatives. Here, the introduction of acceptor-substituents into metal cyclopentadienyl complexes allows the fine-tuning of redox potentials as well as of the Lewis acidity of the metal center. In this context, perfunctionalization of cyclopentadiene is an efficient strategy to reduce possible decomposition pathways *via* (aromatic) C-H bonds. However, the introduction of multiple withdrawing groups is synthetically challenging due to changes of the physicochemical properties of the cyclopentadienyl ligand itself. In the light of the limited perfunctionalization approaches, the first scientific goal of this work is the development of efficient methodologies for the synthesis of acceptor-substituted perfunctionalized cyclopentadienyl compounds.

Studies from the 1990s suggest that Hg(II) undergoes multiple efficient C-H-activations in metallocenes, rendering permercuration as a valid starting point for the synthesis of other persubstituted compounds. The robustness of C-Hg bonds is widely established, therefore, it would be of interest to test the limits of this inert metal carbon bond, for instance, under strongly oxidizing or Brønsted acidic conditions. Generally, permetalated aromatic molecules belong to an extremely rare class of compounds and their structural chemistry is basically unexplored due to their high reactivity or low solubility. Especially, their structural characterization would provide insights into the role of metallophilic interactions or other metal-induced cooperative effects. Therefore, the investigation of permercurated ferrocene derivatives, especially regarding their structural properties and further of their follow-up chemistry, will be a major part of this work.

Related to the follow-up chemistry, efficient halodemercuration approaches will be developed to afford Hg-free perfunctionalized building blocks. The resulting perhalogenated ferrocene derivatives are expected to exhibit high oxidation potentials and will therefore be applied for the synthesis of strongly oxidizing ferrocenium cations. To achieve further derivatization, the synthesis of other reactive permetalated intermediates (e.g. perlithio- or permagnesioferrocene) will be investigated. These highly reactive intermediates will be used for the synthesis of persilylated, overcrowded ferrocenes. The effects of the newly introduced withdrawing groups on the overall electronic structure of ferrocene will be evaluated by electrochemical potentials, UV/VIS absorption spectroscopy and computational calculations.

The second part is focused on the isolation of the elusive cyclopentadienyl cation. Here, the combination of electron deficient groups and the perfunctionalization ap-

proach will be used as a promising approach for its isolation. In this work, the effect of perhalogenation will be investigated to reduce possible side reactions *via* cleavage of C-H bonds. At this point it should be mentioned that structures of highly electrophilic organic carbocations, especially perhalogenated ones, have only been rarely investigated by single-crystal XRD, so far. Hence, the structural characterization of the corresponding cationic intermediates will bring valuable insights into these poorly investigated perhalogenated intermediates.

# 3 Publications

## 3.1 Tenfold Metalation of Ferrocene: Synthesis, Structures, and Metallophilic Interactions in $FeC_{10}(HgX)_{10}$

Susanne Margot Rupf, Gabriel Schröder, Robin Sievers, Moritz Malischewski*
*Chem. J. Eur.* **2021**, *27*, 5125–5129.

DOI: 10.1002/chem.202100261



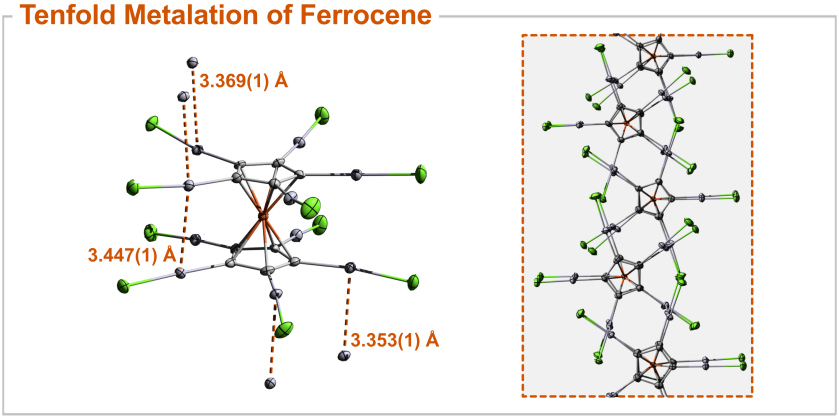


**Author Contribution:**
Susanne M. Rupf designed the project and wrote the manuscript. Furthermore, she performed syntheses and analyzed the spectroscopic data, performed cyclic voltammetry experiments as well as measured and solved the single-crystal XRD data. Gabriel Schröder performed experiments and analyzed data during his bachelor thesis and Robin Sievers performed experiments and analyzed data during his internship course. Both authors were supervised by Susanne M. Rupf. Moritz Malischewski performed quantum chemical calculations, supervised the project and revised the manuscript.

Chemistry–A European Journal
Communication
doi.org/10.1002/chem.202100261
Chemistry Europe
European Chemical Societies Publishing

Metallocenes

# Tenfold Metalation of Ferrocene: Synthesis, Structures, and Metallophilic Interactions in $FeC_{10}(HgX)_{10}$

Susanne Margot Rupf, Gabriel Schröder, Robin Sievers, and Moritz Malischewski*[a]

**Abstract:** The permercuration of ferrocene was achieved by reacting ferrocene with 10 equivalents of mercury(II) butyrate $Hg(O_2CC_3H_7)_2$ in a facile one-pot reaction in multi-gram scale and high yields. The butyrate groups in $FeC_{10}(HgX)_{10}$ ($X = O_2CC_3H_7$) can be exchanged by treatment with trifluoro- or trichloroacetic acid ($X = O_2CCF_3$, $O_2CCCl_3$). Substitution of the trifluoroacetate groups by halides (X = Cl, F) proceeds easily in aqueous THF. The completeness of metalation was confirmed by NMR and vibrational spectroscopy, mass spectrometry, as well as elemental analysis. Additionally, the first crystal structures of permetallated metallocenes are presented: $FeC_{10}(HgX)_{10}$ ($X = Cl$, $O_2CCF_3$, $O_2CCCl_3$).

The functionalization of unreactive C–H bonds is a constant challenge in organometallic chemistry due to their high intrinsic stability.[1] Typically, noble metal complexes are used for the activation of C–H bonds.[2] Unfortunately, these metals are scarce and expensive,[3] and commonly the reactivity of these metal complexes has to be tuned by sophisticated ligands. In the past years, efforts have intensified to use cheaper and more abundant 3d metals for C–H activation.[4] However, in many cases C–H activation relies on the presence of directing groups.[5] One of the most active metals in C–H activation, although nowadays widely ignored, is mercury. Mono- and polymercuration of aromatic compounds,[6–11] olefins,[12] as well as alkanes[13,14] have been observed in reactions involving sources of $Hg^{2+}$. Even unreactive C–H bonds such as methane can be brought to reaction using $Hg(NTf_2)_2$.[14] However, interest in organomercury chemistry has declined during the past decades due to the high toxicity of organomercury compounds. Nevertheless, the utility of such mercurations can be demonstrated by the reaction of ferrocene with mercury(II) carboxylates.

Ferrocene derivatives have found numerous applications, for example, in material science, medicinal chemistry, and catalysis, which can be explained by its unusual stability towards moisture and oxygen as well as its unique redox properties.[15] Consequently, functionalization of the C–H bonds in ferrocene is an active field of research.[16] Although one-pot reactions for the mono- and dilithiation of ferrocene are well established,[17,18] higher degrees of metalation are difficult to achieve. For instance, refluxing a solution of ferrocene with eight equivalents of *n*BuLi for four days and subsequent quenching with $D_2O$ yields only to relatively low degrees of deuteration ($FeC_{10}D_nH_{10-n}$: main products: $n = 2$, 3, 4). The degree of lithiation can be slightly improved by addition of tetramethylethylenediamine (TMEDA).[16] Mulvey and co-workers have shown the use of strong, bimetallic bases for the tetrametalation of ferrocene.[19–22] However, pioneering works of Winter and co-workers demonstrated that much higher degrees of metalation could be accessed by mercuration of ferrocene, ruthenocene, and osmocene using mercury(II) carboxylates.[23–26] Mercuration of aromatic systems by $Hg^{2+}$ proceeds mechanistically via an electrophilic substitution pathway.[27] Surprisingly, the reaction seems to proceed even faster with increasing degree of mercuration.[28] Unfortunately, the insolubility of Winter's highly mercurated metallocenes prevented their full spectroscopic characterization. Moreover, the permercuration of ferrocene seemed also to be incomplete.[29] In a review article, it was mentioned that the solubility and the degree of mercuration could be improved by replacing mercury(II) acetate by mercury(II) butyrate, but details were never published.[7] Although organomercury compounds are highly toxic, they are valuable starting materials for functionalization or transmetalation reactions.[30–32] Therefore, we reinvestigated the permercuration of ferrocene with modern spectroscopic techniques.

$FeC_{10}(HgO_2CC_3H_7)_{10}$ (**2**) was synthesized by reaction of ferrocene with mercury(II) butyrate (**1**) in 1,2-dichloroethane (DCE) under reflux (Scheme 1). The substitution of the butyrate groups was performed by reaction of **2** with trifluoro- or trichloroacetic acid in THF yielding compounds $FeC_{10}(HgO_2CCF_3)_{10}$ (**3a**) and $FeC_{10}(HgO_2CCCl_3)_{10}$ (**3b**), respectively. The trifluoroacetate derivative **3a** could be converted to the insoluble halide derivatives $FeC_{10}(HgX)_{10}$ (**4**) (X = F, Cl) by reaction of NaF/NaCl in aqueous THF mixtures. In contrast to the literature-known permercurated metallocenes, compounds **2** and **3** are soluble in DMSO and tetrahydrothiophene (THT). THF adducts of **3** are even soluble in dichloromethane and methanol. This makes these compounds attractive starting materials for further reactions.

[a] S. M. Rupf, G. Schröder, R. Sievers, Dr. M. Malischewski
Institute of Chemistry and Biochemistry
Freie Universität Berlin
Fabeckstr. 34–36, 14195 Berlin (Germany)
E-mail: moritz.malischewski@fu-berlin.de
Supporting information and the ORCID identification numbers for the authors of this article can be found under: https://doi.org/10.1002/chem.202100261.

Chemistry–A European Journal
Communication
doi.org/10.1002/chem.202100261
Chemistry Europe
European Chemical Societies Publishing

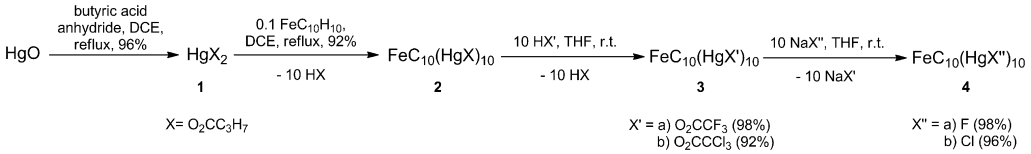


**Scheme 1.** Synthesis of permetalated ferrocene derivatives $FeC_{10}(HgX)_{10}$ starting from mercury(II) oxide and substitution of the butyrate groups (X) by trifluoro- and trichloroacetate (X′) as well as halides (X″).

Compounds **1**, **3a**, **3b**, and **4b** were characterized via single crystal XRD. A detailed description of the crystal structure of mercury(II) butyrate $Hg(O_2CC_3H_7)_2$ **1** can be found in the Supporting Information. Single crystals of compounds **3a**·4THF·2$Et_2O$ and **3b**·10THF·$Et_2O$ were obtained by diffusion of pentane into solutions of **3a** and **3b** in THF/$Et_2O$ mixtures, respectively. The permercurated metallocene with trifluoroacetate groups **3a** (X = $O_2CCF_3$) crystallizes in monoclinic space group $P2_1/n$ and **3b** (X = $O_2CCl_3$) in orthorhombic space group *Pbca*. The structures are shown in Figure 1A,B as well as in the Supporting Information. The asymmetric units of both compounds contain a $[FeC_5(HgO_2CCX_3)_5]$ unit. Due to a center of inversion located at the iron atom the overall formula in both cases is $FeC_{10}(HgO_2CCX_3)_{10}$. A staggered conformation of the two permercurated cyclopentadienyl rings is observed. The cyclopentadienyl-iron distances are similar to ferrocene (Table 1).[33] In both cases, the Cp rings are parallel (tilt angle 0°). In both structures all mercury atoms are coordinated by one Cp carbon atom and one carboxylate ligand. The coordination sphere is almost linear along the C–Hg–O axis. The distortion from linearity is caused by additional Hg–O contacts with carboxylate groups [2.857(8)–3.121(6) Å] and solvent molecules [2.539(6)–2.826(5) Å], all shorter than the sum of the van der Waals radii of oxygen ($r_{vdW}$ = 1.54 Å[34]) and mercury ($r_{vdW}$ = 1.75 Å[35]). Similar Hg–O(solvent) interactions have been reported previously.[36–38] Hg–Hg contacts shorter than twice the van-der-Waals radius of mercury are not observed. Taking all interactions into account the overall coordination number of the mercury atoms is four or five.

By serendipity, crystals of insoluble $FeC_{10}(HgCl)_{10}$ (**4b**) were found in a decomposed sample of the trichloroacetate (**3b**). **4b**·9DMSO crystallizes in the triclinic space group $P\bar{1}$. In contrast to **3a** and **3b** the center of inversion is located outside of the metallocene moiety. Therefore, the asymmetric unit contains the whole molecule. All mercury atoms exhibit a distorted linear symmetry along the C–Hg–Cl axis, which is again a result of Hg–O(solvent) contacts of 2.708(6)–3.119(6) Å. A remarkable feature of the crystal structure is the presence of significant intra- and intermolecular mercurophilic $Hg^{+II}$–$Hg^{+II}$ interactions (Table 1). In contrast to the crystal structures of **3a** and **3b** an eclipsed conformation is observed for the two permercurated cyclopentadienyl rings (Figure 1D). This different conformation could be a result of an intramolecular $Hg^{+II}$–$Hg^{+II}$ interaction between the atoms Hg3 and Hg8 of 3.447(1) Å (Figure 1C), which is in accordance with other examples in the literature for

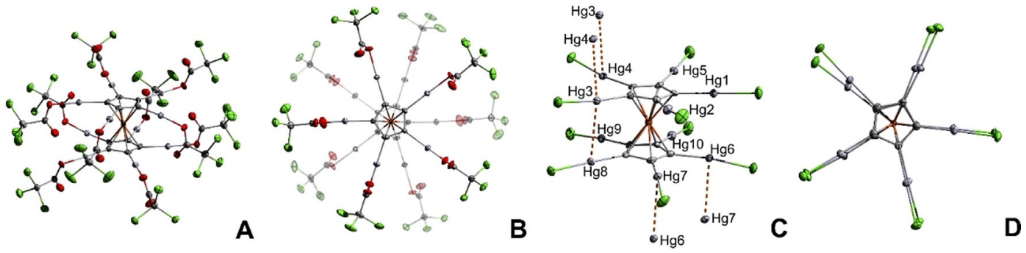


**Figure 1.** Molecular structure in solid state of permercurated ferrocene derivatives with trichloroacetate substituents (A, B) and chloride ligands (C, D) in different perspectives. Solvent molecules are omitted for clarity. Hg–Hg contacts are assigned as dashed lines. Ellipsoids are depicted with a 50% probability level. Color code: light grey—mercury, orange—iron, green—chlorine, red—oxygen, grey—carbon.

**Table 1.** Selected bond lengths [Å] and angles [°].

| Compound | **3a** | **3b** | **4b** |
|---|---|---|---|
| Fe–$Cp^{center}$ | 1.660(1) | 1.657(1) | 1.651(1), 1.658(1) |
| Hg–C | 2.034(9)–2.040(8) | 2.014(6)–2.037(6) | 2.022(10)–2.046(9) |
| Hg–X[a] | 2.082(7)–2.115(6) | 2.082(4)–2.105(5) | 2.326(2)–2.342(3) |
| Hg–$Hg^{intramol.}$ | 3.543(1)–3.748(1) | 3.668(1)–3.878(1) | 3.447(1), 3.517(1)–3.637(1) |
| Hg–$Hg^{intermol.}$ | – | – | 3.353(1), 3.369(1) |
| C–Hg–X[a] | 168.78(31)–176.47(27) | 174.15(21)–178.93(22) | 170.78(21)–176.72(22) |
| Cp–$Cp^{tilt\ angle}$ | 0 | 0 | 1.53(30) |

[a] In case of **3a** and **3b**: X = O; **4b**: X = Cl.

Chemistry–A European Journal
Communication
doi.org/10.1002/chem.202100261
Chemistry Europe
European Chemical Societies Publishing

$Hg^{+II}$–$Hg^{+II}$ interactions. Interestingly, the Cp rings are not completely parallel (tilt angle 1.6°) which might be related to this $d^{10}$–$d^{10}$ interaction. Additionally, intermolecular interactions between Hg3 and Hg4 as well as Hg6 and Hg7 of 3.353(1) and 3.369(1) Å are observed, which are even shorter than the intramolecular interaction. As a consequence, no isolated ferrocene moieties are observed in the solid-state structure, but a polymeric chain of ferrocene units connected by Hg–Hg contacts (Figures S7 and S8), which could explain the insolubility of the compound. In contrast to this, the well soluble derivatives **3** (trihaloacetate) exhibit no significant $Hg^{+II}$–$Hg^{+II}$ contacts. Taking all interactions into account the coordination number of Hg4, Hg6, and Hg7 is five and of Hg3 and Hg8 six for $FeC_{10}(HgCl)_{10}$ (**4b**). At this point it should be noted that short $Hg^{+II}$–$Hg^{+II}$ interactions are usually found when the coordination number of the metal center is small.[39] Therefore, the finding of rather short crystallographically independent $Hg^{+II}$–$Hg^{+II}$ contacts is surprising, since the coordination number of the mercury atoms is relatively high. So far, examples of strong $Hg^{+II}$–$Hg^{+II}$ interactions are relatively rare.[40–42] Only a small number of crystal structures contain shorter contacts than the here reported 3.353(1) Å.[36,43–47] Furthermore, only a few examples of crystal structures of permercurated compounds are known so far.[48–50]

The soluble compounds **2** (butyrate) and **3** (trihaloacetate) were characterized via NMR spectroscopy. The $^{13}C$ NMR spectra of **3a** and **3b** display three signals, respectively. Compound **2** shows five signals. (Figure 2). The most downfield shifted signals chemical shifts (**2**: 177.5, **3a**: 164.2, **3b**: 167.8 ppm) can be assigned to the carbonyl groups. The signals for the cyclopentadienyl rings can be found at (**2**: 97.8, **3a**: 97.4, **3b**: 97.1 ppm), which is similar to those signals of other polymercurated ferrocene derivatives.[38,51] All remaining signals correspond to the alkyl groups of the carboxylates. The fact that only one Cp–C signal is visible for all three compounds confirms the highly symmetric metallocene structure. Furthermore, no Cp–H signals can be found in the $^{1}H$ NMR spectra (see the Supporting Information). Unfortunately, neither a signal in the $^{199}Hg$ NMR spectrum nor $^{199}Hg$ satellites for the Cp–C signals in the $^{13}C$ NMR spectrum could be observed, which is probably a consequence of $^{199}Hg$ line broadening due to chemical shift anisotropy.[52–55] Elemental analysis of the permercurated ferrocenes matches the expected compositions. Electron spray ionization (ESI)-MS shows a peak at $m/z = 3053.05$, which can be unambiguously assigned to $[FeC_{10}(HgO_2CC_3H_7)_{10}]^+$ (calculated: $m/z = 3053.08$). Hence, we conclude that the ten-fold electrophilic substitution of ferrocene by mercury(II) butyrate was successful.

While the IR spectra of all permercurated metallocenes show only bands which correspond to the mercury-bound carboxylates (see the Supporting Information), Raman spectra contain more information especially with respect to Hg–Cp bonds (Figure 3). The bands between 930 and 960 $cm^{-1}$ are present in all spectra which is characteristic for the metallocene backbone and correspond to the vibration of the cyclopentadienyl rings. The bands between 100 and 120 $cm^{-1}$ correspond to Hg–C stretch vibrations. Other bands are associated to vibrations of the Hg-bonded substituents (X). The frequencies of the Hg–X bonds between 300 and 500 $cm^{-1}$ are similar to the analogous vibrations in $HgX_2$.[56–57]

Cyclovoltammetric measurements of the permercurated ferrocene derivatives only revealed one irreversible oxidation process for the trifluoroacetate **3a** at $E_p = +0.87$ V in THF (Figure S38) while the less stable trichloroacetate **3b** visibly decomposed during the measurements under formation of insoluble material. The butyrate derivative **2** did not have enough solubility in THF. When tetrahydrothiophene was used instead to increase the solubility, no oxidation process was observed in the corresponding electrochemical window.

In summary, we demonstrated the synthesis of ten-fold metallated ferrocene derivatives $FeC_{10}(HgX)_{10}$ with mercury(II) carboxylate ($X = O_2CC_3H_7$, $O_2CCF_3$, $O_2CCCl_3$) and halide substituents ($X = F$, Cl). These compounds can be prepared in facile one-pot reactions in multi-gram scale and high yields without

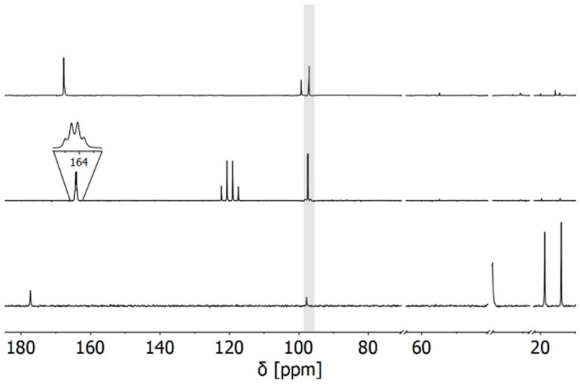


**Figure 2.** $^{13}C$ NMR spectra of $FeC_{10}(HgO_2CC_3H_7)_{10}$ (**2**) (bottom, 176 MHz, $[D_6]$DMSO, r.t.), $FeC_{10}(HgO_2CCF_3)_{10}$ (**3a**) (middle, 176 MHz, $[D_8]$THF, r.t.), and $FeC_{10}(HgO_2CCCl_3)_{10}$ (**3b**) (top, 176 MHz, $[D_8]$THF, r.t.). Signals of the deuterated solvents are omitted for clarity. Cp–C signals are highlighted in grey.

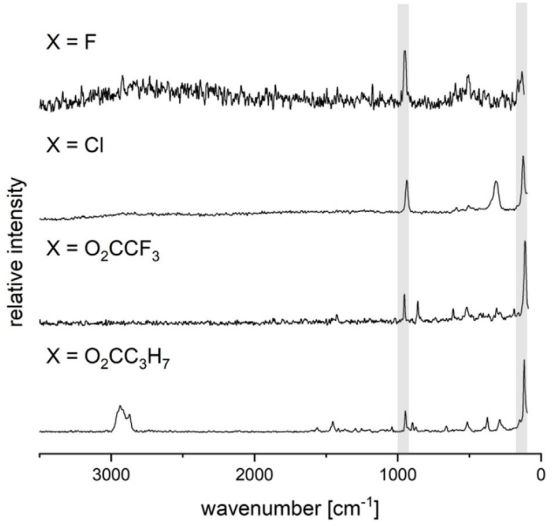


**Figure 3.** Raman spectra (1064 nm) of $FeC_{10}(HgX)_{10}$ derivatives. Characteristic bands for the permercurated metallocene moiety are highlighted in grey.

Chemistry–A European Journal
Communication
doi.org/10.1002/chem.202100261
Chemistry Europe
European Chemical Societies Publishing

the need for inert conditions. The complete metalation as well as the purity of the samples was demonstrated by a variety of spectroscopic methods. Additionally, we present the first crystal structures of permercurated metallocenes. $FeC_{10}(HgO_2CCF_3)_{10}$, $FeC_{10}(HgO_2CCCl_3)_{10}$, and $FeC_{10}(HgCl)_{10}$. Depending on the substituent, different conformers are observed in the solid-state structures. The permercurated ferrocenes with carboxylate groups show good solubility in organic solvents but no significant Hg–Hg interactions. In contrast, $FeC_{10}(HgCl)_{10}$ is completely insoluble. Its crystal structure displays relatively short intra- and intermolecular $Hg^{+II}$–$Hg^{+II}$ contacts.

Beside their aesthetic appearance, the permercurated ferrocenes might be very useful starting materials for further functionalization or transmetalation reactions. From a more general point of view, one can only be amazed about the extreme reactivity of $Hg^{2+}$ in C–H functionalization reactions. However, it might be worthwhile to further investigate this unique behavior with the hope of finding ways to mimic this reactivity with other, less toxic elements.

## *Acknowledgements*

Gefördert durch die Deutsche Forschungsgemeinschaft (DFG)—Projektnummer 387284271—SFB 1349. Computing time was made available by High-Performance Computing at ZEDAT/FU Berlin. We would like to acknowledge the assistance of the Core Facility BioSupraMol supported by the DFG. Open access funding enabled and organized by Projekt DEAL.

## Conflict of interest

The authors declare no conflict of interest.

**Keywords:** C–H activation · mercury · metalation · metallocenes · metal–metal interactions

[1] R. G. Bergman, *Nature* **2007**, *446*, 391 – 393.
[2] N. Kuhl, M. N. Hopkinson, J. Wencel-Delord, F. Glorius, *Angew. Chem. Int. Ed.* **2012**, *51*, 10236 – 10254; *Angew. Chem.* **2012**, *124*, 10382 – 10401.
[3] E. Nakamura, K. Sato, *Nat. Mater.* **2011**, *10*, 158 – 161.
[4] P. Gandeepan, T. Müller, D. Zell, G. Cera, S. Warratz, L. Ackermann, *Chem. Rev.* **2019**, *119*, 2192 – 2452.
[5] C. Sambiagio, D. Schönbauer, R. Blieck, T. Dao-Huy, G. Pototschnig, P. Schaaf, T. Wiesinger, M. F. Zia, J. Wencel-Delord, T. Besset, B. U. W. Maes, M. Schnürch, *Chem. Soc. Rev.* **2018**, *47*, 6603 – 6743.
[6] M. R. Haneline, R. E. Taylor, F. P. Gabbaï, *Chem. Eur. J.* **2003**, *9*, 5188 – 5193.
[7] C. H. Winter, K. N. Seneviratne, A. Bretschneider-Hurley, *Comm. Inorg. Chem.* **1996**, *19*, 1 – 23.
[8] A. Grirrane, I. Resa, D. del Río, A. Rodríguez, E. Álvarez, K. Mereiter, E. Carmona, *Inorg. Chem.* **2007**, *46*, 4667 – 4676.
[9] G. B. Deacon, G. J. Farquharson, *J. Organomet. Chem.* **1974**, *67*, C1 – C3.
[10] R. M. Harrison, T. Brotin, B. C. Noll, J. Michl, *Organometallics* **1997**, *16*, 3401 – 3412.
[11] M. Bausch, M. Vogel, H. Rosenberg, *J. Org. Chem.* **1957**, *22*, 900 – 903.
[12] A. K. Brisdon, I. R. Crossley, R. G. Pritchard, *Organometallics* **2005**, *24*, 5487 – 5490.
[13] B. Korpar-Čolig, Z. Popović, D. Matković-Čalogović, *Organometallics* **1993**, *12*, 4708 – 4713.
[14] N. J. Gunsalus, S. H. Park, B. G. Hashiguchi, A. Koppaka, S. J. Smith, D. H. Ess, R. A. Periana, *Organometallics* **2019**, *38*, 2319 – 2322.
[15] D. Astruc, *Eur. J. Inorg. Chem.* **2017**, 6 – 29.
[16] L. A. López, E. López, *Dalton Trans.* **2015**, *44*, 10128 – 10135.
[17] F. Rebiere, O. Samuel, H. B. Kagan, *Tetrahedron Lett.* **1990**, *31*, 3121 – 3124.
[18] J. J. Bishop, A. Davison, M. L. Katcher, D. W. Lichtenberg, R. E. Merrill, J. C. Smart, *J. Organomet. Chem.* **1971**, *27*, 241 – 249.
[19] W. Clegg, K. W. Henderson, A. R. Kennedy, R. E. Mulvey, C. T. O'Hara, R. B. Rowlings, D. M. Tooke, *Angew. Chem. Int. Ed.* **2001**, *40*, 3902 – 3905; *Angew. Chem.* **2001**, *113*, 4020 – 4023.
[20] P. C. Andrikopoulos, D. R. Armstrong, W. Clegg, C. J. Gilfillan, E. Hevia, A. R. Kennedy, R. E. Mulvey, C. T. O'Hara, J. A. Parkinson, D. M. Tooke, *J. Am. Chem. Soc.* **2004**, *126*, 11612 – 11620.
[21] W. Clegg, E. Crosbie, S. H. Dale-Black, E. Hevia, G. W. Honeyman, A. R. Kennedy, R. E. Mulvey, D. L. Ramsay, S. D. Robertson, *Organometallics* **2015**, *34*, 2580 – 2589.
[22] G. W. Honeyman, D. R. Aarmstrong, W. Clegg, E. Hevia, A. R. Kennedy, R. McLellan, S. A. Orr, J. A. Parkinson, D. L. Ramsay, S. D. Robertson, S. Towie, R. E. Mulvey, *Chem. Sci.* **2020**, *11*, 6510 – 6520.
[23] C. H. Winter, Y.-H. Han, R. L. Ostrander, A. L. Rheingold, *Angew. Chem. Int. Ed. Engl.* **1993**, *32*, 1161 – 1163; *Angew. Chem.* **1993**, *105*, 1247 – 1249.
[24] Y.-H. Han, M. J. Heeg, C. H. Winter, *Organometallics* **1994**, *13*, 3009 – 3019.
[25] S. A. Kur, C. H. Winter, *J. Organomet. Chem.* **1996**, *512*, 39 – 44.
[26] A. F. Neto, A. D. L. Borges, I. P. de Arruda Campos, J. Miller, *Synth. React. Inorg. Met.-Org. Chem.* **1997**, *27*, 1543 – 1551.
[27] J. A. F. Cunningham, *Organometallics* **1997**, *16*, 1114 – 1122.
[28] C. H. Winter, Y.-H. Han, M. J. Heeg, *Organometallics* **1992**, *11*, 3169 – 3171.
[29] S. A. Kur, A. L. Rheingold, C. H. Winter, *Inorg. Chem.* **1995**, *34*, 414 – 416.
[30] M. Olaru, R. Kather, E. Hupf, E. Lork, S. Mebs, J. Beckmann, *Angew. Chem. Int. Ed.* **2018**, *57*, 5917 – 5920; *Angew. Chem.* **2018**, *130*, 6020 – 6023.
[31] M. Olaru, S. Krupke, E. Lork, S. Mebs, J. Beckmann, *Dalton Trans.* **2019**, *48*, 5585 – 5594.
[32] S. Furan, E. Lork, S. Mebs, E. Hupf, J. Beckmann, *Z. Anorg. Allg. Chem.* **2020**, *646*, 856 – 865.
[33] P. Seiler, J. D. Dunitz, *Acta Crystallogr.* **1979**, *35*, 1068 – 1074.
[34] A. Bondi, *J. Phys. Chem. A* **1964**, *68*, 441 – 451.
[35] P. Pyykkö, M. Straka, *Phys. Chem. Chem. Phys.* **2000**, *2*, 2489 – 2493.
[36] H. Schmidbaur, H.-J. Öller, D. L. Wilkinson, B. Huber, G. Müller, *Chem. Ber.* **1989**, *122*, 31 – 36.
[37] M. Tschinkl, A. Schier, J. Riede, F. P. Gabbaï, *Angew. Chem. Int. Ed.* **1999**, *38*, 3547 – 3549; *Angew. Chem.* **1999**, *111*, 3769 – 3771.
[38] K. Venkatasubbaiah, J. W. Bats, A. L. Rheingold, F. Jäkle, *Organometallics* **2005**, *24*, 6043 – 6050.
[39] J. Echeverría, J. Cirera, S. Alvarez, *Phys. Chem. Chem. Phys.* **2017**, *19*, 11645 – 11654.
[40] J. B. King, M. R. Haneline, M. Tsunoda, F. P. Gabbaï, *J. Am. Chem. Soc.* **2002**, *124*, 9350 – 9351.
[41] M. R. Haneline, F. P. Gabbaï, *Angew. Chem. Int. Ed.* **2004**, *43*, 5471 – 5474; *Angew. Chem.* **2004**, *116*, 5587 – 5590.
[42] M. A. Omary, R. M. Kassab, M. R. Haneline, O. Elbjeirami, F. P. Gabbaï, *Inorg. Chem.* **2003**, *42*, 2176 – 2178.
[43] U. Patel, H. B. Singh, G. Wolmershäuser, *Angew. Chem. Int. Ed.* **2005**, *44*, 1715 – 1717; *Angew. Chem.* **2005**, *117*, 1743 – 1745.
[44] E. Hupf, E. Lork, S. Mebs, J. Beckmann, *Inorg. Chem.* **2015**, *54*, 1847 – 1859.
[45] R. Galassi, F. Bachechi, A. Burini, *J. Mol. Struct.* **2006**, *791*, 82 – 88.
[46] P. D. Harvey, K. T. Aye, K. Hierso, E. Isabel, I. Lognot, Y. Mugnier, F. D. Rochon, *Inorg. Chem.* **1994**, *33*, 5981 – 5982.
[47] N. L. Pickett, O. Just, D. G. VanDerveer, W. S. Rees Jr, *Acta Crystallogr.* **2000**, *C56*, 412 – 413.
[48] D. Grdenić, M. Sikirica, B. Korpar-Čolig, *J. Organomet. Chem.* **1978**, *153*, 1 – 7.
[49] D. Grdenić, B. Kamenar, B. Korpar-Čolig, M. Sikirca, G. Jovanovski, *J. Chem. Soc. Chem. Commun.* **1974**, 646 – 647.
[50] D. Grdenić, M. Sikirica, D. Matković-Čalogović, *J. Organomet. Chem.* **1986**, *306*, 1 – 7.

Chemistry–A European Journal
Communication
doi.org/10.1002/chem.202100261
Chemistry Europe
European Chemical Societies Publishing

[51] V. Sathesh, R. V. G. N. Chinta, R. Mamidala, V. Mukundam, K. Dhanunjayarao, K. Venkatasubbaiah, *J. Organomet. Chem.* **2017**, *853*, 74 – 80.
[52] R. E. Wasylishen, R. E. Lenkinski, C. Rodger, *Can. J. Chem.* **1982**, *60*, 2113 – 2117.
[53] J. G. Melnick, K. Yurkerwich, D. Buccella, W. Sattler, G. Parkin, *Inorg. Chem.* **2008**, *47*, 6421 – 6426.
[54] M. Maliarik, I. Persson, *Magn. Reson. Chem.* **2005**, *43*, 835 – 842.
[55] R. Benn, H. Günther, A. Maercker, V. Menger, P. Schmitt, *Angew. Chem. Int. Ed. Engl.* **1982**, *21*, 295 – 296; *Angew. Chem.* **1982**, *94*, 303 – 304.
[56] R. P. J. Cooney, J. R. Hall, *J. Inorg. Nucl. Chem.* **1972**, *34*, 1519 – 1527.
[57] A. J. Downs, E. A. V. Ebsworth, H. J. Emeléus, *J. Chem. Soc.* **1962**, 1254 – 1260.
[58] Deposition numbers 2047737 (for $FeC_{10}(HgCl)_{10}$), 2047740 (for $FeC_{10}(HgO_2CCCl_3)_{10}$), and 2047742 (for $FeC_{10}(HgO_2CCF_3)_{10}$) contain the supplementary crystallographic data for this paper. These data are provided free of charge by the joint Cambridge Crystallographic Data Centre and Fachinformationszentrum Karlsruhe Access Structures service.

Manuscript received: January 22, 2021
Accepted manuscript online: January 25, 2021
Version of record online: February 22, 2021

## 3.2 A Decacationic Ferrocene-Based Metallostar

Susanne Margot Rupf, Amina Mostaha, Moritz Malischewski*
*Chem. Sci.* **2023**, *14*, 1132–1137.

DOI: 10.1039/d2sc06151a



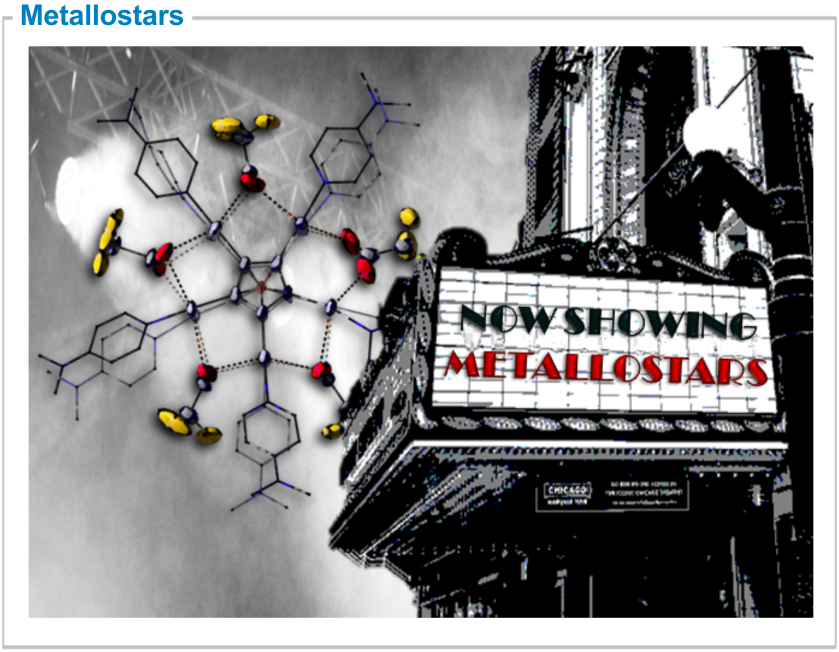


**Author Contribution:**
Susanne M. Rupf designed the project and wrote the manuscript. Furthermore, she performed syntheses and analyzed the spectroscopic data, performed cyclic voltammetry and UV/VIS experiments as well as measured and solved the single-crystal XRD data. Amina L. Moshtaha performed experiments and analyzed data during her internship course with support of Susanne M. Rupf. She performed further NMR, IR and Raman experiments and prepared the single crystals. Moritz Malischewski supervised the project and revised the manuscript.

Chemical Science

ROYAL SOCIETY OF CHEMISTRY

EDGE ARTICLE

View Article Online
View Journal | View Issue



Cite this: *Chem. Sci.*, 2023, **14**, 1132

All publication charges for this article have been paid for by the Royal Society of Chemistry

Received 7th November 2022
Accepted 27th December 2022

DOI: 10.1039/d2sc06151a

rsc.li/chemical-science

# A decacationic ferrocene-based metallostar†

Susanne Margot Rupf, Amina Leoni Moshtaha and Moritz Malischewski *

Decacationic metallostars have been prepared by the reaction of permercurated ferrocene $FeC_{10}(HgO_2CCF_3)_{10}$ with superacidic $(C_5F_5NH)(SbF_6)$ ($pK_a = -11$ estimated in $H_2O$) in multigram scale. In the resulting compound, $[FeC_{10}Hg_{10}(NC_5F_5)_n][SbF_6]_{10}$, the labile pentafluoropyridine ligands are readily displaced by acetonitrile (MeCN) or tetrahydrothiophene (THT). In the X-ray structure of $[FeC_{10}Hg_{10}(THT)_{10}][SbF_6]_{10}\cdot 24$ MeCN no cation–anion contacts between mercury and fluorine were observed. Moreover, cyclic voltammetry measurements of $[FeC_{10}(Hg(MeCN))_{10}]^{10+}$ and $[FeC_{10}(Hg(THT))_{10}]^{10+}$ revealed a (quasi)reversible one-electron oxidation of Fe(II) to Fe(III). From the reaction of $[FeC_{10}(Hg(MeCN))_{10}]^{10+}$ with $MoF_6$ as oxidant the ferrocenium cation $[FeC_{10}(Hg(MeCN))_{10}]^{11+}$ was obtained and characterized *via* single crystal XRD. These electrophilic metallostars are promising potential building blocks for the synthesis of dendritic architectures containing a robust, tenfold functionalized ferrocene core.

## Introduction

The relevance of biological redox processes of metalloproteins for living organisms inspired chemists to design redox active macromolecular compounds.[1] In this context the functionalization of dendrimers with redox active building blocks has received considerable attention as they are well defined macromolecules in terms of size and peripheral chemical functionality.[2] In the last decades these dendrimers have found applications as multielectron redox catalysts as well as reservoirs, in the surface modification of electrodes or in electrochemical sensors.[3,4] Their molecular architecture often resembles star-shaped structures with a core and different ligand building blocks which are not limited to organic moieties but also include examples of p-block and metal(organic) fragments.[5] A widely used redox active building block is the ferrocenyl group due to the reversibility of the $Fe^{+II/+III}$ redox couple and the high thermal stability of the oxidized and the native form in particular.[6] In many molecular stars the metallocene unit is located in the outskirts of the molecule[7–22] despite its $C_5$ symmetry rendering it as an ideal core building block. Examples of ferrocene centered metallostars are rare[23,24] probably due to the synthetic difficulties associated with the poly- or perfunctionalization of ferrocene.[25]

In 2021 we reported a simple perfunctionalization approach by treatment of ferrocene with mercury(II) carboxylates to obtain $FeC_{10}(HgX)_{10}$ ($X = O_2CC_3H_7$, $O_2CCF_3$, $O_2CCCl_3$) in multigram scale.[26] Although these compounds offer relatively weak Hg–C bonds allowing transmetallation[27,28] and electrophilic substitution reactions[29,30] they are chemically inert towards air and strong Brønsted acids (*e.g.* $CF_3CO_2H$ $pK_a = -2.7$ estimated in $H_2O$[31]) caused by the low polarity of the Hg–C bond as well as the low Lewis acidity of the R–Hg–X units to form adducts with increased coordination number.[32] Higher coordination numbers are usually observed in organomercury compounds with electron deficient substituents,[33–35] as shown by the Gabbaï group for $[o\text{-}(HgC_6F_4)_3]$ which forms supramolecular architectures with aromatic hydrocarbons[36,37] or weak Lewis acid/base adducts with a variety of O, N, P and S donors.[38–40] In contrast

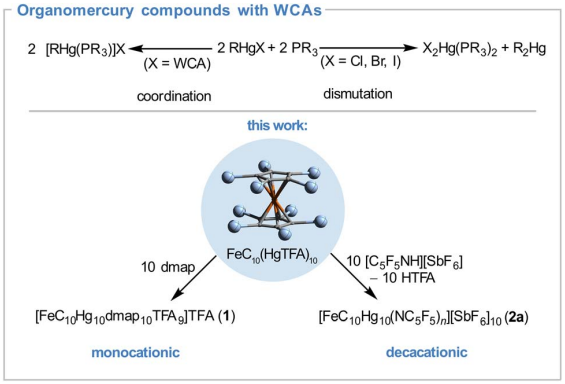


Scheme 1 Reactivity of cationic organomercury compounds towards neutral ligand like phosphine[41–44] and pyridine derivatives (this work) in presence of weakly coordinating anions (WCA). WCA = $ClO_4^-$, $NO_3^-$.[41–43]

*Freie Universität Berlin, Fabeckstr. 34-36, 14195 Berlin, Germany. E-mail: moritz.malischewski@fu-berlin.de*

† Electronic supplementary information (ESI) available. CCDC 2214089, 2213962 and 2213956. For ESI and crystallographic data in CIF or other electronic format see DOI: https://doi.org/10.1039/d2sc06151a

to this, in polar organomercury compounds R–Hg–X the anionic groups can be displaced by neutral ligands, *e.g.* phosphines, to give $[RHg(PR_3)]X$ (Scheme 1) maintaining the linear two-fold coordination.[41–43] The resulting cation $[RHg(PR_3)]^+$ is stable in presence of weakly coordinating anions (*e.g.* $X = ClO_4^-$) but dismutates in presence of halides ($X = Cl^- < Br^- < I^-$).[44] We envisioned that the displacement of anionic ligands in permercurated ferrocenes $FeC_{10}(HgX)_{10}$ would lead to the formation of highly charged species. Moreover, such polycations should be ideal precursors for ferrocene centered metallostars since they offer accessible coordination sites with predominantly linear coordination around the mercury atoms.

## Results and discussion

$FeC_{10}(HgO_2CCF_3)_{10}$ was dissolved in tetrahydrofuran and an excess of 4-(dimethylamino)pyridine (dmap) was added (Scheme 1) yielding an orange precipitate. The solid was analysed by NMR and vibrational spectroscopy as well as elemental analysis. While the IR spectrum of the coordination compound exhibits bands which correspond only to the trifluoroacetate[45] (TFA) as well as the nitrogen based ligand,[46] the Raman spectrum features further information especially with respect to the metallocene framework. $C^{Cp}$–$C^{Cp}$ deformation is found at $\tilde{\nu} = 951\ cm^{-1}$ and Hg–Cp vibrations at $\tilde{\nu} = 100\ cm^{-1}$. Moreover, the Hg–$O^{TFA}$ band ($\tilde{\nu} = 311\ cm^{-1}$ in $FeC_{10}(HgTFA)_{10}$) vanished and new bands at $\tilde{\nu} = 193–158\ cm^{-1}$ appeared, indicating the successful replacement of the carboxylic ligands by the pyridine analogues. $^1H$, $^{19}F$ and $^{13}C$ NMR signals show the intact ligands and anions but as in the starting material the $^{199}Hg$ resonance is not visible. The coordination to the mercury atoms causes a low field shift of $\Delta\delta = 6$ ppm of the $C^{Cp}$ signals in the $^{13}C$ NMR spectrum while all other signals are not significantly affected. The composition was determined by elemental analysis yielding the overall formula $FeC_{10}Hg_{10}dmap_{10}TFA_{10}$ (**1**).

Single crystals were obtained by recrystallization from tetrahydrofuran. Compound **1** crystallized in the monoclinic space group $P2_1/n$ containing one metallocene molecule in the asymmetric unit. All mercury atoms are almost linearly coordinated by one cyclopentadienyl and one dmap ligand with angles of 167.0(3)–178.6(4)° (Table 1), respectively. The distortion from linearity is caused by Hg–$O^{TFA}$ interactions within the sum of van der Waals radii of mercury ($r_{vdW} = 1.75$ Å)[47] and oxygen ($r_{vdW} = 1.52$ Å).[48] The Hg–O distances display a broad range of 2.24(1)–3.28(4) Å and are longer than in $FeC_{10}(HgO_2CCF_3)_{10}$ (Table 1). The TFA anions serve as bridging ligands between two to three metal centers (Fig. 1A) similarly to the structure of $Hg(TFA)_2 \cdot 2$ dmap which crystallizes as a dimer bridged by two TFA anions with a distorted octahedral coordination environment around the mercury atoms.[46] This coordination motif causes an eclipsed conformation in **1a** ($Cp^{torsion} = 3.6(1)°$) in contrast to $FeC_{10}(HgO_2CCF_3)_{10}$ which exhibits a staggered conformation in solid state. As a result, one intramolecular Hg–Hg contact of 3.440(2) Å is observed. Taking all interactions into account the total coordination number of the mercury atoms is four to six. As only two non-coordinating (distorted) TFA units within the

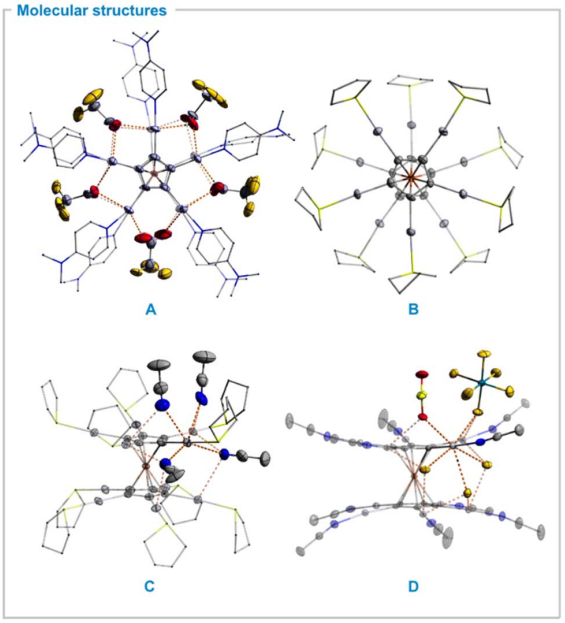


Fig. 1 Molecular structures of selected star-shaped permercurated metallocene cations in solid state. Ellipsoids with 50% probability level. Color code: mercury – light grey, antimony – turquoise, iron – orange, sulfur – neon yellow, fluorine – yellow, oxygen – red, nitrogen – blue, carbon – dark grey. Metal-anion or solvent interactions are shown as dashed orange lines. Hydrogen atoms, selected solvents and counter anions as well as disorder is omitted for clarity. (A) Inner sphere coordination of bridging TFA anions in $FeC_{10}Hg_{10}dmap_{10}(O_2CCF_3)_{10}$. (B) $[FeC_{10}(HgTHT)_{10}]^{10+}$ molecular fragment. (C) Solvent coordination motif in $[FeC_{10}(HgTHT)_{10}]^{10+}$ structure. (D) $[FeC_{10}(HgMeCN)_{10}]^{11+}$ molecular fragment as well as coordination of selected solvents and counter anion.

Table 1 Selected bond distances [Å] and angles [°] within the sum of van der Waals radii

| Compound | $FeC_{10}(HgO_2CCF_3)$[26] ($X = O^{TFA}$) | **1a** ($X = O^{TFA}$) | **2b** ($X = S^{THT}$) | **2c[$MoF_6$]** ($X = N^{MeCN}$) |
|---|---|---|---|---|
| Fe–$Cp^{center}$ | 1.660(1) | 1.672(2) | 1.651(1), 1.658(1) | 1.738(1) |
| Hg–C | 2.034(9)–2.040(8) | 2.009(10)–2.062(8) | 2.022(10)–2.046(9) | 2.023(6)–2.039(7) |
| Hg–X | 2.082(7)–2.115(6) | 2.241(17)–3.286(36) | 2.395(2)–2.405(2) | 2.050(6)–2.062(5) |
| $Hg–Hg^{intramol.}$ | — | 3.440(2) | — | — |
| C–Hg–X | 168.8(3)–176.5(3) | 167.0(3)–178.6(4) | 170.8(2)–176.7(2) | 171.2(3)–175.1(2) |
| Conformation | Staggered | Eclipsed | Staggered | Staggered |

View Article Online
Chemical Science Edge Article

unit cell with an overall occupancy of 1.33 are observed, this metallocene is better described as a "monocation" $[FeC_{10}(HgdmapH)_{10}(TFA)_{8.66}][TFA]_{1.33}$.

In order to reduce cation anion interactions, we introduced more weakly coordinating anions by protonation of the TFA anions with protonated pentafluoropyridine $[C_5F_5NH][SbF_6]$ ($pK_a \approx -11$ estimated in $H_2O$[49]) in liquid $SO_2$ (Scheme 1) yielding $[FeC_{10}Hg_{10}(NC_5F_5)_n][SbF_6]_{10}$ (**2a**) quantitatively as an insoluble orange solid whereas trifluoroacetic acid can be removed in vacuum. The completeness of the protonation was confirmed by the absence of TFA vibrations in the corresponding IR as well as Raman spectra (Fig. S7†). Instead, additional Sb–F bands are present at $\tilde{\nu} = 660$ and 633 $cm^{-1}$ in the infrared spectrum as well as C–C and C–F vibrations in the Raman and infrared spectrum which could be assigned to $C_5F_5N$[50] indicating coordination to the metal center. Protodemercuration is negligible as neither $\nu$(Cp–H) in the 3100 $cm^{-1}$ region nor (intense) $\delta$(Cp–H) vibrations in the 1100 $cm^{-1}$ region are visible in both spectra which again confirms the stability of the Cp–Hg bonds. Unfortunately, the total composition could not be determined by elemental analysis due to the sensitivity of the compound.

Substitution of the $C_5F_5N$ ligands improves the solubility of the corresponding compounds considerably and enables the full characterization of the compounds $[FeC_{10}(Hg\,solv.)_{10}][SbF_6]_{10}$ (solv. = tetrahydrothiophene (THT) **2b**, MeCN **2c**). Both metallocenes show similar features in the vibrational spectra as discussed for compound **2a**. The $C^{Cp}$ signals in the $^{13}C$ NMR spectra ($\delta = 111.8$ (**2b**) and 97.7 ppm (**2c**)) are again low field shifted in comparison to the signal of $FeC_{10}(HgTFA)_{10}$ as shown for compound **1**, previously.

Single crystals of the THT-complex **2b**·24 MeCN were obtained upon recrystallization from acetonitrile at −30 °C. It crystallized in the space group *C*2/*c*. The asymmetric unit contains a $\{Fe(CHgTHT)_5\}$ fragment with the iron position located at a center of inversion. The Cp ligands are aligned in a staggered conformation with torsion angles between 30.3(4) and 34.1(4)° (Fig. 1B). Again, the mercury atoms are linearly coordinated by a cyclopentadienyl and a THT ligand. In contrast to the structure of **1** no mercury anion contacts are visible (Fig. 1C). Instead, the decacationic fragment $[FeC_{10}(HgTHT)_{10}]^{10+}$ is fully solvated by 20 acetonitrile molecules. Ten of those are coordinating systematically two to three different mercury atoms from the space within both Cp rings and the other ten from the outer-sphere of the metallocene framework yielding a distorted octahedral geometry for all mercury atoms. The Hg–N distances are in range of 2.941(8)–3.289(8) Å. The interactions between cations and anions are mainly a consequence of hydrogen bonding to the solvent as well as the THT ligand. A detailed discussion of the packing motif of the decacation (**2b**) can be found in the ESI.†

Since $[FeC_{10}(HgTHT)_{10}][SbF_6]_{10}$ can be regarded as a ferrocene with ten cationic $[Hg(THT)]^+$ substituents the oxidation potentials of the metallocene are expected to be higher than in unsubstituted ferrocene as similar observations were reported for a series of acceptor substituted metallocenes.[51] Herein, Sundermeyer *et al.* observed increasing oxidation potentials of up to $\Delta E = 474$ mV per cationic group $\{SR_2\}^+$ group. The electrochemical properties of the compounds **1** and **2b,c** were determined by cyclic voltammetry. Unfortunately, the metallocene **1** decomposed upon oxidation preventing the determination of the oxidation potentials. The measurements of the soluble decacationic THT and MeCN complexes **2b** and **2c** were performed in acetonitrile and referenced against the $FcH/FcH^+$ redox couple (Fig. 2). Both compounds exhibit a reversible one-electron oxidation of the redox couple $Fe^{+II/+III}$ at $E_{1/2}{}^{THT} = 0.522$ V and $E_{1/2}{}^{MeCN} = 0.713$ V as well as irreversible oxidations above $E_a > 1.3$ V (Fig. S24 and S25, ESI†). The comparison of the $Fe^{+II/+III}$ potentials with the starting material $FeC_{10}(HgTFA)_{10}$ ($E_{1/2} = 0.450$ V) shows increasing oxidation potentials depending on the coordination strength of the ligand (TFA > THT > MeCN). Therefore, $[FeC_{10}Hg_{10}(NC_5F_5)_n][SbF_6]_{10}$, is expected to exhibit the highest oxidation potential in the series TFA < THT < MeCN < $NC_5F_5$ although its insolubility prevented its electrochemical characterization. A similar trend was already observed in Ag(I) compounds which vary enormously in oxidation potentials depending on the ligands at the metal center or simply the solvation ability of the solvents.[52] The surprisingly low potentials of the 10+/11+ redox couple are probably a consequence of the large size and effective solvation of these highly charged species as in multicationic ferrocenyl dendrimers.[53]

To realise the chemical oxidation of the permercurated ferrocene decacations we used different moderate oxidants in liquid $SO_2$ which allow solely oxidation to the desired ferrocenium compounds. The oxidations were tested with $Ag[SbF_6]$, $NO[BF_4]$, $NO_2[SbF_6]$ as well as $MoF_6$. Unfortunately, the presence of coordinating ligands seemed to reduce the reactivity of silver salts as no reaction of none of the compounds was observed with $AgSbF_6$. Moreover, $[FeC_{10}Hg_{10}(NC_5F_5)_n][SbF_6]_{10}$

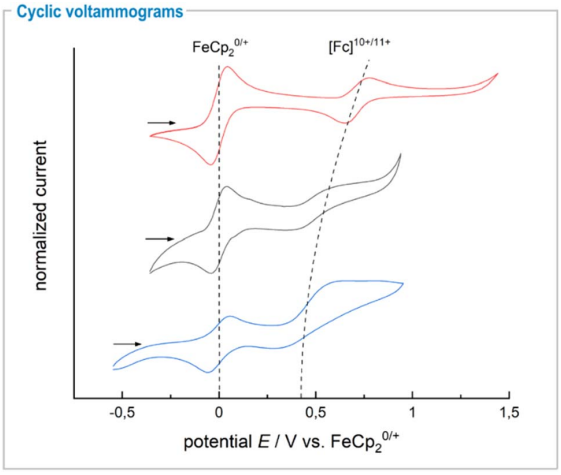


Fig. 2 Cyclic voltammograms of compounds $FeC_{10}(HgO_2CCF_3)_{10}$ in THF with 0.1 M $TBAPF_6$ as supporting electrolyte (bottom),[26] $[FeC_{10}(HgTHT)_{10}][SbF_6]_{10}$ (**2b**, middle) and $[FeC_{10}(HgMeCN)_{10}][SbF_6]_{10}$ (**2c**, top) in acetonitrile without supporting electrolyte at 100 mV $s^{-1}$ scan rate and room temperature.

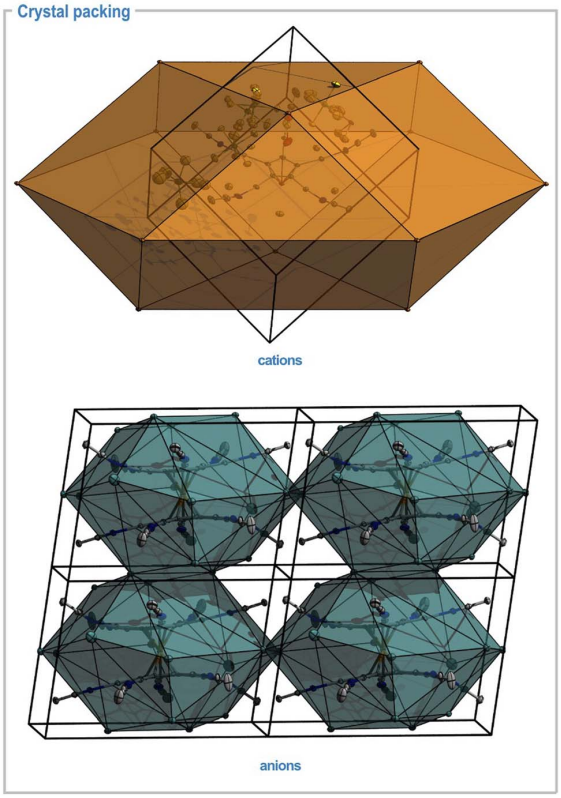


Fig. 3 Packing motifs of anions and cations in the crystal structure of $[FeC_{10}Hg(MeCN)_{10}][SbF_6]_{10}[MoF_6]$ 2 $SO_2$·10 HF. Top: asym. unit and closest iron positions forming a cuboctahedron. Bottom: four units cells containing heavy metal positions forming distorted square orthobicupolas around the undecacation. Ellipsoids drawn with 50% probability level. Color code: mercury – light grey, molybdenum – purple, antimony – turquoise, iron – orange, sulphur – neon yellow, fluorine – yellow, oxygen – red, carbon – dark – grey.

showed no reaction with $(NO)^+$ but with $(NO_2)^+$ indicating high oxidation potentials which perfectly fits to the correlation between ligand strength and redox potential. Reactions with $(NO_2)^+$ and $MoF_6$ were successful in all cases.

Single crystals of **2c[MoF$_6$]**·10 HF·2 $SO_2$ were obtained upon recrystallisation from HF/$SO_2$ at −74 °C. The compound crystallized in the space group $P\bar{1}$. The asymmetric unit consists of one $\{FeC_5(HgMeCN)_5\}$ moiety with a center of inversion located at the iron atom. The oxidation of the iron center is indicated by an elongated iron-cyclopentadienyl distance of 1.738(1) Å which is in the same order of magnitude as other substituted ferrocenium salts but significantly longer than those of non-substituted ferrocenium cations.[54] The metallocene cation is again fully solvated by 10 HF molecules with Hg–F$^{HF}$ distances of 2.817(5)–2.956(4) Å within the inner-sphere of the metallocene framework in a similar fashion as discussed for compound **2b** triggering a staggered conformation with torsion angles in the range of 31.1(1)° to 35.9(1). However, the structure features several additional Hg–F cation–anion interactions of 2.824(5)–3.090(5) Å length yielding a coordination number of four to six for all mercury atoms (Fig. 1D). The Hg–F contacts to the $[SbF_6]^-$ counter anions are present due to the low solvation of the undecacation in HF, in contrast to the THT complex **2b** which was recrystallized from acetonitrile.

Both, the solid-state structure of $[FeC_{10}(HgTHT)_{10}]^{10+}$ and $[FeC_{10}(HgMeCN)_{10}]^{11+}$ are rare examples of isolated organometallic deca- and undecacations. Although the large variety of multicationic organic or organometallic compounds,[55–60] only a few examples for crystallographically characterized octa-,[61] nona-,[62] deca-,[63–65] dodeca[66] and even hexadecacations[67] have been reported in the past years. In such multications, the positive charges are kinetically stabilized by organic ligands *via* formation of large aggregates.[68] These so-called "lipophilically wrapped polyion aggregates" are usually not perfectly spheric causing voids within the crystal packing. Therefore, the formation of a closest packing arrangements or typical structure types as observed for (pseudo-)spherical components of low charge is prevented. In the crystal structure of $[FeC_{10}Hg(MeCN)_{10}][SbF_6]_{10}[MoF_6]\cdot 2\ SO_2\cdot 10$ HF the iron atoms produce a distorted hexagonal distorted arrangement along the [111] direction but with a ABC-stacking pattern similar to the face-centered cubic structure of copper causing a distorted cuboctahedral geometry around each iron position (Fig. 3, top). Considering only the centers of gravity for all molecular entities, no simple packing arrangement is observed for the anionic units. The undecacation is surrounded by 16 anions in a distorted square orthobicupolar geometry (Fig. 3, bottom). These polyhedra are edge-sharing with the same polyhedra of adjacent unit cells along *a* and *b* and corner-sharing along *c* resulting in a 1 : 11 composition of cations and anions. Sulphur moieties from $SO_2$ solvates are capping two adjacent faces on both apical sides of the bicupolas.

## Conclusions

In summary, we investigated the reactivity of permercurated ferrocene derivatives towards neutral ligands in standard organic solvents as well as in superacidic medium.[69] We demonstrated that in the compound $FeC_{10}(HgTFA)_{10}$ all mercury atoms are accessible to Lewis bases. The Lewis acidity of the $\{FeC_{10}Hg_{10}\}^{10+}$ framework was tuned by variation of the counter anions. While the TFA salt only binds to strong σ-donors like dmap, the presence of weakly coordinating anions allows to isolate solvent adducts $[FeC_{10}(HgL)_{10}][SbF_6]_{10}$ (with L = $C_5F_5N$, MeCN, THT). Surprisingly, in those compounds the Hg–C bonds are inert to Brønsted acids, such as $[C_5F_5NH][SbF_6]$. Moreover, we report the preparation of undecacations $[FeC_{10}(HgMeCN)_{10}]^{11+}$ and $[FeC_{10}(HgTHT)_{10}]^{11+}$ as stable solids. Both, the solid-state structure of $[FeC_{10}(HgTHT)_{10}]^{10+}$ and $[FeC_{10}(HgMeCN)_{10}]^{11+}$ are rare examples of isolated organometallic deca- and undecacations.[70] The combination of the accessible coordination sites, electrochemical properties as well as their reliable multigram synthesis renders these

deca- and undecacations as promising precursors for even larger star-shaped molecular architectures (*e.g.* dendrimers).

## Data availability

Besides the ESI† and the crystal structures in CCDC we have not deposited any data in other repositories.

## Author contributions

The project was developed by S. M. R. and M. M. Both authors wrote the manuscript with main contributions from S. M. R. The synthetic work was carried out by S. M. R. and A. L. M, S. M. R. performed cyclic voltammetry and UV/vis experiments as well as measured and solved the SCXRD data. A. L. M. performed further NMR, IR and Raman experiments and prepared the single crystals.

## Conflicts of interest

There are no conflicts to declare.

## Acknowledgements

Gefördert durch Deutsche Forschungsgemeinschaft (DFG) – Projektnummer: 387284271 – SFB 1349. Funded by Deutsche Forschungsgemeinschaft (DFG) – project number: 387284271 – SFB 1349. Computing time was made available by High-Performance Computing at ZEDAT/FU Berlin. We would like to acknowledge the assistance of the Core Facility BioSupraMol supported by the DFG. The authors thank Prof. Dr Florian Kraus (Philipps-Universität Marburg) and Dr Günther Thiele (Freie Universität Berlin) for helpful discussions.

## Notes and references

1 D. Astruc, *J. Leather Sci. Eng.*, 2020, **2**, 1–17.
2 C. Gorman, *Adv. Mater.*, 1998, **10**, 295–309.
3 D. Astruc, C. Ornelas and J. Ruiz, *Acc. Chem. Res.*, 2008, **41**, 841–856.
4 G. R. Newkome, E. He and C. N. Moorefield, *Chem. Rev.*, 1999, **99**, 1689–1746.
5 H. Detert, M. Lehmann and H. Meier, *Materials*, 2010, **3**, 3218–3330.
6 D. Astruc, *Eur. J. Inorg. Chem.*, 2017, 6–29.
7 B. Kayser, J. Altman, H. Nöth, J. Knizek and W. Beck, *Eur. J. Inorg. Chem.*, 1998, 1791–1798.
8 M. Iyoda, T. Kondo, T. Okabe, H. Masuyama, S. Sasaki and Y. Kuwatani, *Chem. Lett.*, 1997, **26**, 35–36.
9 R. Misra, R. Maragani, C. P. Singh and R. Chari, *Dye Pigm.*, 2016, **126**, 110–117.
10 A. K. Diallo, C. Absalon, J. Ruiz and D. Astruc, *J. Am. Chem. Soc.*, 2011, **133**, 629–641.
11 J. C. Santos, F. Madrid-Moliné, C. A. Cisternas, F. Paul, C. A. Escobar, P. Jara-Ulloa and A. Trujillo, *Inorg. Chim. Acta*, 2018, **486**, 95–100.
12 G. Erbland, S. Abid, Y. Gisbert, N. Saffon-Merceron, Y. Hashimoto, L. Anderoni, T. Guérin, C. Kammerer and G. Rapenne, *Chem.–Eur. J.*, 2019, **25**, 16328–16339.
13 A. Hildebrandt, T. Rüffer, E. Erasmus, J. C. Swarts and H. Lang, *Organometallics*, 2010, **29**, 4900–4905.
14 G. Vives, A. Carella, J.-P. Launay and G. Rapenne, *Chem. Commun.*, 2006, 2283–2285.
15 J.-L. Fillaut, J. Lineares and D. Astruc, *Angew. Chem., Int. Ed. Engl.*, 1994, **33**, 2460–2462.
16 V. Mamane, I. Ledoux-Rak, S. Deveau, J. Zyss and O. Riant, *Synthesis*, 2003, **3**, 433–467.
17 V. Mamane, A. Gref and O. Riant, *New J. Chem.*, 2004, **28**, 585–594.
18 Y. Yu, A. D. Bond, P. W. Leonard, K. P. C. Vollhardt and G. D. Whitener, *Angew. Chem., Int. Ed.*, 2006, **45**, 1794–1799.
19 B. Alonso, I. Cuadrado, M. Morán and J. Losada, *J. Chem. Soc., Chem. Commun.*, 1994, 2575–2576.
20 Y. Yu, A. D. Bond, P. W. Leonard, U. J. Lorenz, T. V. Timofeeva, K. P. C. Vollhardt, G. D. Whitener and A. A. Yakovenko, *Chem. Commun.*, 2006, 2572–2574.
21 R. Misra, R. Sharma and S. M. Mobin, *Dalton Trans.*, 2014, **43**, 6891–6896.
22 R. Misra, R. Maragani, B. Pathak, P. Gautam and S. M. Mobin, *RCS Adv.*, 2015, **5**, 71046–71051.
23 K. Rahimpour and R. Teimuri-Mofrad, *Appl. Organomet. Chem.*, 2020, **34**, e5943.
24 P. Jutzi, C. Batz, B. Neumann and H.-G. Stammler, *Angew. Chem., Int. Ed. Engl.*, 1996, **35**, 2118–2121.
25 H. Butenschön, *Synthesis*, 2018, **50**, 3787–3808.
26 S. M. Rupf, G. Schröder, R. Sievers and M. Malischewski, *Chem.–Eur. J.*, 2021, **27**, 5125–5129.
27 K. N. Seneviratne, A. Bretschneider-Hurley and C. H. Winter, *J. Am. Chem. Soc.*, 1996, **118**, 5506–5507.
28 A. Bretschneider-Hurley and C. H. Winter, *J. Am. Chem. Soc.*, 1994, **116**, 6468–6469.
29 S. M. Rupf, I. S. Dimitrova, G. Schröder and M. Malischewski, *Organometallics*, 2022, **41**, 1261–1267.
30 Y.-H. Han, M. J. Heeg and C. H. Winter, *Organometallics*, 1994, **13**, 3009–3019.
31 S. Saito, S. Saito, T. Ohwada and K. Shudo, *Chem. Pharm. Bull.*, 1991, **39**, 2718–2720.
32 I. P. Beletskaya, K. P. Butin, A. N. Ryabtsev and O. A. Reutov, *J. Organomet. Chem.*, 1973, **59**, 1–44.
33 T.-P. Lin, R. C. Nelson, R. Wu, J. T. Miller and F. P. Gabbaï, *Chem. Sci.*, 2012, **3**, 1128–1136.
34 P. Nockemann, F. Schulz, D. Maumann and G. Meyer, *Z. Anorg. Allg. Chem.*, 2005, **631**, 649–653.
35 M. Nolte, I. Patenburg and G. Meyer, *Z. Anorg. Allg. Chem.*, 2007, **634**, 362–368.
36 M. Tsunoda and F. P. Gabbaï, *J. Am. Chem. Soc.*, 2000, **122**, 8335–8336.
37 M. R. Haneline, M. Tsunoda and F. P. Gabbaï, *J. Am. Chem. Soc.*, 2002, **124**, 3737–3742.
38 M. Fleischmann, J. S. Jones, G. Balázs and F. P. Gabbaï, *Dalton Trans.*, 2016, **45**, 13742–13749.
39 M. R. Haneline, R. E. Taylor and F. P. Gabbaï, *Chem.–Eur. J.*, 2003, **9**, 5188–5193.

40 T. J. Taylor, C. N. Burress and F. P. Gabbaï, *Organometallics*, 2007, **26**, 5252–5263.
41 G. E. Coates and A. Lauder, *J. Chem. Soc.*, 1965, 1857–1864.
42 T. S. Lobana, M. K. Sandhu, D. C. Povey and G. W. Smith, *J. Chem. Soc., Dalt. Trans.*, 1988, 2913–2914.
43 T. S. Lobana and M. K. Sandhu, *J. Chem. Soc., Dalt. Trans.*, 1989, 2339–2341.
44 G. Schwarzenbach and M. Schellenberg, *Helv. Chim. Acta*, 1965, **48**, 28–46.
45 A. J. Downs, E. A. V. Ebsworth and H. J. Emeléus, *J. Chem. Soc.*, 1962, 1254–1260.
46 W. Tyrra, D. Naumann and I. Pantenburg, *J. Fluorine Chem.*, 2003, **120**, 13–19.
47 P. Pyykkö and M. Straka, *Phys. Chem. Chem. Phys.*, 2000, **2**, 2489–2493.
48 A. Bondi, *J. Phys. Chem.*, 1964, **68**, 441–451.
49 S. L. Bell, R. D. Chambers, K. R. Musgrave and J. G. Thorpe, *J. Fluorine Chem.*, 1971, **1**, 51–57.
50 K. Züchner, T. J. Richardson, O. Glemser and N. Bartlett, *Angew. Chem., Int. Ed. Engl.*, 1980, **19**, 944–945.
51 A. Venker, T. Vollgraff and J. Sundermeyer, *Dalton Trans.*, 2018, **47**, 1933–1941.
52 N. G. Connelly and W. E. Geiger, *Chem. Rev.*, 1996, **96**, 877–910.
53 D. Astruc, *New J. Chem.*, 2011, **35**, 764–772.
54 R. Martinez and A. Tiripicchio, *Acta Cryst.*, 1990, **C46**, 202–205.
55 D. Astruc, M.-C. Daniel and J. Ruiz, *Chem. Commun.*, 2004, 2637–2649.
56 D. Astruc, C. Ornelas and J. Ruiz, *Chem.–Eur. J.*, 2009, **15**, 8936–8944.
57 J. Chen, J. Shan, Y. Xu, P. Su, L. Tong, L. Yuwen, L. Weng, B. Bao and L. Wang, *ACS Appl. Mater. Interfaces*, 2018, **10**, 34455–34463.
58 K.-Y. Pu, K. Li and B. Liu, *Adv. Mater.*, 2010, **22**, 643–646.
59 C. McCusker, J. B. Caroll and V. M. Rotello, *Chem. Commun.*, 2005, 996–998.
60 L.-I. Rodríguez, O. Rossell, M. Seco and G. Muller, *J. Organomet. Chem.*, 2007, **692**, 851–858.
61 D. M. L. Goodgame, S. Kealey, P. D. Lickiss and A. J. P. White, *J. Mol. Struct.*, 2008, **890**, 232–239.
62 M. A. Little, M. A. Halcrow, L. P. Harding and M. J. Hardie, *Inorg. Chem.*, 2010, **49**, 9486–9496.
63 C. S. Campos-Fernandez, R. Clerac, J. M. Koomen, D. H. Russell and K. R. Dunbar, *J. Am. Chem. Soc.*, 2001, **123**, 773–774.
64 C. S. Campos-Fernandez, B. L. Schottel, H. T. Chifotides, J. K. Bera, J. Bacsa, J. M. Koomen, D. H. Russell and K. R. Dunbar, *J. Am. Chem. Soc.*, 2005, **127**, 12909–12923.
65 I. D. Giles, H. T. Chifotides, M. Shatruk and K. R. Dunbar, *Chem. Commun.*, 2011, **47**, 12604–12606.
66 R. Lavendomme, T. K. Ronson and J. R. Nitschke, *J. Am. Chem. Soc.*, 2019, **141**, 12147–12158.
67 J. Yang, X.-Y. Chang, K.-C. Sham, S.-M. Yui, H.-L. Kwong and C.-M. Che, *Chem. Commun.*, 2016, **52**, 5981–5984.
68 H. Bock, A. John, C. Näther and Z. Havlas, *J. Am. Chem. Soc.*, 1995, **117**, 9367–9368.
69 A previous version of this manuscript has been deposited on a preprint server: S. M. Rupf, A. L. Moshtaha, and M. Malischewski, *ChemRxiv*, 2022, DOI: 10.26434/chemrxiv-2022-5rxlm.
70 Deposition numbers CCDC 2214089 ($[FeC_{10}(HgDMAP)_{10}][TFA]_{10}$), 2213962 ($[FeC_{10}(HgTHT)_{10}][SbF_6]_{10}\cdot 24$ MeCN) and 2213956 ($[FeCp_2(HgMeCN)_{10}][SbF_6]_{10}[MoF_6]\cdot 2SO_2\cdot 10$ HF) contain the supplementary crystallographic data for this paper. These data are provided free of charge by the joint Cambridge Crystallographic Data Centre and Fachinformationszentrum Karlsruhe Access Structures service.**https://www.ccdc.cam.ac.uk/structures**.

## 3.3 Preparation and One-Electron Oxidation of Decabromoferrocene

Susanne Margot Rupf, Irina Savova Dimitrova, Gabriel Schröder, Moritz Malischewski*
*Organometallics* **2022**, *41*, 1261–1267.

DOI: 10.1021/acs.organomet.2c00157



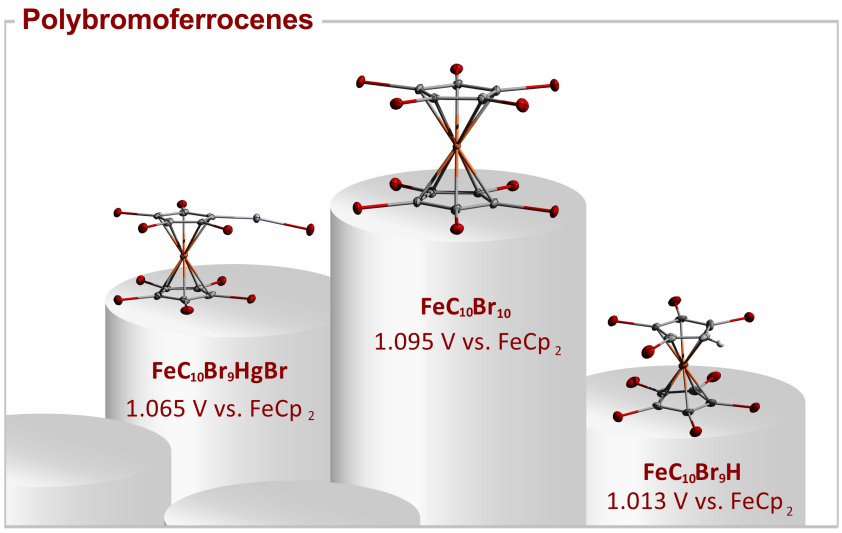


**Author Contribution:**
Susanne M. Rupf designed the project and wrote the manuscript. Furthermore, she performed syntheses and analyzed the spectroscopic data, performed cyclic voltammetry experiments as well as measured and solved the single-crystal XRD data. Gabriel Schröder performed experiments and analyzed data during his bachelor thesis and Irina S. Dimitrova performed experiments and analyzed data during her internship course. Both authors were supervised by Susanne M. Rupf. Moritz Malischewski supervised the project and revised the manuscript.

ORGANOMETALLICS

pubs.acs.org/Organometallics Article

# Preparation and One-Electron Oxidation of Decabromoferrocene

Susanne M. Rupf, Irina S. Dimitrova, Gabriel Schröder, and Moritz Malischewski*

Cite This: *Organometallics* 2022, 41, 1261−1267 Read Online

ACCESS | Metrics & More | Article Recommendations | Supporting Information

**ABSTRACT:** We report an improved synthesis as well as a spectroscopical, structural, and electrochemical characterization of decabromoferrocene ($FeC_{10}Br_{10}$) and relevant side products. One-electron oxidation of decabromoferrocene ($E_{1/2}$ = 1.095 V vs $FeCp_2^{0/+}$) was achieved by $AsF_5$ in liquid $SO_2$. The crystal structure of decabromoferrocenium hexafluoroarsenate, $[FeC_{10}Br_{10}][AsF_6]$, represents the first example of an isolated and structurally characterized perhalogenated ferrocenium salt.

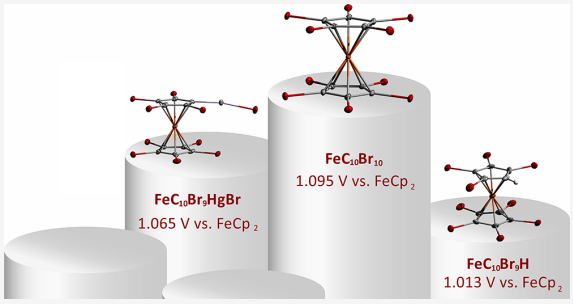


## INTRODUCTION

Since the discovery of ferrocene in 1951,[1] ferrocene derivatives have found wide applications ranging from materials science and medicinal chemistry to catalysis.[2] This can be explained by its unusual high metal carbon bond stability and unique redox properties. Ferrocene can be easily oxidized by mild oxidizers ($FeCp_2^{0/+}$ $E_{1/2}$ = 0.41 V vs SCE[3]) forming the deep blue ferrocenium cation $[Fe^{III}Cp_2]^+$. While numerous ferrocenium compounds have been isolated so far, two-electron oxidations ($FeCp_2^{+/2+}$) and one-electron reductions ($FeCp_2^{-/0}$) are hard to achieve due to the extreme redox potentials of these processes.[4,5] Changing the substitution pattern allows for a fine-tuning of the electrochemical properties, enabling the isolation of Fe(IV) and Fe(I) species.[6,7] For instance, while the permethylation of the cyclopentadienyl ligands lowers the first oxidation to $E_{1/2}$ = −0.096 V vs SCE,[3] electron-withdrawing groups, e.g., carboxylic or sulfonyl groups, increase the oxidation potentials drastically.[8]

Functionalized ferrocenes are typically derived from haloferrocenes. However, direct reaction of ferrocenes with elemental halogens is often synthetically not useful to prepare halogenated derivatives. Instead, one-electron oxidation to ferrocenium cations or total decomposition is typically observed.[9] Therefore, monohaloferrocenes $FeC_{10}H_9X$ (X = F, Cl, Br, I) are instead synthesized by monometalation followed by quenching with an electrophilic halogenation agent.[10−12] Higher halogenation degrees ($FeC_{10}H_nX_{10-n}$; $n$ = 2−8) lead to a large number of possible isomers. So far only a small number of halogenated ferrocenes have been reported.[13] Isomerically pure polyfunctionalizations were achieved by iterative *ortho*-lithiation with, for example, LiTMP or LDA followed by halogenation.[14−19] Via this approach the perhalogenated ferrocene $FeC_{10}Cl_{10}$ was isolated as well,[20] but a more efficient approach proceeds via one-pot permercuration followed by halogenation to yield $FeC_{10}X_{10}$ (X = Cl, Br, I) (Scheme 1).[21,22] However, the mercuration step was incomplete, raising doubts about the subsequent perhalogenation.[23]

**Scheme 1. Perhalogenation of Ferrocene via the Permercuration Approach (Winter 1994[21])**

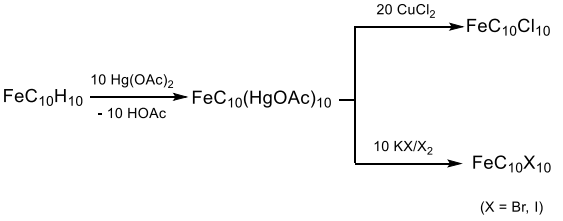


Perhalogenated metallocenes are not only valuable precursors for other persubstituted ferrocenes but also exhibit interesting electrochemical properties themselves. Brown et al. observed unusually high oxidation potentials for $FeC_{10}Cl_{10}$ ($E_{1/2}$ = 1.246 V[24] vs $FeCp_2^{0/+}$) in comparison to other acceptor-substituted metallocenes.[25] The oxidation potentials of the neutral compounds $FeC_{10}H_{10-n}Cl_n$ ($n$ = 1, 2, 5, 10) increase gradually by $\Delta E$ = 0.12−0.16 V per Cl (Scheme 2). Due to the absence of hydrogen atoms and consequently

**Received:** March 31, 2022
**Published:** May 5, 2022

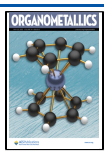





https://doi.org/10.1021/acs.organomet.2c00157
*Organometallics* 2022, 41, 1261−1267

**Scheme 2. Electrochemical Potentials in Volts versus the Redox Couple $FeCp_2^{0/+}$ of Selected Literature-Known Metallocenes**

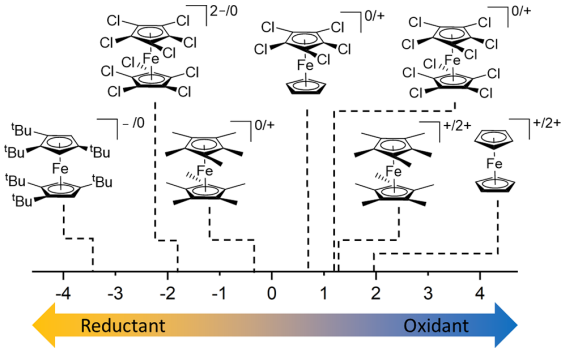


blocked decomposition pathways, a high stability of the corresponding perhalogenated ferrocenium cations is expected. Unfortunately, the electrochemical behavior of other fully halogenated ferrocene derivatives $FeC_{10}X_{10}$ (X = F, Br, I) is unknown. Therefore, we revised the synthesis of $FeC_{10}Br_{10}$ and investigated its electrochemical behavior.

## RESULTS AND DISCUSSION

$FeC_{10}(HgOAc)_{10}$ was treated with $KBr_3$ as described in previous literature,[21] and the resulting product was analyzed by IR and NMR spectroscopy. The obtained infrared spectrum of the product is in agreement with the literature data in which the absence of $\nu$(C−H) absorptions was interpreted as proof for the completeness of the halogenation reaction. However, we found this conclusion to be erroneous based on the $^{13}C$ NMR spectra (Figure 1). The spectrum reveals a mixture of polyhalogenated compounds (Figure 1, top). Apart from the signal of the perhalogenated Cp moiety at $\delta$ = 85.4 ppm (orange) the spectrum shows three doublets at $\delta$ = 86.4, 84.1, and 78.2 ppm (blue), which were assigned to the $\{C_5Br_4H\}$ fragment, indicating that one main product is $FeC_{10}Br_9H$. The corresponding $^1H$ NMR signal was found at $\delta$ = 4.92 ppm (SI). The formation of $FeC_{10}Br_9H$ can be explained either by incomplete mercuration of ferrocene ($FeC_{10}H(HgOAc)_9$) or by protodemercuration of $FeC_{10}(HgOAc)_{10}$ as a competing reaction, which could prevent the perhalogenation.[26]

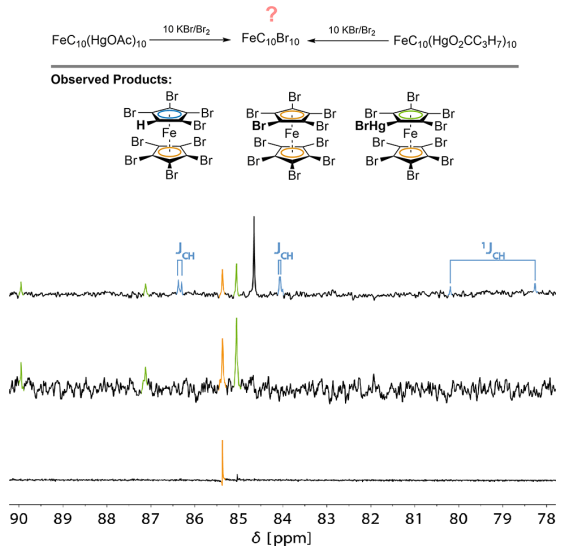


**Figure 1.** $^{13}C$ NMR spectra in THF-$d_8$ of the bromination products after reaction of $FeC_{10}(HgOAc)_{10}$ with $KBr_3$ (top), $FeC_{10}(HgO_2CC_3H_7)_{10}$ with $KBr_3$ (middle), and $FeC_{10}Br_9HgBr$ with elemental bromine and iron powder (bottom). Assigned signals: orange, $\{C_5Br_5\}$ fragment; green, $\{C_5Br_4HgBr\}$ fragment; blue, $\{C_5Br_4H\}$ fragment; black, unknown impurity.

To answer this question, the bromination experiments were repeated with $FeC_{10}(HgO_2CC_3H_7)_{10}$, for which a synthetic approach with high purity and 92% yield was reported recently by us.[27] After the bromination, the $^1H$ NMR spectrum shows no Cp-H signals, indicating that the protohaloferrocenes in reaction (a) are derived from incomplete mercuration. Surprisingly, the $^{13}C$ NMR spectrum of the corresponding product mixture shows, apart from the signal of the $\{C_5Br_5\}$ ring, three singlets at $\delta$ = 90.0, 87.1, and 85.1 ppm (Figure 1, middle), which were assigned to the $\{C_5Br_4HgBr\}$ fragment. The desired perhalogenated species could be isolated only in low yields out of this mixture. The incomplete perhalogenation of permercurated compounds by reaction with $KBr_3$ was already observed in the perbromination of $C_6(HgO_2CCF_3)_6$, $C_6(HgO_2CCF_3)_5OMe$, and other permercurated benzene derivatives and seems to be a common difficulty.[28,29] To achieve a complete halogenation, $FeC_{10}Br_9HgBr$ was treated with Fe powder and elemental bromine. Due to the increased stability of $FeC_{10}Br_9HgBr$ toward oxidizing agents, $FeC_{10}Br_{10}$ was isolated in high purity in this second step (Figure 1, bottom). The compound is soluble in dichloromethane, tetrahydrofuran, and dimethylsulfoxide.

In addition to NMR spectroscopy, the purity of the reaction product was checked via vibrational spectroscopy. The infrared spectrum of pure $FeC_{10}Br_9HgBr$ shows four bands at $\tilde{\nu}$ = 1309, 1280, 1264, and 583 $cm^{-1}$ (Figure 2, green). While the last band can be assigned to the $\nu$(C−Br) vibration, the remaining resonances correspond to C−C vibrations of the Cp moiety. The compounds $FeC_{10}Br_9HgBr$ and $FeC_{10}Br_{10}$ can be differentiated by the absence of a band at $\tilde{\nu}$ = 1265 $cm^{-1}$ due to higher symmetry of decabromoferrocene (Figure 2,

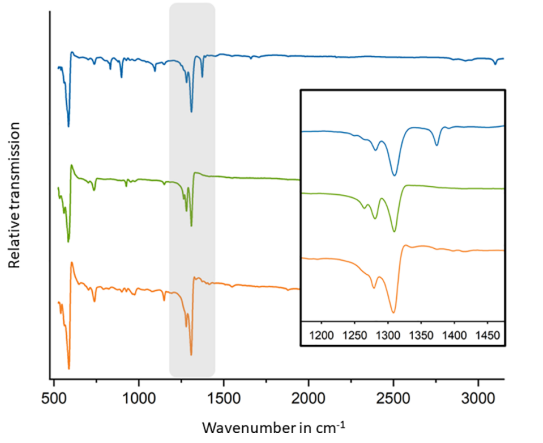


**Figure 2.** Infrared spectra of $FeC_{10}Br_{10}$ (orange), $FeC_{10}Br_9HgBr$ (green), and products of reaction of $FeC_{10}(HgOAc)_{10}$ with $KBr_3$ (blue).



https://doi.org/10.1021/acs.organomet.2c00157
Organometallics 2022, 41, 1261−1267

orange). This is in contrast to the published infrared data of Winter and co-workers, who reported four vibrations at $\tilde{\nu}$ = 1379, 1302, 1274, and 580 $cm^{-1}$ for $FeC_{10}Br_{10}$.[21] The additional band at $\tilde{\nu}$ = 1379 $cm^{-1}$ was only visible in the presence of $FeC_{10}Br_9H$ (Figure 2, blue). Therefore, we conclude that the synthetic approach by Winter and co-worker never yielded pure $FeC_{10}Br_{10}$ but a mixture of most likely $FeC_{10}Br_{10}$, $FeC_{10}Br_9H$, and $FeC_{10}Br_9HgBr$.

The electrochemical properties of these compounds were investigated by cyclic voltammetric measurements in dry and oxygen-free dichloromethane and tetrahydrofuran as well as $[nBu_4N][PF_6]$ as supporting electrolyte. In tetrahydrofuran, no oxidation process of either $FeC_{10}Br_9H$ or $FeC_{10}Br_{10}$ was observed within the electrochemical window. In dichloromethane, one reversible one-electron oxidations at $E_{1/2}$ = 1.013 ($FeC_{10}Br_9H$) and 1.095 V ($FeC_{10}Br_{10}$) vs $FeCp_2^{0/+}$ were observed, respectively. The comparison of these results with less brominated metallocenes ($FeC_{10}BrH_9$, $E_{1/2}$ = 0.110 V vs $FeCp_2^{0/+}$; see Table 1) shows that the oxidation potentials

**Table 1. Electrochemical Potentials vs $FeCp_2^{0/+}$ of Selected Brominated Metallocenes in Dichloromethane**

| compound | $E_{1/2}$/V | ref |
|---|---|---|
| $FeC_{10}BrH_9$ | 0.110 | this work |
| 1,1-$FeC_{10}Br_2H_8$ | 0.276 | this work |
| 1,1′,2,2′-$FeC_{10}Br_4H_6$ | 0.559[a] | 34 |
| $FeC_{10}Br_9H$ | 1.013 | this work |
| $FeC_{10}Br_9HgBr$ | 1.065 | this work |
| $FeC_{10}Br_{10}$ | 1.095 | this work |

[a]+0.99 V vs AgCl/Ag (KCl saturated).

continuously increase with the level of bromination. This finding is consistent with the results for polyfluorinated $FeC_{10}F_nH_{10-n}$ ($n$ = 0, 1, 2, 3, 4, 5)[30] and polychlorinated metallocenes $FeC_{10}H_{10-n}Cl_n$ ($n$ = 1, 2, 5, 10).[24] This correlation was found to be linear for ferrocenes bearing the lighter halogens atoms (F, Cl) but not for brominated ferrocenes (this work). This observation demonstrates that the change in the electrochemical potentials cannot be explained by the electronegativity of the halogen atoms alone. Inkpen and co-workers systematically studied the effect of mono- and dihalogenation of ferrocene on the redox potentials, showing the following trend: Cl ∼ Br > I > F.[31] As a result, they assumed that besides inductive effects, resonance effects have to be taken into account, which are combined with the Hammett parameter by $\sigma = \alpha F + R$.[32] A linear correlation was found for the electrochemical potentials of the mono- and dihalogenated series with respect to the resonance factor $R$. Similar observations were reported for a series of non-halogenated, substituted ferrocenes.[3,33] This seemingly linear correlation should allow the prediction of redox potentials of (poly)substituted ferrocenes, but should be considered carefully. While for mono- and disubstituted ferrocenes these correlations fit quite well (Figure 3), the discrepancies become most visible at high halogenation levels. This is consistent with the results of Erb and co-workers, who showed that in the case of (poly)halogenated ferrocenes the correlation between the redox potentials and $R$ falls into distinct groups depending on the substitutional pattern but is nonlinear over all investigated metallocenes.[30] Therefore, the explanation cannot be restricted to Hammett constants but should consider, as discussed by Erb and Inkpen previously, orbital reordering, changes in hybrid-

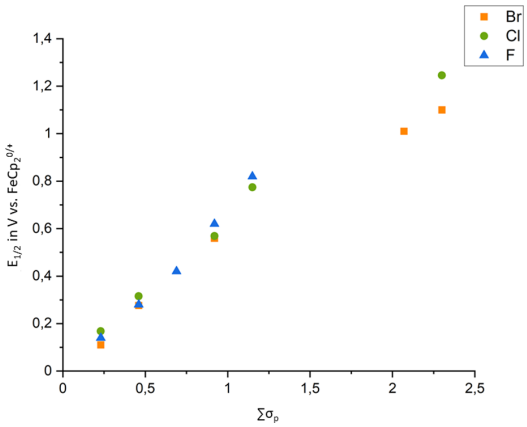


**Figure 3.** $E$ (V) vs $\sum\sigma_p$ for mono- and polyhalogenated metallocenes. Blue, fluorine; green, chlorine; orange, bromine.

ization and frontier orbital composition, electrostatic repulsion between metal and Cp ring orbitals, and through-space interactions between the iron center and halogen atoms.[30,31]

Since electrochemical measurements suggest the existence of the polybrominated ferrocenium cations, we were interested in the isolation of the oxidized species. $FeC_{10}Br_9HgBr$ and $FeC_{10}Br_{10}$ are oxidized by strong oxidants, such as $AsF_5$, and isolated as moisture-sensitive green solids at room temperature. Due to the paramagnetic character of the compounds, the bulk characterization was performed only by vibrational spectroscopy. The oxidation causes no visible changes in the vibrational spectra except of additional bands caused by the corresponding counteranions.

Additionally, the compounds $[FeC_{10}Br_{10}][AsF_6]\cdot 2HF$ and $[FeC_{10}Br_9HgBr][AsF_6]\cdot SO_2$ were analyzed by single-crystal XRD, and their structures compared with $FeC_{10}Br_9H$ and $FeC_{10}Br_{10}$, (also this study). All investigated metallocenes exhibit parallel Cp rings (0.1(4)−1.1(3)° $Cp_{plane1}$ vs $Cp_{plane2}$). In the neutral compounds, the iron Cp bonds are 0.03 Å shorter than in unsubstituted ferrocene, which was already observed in other halogenated metallocenes.[31,35−38] This effect is not visible in the oxidized species. The oxidation of $Fe^{+II}$ to $Fe^{+III}$ increases the Fe−C bond lengths up to 0.07 Å and shortens the C−Br bonds up to 0.04 Å (Table 2) and is consequently another example of the $\alpha$-halogen effect, which is also observed in perhalogenated cyclopentadienyl cations.[39] In contrast to most (poly)halogenated derivatives[31,37,38,40−42] as well as perhalogenated metallocenes (M = Ru, Os)[43−45] the cyclopentadienyl ligands exhibit a staggered conformation instead of an eclipsed one in the solid state. Intramolecular interactions are mostly of halogen bond nature between halogenated ferrocene and solvent molecules, counteranions, or other halogenated ferrocene moieties (Figure 4, SI). Typically for halogen bonds the C−Br-donor angles are close to 180°. The Br···Br contacts are weakened upon oxidation due to cation−anion interactions as well as reduced electron density on the halogen bond acceptor. Intramolecular Br···Br contacts were not observed.

The crystal structure of $[FeC_{10}Br_9HgBr]_2[AsF_6]_2\cdot 2SO_2$ demonstrates the considerable stability of Cp−Hg bonds toward strong Lewis acids, such as $AsF_5$ (Figure 5). The compound forms a dimer in the solid state. The mercury atom is linearly coordinated along the Cp−Hg−Br axis. Two [Hg−



https://doi.org/10.1021/acs.organomet.2c00157
Organometallics 2022, 41, 1261−1267

**Table 2. Selected Structural Information**

| compound | $d$(C−Br) in Å | $d$(Fe-$Cp_{center}$) in Å | $d$(Br···Br) in Å | Cp−Br···Br in deg | $Cp_{torsion\ angle}$ in deg | $Cp_{tilt\ angle}$ in deg |
|---|---|---|---|---|---|---|
| $FeC_{10}Br_9H$ | 1.861(10)−1.888(11) | 1.637(1), 1.642(1) | 3.405(2)−3.621(2) | 140.7(4), 162.0(3) | 33.4(5) | 0.4(4) |
| $FeC_{10}Br_{10}$ | 1.863(4) −1.874(4) | 1.644(1) | 3.499(1), 3.536(1) | 169, 156 | 33.8(2) | 0.0(2) |
| $[FeC_{10}Br_9HgBr]^+$ | 1.845(8)−1.865(8) | 1.702(1), 1.708(1) | 3.395(1), 3.632(1) | 165.6(3), 153.3(3) | 32.5(4) | 1.1(3) |
| $[FeC_{10}Br_{10}]^+$ | 1.853(9)−1.864(6) | 1.706(1) | 3.582(8) | 153.1(2) | 34.9(3) | 0.0(3) |

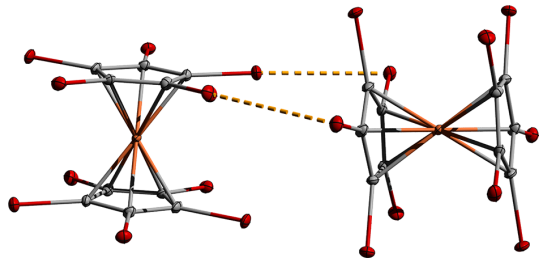

**Figure 4.** Molecular structure of $FeC_{10}Br_{10}$·DMSO. Ellipsoids with 50% probability level. Solvent molecules are omitted for clarity. Red, bromine; orange, iron; gray, carbon; dashed, halogen contacts. $FeC_{10}Br_{10}$ as halogen bond donor (left) and acceptor (right).

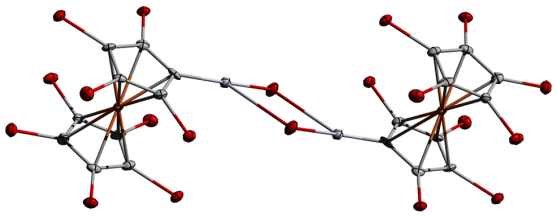

**Figure 5.** Molecular structure of dimeric $[FeC_{10}Br_9HgBr]_2[AsF_6]_2$·$2SO_2$. Ellipsoids with 50% probability level. Solvent molecules are omitted for clarity. Red, bromine; orange, iron; gray, carbon; mercury, light gray.

Br] units are connected via the Lewis acidic sites at the mercury atom, forming a $[Hg-Br]_2$ four-membered ring ($d$(Hg−Br) = 2.426(1), 3.061(1) Å). The coordination number at the mercury center is three in total. The dimerization of linear organomercury compounds is common, but examples of a coordination number of three are rare.[46,47]

## CONCLUSION

In summary, an improved synthetic protocol was developed for decabromoferrocene, and in contrast to previous reports, we demonstrate that the metallocene was obtained in high purity. Its crystal structure and electrochemical behavior were determined and compared to less brominated analogues, showing an increased oxidation potential of the fully brominated ferrocene. Moreover, we report the preparation and structural characterization of the strongest ferrocenium-based oxidant, $[FeC_{10}Br_{10}][AsF_6]$, that has been isolated so far. We are confident that this improved synthetic methodology for the valuable precursor decabromoferrocene will facilitate the preparation of other fully substituted ferrocene-based materials.

## EXPERIMENTAL SECTION

The halogenation reactions were carried out under open-atmosphere laboratory conditions. $FeC_{10}(HgOAc)_{10}$[21] and $FeC_{10}(HgO_2CC_3H_7)_{10}$[27] were synthesized as described in previous literature. All other chemicals and solvents were used as purchased, unless otherwise noted. (Organo)mercury compounds are highly toxic. Therefore, the chemicals should be handled under a well-ventilated fume hood. Great care must be taken that organomercury compounds are not spilled on the skin. It is advisable to use multiple layers of impenetrable gloves and to remove the outer layer immediately if material is spilled on it. The face can be protected against splashes by using a face shield. Due to the hazardous effects of mercury on the environment, great care must be taken to prevent contamination of the wastewater with mercury. Reactions involving $AsF_5$, $SO_2$, and aHF were performed in PFA (tetrafluoroethene−perfluoroalkoxyvinyl copolymer) tubes connected to a stainless-steel line. Instead of stirring, the mixtures were agitated with the help of a mini-vortex mixer PV-1. $SO_2$, $AsF_5$, and HF are (toxic) gases at room temperature. They should be handled only by trained personnel with suitable protective equipment. $AsF_5$ was prepared as described in previous literature.[48] $SO_2$ was distilled from $CaH_2$, and HF was dried with elemental fluorine. Both solvents were stored in a stainless-steel cylinder. $^1H$, $^{13}C$, and $^{19}F$ NMR spectra were recorded on a Bruker AVANCE III 700 spectrometer by using 6 mm NMR glass tubes. All reported chemical shifts ($\delta$) are referenced to the Ξ values given in IUPAC recommendations of 2008 using the $^2H$ signal of the deuterated solvent as an internal reference.[49] All chemical shifts ($\delta$) are given in parts per million (ppm), and the signals are specified according to the multiplicity (s = singlet, d = doublet, t = triplet, q = quartet, m = multiplet, br = broad) and the coupling constants $J$ in Hz. The program MestRe Nova version 14.0.1 was used to evaluate and plot the data.[50] Mass spectrometry was performed on a Waters Autospec Premier with an Agilent 7890B GC spectrometer. The evaluation of the resulting data occurred by using Mmass 5.5.0.[51] Infrared spectra were measured either using a Thermo-Scientific Nicolet iS10 FTIR spectrometer with a DuraSamplIR accessory in attenuated total reflection at room temperature or on a Bruker ALPHA FTIR spectrometer inside a glovebox equipped with a diamond ATR attachment. The software OriginPro 2017G was used to plot the data.[52] Cyclic voltammetry was performed on an Interface 1010 B potentiostat/galvanostat/ZRA from Gamry Instruments. The investigations were carried out starting from 0 V going to the oxidation first and then to the reduction. The measurements were performed in anhydrous and oxygen-free solvents under an argon atmosphere using tetrabutylammonium hexafluorophosphate as the supporting electrolyte and platinum wires as working, counter, and quasi-reference electrodes. The voltammograms were internally referenced against $FeCp_2^{0/+}$. The software OriginPro 2017G was used to plot the data.[52] Tetrahydrofuran (THF) was distilled over Na and stored in Young flasks under an argon atmosphere over a molar sieve (3 Å), which was dried beforehand at 250 °C under high vacuum. The conducting salt was dried at 250 °C under high vacuum. The solvents were condensed on the conducting salt in the cyclic voltammetry cells via a vacuum line.

**Nonabromoferrocene.** Potassium bromide (0.60 g, 5.1 mmol, 20 equiv) was dissolved in deionized water (100 mL). Then, bromine (0.49 g, 3 mmol, 12 equiv) and $FeC_{10}(HgOAc)_{10}$ (0.70 g, 0.25 mmol, 1 equiv) were added. The mixture was stirred at room temperature for 5 h. Afterward, the suspension was filtered over a porous glass frit and the residue was washed with deionized water (100 mL) and methanol (100 mL). The yellow solid was than extracted in 100 mL of dichloromethane. The solvent was removed under reduced pressure and washed with (a few milliliters of) dichloromethane and $n$-hexane. The resulting yellow crude product (100 mg) was dried under high



https://doi.org/10.1021/acs.organomet.2c00157
Organometallics 2022, 41, 1261−1267

vacuum. $IR_{bulk}$ (ATR, RT): $\tilde{\nu}$ ($cm^{-1}$) = 1373, 1132, 1282, 896, 584. MS (EI): calcd for $[FeC_{10}Br_9H]^+$ 895.1996; found 895.1746.

Single crystals of $FeC_{10}Br_9H$ were obtained by slow evaporation of a mixture of tetrahydrofuran and dichloromethane at room temperature over weeks. $^1H$ NMR ($d_8$-THF, RT, 400 MHz): $\delta$ 4.92 ppm. $^{13}C$ NMR ($d_8$-THF, RT, 176 MHz): $\delta$ 86.4 (d, $J$ = 7.5 Hz), 85.4 (s), 84.1 (d, $J$ = 2.5 Hz), 79.2 ppm (d, $J$ = 193.8 Hz).

**Pentabromocyclopentadienyl(2,3,4,5-tetrabromo-(bromidomercurio)cyclopentadienyl)iron(II).** Potassium bromide (3.97 g, 33.4 mmol, 20 equiv) was dissolved in deionized water (200 mL). Then, bromine (3.60 g, 22.5 mmol, 12 equiv) and $FeC_{10}(HgO_2CC_3H_7)_{10}$ (5.00 g 1.7 mmol, 1 equiv) were added. The mixture was stirred at room temperature for 5 h. Afterward, the suspension was filtered over a porous glass frit, and the residue was washed with deionized water (1 L) and methanol (1 L). The yellow solid was than extracted with 500 mL of dichloromethane in a 100 mL Soxhlet apparatus for 4 days. The resulting suspension was reduced to 100 mL, filtered off, and dried under high vacuum. The compound was obtained as yellow solid (1.5 g, 75%). $^{13}C$ NMR ($d_8$-THF, RT, 176 MHz): $\delta$ 90.0 (s), 87.1 (s), 85.4, 85.1 (s) ppm. IR (ATR, RT): $\tilde{\nu}$ ($cm^{-1}$) 1309, 1281, 1265, 584. MS (EI): calcd for $[FeC_{10}Br_{10}Hg]^+$ 1175.0808; found 1175.0771. Anal. Calcd for $FeC_{10}Br_{10}Hg$: N, 0.00; C, 10.22; H, 0.00. Found: N, 0.01; C, 10.29; H, 0.00.

**Bis(pentabromocyclopentadienyl)iron(II).** $FeC_{10}Br_9HgBr$ (5.85 g, 5.0 mmol, 1 equiv), iron powder (0.28 g, 5.0 mmol, 1 equiv), and bromine (7.96 g, 49.8 mmol, 10 equiv) were suspended in dichloromethane (500 mL). The mixture was stirred at room temperature over 3 days. Afterward, all volatile compounds were removed under reduced pressure. The resulting suspension was filtered in a porous glass frit. The residue was then washed with deionized water (2 L) and methanol (2 L). The yellow solid was than extracted with 500 mL of dichloromethane in a 100 mL Soxhlet apparatus for 1 week. The resulting suspension was reduced to 50 mL, filtered off, and dried under high vacuum. The compound was obtained as a yellow solid (2.07 g, 43%). Single crystals of $FeC_{10}Br_{10}\cdot 2DMSO$ were obtained by crystallization from DMSO at room temperature after three months. $^{13}C$ NMR ($d_8$-THF, RT, 176 MHz): $\delta$ 85.4 (s). IR (ATR, RT): $\tilde{\nu}$ ($cm^{-1}$) 1309, 1279, 588. MS (EI): calcd for $[FeC_{10}Br_{10}]^+$ 975.1081; found 975.0871. Anal. Calcd for $FeC_{10}Br_{10}$: N, 0.00; C, 12.32; H, 0.00. Found: N, 0.01; C, 13.05; H, 0.00.

**Pentabromocyclopentadienyl(2,3,4,5-tetrabromo-(bromidomercurio)cyclopentadienyl)iron(III) Hexafluoroarsenate.** $FeC_{10}Br_9HgBr$ (20 mg, 0.02 mmol, 1 equiv) was suspended in $SO_2$ (1 mL) at −20 °C. To the suspension was condensed $AsF_5$ (75 mg, 0.44 mmol, 22 equiv). After several minutes a green solution was obtained. All volatile compounds were removed under reduced pressure, yielding $[FeC_{10}Br_9HgBr][AsF_6]$ (26 mg, 99%) as a green solid. Single crystals of $[FeC_{10}Br_9HgBr][AsF_6]\cdot SO_2$ were obtained by cooling a solution in $SO_2$ from −20 °C to −75 °C over 3 days. IR (ATR, RT): $\tilde{\nu}$ ($cm^{-1}$) 1309, 1278, 717, 691, 589.

**Bis(pentabromocyclopentadienyl)iron(III) Hexafluoroarsenate.** $FeC_{10}Br_{10}$ (20 mg, 0.02 mmol, 1 equiv) was suspended in $SO_2$ (1 mL) at −20 °C. To the suspension was condensed $AsF_5$ (55 mg, 0.32 mmol, 16 equiv). After several minutes a green solution was obtained. All volatile compounds were removed under reduced pressure, yielding $[FeC_{10}Br_{10}][AsF_6]$ (23 mg, 99%) as a green solid. Single crystals of $[FeC_{10}Br_{10}][AsF_6]\cdot 2HF$ were obtained by layering HF on the $SO_2$ solution at −40 °C over 2 days. IR (ATR, RT): $\tilde{\nu}$ ($cm^{-1}$) 1311, 1280, 689, 664, 587.

## ■ ASSOCIATED CONTENT

### Supporting Information

The Supporting Information is available free of charge at https://pubs.acs.org/doi/10.1021/acs.organomet.2c00157.

Cyclic voltammetry plots (Figures S1−S5), crystal structure information (Figures S6−S11), NMR characterization (Figures S12−S16); IR spectra (Figures S17 and S18) (PDF)

### Accession Codes

CCDC 2162547−2162548, 2162554, and 2162561 contain the supplementary crystallographic data for this paper. These data can be obtained free of charge via www.ccdc.cam.ac.uk/data_request/cif, or by emailing data_request@ccdc.cam.ac.uk, or by contacting The Cambridge Crystallographic Data Centre, 12 Union Road, Cambridge CB2 1EZ, UK; fax: +44 1223 336033.

## ■ AUTHOR INFORMATION

### Corresponding Author

**Moritz Malischewski** − *Freie Universität Berlin, 14195 Berlin, Germany;* orcid.org/0000-0002-6756-2951; Email: moritz.malischewski@fu-berlin.de

### Authors

**Susanne M. Rupf** − *Freie Universität Berlin, 14195 Berlin, Germany;* orcid.org/0000-0002-1577-1743

**Irina S. Dimitrova** − *Freie Universität Berlin, 14195 Berlin, Germany*

**Gabriel Schröder** − *Freie Universität Berlin, 14195 Berlin, Germany*

Complete contact information is available at: https://pubs.acs.org/10.1021/acs.organomet.2c00157

### Notes

The authors declare no competing financial interest.

## ■ ACKNOWLEDGMENTS

Gefördert durch die Deutsche Forschungsgemeinschaft (DFG), Projektnummer 387284271−SFB1349. We would like to acknowledge the assistance of the Core Facility BioSupraMol supported by the DFG.

## ■ REFERENCES

(1) Kealy, T. J.; Pauson, P. L. A New Type of Organo-Iron Compound. *Nature* **1951**, *168*, 1039−1040.

(2) Astruc, D. Why Is Ferrocene so Exceptional? *Eur. J. Inorg. Chem.* **2017**, *2017*, 6−29.

(3) Paul, A.; Borrelli, R.; Bouyanfif, H.; Gottis, S.; Sauvage, F. Tunable Redox Potential, Optical Properties, and Enhanced Stability of Modified Ferrocene-Based Complexes. *ACS Omega* **2019**, *4*, 14780−14789.

(4) Walawalkar, M. G.; Pandey, P.; Murugavel, R. The Redox Journey of Iconic Ferrocene: Ferrocenium Dications and Ferrocenate Anions. *Angew. Chem. Int. Ed* **2021**, *60*, 12632−12635.

(5) Sharp, P. R.; Bard, A. J. Electrochemistry in Liquid Sulfur Dioxide. 4. Electrochemical Production of Highly Oxidized Forms of Ferrocene, Decamethylferrocene, and Iron Bis(Tris(l-Pyrazolyl)-Borate). *Inorg. Chem.* **1983**, *22*, 2689−2693.

(6) Malischewski, M.; Adelhardt, M.; Sutter, J.; Meyer, K.; Seppelt, K. Isolation and Structural and Electronic Characterization of Salts of the Decamethylferrocene Dication. *Science* **2016**, *353*, 678−682.

(7) Goodwin, C. A. P.; Giansiracusa, M. J.; Greer, S. M.; Nicholas, H. M.; Evans, P.; Vonci, M.; Hill, S.; Chilton, N. F.; Mills, D. P. Isolation and Electronic Structures of Derivatized Manganocene, Ferrocene and Cobaltocene Anions. *Nat. Chem.* **2021**, *13*, 243−248.

(8) Khobragade, D. A.; Mahamulkar, S. G.; Pospísil, L.; Císarová, I.; Rulísek, L.; Jahn, U. Acceptor-Substituted Ferrocenium Salts as Strong, Single-Electron Oxidants: Synthesis, Electrochemistry, Theoretical Investigations, and Initial Synthetic Application. *Chem.—Eur. J.* **2012**, *18*, 12267−12277.

(9) Voßnacker, P.; Keilhack, T.; Schwarze, N.; Sonnenberg, K.; Seppelt, K.; Malischewski, M.; Riedel, S. From Missing Links to New

Records: A Series of Novel Polychlorine Anions. *Eur. J. Inorg. Chem.* **2021**, *2021*, 1034−1040.
(10) Popov, V. I.; Lib, M.; Kaas, A. Novel Synthesis of Fluoroferrocene and Pentafluoroanisole. *A. Ukr. Khim. Zh. (Russ. Ed.)* **1990**, *56*, 1115.
(11) Nesmeyanov, A. N.; Sazonova, V. A.; Drosd, V. N. Synthese von Ferrocenderivaten Mittels Bor- Und Halogensubstituierter Ferrocene. *Chem. Ber.* **1960**, *93*, 2717−2729.
(12) Fish, R. W.; Rosenblum, M. A Convenient Synthesis of Some Haloferrocenes. *J. Org. Chem.* **1965**, *30*, 1253−1254.
(13) Butenschön, H. Haloferrocenes: Syntheses and Selected Reactions. *Synthesis* **2018**, *50*, 3787−3808.
(14) Butler, I. R. Sitting Out the Halogen Dance. Room-Temperature Formation of 2,2′-Dilithio-1,1′-Dibromoferrocene. TMEDA and Related Lithium Complexes: A Synthetic Route to Multiply Substituted Ferrocenes. *Organometallics* **2021**, *40*, 3240−3244.
(15) Butler, I. R. 1,2,3,4,5-Pentabromoferrocene and Related Compounds: A Simple Synthesis of Useful Precursors. *Inorg. Chem. Commun.* **2008**, *11*, 484−486.
(16) Sünkel, K.; Bernhartzeder, S. Coordination Chemistry of Perhalogenated Cyclopentadienes and Alkynes. XXVIII New High-Yield Synthesis of Monobromoferrocene and Simplified Procedure for the Synthesis of Pentabromoferrocene. Molecular Structures of 1,2,3-Tribromoferrocene and 1,2,3,4,5-P. *J. Organomet. Chem.* **2011**, *696*, 1536−1540.
(17) Bernhartzeder, S.; Sünkel, K. Coordination Chemistry of Perhalogenated Cyclopentadienes and Alkynes. Part 30. New High-Yield Syntheses of Monochloroferrocene and 1, 2, 3, 4, 5-Pentachloroferrocene. Molecular Structures of 1,2-Dichloroferrocene and 1,2,3-Trichloroferrocene. *J. Organomet. Chem.* **2012**, *716*, 146−149.
(18) Butler, I. R. The Conversion of 1,1′-Dibromoferrocene to 1,2-Dibromoferrocene: The Ferrocene-Chemist's Dream Reaction. *Inorg. Chem. Commun.* **2008**, *11*, 15−19.
(19) Sünkel, K.; Weigand, S.; Hoffmann, A.; Blomeyer, S.; Reuter, C. G.; Vishnevskiy, Y. V.; Mitzel, N. W. Synthesis and Characterization of 1,2,3,4,5-Pentafluoroferrocene. *J. Am. Chem. Soc.* **2015**, *137*, 126−129.
(20) Hedberg, F. L.; Rosenberg, H. Preparation and Reactions of Decachloroferrocene and Decachlororuthenocene. *J. Am. Chem. Soc.* **1973**, *95*, 870−875.
(21) Han, Y.-H.; Heeg, M. J.; Winter, C. H. Permercuration of Ferrocenes and Ruthenocenes. New Approaches to Complexes Bearing Perhalogenated Cyclopentadienyl Ligands. *Organometallics* **1994**, *13*, 3009−3019.
(22) Boev, V. I.; Dombrovskii, A. V. Decakis-(Trifluoroacetylmercurio)Ferrocene and Decaiodoferrocene. *Zh. Obshch. Khim* **1977**, *47*, 727−728.
(23) Kur, S. A.; Winter, C. H. Permercuration of Substituted Ferrocenes: Assessment of the Degree of Mercuration. *J. Organomet. Chem.* **1996**, *512*, 39−44.
(24) Brown, K. N.; Gulyas, P. T.; Lay, P. A.; McAlpine, N. S.; Masters, A. F.; Phillips, L. Electrochemistry of Chlorinated Ferrocenes: Stability of Chlorinated Ferrocenium Ions. *J. Chem. Soc., Dalt. Trans* **1993**, 835−840.
(25) Venker, A.; Vollgraff, T.; Sundermeyer, J. Ferrocenyl-Sulfonium Ionic Liquids-Synthesis, Characterization and Electrochemistry. *Dalton Trans* **2018**, *47*, 1933−1941.
(26) Deacon, G. B.; Farquharson, G. J. Permercurated Arenes. III Synthesis of Periodoarenes and Perchloroarenes by Iodo- and Chloro-Demercuration of Some Permercurated Arenes. *Aust. J. Chem.* **1977**, *30*, 1701−1713.
(27) Rupf, S. M.; Schröder, G.; Sievers, R.; Malischewski, M. Tenfold Metalation of Ferrocene: Synthesis, Structures, and Metallophilic Interactions in $FeC_{10}(HgX)_{10}$. *Chem.—Eur. J.* **2021**, *27*, 5125−5129.
(28) Deacon, G. B.; Farquharson, G. J. Synthesis of Perbromobenzoic Acids and Perbromobenzenes from Aromatic Carboxylic Acids by Permercuration and Bromodemercuration. *Aust. J. Chem.* **1977**, *30*, 293−303.
(29) Deacon, G. B.; Farquharson, G. J. Synthesis an Bromodemercuration of Some Permercurated Arenes. *Aust. J. Chem.* **1976**, *29*, 672−635.
(30) Erb, W.; Richy, N.; Hurvois, J.-P.; Low, P. J.; Mongin, F. From Ferrocene to 1,2,3,4,5-Pentafluoroferrocene: Halogen Effect on the Properties of Metallocene. *Dalton Trans* **2021**, *50*, 16933−16938.
(31) Inkpen, M. S.; Du, S.; Hildebrand, M.; White, A. J. P.; Harrison, N. M.; Albrecht, T.; Long, N. J. The Unusual Redox Properties of Fluoroferrocenes Revealed through a Comprehensive Study of the Haloferrocenes. *Organometallics* **2015**, *34*, 5461−5469.
(32) Hansch, C.; Leo, A.; Taft, R. W. A Survey of Hemmett Substituent Constants and Resonance and Field Parameters. *Chem. Rev.* **1991**, *91*, 165−195.
(33) Little, W. F.; Reilley, C. N.; Johnson, J. D.; Sanders, A. P. Chronopotentiometric Studies of Ferrocenes Derivatives. II. Directly Substituted Ferrocenes. *J. Am. Chem. Soc.* **1964**, *86*, 1382−1386.
(34) Evans, D. M.; Hughes, D. D.; Murphy, P. J.; Horton, P. N.; Coles, S. J.; Biani, F. F. de; Corsini, M.; Butler, I. R. Synthetic Route to 1,1′,2,2′-Tetraiodoferrocene That Avoids Isomerization and the Electrochemistry of Some Tetrahaloferrocenes. *Organometallics* **2021**, *40*, 2496−2503.
(35) Romanov, A. S.; Mulroy, J. M.; Khrustalev, V. N.; Antipin, M. Y.; Timofeeva, T. V. Monohalogenated Ferrocenes $C_5H_5FeC_5H_4X$ (X = Cl, Br and I) and a Second Polymorph of $C_5H_5FeC_5H_4I$. *Acta Crystallogr., Sect. C Cryst. Struct. Commun.* **2009**, *65*, m426−m430.
(36) Laus, G.; Wurst, K.; Stolz, W.; Schottenberger, H. Crystal Structure of Iodoferrocene, $Fe(C_5H_4I)(C_5H_5)$. *Z. Krist. NCS* **2005**, *220*, 229−230.
(37) Hnetinka, C. A.; Hunter, A. D.; Zeller, M.; Lesley, M. J. G. 1,1'-Dibromoferrocene. *Acta Crystallogr.* **2004**, *E60*, m1806−m1807.
(38) Roemer, M.; Nijhuis, C. A. Syntheses and Purification of the Versatile Synthons Iodoferrocene and 1,1′-Diiodoferrocene. *Dalton Trans* **2014**, *43*, 11815−11818.
(39) Rupf, S. M.; Pröhm, P.; Malischewski, M. The [2 + 2] Cycloaddition Product of Perhalogenated Cyclopentadienyl Cations: Structural Characterization of Salts of the $[C_{10}Cl_{10}]^{2+}$ and $[C_{10}Br_{10}]^{2+}$ Dications. *Chem. Commun.* **2020**, *56*, 9834−9837.
(40) Roemer, M.; Heinrich, D.; Kang, Y. K.; Chung, Y. K.; Lentz, D. No TitleBulky-Alkyl-Substituted Bis(Trifluorovinyl)Ferrocenes: Redox-Autocatalytic Formation of Fluorinated Ferrocenophanes. *Organometallics* **2012**, *31*, 1500−1510.
(41) Kumiko, S.; Michiko, K.; Hirotoshi, S. Studies on the Crystal Structure and the Plastic Crystalline Phase of Tetrachloroferrocene. *Chem. Lett.* **1984**, *13*, 17−20.
(42) Hess, J.; Konatschnig, S.; Morard, S.; Pierroz, V.; Farrari, S.; Spingler, B.; Gasser, G. Novel, Mercury-Free Synthetic Pathway for Trifluoromethylthio-Substituted Metallocenes. *Inorg. Chem.* **2012**, *53*, 3662−3667.
(43) Brown, G. M.; Hedberg, F. L.; Rosenberg, H. Crystal Structure of Decachlororuthenocene. Noncoplanarity of Carbon and Chlorine Atoms Arising from Valence Forces. *J. Chem. Soc., Chem. Commun.* **1972**, 5−6.
(44) Kur, S. A.; Reingold, A. L.; Winter, C. H. Synthesis, Characterization, and Halogenation of Decakis(Acetoxymercurio)-Osmocene. Crystal and Molecular Structure of Decachloroosmocene. *Inorg. Chem.* **1995**, *34*, 414−416.
(45) Winter, C. H.; Han, Y.-H.; Ostrander, R. L.; Rheingold, A. L. Decamercuration of Ruthenocene. *Angew. Chem. Int. Ed* **1993**, *32*, 1161−1163.
(46) Grirrane, A.; Resa, I.; del Río, D.; Rodríguez, A.; Álvarez, E.; Mereiter, K.; Carmona, E. Solid-State Structures and Solution Studies of Novel Cyclopentadienyl Mercury Compounds. *Inorg. Chem.* **2007**, *46*, 4667−4676.
(47) Resa, I.; Carmona, E.; Mereiter, K. CCDC 909073 (GOGHUH): Experimental Crystal Structure Determination *CCDC* **2012**.



https://doi.org/10.1021/acs.organomet.2c00157
*Organometallics* 2022, 41, 1261−1267

(48) Aris, D. R.; Knapp, C.; Passmore, J.; Wang, X. A Detailed Account of a Convenient Lab-Scale Preparation of $AsF_5$ via Direct Fluorination of $AsF_3$. *J. Fluor. Chem.* **2005**, *126*, 1368−1372.
(49) Harris, R. K.; Becker, E. D.; Menezes, S. M. C. de; Granger, P.; Hoffmann, R. E.; Zilm, K. W. Further Conventions for NMR Shielding and Chemical Shifts (IUPAC Recommendations 2008). *Pure Appl. Chem.* **2008**, *80*, 59−84.
(50) Willcott, M. R. MestRe Nova. *J. Am. Chem. Soc.* **2009**, *131*, 13180.
(51) Niedermeyer, T. H. J.; Strohalm, M. Mass as a Software Tool for the Annotation of Cyclic Peptide Tandem Mass Spectra. *PLoS One* **2012**, *7*, No. e44913.
(52) *Origin(Pro), Version 2016*; OriginLab Corporation: Northhampton, MA, USA, 2016.



https://doi.org/10.1021/acs.organomet.2c00157
*Organometallics* 2022, 41, 1261−1267

## 3.4 Persilylation of Ferrocene: The Ultimate Discipline in Sterically Overcrowded Metal Complexes

Susanne Margot Rupf, Robin Sievers, Paulin Riemann, Marc Reimann, Martin Kaupp, Carlo Fasting, Moritz Malischewski*
*Dalton Trans.* **2023**, *52*, 6870–6875.

DOI: 10.1039/D3DT01133J



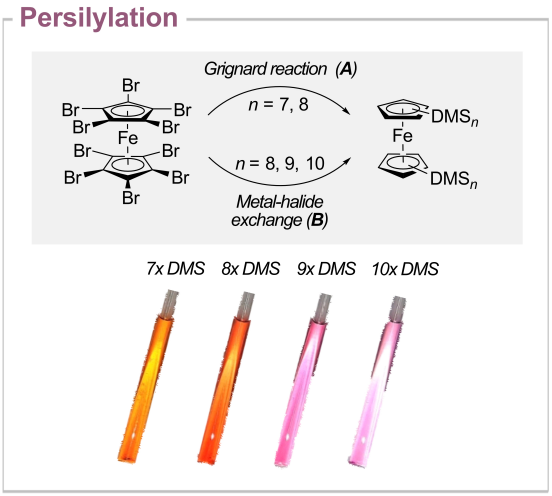


**Author Contribution:**
Susanne M. Rupf designed the project and wrote the manuscript. Furthermore, she performed syntheses and analyzed the spectroscopic data, determined cyclic voltammetry and UV/VIS data as well as prepared, measured and solved the single-crystal XRD data. Robin Sievers performed experiments and analyzed data during his internship course and Paulin S. Riemann performed experiments and analyzed data during her bachelor thesis. Both authors were supervised by Susanne M. Rupf. Marc Riemann and Martin Kaupp performed quantum chemical calculations. Carlo Fasting designed the HPLC experiments. Susanne M. Rupf performed HPLC experiments with support of Carlo Fasting. Moritz Malischewski supervised the project and revised the manuscript.

Dalton Transactions

ROYAL SOCIETY OF CHEMISTRY

PAPER

View Article Online
View Journal | View Issue



Cite this: *Dalton Trans.*, 2023, **52**, 6870

# Persilylation of ferrocene: the ultimate discipline in sterically overcrowded metal complexes†

Susanne M. Rupf, [a] Robin Sievers,[a] Paulin S. Riemann,[a] Marc Reimann, [b] Martin Kaupp, [b] Carlo Fasting[a] and Moritz Malischewski *[a]

Received 14th April 2023,
Accepted 19th April 2023

DOI: 10.1039/d3dt01133j

rsc.li/dalton

We report the preparation and structural characterization of the first persilylated metallocene *via* the metalation of decabromoferrocene. Although Grignard conditions turned out to be insufficient due to the steric and electronic effects of silyl groups causing a decreased nucleophilicity of the metalated intermediates, stepwise lithium–halogen exchange yields complex mixtures of polysilylated compounds $FeC_{10}DMS_nH_{10-n}$ ($n$ = 10, 9, 8) including the targeted decasilylated ferrocene. These mixtures were successfully separated allowing a systematic study of silylation effects on ferrocene by XRD, CV, NMR and UV/vis spectroscopy supported by DFT calculations. The findings were used to develop a high-yielding and simple preparation method to generate a tenfold substituted overcrowded ferrocene, $FeC_{10}DMS_8Me_2$.

## Introduction

Given the outstanding variety of possible cyclopentadienyl (Cp) complexes reported so far, cyclopentadienyl ligands with dimethylsilyl (DMS) or trimethylsilyl (TMS) groups have found widespread synthetic applications. As they are superior in steric demand to the corresponding carbon containing analogues, iso-propyl and *tert*-butyl,[1,2] they allow the isolation of reactive f-block[3–7] and main group complexes[8–12] and improve hydrocarbon solubility.[13] Moreover, the introduction of silyl groups allows the generation of sensitive (redox) species due to hyperconjugation effects, allowing the isolation of highly reduced organic compounds[14–18] or low-valent actinide and lanthanide compounds, like $\{[C_5H_{5-n}(SiMe_3)_n]_3M\}^{1-}$ ($n$ = 1, 2), containing metal centers with a formal oxidation state of +II as demonstrated by the Evans group.[19–24] Although higher degrees of silylation are expected to result in an increased kinetic stability of low-valent species due to steric demand and changed electronic properties of the Cp ligand, the steric overload required and the further changed electronic properties of the Cp ligands pose a formidable synthetic challenge.

So far, only one transition metal complex with a pentakis (dimethylsilyl) substituted Cp ligand is known in the literature. Sünkel and Hofmann prepared $[Mn(CO)_3(C_5DMS_5)]$ by iterative lithiation and silylation of $[Mn(CO)_3(C_5Br_5)]$ (Scheme 1, top).[25]

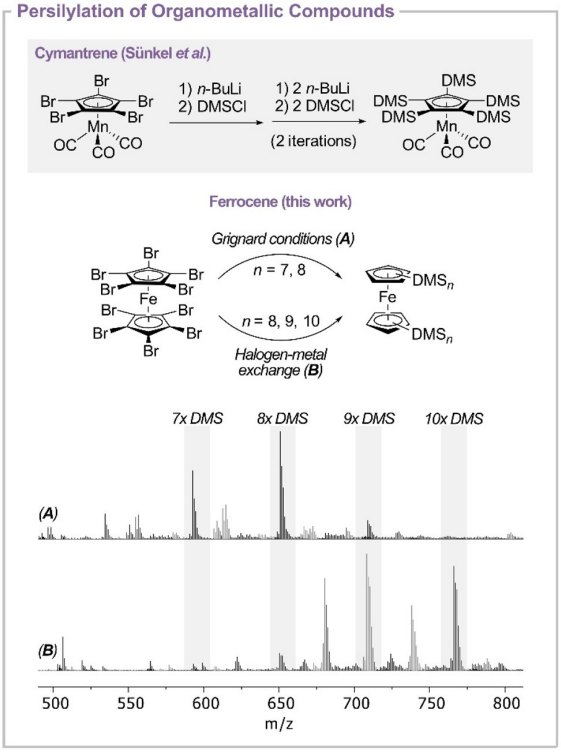


**Scheme 1** Overview of synthetically prepared persilylated compounds. Top: persilylation of $[Mn(CO)_3(C_5Br_5)]$ by iterative lithium–halide exchange and reaction with DMSCl. Middle: silylation of $[FeC_{10}Br_{10}]$ with DMSCl *via* lithium–halogen exchange and Grignard reaction. Bottom: the corresponding mass spectra of the conversions.

[a]*Freie Universität Berlin, Fabeckstr. 34-36, 14195 Berlin, Germany. E-mail: moritz.malschewski@fu-berlin.de*
[b]*Technische Universität Berlin, Straße des 17. Juni 135, 10623 Berlin, Germany*

†Electronic supplementary information (ESI) available. CCDC 2248053 (**1**), 2248054 (**2**), 2248060 (**3a**), 2248059 (**3b**), 2248057 (**4a**), 2248058 (**4b**), 2248056 (**5**) and 2248055 (**6**). For ESI and crystallographic data in CIF or other electronic format see DOI: https://doi.org/10.1039/d3dt01133j

View Article Online

Dalton Transactions Paper

Although the preparation of $[C_5DMS_5]^-$ by the reaction of $C_5DMS_6$ with MeLi has been reported,[26] it has never been used for follow-up chemistry. Here, the corresponding $C_5DMS_6$ was prepared by the reaction of $C_5Br_6$ with Mg and DMSCl. Claims in the Russian literature regarding the preparation of $C_5TMS_6$ [27] were not reproducible. In contrast, the synthesis of $[C_5TMS_3H_2]^-$ is well established and the ligand is easily coordinated in reactions with metal halides.[28–31] However, the synthetic challenge becomes more demanding for metallocenes due to the repulsion of the sterically crowded Cp ligands in the "sandwich" structure. Okuda achieved high silylation degrees by the reaction of iron(II) halides with tris(1,2,4-TMS) cyclopentadienyllithium to yield 1,1′,2,2′,4,4′-hexakis(trimethylsilyl)ferrocene. As a consequence of the steric demand, a distorted structure of the silylated Cp ligands is observed.[32] Butler *et al.* reported an alternative approach for hexakis(trimethylsilyl)ferrocene including a lithium–halogen exchange of 1,1′,2,2′,3,3′-hexabromoferrocene followed by silylation with TMSCl.[33] Recently, some of us reported an improved synthetic protocol for decabromoferrocene[34] by the bromination of $[FeC_{10}(Hg(O_2CC_3H_7)_{10}]$.[35] The reaction pathway emerging from perbrominated ferrocene is supposed to be a promising route to persilylation. In the context of ferrocene as a highly versatile model compound in organometallic chemistry,[36] we were interested in synthesizing the first persilylated ferrocene to investigate the resulting steric and electronic effects.

## Results and discussion

### Unsubstituted ferrocene

One major challenge in converting $[FeC_{10}Br_{10}]$ effectively into the subsequent silylated ferrocene was to avoid trapping of protons by basic intermediates. Therefore, the reaction itself and especially the used solvents and silanes as well as the glassware had to be made as dry as possible (ESI, S1†). The persilylation of $[FeC_{10}Br_{10}]$ was carried out by a direct reaction with elemental magnesium or by bromine–lithium exchange followed by subsequent trapping with a suitable DMS electrophile (Scheme 1, bottom). Herein, the degree of silylation was followed by mass spectrometry.

All reactions including Grignard formation were carried out using DMSCl or DMSOTf in tetrahydrofuran (THF) by varying the conditions like temperature and reaction time (ESI, Table S1†). For all reactions, mass spectrometry revealed that the Grignard formation was complete as no brominated species were observed. However, the silylation step seems to proceed very slowly at high degrees of silylation, as the formation of decasilylferrocene ($m/z$ = 766.2530 for $[FeC_{10}DMS_{10}]^+$) was only observed in traces. Instead, mixtures of $[FeC_{10}DMS_7H_3]$ ($m/z$ = 592.1711 for $[FeC_{10}DMS_7H_3]^+$) and $[FeC_{10}DMS_8H_2]$ ($m/z$ = 650.1946 for $[FeC_{10}DMS_8H_2]^+$) as main products were obtained (Scheme 1, bottom) in the presence of DMSCl indicating that the nucleophilicity of the Grignard species $\{FeC_{10}DMS_n(MgBr)_{10-n}\}$ ($n$ = 8, 9, 10) is decreased with every DMS group attached to it. Therefore, additional reactions were carried out with DMSOTf as a more electrophilic silylation reagent. In the reactions including DMSOTf, however, silylation of the attached DMS groups takes place rather than the formation of persilylferrocene, causing oligomerization of the attached silyl groups as well as polymerization of the solvent.

As the generated silylated Grignard intermediates seem to be too unreactive for further silylation, to give the target $[FeC_{10}DMS_{10}]$, organolithium compounds were used instead. Herein, lithium is introduced by lithium–halogen exchange with $^t$BuLi and $FeC_{10}Br_{10}$ followed by the addition of DMSCl. The introduction of lithium in the *ortho*-position to bromine can cause a subsequent elimination of lithium bromide, which is known for several aryls followed by aryne formation and decomposition.[37,38] Therefore, a lithiation agent and an electrophile were added at −100 °C. The stability of the lithiated species varies depending on the solvents. While in *n*-pentane the compounds only decompose slowly at room temperature, which can be explained by the low solubility in alkanes, in THF and $Et_2O$ decomposition was observed above *ca.* −80 °C. The silylation itself was mainly observed between *ca.* −80 °C and room temperature in THF and in *n*-pentane between −50 °C to room temperature indicating that the silylation proceeds faster in THF. However, in $Et_2O$ the lithiated intermediates decompose before the silylation process starts. The mass spectra of the reactions in THF and *n*-pentane still revealed incomplete substitution as after the first lithiation attempt with up to 80 equivalents of $^t$BuLi, in both cases brominated species were still visible at $m/z$ = 672.0876 for $[FeC_{10}DMS_7BrH_2]^+$, $m/z$ = 730.1196 for $[FeC_{10}DMS_8BrH]^+$, $m/z$ = 750.0010 for $[FeC_{10}DMS_7Br_2H]^+$, $m/z$ = 788.1330 for $[FeC_{10}DMS_9Br]^+$ and $m/z$ = 808.0328 for $[FeC_{10}DMS_8Br_2]^+$ (ESI, Fig. S57†). Here, the compounds $[FeC_{10}DMS_8Br_2]$ (**1**) and $[FeC_{10}DMS_9Br]$ (**2**) were isolated and characterized (see the ESI†). Due to the presence of brominated species in the mass spectra, we exclude the formation of $[FeC_{10}Li_{10}]$ as the main intermediate of the reaction. Improved conversion is achieved by multiple metalation cycles. Here, the choice of the solvent becomes more important after multiple lithiation and silylation iterations. While after four iterations in *n*-pentane brominated species are still visible in the mass spectra, in THF three iterations are sufficient to transform all brominated compounds. However, the formation of side products at $m/z$ = 606.1510 ($FeC_{25}H_{54}Si_7$), $m/z$ = 680.2075 ($FeC_{28}H_{64}Si_8$) and $m/z_{found}$ = 738.2315 ($FeC_{30}H_{70}Si_9$) is observed (Fig. 1, bottom). As *n*-pentane still offers sufficient reaction speed it was chosen to be the most suitable solvent for the first lithiation and later changed to THF to reduce side reactions. Nevertheless, *via* this approach we were able to isolate the desired $[FeC_{10}(DMS)_{10}]$ (**6**) in milligram amounts.

The persilylated derivative is only poorly soluble in most organic solvents but can consequently be easily separated by crystallization from THF or *n*-pentane to afford compound **6** as a purple solid. Further purification of the remaining polysilylated metallocene mixtures was accomplished by reverse phase HPLC, using methanol/water as the eluent. Starting from the crude mixture not only were the hepta-, octa-, nona- and

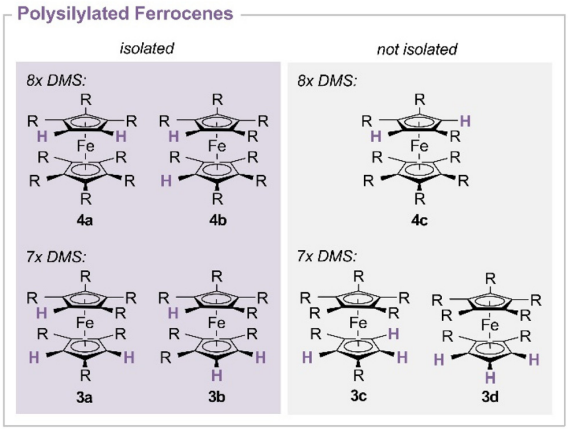


**Fig. 1** Possible regioisomers of $[FeC_{10}DMS_8H_2]$ and $[FeC_{10}DMS_7H_3]$.

decakis(dimethylsilyl)ferrocene separated, but also their corresponding regioisomers in milligram scale. Considering the heptakis- and octakis(dimethylsilyl)ferrocene, in principle four or three possible regioisomers, respectively, exist. However, only four of the seven possible compounds were isolated. The distribution of the observed substitutional pattern reveals that silylation occurs equally at both Cp ligands rather than a consecutive silylation of only one Cp ligand, as metallocenes **3c**, **3d** and **4c** with a tetrakis(dimethylsilyl)cyclopentadienyl ligand were dominantly formed (Fig. 1, purple). This indicates that silylation might have been hampered due to strong steric hindrance.

Single crystals of all isolated compounds were obtained by recrystallization from $MeOH/H_2O$ or THF mixtures and analyzed *via* single-crystal XRD. The steric influence of the polysilylated cyclopentadienyl ligands becomes clear from several features: for the sterically overcrowded metallocenes a staggered conformation is preferred. In the solid state structures extraordinarily large Fe–C bond lengths up to 2.118(1) Å in comparison with that of unsubstituted ferrocene (Fe–C: 2.051(2)–2.063(2) Å (ref. 39)) are observed, indicating repulsion of the parallel cyclopentadienyl ligands. Furthermore, a bent structure for the cyclopentadienyl ligands is observed, as almost all Si atoms are found out of the Cp plane (Table 1, Si–$Cp^{plane}$). This effect is the most pronounced in the $[FeC_{10}DMS_{10}]$ (**6**) and $[FeC_{10}DMS_9H]$ (**5**) structures which exhibit even larger angulations in 1,1′,2,2′,4,4′-hexakis(trimethylsilyl)ferrocene (12.8° (ref. 40)). Moreover, the DMS groups on the persilylated ligand prefer to order in a highly symmetric circular manner. As a result, two sets of methyl groups are found pointing towards or away from the iron center while the silicon–hydrogen bond is in the same plane as the Cp ligand. In unsymmetrically silylated ferrocenes (*e.g.* **3a**, **4a**), the repulsive interaction is compensated by tilting of the respective ferrocene (Table 1, Cp–$Cp'^{tilt}$), whereupon the parallel orientation of the DMS substituents on the less substituted Cp ligands is repealed (Fig. 2).

**Table 1** Selected structural parameters

| Compound | Distances/Å Fe–C | Angles/° Cp–$Cp'^{tilt}$ | Si–$Cp^{plane}$ |
|---|---|---|---|
| $FeC_{10}DMS_{10}$ (**6**) | 2.000(8)–2.118(2) | 0.0(1) | 15.1(2)–13.2(1) |
| $FeC_{10}DMS_9H$ (**5**)[a] | 2.044(17)–2.115(3) | 3.0(4), 3.5(1) | 31.7(3)–9.5(3) |
| $FeC_{10}DMS_8H_2$ (**4a**) | 2.055(5)–2.111(6) | 8.0(2) | 20.4(2)–5.4(2) |
| $FeC_{10}DMS_8H_2$ (**4b**)[a] | 2.051(3)–2.115(3) | 2.5(1), 3.8(1) | 10.1(1)–3.6(1) |
| $FeC_{10}DMS_7H_3$ (**3a**) | 2.056(2)–2.097(2) | 5.0(1) | 10.4(1)–1.3(1) |
| $FeC_{10}DMS_7H_3$ (**3b**) | 2.057(2)–2.099(2) | 3.1(1) | 11.4(1)–3.3(1) |

[a] Multiple metallocene molecules are found within the asymmetric unit.

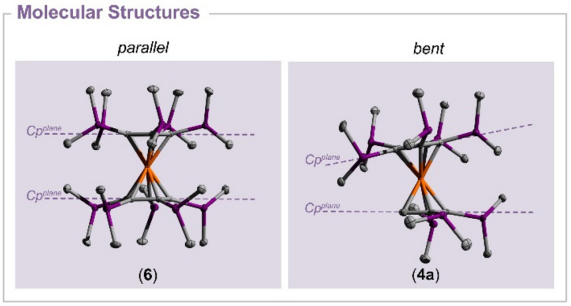


**Fig. 2** Molecular structures in solid state of compounds $[FeC_{10}DMS_8H_2]$ (**4a**) and $[FeC_{10}DMS_{10}]$ (**6**). Ellipsoids are drawn with a 50% probability level. Hydrogen atoms and disorder were omitted for clarity. Dashed lines display the plane of the five-membered Cp ring. Color code: purple – silicon, orange – iron, grey – carbon.

The repulsive interactions cause signs of rotational hindrance regarding the DMS groups in the $^1H$ and $^{13}C\{^1H\}$ NMR spectra. Considering rotatable silyl groups, the compound $[FeC_{10}DMS_{10}]$ (**6**) should show one signal for the magnetically equivalent DMS methyl protons in the $^1H$ and $^{13}C\{^1H\}$ NMR spectra, respectively. However, two signals at $\delta$ = 0.76 and 0.09 ppm with an integral ratio of 1 : 1 in the $^1H$ spectrum and at $\delta$ = 2.41 and −0.18 ppm in the $^{13}C\{^1H\}$ spectrum are observed instead, as the pairs of methyl groups do not resolve together and are consequently chemically inequivalent. A similar behavior is observed for compounds **5** and **4b** with $[C_5(DMS)_4H]^-$ ligands. The metallocenes with threefold silylated cyclopentadienyl ligands exhibit lower rotational barriers for the silyl groups next to the unsubstituted position. Hence, heptasilyl isomers **3a** and **3b** do not show the expected four methyl signals in their $^{13}C\{^1H\}$ NMR spectra, but instead six signals, while the octasilyl compound **4a** exhibits four differentiated $^{13}C\{^1H\}$ signals instead of three expected in the absence of rotational hindrance.

Substitution of the cyclopentadienyl protons typically results in significant electronic and electrochemical changes in metallocenes as HOMO and LUMO energies are shifted. In classical acceptor-substituted compounds, *e.g.* haloferrocenes, the substituents mainly stabilize the HOMO while weakly de-

stabilizing the LUMO,[41] resulting in high redox potentials for the reversible redox couple $Fe^{+II/+III}$.[42] In silylated ferrocenes, *e.g.* $[Fe(C_5(TMS)H_4)_2]$ (0.01 V *vs.* FcH), similar redox potentials to those of unsubstituted ferrocene are observed.[43] The electrochemical properties of the polysilylated metallocenes **3** to **6** were determined by cyclic voltammetry in THF and referenced against the $FcH/FcH^+$ redox couple. All compounds exhibit a reversible one-electron oxidation with half-wave potentials between $E_{1/2}$ = 0.161 V and 0.172 V, indicating that the silyl groups do not affect the HOMO energies significantly.

In contrast to this, the UV/VIS spectra of isolated silylferrocenes **3** to **6** indicate decreasing HOMO–LUMO energy gaps. Those spectra were recorded in *n*-hexane (Fig. 3). Unsubstituted ferrocene exhibits an absorption band at $\lambda$ = 441 nm in the visible regime corresponding to the unresolved $^1A_1 \rightarrow {}^1E_1$ and $^1A_1 \rightarrow {}^1E_2$ spin-allowed d–d transitions, explaining the orange color of this compound.[41,44] Incorporation of dimethylsilyl groups causes a bathochromic shift yielding a color transition from red to purple from heptakis- to decakis (dimethylsilyl)ferrocene. This shift has been observed in previously reported polysilylated ferrocenes[2,45,46] as well. However, in the spectra of silylferrocenes **3** to **6** this band is accompanied by a shoulder which is most pronounced in the spectrum of $[FeC_{10}DMS_{10}]$ (**6**).

To explain these findings, density functional theory (DFT) calculations were performed, comparing unsubstituted ferrocene, $[FeCp_2]$, with the persilylated derivative (**6**) (ωB97X-D/def2-TZVPP(D)//r$^2$SCAN-3c level, see the ESI† for details). For $[FeCp_2]$, the expected $D_{5h}$ symmetric minimum is found, with the usual $D_{5d}$ transition state for the rotation of the Cp ligands (at a free energy of about 5 kJ mol$^{-1}$, consistent with the well-known free rotation in solution[47]). Time-dependent DFT calculations of the lowest excitation energies give a band at $\lambda$ = 461 nm, for a $^1A_1 \rightarrow {}^1E_1$ transition (in $D_5$ notation) and two additional bands at $\lambda$ = 351 nm and 512 nm, arising from the second $^1A_1 \rightarrow {}^1E_1$ and the formally forbidden $^1A_1 \rightarrow {}^1E_2$ transitions, respectively (ESI, Fig. S78†). The overall spectrum agrees very well with the experimentally determined spectrum.

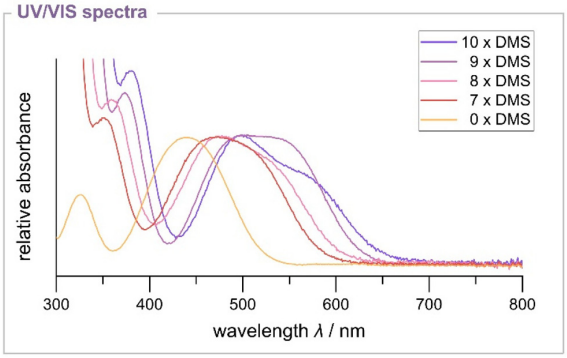


**Fig. 3** Normalized UV/VIS spectra of compounds $[FeC_{10}DMS_{10}]$ (**6**), $[FeC_{10}DMS_9H]$ (**5**), $[FeC_{10}DMS_8H_2]$ (**4b**), $[FeC_{10}DMS_7H_3]$ (**3b**) and ferrocene in *n*-hexane.

It is likely that the closeness of the two lowest excitation energies and the similar intensities (when also considering contributions from the $D_{5d}$ transition state) lead to a broadening of the peak, without a clearly discernible shoulder.

Replacing the Cp–hydrogen atoms with DMS groups so that the fivefold axis of the Cp ligand is retained results in two possible conformers (of $D_5$ and $S_{10}$ symmetry, respectively) which differ in the relative orientation of the Si–H bonds on the two rings. The electronic energy difference between the two conformers vanishes, consistent with the experimentally observed disorder in the crystal structure of **6** (ESI, Fig. S79†). Based on our calculations, these two conformers lead to qualitatively different spectra (ESI, Fig. S78†). A low-energy shoulder is found for the $S_{10}$ structure but not for the $D_5$ structure. However, the $D_5$ conformer exhibits much larger intensities, as the $^1A_1 \rightarrow {}^1E_1$ transition becomes dipole-allowed. We suspect that the shoulder observed experimentally (Fig. 3) may be due to a significant contribution to these low-energy regions of the spectrum from further areas on the conformational energy surface that are accessed dynamically at experimental temperatures. Contributions from different, energetically similar structures may be expected also for the hepta-, octa- and nonasilylated compounds, explaining their comparable band shapes.

Most notably, the TDDFT calculations clearly confirm the overall bathochromic shift of the spectrum upon silylation. NPA charges (ESI, Table S78†) become more positive from $[FeCp_2]$ to **6**. Most of this substituent effect seems to be structural, caused by the substantially longer Fe–C distances in **6**. Computations on $[FeCp_2]$ with the carbon positions of **6** do already provide most of the changes in charges and band positions, while finally adding the DMS substituents has a relatively small effect.

Closer analysis of the MOs and of the character of the electronic excitations shows that the degenerate HOMO in **6** is genuinely nonbonding (with $d_{xy}$ and $d_{x^2-y^2}$ character) and thus also changes very little (by less than 0.15 eV) upon expanding the Fe–C distances and upon finally adding the DMS substituents. This is consistent with the small effect of the silyl substituents on the redox potentials (see above). The low-lying excitations are out of this HOMO and out of another high-lying occupied MO with predominant metal $d_{z^2}$ character. This MO, which is very slightly σ-antibonding, drops in energy by about 0.25 eV upon bond expansion but goes up by 0.17 eV when adding the DMS substituents, thus staying also almost unchanged overall compared to $[FeCp_2]$. The changes in the band gap and low-lying excitation energies from $[FeCp_2]$ to **6** are thus largely due to changes in the virtual MO energies. In particular, the (twofold degenerate) LUMO comes down by 0.47 eV upon bond lengthening and by another 0.20 eV upon adding the DMS substituents. The LUMO is clearly π-antibonding and becomes less antibonding for the silyl-substituted ferrocenes, thus explaining the bathochromic shifts.

### 1,1-Substituted ferrocenes

Although we were able to isolate the persilylated derivative $[FeC_{10}DMS_{10}]$ (**6**) the demonstrated synthetic approach is

inconvenient for further synthetic applications in terms of selectivity and experimental effort. In order to generate highly overcrowded metallocenes in a selective manner we modified the substitutional pattern to 1,1′-disubstituted ferrocenes. Here the presence of methyl groups should in part compensate the electron-withdrawing and steric effects of the silyl substituents. The polybrominated compound $[FeC_{10}Br_8Me_2]$ (**7**) was synthesized by eightfold mercuration of 1,1′-dimethylferrocene followed by bromination with $KBr_3$, analogous to the synthetic protocol for decabromoferrocene.[34] The silylation of the corresponding metallocene was carried out with elemental magnesium and DMSCl in anhydrous THF. In contrast to the analogous reaction of decabromoferrocene the perfunctionalized derivative was obtained selectively in high yields (88%). Due to the high selectivity of the reaction step the purification of the substrates is accomplished easily by recrystallization instead of complex chromatographic methods. The obtained compound $[FeC_{10}DMS_8Me_2]$ (**8**) was analyzed by NMR, UV/VIS and single-crystal XRD. The polysilylated metallocenes show similar features as $[FeC_{10}DMS_{10}]$ (**6**). In the $^1H$ and $^{13}C\{^1H\}$ NMR spectra the signals which were assigned to the methyl groups attached to silicon split into a set of four signals indicating again a hindered rotation along the $Si–C^{Cp}$ axis. In the UV/VIS spectra the observed absorption maximum in the visible region at $\lambda_{max}$ = 490 nm is again red-shifted, indicating decreased HOMO–LUMO energy gaps. The observed wavelengths are similar to those of $[FeC_{10}DMS_8H_2]$ (**4b**: $\lambda_{max}$ = 495 nm) with tetrasilylated Cp ligands. Single crystals of compound **8** were obtained upon crystallization from MeOH/THF mixtures. The molecular structure shows again elongated metal–Cp bonds of 2.082(4)–2.099(4) Å compared to those of unsubstituted ferrocene (Fe–C: 2.051(2)–2.063(2) Å 39). The Cp rings deviate from a parallel arrangement by only 4.6(2)° due to the lower steric demand of the methyl groups. The silyl groups are found out of the Cp plane (5.3–20.9°) in spite of the reduced steric demand induced by the methyl groups.

## Conclusions

The focus of this work was to find appropriate methods for the generation of highly silylated ferrocenes to investigate the effects of steric overload and charge stabilization by the silyl groups.[48] Reactions were carried out by metalation of bromoferrocenes $[FeC_{10}Br_{10}]$ and $[FeC_{10}Br_8Me_2]$ followed by quenching with DMSCl. We observed that the introduction of silyl groups inhibits further silylation yielding only a mixture of polysilylated compounds $[FeC_{10}DMS_nH_{10-n}]$ ($n$ = 10, 9, 8) containing the targeted decasilylated ferrocene in low yields. The reactivity of the polymetalated intermediates and the selectivity of the products drastically improved when electron donating groups were applied and the corresponding octasilylated metallocenes $[FeC_{10}DMS_8Me_2]$ were isolated purely in good yields despite the sterically demanding substituents.

Mixtures of polysilylated metallocenes $[FeC_{10}DMS_nH_{10-n}]$ ($n$ = 10, 9, 8, 7) were successfully separated by HPLC allowing a systematic study on silylation effects on ferrocene by XRD, CV, NMR and UV/VIS spectroscopy. Here, the steric overcrowding is reflected by significant rotational hindrance of the tetra- and pentasilylated cyclopentadienyl ligands regarding the DMS groups and greater ordering. Furthermore, the cyclopentadienyl ligands are found to exhibit distortions from planarity within the molecular structure.[49] The maximum UV/VIS absorbances are systematically red-shifted with further silylation indicating decreased energy gaps between occupied and virtual MOs. DFT calculations show that this is largely due to the lengthening of the Fe–C bonds caused by the steric crowding induced by the silyl substituents. The occupied frontier MOs are largely nonbonding in nature and thus not affected much by the substitution, in agreement with small changes in the redox potentials. But the metal–ligand antibonding character of the lowest-lying virtual MOs is reduced compared to that of the parent ferrocene, giving rise to the observed red shifts.

The approach of exploiting sterically demanding and electron donating groups to force high degrees of silylation allows the isolation of sterically overcrowded cyclopentadienyl compounds on multigram scale. Even a subsequent methylation to obtain the trimethylsilyl substituted analogues should be feasible to obtain chemically more inert and increasingly overloaded compounds. In the future, the syntheses of other main group, transition metal or lanthanide or actinide complexes with persilylated cyclopentadienyl ligands could be of great interest.

## Author contributions

S. M. R. designed the project and wrote the manuscript. Furthermore, she performed the synthesis, recorded cyclic voltammetry and UV/VIS data as well as prepared, measured and solved the single-crystal XRD data. R. S. and P. S. R. performed experiments and analyzed the data. Both authors were supervised by S. M. R. M. R. and M. K. performed the quantum chemical calculations and revised the manuscript. C. F. designed the HPLC experiments. M. M. supervised the project and revised the manuscript.

## Conflicts of interest

There are no conflicts to declare.

## Acknowledgements

This study was funded by Deutsche Forschungsgemeinschaft (DFG) – project number: 387284271 – SFB 1349. We would like to acknowledge the assistance of the Core Facility BioSupraMol supported by the DFG.

View Article Online
Dalton Transactions Paper

## References


1 J. Okuda, *Chem. Ber.*, 1989, **122**, 1075–1077.
2 J. Okuda and E. Herdtweck, *J. Organomet. Chem.*, 1989, **373**, 99–105.
3 M. P. Plesniak, X. Just-Baringo, F. Ortu, D. P. Mills and D. J. Procter, *Chem. Commun.*, 2016, **52**, 13503–13506.
4 D. Cui, O. Tardif and Z. Hou, *J. Am. Chem. Soc.*, 2004, **126**, 1312–1313.
5 F. Ortu, J. Lui, M. Burton, M. Fowler, A. Formanuik, M.-E. Boulon, N. F. Chilton and D. P. Mills, *Inorg. Chem.*, 2017, **56**, 2496–2505.
6 D. Cui, M. Nishiura and Z. Hou, *Angew. Chem., Int. Ed.*, 2005, **44**, 959–962.
7 W.-X. Zhang, Z. Wang, M. Nishiura, Z. Xi and Z. Hou, *J. Am. Chem. Soc.*, 2011, **133**, 5712–5715.
8 L. M. Engelhardt, P. C. Junk, C. L. Raston and A. H. White, *J. Chem. Soc., Chem. Commun.*, 1988, 1500–1501.
9 A. H. Cowley, P. Jutzi, F. X. Kohl, J. G. Lasch, N. C. Norman and E. Schlüter, *Angew. Chem.*, 1984, **96**, 603–604.
10 M. J. Harvey, T. P. Hanusa and M. Pink, *J. Chem. Soc., Dalton Trans.*, 2001, 1128–1130.
11 P. Jutzi, E. Schlüter, M. B. Hursthouse, A. M. Arif and R. L. Short, *J. Organomet. Chem.*, 1986, **299**, 285–295.
12 M. Westerhausen, S. Schneiderbauer, N. Makropoulos, M. Warchhold, H. Nöth, H. Piotrowski and K. Karaghiosoff, *Organometallics*, 2002, **21**, 4335–4341.
13 C. H. Winter, X. X. Zhou and M. J. Heeg, *Inorg. Chem.*, 1992, **31**, 1808–1815.
14 A. Sekiguchi, T. Nakanishi, C. Kabuto and H. Sakurai, *J. Am. Chem. Soc.*, 1989, **111**, 3748–3750.
15 A. Sekiguchi, M. Ichinohe, C. Kabuto and H. Sakurai, *Organometallics*, 1995, **14**, 1092–1094.
16 A. Sekiguchi, T. Matsuo, K. Ebata and H. Sakurai, *Chem. Lett.*, 1996, **25**, 1133–1134.
17 A. Sekiguchi, T. Matsuo and H. Watanabe, *J. Am. Chem. Soc.*, 2000, **122**, 5652–5653.
18 A. Sekiguchi, K. Ebata, C. Kabuto and H. Sakurai, *J. Am. Chem. Soc.*, 1991, **113**, 1465–1466.
19 J. C. Wedal, J. M. Barlow, J. W. Ziller, J. Y. Yang and W. J. Evans, *Chem. Sci.*, 2021, **12**, 8501–8511.
20 M. R. Trinh, J. C. Wedal and W. J. Evans, *Dalton Trans.*, 2021, **50**, 14384–14389.
21 R. R. Langeslay, M. E. Fieser, J. W. Ziller, F. Furche and W. J. Evans, *Chem. Sci.*, 2015, **6**, 517–521.
22 R. R. Langeslay, M. E. Fieser, J. W. Ziller, F. Furche and W. J. Evans, *J. Am. Chem. Soc.*, 2016, **138**, 4036–4045.
23 M. R. MacDonald, J. E. Bates, J. W. Ziller, F. Furche and W. J. Evans, *J. Am. Chem. Soc.*, 2013, **135**, 9857–9868.
24 M. E. Fieser, M. R. MacDonald, B. T. Krull, J. E. Bates, J. W. Ziller, F. Furche and W. J. Evans, *J. Am. Chem. Soc.*, 2015, **137**, 369–382.
25 K. Sünkel and J. Hofmann, *Organometallics*, 1992, **11**, 3923–3925.
26 A. Sekiguchi, Y. Sugai, K. Ebata, C. Kabuto and H. Sakurai, *J. Am. Chem. Soc.*, 1993, **115**, 1144–1146.
27 M. S. Miftakhov, G. A. Tolstikov and S. I. Lomakina, *Zh. Obshch. Khim.*, 1976, **46**, 2754–2754.
28 P. Jutzi, E. Schlüter, C. Krüger and S. Pohl, *Angew. Chem., Int. Ed. Engl.*, 1983, **22**, 944–944.
29 M. A. Edelman, P. B. Hitchcock, M. F. Lappert, D.-S. Liu and S. Tian, *J. Organomet. Chem.*, 1998, **550**, 397–808.
30 H. Chen, P. Jutzi, W. Leffers, M. M. Olmstead and P. P. Power, *Organometallics*, 1991, **10**, 1282–1286.
31 C. P. Morley and P. Jutzi, *Organometallics*, 1987, **6**, 1084–1090.
32 J. Okuda and E. Herdtweck, *Chem. Ber.*, 1988, **121**, 1899–1905.
33 I. R. Butler, D. M. Evans, P. N. Horton, S. J. Coles and P. J. Murphy, *Organometallics*, 2021, **40**, 600–605.
34 S. M. Rupf, I. S. Dimitrova, G. Schröder and M. Malischewski, *Organometallics*, 2022, **41**, 1261–1267.
35 S. M. Rupf, G. Schröder, R. Sievers and M. Malischewski, *Chem. – Eur. J.*, 2021, **27**, 5125–5129.
36 P. Štěpnička, *Dalton Trans.*, 2022, **51**, 8085–8102.
37 C. H. Winter and K. N. Seneviratne, *Comments Inorg. Chem.*, 1996, **19**, 1–23.
38 J. R. Baran Jr., C. Hendrickson, D. A. Laude Jr. and R. J. Lagow, *J. Org. Chem.*, 1992, **57**, 3759–3760.
39 P. Seiler and J. D. Dunitz, *Acta Crystallogr., Sect. B: Struct. Crystallogr. Cryst. Chem.*, 1982, **38**, 1741–1745.
40 J. Okuda, *J. Organomet. Chem.*, 1989, **376**, C1–C4.
41 M. S. Inkpen, S. Du, M. Hildebrand, A. J. P. White, N. M. Harrison, T. Albrecht and N. J. Long, *Organometallics*, 2015, **34**, 5461–5469.
42 D. A. Khobragade, S. G. Mahamulkar, L. Pospíšil, I. Císařová, L. Rulísek and U. Jahn, *Chem. – Eur. J.*, 2012, **18**, 12267–12277.
43 A. Abri and A. abbaszad Rafe, *J. Chin. Chem. Soc.*, 2015, **62**, 273–279.
44 Y. S. Sohn, D. N. Hendrickson and H. B. Gray, *J. Am. Chem. Soc.*, 1971, **93**, 3603–3612.
45 O. J. Curnow, G. M. Fern, S. Klaib, U. Böhme, H. Lang and R. Holze, *J. Electroanal. Chem.*, 2005, **585**, 167–171.
46 J. Okuda, R. W. Albach and E. Herdtweck, *Polyhedron*, 1991, **10**, 1741–1748.
47 M. Rosenblum and R. B. Woodward, *J. Am. Chem. Soc.*, 1958, **80**, 5443–5449.
48 A previous version of the manuscript has been deposited on a preprint server: S. M. Rupf, R. Sievers, P. S. Riemann, M. Reimann, K. Kaupp, C. Fasting and M. Malischewski, *ChemRxiv*, 2023, DOI: **10.26434/chemrxiv-2023-538rg**.
49 Deposition numbers CCDC 2248053–2248061 contain the supplementary crystallographic data for this paper.†

## 3.5 The [2+2] Cycloaddition Product of Perhalogenated Cyclopentadienyl Cations: Structural Characterization of Salts of the $[C_{10}Cl_{10}]^{2+}$ and $[C_{10}Br_{10}]^{2+}$ Dications

Susanne Margot Rupf, Patrick Pröhm, Moritz Malischewski*
*Chem. Commun.* **2020**, *56*, 9834–9837.

DOI: 10.1039/d0cc04226a



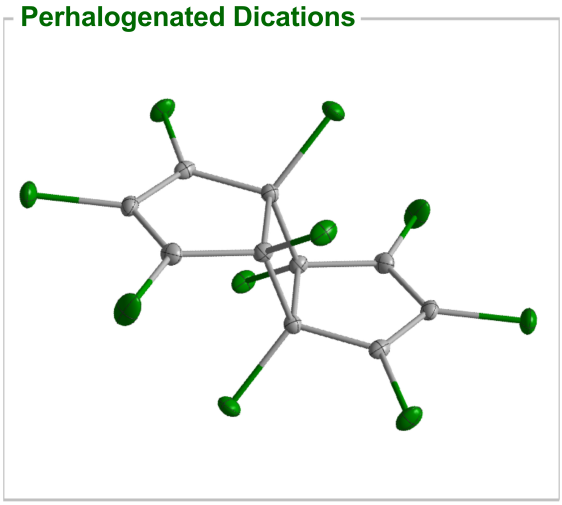


**Author Contribution:**
Susanne M. Rupf and Moritz Malischewski designed the project and wrote the manuscript with main contribution of Susanne M. Rupf. Susanne M. Rupf performed the syntheses and analyzed the spectroscopic data as well as prepared, measured and solved the single crystals. Patrick Pröhm performed low-temperature NMR experiments. Moritz Malischewski supervised the project and revised the manuscript.

ChemComm

COMMUNICATION

View Article Online
View Journal | View Issue



Cite this: *Chem. Commun.*, 2020, **56**, 9834

Received 17th June 2020,
Accepted 20th July 2020

DOI: 10.1039/d0cc04226a

rsc.li/chemcomm

# The [2+2] cycloaddition product of perhalogenated cyclopentadienyl cations: structural characterization of salts of the $[C_{10}Cl_{10}]^{2+}$ and $[C_{10}Br_{10}]^{2+}$ dications†

Susanne Margot Rupf, Patrick Pröhm and Moritz Malischewski *

**Instead of monomeric cyclopentadienyl cations, the low-temperature reaction of hexachloro- and hexabromocyclo-pentadiene ($C_5Cl_6$ and $C_5Br_6$) with powerful Lewis acids $SbF_5$ and $AsF_5$ in $SO_2ClF$ yields salts of perhalogenated dications $[C_{10}Cl_{10}][Sb_3F_{16}]_2$ and $[C_{10}Br_{10}][As_2F_{11}]_2$ which are characterized *via* single crystal X-ray diffraction and NMR spectroscopy. Additionally, this reactivity is rationalized by quantum-chemical calculations.**

Carbocations have been an equally important and fascinating research field in organic chemistry for many decades.[1] But even lately, important landmarks have been reported, *e.g.* the structural characterization of the 2-norbornyl cation and of the pentagonal pyramidal hexamethylbenzene dication with a hexacoordinated carbon atom.[2,3] One important carbocation that so far has resisted all attempts at isolation and crystallization due to its instability is the cyclopentadienyl cation. As the cyclopentadienyl cation has an antiaromatic 4-π electron system the ground state of $[C_5H_5]^+$ is a (diradical) triplet state.[4] This is also the case for $[C_5(^iPr)_5]^+$[5] and $[C_5Cl_5]^+$,[6] while for $[C_5Ph_5]^+$ a singlet ground state seems to be favored although in general the singlet–triplet energy gap is usually very small in these systems.[6,7] While $[C_5H_5]^+$ dimerizes,[8] the pentaphenyl cyclopentadienyl cation decomposes *via* C–H cleavage and formation of additional C–C bonds – some of the decomposition products have been identified.[9] Although permethylation is an effective strategy to stabilize highly electrophilic cations[3,10–13] this is not the case for the cyclopentadienyl cation. Jutzi reported that $[C_5Me_5]^+$ decomposes *via* loss of a proton and subsequent polymerization of the resulting tetramethylfulvene.[14] Surprisingly, in 2002 the structural characterization of the stable $[C_5Me_5]^+$ cation was reported but this result turned out to be erroneous.[15] The reduced species that had been isolated instead, turned out to be $[C_5Me_5H_2]^+$,[16–19] being a rare example of an allylic cation without stabilizing heteroatoms or additional π-systems.[20–22] Hydrogen-abstraction from the organic solvent also seems to cause the decomposition of $[C_5(i\text{-}Pr)_5]^+$.[5]

In order to block decomposition pathways *via* the hydrogen atoms, the synthetic target of a perhalogenated cyclopentadienyl cation is very appealing.[23] Breslow *et al.* observed the formation of a triplet state cyclopentadienyl cation after reaction of $C_5Cl_6$ with neat antimony pentafluoride by EPR spectroscopy.[6,24] However, the triplet signal of the presumed $[C_5Cl_5]^+$ in the $SbF_5$ matrix vanishes rapidly above the freezing point of $SbF_5$. Quenching experiments with methanol resulted only in $<5\%$ $C_5Cl_5OCH_3$ but $>90\%$ dimeric perchlorinated ketones.[6] This can be explained by the tendency of $C_5Cl_6$ to either dimerize or polymerize in presence of Lewis acids (*e.g.* $AlCl_3$).[25–27]

For this study, we decided to (re-)investigate the reaction of $C_5Cl_6$ and $C_5Br_6$ with the powerful Lewis acids $SbF_5$ and $AsF_5$ in the non-coordinating solvent $SO_2ClF$ at low temperatures (Scheme 1). Single crystals of compounds $[C_{10}Cl_{10}][Sb_3F_{16}]_2 \cdot SO_2ClF$ (**4a**) and $[C_{10}Br_{10}][As_2F_{11}]_2 \cdot 2SO_2ClF$ (**4b**) were obtained from the reaction mixtures at −75 °C. The compound **4a** crystallizes in monoclinic space group $P2_1/n$ and **4b** in triclinic space group $P\bar{1}$. The asymmetric units contain a $[C_5X_5]$ unit as well as one monoanion, respectively (Fig. 1). Due to a center of inversion the overall formulas are $[C_{10}Cl_{10}][Sb_3F_{16}]_2$ and $[C_{10}Br_{10}][As_2F_{11}]_2$. Based on the variations in C–C bond lengths,

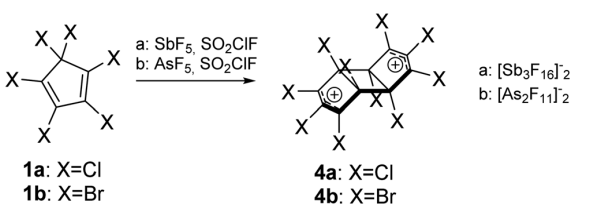


**1a**: X=Cl
**1b**: X=Br

**4a**: X=Cl
**4b**: X=Br

Scheme 1 Reaction of $C_5X_6$ (X = Cl, Br) with strong Lewis acids in $SO_2ClF$ to [2+2] cycloaddition products $[C_{10}X_{10}]^{2+}$ of two cyclopentadienyl cations $[C_5X_5]^+$.

*Freie Universität Berlin, Institut für Chemie und Biochemie, Institut für Anorganische Chemie, Fabeckstraße 34-36, 14195 Berlin, Germany. E-mail: moritz.malischewski@fu-berlin.de*

† Electronic supplementary information (ESI) available: Experimental, NMR and X-ray data, calculations. CCDC 2009907–2009910. For ESI and crystallographic data in CIF or other electronic format see DOI: 10.1039/d0cc04226a

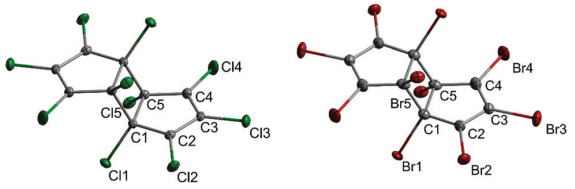


Fig. 1 Ellipsoid (50% probability at 100 K) plot of compounds $[C_{10}Cl_{10}][Sb_3F_{16}]_2 \cdot SO_2ClF$ (left; **4a**) and $[C_{10}Br_{10}][As_2F_{11}]_2 \cdot 2SO_2ClF$ (right, **4b**). Counterions and solvent molecules are omitted for clarity. Color code: red – bromine, green – chlorine, grey – carbon.

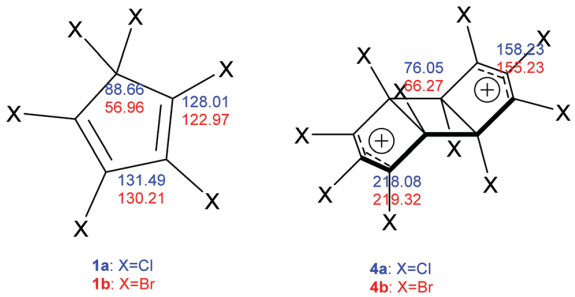


Fig. 2 $^{13}C$ NMR chemical shifts of compounds (**1**) and (**4**) in [ppm]. $C_{10}Cl_{10}^{2+}$ and $C_{10}Br_{10}^{2+}$: 100 MHz, $SO_2$, ext. acetone-$d_6$, −60 °C. $C_5Cl_6$: 100 MHz, $CH_2Cl_2$, ext. acetone-$d_6$, room temperature. $C_5Br_6$: 100 MHz, $CDCl_3$, room temperature.

the bonding situation in these dications is best described as two allyl cations separated by a saturated four-membered ring (see ESI,† Table S3).

Interestingly, the C–Cl bond lengths vary considerably within the dication. In comparison with the C–Cl bond lengths in $C_5Cl_6$ ($C_{sp^3}$–Cl: 1.780(2)–1.781(2) Å; $C_{sp^2}$–Cl: 1.696(1)–1.699(2) Å) the C–Cl bonds C1–Cl1 and C5–Cl5 from the saturated four-membered ring in **4a** are slightly shortened (1.739(2)–1.740(2) Å). However, the so-called α-chlorine effect is even more evident in the allyl cation: Here, the C2–Cl2 and C4–Cl4 bonds are shortened to 1.643(2) and 1.634(2) Å while the effect is less pronounced for C3–Cl3 (1.678(2) Å). This finding is in accordance with calculated NBO charges (see ESI†) which are the highest for Cl2 and Cl4. In general, the high electrophilicity of the allyl cation is reduced by chlorine as a π-donor (+M-effect). The same effects can be observed for the perbrominated dication **4b** (Table 1). The resulting bond-shortening of the C–halogen bond in carbocations has been observed before.[28–34]

Only few examples of crystal structures containing $[Sb_3F_{16}]^-$ ions are known, in which it can exist as either *cis* or *trans* isomer.[34–38] In **4a** the $SbF_5$ groups are attached to neighbouring *cis*-fluorine atoms of a central $[SbF_6]^-$ unit. The number of structures containing $[As_2F_{11}]^-$ is similarly scarce.[3,12,29,34,39–43] The structures of **4a** and **4b** show only weak contacts between anion $[Sb_3F_{16}]^-$ and $[As_2F_{11}]^-$ to the allylic carbon centres. The present C···F contact distances of 3.031 and 3.110 Å in the **4a** and 3.096 and 3.158 Å in the **4b** structure are comparable to those observed in $[CCl_3]^+$[17] (2.962(9) Å), $[CBr_3]^+$[17] (3.09(2) Å), $[C_6Cl_6]^+$[19] (3.003(1) Å) and $[C_6Br_6]^+$ (2.994(1) Å).[34] The chlorine and bromine atoms also interact with the fluorine atoms of the anion as well as the oxygen atoms of the $SO_2ClF$ molecules (Cl···F: 2.843 to 3.212 Å; Br···F: 2.877 to 3.310 Å; Cl···O: 3.268 Å, Br···O: 2.975 and 3.196 Å).

Table 1 Selected bond lengths of the compounds **1a**, **1b**, **4a** and **4b** in [Å]

| | $C_{10}X_{10}^{2+}$ (X = Cl) **4a** | $C_{10}X_{10}^{2+}$ (X = Br) **4b** |
|---|---|---|
| C1–X1 | 1.740(2) | 1.908(4) |
| C2–X2 | 1.643(2) | 1.803(6) |
| C3–X3 | 1.678(2) | 1.833(5) |
| C4–X4 | 1.634(2) | 1.797(4) |
| C5–X5 | 1.739(2) | 1.912(5) |
| | $C_5X_6$ (X = Cl) **1a** | $C_5X_6$ (X = Br) **1b** |
| $C_{sp^3}$–X | 1.780(2)–1.781(2) | 1.950(6) |
| $C_{sp^2}$–X | 1.696(1)–1.699(2) | 1.838(11)–1.875(11) |

$^{13}C$ and $^{19}F$ NMR spectra of **4a** and **4b** were recorded in liquid $SO_2$ at −60 °C while the spectra of **1a** and **1b** were measured in organic solvents at room temperature. The difference in $^{13}C$ chemical shifts between **1a** and **1b**, as well as **4a** and **4b** is most pronounced for the $sp^3$ hybridized carbon atoms. The $^{13}C$ NMR spectra of **4a** and **4b** display three signals, respectively (see ESI†) which is consistent with the symmetry of the compounds (Fig. 2). The most downfield shifted chemical shifts (**4a**: 218.08, **4b**: 219.32 ppm) correspond to the carbon atoms C2 and C4 which are mostly affected by the positive charges. These signals are significantly deshielded compared to the starting materials (**1a**: 131.49, **1b**: 130.21 ppm) which confirms carbocation formation.[44] The inner carbon of the allyl cation (C3) resonates at 158.23/155.23 ppm (**4a**/**4b**). The four-membered saturated ring is characterized by one signal at 76.05/66.27 ppm (**4a**/**4b**). Very similar chemical shifts are observed for $[C_{10}(cyclopropyl)_{10}]^{2+}$ and the less-symmetric $[C_{10}H_8Me_2]^{2+}$ which both have not been structurally characterized so far.[45,46] The $^{13}C$ NMR spectrum of the former displays three signals at $\delta$ = 222.6, 148.3 and 83.2 ppm. The $^{19}F$ NMR spectrum of **4a** (see ESI†) shows five signals consistent with the counter ion $[Sb_3F_{16}]^-$. The $^{19}F$ NMR spectrum of **4b** only shows a broad singlet for $[As_2F_{11}]^-$ due to fast exchange processes.[47,48]

The isolation of the $[C_{10}X_{10}]^{2+}$ dications instead of $[C_5X_5]^+$ poses the question how energetically favorable this dimerization is. Although dimerization of the 4π-electron systems and diradicals $[C_5X_5]^+$ appears reasonable, Coulomb-repulsion should destabilize the dication. Structure optimizations and frequency calculations were performed on the B3LYP-GD3BJ/def2-TZVP and MP2/cc-PVTZ level of theory. The optimized structures are in accordance with the crystal structures and the variations in C–C and C–X bond lengths are well reproduced. As expected, the shortest C–X bond lengths are those where the halogen atom (X) carries the highest positive charge (see ESI†). Calculation of Gibbs free energies for the dimerization of (triplet) $[C_5Cl_5]^+$ (**2a**) to $[C_{10}Cl_{10}]^{2+}$ and its isomers (**4a**, **5a** and **5b**) were performed for a temperature of 213.15 K (Fig. 3 and Table 2). While the dimerization of **2a** to **4a** is endergonic by 225 kJ $mol^{-1}$ (using B3LYP-GD3BJ/def2-TZVP), formation of the [4+2] Diels–Alder-products **5a** and **5b** is even less favorable

View Article Online
ChemComm Communication

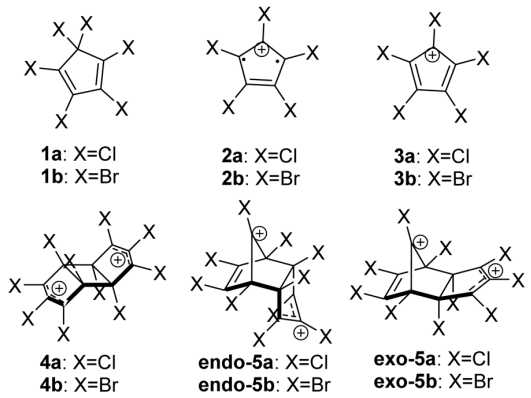


Fig. 3 Top: Perhalogenated cyclopentadiene derivatives (**1**) as well as triplet state (**2**) and singlet state (**3**) cyclopentadienyl cations. Bottom: [2+2] cycloaddition product (**4**) and [2+4] cycloaddition products of two cyclopentadienyl cations.

Table 2 Calculated energy differences $\Delta G$ in kJ mol$^{-1}$ at 213.15 K. $\varepsilon_r$ is the dielectric constant, used for calculations with the Polarizable Continuum Model (PCM) for solvent effects

| | B3LYP-GD3BJ/ def2-TZVP | MP2/cc-pVTZ |
|---|---|---|
| **2a**/**3a** | 0/+32 | 0/+15 |
| **2a** + **2a** → **4a**/***exo*-5a**/***endo*-5a** | +225/+317/+316 | +102/+156/+165 |
| **2a** + **2a** → **4a**/***exo*-5a**/***endo*-5a**; $\varepsilon_r$ = 2 | +108/+195/+201 | −13/+37/+41 |
| **2a** + **2a** → **4a**/***exo*-5a**/***endo*-5a**; $\varepsilon_r$ = 10 | +35/+103/+101 | −109/−61/−61 |
| **2a** + **2a** → **4a**/***exo*-5a**/***endo*-5a**; $\varepsilon_r$ = 23 | +5/+89/+90 | −123/−75/−76 |

(317/316 kJ mol$^{-1}$). However, these values contradict common chemical experience, especially since the dimerization already takes place at very low temperatures. It is important to note that these calculated values refer to isolated molecules in vacuum. In order to obtain a better description for the experimental parameters, the calculations were repeated with a solvation model, using dielectric constants (relative permittivity) of $\varepsilon_r$ = 2 and $\varepsilon_r$ = 10 to simulate the influence of solvents of very low or medium polarity. Additionally, $\varepsilon_r$ = 23 was used to model the dielectric constant of liquid $SO_2$ at 213.15 K.[49] Taking solvation into account the dications become significantly more stable, reducing the overall Gibbs free energy of the formation of $[C_{10}Cl_{10}]^{2+}$ (**4a**) to +108, +35 and +5 kJ mol$^{-1}$, respectively (for $\varepsilon_r$ = 2; 10; 23). The Diels–Alder-products ***exo*-5a** and ***endo*-5a** remain about 100 kJ mol$^{-1}$ less stable than **4a**. If MP2/cc-PVTZ instead of DFT is used for the calculations, all Gibbs free energies are roughly shifted by 100–150 kJ mol$^{-1}$ in favor of the dications. Consequently, dimerization is slightly favorable even for extremely non-polar solvents ($\varepsilon_r$ = 2) but becomes significantly exergonic for **4a** and **5a** in medium-polar solvents ($\varepsilon_r$ = 10 and 23). For $[C_{10}Br_{10}]^{2+}$ the general trend is clearly the same for the DFT calculations, although the calculations using MP2/cc-PVTZ were not performed for $[C_{10}Br_{10}]^{2+}$ due to the enormous demand of computational resources (see ESI†).

Dutton proposed a series of possible substitution patterns (typically, $CH_3$, $CF_3$, $C_6H_5$, $C_6F_5$ substituents) which could give rise to a stable cyclopentadienyl cation.[50] Possible side-reactions (proton loss, addition of fluoride, *etc.*) were taken into account. By using M06-2X/def2-TZVP, B3LYP/def2-TZVP and the polarizable continuum model to account for solvent effects of dichloromethane ($\varepsilon_r \approx 9$), he calculated that the dimerization to dicationic (*exo*/*endo*)-Diels–Alder-products similar to **5a** is endergonic by about 195–212 kJ mol$^{-1}$ which is similar to our calculations. Since we can experimentally prove that dimerization occurs (however to products that are even about 50–100 kJ mol$^{-1}$ more stable), we have to assume that the probability is low to achieve a stable, monomeric cyclopentadienyl cation with this approach. Even worse, also lattice energies work against isolation of the monomeric cation in the solid state, since an $A^+X^-$ salt has a significantly lower lattice energy than an $A^{2+}[X]_2^-$ salt. So even in case of a mildly endergonic dimerization, the gain of the higher lattice energy could lead to the isolation of the dimerization products. Only for extremely large weakly-coordinating anions the energy differences between these different stoichiometries would become relatively small and could in principal be overcome by a highly endergonic dimerization reaction. However, the numbers of our MP2 calculations suggest that this is definitely not the case here.

These results suggest that in order to isolate a monomeric cyclopentadienyl cation the most promising strategy is to design sterically bulky Cp rings, where sterics destabilize the dication. Additionally, the larger molecular volume of the cation also beneficially reduces the lattice energies. However, as stated in the introduction, this is very difficult from a synthetic point of view since C–H containing systems seem to be very prone to all sorts of decomposition reactions.

In summary, $[C_{10}Cl_{10}][Sb_3F_{16}]_2$ and $[C_{10}Br_{10}][As_2F_{11}]_2$ are the first structurally characterized dications which are derived from the dimerization of a substituted cyclopentadienyl cation. To our knowledge, only one perhalogenated dication had been structurally characterized so far ($[C_{14}F_{10}]^{2+}$).[42] The bonding situation in $C_{10}X_{10}^{2+}$ is best described as two allyl cations that are separated by a four-membered saturated ring. The chlorine and bromine atoms act as efficient π-donors into the allyl-cation, which is reflected by significant shortening of C–Cl and C–Br bonds.

Gefördert durch die Deutsche Forschungsgemeinschaft (DFG) – Projektnummer 387284271 – SFB 1349. Computing time was made available by HPC Service of ZEDAT, FU Berlin.

## Conflicts of interest

There are no conflicts to declare.

## References

1 G. A. Olah, *J. Org. Chem.*, 2001, **66**, 5943–5957.
2 F. Scholz, D. Himmel, F. W. Heinemann, P. V. R. Schleyer, K. Meyer and I. Krossing, *Science*, 2013, **341**, 62–64.
3 M. Malischewski and K. Seppelt, *Angew. Chem., Int. Ed.*, 2017, **56**, 368–370.
4 M. Saunders, R. Berger, A. Jaffe, J. M. McBride, J. O'Neill, R. Breslow, J. M. Hoffmann Jr, C. Perchonock, E. Wasserman, R. S. Hutton and V. J. Kuck, *J. Am. Chem. Soc.*, 1973, **95**, 3017–3018.

 

5 H. Sitzmann, H. Bock, R. Boese, T. Dezember, Z. Havlas, W. Kaim, M. Moscherosch and L. Zanathy, *J. Am. Chem. Soc.*, 1993, **115**, 12003–12009.
6 R. Breslow, H. W. Chang, R. Hill and E. Wasserman, *J. Am. Chem. Soc.*, 1967, **89**, 1112–1119.
7 R. Breslow, H. W. Chang and W. A. Yager, *J. Am. Chem. Soc.*, 1963, **85**, 2033–2034.
8 R. Breslow and J. M. Hoffman Jr, *J. Am. Chem. Soc.*, 1972, **94**, 2110–2111.
9 R. Breslow and H. W. Chang, *J. Am. Chem. Soc.*, 1961, **83**, 3727–3728.
10 M. Malischewski and K. Seppelt, *Angew. Chem., Int. Ed.*, 2017, **56**, 16495–16497.
11 M. Schorpp, S. Rein, S. Weber, H. Scherer and I. Krossing, *Chem. Commun.*, 2018, **54**, 10036–10039.
12 M. Malischewski, M. Adelhardt, J. Sutter, K. Meyer and K. Seppelt, *Science*, 2016, **353**, 678–682.
13 M. Malischewski, K. Seppelt, J. Sutter, D. Munz and K. Meyer, *Angew. Chem., Int. Ed.*, 2018, **57**, 14597–14601.
14 P. Jutzi and A. Mix, *Chem. Ber.*, 1992, **125**, 951–954.
15 J. B. Lambert, L. Lin and V. Rassolov, *Angew. Chem., Int. Ed.*, 2002, **41**, 1429–1431.
16 M. Otto, D. Scheschkewitz, T. Kato, M. M. Midland, J. B. Lambert and G. Bertrand, *Angew. Chem., Int. Ed.*, 2002, **41**, 2275–2276.
17 T. Müller, *Angew. Chem., Int. Ed.*, 2002, **41**, 2276–2278.
18 J. B. Lambert, *Angew. Chem., Int. Ed.*, 2002, **41**, 2278.
19 J. N. Jones, A. H. Cowley and C. L. B. Macdonald, *Chem. Commun.*, 2002, 1520–1521.
20 G. Maier, R. Emrich, K.-D. Malsch, K.-A. Schneider, M. Nixdorf and H. Irngartinger, *Chem. Ber.*, 1985, **118**, 2798–2810.
21 K. Ogawa, S. Minegishi, K. Komatsu and T. Kitagawa, *J. Org. Chem.*, 2008, **73**, 5248–5254.
22 S. Duttwyler, Y. Zhang, A. Linden, C. A. Reed, K. K. Baldridge and J. S. Siegel, *Angew. Chem., Int. Ed.*, 2009, **48**, 3787–3790.
23 H. Vančik, I. Novak and D. Kidemet, *J. Phys. Chem. A*, 1997, **101**, 1523–1525.
24 R. Breslow, R. Hill and E. Wasserman, *J. Am. Chem. Soc.*, 1964, **86**, 5349–5350.
25 J. S. Newcomer and E. T. McBee, *J. Am. Chem. Soc.*, 1949, **71**, 952–956.
26 H. P. Fritz and L. Schäfer, *J. Organomet. Chem.*, 1964, **1**, 318–322.
27 R. West, *Acc. Chem. Res.*, 1970, **3**, 130–138.
28 T. Laube, E. Bannwart and S. Hollenstein, *J. Am. Chem. Soc.*, 1993, **115**, 1731–1733.
29 K. O. Christe, X. Zhang, R. Bau, J. Hegge, G. A. Olah, G. K. S. Prakash and J. A. Sheehy, *J. Am. Chem. Soc.*, 2000, **122**, 481–487.
30 H. P. A. Mercier, M. D. Moran, G. J. Schrobilgen, C. Steinberg and R. J. Suontamo, *J. Am. Chem. Soc.*, 2004, **126**, 5533–5548.
31 I. Krossing, A. Bihlheimer, I. Raabe and N. Trapp, *Angew. Chem., Int. Ed.*, 2003, **42**, 1531–1534.
32 H. Shorafa, D. Mollenhauer, B. Paulus and K. Seppelt, *Angew. Chem., Int. Ed.*, 2009, **48**, 5845–5847.
33 M. J. Molski, D. Mollenhauer, S. Gohr, B. Paulus, M. A. Khanfar, H. Shorafa, S. H. Strauss and K. Seppelt, *Chem. – Eur. J.*, 2012, **18**, 6644–6654.
34 M. J. Molski, M. A. Khanfar, H. Shorafa and K. Seppelt, *Eur. J. Org. Chem.*, 2013, 3131–3136.
35 I. Bernhardi, T. Drews and K. Seppelt, *Angew. Chem., Int. Ed.*, 1999, **38**, 2232–2233.
36 R. Faggiani, D. K. Kennepohl, C. J. L. Lock and G. J. Schrobilgen, *Inorg. Chem.*, 1986, **25**, 563–571.
37 T. Drews, W. Koch and K. Seppelt, *J. Am. Chem. Soc.*, 1999, **121**, 4379–4384.
38 V. A. Petrov, A. Marchione and W. Marshall, *J. Fluorine Chem.*, 2008, **129**, 1011–1017.
39 R. Minkwitz and F. Neikes, *Inorg. Chem.*, 1999, **38**, 5960–5963.
40 R. Minkwitz, C. Hirsch and T. Berends, *Eur. J. Inorg. Chem.*, 1999, 2249–2254.
41 N. Kuhn, S. Fuchs, R. Minkwitz and T. Berends, *Z. Naturforsch., B: J. Chem. Sci.*, 2001, **56**, 626–629.
42 M. A. Khanfar and K. Seppelt, *J. Fluorine Chem.*, 2015, **179**, 193–197.
43 O. Mallow, M. A. Khanfar, M. Malischewski, P. Finke, M. Hesse, E. Lork, T. Augenstein, F. Breher, J. R. Harmer, N. V. Vasilieva, A. Zibarev, A. S. Bogomyakov, K. Seppelt and J. Beckmann, *Chem. Sci.*, 2015, **6**, 497–504.
44 G. A. Olah, L. Heiliger and G. K. S. Prakash, *J. Am. Chem. Soc.*, 1989, **111**, 8020–8021.
45 S. Redlich, PhD thesis, Georg-August-Universität zu Göttingen, 2004.
46 G. A. Olah, M. Arvanaghi and G. K. S. Prakash, *Angew. Chem., Int. Ed. Engl.*, 1983, **22**, 712–713.
47 J.-C. Culmann, M. Fauconet, R. Jost and J. Sommer, *New J. Chem.*, 1999, **23**, 863–867.
48 P. A. W. Dean, R. J. Gillespie, R. Hulme and D. A. Humphreys, *J. Chem. Soc. A*, 1971, 341–346.
49 *CRC Handbook of Chemistry and Physics*, ed. D. R. Lide, CRC Press, Boca Raton, FL, 2004, Section 6, p. 156.
50 K. J. Iversen, D. J. D. Wilson and J. L. Dutton, *Chem. – Eur. J.*, 2014, **20**, 14132–14138.

## 3.6 Structural Characterization and Reactivity of a Room Temperature-Stable, Antiaromatic Cyclopentadienyl Cation Salt

Yannick Schulte, Christoph Wölper, Susanne M. Rupf, Moritz Malischewski, Gebhard Haberhauer,* Stephan Schulz*, *ChemRxiv*, **17 March 2023**, Version 1.

DOI: 10.26434/chemrxiv-2023-qnstd



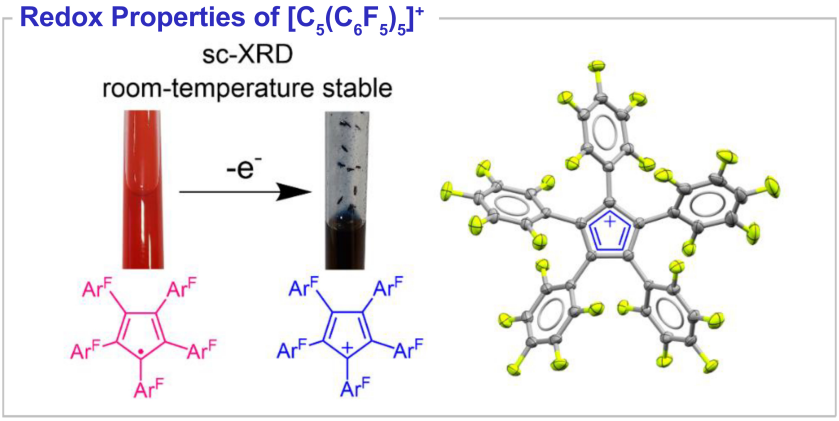


**Author Contribution:**
Susanne M. Rupf performed cyclic voltammetry experiments in liquid $SO_2$ and revised the manuscript. Yannick Schulte designed the project and performed experiments and analyzed data. Furthermore, he wrote the manuscript. Christoph Wölper measured and solved single-crystal X-ray data. Moritz Malischewski supervised the cyclic voltammetry experiments and revised the manuscript. Gebhard Haberhauer performed quantenchemical calculations, wrote and revised the manuscript. Stephan Schulz supervised the project, designed experiments and wrote and revised the manuscript.

**Structural Characterization and Reactivity of a Room Temperature-Stable, Antiaromatic Cyclopentadienyl Cation Salt**

Yannick Schulte,[a] Christoph Wölper,[a] Susanne M. Rupf,[b] Moritz Malischewski,[b] Gebhard Haberhauer,[c]* and Stephan Schulz[a;d]*

[a] Institute of Inorganic Chemistry, University of Duisburg-Essen, Universitätsstraße 5-7, D-45141 Essen

E-mail: stephan.schulz@uni-due.de; https://www.uni-due.de/ak_schulz/index_en.php

[b] Institute of Inorganic Chemistry, Freie Universität Berlin, Fabeckstraße 34-36, D-14195 Berlin

[c] Institute of Organic Chemistry, University of Duisburg-Essen, Universitätsstraße 5-7, D-45141 Essen

E-mail: gebhard.haberhauer@uni-due.de; https://www.uni-due.de/akhaberhauer/

[d] Institute of Inorganic Chemistry and Center for Nanointegration Duisburg-Essen (CENIDE), University of Duisburg-Essen, Carl-Benz-Straße 199, D-47057 Duisburg.

**E-mail corresponding authors:** stephan.schulz@uni-due.de; gebhard.haberhauer@uni-due.de

**Graphic TOC**

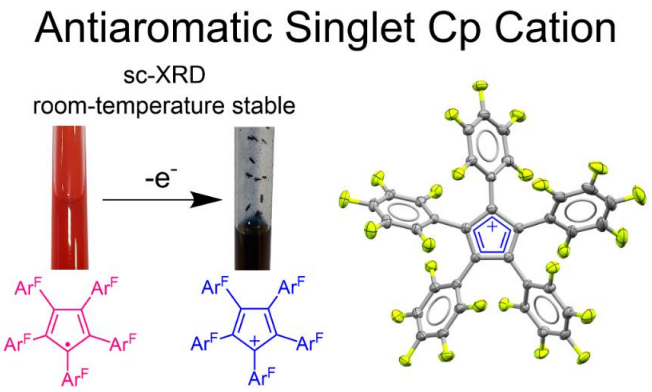


**Abstract**. **The singlet states of cyclopentadienyl (Cp) cations are considered as true prototypes of an antiaromatic system. Due to their high reactivity, their isolation in the solid state as a salt has so far failed. We present here the synthesis of the first room temperature-stable Cp cation salt $Cp(C_6F_5)_5Sb_3F_{16}$ ($1{\cdot}Sb_3F_{16}$) by single electron oxidation of the corresponding Cp radical $Cp(C_6F_5)_5{\cdot}$ (2) with either an excess of $XeF_2$ and $SbF_5{\cdot}SO_2$ or by hydroxide abstraction from $Cp(C_6F_5)_5OH$ (D) with $SbF_5{\cdot}SO_2$ in hexafluorobenzene. $1{\cdot}Sb_3F_{16}$ was characterized by sc-XRD, SQUID, UV-vis, and EPR spectroscopy. Although the aromatic triplet state of the $Cp(C_6F_5)_5$ cation 1 is energetically favored in the gas phase according to quantum chemical calculations, the coordination of the cation by either $Sb_3F_{16}^-$ ($1a{\cdot}Sb_3F_{16}$) or $C_6F_6$ ($1b{\cdot}Sb_3F_{16}$) in the crystal lattice stabilizes the antiaromatic singlet state, which is present in the solid state. The calculated hydride and fluoride ion affinities of 1 are higher than those of the tritylium cation $C(C_6F_5)_3^+$. In addition, results from reactions of $1{\cdot}Sb_3F_{16}$ with CO, which most likely yields the corresponding carbonyl complex, and 2 with selected model substrates ($Cp_2Fe$, $(Ph_3C{\cdot})_2$, and Cp*Al) are presented.**

Faraday's discovery of benzene was quickly recognized as "the most important chemical result of 1825".[1,2] At that time, the understanding of chemical structure was still in its infancy and more than 30 years passed before Kekulé's famous daydream in front of the fireplace in his dark apartment shed light on the bonding situation in this unique compound.[3,4,5] Nevertheless, the relative inertness and low enthalpy of the hydrogenation of benzene were difficult to explain in the 19th century. This became even more puzzling in 1911, when Willstätter prepared 1,3,5,7-cyclooctatetraene and showed that it reacted like an alkene, rendering the hypothesis that all cyclic conjugated polyenes would behave like aromatics implausible.[6] It was soon recognized that the exact number of π-electrons was important for the chemical behavior of these cyclic molecules,[7] but an explanation for this phenomenon was lacking until the seminal work of Hückel, who applied the rather new theory of quantum mechanics to the π electrons of cyclic alkenes.[8] He formulated what came to be known as “Hückel's rule” and explained why those systems with (4n+2) π electrons (n being a natural number) were particularly stable. At that time, only representatives with n = 1 like benzene and the cyclopentadienyl anion were known. The experimental evidence for cyclic π systems was greatly expanded in 1958 and 1960 by Breslow's cyclopropenyl cation[9,10] (n = 0) and Katz's cyclooctatetraene dianion[11] (n = 2), which were found to be stabilized by aromaticity, supporting Hückel's predictions. It is now textbook knowledge that planar, conjugated cycles with (4n + 2) π electrons are aromatic systems that exhibit high thermodynamic stability, tend to equalize bond lengths, and maintain their cyclic delocalization of electrons during a chemical reaction.

However, much more difficult to define and quantify is the concept of antiaromaticity, introduced by Breslow in the 1960s to describe the destabilization of planar, conjugated cycles with 4n π electrons.[12] In antiaromatic molecules, cyclic π conjugation has a destabilizing effect on the system. Accordingly, the system tries to avoid this destabilization by distortion and, therefore, antiaromatic systems often represent only transition states. Local minima on the potential hypersurface, *i.e*., molecules that may, in principle, be isolated, (only) partially retain their antiaromaticity and are unstable and highly reactive, making isolation an enormous challenge. Another obstacle in isolating antiaromatic systems with 4n π electrons is the fact that the triplet states of these systems are aromatic. Thus, in some cases, the (aromatic) triplet state is energetically lower than the (antiaromatic) singlet state, making isolation of the antiaromatic state almost impossible. Textbook examples of 4n π electron systems with antiaromatic character used to be the cyclopropenyl anion, the cyclobutadiene molecule, and the cyclopentadienyl cation. However, it has now been shown that the cyclopropenyl anion is a non-aromatic system[13] and the cyclobutadiene molecule should be considered as a maverick (and thus not antiaromatic).[14] This leaves only the cyclopentadienyl cation as a possible prototype of an antiaromatic system.

Unfortunately, the cyclopentadienyl cation ($C_5H_5^+$) is an unstable compound,[15] that has a triplet ground state as demonstrated by low temperature EPR[16] as is also true for substituted Cp cations such as $C_5Cl_5^+$.[17,18] According to Baird’s rule, “the lowest triplet state for 4n rings is aromatic since the bonding energy is significantly greater than for the diradical reference structure”.[19,20] Therefore, the ground states of $C_5H_5^+$ and $C_5Cl_5^+$ must be considered as aromatic and not antiaromatic. In contrast, the singlet ground state seems to be more favored for pentaaryl-substituted Cp cations although the singlet-triplet energy gap is very small.[21-24] They persist as long-lived species in solution due to the substantial delocalization of the positive charge (electronic effect) and steric shielding (kinetic effect).

To the best of our knowledge, Cp cations have not yet been structurally characterized by single-crystal X-ray diffraction (sc-XRD), as they are typically highly labile species,[12] *i.e*. according to the thermodynamic criteria for $C_5H_5^+$.[25-27] Only Cp cations with strongly electron-donating substituents are stable species,[28] but to the best of our knowledge, all attempts to isolate a crystalline salt of a Cp cation have so far failed due

to the occurrence of a number of side reactions (Scheme S42, electronic supplementary material), which led to the decomposition of the target molecules.[29-36] For example, heating a solution of the $C_5Me_5^+$ cation to room temperature yielded tetramethylpentafulvene by deprotonation,[36] whereas the $C_5Ph_5^+$ cation decomposed by C–H cleavage and formation of additional C–C bonds,[34] and the $C_5Cl_5^+$ and $C_5Br_5^+$ cations were found to dimerize.[35] In 2002, the structure of a stable $B(C_6F_5)_4$ salt of the pentamethylcyclopendadienyl cation ($C_5Me_5^+$) was reported,[29] however this was later shown to be the pentamethylcyclopentenyl cation.[30-33] More recently, the reaction of triplet tetrachlorocyclopentadienylidene with $BF_3$ in low-temperature noble gas matrices has been reported, yielding a zwitterion consisting of a positively charged antiaromatic singlet cyclopentadienyl cation and a negatively charged $BF_3$ unit (Scheme 1).[37]

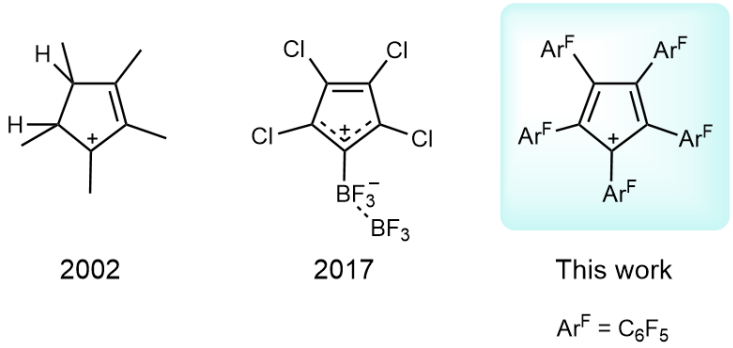


**Scheme 1**: The pentamethylcyclopentenyl cation that was first misidentified as the Cp* cation,[29-33] the cyclopentadienyl zwitterion obtained by Sander *et al.* in rare gas matrices,[37] and this work featuring a room temperature-stable and crystalline Cp cation.

In order to be able to isolate a stable cyclopentadienyl cation, a number of requirements for the substitution pattern of the Cp ring must be met: C-H bonds are potential weak points of possible decomposition reactions and should therefore be avoided. Furthermore, the substituents should be sterically demanding in order to suppress dimerization reactions. In 2014 Dutton *et al*. suggested in a computational study that electron-withdrawing substituents (*e.g*. $CF_3$ or $C_6F_5$) could be advantageous for the isolation of stable cyclopentadienyl cations since the cation would then be similar to the isoelectronic neutral borole.[38] As perfluoropentaphenylborole $BC_4(C_6F_5)_5$ is a stable (although highly reactive) compound,[39] $Cp(C_6F_5)_5^+$ seemed to be a worthwhile target even if the high electron deficiency would make the synthesis of this compound realistic only under strongly oxidizing or highly Lewis acidic conditions.

We report here the isolation of a room temperature-stable cyclopentadienyl cation containing five chemically very robust and bulky pentafluorophenyl substituents ($C_6F_5$) and its structural characterization by sc-XRD. Detailed quantum chemical studies revealed that these Cp cations adopt singlet ground states.

**Results and Discussion**

**Synthesis and Characterization of 1·$Sb_3F_{16}$ and 2. 1·$Sb_3F_{16}$** was synthesized in a 4-step reaction starting from commercially available bromopentafluorobenzene **A** *via* the formation of the known perfluorotolane **B**[40-41] and tetrakis(pentafluorophenyl)tetracyclone **C** (Scheme 2).[42] Temperature-controlled reaction of **C** with $C_6F_5MgBr$ gave pentakis(pentafluorophenyl)cyclopentadienole **D** in good yield (58 %).

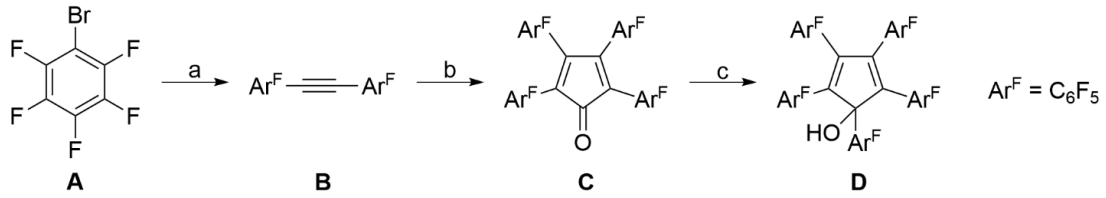


**Scheme 2**: Synthesis of pentakis(pentafluorophenyl)cyclopentadienole **D**. a) EtMgBr in thf/$Et_2O$ (*i*), diglyme, CuBr (*ii*), tribromoethylene, diglyme, 120 °C (*iii*); b) $Co_2(CO)_8$, decaline, 25 °C, then 190 °C (*i*), $I_2$ (ii); c) $C_6F_5MgBr$, thf, - 78 °C to 25 °C.

Our attempts to functionalize **D** were hindered by its remarkably low reactivity. We attribute this both to the appearance of the energetically unfavorable Cp cation intermediate **1** in nucleophilic substitution reactions and to the steric protection by the bulky $C_6F_5$ substituents. For example, **D** is stable to triflic anhydride in the presence/absence of strong bases (pyridine, 4-dimethylaminopyridine), to HBr in acetic acid and to $PCl_5$ at temperatures up to 110 °C in toluene, respectively. In marked contrast, **D** reacts under superacidic conditions with $SbF_5{\cdot}SO_2$ to form **1·Sb₃F₁₆** containing the desired Cp cation **1**, whereas the corresponding cyclopentadienyl radical **2** is formed in the reaction with the Friedel-Crafts-type superacid system $AlBr_3$/EtBr/benzene (Scheme 3). The high oxidation potential of **1·Sb₃F₁₆** requires the use of solvents resistant to these constraining conditions ($SO_2$, hexafluorobenzene). Oxidation of radical **2** with an excess of $XeF_2$ and $SbF_5{\cdot}SO_2$ in $C_6F_6$ also yielded **1·Sb₃F₁₆**, while reactions of **1·Sb₃F₁₆** with very weak reducing agents, *i.e*. alkanes, dichloromethane (DCM), difluorobenzene and even polypropylene syringes, yielded radical **2**.

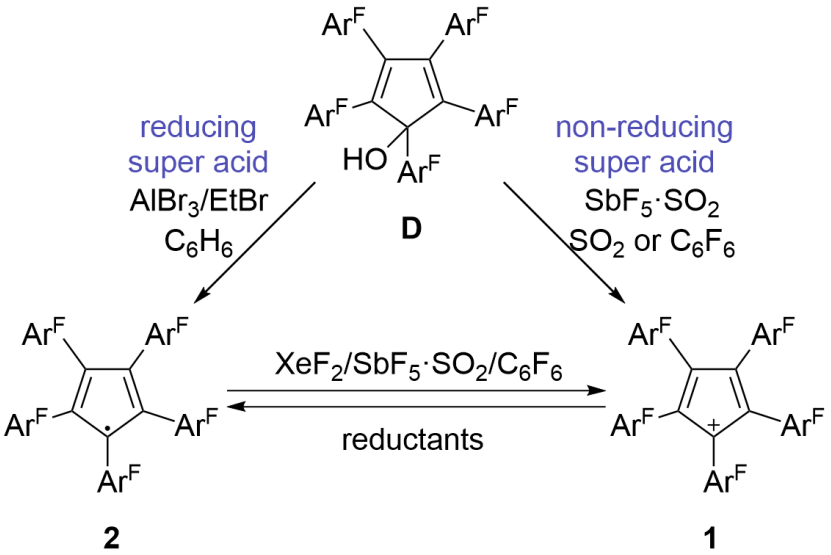


**Scheme 3**: Preparation of **1·Sb₃F₁₆** and radical **2** by reaction of alcohol **D** with reducing or non-reducing Lewis acids and their interconversion by oxidation or reduction.

The reaction of **D** with $SbF_5{\cdot}SO_2$ in $SO_2$ was monitored by *in situ* NMR spectroscopy, which showed the complete conversion of **D** (Figure S8). Alcohol **D**, **1·Sb₃F₁₆**, and radical **2** were also distinguished by UV-vis spectroscopy. While the pale yellow alcohol **D** shows no strong absorption in the visible region, **1·Sb₃F₁₆**

and **2** have absorption maxima at 977 nm and 546 nm, respectively (Figure S7). Solutions of **1·Sb₃F₁₆** and **2** in $SO_2$ and toluene, respectively, were also investigated by EPR spectroscopy. **2** gives a signal that is typical for a Cp radical with a g value of 2.0033 and a line width of 0.75 mT (Figure S11), while no EPR signal was detected for **1·Sb₃F₁₆**. A SQUID measurement on solid $Cp(C_6F_5)_5Sb_3F_{16}$·1.5 $C_6F_5$ also showed no evidence of paramagnetism. Cyclic voltammetry ($SO_2$, $NBu_4SbF_6$) showed that the interconversion of **2** and **1** occurs at an anodic peak potential of $E_{pa}$ = +2.30 V vs. ferrocene (Figure S9). This value is significantly higher than the anodic peak potential of the perfluorotritylium cation $C(C_6F_5)_3^+$ (+1.11 V vs. $Cp_2Fe$ in o-difluorobenzene).[43]

**Solid State Structures of 1·Sb₃F₁₆.** Crystallization of **1·Sb₃F₁₆** from a solution in hexafluorobenzene at 6 °C yielded two distinct solvates, $Cp(C_6F_5)_5Sb_3F_{16}$·1.5$C_6F_6$ (**1a·Sb₃F₁₆**) and $Cp(C_6F_5)_5Sb_3F_{16}$·2$C_6F_6$ (**1b·Sb₃F₁₆**, Figure 1).

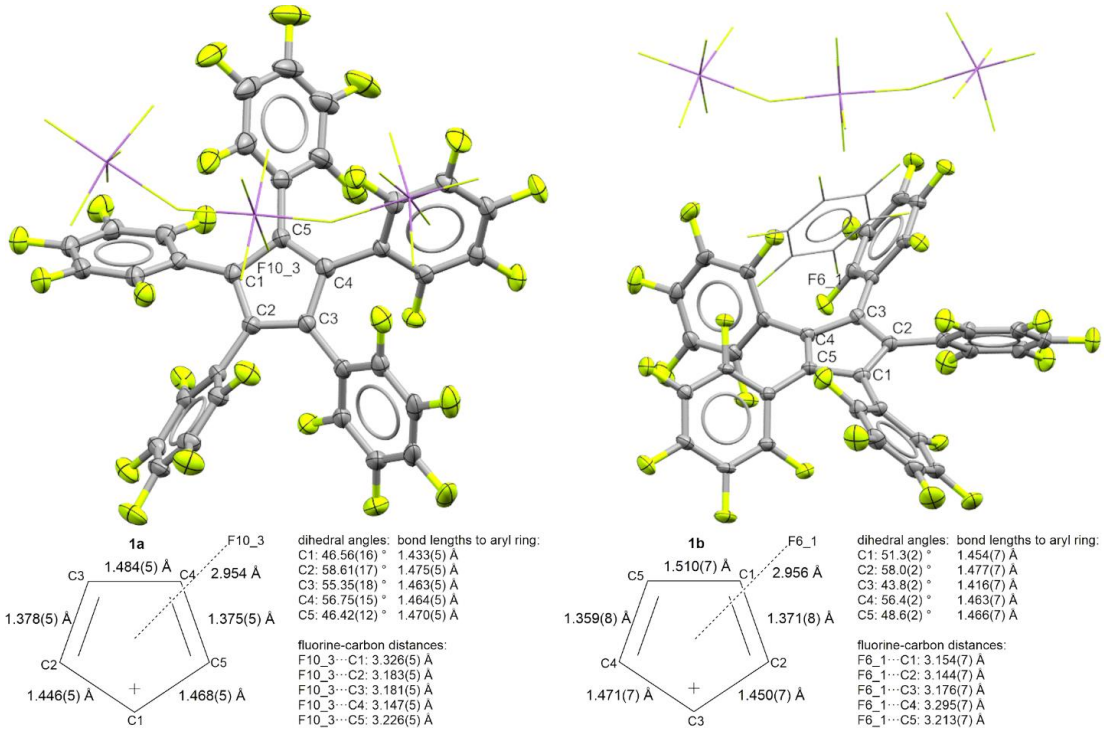


**Figure 1**. Molecular structures of **1a·Sb₃F₁₆** (left) and **1b·Sb₃F₁₆** (with counter anion, right), including selected bond lengths and dihedral angles between the Cp plane and the aryl groups (defined as best fit planes of the five Cp carbon atoms and six aryl carbon atoms). Anions and solvent molecules are depicted as wireframe models. Ellipsoids are drawn at a probability level of 50%. Non-participating solvent molecules are omitted for clarity.

Despite the intentionally low nucleophilicity of both the solvent ($C_6F_6$) and the counteranion ($Sb_3F_{16}^-$), the Cp cations in both structures show a weak interaction with a negatively polarized fluorine atom of the counter anion ($Cp(C_6F_5)_5Sb_3F_{16}$ **1a·Sb₃F₁₆** in $Cp(C_6F_5)_5Sb_3F_{16}$·1.5 $C_6F_6$) or the solvent ($Cp(C_6F_5)_5C_6F_6$ **1b·Sb₃F₁₆** in $Cp(C_6F_5)_5Sb_3F_{16}$·2 $C_6F_6$). The distances between the carbon atoms of the Cp ring and these fluorine atoms are in the same range as the sum of the van-der-Waals radii of carbon and fluorine (3.17 Å)[44]. The different solvates were distinguished by their crystal habit (**1a·Sb₃F₁₆** platelets, **1b·Sb₃F₁₆** needles), but

unfortunately, crystals of **1b·$Sb_3F_{16}$** suitable for a sc-XRD study were only obtained in a single experiment and the large size of the crystal resulted in uneven irradiation by the X-ray beam. The bond lengths and angles of **1a·$Sb_3F_{16}$** should therefore be considered more reliable than those of **1b·$Sb_3F_{16}$**. Both structures show a planar (rms deviation 0.018 Å) Cp cation. The C–C bond lengths of the central Cp rings show the characteristic bond length alternation that is expected for an antiaromatic singlet Cp cation (*vide infra*). The angles between the planes of the aryl groups bonded to a carbon atom with a higher calculated charge (C1, C3, C5; see 1a_singlett, Fig. S44) and the plane of the Cp ring are smaller and show a shorter aryl-Cp bond due to a better π-conjugation.

**Quantum Chemical Calculations.** For a better understanding of the electronic structures, we have calculated the key structures and energies of the singlet and triplet states of the cyclopentadienyl cation **1** using density functional theory (DFT) approaches. Geometry optimizations were performed using (U)B3LYP[45-46]-D3BJ[47] and (U)CAM-B3LYP[48]-D3BJ calculations, and the 6-31G(d), 6-311++G(d,p) and TZP basis sets were applied. In addition, the open-shell singlet states were calculated using UB3LYP-D3BJ/6-31G(d), UCAM-B3LYP-D3BJ/6-31G(d) and UB3LYP-D3BJ/6-311++G(d,p) with the "guess = mix" keyword. In all cases these calculations converged to the closed-shell states. Single-point calculations were performed with the double-hybrid method B2PLYP[49]-D3BJ and the TZ2P basis set. The S-T gaps calculated with B3LYP and CAM-B3LYP range from -5 to -6 kcal/mol (Table S3). That is, in agreement with calculations for other cyclopentadienyl cations, the triplet state is expected to be energetically more favored than the singlet state. Single-point calculations using the double-hybrid method B2PLYP-D3BJ also lead to the same result, although the S-T gap here is only -2.3 kcal/mol (Table S3).

**Discussion.** Comparing the calculated C–C bond lengths in the triplet state cyclopentadienyl cation **1**, almost identical bond lengths are found (1.431–1.434 Å for B3LYP-D3BJ/TZP; see Table S4), emphasizing the aromatic state of the triplet system. In marked contrast, the singlet state of cation **1**, shows a strong C–C bond length alternation (1.366–1.539 Å for B3LYP-D3BJ/TZP; see Table S4), as was also observed in the solid-state structures of the cyclopentadienyl cations **1a** (1.375–1.484 Å) and **1b** (1.359–1.510 Å) as determined by sc-XRD. Thus, the experimental results of the sc-XRD studies indicate that the cyclopentadienyl cations (**1a·$Sb_3F_{16}$** and **1b·$Sb_3F_{16}$**) in **1·$Sb_3F_{16}$** adopt singlet states in the solid state. A similar bond lengths alternation was observed in the isoelectronic perfluoropentaphenylborole (1.356–1.585 Å), which also has a singlet ground state.[39] In addition, EPR studies of **1·$Sb_3F_{16}$** gave no evidence for the presence of a triplet (radical) species under EPR conditions. In contrast, the singlet state is energetically less favorable than the triplet state according to quantum chemical calculations. A possible reason for these findings is that the counterions strongly influence the structure of the Cp cation in the solid: The negatively charged counterion localizes the positive charge on one carbon atom by spatial approach. The interaction of the anion with the differently positively polarized centers is then greater than the interaction of the anion with five equally positively polarized carbon atoms due to the shorter distance to one carbon atom. The calculated APT (atomic polar tensor) and NBO (natural bond orbitals) charges show that in the singlet cation there is a strong localization of the positive charge at C1, whereas in the triplet cation the charge is delocalized over the five carbon atoms (Figure S44). Accordingly, the approach of a negatively charged counterion can lead to an inversion of the S-T gap.

To verify this, the S-T gap of the **1·$SbF_6$** ion pair was also calculated using B2PLYP-D3BJ/TZ2P//B3LYP-D3BJ/TZP. Indeed, there is a preference, albeit very small, for the singlet state over the triplet state ($\Delta G$ = 0.36 kcal/mol; Table S3). In addition, single point calculations of **1a·$Sb_3F_{16}$** and **1b·$Sb_3F_{16}$** were performed using B2PLYP-D3BJ/TZ2P, with geometric data obtained from the X-ray structure analyses of **1a·$Sb_3F_{16}$** and

**1b·$Sb_3F_{16}$**. The obtained S-T gaps are 4.2 kcal/mol for **1a·$Sb_3F_{16}$** and 8.1 kcal/mol for **1b·$Sb_3F_{16}$**, showing that the singlet states are unambiguously present in the solid state.

The degree of (anti)aromaticity can also be evaluated using geometric criteria.[50] For example, the harmonic oscillator model of aromaticity (HOMA) index can be applied:[51,53]

$$HOMA = 1 - \frac{\alpha}{n}\sum_{i}^{n}(R_{opt} - R_i)^2$$

In this equation, $R_{opt}$ corresponds to the optimal bond length, which is assumed to be 1.388 Å for a C–C bond. $R_i$ represents an individual bond length; $n$ is the number of bonds included in the sum and $\alpha$ is an empirical constant (257.7 $Å^{-2}$).[52] For aromatic systems the HOMA equals 1 and for non-aromatic systems it is zero. Antiaromatic molecules usually have negative HOMA values. Inserting the calculated (B3LYP-D3BJ/TZP) values for **1**(S) and **1**(T) and the experimentally determined data for **1a** and **1b** into this equation gives the following result: HOMA(**1**(S)) = -0.69, HOMA(**1**(T)) = +0.49, HOMA(**1a**) = +0.01 and HOMA(**1b**) = -0.39. That is, while the triplet state of **1** should be aromatic, the singlet state of **1** and the cyclopentadienyl cation **1b** found in the solid state are anti-aromatic.

These findings are further supported by the application of another criterion of aromaticity, the nucleus independent chemical shift (NICS).[50,53] Negative NICS values indicate diatropic ring currents and aromaticity, positive values indicate paratropic ring currents and antiaromaticity, and values close to zero indicate a non-aromatic molecule. Therefore, the NICS values were calculated using CAM-B3LYP/def2-TZVP//CAM-B3LYP-D3BJ/6-311++G(d,p) along a line perpendicular from the center of the ring plane to 5 Å, with a step size of 0.1 Å for the singlet and triplet state of cyclopentadienyl cation **1** (Figure S43). In agreement with the HOMA values, the triplet state of cyclopentadienyl cation **1** is found to be aromatic, while the singlet state shows anti-aromatic behavior.

In order to quantify the Lewis acidity of $Cp(C_6F_5)_5^+$, its hydride (HIA) and fluoride ion affinities (FIA) were calculated. The resulting very high values of 1021 kJ/mol (HIA) and 771 kJ/mol (FIA) even exceed those of the recently isolated highly reactive perfluorotritylium cation $C(C_6F_5)_3^+$ (HIA: 955 kJ $mol^{-1}$; FIA: 697 kJ $mol^{-1}$),[43] rendering cyclopentadienyl cation **1** an extremely superacidic species. The FIA of $Cp(C_6F_5)_5^+$ also exceeds that of SbF5, explaining why $SbF_5$ (FIA: 496 kJ $mol^{-1}$)[54] must be used in excess for its synthesis.

***Reactivity Studies of 1·$Sb_3F_{16}$ and 2.*** In addition to their structural and spectroscopic characterization, we investigated the reactivity of **1·$Sb_3F_{16}$** and radical **2** in more detail. **1·$Sb_3F_{16}$** was found to react readily with the weak Lewis base carbon monoxide in $C_6F_6$ or $SO_2$, but unfortunately, we could not isolate a crystalline product. However, we propose the formation of the carbonyl complex **4** in analogy to the previously reported synthesis of an isoelectronic borole carbonyl complex, which was formed in the reaction of CO with the highly Lewis acidic perfluoropentaphenylborole.[55] The formation of **4** was indirectly confirmed by its reaction with water to the corresponding carboxylic acid **5**, which was identified by $^{19}F$ NMR spectroscopy and sc-XRD. **5** decarboxylates already under the hydrolysis conditions ($H_2O$, 25 °C) with formation of the novel pentakis(pentafluorophenyl)cyclopentadiene **6** (Scheme 4)

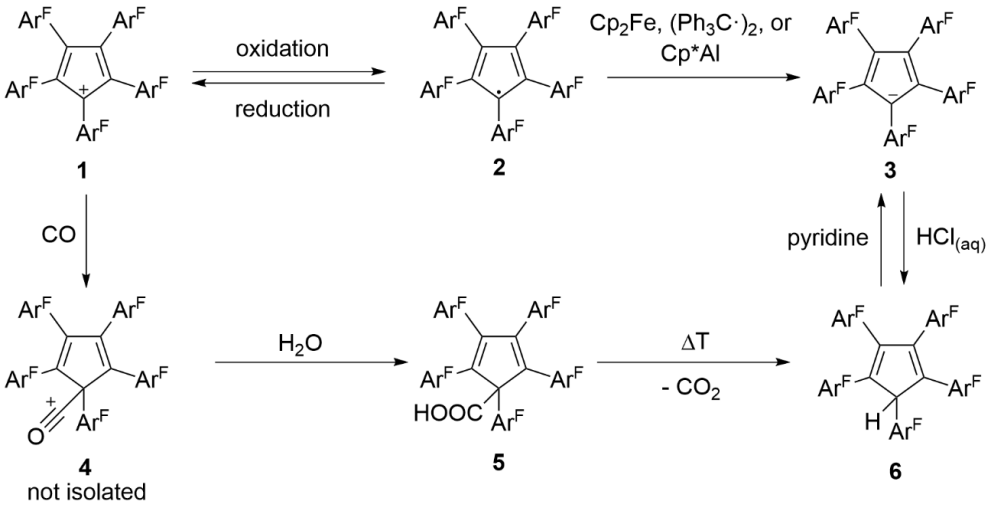


**Scheme 4**: Reactions of **1**·$Sb_3F_{16}$ and **2**.

Pentakis(pentafluorophenyl)cyclopentadienide **3**, the conjugated base of **6**, was proposed by Reed and Richardson as a "carbon-based weakly coordinating anion", but has not yet been prepared.[56] Compared to the more electron-deficient pentacyanocyclopentadiene[56] and pentakis(trifluoromethyl)-cyclopentadiene,[57,58] compound **6** is expected to be less acidic. However, its larger size and the presence of non-basic $C_6F_5$ side arms as well as its stability to polymerization and HF formation, make it nonetheless an interesting choice as a strong carbon acid, which forms a weakly coordinating anion (WCA). We have roughly estimated the $pK_a$ value of **6** by chemical means to be between -1 and 4.76,[59] because **3** is protonated by hydrochloric acid, but not by acetic acid, while **6** can be deprotonated with pyridine to give the pyridinium salt pyrH-**3**.

Another promising approach to the formation of salts of anion **3** is the direct reaction of radical **2** with reducing agents. To investigate the scope of this reaction, we performed cyclic voltammetry studies with **2** (o-difluorobenzene, $NBu_4B(Ph\text{-}3,5(CF_3)_2)_4$), which showed a reversible reduction to **3** at a half wave potential of 0.48 V *vs.* ferrocene. Thus, the oxidizing ability of **2** is in a synthetically useful range between $NO^+$ and $Cp_2Fe^+$.[60] "Innocent" oxidants, i.e. oxidants that produce no adverse byproducts, have recently gained increased interest because traditional one-electron oxidants such as $NO^+$ or $Ag^+$ can induce side reactions due to their Lewis acidity or participation in ligand exchange.[61] Therefore, **2** is a potentially good candidate for such a reagent and has the added advantage of not producing byproducts such as silver metal, NO, or ferrocene, thus avoiding separation difficulties, and reactions of **2** can be monitored visually due to its intense pink color. **2** is purified by sublimation and can be stored for several months even in contact with air and moisture and can be washed with water without significant decomposition (see synthetic details). To investigate its practical usefulness, we have reacted **2** with ferrocene, Gomberg's dimer $(Ph_3C\cdot)_2$, and Cp*Al (Scheme 4), in all cases yielding the respective salts of anion **3** ($FeCp_2$ **3** (**3a**), $Ph_3C$ **3** (**3b**), $(Cp^*)_2Al$ **3** (**3c**)) in single-crystalline and pure form. The molecular structures of **3a-c** have been determined by sc-XRD. They show the expected nearly symmetrical Cp rings with C–C bond lengths ranging from 1.405 Å to 1.415 Å (Table S1). The cations are located near the negatively charged Cp ring with shortest Cp(centroid)-H distances of 2.546 Å, 2.683 Å, and 3.131 Å, respectively (Table S1, Figures S37-39).

**Conclusion.** The synthesis and structural characterization (sc-XRD) of **1·$Sb_3F_{16}$** containing the first room-temperature stable cyclopentadienyl cation **1** is reported. sc-XRD, EPR, and SQUID studies prove that **1** adopts the singlet state in the solid state, which is stabilized most likely due to weak intermolecular contacts with solvent or anion molecules. In contrast, the triplet ground state is energetically favored in the gas phase according to quantum chemical calculations. **1·$Sb_3F_{16}$** shows a high oxidation potential and a very high Lewis acidity. In addition, it reacts readily to the corresponding radical **2**, while the reaction with CO and hydrolytic work-up finally afforded the corresponding pentakis(pentafluorophenyl)cyclopentadiene **6**. The unprecedented access to Cp anions with five $C_6F_5$ substituents could also enable the preparation of perfluorinated metal complexes in the future and thus provide new impulses in the hitherto poorly explored field of coordination chemistry with fluorinated Cp ligands.[62]

**Methods & Protocols**

Manipulations were performed under a dry, oxygen-free argon atmosphere, with anhydrous solvents, using cannula and glove-box techniques. **1·$Sb_3F_{16}$** was synthesized by the reaction of pentakis(pentafluorophenyl)cyclopentadienole **D** with $SbF_5{\cdot}SO_2$ under superacidic conditions, while the reaction of **D** with the Friedel-Crafts-type superacid system $AlBr_3$/EtBr/benzene afforded the corresponding radical **2** in a single step. Oxidation of radical **2** with an excess of $XeF_2$ and $SbF_5$ in $C_6F_6$ also gave the cyclopentadienyl cation **1**, while reactions of **1** with very weak reducing agents gave radical **2**. Hydrolysis of the product obtained from the reaction of **1·$Sb_3F_{16}$** with carbon monoxide gave the carboxylic acid **5**, which decarboxylates to form pentaphenylcyclopentadiene **6**. The products were characterized by multinuclear NMR (**D**, **3a-d**, **5**, **6**), IR (**D**, **2**, **3a-d**, **5**, **6**), and UV-Vis spectroscopy (**D**, **1**, **2**), and sc-XRD (**B**, **1**, **2**, **3a-c**, **5**, **6**) and details are given in the electronic supplementary material.

**Data availability**

All data generated or analyzed during this study are included in this published article (and its supplementary information files). The structures of **B**, **1a-b**, **2a-b**, **3a-c**, **5**, and **6** in the solid state were determined by single-crystal X-ray diffraction and the crystallographic data have been deposited with the Cambridge Crystallographic Data Centre as supplementary publication nos. CCDC-2246848 (ys_712a, **1a**), -2246849 (ys_712, **1b**), -2246850 (ys_631a_tw4, **2a**), -2246851 (ys_681, **2b**), -2246852 (ys_679a, **3a**), -2246853 (ys_682am_sq, **3b**), -2246854 (ys_695c, **3c**), -2246857 (ys_719m_sq, **5**), -2246858 (ys_705, **6**), -2246859 (ys_584, **B**), and -2246860 (ys_586 hexakis(pentafluorophenyl)benzene). Copies of the data can be obtained free of charge on application to CCDC, 12 Union Road, Cambridge, CB21EZ (fax: (+44) 1223/336033; e-mail: deposit@ccdc.cam-ak.uk).

**Code Availability**

DFT and double-hybrid DFT methods, as implemented in the quantum chemistry program packages Gaussian16 Amsterdam Density Functional (ADF), were employed to calculate molecular geometries, orbital energies, charges, NBOs and NICS values. All data generated or analyzed are included in the supplementary information file.

**References**

1. Faraday M. XX. On new compounds of carbon and hydrogen, and on certain other products obtained during the decomposition of oil by heat. *Phil. Trans. R. Soc.* **115**, 440-466; 10.1098/rstl.1825.0022 (1825).

2. Kaiser, R. “Bicarburet of Hydrogen”. Reappraisal of the Discovery of Benzene in 1825 with the Analytical Methods of 1968. *Angew. Chem. Int. Ed. Engl.* **7**, 345-350; 10.1002/anie.196803451 (1968).
3. Kekulé, A. Ueber die s. g. gepaarten Verbindungen und die Theorie der mehratomigen Radicale. *Justus Liebigs Ann. Chem.* **104**, 129–150; 10.1002/jlac.18571040202 (1857).
4. Kekulé, A. Ueber die Constitution und die Metamorphosen der chemischen Verbindungen und über die chemische Natur des Kohlenstoffs. *Justus Liebigs Ann. Chem.* **106**, 129–159; 10.1002/jlac.18581060202 (1858).
5. Schultz, G. Feier der Deutschen Chemischen Gesellschaft zu Ehren August Kekulé's. *Ber. Dtsch. Chem. Ges.* **23**, 1265–1312; 10.1002/cber.189002301204 (1890).
6. Willstätter, R. & Waser, E. Über Cyclooctatetraen. *Ber. Dtsch. Chem. Ges.* **44**, 3423–3445; 10.1002/cber.191104403216 (1911).
7. Balaban, A. T., Schleyer, P. v. R. & Rzepa, H. S. Crocker, not Armit and Robinson, begat the six aromatic electrons. *Chem. Rev.* **105**, 3436–3447; 10.1021/cr0300946 (2005).
8. Hückel, E. Quantentheoretische Beiträge zum Benzolproblem. *Z. Physik* **70**, 204–286; 10.1007/BF01339530 (1931).
9. Breslow, R. & Yuan, C. The sym-Triphenylcyclopropenyl Cation, a Novel Aromatic System. *J. Am. Chem. Soc.* **80**, 5991–5994; 10.1021/ja01555a026 (1958).
10. Breslow, R., Groves, J. T. & Ryan, G. Cyclopropenyl cation. *J. Am. Chem. Soc.* **89**, 5048; 10.1021/ja00995a042 (1967).
11. Katz, T. J. The Cycloöctatetraenyl Dianion. *J. Am. Chem. Soc.* **82**, 3784–3785; 10.1021/ja01499a077 (1960).
12. Breslow, R. Novel aromatic and antiaromatic systems. *Chem. Rec.* **14**, 1174-1182; 10.1002/tcr.201402070 (2014).
13. Kass, S. R. Cyclopropenyl Anion: An Energetically Nonaromatic Ion. *J. Org. Chem.* **78**, 7370-7372; (10.1021/jo401350m) (2013).
14. Wu, J. I. C., Mo, Y., Evangelista, F. A. & Schleyer, P. v. R. Is cyclobutadiene really highly destabilized by antiaromaticity? *Chem. Commun.* **48**, 8437-8439; (10.1039/C2CC33521B) (2012).
15. Breslow, R. & Hoffman, J. M. Antiaromaticity in the parent cyclopentadienyl cation. Reaction of 5-iodocyclopentadiene with silver ion. *J. Am. Chem. Soc.* **94**, 2110–2111; 10.1021/ja00761a051 (1972).
16. Saunders, M. *et al.* Unsubstituted cyclopentadienyl cation, a ground-state triplet. *J. Am. Chem. Soc.* **95**, 3017–3018; 10.1021/ja00790a049 (1973).
17. Breslow, R., Hill, R. & Wasserman, E. Pentachlorocyclopentadienyl Cation, a Ground-State Triplet. *J. Am. Chem. Soc.* **86**, 5349–5350; 10.1021/ja01077a072 (1964).
18. Vančik, H., Novak, I. & Kidemet, D. IR Matrix Spectroscopy of Pentachlorocyclopentadienyl Cation $C_5Cl_5^+$. Effect of Chlorine as a Substituent. *J. Phys. Chem. A* **101**, 1523–1525; 10.1021/jp961610h (1997).
19. Baird, N. C. Quantum organic photochemistry. II. Resonance and aromaticity in the lowest 3.pi.pi.* state of cyclic hydrocarbons. *J. Am. Chem. Soc.* **94**, 4941–4948; 10.1021/ja00769a025 (1972).
20. Karas, L. J. & Wu, J. I. Baird’s rules at the tipping point. *Nat. Chem.* **14**, 723–725; 10.1038/s41557-022-00988-z (2022).
21. Yager, W. A. A Stable Triplet State of Pentaphenylcyclopentadienyl Cation. *J. Am. Chem. Soc.* **85**, 2033–2034; 10.1021/ja00896a042 (1963).
22. Breslow, R., Chang, H. W., Hill, R. & Wasserman, E. Stable Triplet States of Some Cyclopentadienyl Cations. *J. Am. Chem. Soc.* **89**, 1112–1119; 10.1021/ja00981a015 (1967).

23. Broser, W., Siegle, P. & Kurreck, H. Über substituierte Pentaphenyl-cyclopentadienyl-Verbindungen und Tetracyclone, IV Unsymmetrischp-methyl- und *p*-phenyl-substituierte Pentaphenyl-cyclopentadienyl-Kationen und -Radikale. *Chem. Ber.* **101**, 69-83; 10.1002/cber.19681010111 (1968).
24. Broser, W., Kurreck, H. & Siegle, P. Über substituierte Pentaphenylcyclopentadienyl-Verbindungen und Tetracyclone, III. Symmetrische Cyclopentadienyl-Kationen mit nachweisbaren Triplettzuständen. *Chem. Ber.* **100**, 788-794; 10.1002/cber.19671000312 (1967).
25. Breslow, R. & Mazur, S. Electrochemical determination of $pK_{R^+}$ for some antiaromatic cyclopentadienyl cations. *J. Am. Chem. Soc.* **95**, 584–585; 10.1021/ja00783a046 (1973).
26. Breslow, R. Quantitative studies on aromaticity and antiaromaticity. *Pure Appl. Chem.* **28**, 111–130; 10.1351/pac197128020111 (1971).
27. Lossing, F. P. & Traeger, J. C. Stabilization in cyclopentadienyl, cyclopentenyl, and cyclopentyl cations. *J. Am. Chem. Soc.* **97**, 1579–1580; 10.1021/ja00839a053 (1975).
28. Gompper, R. & Glöckner, H. Stable Cyclopentadienylium Salts. *Angew. Chem. Int. Ed. Engl.* **23**, 53–54; 10.1002/anie.198400532 (1984).
29. Lambert, J. B., Lin, L. & Rassolov, V. The Stable Pentamethylcyclopentadienyl Cation. *Angew. Chem. Int. Ed. Engl.* **41**, 1429-1431; 10.1002/1521-3773(20020415)41:8<1429::AID-ANIE1429>3.0.CO;2-J (2002).
30. Otto, M. *et al.* The Stable Pentamethylcyclopentadienyl Cation Remains Unknown. *Angew. Chem. Int. Ed. Engl.* **41**, 2275; 10.1002/1521-3773(20020703)41:13<2275::AID-ANIE2275>3.0.CO;2-1 (2002).
31. Jones, J. N., Cowley, A. H. & Macdonald, C. L. B. The crystal structure of the 'pentamethylcyclopentadienyl cation' is that of the pentamethylcyclopentenyl cation. *Chem. Commun.,* 1520–1521; 10.1039/b205081a (2002).
32. Müller, T. Comment on the X-Ray Structure of Pentamethylcyclopentadienyl Cation. *Angew. Chem. Int. Ed. Engl.* **41**, 2276–2278; 10.1002/1521-3773(20020703)41:13<2276::AID-ANIE2276>3.0.CO;2-W (2002).
33. Lambert, J. B. Statement. *Angew. Chem. Int. Ed. Engl.* **41**, 2278; 10.1002/1521-3773(20020703)41:13<2278::AID-ANIE2278>3.0.CO;2-K (2002).
34. Breslow, R. & Chang, H. W. The Rearrangement of the Pentaphenylcyclopentadienyl Cation. *J. Am. Chem. Soc.* **83**, 3727-3728; 10.1021/ja01478a046 (1961).
35. Rupf, S. M., Pröhm, P. & Malischewski, M. The 2+2 cycloaddition product of perhalogenated cyclopentadienyl cations: structural characterization of salts of the $C_{10}Cl_{10}^{2+}$ and $C_{10}Br_{10}^{2+}$ dications. *Chem. Commun.* **56**, 9834-9837; 10.1039/d0cc04226a (2020).
36. Jutzi, P. & Mix, A. Synthesen mit dem Reagenz Pentamethylcyclopentadienylbromid/Silbertetrafluoroborat: Das Pentamethylcyclopentadienyl-Kation als reaktive Zwischenstufe. *Chem. Ber.* **125**, 951–954; 10.1002/cber.19921250429 (1992).
37. Costa, P., Trosien, I., Mieres-Perez, J. & Sander, W. Isolation of an Antiaromatic Singlet Cyclopentadienyl Zwitterion. *J. Am. Chem. Soc.* **139**, 13024-13030; 10.1021/jacs.7b05807 (2017).
38. Kalon J. Iversen, David J. D. Wilson & Jason L. Dutton. A Computational Study on a Strategy for Isolating a Stable Cyclopentadienyl Cation. *Chem. Eur. J.* **20**, 14132–14138; 10.1002/chem.201403748 (2014).
39. Fan, C., Piers, W. E. & Parvez, M. Perfluoropentaphenylborole. *Angew. Chem. Int. Ed. Engl.* **48**, 2955–2958; 10.1002/anie.200805865 (2009).
40. Webb, A. F. & Gilman, H. Reactions of some perhaloarenes with metals and metal halides. *J. Organomet. Chem.* **20**, 281–283; 10.1016/S0022-328X(00)80121-7 (1969).
41. Cairncross, A., Sheppard, W. A. & Wonchoba, E. Pentafluorophenylcopper tetramer, a reagent for synthesis of fluorinated aromatic compounds. *Org. Synth.* **59**, 122; 10.15227/orgsyn.059.0122 (1979).

42. Birchall, J. M., Bowden, F. L., Haszeldine, R. N. & Lever, A. B. P. Polyfluoroarenes. Part IX. Decafluorotolan: synthesis, properties, and use as an organometallic ligand. *J. Chem. Soc., A,* 747; 10.1039/j19670000747 (1967).
43. Hoffmann, K. F. *et al.* The Tris(pentafluorophenyl)methylium Cation: Isolation and Reactivity. *Angew. Chem. Int. Ed. Engl.* **61**, e202203777; 10.1002/anie.202203777 (2022).
44. Bondi, A. van der Waals Volumes and Radii. *J. Phys. Chem.* **68**, 441–451; 10.1021/j100785a001 (1964).
45. Becke, A. D. Density-functional exchange-energy approximation with correct asymptotic behavior. *Phys. Rev. A* **38**, 3098–3100; 10.1103/physreva.38.3098 (1988).
46. Lee, C., Yang, W. & Parr, R. G. Development of the Colle-Salvetti correlation-energy formula into a functional of the electron density. *Phys. Rev. B* **37**, 785–789; 10.1103/physrevb.37.785 (1988).
47. Grimme, S., Ehrlich, S. & Goerigk, L. Effect of the damping function in dispersion corrected density functional theory. *J. Comp. Chem.* **32**, 1456–1465; 10.1002/jcc.21759 (2011).
48. Yanai, T., Tew, D. P. & Handy, N. C. A new hybrid exchange–correlation functional using the Coulomb-attenuating method (CAM-B3LYP). *Chem. Phys. Lett.* **393**, 51–57; 10.1016/j.cplett.2004.06.011 (2004).
49. Grimme, S. Semiempirical hybrid density functional with perturbative second-order correlation. *J. Chem. Phys.* **124**, 34108; 10.1063/1.2148954 (2006).
50. Gleiter, R. & Haberhauer, G. *Aromaticity and Other Conjugation Effects*. (Wiley-VCH, 2012).
51. Julg, A. & Franois, P. Recherches sur la géomtrie de quelques hydrocarbures non-alternants: son influence sur les énergies de transition, une nouvelle définition de l'aromaticité. *Theoret. Chim. Acta* **8**, 249–259; 10.1007/BF00527311 (1967).
52. Krygowski, T. M. & Cyrański, M. Separation of the energetic and geometric contributions to the aromaticity of π-electron carbocyclics. *Tetrahedron* **52**, 1713–1722; 10.1016/0040-4020(95)01007-6 (1996).
53. Chen, Z., Wannere, C. S., Corminboeuf, C., Puchta, R. & Schleyer, P. v. R. Nucleus-independent chemical shifts (NICS) as an aromaticity criterion. *Chem. Rev.* **105**, 3842–3888; 10.1021/cr030088 (2005).
54. Erdmann, P., Leitner, J., Schwarz, J. & Greb, L. An Extensive Set of Accurate Fluoride Ion Affinities for p-Block Element Lewis Acids and Basic Design Principles for Strong Fluoride Ion Acceptors. *Chemphyschem* **21**, 987–994; 10.1002/cphc.202000244 (2020).
55. Fukazawa, A. *et al.* Reaction of pentaarylboroles with carbon monoxide: an isolable organoboron carbonyl complex. *Chem. Sci.* **3**, 1814; 10.1039/c2sc20336g (2012).
56. Richardson, C. & Reed, C. A. Exploration of the pentacyano-cyclo-pentadienide ion, C(5)(CN)(5)(-), as a weakly coordinating anion and potential superacid conjugate base. Silylation and protonation. *Chem. Commun.* 706-707; 10.1039/b316122f (2004).
57. Sievers, R., Sellin, M., Rupf, S. M., Parche, J. & Malischewski, M. Introducing the Perfluorinated Cp* Ligand into Coordination Chemistry. *Angew. Chem. Int. Ed. Engl.* **61**, e202211147; 10.1002/anie.202211147 (2022).
58. Laganis, E. D. & Lemal, D. M. 5H-(Perfluoropentamethyl)cyclopentadiene, an extraordinary carbon acid. *J. Am. Chem. Soc.* **102**, 6633–6634; 10.1021/ja00541a075 (1980).
59. Goldberg, R. N., Kishore, N. & Lennen, R. M. Thermodynamic Quantities for the Ionization Reactions of Buffers. *J. Phys. Chem. Ref. Data* **31**, 231-370; 10.1063/1.1416902 (2002).
60. Connelly, N. G. & Geiger, W. E. Chemical Redox Agents for Organometallic Chemistry. *Chem. Rev.* **96**, 877–910; 10.1021/cr940053x (1996).
61. Schorpp, M. *et al.* Synthesis and Application of a Perfluorinated Ammoniumyl Radical Cation as a Very Strong Deelectronator. *Angew. Chem. Int. Ed. Engl.* **59**, 9453-9459; 10.1002/anie.202002768 (2020).

62. Sievers, R., Parche, J., Kub, N. G. & Malischewski, M. Synthesis and Coordination Chemistry of Fluorinated Cyclopentadienyl Ligands. *Synlett*; 10.1055/s-0042-1751426 (2023).

## Acknowledgements

The University of Duisburg-Essen is acknowledged for generous financial support. We thank B. Geoghegan and G. E. Cutsail III (MPI CEC, Mülheim an der Ruhr, Germany), for EPR and SQUID measurements, M. Weinert for CV studies, and T. Schaller, F. Niemeyer, and B. Römer (University of Duisburg-Essen) for NMR measurements. M.M and S.M.R. thank the Deutsche Forschungsgemeinschaft (DFG, German Research Foundation) for financial support (project ID 387284271, SFB 1349).

## Author contributions

Y. Schulte: Conceptualization, Investigation, Validation, Formal Analysis, Writing - Original Draft, Visualization. C. Wölper: Single Crystal X-ray Analysis. S. M. Rupf / M. Malischewski: cyclic voltammetry studies in liquid $SO_2$. G. Haberhauer: Writing – Original Draft – Review and Editing, Visualization, performing calculations. S. Schulz: Conceptualization, Writing – Original Draft – Review and Editing, Visualization, Supervision, Project administration.

## Additional Information

Supplementary information (general experimental procedures, experimental details synthesis and characterization, quantum chemical details) is available in the online version of the paper. Reprints and permissions information is available online at www.nature.com/reprints.

## Competing financial interests

The authors declare no competing financial interests.

# 4 Conclusion and Outlook

## 4.1 Conclusion

The first part of this thesis was focused on the development of synthetic protocols to novel acceptor-substituted perfunctionalized ferrocenes (Figure 17). For this purpose, the reactivity of ferrocene towards mercury(II) carboxylates was investigated by modern spectroscopic techniques. A convenient one-pot, multi-gram synthesis to afford the pure permetalated product, $[FeC_{10}(HgO_2CC_3H_7)_{10}]$, was developed by use of mercury(II) butyrate instead of $Hg(OAc)_2$ due to increased solubility of the polymercurated intermediates in organic solvents (Figure 17, left box). This improved synthetic methodology for the simple preparation of a permercurated ferrocene enabled the first X-ray structures of permetalated aromatic compounds as well as the investigation of their follow-up chemistry.

In the permercurated metallocene $[FeC_{10}(HgO_2CC_3H_7)_{10}]$, the Hg-C bonds were found to resist oxygen, moisture and even strong Brønsted acids like trifluoroacetic acid ($CF_3CO_2H$) and pentafluoropyridinium hexafluoroantimonate ($[C_5F_5NH][SbF_6]$). Instead of metal carbon bond cleavage, the complete protonation followed by displacement of the butyrate groups was observed, allowing the introduction of weakly coordinating anions and further leading to the formation of highly charged cations. The coordinating behavior of the corresponding compounds, $[FeC_{10}(HgO_2CCF_3)_{10}]$ and $[FeC_{10}Hg_{10}(C_5F_5N)_n][SbF_6]_{10}$, towards anionic and neutral ligands were subject of study. Here, the Lewis acidity of the Hg-sites was tuned by variation of the counter anions. In $[FeC_{10}(HgO_2CCF_3)_{10}]$ the trifluoroacetate anion is not fully displaced by the strongly $\sigma$-donating ligand 4-(dimethylamino)pyridine (dmap), however, weakly coordinating anions such as $[SbF_6]^-$ can be displaced by significantly weaker bases such as acetonitrile or tetrahydrothiophene under formation of $[FeC_{10}(HgL)_{10}][SbF_6]_{10}$ (L = MeCN, THT).

All investigated (soluble) permercurated ferrocenes reveal (quasi)reversible one-electron oxidations. Here, the combination of neutral ligands with weakly coordinating anions increased the overall withdrawing character of the corresponding Cp ligands, resulting in increased electrochemical potentials of the metallocenes. The compound $[FeC_{10}Hg_{10}(C_5F_5N)_n]^{11+}$ was determined to be the strongest oxidizing agent in the series of isolated permercurated ferrocenes with an estimated potential of $E_{1/2} > 1\,V$ vs. ferrocene. Generally, the observed electrochemical potentials of the permercurated derivatives varied considerably (Figure 18). The corresponding ferrocenium cations $[FeC_{10}(HgL)_{10}]^{11+}$ (L = $C_5F_5N$, MeCN, THT) were isolated and characterized.

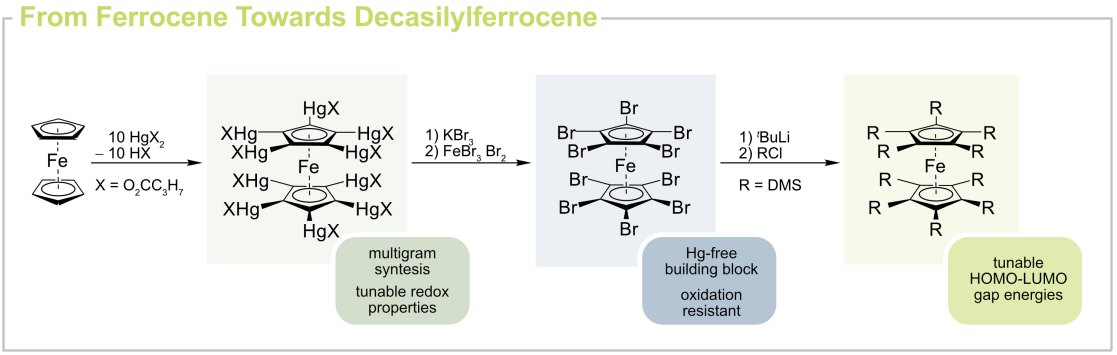


**Figure 17.** Reaction sequence towards permercurated, perbrominated and persilylated metallocenes starting from ferrocene.

The crystallographic characterization of the permercurated ferrocene derivatives $[FeC_{10}(HgX)_{10}]$ (X = Cl, $O_2CCF_3$, $O_2CCCl_3$), $[FeC_{10}(HgL)_{10}]^{10+}$ (L = dmap, THT) and $[FeC_{10}(HgMeCN)_{10}]^{11+}$ was realized by single-crystal XRD. In the permercurated ferrocenes with carboxylate or chloride ligands, the Hg(II) centers were linearly coordinated by a Cp carbon atom and the substituent. Intermolecular mercurophilic interactions, evident from the formation of polymeric chains in the solid-state, rendered the ferrocene compounds $[FeC_{10}(HgX)_{10}]$ (X = Cl, F) insoluble. In contrast, in the structures of the polycationic compounds no mercurophilic interactions were observed probably due to electrostatic reasons. Here, the coordination sphere of the Hg atoms was saturated by organic neutral ligands and solvent molecules, leading to an overall net charge of 10+ or 11+ (depending on the iron oxidation state). Nevertheless, the influence of the (neutral or anionic) ligands at the Hg(II) centers on its ability to form mercurophilic contacts is not fully understood and requires further investigation. In this context, sterical factors, polarizabilities of the Hg-X or Hg-L bonds as well as Coulomb repulsion of oligomeric fragments have to be considered.

In addition, the C-Hg moiety is useful for further functionalization, giving access to a variety of tenfold functionalized ferrocenes. In this work, the reactivity towards brominating agents was investigated (Figure 17, center). It was demonstrated that the literature known synthetic way to decabromoferrocene by reaction of $[FeC_{10}(HgOAc)_{10}]$ with $K[Br_3]$ does not yield the clean product but a mixture of polybrominated ferrocenes. Complete halogenation was realized by a two-step reaction of $[FeC_{10}(HgO_2CC_3H_7)_{10}]$ with $K[Br_3]$ followed by reaction with $FeBr_3$ and elemental bromine. Oxidation to the corresponding decabromoferrocenium salt was achieved by reaction with $AsF_5$. The electrochemical and structural properties of $[FeC_{10}Br_{10}]$ were compared to other polybrominated ferrocenes $[FeC_{10}Br_nH_{10-n}]$ ($n$ = 1, 2, 5, 9) and $[FeC_{10}Br_9(HgBr)]$. The findings contribute to recent debates about polyhalogenation effects by the groups of Butler, Long and Low. It was confirmed that the increase in redox potentials behaves non-linearly with the degree of halogenation, indicating synergistic effects. Here, a possible resonance stabilization was implied by a systematic shortening of all C-Br bonds as

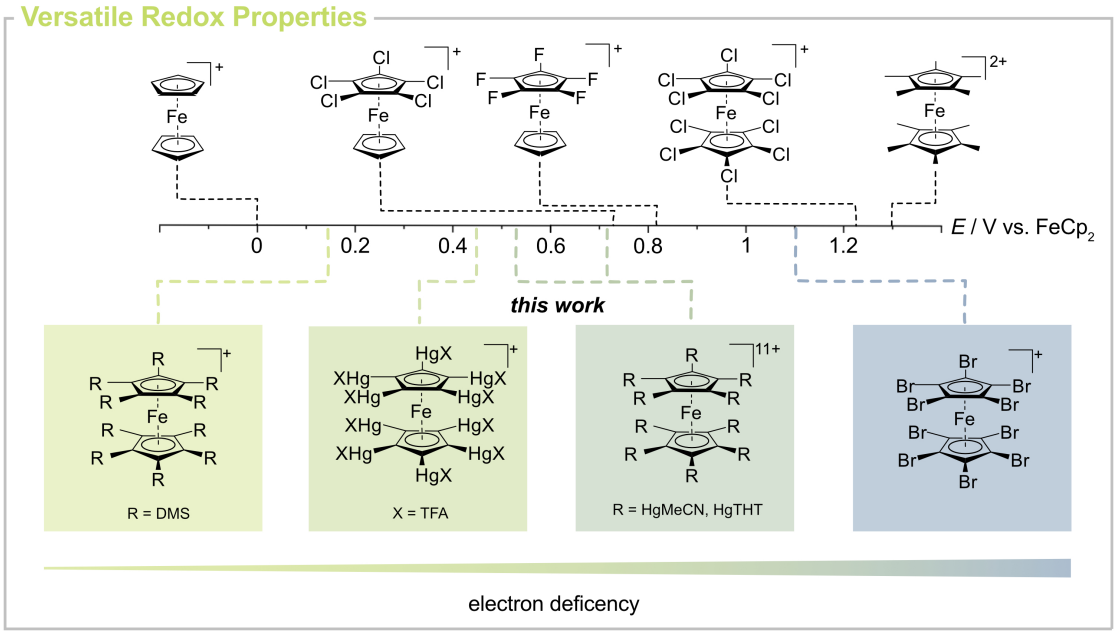


**Figure 18.** Ranking of electrochemical potentials of literature-known acceptor-substituted ferrocene derivatives bearing a perfunctionalized Cp ligand.

well as decreased intermolecular halogen bond contacts upon oxidation. However, the influence of resonance effects and halogen bonding interactions on the oxidation potentials requires further investigations. In the series of polybrominated ferrocenes the $[FeC_{10}Br_{10}]^+$ is a potent one-electron oxidizer with a redox potential of $\Delta E_{1/2}$ = 1.1 V and the strongest ferrocenium-based oxidant that has been isolated so far. The reported crystal structures of the perbrominated ferrocene and ferrocenium are the first examples of perhalogenated ferrocenes.

The perbrominated ferrocene itself is a versatile starting material for other perfunctionalization reactions such as cross-coupling, halogen-metal exchange or Grignard reactions. In this work, the permetalation *via* bromine-lithium exchange as well as under Grignard conditions was investigated. However, subsequent quenching experiments with DMSCl suggested only partial metalation. Using a cascade of multiple metalation-silylation iterations, allowed the first synthesis and structural characterization of a persilylated metallocene $[FeC_{10}DMS_{10}]$ (Figure 17, right box). Furthermore, a series of polysilylated metallocenes $[FeC_{10}DMS_nH_{10-n}]$ ($n$ = 7, 8, 9, 10) was investigated in terms of systematic silylation effects. Here, UV/VIS spectroscopy as well as electrochemical and DFT methods were used to show that the introduction of silyl groups only marginally affected the HOMO energies while the metallocenes' LUMO energies were successively decreased. In the UV/VIS spectra, the intensities of the observed bands associated with the d-d-transitions are highly sensitive towards silylation. This finding was explained by conformational distortions due to the steric overcrowding on the Cp ligand (for tetra- and pentasubstituted Cp ligands).

In the last part of this thesis, the reactivity of perhalogenated Cp compounds towards strong Lewis acids was investigated. Here, the combination of electron deficient groups with the absence of (aromatic) protons was expected to yield a sufficient stabilization of the elusive Cp cation. In order to obtain $[C_5Cl_5]^+$ and $[C_5Br_5]^+$, the reactions of $C_5X_6$ (X = Cl, Br) with the highly reactive Lewis acids $SbF_5$ and $AsF_5$ were studied. However, instead of the desired monocations, salts containing the unprecedented dications $[C_{10}X_{10}]^{2+}$ were isolated. These thermally unstable dications were characterized by single crystal XRD and NMR spectroscopy. Here it should be mentioned that structures of highly electrophilic organic intermediates, especially perhalogenated ones, have only been rarely investigated *via* single-crystal XRD so far. The crystal structures revealed large differences in C-Cl and C-Br bond lengths demonstrating the $\pi$-donor ability of the halogen atoms. The differences in the C-X bonds were rationalized by calculations of the NPA charges, showing higher positive charges on halogens with shorter C-X bond lengths. The thermodynamics of the dimerization process were calculated by second order Møller-Plesset perturbation theory showing firstly that the perhalogenation strategy is inefficient for the isolation of the monomeric species. Secondly, the dimeric [2+2]-cycloaddition products were predicted to be thermodynamically favored over the [2+4]-Diels-Alder products due to the formation of two allylic $\pi$-electron systems.

The obtained results demonstrate the efficiency of the perhalogenation approach to stabilize highly electrophilic cations. However, to achieve the isolation of a Cp cation, further developments on sterically demanding substituents to suppress dimerization reactions will be required. Based on these results, the Schulz group designed perhalogenated Cp precursors containing $C_6F_5$ groups. Here, the $C_6F_5$ substituents combine both requirements as they are sufficiently inert towards strong electrophiles but also exhibit superior steric demand in comparison to pure halides. The isolation of the Cp cation was achieved by reaction of $C_5(C_6F_5)_5OH$ with $SbF_5$. The corresponding room-temperature stable salt $[C_5(C_6F_5)_5][Sb_3F_{16}]$ was analyzed by single-crystal XRD, EPR and SQUID studies revealing an (antiaromatic) singlet state in the solid state. The compound exhibits versatile redox properties and can be easily reduced to the corresponding neutral radical and further to the corresponding anion. In this work, the cation formation from the radical species was investigated by CV in liquid $SO_2$. The cation exhibit an irreverible one-electron process. The high oxidation potential of $E_{pa}$ = 2.3 V vs. ferrocene renders this cations oxidation power superior to other perfluorinated organic cations, like the perfluortrityl cation, or other potent inorganic oxidants such as $SbF_5$ or $MoF_6$. The observed irreversibility could be a result of the high Lewis acidity of the cationic species which probably decomposed the conducting salt, $[NBu_4][SbF_6]$.

To summarize this thesis, reaction procedures were optimized to yield clean, persubstituted ferrocenes and these products were subjected to further functionalization reactions, to improve the access to perfunctionalized ferrocenes. Systematic effects of (per)mercuration, (per)halogenation and (per)silylation on ferrocene or cyclopentadienyl cations were investigated. The gained insights into substitutional effects as well as their

follow-up chemistry allowed the isolation of potent organometallic oxidizing agents as well as highly electrophilic organic mono- and dications.

## 4.2 Outlook

This work established efficient routes to highly functionalized metallocenes. Especially, the mercuration reactions were found to be ideal for multiple metalations of C-H bonds. The isolated ferrocenes display a promising starting point to expand the rarely explored chemistry of permetalated compounds. Generally, organomercury compounds are ideally suited as starting materials for transmetalation reactions since the mercury atom in C-Hg bonds can be replaced, in theory, by many other metals. Possible transmetalations could involve reductive demercuration (e.g. by elemental Mg or Li) or by salt metathesis reactions of the corresponding metal chlorides. Hence, the combination of the perfunctionalization approach as well as the possibility to undergo transmetalations could lead to unprecedented permetalated species.

The observed reactivity as well as the unusual structural features of the isolated permercurated compounds open up further exciting perspectives for future investigations. The permercurated framework $\{FeC_{10}Hg_{10}\}$ is extremely inert under strongly oxidizing and Brønsted acidic conditions. The Lewis acidity of the corresponding compounds is easily modified by variation of the counter anions or by oxidation of the metallocene. Here, coordination or activation of small molecules by the permercurated metallocenes is reasonable. Olefinic or aromatic compounds can be activated for the reaction with nucleophiles by coordination to Hg centers. Obviously, the electronic situation of the mercury atoms has an important influence on this type of reaction, making a finely tunable ligand system, such as the permercurated ferrocenyl moiety, desirable. Further on, the tunable redox properties, the accessible coordination sites as well as the simple multi-gram approach render these compounds as ideal precursors in coordination chemistry for the synthesis of larger star-shaped molecular architectures or even dendrimers, e.g. *via* pyridinyl-, phosphine- or metallocenyl-containing linkers. The latter approach might be useful for the development of redox carriers. In addition, further functionality is provided by the formation of metallophilic interactions. The tendency to form metallophilic contacts allows to control structural motifs in solid state and further provides potential applications in the coordination of small metalloligands (e.g. metal carbonyls) or in the modulation of metallic surfaces. In addition, mercurophilic interactions are known to influence the photochemical properties of the corresponding material and could be part of further investigations.

Especially the synthesis and electrochemical properties of a perfluorinated derivative would be of great interest. The $[FeC_{10}F_{10}]^+$ would display a rare example of a perfluorinated cation and could contribute to the isolation of exotic anions like $[XeF_3]^-$ or the elusive $[F_3]^-$. Furthermore, the corresponding metallocene dication would be a strong Lewis acid and its coordination ability towards small molecules like CO, $CO_2$ or elemen-

tal xenon would be of interest. As already demonstrated in this thesis, all Hg-C bonds in $[FeC_{10}(HgO_2CC_3H_7)_{10}]$ are efficiently transformed into C-Br moieties in two steps. Hence, the fluorination of the permercurated ferrocenes appears reasonable. However, due to the kinetic stability of the Hg-C bond fluorination with sources of electrophilic fluorine is challenging while stronger fluorination agents such as elemental fluorine decompose the metallocene framework itself. Here, the influence of other assisting ligands on the lability of the Hg-C bonds should be studied to facilitate fluorination. More generally, insights into the nature of the Hg-C bond could contribute to the development of other efficient demercuration reactions leading to novel perfunctionalized metallocenes.

To summarize, the obtained persubstituted ferrocenes offer new pathways to unprecedented perfunctionalized compounds. Hence, continued research should focus on the derivatization of these molecules. Especially, the knowledge on demercuration strategies is valuable with regard to the removal of organomercury compounds from the environment. So far, similar literature known procedures exploit sulfur- or selenium-containing chelating ligands in order to activate the decomposition of dimethylmercury into $Hg^{2+}$ and methane.[343–345] Albeit the advances demonstrated in this thesis, the perfunctionalization approach and consequently all obtained persubstituted compounds exploit the reactivity of toxic elements which displays a major drawback in this research field. So far, the observed reactivity of Hg(II) compounds towards non-activated C-H bonds is unique within the periodic table, hence, difficult to replace. However, catalytic mercuration could be accomplished due to the reversibility of the aromatic metalation step and should be part of further investigation. Furthermore, less toxic metal complexes should be developed which are able to mimic the reactivity of Hg(II) compounds. However, their replacement by non-toxic and abundant metals, is non-trivial and will require complex ligand designs.

A completely different approach would either focus on the perfunctionalization of metal-free Cp moieties, or the direct built-up of the perfunctionalized Cp framework. The resulting Cp derivatives should be versatile precursors as they can be converted into metallocenes and other metal complexes. In this context, the generation of a persilylated metal-free Cp anion, which is one of the most sterical overcrowded Cp ligands, could be of interest in d-block, f-block or main group chemistry. The persilylation reaction established in this work is probably not easily transferable to other, potentially more sensitive, organometallic compounds. Hence, the fully functionalized pure ligand that is easily attachable to many different metal centers would be useful for the systematic development of this chemistry.

# References


[1] H. Werner, *Angew. Chem. Int. Ed.* **2012**, *51*, 6052–6058.

[2] T. J. Kealy, P. L. Pauson, *Nature* **1951**, *168*, 1039–1040.

[3] S. A. Miller, J. A. Tebboth, J. F. Tremaine, *J. Chem. Soc.* **1952**, 632–635.

[4] G. Wilkinson, M. Rosenblum, M. C. Whiting, R. B. Woodward, *J. Am. Chem. Soc.* **1952**, *74*, 2125–2126.

[5] E. O. Fischer, W. Pfab, *Z. Naturforsch. B* **1952**, *7*, 377–379.

[6] L. E. Orgel, J. D. Dunitz, *Nature* **1953**, *171*, 121–122.

[7] M.-L. Hu, M. Abbasi-Azad, B. Habibi, F. Rouhani, H. Moghanni-Bavil-Olyaei, K.-G. Liu, A. Morsali, *ChemPlusChem* **2020**, *85*, 2397–2418.

[8] S. Toma, R. Šebesta, *Synthesis* **2015**, *47*, 1683–1695.

[9] R. C. J. Atkinson, V. C. Gibson, N. J. Long, *Chem. Soc. Rev.* **2004**, *33*, 313–328.

[10] L.-X. Dai, T. Tu, S.-L. You, W.-P. Deng, X.-L. Hou, *Acc. Chem. Res.* **2003**, *36*, 659–667.

[11] X. Liu, A. Rapakousiou, C. Deraedt, R. Ciganda, Y. Wang, J. Ruiz, H. Gu, D. Astruc, *Chem. Commun.* **2020**, *56*, 11374–11385.

[12] R. D. A. Hudson, *J. Organomet. Chem.* **2001**, *637-639*, 47–69.

[13] M. Kurosawa, T. Nankawa, T. Matsuda, K. Kubo, M. Kurihara, H. Nishihara, *Inorg. Chem.* **1999**, *38*, 5113–5123.

[14] D. Astruc, *J. Leather Sci. Eng.* **2020**, *2*, 1–17.

[15] C. Gorman, *Adv. Mater.* **1998**, *10*, 295–309.

[16] D. Astruc, C. Ornelas, J. Ruiz, *Acc. Chem. Res.* **2008**, *41*, 841–856.

[17] G. R. Newkome, E. He, C. N. Moorefield, *Chem. Rev.* **1999**, *99*, 1689–1746.

[18] A. Nazemi, C. E. Boott, D. J. Lunn, J. Gwyther, D. W. Hayward, R. M. Richardson, M. A. Winnik, I. Manners, *J. Am. Chem. Soc.* **2016**, *138*, 4484–4493.

[19] P. D. Beer, P. A. Gale, *Angew. Chem. Int Ed.* **2001**, *40*, 486–516.

[20] H. Yang, Z. Zhou, K. Huang, M. Yu, F. Li, T. Yi, C. Huang, *Org. Lett.* **2007**, *9*, 4729–4732.

[21] A. J. Plajer, F. J. Rizzuto, L. K. S. von Krbek, Y. Gisbert, V. Martínez-Agramunt, J. R. Nitschke, *Chem. Sci.* **2020**, *11*, 10399–10404.

[22] G. Jaouen, A. Vessières, S. Top, *Chem. Soc. Rev.* **2015**, *44*, 8802–8817.

[23] B. S. Ludwig, J. D. G. Correia, F. E. Kühn, *Coord. Chem. Rev.* **2019**, *396*, 22–48.

[24] C. Bruyère, V. Mathieu, A. Vessières, P. Pigeon, S. Top, G. Jaouen, R. Kiss, *J. Inorg. Biochem.* **2014**, *141*, 144–151.

[25] C. Biot, G. Glorian, L. A. Maciejewski, J. S. Brocard, O. Domarle, G. Blampain, P. Millet, A. J. Georges, H. Abessolo, D. Dive, J. Lebibi, *J. Med. Chem.* **1997**, *40*, 3715–3718.

[26] F. D'Orchymont, J. Hess, G. Panic, M. Jakubaszek, L. Gemperle, J. Keiser, G. Gasser, *Med. Chem. Commun.* **2018**, *9*, 1905–1909.

[27] I. Langmuir, *Science* **1923**, *926*, 59–67.

[28] N. V. Sidgwick, *Trans. Faraday Soc.* **1923**, *19*, 469–475.

[29] D. Astruc, *Eur. J. Inorg. Chem.* **2017**, *2017*, 6–29.

[30] J. P. Hurvois, C. Moinet, *J. Organomet. Chem.* **2005**, *690*, 1829–1839.

[31] A. Paul, R. Borrelli, H. Bouyanfif, S. Gottis, F. Sauvage, *ACS Omega* **2019**, *4*, 14780–14789.

[32] D. A. Khobragade, S. G. Mahamulkar, L. Pospíšil, I. Císařová, L. Rulísek, U. Jahn, *Chem. Eur. J.* **2012**, *18*, 12267–12277.

[33] C. A. P. Goodwin, M. J. Giansiracusa, S. M. Greer, H. M. Nicholas, P. Evans, M. Vonci, S. Hill, N. F. Chilton, D. P. Mills, *Nat. Chem.* **2021**, *13*, 243–248.

[34] M. Malischewski, M. Adelhardt, J. Sutter, K. Meyer, K. Seppelt, *Science* **2016**, *353*, 678–682.

[35] D. W. Macomber, W. P. Hart, M. D. Rausch, *Adv. Organomet. Chem.* **1982**, *21*, 1–55.

[36] M. A. Radtke, T. H. Lambert, *Chem. Sci.* **2018**, *9*, 6406–6410.

[37] L. A. López, E. López, *Dalton Trans.* **2015**, *44*, 10128–10135.

[38] K. Sünkel, S. Weigand, A. Hoffmann, S. Blomeyer, C. G. Reuter, Y. V. Vishnevskiy, N. W. Mitzel, *J. Am. Chem. Soc.* **2015**, *137*, 126–129.

[39] R. D. Chambers, W. K. Gray, J. F. S. Vaughan, S. R. Korn, M. Médebielle, A. S. Batsanov, C. W. Lehmann, J. A. K. Howard, *J. Chem. Soc. Perkin Trans. 1* **1997**, 135–145.

[40] T. Olsson, O. Wennerström, *Acta Chem. Scand.* **1978**, *B 32*, 293–296.

[41] R. J. Less, T. C. Wilson, M. McPartlin, P. T. Wood, D. S. Wright, *Chem. Commun.* **2011**, *47*, 10007–10009.

[42] R. J. Less, B. Guan, N. M. Muresan, M. McPartlin, E. Reisner, T. C. Wilson, D. S. Wright, *Dalton Trans.* **2012**, *41*, 5919–5924.

[43] R. B. Woodward, M. Rosenblum, M. C. Whiting, *J. Am. Chem. Soc.* **1952**, *74*, 3458–3459.

[44] R. Sievers, M. Sellin, S. M. Rupf, J. Parche, M. Malischewski, *Angew. Chem. Int. Ed.* **2022**, *61*, e202211147.

[45] M. Lein, J. Frunzke, A. Timoshkin, G. Frenking, *Chem. Eur. J.* **2001**, *7*, 4155–4163.

[46] J. Frunzke, M. Lein, G. Frenking, *Organometallics* **2002**, *21*, 3351–3359.

[47] Q. M. Phung, S. Vancoillie, K. Pierloot, *J. Chem. Theory Comput.* **2012**, *8*, 883–892.

[48] M. S. Inkpen, S. Du, M. Hildebrand, A. J. P. White, N. M. Harrison, T. Albrecht, N. J. Long, *Organometallics* **2015**, *34*, 5461–5469.

[49] O. J. Curnow, G. M. Fern, S. Klaib, U. Böhme, H. Lang, R. Holze, *J. Electroanal. Chem.* **2005**, *585*, 167–171.

[50] J. Okuda, E. Herdtweck, *J. Organomet. Chem.* **1989**, *373*, 99–105.

[51] T. Ziegler, J. Autschbach, *Chem. Rev.* **2005**, *105*, 2695–2722.

[52] G. Frenking, A. Krapp, *J. Comput. Chem.* **2007**, *28*, 15–24.

[53] V. M. Rayón, G. Frenking, *Organometallics* **2003**, *22*, 3304–3308.

[54] D. V. Muratov, A. S. Romanov, A. R. Kudinov, *Russ. Chem. Bull. Int. Ed.* **2014**, *63*, 2485–2492.

[55] H. Sitzmann, H. Bock, R. Boese, T. Dezember, Z. Havlas, W. Kaim, M. Moscherosch, L. Zanathy, *J. Am. Chem. Soc.* **1993**, *115*, 12003–12009.

[56] P. R. Nimax, F. Zoller, T. Blockhaus, T. Küblböck, D. Fattakhova-Rohlfing, K. Sünkel, *New. J. Chem.* **2020**, *44*, 72–78.

[57] N. G. Connelly, W. E. Geiger, *Chemical Reviews* **1996**, *96*, 877–910.

[58] C. Janiak, R. Weimann, F. Görlitz, *Organometallics* **1997**, *16*, 4933–4936.

[59] H. Sitzmann, R. Boese, *Angew. Chem. Int. Ed. Engl.* **1991**, *30*, 971–973.

[60] N. Jux, Y. Rubin, K. Holczer, *Angew. Chem. Int. Ed. Engl.* **1996**, *35*, 1986–1990.

[61] T. Kitagawa, K. Ogawa, K. Komatsu, *J. Am. Chem. Soc.* **2004**, *126*, 9930–9931.

[62] R. Breslow, *Acc. Chem. Res.* **1973**, *6*, 393–398.

[63] F. Feixas, E. Matito, J. Poater, M. Solà, *Chem. Soc. Rev.* **2015**, *44*, 6434–6451.

[64] N. C. Baird, *J. Am. Chem. Soc.* **1972**, *94*, 4941–4948.

[65] P. B. Karadakov, *J. Phys. Chem. A* **2008**, *112*, 7303–7309.

[66] K. J. Iversen, D. J. D. Wilson, J. L. Dutton, *Chem. Eur. J.* **2014**, *20*, 14132–14138.

[67] W. Zou, M. Filatov, D. Cremer, *Int. J. Quantum Chem.* **2012**, *112*, 3277–3288.

[68] M. Alonso, B. Herradón, *Phys. Chem. Chem. Phys.* **2010**, *12*, 1305–1317.

[69] M. J. S. Dewar, R. C. Haddon, *J. Am. Chem. Soc.* **1973**, *95*, 5837–5839.

[70] B. Reindl, P. v. R. Schleyer, *J. Comput. Chem.* **1998**, *19*, 1402–1420.

[71] S. Zilberg, Y. Haas, *J. Am. Chem. Soc.* **2002**, *124*, 10683–10691.

[72] E. P. F. Lee, T. G. Wright, *Phys. Chem. Chem. Phys.* **1999**, *1*, 219–225.

[73] M. Stojanović, J. Aleksić, M. Baranac-Stojanović, *Chemistry* **2021**, *3*, 765–782.

[74] M. Saunders, R. Berger, A. Jaffe, J. M. McBride, J. O'Neill, R. Breslow, J. M. Hoffman, C. Perchonock, E. Wasserman, R. S. Hutton, V. J. Kuck, *J. Am. Chem. Soc.* **1973**, *95*, 3017–3018.

[75] R. Breslow, H. W. Chang, R. Hill, E. Wasserman, *J. Am. Chem. Soc.* **1967**, *89*, 1112–1119.

[76] R. Breslow, H. W. Chang, W. A. Yager, *J. Am. Chem. Soc.* **1963**, *85*, 2033–2034.

[77] R. Breslow, J. M. Hoffman, *J. Am. Chem. Soc.* **1972**, *94*, 2110–2111.

[78] R. Breslow, H. W. Chang, *J. Am. Chem. Soc.* **1961**, *83*, 3727–3728.

[79] P. Jutzi, A. Mix, *Chem. Ber.* **1992**, *125*, 951–954.

[80] J. B. Lambert, L. Lin, V. Rassolov, *Angew. Chem. Int. Ed.* **2002**, *41*, 1429–1431.

[81] M. Otto, D. Scheschkewitz, T. Kato, M. M. Midland, J. B. Lambert, G. Bertrand, *Angew. Chem. Int. Ed.* **2002**, *41*, 2275–2276.

[82] J. N. Jones, A. H. Cowley, C. L. B. Macdonald, *Chem. Commun.* **2002**, 1520–1521.

[83] T. Müller, *Angew. Chem. Int. Ed.* **2002**, *41*, 2276–2278.

[84] R. S. Threlkel, J. E. Bercaw, P. F. Seidler, J. M. Stryker, R. G. Bergman, *Org. Synth.* **1987**, *65*, 42–46.

[85] M.-H. Hung, *e-EROS* **2005**, 1–4.

[86] I. P. Saveleva, M. B. Skbinskaya, V. I. Kolbasov, L. I. Virin, *Russ. J. Appl. Chem.* **1980**, *53*, 2384–2386.

[87] O. Diels, K. Alder, *Justus Liebigs Ann. Chem.* **1928**, *460*, 98–122.

[88] K. Alder, G. Stein, *Angew. Chem.* **1937**, *50*, 510–519.

[89] J. Sauer, *Angew. Chem. Int. Ed. Engl.* **1967**, *6*, 16–33.

[90] B. Raistrick, R. H. Sapiro, D. M. Newitt, *J. Chem. Soc.* **1939**, 1761–1769.

[91] A. G. Turnbull, H. S. Hull, *Aust. J. Chem.* **1968**, *21*, 1789–1797.

[92] B. Rickborn, *Org. React.* **2004**, *52*, 1–79.

[93] J. Blümel, F. H. Köhler, G. Müller, D. L. Wilkinson, *Angew. Chem. Int. Ed. Engl.* **1988**, *27*, 977–979.

[94] F. A. Carey, R. J. Sundberg, *Organic Chemistry*, Wiley-VCH, Weinheim, **1995**.

[95] A. Streitweiser Jr., P. J. Scannon, H. M. Niemeyer, *J. Am. Chem. Soc.* **1972**, *94*, 7936–7937.

[96] K. Daasbjerg, *Acta Chem. Scand.* **1995**, *49*, 878–887.

[97] A. Sievers, R. Wolfenden, *J. Am. Chem. Soc.* **2002**, *124*, 13986–13987.

[98] R. D. Chambers, A. J. Roche, J. F. S. Vaughan, *Can. J. Chem.* **1996**, *74*, 1925–1929.

[99] O. T. Beachley, J. C. Pazik, T. E. Glassman, M. R. Churchill, J. C. Fettinger, R. Blom, *Organometallics* **1988**, *7*, 1051–1059.

[100] C. Janiak, H. Schumann, C. Stader, B. Wrackmeyer, J. J. Zuckerman, *Chem. Ber.* **1988**, *121*, 1745–1751.

[101] T. K. Panda, M. T. Gamer, P. W. Roesky, *Organometallics* **2003**, *22*, 877–878.

[102] F. H. Köhler, W. A. Geike, N. Hertkorn, *J. Organomet. Chem.* **1987**, *334*, 359–367.

[103] M. P. Thornberry, C. Slebodnick, P. A. Deck, *Organometallics* **2000**, *19*, 5352–5369.

[104] M. P. Thornberry, C. Slebodnick, P. A. Deck, F. R. Fronczek, *Organometallics* **2001**, *20*, 920–926.

[105] Z. J. Tonzetich, R. Eisenberg, *Inorg. Chim. Acta* **2003**, *345*, 340–344.

[106] W. J. Evans, J. M. Perotti, J. C. Brady, J. W. Ziller, *J. Am. Chem. Soc.* **2003**, *125*, 5204–5212.

[107] G. E. Herberich, A. Fischer, *Organometallics* **1996**, *15*, 58–67.

[108] R. M. Bellabarba, G. P. Clancy, P. T. Gomes, A. M. Martins, L. H. Rees, M. L. H. Green, *J. Organomet. Chem.* **2001**, *640*, 93–112.

[109] J. M. Birmingham, *Adv. Organomet. Chem.* **1965**, *2*, 365–413.

[110] G. Wilkinson, F. A. Cotton, J. M. Birmingham, *J. Inorg. Nucl. Chem.* **1956**, *2*, 95–113.

[111] P. Jutzi, N. Burford, *Chem. Rev.* **1999**, *99*, 969–990.

[112] P. Jutzi, *Pure Appl. Chem.* **1989**, *61*, 1731–1736.

[113] S. Arndt, J. Okuda, *Chem. Rev.* **2002**, *102*, 1953–1976.

[114] M. Ephritikhine, *Organometallics* **2013**, *32*, 2464–2488.

[115] M. Green, I. R. Butler in *Organometallic Chemistry*, *Vol. 31*, The Royal Society of Chemistry, **2004**, pp. 393–444.

[116] C. Elschenbroich, *Organometallchemie*, 6th ed., (Eds.: C. Elschenbroich, F. Hensel, H. Hopf), B. G. Teubner Verlag, Wiesbaden, **2008**.

[117] P. A. Deck, *Coord. Chem. Rev.* **2006**, *250*, 1032–1055.

[118] M. D. Rausch, *Can. J. Chem.* **1962**, *41*, 1289–1314.

[119] C. W. Fung, R. M. G. Roberts, *Tetrahedron* **1980**, *36*, 3289–3293.

[120] G. Cerichelli, B. Floris, G. Illuminati, G. Ortaggi, *J. Org. Chem.* **1974**, *39*, 3948–3950.

[121] Y. Fujiwara, R. Asano, I. Moritani, S. Teranishi, *J. Org. Chem.* **1976**, *41*, 1681–1683.

[122] M. Rosenblum, R. B. Woodward, *J. Am. Chem. Soc.* **1958**, *80*, 5443–5449.

[123] S. Y. Caille, R. J. P. Corriu, *Chem. Commun.* **1967**, 1251–1252.

[124] T. J. Curphey, J. O. Santer, M. Rosenblum, J. H. Richards, *J. Am. Chem. Soc.* **1960**, *82*, 5249–5250.

[125] M. Malischewski, K. Seppelt, J. Sutter, F. W. Heinemann, B. Dittrich, K. Meyer, *Angew. Chem. Int. Ed.* **2017**, *56*, 13372–13376.

[126] M. Rosenblum, F. W. Abbate, *J. Am. Chem. Soc.* **1966**, *88*, 4178–4184.

[127] M. Vogel, M. Rausch, H. Rosenberg, *J. Org. Chem.* **1957**, *22*, 1016–1018.

[128] M. Sato, H. Kono, M. Shiga, I. Motoyama, K. Hata, *Bull. Chem. Soc. Jpn.* **1968**, *41*, 252–252.

[129] G. D. Broadhead, J. M. Osgerby, P. L. Pauson, *J. Chem. Soc.* **1958**, 650–656.

[130] R. E. Bozak, *J. Chem. Educ.* **1966**, *43*, 73–73.

[131] C. J. Donahue, E. R. Donahue, *J. Chem. Educ.* **2013**, *90*, 1688–1691.

[132] M. Herberhold, *Ferrocenes: Homogeneous Catalysis, Organic Synthesis, Materials Science*, (Eds.: A. Togni, T. Hayashi), VCH Verlagsgesellschaft GmbH, **1994**, pp. 219–278.

[133] J. G. O'Shea, *J. R. Soc. Med.* **1990**, *83*, 392–395.

[134] D. Cirri, L. Chiaverini, A. Pratesi, T. Marzo, *Comments Inorg. Chem.* **2022**, 1–14.

[135] D. J. Dempsey, R. R. Thirucote, *J. Biomater. Appl.* **1988**, *3*, 454–523.

[136] N. A. Smart, *Use and residues of mercury compounds in agriculture*, (Ed.: F. A. Gunther), Springer New York, New York, **1968**, pp. 1–36.

[137] M. Richardson, I. M. Trakhtenberg, M. N. Korshun, *Environmental Management and Health* **1993**, *4*, 16–20.

[138] K. Eto, *Neuropathol.* **2000**, *20*, 14–19.

[139] J. M. Wood, *Science* **1974**, *183*, 1049–1052.

[140] A. L. Hammond, *Science* **1971**, *171*, 788–789.

[141] D. A. Geier, L. K. Sykes, M. R. Geier, *J. Toxicol. Environ. Heal. Part B* **2007**, *10*, 575–596.

[142] D. A. Geier, P. G. King, B. S. Hooker, J. G. Dórea, J. K. Kern, L. K. Sykes, M. R. Geier, *Clin. Chim. Acta* **2015**, *444*, 212–220.

[143] X. Zheng, M. E. Mulcahy, D. Horinek, F. Galeotti, T. F. Magnera, J. Michl, *J. Am. Chem. Soc.* **2004**, *126*, 4540–4542.

[144] M. E. Mulcahy, Z. Bastl, K. F. Stensrud, T. F. Magnera, J. Michl, *J. Phys. Chem. C* **2010**, *114*, 14050–14060.

[145] D. Horinek, J. Michl, *Proc. Natl. Acad. Sci. U.S.A.* **2005**, *102*, 14175–14180.

[146] T. Brotin, L. Pospisil, J. Fiedler, B. T. King, J. Michl, *J. Phys. Chem. B* **1998**, *102*, 10062–10070.

[147] L. Pospisil, N. Varaksa, T. F. Magnera, T. Brotin, J. Michl, *Langmuir* **2007**, *23*, 930–935.

[148] R. C. Larock, *Organomercury compounds in organic synthesis*, 22nd ed., Springer Science and Business Media, **2012**.

[149] D. W. Nierenberg, R. E. Nordgren, M. B. Chang, R. W. Siegler, M. B. Blayney, F. Hochberg, T. Y. Toribara, E. Cernichiari, T. Clarkson, *N. Engl. J. Med.* **1998**, *338*, 1672–1676.

[150] T. Syversen, P. Kaur, *Perspectives in Medicine* **2014**, *2*, 133–150.

[151] T. W. Clarkson, *Annu. Rev. Pharmacol.* **1972**, *12*, 375–406.

[152] M. Rausch, M. Vogel, H. Rosenberg, *J. Org. Chem.* **1957**, *22*, 900–903.

[153] M. R. Haneline, R. E. Taylor, F. P. Gabbaï, *Chem. Eur. J.* **2003**, *9*, 5188–5193.

[154] C. H. Winter, K. N. Seneviratne, A. Bretschneider-Hurley, *Comm. Inorg. Chem.* **1996**, *19*, 1–23.

[155] A. Grirrane, I. Resa, D. del Río, A. Rodríguez, E. Álvarez, K. Mereiter, E. Carmona, *Inorg. Chem.* **2007**, *46*, 4667–4676.

[156] R. M. Harrison, T. Brotin, B. C. Noll, J. Michl, *Organometallics* **1997**, *16*, 3401–3412.

[157] A. K. Brisdon, I. R. Crossley, R. G. Pritchard, *Organometallics* **2005**, *24*, 5487–5490.

[158] B. Korpar-Colig, Z. Popovic, D. Matkovic-Calogovic, D. Vikic-Topic, *Organometallics* **1993**, *12*, 4708–4713.

[159] N. J. Gunsalus, S. H. Park, B. G. Hashiguchi, A. Koppaka, S. J. Smith, D. H. Ess, R. A. Periana, *Organometallics* **2019**, *38*, 2319–2322.

[160] M. Olaru, R. Kather, E. Hupf, E. Lork, S. Mebs, J. Beckmann, *Angew. Chem. Int. Ed.* **2018**, *57*, 5917–5920.

[161] M. Olaru, S. Krupke, E. Lork, S. Mebs, J. Beckmann, *Dalton Trans.* **2019**, *48*, 5585–5594.

[162] S. Furan, E. Lork, S. Mebs, E. Hupf, J. Beckmann, *Z. Anorg. Allg. Chem.* **2020**, *646*, 856–865.

[163] J. Vicente, J.-A. Abad, B. Rink, F.-S. Hernández, M. C. Ramírez de Arellano, *Organometallics* **1997**, *16*, 5269–5282.

[164] R. C. Larock, S. S. Hershberger, *Tetrahedron Lett.* **1981**, *22*, 2443–2446.

[165] G. B. Deacon, G. J. Farquharson, *Aust. J. Chem.* **1977**, *30*, 293–303.

[166] G. B. Deacon, G. J. Farquharson, *Aust. J. Chem.* **1976**, *29*, 627–635.

[167] G. B. Deacon, G. J. Farquharson, *Aust. J. Chem.* **1977**, *30*, 1701–1713.

[168] S. H. Kang, J. H. Lee, S. B. Lee, *Tetrahedron Lett.* **1998**, *39*, 59–62.

[169] E. Bettelli, P. Cherubini, P. D'Andrea, P. Passacantilli, G. Piancatelli, *Tetrahedron* **1998**, *54*, 6011–6018.

[170] Y. S. Shabarov, S. S. Mochalov, T. S. Oretskaya, V. V. Karpova, *J. Organomet. Chem.* **1978**, *150*, 7–20.

[171] H. Schmidbaur, H.-J. Öller, D. L. Wilkinson, B. Huber, G. Müller, *Chem. Ber.* **1989**, *122*, 31–36.

[172] H. Schmidbaur, A. Schier, *Organometallics* **2015**, *34*, 2048–2066.

[173] J. Echeverría, J. Cirera, S. Alvarez, *Phys. Chem. Chem. Phys.* **2017**, *19*, 11645–11654.

[174] P. Pyykkö, *Chem. Rev.* **1997**, *97*, 597–636.

[175] R. Schwerdtfeger, G. A. Heath, M. Dolg, M. A. Bennett, *J. Am. Chem. Soc.* **1992**, *114*, 7518–7527.

[176] R. Schwerdtfeger, P. D. W. Boyd, S. Brienne, J. S. McFeaters, M. Dolg, M.-S. Liao, W. H. E. Schwarz, *Inorg. Chim. Acta* **1993**, *213*, 233–246.

[177] H. Schmidbaur, W. Graf, G. Müller, *Angew. Chem. Int Ed. Engl.* **1988**, *27*, 417–419.

[178] H. Schmidbaur, K. Dziwok, A. Grohmann, G. Müller, *Chem. Ber.* **1989**, *122*, 893–895.

[179] K. Dziwok, J. Lachmann, D. L. Wilkinson, G. Müller, H. Schmidbaur, *Chem. Ber.* **1990**, *123*, 423–431.

[180] R. Narayanaswamy, M. A. Young, E. Parkhurst, M. Ouellette, M. E. Kerr, D. M. Ho, R. C. Elder, A. E. Bruce, M. R. M. Bruce, *Inorg. Chem.* **1993**, *32*, 2506–2517.

[181] D. E. Harwell, M. D. Mortimer, C. B. Knobler, F. A. L. Anet, M. F. Hawthorne, *J. Am. Chem. Soc.* **1996**, *118*, 2679–2685.

[182] A. Burini, J. P. J. Fackeler, R. Galassi, T. A. Grant, M. A. Omary, M. A. Rawashdeh-Omary, B. R. Pietroni, R. J. Staples, *J. Am. Chem. Soc.* **2000**, *122*, 11264–11265.

[183] A. Bondi, *J. Phys. Chem.* **1964**, *68*, 441–451.

[184] J. Donohue, *The Structure of the Elements*, John Wiley and Sons, New York, **1974**, pp. 231–231.

[185] R. Galassi, F. Bachechi, A. Burini, *J. Mol. Struct.* **2006**, *791*, 82–88.

[186] L. Liu, W.-Y. Wong, Y.-W. Lam, W.-Y. Tam, *Inorg. Chim. Acta* **2007**, *360*, 109–121.

[187] W.-Y. Wong, K.-H. Choi, G.-L. Lu, J.-X. Shi, P.-Y. Lai, S.-M. Chan, Z. Lin, *Organometallics* **2001**, *20*, 5446–5454.

[188] W.-Y. Wong, L. Liu, J.-X. Shi, *Angew. Chem. Int. Ed.* **2003**, *42*, 4064–4068.

[189] L. Liu, S.-Y. Poon, W.-Y. Wong, *J. Organomet. Chem.* **2005**, *690*, 5036–5048.

[190] F. Zamora, M. Sabat, M. Janik, C. Siethoff, B. Lippert, *Chem. Commun.* **1997**, 485–486.

[191] M. A. Omary, M. A. Rawashdeh-Omary, M. W. A. Gonser, O. Elbjeirami, T. Grimes, T. R. Cundari, H. V. K. Diyabalanage, C. S. P. Gamage, H. V. R. Dias, *Inorg. Chem.* **2005**, *44*, 8200–8210.

[192] M. A. Omary, R. M. Kassab, M. R. Haneline, O. Elbjeirami, F. P. Gabbaï, *Inorg. Chem.* **2003**, *42*, 2176–2178.

[193] M. R. Haneline, M. Tsunoda, F. P. Gabbaï, *J. Am. Chem. Soc.* **2002**, *124*, 3737–3742.

[194] O. Dimroth, *Ber. d. Dt. Chem. Ges.* **1898**, *31*, 2154–2156.

[195] L. Pesci, *Z. Anorg. Allg. Chem.* **1902**, *32*, 227–234.

[196] O. Dimroth, *Z. Anorg. Allg. Chem.* **1902**, *22*, 311–316.

[197] W. J. Klapproth, F. H. Westheimer, *J. Am. Chem. Soc.* **1950**, *72*, 4461–4465.

[198] R. M. Schramm, W. Klapproth, F. H. Westheimer, *J. Phys. Chem.* **1951**, *55*, 843–860.

[199] M. Malaiyandi, H. Sawatzky, G. F. Wright, *Can. J. Chem.* **1961**, *39*, 1827–1835.

[200] K. A. Kobe, T. F. Doumani, *Ind. Eng. Chem. Res.* **1941**, *33*, 170–176.

[201] G. B. Deacon, G. J. Farquharson, *J. Organomet. Chem.* **1974**, *67*, C1–C3.

[202] G. N. O'Connor, J. V. Crawford, C.-H. Wang, *J. Org. Chem.* **1965**, *30*, 4090–4091.

[203] R. Ciusa, G. Grilla, *Gazz. Chim. Ital.* **1927**, *57*, 323–329.

[204] H. Scheibler, J. Jeschke, W. Beiser, *J. Prakt. Chem.* **1933**, *136*, 232–240.

[205] N. P. Buu-Hoi, *Bull. Soc. Chim. Fr.* **1958**, 1407–1408.

[206] W. Steinkopf, M. Boetius, *Liebigs Ann.* **1941**, *546*, 208–210.

[207] G. W. Watt, L. J. Baye, *J. Inorg. Nucl. Chem.* **1964**, *26*, 1531–1534.

[208] S. A. Kur, M. J. Heeg, C. H. Winter, *Organometallics* **1994**, *13*, 1865–1869.

[209] U. H. F. Bunz, V. Enkelmann, J. Räder, *Organometallics* **1993**, *12*, 4745–4747.

[210] V. I. Boev, A. V. Dombrovskii, *Zh. Obshch. Khim.* **1977**, *47*, 727–728.

[211] A. F. Neto, A. Donizete, A. D. L. Borges, I. P. de Arruda Campos, J. Miller, *Synth. React. Inorg. Met.-Org. Chem.* **1997**, *27*, 1543–1551.

[212] C. H. Winter, Y.-H. Han, M. J. Heeg, *Organometallics* **1992**, *11*, 3169–3171.

[213] C. H. Winter, Y.-H. Han, R. L. Ostrander, A. L. Rheingold, *Angew. Chem. Int. Ed.* **1993**, *32*, 1161–1163.

[214] S. A. Kur, A. L. Reingold, C. H. Winter, *Inorg. Chem.* **1995**, *34*, 414–416.

[215] Y.-H. Han, M. J. Heeg, C. H. Winter, *Organometallics* **1994**, *13*, 3009–3019.

[216] M. D. Rausch, E. O. Fischer, H. Grubert, *J. Am. Chem. Soc.* **1960**, *82*, 76–82.

[217] M. D. Rausch, V. Mark, *J. Org. Chem.* **1963**, *28*, 3225–3228.

[218] S. A. Kur, C. H. Winter, *J. Organomet. Chem.* **1996**, *512*, 39–44.

[219] H. V. Carter, E. I. Chappell, E. Warhurst, *J. Chem. Soc.* **1956**, 106–115.

[220] I. P. Beletskaya, K. P. Butin, A. N. Ryabtsev, O. A. Reutov, *J. Organomet. Chem.* **1973**, *59*, 1–44.

[221] A. Bretschneider-Hurley, C. H. Winter, *J. Am. Chem. Soc.* **1994**, *116*, 6468–6469.

[222] K. N. Seneviratne, A. Bretschneider-Hurley, C. H. Winter, *J. Am. Chem. Soc.* **1996**, *118*, 5506–5507.

[223] E. C. Brehm, J. K. Stille, A. I. Meyers, *Organometallics* **1992**, *11*, 938–942.

[224] S. Purser, P. R. Moore, S. Swallow, V. Gouverneur, *Chem. Soc. Rev.* **2008**, *37*, 320–330.

[225] Z. Xu, Z. Yang, Y. Lui, Y. Lu, K. Chen, W. Zhu, *J. Chem. Inf. Model.* **2014**, *54*, 69–78.

[226] P. Jeschke, *Pest. Manag. Sci.* **2010**, *66*, 10–27.

[227] E. J. Lien, Z.-R. Guo, R.-L. Li, C.-T. Su, *J. Pharm. Sci.* **1982**, *71*, 641–655.

[228] K. R. Hiraoka, R. Yamdagni, P. Kebarle, *J. Am. Chem. Soc.* **1973**, *95*, 6833–6835.

[229] G. A. Olah, G. Rasul, L. Heiliger, G. K. S. Prakash, *J. Am. Chem. Soc.* **1996**, *118*, 3580–3583.

[230] G. Frenking, S. Fau, C. M. Marchand, H. Grützmacher, *J. Am. Chem. Soc.* **1997**, *119*, 6648–6655.

[231] T. Laube, E. Bannwart, S. Hollenstein, *J. Am. Chem. Soc.* **1993**, *115*, 1731–1733.

[232] K. O. Christe, X. Zhang, R. Bau, J. Hegge, G. A. Olah, G. K. S. Prakash, J. A. Sheehy, *J. Am. Chem. Soc.* **2000**, *122*, 481–487.

[233] H. P. A. Mercier, M. D. Moran, G. J. Schrobilgen, C. Steinberg, R. J. Suontamo, *J. Am. Chem. Soc.* **2004**, *126*, 5533–5548.

[234] I. Krossing, A. Bihlmeier, I. Raabe, N. Trapp, *Angew. Chem. Int Ed.* **2003**, *42*, 1531–1534.

[235] H. Shorafa, D. Mollenhauer, B. Paulus, K. Seppelt, *Angew. Chem. Int. Ed.* **2009**, *48*, 5845–5847.

[236] M. J. Molski, D. Mollenhauer, S. Gohr, B. Paulus, M. A. Khanfar, H. Shorafa, S. H. Strauss, K. Seppelt, *Chem. Eur. J.* **2012**, *18*, 6644–6654.

[237] M. J. Molski, M. A. Khanfar, H. Shorafa, K. Seppelt, *Eur. J. Org. Chem.* **2013**, 3131–3136.

[238] W. T. Borden, *Chem. Commun.* **1998**, 1919–1925.

[239] I. M. Riddlestone, A. Kraft, J. Schaefer, I. Krossing, *Angew. Chem. Int. Ed.* **2018**, *57*, 13982–14024.

[240] T. A. Engesser, M. R. Lichtenthaler, M. Schleep, I. Krossing, *Chem. Soc. Rev.* **2016**, *45*, 789–899.

[241] W. D. Good, D. R. Douslin, D. W. Scott, A. George, J. L. Lacina, J. P. Dawson, G. Waddington, *J. Phys. Chem.* **1959**, *63*, 1133–1138.

[242] T. Brink, J. S. Murray, P. Politzer, *Int. J. Quantum Chem.* **1992**, *44*, 57–64.

[243] J. S. Murray, K. Paulsen, P. Politzer, *Proc. Indian Acad. Sci. (Chem. Sci.)* **1994**, *106*, 267–275.

[244] T. D. Paolo, C. Sandorfy, *Can. J. Chem.* **1974**, *52*, 3612–3622.

[245] G. Cavallo, P. Metrangolo, R. Milani, T. Pilati, A. Priimagi, G. Resnati, G. Terraneo, *Chem. Rev.* **2016**, *116*, 2478–2601.

[246] P. Politzer, J. S. Murray, T. Clark, *Phys. Chem. Chem. Phys.* **2013**, *15*, 11178–11189.

[247] P. Politzer, P. Lane, M. C. Concha, Y. Ma, J. S. Murray, *J. Mol. Model.* **2007**, *13*, 305–311.

[248] P. Metrangolo, F. Meyer, T. Pilati, G. Resnati, G. Terraneo, *Angew. Chem. Int. Ed.* **2008**, *47*, 6114–6127.

[249] P. Metrangolo, J. S. Murray, T. Pilati, P. Politzer, G. Resnati, G. Terraneo, *Cryst. Growth Des.* **2011**, *11*, 4238–4246.

[250] L. Muzangwa, S. Nyambo, B. Uhler, S. A. Reid, *J. Chem. Phys.* **2012**, *137*, 184307.

[251] P. Politzer, J. S. Murray, M. C. Concha, *J. Mol. Model.* **2008**, *14*, 659–665.

[252] G. Paprott, D. Lentz, K. Seppelt, *Chem. Ber.* **1984**, *117*, 1153–1160.

[253] J. A. Krynitsky, R. W. Bost, *J. Am. Chem. Soc.* **1947**, *69*, 1918–1920.

[254] E. T. McBee, C. F. Baranauckas, *Ind. Eng. Chem. Res.* **1949**, 806–809.

[255] J. Kovacs, C. S. Marvel, *J. Polym. Sci. Part A-1: Polym. Chem.* **1967**, *5*, 1279–1287.

[256] G. A. Ungefug, *J. Org. Chem.* **1973**, *38*, 153–155.

[257] V. L. Heasley, P. D. Davis, D. M. Ingle, K. D. Rold, G. E. Heasley, *J. Org. Chem.* **1974**, *39*, 736–737.

[258] W. G. Young, H. K. Hall Jr., S. Winstein, *J. Am. Chem. Soc.* **1956**, *78*, 4338–4344.

[259] D. F. Shellhamer, M. C. Chiaco, K. M. Gallego, W. S. C. Low, B. Carter, V. L. Heasley, R. D. Chapman, *J. Fluor. Chem.* **1995**, *72*, 83–87.

[260] R. Riemschneider, K. D. Albrecht, *Monatsh. fur Chem.* **1963**, *94*, 922–923.

[261] I. V. Ekhato, C. C. Huang, *J. Label. Compd. Radiopharm.* **1993**, *33*, 869–880.

[262] G.-P. Blümer, M. Zander, *Monatsh. fur Chem.* **1979**, *110*, 1233–1236.

[263] B. Fuchs, Y. Belsky, E. Tartakovsky, J. Zizuashvili, S. Weinman, *J. Chem. Soc. Chem. Commun.* **1982**, 778–779.

[264] M. A. Wellman, L. C. Burry, J. E. Letourneau, J. N. Bridson, D. O. Miller, D. J. Burnell, *J. Org. Chem.* **1997**, *62*, 939–946.

[265] Y. Kitahara, I. Murata, M. Funamizu, T. Asano, *Bull. Chem. Soc. Jpn.* **1964**, *37*, 1399–1403.

[266] G. Paprott, S. Lehmann, K. Seppelt, *Chem. Ber.* **1988**, *121*, 727–733.

[267] E. T. McBee, D. K. Smith, *J. Am. Chem. Soc.* **1954**, *77*, 389–391.

[268] R. West, T. Kwitowski, *J. Am. Chem. Soc.* **1968**, *90*, 4697–4701.

[269] E. T. McBee, J. D. Idol Jr., C. W. Roberts, *J. Am. Chem. Soc.* **1955**, *77*, 4375–4379.

[270] J. S. Newcomer, E. T. McBee, *J. Am. Chem. Soc.* **1949**, *71*, 952–956.

[271] H. P. Fritz, L. Schäfer, *J. Organomet. Chem.* **1964**, *1*, 318–322.

[272] R. Breslow, R. Hill, E. Wasserman, *J. Am. Chem. Soc.* **1964**, *86*, 5349–5350.

[273] G. Wulfsberg, R. West, *J. Am. Chem. Soc.* **1972**, *94*, 6069–6067.

[274] K. J. Reimer, A. Shaver, *Inorg. Chem.* **1975**, *14*, 2707–2716.

[275] K. Sünkel, C. Stramm, M. Lang, W. Kempinger, J. Hofmann, *Inorg. Chim. Acta.* **1998**, *269*, 111–116.

[276] L. V. Dinh, F. Hampel, J. A. Gladysz, *J. Organomet. Chem.* **2005**, *690*, 493–503.

[277] P. Voßnacker, T. Keilhack, N. Schwarze, K. Sonnenberg, K. Seppelt, M. Malischewski, S. Riedel, *Eur. J. Inorg. Chem.* **2021**, 1034–1040.

[278] H. Butenschön, *Synthesis* **2018**, *50*, 3787–3808.

[279] S. Bernhartzeder, K. Sünkel, *J. Organomet. Chem.* **2012**, *716*, 146–149.

[280] K. Sünkel, S. Bernhartzeder, *J. Organomet. Chem.* **2011**, *696*, 1536–1540.

[281] I. R. Butler, *Inorg. Chem. Commun.* **2008**, *11*, 484–486.

[282] K. N. Brown, P. T. Gulyas, P. A. Lay, N. S. McAlpine, A. F. Masters, L. Phillips, *J. Chem. Soc. Dalton Trans.* **1993**, 835–840.

[283] F. L. Hedberg, H. Rosenberg, *J. Am. Chem. Soc.* **1973**, *95*, 870–875.

[284] W. Erb, N. Richy, J.-P. Hurvois, P. J. Low, F. Mongin, *Dalton Trans.* **2021**, *50*, 16933–16938.

[285] C. Hansch, A. Leo, R. W. Taft, *Chem. Rev.* **1991**, *91*, 165–195.

[286] W. F. Little, C. N. Reilley, J. D. Johnson, A. P. Sanders, *J. Am. Chem. Soc.* **1964**, *86*, 1382–1386.

[287] D. M. Evans, D. D. Hughes, P. J. Murphy, P. N. Horton, S. J. Coles, F. F. de Biani, M. Corsini, I. R. Butler, *Organometallics* **2021**, *40*, 2496–2503.

[288] W. E. Britton, R. Kashyap, M. El-Hashash, M. El-Kady, M. Herberhold, *Organometallics* **1986**, *5*, 1029–1031.

[289] M. A. Khanfar, K. Seppelt, *J. Fluor. Chem.* **2015**, *179*, 193–197.

[290] J. O. Howell, J. M. Goncalves, C. Amatore, L. Klasnic, R. M. Wightman, J. K. Kochi, *J. Am. Chem. Soc.* **1984**, *106*, 3968–3976.

[291] R. J. Maldanis, J. C. W. Chien, M. D. Rausch, *J. Organomet. Chem.* **2000**, *599*, 107–111.

[292] M. P. Thornberry, N. T. Reynolds, P. A. Deck, *Organometallics* **2004**, *23*, 1333–1339.

[293] R. Wahren, *J. Organomet. Chem.* **1973**, *57*, 415–422.

[294] A. Roloff, K. Meier, M. Reidiker, *Pure Appl. Chem.* **1986**, *58*, 1267–1272.

[295] B. Klingert, A. Roloff, B. Urwyler, J. Wirz, *Helv. Chim. Acta* **1988**, *71*, 1858–1867.

[296] P. A. Deck, K. C. Jantunen, F. L. Taw, J. L. Kiplinger in *Inorganic Syntheses*, *Vol. 36*, (Eds.: G. S. Girolami, A. P. Sattelberger), **2014**, Chapter 8, pp. 38–42.

[297] P. A. Deck, W. F. Jackson, F. R. Froczek, *Organometallics* **1996**, *15*, 5287–5291.

[298] S. Becke, U. Denninger, S. Kahlert, W. Obrecht, C. Schmid, H. Windisch, *Metal-free cyclopentadienide anions as co-catalysts for olefin polymerization*, **2002**, WO2002012154.

[299] M. I. Bruce, M. J. Melvin, *J. Chem. Soc.* **1969**, 2107–2112.

[300] J. E. Sheats, W. Miller, M. D. Rausch, S. A. Gardner, P. S. Andrews, F. A. Higbie, *J. Organomet. Chem.* **1975**, *96*, 115–121.

[301] Y. K. Kang, H.-K. Lee, S. S. Lee, Y. K. Chung, G. Carpenter, *Inorg. Chim. Acta* **1997**, *261*, 37–44.

[302] S. Tannenbaum, *J. Am. Chem. Soc.* **1954**, *76*, 1027–1027.

[303] M. S. Gordon, D. R. Gano, J. S. Binkley, M. J. Frisch, *J. Am. Chem. Soc.* **1986**, *108*, 2192–2195.

[304] S. W. Benson, *J. Chem. Educ.* **1965**, *42*, 502–518.

[305] M. P. Plesniak, X. Just-Baringo, F. Ortu, D. P. Mills, D. J. Procter, *Chem. Commun.* **2016**, *52*, 13503–13506.

[306] D. Cui, O. Tardif, Z. Hou, *J. Am. Chem. Soc.* **2004**, *126*, 1312–1313.

[307] F. Ortu, J. Lui, M. Burton, M. Fowler, A. Formanuik, M.-E. Boulon, N. F. Chilton, D. P. Mills, *Inorg. Chem.* **2017**, *56*, 2496–2505.

[308] D. Cui, M. Nishiura, Z. Hou, *Angew. Chem. Int. Ed.* **2005**, *44*, 959–962.

[309] W.-X. Zhang, Z. Wang, M. Nishiura, Z. Xi, Z. Hou, *J. Am. Chem. Soc.* **2011**, *133*, 5712–5715.

[310] L. M. Engelhardt, P. C. Junk, C. L. Raston, A. H. White, *J. Chem. Soc. Chem. Commun.* **1988**, 1500–1501.

[311] A. H. Cowley, P. Jutzi, F. X. Kohl, J. G. Lasch, N. C. Norman, E. Schlüter, *Angew. Chem.* **1984**, *96*, 603–604.

[312] M. J. Harvey, T. P. Hanusa, M. Pink, *J. Chem. Soc. Dalton Trans.* **2001**, 1128–1130.

[313] P. Jutzi, E. Schlüter, M. B. Hursthouse, A. M. Arif, R. L. Short, *J. Organomet. Chem.* **1986**, *299*, 285–295.

[314] M. Westerhausen, S. Schneiderbauer, N. Makropoulos, M. Warchhold, H. Nöth, H. Piotrowski, K. Karaghiosoff, *Organometallics* **2002**, *21*, 4335–4341.

[315] C. H. Winter, X. X. Zhou, M. J. Heeg, *Inorg. Chem.* **1992**, *31*, 1808–1815.

[316] E. J. Little, M. M. Jones, *J. Chem. Educ.* **1960**, *37*, 231–233.

[317] S. Kyushin, T. Kitahara, H. Matsumoto, *Chem. Lett.* **1998**, 471–472.

[318] S. Kyushin, T. Matsuura, H. Matsumoto, *Organometallics* **2006**, *25*, 2761–2765.

[319] J. Okuda, R. W. Albach, E. Herdtweck, *Polyhedron* **1991**, *10*, 1741–1748.

[320] J. C. Wedal, J. M. Barlow, J. W. Ziller, J. Y. Yang, W. J. Evans, *Chem. Sci.* **2021**, *12*, 8501–8511.

[321] M. R. Trinh, J. C. Wedal, W. J. Evans, *Dalton Trans.* **2021**, *50*, 14384–14389.

[322] R. R. Langeslay, M. E. Fieser, J. W. Ziller, F. Furche, W. J. Evans, *Chem. Sci.* **2015**, *6*, 517–521.

[323] R. R. Langeslay, M. E. Fieser, J. W. Ziller, F. Furche, W. J. Evans, *J. Am. Chem. Soc.* **2016**, *138*, 4036–4045.

[324] M. R. MacDonald, J. E. Bates, J. W. Ziller, F. Furche, W. J. Evans, *J. Am. Chem. Soc.* **2013**, *135*, 9857–9868.

[325] M. E. Fieser, M. R. MacDonald, B. T. Krull, J. E. Bates, J. W. Ziller, F. Furche, W. J. Evans, *J. Am. Chem. Soc.* **2015**, *137*, 369–382.

[326] A. Sekiguchi, Y. Sugai, K. Ebata, C. Kabuto, H. Sakurai, *J. Am. Chem. Soc.* **1993**, *115*, 1144–1146.

[327] P. Jutzi, E. Schlüter, C. Krüger, S. Pohl, *Angew. Chem. Int. Ed. Engl.* **1983**, *22*, 944–944.

[328] M. D. Walter, C. D. Sofield, C. H. Booth, R. A. Andersen, *Organometallics* **2009**, *28*, 2005–2019.

[329] M. H. Kuiper, H. Lueken, *Z. Anorg. Allg. Chem.* **2007**, *633*, 1407–1409.

[330] K. Sünkel, J. Hofmann, *Organometallics* **1992**, *11*, 3923–3925.

[331] K. Sünkel, J. Hofmann, *Chem. Ber.* **1993**, *126*, 1791–1795.

[332] K. Sünkel, J. Hofmann, *J. Coord. Chem.* **1993**, *30*, 261–264.

[333] J Okuda, E Herdtweck, *Chem. Ber.* **1988**, *121*, 1899–1905.

[334] I. R. Butler, D. M. Evans, P. N. Horton, S. J. Coles, P. J. Murphy, *Organometallics* **2021**, *40*, 600–605.

[335] H. Bauer, J. Weismann, D. Saurenz, C. Färber, M. Schär, W. Gidt, I. Schädlich, G. Wolmershäuser, Y. Sun, S. Harder, H. Sitzmann, *J. Organomet. Chem.* **2016**, *809*, 63–73.

[336] F. Jaroschik, F. Nief, X.-F. L. Goff, L. Ricard, *Organometallics* **2007**, *26*, 3552–3558.

[337] M. J. Harvey, K. T. Quisenberry, T. P. Hanusa, V. G. Y. Jr., *Eur. J. Inorg. Chem.* **2003**, 2282–2290.

[338] C. P. Morley, P. Jutzi, *Organometallics* **1987**, *6*, 1084–1090.

[339] A. H. Cowley, P. Jutzi, F. X. Kohl, J. G. Lasch, N. C. Norman, E. Schlüter, *Angew. Chem. Int. Ed. Engl.* **1984**, *23*, 616–616.

[340] W. D. Luke, A. Streitwieser Jr., *J. Am. Chem. Soc.* **1981**, *103*, 3241–3243.

[341] J. Okuda, *J. Organomet. Chem.* **1989**, *376*, C1–C4.

[342] J. Okuda, *Chem. Ber.* **1989**, *122*, 1075–1077.

[343] R. Karri, A. Chalana, R. Das, R. K. Rai, G. Roy, *Metallomics* **2019**, *11*, 213–225.

[344] R. Karri, M. Banerjee, A. Chalana, K. K. Jha, G. Roy, *Inorg. Chem.* **2017**, *56*, 12102–12115.

[345] R. Karri, A. Chalana, B. Kumar, S. K. Jayadev, G. Roy, *Chem. Eur. J.* **2019**, *25*, 2810–12819.

# 5 List of Publications

## Publications – Peer Reviewed

**A decacationic ferrocene-based metallostar**
Susanne M. Rupf, Amina L. Moshtaha, Moritz Malischewski, *Chem. Sci.* **2023**, *14*, 1132–1137.

**Persilylation of Ferrocene: The Ultimate Discipline in Sterically Overcrowded Metal Complexes**
Susanne M. Rupf, Robin Sievers, Paulin S. Riemann, Marc Reimann, Martin Kaupp, Carlo Fasting, Moritz Malischewski, *Dalton Trans.* **2023**, *52*, 6870–6875.

**Structural characterization and bonding analysis of $[Hg\{Fe(CO)_5\}_2]^{2+}$ $[SbF_6]_2^-$**
Susanne M. Rupf,‡ Sudip Pan,‡ Amina L. Moshtaha, Gernot Frenking, Moritz Malischewski, *J. Am. Chem. Soc.*, **2023**, *accepted manuscript*. DOI: 10.1021/jacs.3c03064

**On pyridine chloronium cations**
Patrick Pröhm, Willi Berg, Susanne M. Rupf, Carsten Müller, Sebastian Riedel, *Chem. Sci.* **2023** *14*, 2325–2329.

**Lithium catalysed sequence selective ring opening terpolymerisation: a mechanistic study**
Peter Deglmann, Sara Machleit, Cesare Gallizioli, Susanne M. Rupf, Alex J. Plajer, *Catal. Sci. Technol.* **2023**, *13*, 2937–2945.

**Increasing oxidation power of TCNQ by coordination of $B(C_6F_5)_3$**
Paul A. Albrecht, Susanne M. Rupf, Malte Sellin, Johanna Schlögl, Sebastian Riedel, Moritz Malischewski, *Chem. Commun.* **2022**, *56*, 4958–4961.

**Lithium achieves sequence selective ring-opening terpolymerisation (ROTERP) of ternary monomer mixtures**
Susanne M. Rupf,‡ Patrick Pröhm,‡ Alex J. Plajer, *Chem. Sci.* **2022**, *13*, 6355–6365.

‡Authors contributed equally.

**Preparation and one-electron oxidation of decabromoferrocene**
Susanne M. Rupf, Irina S. Dimitrova, Gabriel Schröder, and Moritz Malischewski, *Organometallics* **2022**, *41*, 1261–1267.

**Sequence-sorted redox-switchable hetero[3]rotaxanes**
Marius Gaedke,‡ Henrik Hupatz,‡ Felix Witte, Susanne M. Rupf, Clara Douglas, Hendrik H. Schröder, Lukas Fischer, Moritz Malischewski, Beate Paulus, Christoph A. Schalley, *Org. Chem. Front.* **2022**, *9*, 64–74.

**Introducing the perfluorinated Cp* ligand into coordination chemistry**
Robin Sievers, Malte Sellin, Susanne M. Rupf, Joshua Parche, Moritz Malischewski, *Angew. Chem. Int. Ed.* **2022**, *61*, e202211147.

**The tris(pentafluorophenyl)methylium cation: isolation and reactivity**
Kurt F. Hoffmann, David Battke, Paul Golz, Susanne M. Rupf, Moritz Malischewski, Sebastian Riedel, *Angew. Chem. Int. Ed.* **2022**, *61*, e202203777.

**Non-classical polyinterhalides of chlorine monofluoride: experimental and theoretical characterization of $[F(ClF)_3]^-$**
Patrick Pröhm, Nico Schwarze, Carsten Müller, Simon Steinhauer, Helmut Beckers, Susanne M. Rupf, Sebastian Riedel, *Chem. Commun.* **2021**, *57*, 4843–4846.

**Investigation of bis(perfluoro-*tert*-butoxy) halogenates(I/III)**
Patrick Pröhm, Willi Berg, Susanne M. Rupf, Patrick Voßnacker, Sebastian Riedel, *Chem. Eur. J.* **2021**, *27*, 17676–17681.

**Cubic three-dimensional networks of the cyanometalate $[Fe(CN)_6]^{3-}$ with the ditopic halogen bond donor diiodoacetylene $C_2I_2$**
Malte Sellin,‡ Susanne M. Rupf,‡ Moritz Malischewski, *Cryst. Growth Des.* **2021**, *21*, 5515–5520.

**Eightfold electrophilic methylation of octacyanotungstate $[W(CN)_8]^{4-/3-}$: preparation of homoleptic, eight-coordinate methyl isocyanide complexes $[W(CNMe)_8]^{4+/5+}$**
Malte Sellin, Susanne M. Rupf, Ulrich Abram, Moritz Malischewski, *Inorg. Chem.* **2021**, *60*, 5917–5924.

**Tenfold metalation of ferrocene: synthesis, structures, and metallophilic interactions in $FeC_{10}(HgX)_{10}$**
Susanne M. Rupf, Gabriel Schröder, Robin Sievers, Moritz Malischewski, *Chem. Eur. J.* **2021**, *27*, 5125–5129.

**The [2+2] cycloaddition product of perhalogenated cyclopentadienyl cations: structural characterization of salts of the $[C_{10}Cl_{10}]^{2+}$ and $[C_{10}Br_{10}]^{2+}$ dications**
Susanne M. Rupf, Patrick Pröhm, Moritz Malischewski, *Chem. Commun.* **2020**, *56*, 9834–9837.

**Bi- and trifurcated halogen bonding M–C≡N···I in 1D, 2D, and 3D supramolecular network structures of co-crystallized diiodoacetylene $C_2I_2$ and tetracyanonickelate $[Ni(CN)_4]^{2-}$**
Malte Sellin,‡ Susanne M. Rupf,‡ Yuyin Zhang, Moritz Malischewski, *Cryst. Growth Des.* **2020**, *20*, 7104–7110.

**The power of ferrocene, mesoionic carbenes, and gold: redox-switchable catalysis**
Sinja Klenk, Susanne M. Rupf, Lisa Suntrup, Margarethe van der Meer, Biprajit Sarkar, *Organometallics* **2017**, *36*, 2026–2035.

## Publications – Preprint

**Structural Characterization and Reactivity of a Room Temperature-Stable, Antiaromatic Cyclopentadienyl Cation Salt**
Yannick Schulte, Christoph Wölper, Susanne M. Rupf, Moritz Malischewski, Gebhard Haberhauer, Stephan Schulz.
DOI: 10.26434/chemrxiv-2023-qnstd

**From $CO_2$ to $CS_2$: mechanistic mapping of cooperative ($CS_2$/$CO_2$)/epoxide ring-opening copolymerisation catalysis**
Alex J. Plajer, Jenny Stephan, Merlin Stühler, Susanne M. Rupf, Samuel Neal.
DOI: 10.26434/chemrxiv-2023-t7bcd

## Conferences

| | |
|---|---|
| 09/2022 | 21st Conference on Inorganic Chemistry<br>**Poster: Synthesis of a Ferrocene Deca- and Undecacation** (Poster Prize) |
| 09/2022 | 19. Deutscher Fluortag<br>**Presentation: Synthesis of a Ferrocene Deca- and Undecacation** |
| 08/2022 | European Symposium of Fluorine Chemistry 2022<br>**Presentation: Perhalogenated Organic Mono- and Dications** |
| 08/2021 | GDCh-Wissenschaftsforum Chemie (online)<br>**Poster: Tenfold Metalation and Functionalization of Ferrocene, Ruthenocene and Osmocene** (Poster prize) |

July 11, 2023

# A Supporting Information of Publications

## A.1 Tenfold Metalation of Ferrocene: Synthesis, Structures, and Metallophilic Interactions in $FeC_{10}(HgX)_{10}$

Chemistry–A European Journal

Supporting Information

# Tenfold Metalation of Ferrocene: Synthesis, Structures, and Metallophilic Interactions in $FeC_{10}(HgX)_{10}$

Susanne Margot Rupf, Gabriel Schröder, Robin Sievers, and Moritz Malischewski*[a]

WILEY-VCH

# SUPPORTING INFORMATION

## Table of Contents

WILEY-VCH

# SUPPORTING INFORMATION

## Experimental Procedures

### General Procedures

**CAUTION:** Mercury compounds are highly toxic. Therefore, the chemicals should be handled under a well-ventilated fume hood. Great care must be taken that organomercury compounds are not spilled on the skin. It is advisable to use multiple layers of impenetrable gloves and to remove the outer layer immediately if material is spilled on it. The face might be protected against splashes by using a face shield. Due to the hazardous effects of mercury on the environment, great care must be taken to prevent contamination of the wastewater with mercury.

Commercially available chemicals were used as received, unless otherwise noted. All manipulations were performed in air. Yellow and red mercury oxide as well as 1,2-dichloroethane (carcinogenic) was purchased from abcr GmbH. Sodium chloride was purchased from Carl Roth GmbH + Co. KG, sodium fluoride from Riedel de Haen AG, butyric acid anhydride from Sigma-Aldrich, 1,1,1-trifluoroacetic acid from Fluorochem, 1,1,1-trichloroacetic acid from Merck KGaA, and ferrocene from Alfa Aesar.

$^{1}$H, $^{13}$C and $^{19}$F NMR spectra were recorded on a Bruker AVANCE III 700 spectrometer by using 6mm NMR glass tubes. All reported chemical shifts (δ) are referenced to the Ξ values given in IUPAC recommendations of 2008 using the $^{2}$H signal of the deuterated solvent as internal reference.[1] All chemical shifts (δ) are given in parts per million (ppm) and the signals are specified according to the multiplicity (s = singlet, d = doublet, t = triplet, q = quartet, m = multiplet, br = broad) and the coupling constants *J* in Hz. Mass spectrometry was performed on a Agilent 6210 ESI TOF (electrospray ionization time-of-flight spectrometer) of Aglient Technologies, Santa Clara, CA in negative mode. Flow rates were set to 10 µL·min$^{-1}$. The evaluation of the resulting data occurred by using Mmass 5.5.0.[2] The program MestRe Nova Version 14.0.1 was used to evaluate and plot the data.[3]

Infrared spectra were measured using a Thermo-Scientific Nicolet iS10 FTIR spectrometer with DuraSamplIR accessory in attenuated total reflection at room temperature. Raman spectra were recorded on a Bruker MultiRAM II equipped with a low-temperature Ge detector (1064 nm, 30-80 mW, resolution 2 cm$^{-1}$). The software OriginPro 2017G was used to plot the data.[4]

Cyclic voltammetry was performed on a Interface 1010 B Potentiostat/Galvanostat/ZRA from Gamry Instruments. The investigations were carried out starting from 0 V going to the oxidation first and then to the reduction. The measurements were performed at a scan rate of 100 mV/s in anhydrous solvents under argon atmosphere using tetrabutylammonium hexafluorophosphate as the supporting electrolyte and platinum wires as working-, counter-, and quasi-reference electrodes. The voltammograms were internally referenced against $Fc^{0/+}$. The software OriginPro 2017G was used to plot the data.[4] Anhydrous THF was stored in Young flasks under argon atmosphere over molar sieve (3 Å) which was dried beforehand at 250 °C under high vacuum. The conducting salt was dried at 250 °C under high vacuum. The solvents were condensed on the conducting salt in the cyclic voltammetry cells via a vacuum line.

X-Ray data were collected on a BRUKER D8 Venture system. Data were collected at 100(2) K using graphite-monochromated Mo $K_\alpha$ radiation ($\lambda_\alpha$ = 0.71073 Å). The strategy for the data collection was evaluated by using the Smart software. The data were collected by the standard "*ψ-ω* scan techniques" and were scaled and reduced using Saint+software. The structures were solved by using Olex2,[5] the structure was solved with the XT[6] structure solution program using Intrinsic Phasing and refined with the XL refinement package[7,8] using Least Squares minimization. If it is noted, bond length and angles were measured with Diamond Crystal and Molecular Structure Visualization Version 4.6.2.[9] Drawings were generated with POV-Ray.[10] Deposition numbers CCDC 2047737 ($FeC_{10}(HgCl)_{10}$), 2047740 ($FeC_{10}(HgO_2CCCl_3)_{10}$) and 2047742 ($FeC_{10}(HgO_2CCF_3)_{10}$) contains the supplementary crystallographic data for this paper. These data are provided free of charge by the joint Cambridge Crystallographic Data Centre and Fachinformationszentrum Karlsruhe Access Structures service www.ccdc.cam.ac.uk/structures.

### Synthesis

*Bis(butyryloxy)mercury(II) – "Mercury(II) butyrate"* ***1***

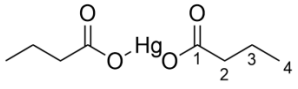


Butyric acid anhydride (18.5 mL, 113 mmol, 1.1 eq.) and 1,2-dichloroethane (600 mL) were placed in a 1000 mL round bottom flask. Mercury(II)oxide (22.2 g, 103 mmol, 1.0 Eq.) was added and the suspension was stirred under reflux for 12 h (Note: yellow HgO dissolves faster than red HgO). After cooling to room temperature the product was obtained as a colourless, crystalline solid. The

precipitate was filtered off and washed with 1,2-dichloroethane (400 mL) and *n*-pentane (600 mL). The residue was dried in high vacuum to afford compound **1** (37.2 g, 96%) as a colorless, crystalline solid.

$^{1}$H NMR (400 MHz, dmso-$d_6$, r.t.): $\delta$ [ppm] = 3.04 (t, *J* = 7.4 Hz, 2H), 2.39 (qt, *J* = 7.4, 7,4 Hz, 2H), 1.71 (t, *J* = 7.4 Hz, 3H).

$^{13}$C{$^{1}$H} NMR (101 MHz, dmso-$d_6$, r.t.): $\delta$ [ppm] = 191.2 (s, C1), 50.5 (s, C2), 34.4 (s, C3), 28.3 (s, C4).

FT-IR (ATR): $\tilde{\nu}$ [cm$^{-1}$] = 2964 ($\nu$ $CH_3$), 2932 ($\nu$ $CH_2$), 2871 ($\nu$ $CH_2$), 1600 ($\nu_s$ COO), 1572 ($\nu_{as}$ COO), 1465 ($\delta$ $CH_2$), 1373 ($\delta$ $CH_3$), 1327, 1290, 1240, 1121, 1100, 896, 756, 727 ($\delta$ $CH_2$).

Raman (1064 nm, r.t.): $\tilde{\nu}$ [cm$^{-1}$] = 2971 ($\nu$ $CH_3$), 2938 ($\nu$ $CH_2$), 2880 ($\nu$ $CH_2$), 1606 ($\nu_{sym}$ COO), 1449 ($\nu_{asym}$ COO)

MS (ESI+, r.t.): $[Hg(O_2C_4H_7)_2 + Na]^+$ calculated: 399.05, found: 399.05.

Elemental analysis: m [%] = calculated: N: 0.00, C: 25.64, H: 3.765, found: N: 0.01, C: 25.89, H: 3.817.

*Decakis(butyryloxymercury(II))ferrocene* ***2***

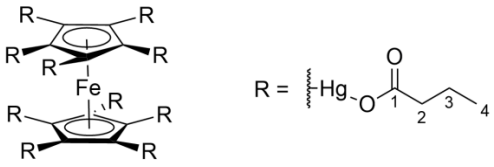


Mercury(II) butyrate (32.5 g, 86.7 mmol, 11 eq.) and 1,2-dichloroethane (600 mL) were placed in a 1000 mL round bottom flask. Ferrocene (1.47 g, 7.88 mmol, 1.0 Eq.) was added and the suspension was stirred under reflux for 18 h. The suspension was filtered while still hot and the precipitate was washed with 1,2-dichloroethane (300 mL) and *n*-pentane (400 mL). The solid was dried in high vacuum to afford compound **2** (22.1 g, 92%) as an orange, amorphous solid.

$^{1}$H NMR (700 MHz, dmso-$d_6$, r.t.) δ [ppm] = 2.11 (t, J = 7.4 Hz, 2H), 1.53 (qt, J = 7.4 Hz, 2H), 0.91 (t, J = 7.4 Hz, 3H).

$^{13}$C{$^{1}$H} NMR (176 MHz, dmso-$d_6$, r.t.) δ [ppm] = 177.5 (s, C1), 97.6 (s, $C_{Cp}$), 38.7 (s, C2), 18.9 (s, C3), 13.9 (s, C4).

FT-IR (ATR): $\tilde{\nu}$ [cm$^{-1}$] = 2960 ($\nu$ $CH_3$), 2931 ($\nu$ $CH_2$), 2872 ($\nu$ $CH_2$), 1610 ($\nu_s$ C=O), 1561 (s, $\nu_{as}$ C=O), 1368 ($\delta$ $CH_3$), 1338, 1241, 1216, 661.

Raman (1064 nm, r.t.): $\tilde{\nu}$ [cm$^{-1}$] = 2935 ($\nu$ $CH_3$), 2870 ($\nu$ $CH_2$), 1559, 1459, 950 ($\delta$ Cp), 892 ($\delta$ C-C), 869 ($\delta$ C-C), 664, 501, 377 ($\nu$ Hg-X), 285, 123 ($\nu$ Hg-Cp).

MS (ESI+, r.t.): $[FeC_{10}(HgO_2C_4H_7)_{10}]^+$ calculated: 3053.08, found: 3053.05.

Elemental analysis: m [%] = calculated: N: 0.00, C: 19.67, H: 2.31, found: N: 0.01, C: 20.37, H: 2.34.

*Decakis(trifluoroacetoxymercury(II))ferrocene* ***3a***

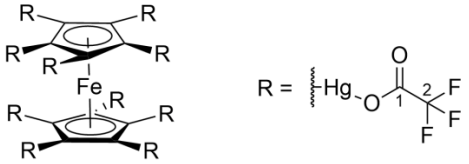


To a suspension of decakis(butyryloxymercury)ferrocene **2** (30 g, 9.83 mmol, 1 Eq.) in THF (50 mL) trifluoroacetic acid (ca. 10 mL) was added dropwise under vigorous stirring until the suspension became clear. The mixture was then concentrated under reduced pressure yielding a red solution. The product was precipitated by addition of *n*-pentane (500 mL) and filtered off. Afterwards the solid was washed with *n*-pentane and dichloromethane. This procedure was repeated three times. The product was obtained as an orange solid (31.98 g, 98%). Single crystals of $FeC_{10}(HgO_2CCF_3)_{10}$ · 4 THF · 2 $OEt_2$ were obtained by diffusion of *n*-pentane into a solution of compound **3a** in a mixture of THF and diethylether.

## SUPPORTING INFORMATION

$^{19}$F NMR (564 MHz, THF-$d_8$, r.t.) δ [ppm] = −74.5 (s, $CF_3$).

$^{13}$C{$^1$H} NMR (176 MHz, dmso-$d_6$, r.t.) δ [ppm] = 164.2 (q, *J* = 39.5 MHz, C1), 119.9 (q, *J* = 287.6 MHz, C2), 97.4 (s, $C_{Cp}$).

FT-IR (ATR): $\tilde{\nu}$ [cm$^{-1}$] = 1646 ($\nu_{asym}$ COO), 1429 ($\nu_{sym}$ COO), 1173 ($\nu$ C-C), 1144 ($\nu$ C-C), 862 ($\nu_{asym}$ $CF_3$), 794 ($\nu_{asym}$ $CF_3$), 733 ($\nu_{sym}$ $CF_3$).

Raman (1064 nm, r.t.): $\tilde{\nu}$ [cm$^{-1}$] = 1423 ($\nu_{asym}$ COO), 954 ($\delta$ Cp), 856 ($\delta$ C-C), 615 ($\delta$ C-F), 514 ($\delta$ C-F), 311 ($\nu$ Hg-X), 116 ($\nu$ Hg-Cp).

Elemental analysis: m [%] = calculated: N: 0.00, C: 10.88, H: 0.00, found: N: 0.01, C: 11.30, H: 0.01.

*Decakis(trichloroacetoxymercury(II))ferrocene* ***3b***

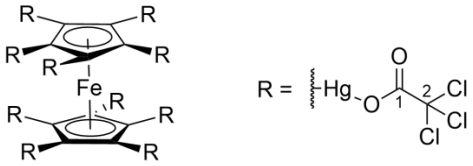


To a suspension of decakis(butyryloxymercury)ferrocene **2** (0.92 g, 0.31 mmol, 1 Eq.) in THF (10 mL) trichloroacetic acid (ca. 1 g) was added portion wise under vigorous stirring until the suspension became clear. THF was removed under reduced pressure yielding a red solid. The crude product was dissolved in 3 mL THF. Then, the solution was precipitated by addition of *n*-pentane (ca. 200 mL). Afterwards the precipitate was filtered off and washed with *n*-pentane and dichloromethane. This procedure was repeated three times. The product was obtained as an orange solid (1.09 g ,92%). Single crystals of $FeC_{10}(HgO_2CCCl_3)_{10}$ · 10 THF · $OEt_2$ were obtained by diffusion of *n*-pentane into a solution of compound **3b** in a THF/$Et_2O$ mixture.

$^{13}$C{$^1$H} NMR (176 MHz, dmso-$d_6$, r.t.) δ [ppm] = 167.8 (s, C1), 99.4 (s, C2), 97.2 (s, $C_{Cp}$).

FT-IR (ATR): $\tilde{\nu}$ [cm$^{-1}$] = 1640 ($\nu_{asym}$ COO), 1326 ($\nu_{sym}$ COO), 827 ($\nu_{asym}$ $CCl_3$), 751 ($\nu_{asym}$ $CCl_3$), 669 ($\nu_{sym}$ $CCl_3$).

Raman (1064 nm, r.t.): $\tilde{\nu}$ [cm$^{-1}$] = 1341 ($\nu_{asym}$ COO), 960 ($\delta$ Cp), 852 ($\delta$ C-C), 774 ($\nu_{asym}$ $CCl_3$), 441, 374 ($\nu$ Hg-O), 94 ($\nu$ Hg-Cp).

Elemental analysis: m [%] = calculated: N: 0.00, C: 9.47, H: 0.00, found: N: 0.01, C: 9.37, H: 0.01.

*Decakis(fluoridomercury(II))ferrocene* ***4a***

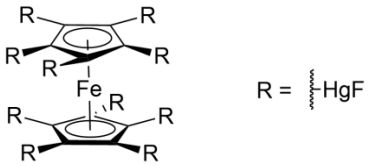


To solution of decakis(trifluoroacetoxymercury(II))ferrocene **3a** (1.40 g, 0.42 mmol) in THF (5 mL) sodium fluoride (200 mg, 4.76 mmol, 11 Eq.) was added. After addition of water (5 mL) a red precipitate formed. The precipitate was filtered off and washed with water, THF and dichloromethane. After drying in high vacuum, the product was obtained as a red solid (0.98 g, 98%).

Raman (1064 nm, r.t.): $\tilde{\nu}$ [cm-$^1$] = 947 ($\delta$ Cp), 507 ($\nu$ Hg-F) 122 ($\nu$ Hg-Cp).

Elemental analysis: m [%] = calculated: N: 0.00, C: 5.06, H: 0.00, found: N: 0.01, C: 5.16, H: 0.01.

*Decakis(chloridomercury(II))ferrocene* ***4b***

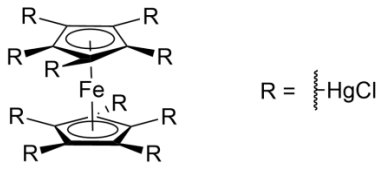


To solution of decakis(trifluoroacetoxymercury(II))ferrocene **3a** (1.40 g) in THF (5 mL) sodium chloride (300 mg, 5.17 mmol, 12 Eq.) was added. After addition of water (5 mL) a red precipitate formed. The precipitate was filtered off and washed with water, THF and dichloromethane. After drying in high vacuum, the product was obtained as a red solid (1.02 g, 96 %). Single crystals of $FeC_{10}(HgCl)_{10} \cdot 9$ DMSO formed upon decomposition of decakis(mercury(II) trichloroacetate)ferrocene in dimethylsulfoxide at room temperature over weeks.

Raman (1064 nm, r.t.): $\tilde{\nu}$ [cm$^{-1}$] = 937 ($\delta$ Cp), 318 ($\nu$ Hg-Cl), 119 ($\nu$ Hg-Cp).

Elemental analysis: m [%] = calculated: N: 0.00, C: 5.33, H: 0.00, found: N: 0.01, C: 5.53, H: 0.01.

WILEY-VCH

# SUPPORTING INFORMATION

## Crystallographic Data

**Table S1**. Crystallographic data.

| Compound | $FeC_{10}(HgO_2CCF_3)_{10}$ · 4 THF · 2 $OEt_2$ | $FeC_{10}(HgO_2CCCl_3)_{10}$ · 10 THF · $OEt_2$ | $FeC_{10}(HgCl)_{10}$ · 9 DMSO |
|---|---|---|---|
| **Empirical formula** | $C_{54}H_{52}F_{30}FeHg_{10}O_{26}$ | $C_{74}H_{90}Cl_{30}FeHg_{10}O_{31}$ | $C_{28}H_{54}Cl_{10}FeHg_{10}O_9S_9$ |
| **Formula weight** | 2748.70 | 4600.70 | 3239.50 |
| **Temperature/K** | 100.0 | 100.0 | 100.0 |
| **Crystal system** | monoclinic | orthorhombic | triclinic |
| **Space group** | $P2_1/n$ | Pbca | $P\bar{1}$ |
| **a/Å** | 10.2188(5) | 22.3645(8) | 15.6348(8) |
| **b/Å** | 26.8902(12) | 19.9277(6) | 16.8576(9) |
| **c/Å** | 14.8988(6) | 26.6101(9) | 17.3256(9) |
| **α/°** | 90 | 90 | 105.992(2) |
| **β/°** | 98.1234(15) | 90 | 114.194(2) |
| **γ/°** | 90 | 90 | 102.216(2) |
| **Volume/Å³** | 4052.9(3) | 11859.4(7) | 3719.8(3) |
| **Z** | 2 | 4 | 2 |
| **$\rho_{calc}$/g·cm³** | 3.072 | 2.577 | 2.892 |
| **μ/mm⁻¹** | 19.173 | 13.753 | 21.383 |
| **F(000)** | 3360.0 | 8472.0 | 2868.0 |
| **Crystal size/mm³** | 0.331 x 0.254 x 0.194 | 0.27 × 0.26 × 0.25 | 0.65 × 0.159 × 0.098 |
| **Crystal shape** | block | cube | Needle |
| **Radiation** | MoKα (λ = 0.71073) | MoKα (λ = 0.71073) | MoKα (λ = 0.71073) |
| **2Θ range for data collection/°** | 4.1 to 51.516 | 4.106 to 56.598 | 4.016 to 50.832 |
| **Index ranges** | -12 ≤ h ≤ 12, -32 ≤ k ≤ 32, -17 ≤ l ≤ 18 | - 29 ≤ h ≤ 29, -26 ≤ k ≤ 26, -35 ≤ l ≤ 35 | -18 ≤ h ≤ 17, -20 ≤ k ≤ 20, -20 ≤ l ≤ 20 |
| **Reflections collected** | 116438 | 189726 | 180244 |
| **Independent reflections** | 7763 [$R_{int}$ = 0.0623, $R_{sigma}$ = 0.0257] | 14717 [$R_{int}$ = 0.0615, $R_{sigma}$ = 0.0243] | 13670 [$R_{int}$ = 0.0511, $R_{sigma}$ = 0.0221] |
| **Data/restrains/parameters** | 7763/0/532 | 14717/0/700 | 13670/1/663 |
| **Goodness-of-fit on $F^2$** | 1.119 | 1.127 | 1.033 |
| **Final R indexes [I>=2σ(I)]** | $R_1$ = 0.0332, $wR_2$ = 0.0861 | $R_1$ = 0.0313, $wR_2$ = 0.0663 | $R_1$ = 0.0291, $wR_2$ = 0.0755 |
| **Final R indexes [all data]** | $R_1$ = 0.0345, $wR_2$ = 0.0869 | $R_1$ = 0.0459, $wR_2$ = 0.0755 | $R_1$ = 0.0330, $wR_2$ = 0.0791 |
| **Largest diff. peak/hole / e·Å³** | 2.31/−1.81 | 1.86/−1.32 | 2.55/−1.81 |

**Table 2. Crystallographic data.**

| **Compound** | **$Hg(O_2CC_3H_7)$** |
|---|---|
| **Empirical formula** | $C_8H_{14}HgO_4$ |
| **Formula weight** | 372.78 |
| **Temperature/K** | 295 |
| **Crystal system** | triclinic |
| **Space group** | $P\bar{1}$ |
| **a/Å** | 4.6153(7) |
| **b/Å** | 8.5983(14) |
| **c/Å** | 13.661(2) |
| **α/°** | 97.157(6) |
| **β/°** | 99.537(5) |
| **γ/°** | 102.882(5) |
| **Volume/Å³** | 513.76(14) |
| **Z** | 2 |
| **$\rho_{calc}$/g·cm³** | 2.423 |
| **μ/mm⁻¹** | 14.961 |
| **F(000)** | 348.0 |
| **Crystal size/mm³** | 0.871 x 0.531 x 0.381 |
| **Crystal shape** | Needle |
| **Radiation** | MoKα (λ = 0.71073) |
| **2Θ range for data collection/°** | 4.93 to 56.89 |
| **Index ranges** | -6 ≤ h ≤ 6, -11 ≤ k ≤ 11, -18 ≤ l ≤ 18 |
| **Reflections collected** | 28054 |
| **Independent reflections** | 2577 [$R_{int}$ = 0.0433, $R_{sigma}$ = 0.0206] |
| **Data/restrains/parameters** | 2577/0/123 |
| **Goodness-of-fit on $F^2$** | 1.120 |
| **Final R indexes [I>=2σ(I)]** | $R_1$ = 0.0233, $wR_2$ = 0.0521 |
| **Final R indexes [all data]** | $R_1$ = 0.0373, $wR_2$ = 0.0596 |
| **Largest diff. peak/hole / e·Å³** | 1.55/−0.75 |

Single crystals of $Hg(OOCC_3H_7)_2$ were obtained by crystallization from a hot solution in 1,2-dichloroethane. The compound crystallizes in triclinic space group $P\bar{1}$. The asymmetric unit contains two $Hg(OCC_3H_7)$ fragments. Due to a center of inversion located at both mercury atoms the overall formula is $Hg(O_2CC_3H_7)_2$. The mercury atoms are coordinated by 4 different carboxylic groups forming two short Hg-O bonds (2.054(4), 2.056(4) Å) in a linear fashion (O-Hg-O: 180°) and six weaker Hg-O contacts (2.680(4) – 3.086(4) Å) within the sum of the van-der-Waals radii of mercury[11] and oxygen,[12] respectively. Therefore, the coordination number for both metal centers is eight. The carboxylic groups are connecting up to three different mercury atoms yielding a polymeric network. Hg-Hg contacts shorter than twice the van-der-Waals radius of mercury are not observed. So far only a few examples of mercury complexes with a coordination number of eight are reported in the literature.[13–15]

WILEY-VCH

## SUPPORTING INFORMATION

*$FeC_{10}(HgO_2CCF_3)_{10} \cdot 4\ THF \cdot 2\ OEt_2$*

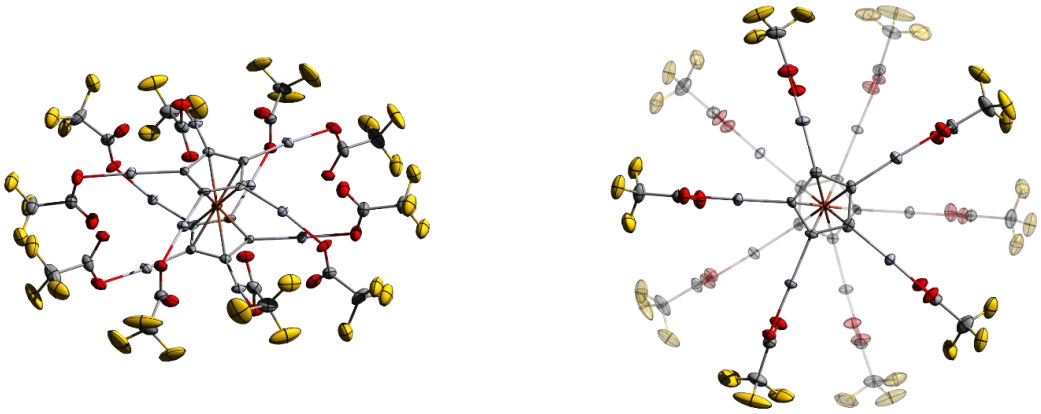

**Figure S1.** Molecular structure of $FeC_{10}(HgO_2CCF_3)_{10} \cdot 4$ THF $\cdot$ 2 $OEt_2$ in the solid state. Solvent molecules and distorted atoms are omitted for clarity. Ellipsoids (50% probability level). Left: front view. Right: top view. The second cyclopentadienyl ligand is drawn in a transparent fashion. Color code: light grey – mercury, orange – iron, yellow – fluorine, red – oxygen, grey – carbon.

*$FeC_{10}(HgO_2CCCl_3)_{10} \cdot 10\ THF \cdot OEt_2$*

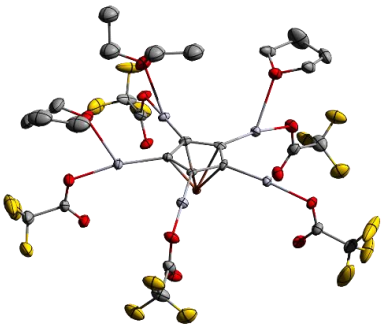

**Figure S2.** Asymmetric unit in the crystal structure of $FeC_{10}(HgO_2CCF_3)_{10} \cdot 4$ THF $\cdot$ 2 $OEt_2$. Hydrogen and distorted atoms are omitted for clarity. Ellipsoids (50% probability level). Color code: light grey – mercury, orange – iron, yellow – fluorine, red – oxygen, grey – carbon.

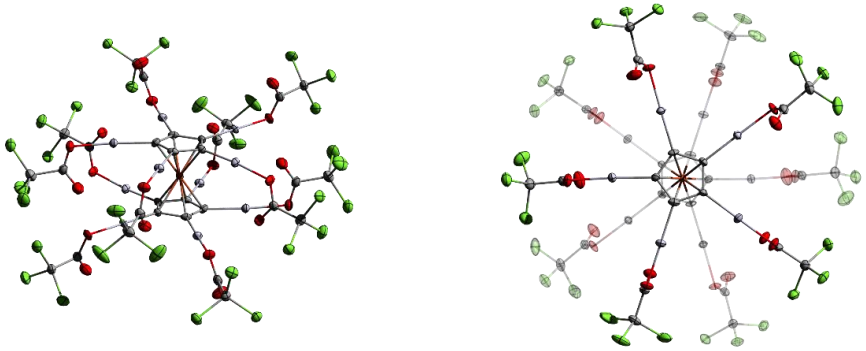

**Figure S3.** Molecular structure of $FeC_{10}(HgO_2CCCl_3)_{10} \cdot 10$ THF $\cdot$ $OEt_2$ in the solid state. Solvent molecules are omitted for clarity. Ellipsoids (50% probability level). Left: front view. Right: top view. The second cyclopentadienyl ligand is drawn in a transparent fashion. Color code: light grey – mercury, orange – iron, green – chlorine, red – oxygen, grey – carbon.

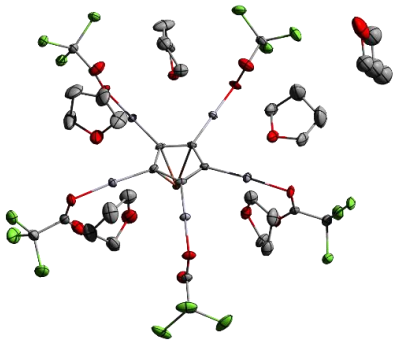

**Figure 4.** Asymmetric unit in the crystal structure of $FeC_{10}(HgO_2CCCl_3)_{10}$ · 10 THF · $OEt_2$. Hydrogen and distorted atoms are omitted for clarity. Ellipsoids (50% probability level). Color code: light grey – mercury, orange – iron, green – chlorine, red – oxygen, grey – carbon.

*$FeC_{10}(HgCl)_{10}$ · 9 DMSO*

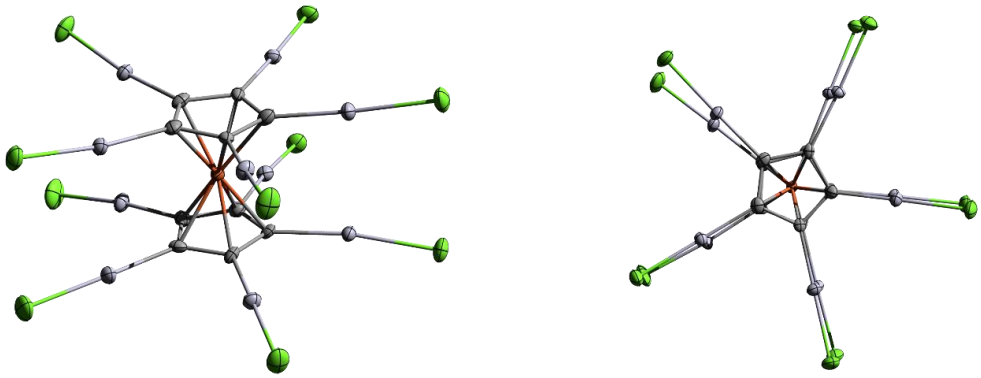

**Figure S5.** Molecular structure of $FeC_{10}(HgCl)_{10}$ · 9 DMSO in the solid state. Solvent molecules are omitted for clarity. Ellipsoids (50% probability level). Left: front view. Right: top view. Color code: light grey – mercury, orange – iron, green – chlorine, red – oxygen, grey – carbon.

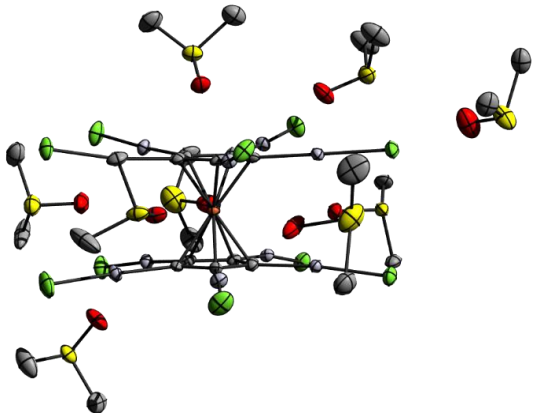

**Figure 6.** Asymmetric unit in the crystal structure of $FeC_{10}(HgCl)_{10}$ · 9 DMSO. Hydrogen and distorted atoms are omitted for clarity. Ellipsoids (50% probability level). Color code: light grey – mercury, orange – iron, green – chlorine, yellow – sulphur, red – oxygen, grey – carbon.

WILEY-VCH

## SUPPORTING INFORMATION

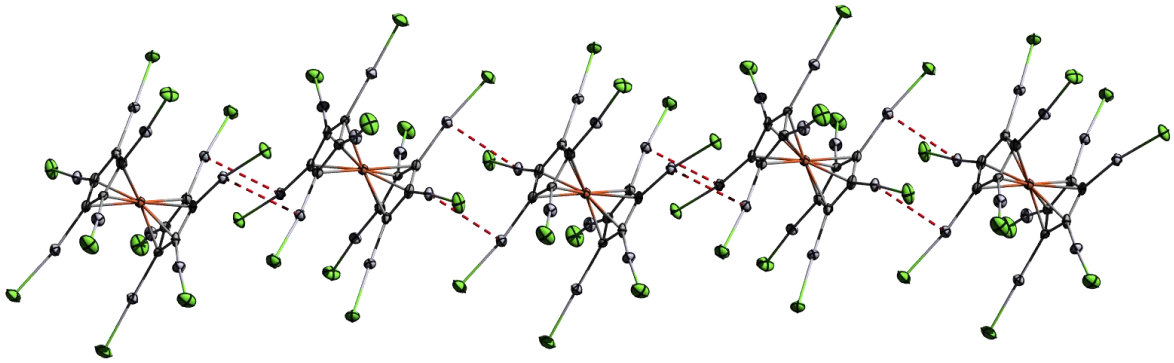

**Figure S7.** Crystal structure of $FeC_{10}(HgCl)_{10} \cdot 9$ DMSO. Front perspective. Ellipsoids (50% probability level). Solvent molecules are omitted for clarity. Color code: light grey – mercury, orange – iron, green – chlorine, grey – carbon.

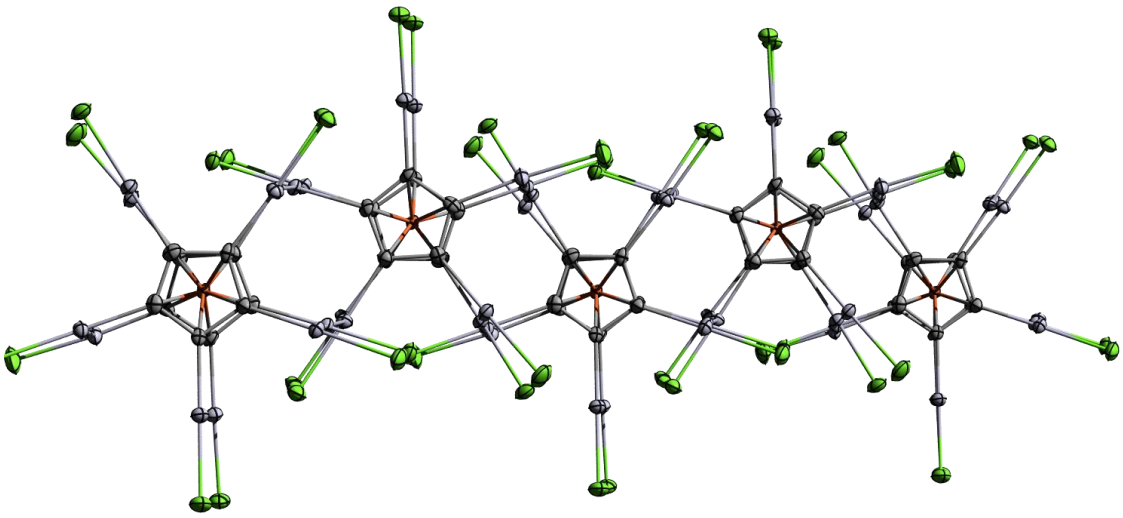

**Figure S8.** Crystal structure of $FeC_{10}(HgCl)_{10} \cdot 9$ DMSO. Top perspective. Ellipsoids (50% probability level). Solvent molecules are omitted for clarity. Color code: light grey – mercury, orange – iron, green – chlorine, grey – carbon.

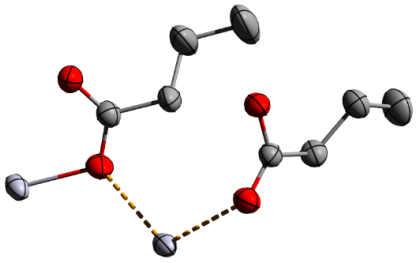

**Figure S9.** Asymmetric unit of the crystal structure of $Hg(O_2CC_3H_7)_2$. Hydrogen atoms are omitted for clarity. Ellipsoids (50% probability level). Color code: light grey – mercury, red – oxygen, grey – carbon.

## References

[1] R. K. Harris, E. D. Becker, S. M. C. de Menezes, P. Granger, R. E. Hoffmann, K. W. Zilm, *Pure Appl. Chem.* **2008**, *80*, 59.
[2] N. T. H. J., S. M., *PLoS One* **2012**, *7*, e44913.
[3] M. R. Willcott, *J. Am. Chem. Soc.* **2009**, *131*, 13180.
[4] OriginLab, *No Title*, OriginLab Corp., Northhampton, Massachusetts, USA, **2016**.
[5] O. V. Dolomanov, L. J. Bourhis, R. J. Gildea, J. A. K. Howard, H. Puschmann, *J. Appl. Cryst.* **2009**, *42*, 339–341.
[6] G. M. Sheldrick, *Acta Cryst.* **2015**, *A71*, 3–8.
[7] G. M. Sheldrick, *SHELXL Version 2014/7, Program for Chrystal Structure Solution and Refinement*, Göttingen, Germany, **2014**.
[8] G. M. Sheldrick, *Acta Cryst.* **2008**, *A64*, 112–122.
[9] K. Brandenburg, "Diamond: Crystal and Molecular Structure Visualization," can be found under http://www.crystalimpact.com/diamond, **2017**.
[10] Persistance of Version Pty. Ltd., **2004**, Retrieved from http://www.povray.org/download/.
[11] P. Pyykkö, M. Straka, *Phys. Chem. Chem. Phys.* **2000**, *2*, 2489–2493.
[12] A. Bondi, *J. Phys. Chem.* **1964**, *68*, 441–451.
[13] N. J. Williams, R. D. Hancock, J. H. Riebenspies, M. A. Fernandes, A. S. de Sousa, *Inorg. Chem.* **2009**, *48*, 11724–11733.
[14] C. Kimblin, V. J. Murphy, T. Hascall, B. M. Bridgewater, J. B. Bonanno, G. Parkin, *Inorg. Chem.* **2000**, *39*, 967–974.
[15] J. Halfpenny, R. W. H. Small, *Acta Crystallorgr., Sect. C Cryst. Struct. Commun.* **1997**, *53*, 438–443.

WILEY-VCH



## Appendix

### Spectra

*Bis(butyryloxy)mercury(II)*

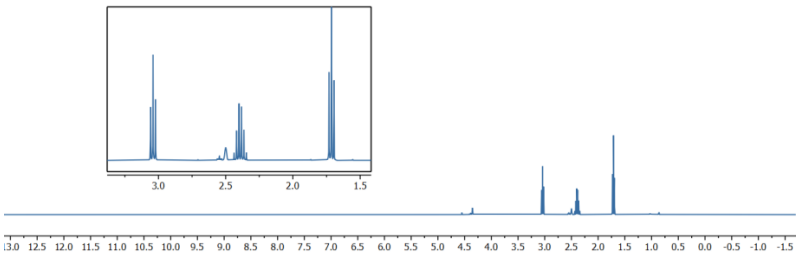


**Figure S10.** $^{1}$H NMR spectrum of bis(butyryloxy)mercury(II) (400 MHz, dmso-$d_6$, r.t.).

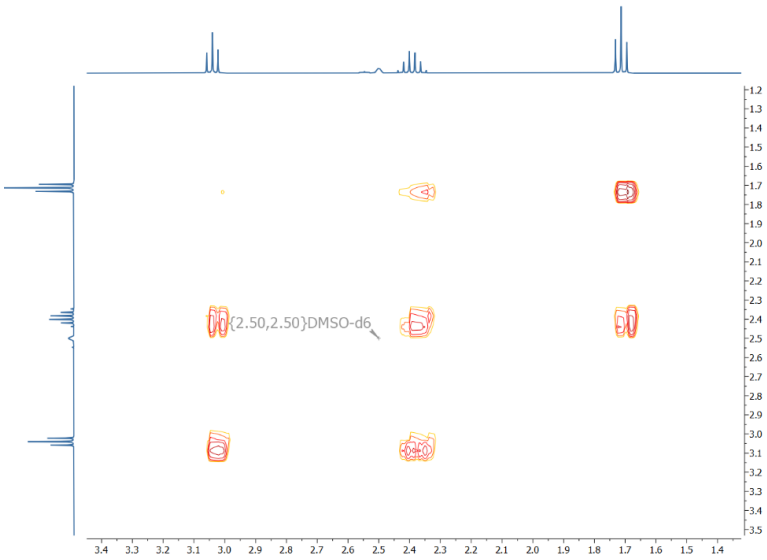


**Figure S11.** $^{1}$H,$^{1}$H COSY NMR spectrum (400 MHz, dmso-$d_6$, r.t.).

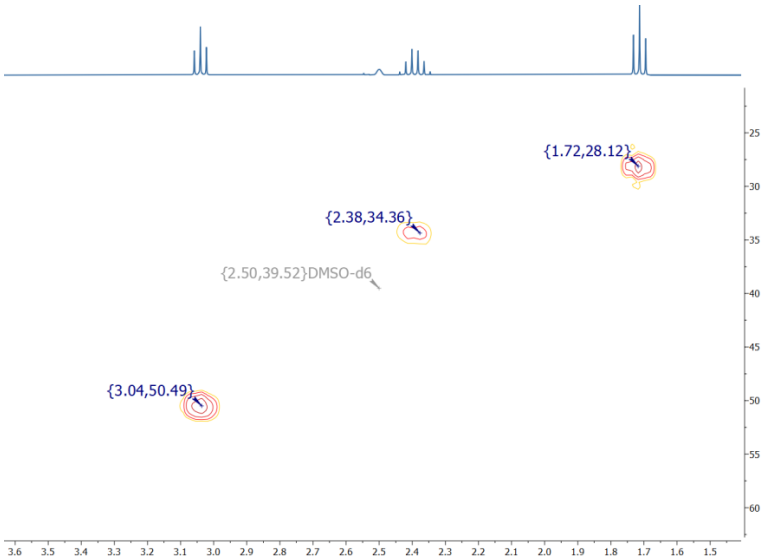


**Figure S12.** $^{1}H,^{13}C$ HMQC NMR spectrum (400 MHz, dmso-$d_6$, r.t.).

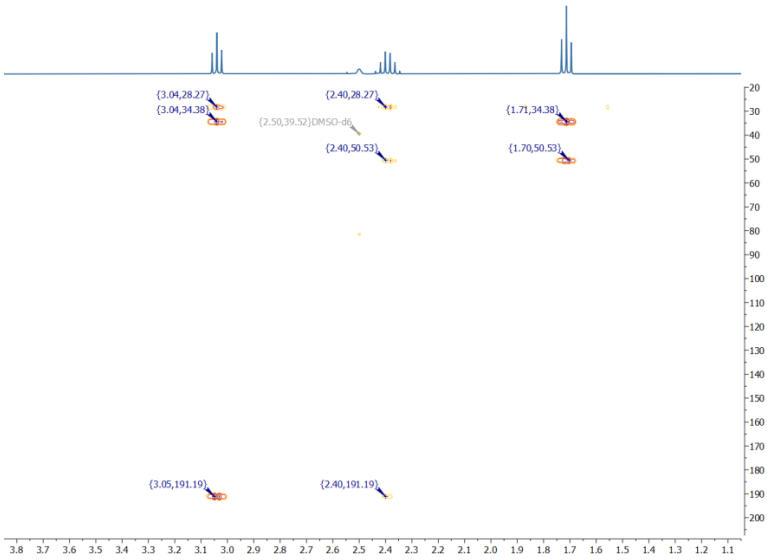


**Figure S13.** $^{1}H,^{13}C$ HMBC NMR spectrum (400 MHz, dmso-$d_6$, r.t.).

WILEY-VCH

SUPPORTING INFORMATION

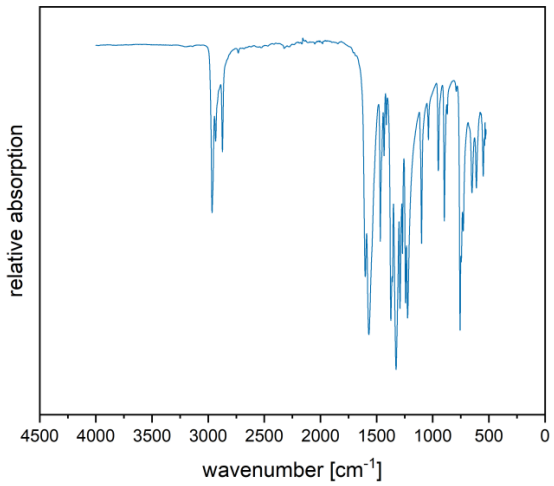


**Figure S14.** Infrared spectrum (ATR) of compound $Hg(O_2CC_3H_7)_2$.

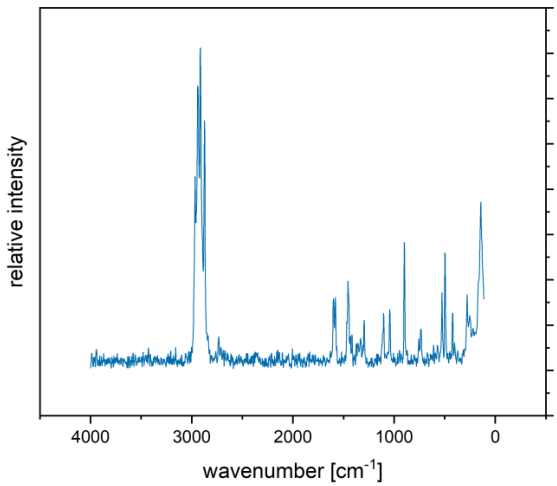


**Figure S15.** Raman spectrum (1064 nm) of $Hg(O_2CC_3H_7)_2$.

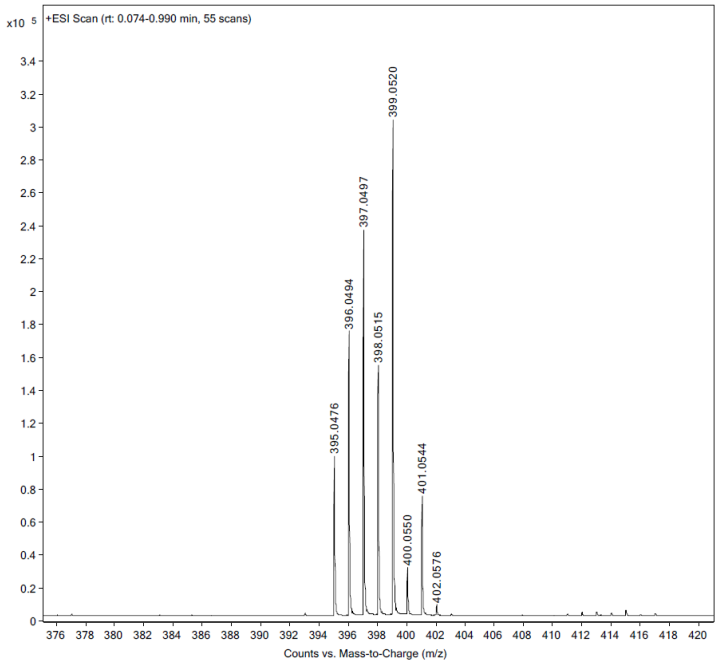


**Figure S16.** Mass spectrum of $Hg(O_2CC_3H_7)_2$, RT, ESI+, DCM/MeOH.

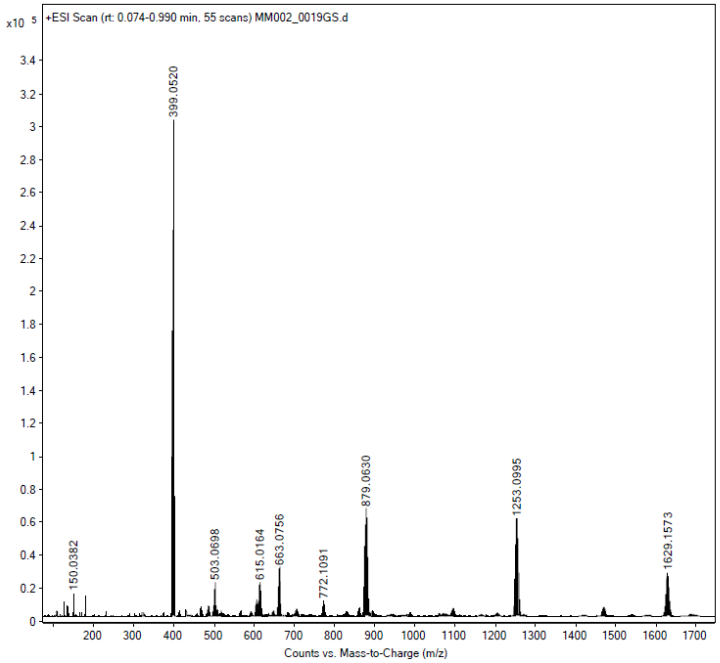


**Figure S17.** Mass spectrum of $Hg(O_2CC_3H_7)_2$, RT, ESI+, DCM/MeOH.

*Decakis(butyryloxymercury(II))ferrocene* ***2***

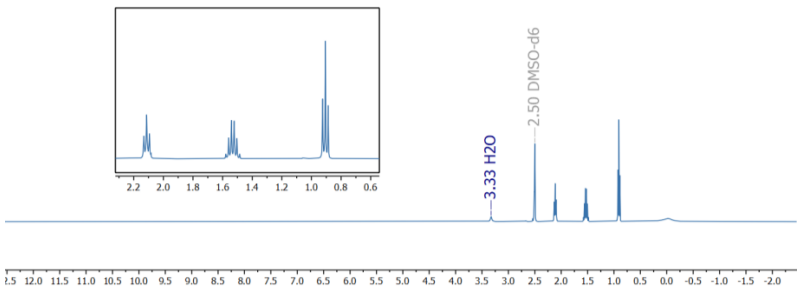


**Figure S19.** $^{1}$H NMR spectrum of $FeC_{10}(HgO_2CC_3H_7)_{10}$ (700 MHz, dmso-$d_6$, r.t.).

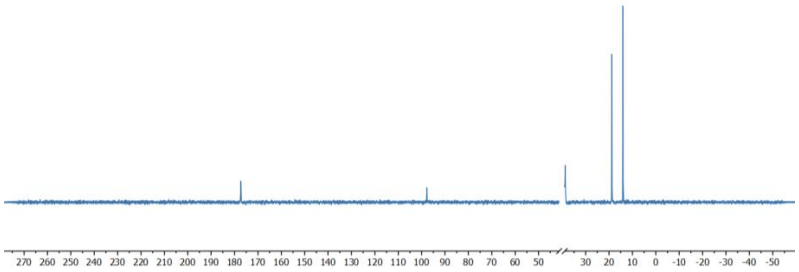

**Figure S20.** $^{13}$C NMR spectrum of $FeC_{10}(HgO_2CC_3H_7)_{10}$ (176 MHz, dmso-$d_6$, r.t.). The signal of the deuterated solvent is omitted for clarity.

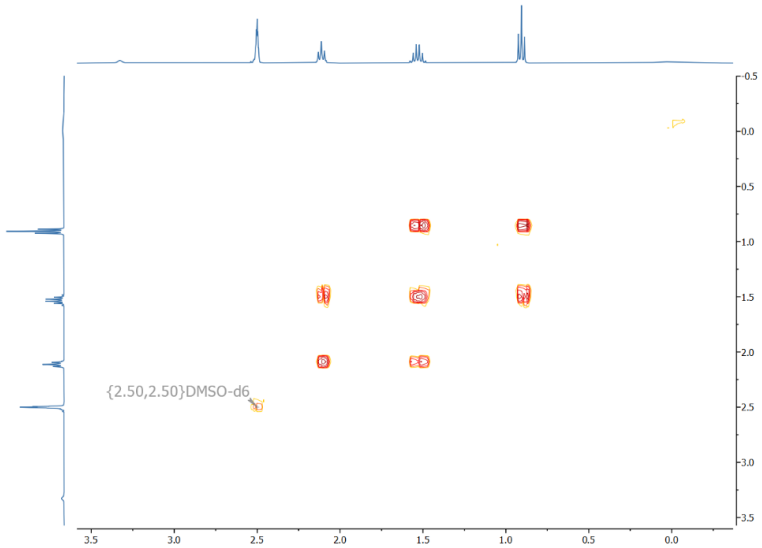


**Figure S18.** $^{1}$H,$^{1}$H COSY NMR spectrum of $FeC_{10}(HgO_2CC_3H_7)_{10}$ (700 MHz, dmso-$d_6$, r.t.).

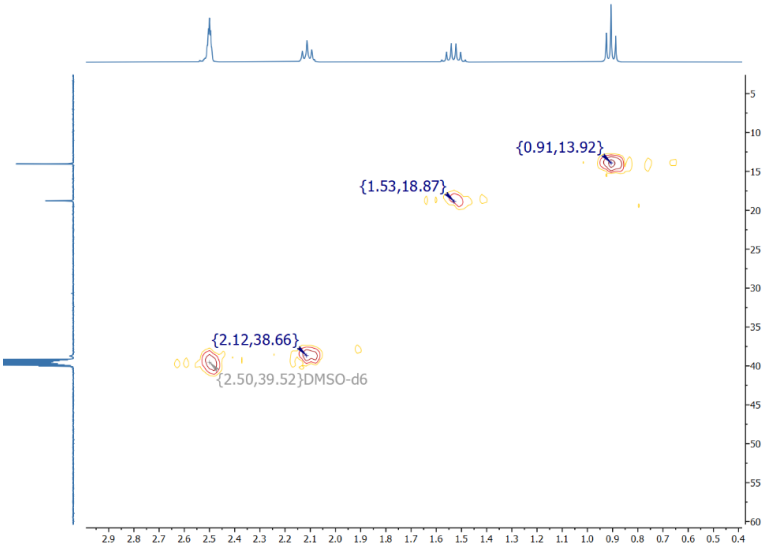


**Figure S21.** $^{1}H,^{13}C$ HMQC NMR spectrum of $FeC_{10}(HgO_2CC_3H_7)_{10}$ (700 MHz, dmso-$d_6$, r.t.).

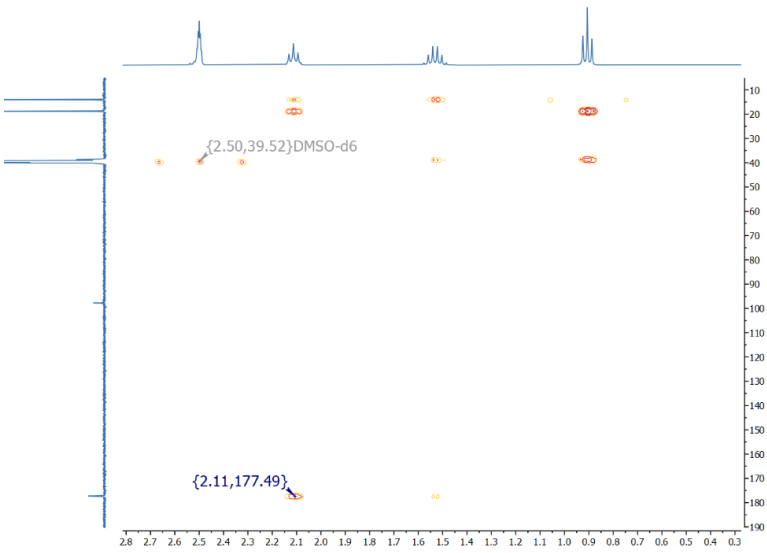


**Figure S22.** $^{1}H,^{13}C$ HMBC NMR spectrum of $FeC_{10}(HgO_2CC_3H_7)_{10}$ (700 MHz, dmso-$d_6$, r.t.).

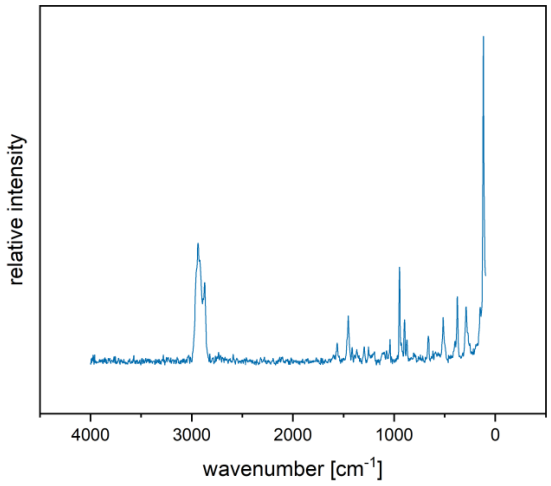


**Figure S23.** Raman spectrum of $FeC_{10}(HgO_2CC_3H_7)_{10}$ (1064 nm, r.t.).

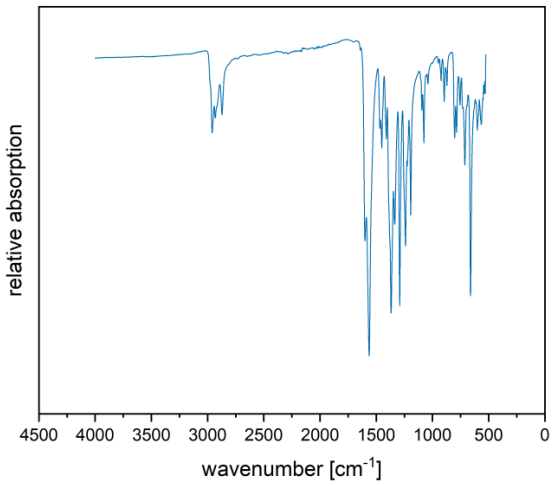


**Figure S24.** Infrared spectrum (ATR) of compound $FeC_{10}(HgO_2CC_3H_7)_{10}$.

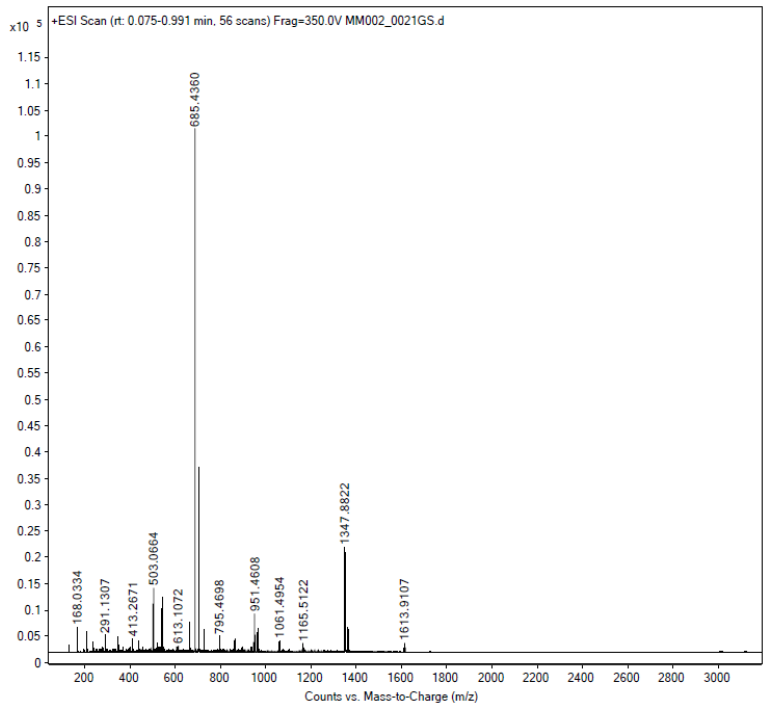


**Figure S25.** Mass spectrum of $FeC_{10}(HgO_2CC_3H_7)_{10}$, RT, ESI+, DCM/MeOH.

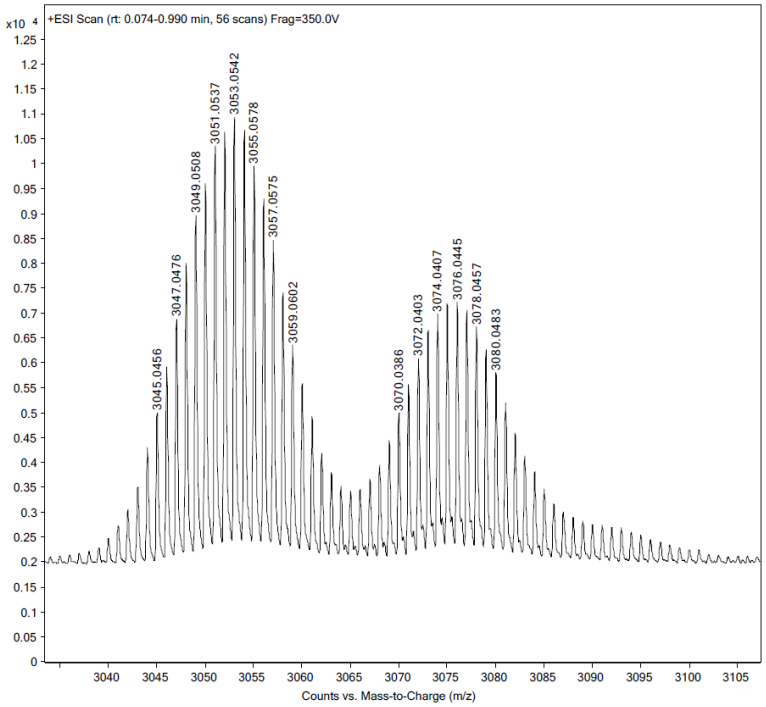


**Figure S26.** Mass spectrum of $FeC_{10}(HgO_2CC_3H_7)_{10}$, RT, ESI+, DCM/MeOH.

WILEY-VCH

## SUPPORTING INFORMATION

*Decakis(trifluoroacetoxymercury(II))ferrocene*

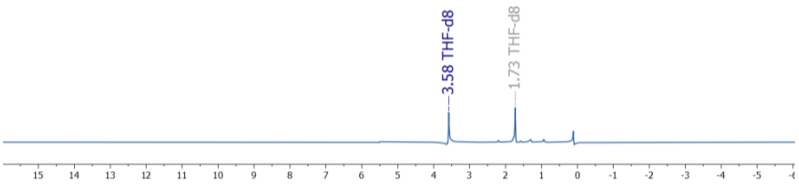


**Figure S27.** $^{1}H$ NMR spectrum of $FeC_{10}(HgO_2CCF_3)_{10}$ (700 MHz, THF-$d_8$, r.t.).

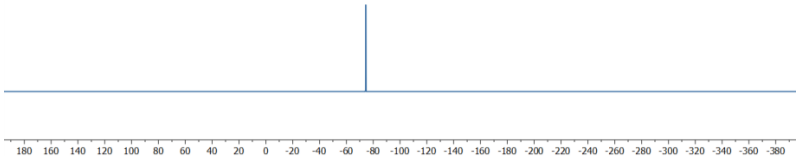

**Figure S28.** $^{19}F$ NMR spectrum of $FeC_{10}(HgO_2CCF_3)_{10}$ (564 MHz, THF-$d_8$, r.t.).

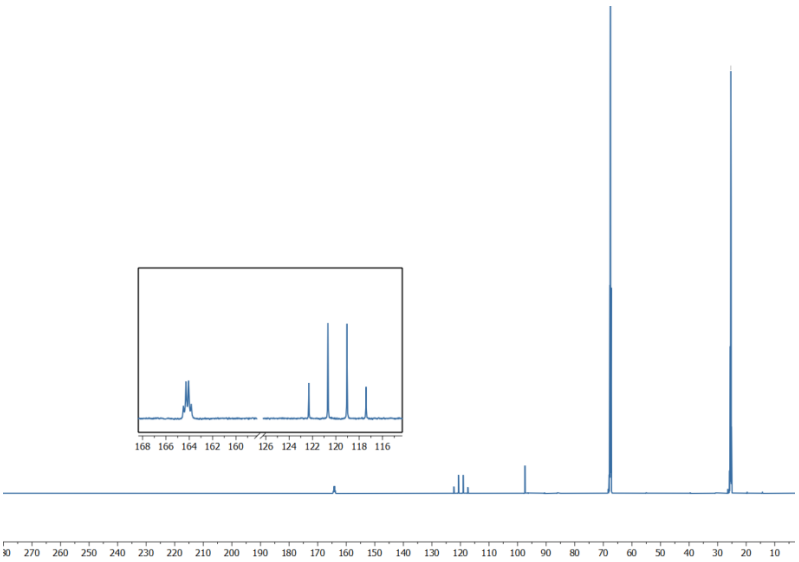

**Figure S29.** $^{13}C\{^{1}H\}$ NMR spectrum of $FeC_{10}(HgO_2CCF_3)_{10}$ (176 MHz, THF-$d_8$, r.t.).

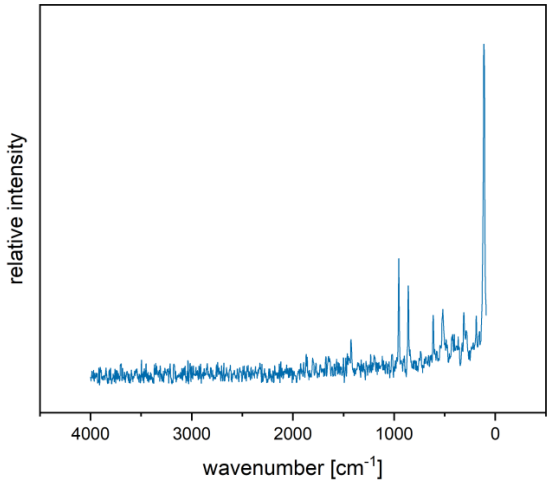


**Figure S30.** Raman spectrum of of $FeC_{10}(HgO_2CCF_3)_{10}$ (1064 nm, r.t.).

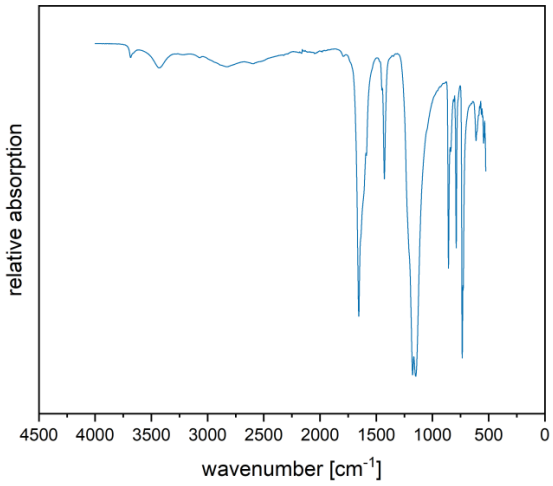


**Figure S31.** Infrared spectrum (ATR) of compound $FeC_{10}(HgO_2CCF_3)_{10}$.

*Decakis(trichloroacetoxymercury(II))ferrocene*

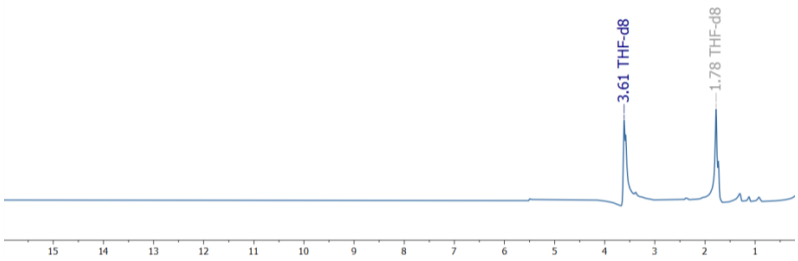


**Figure S32.** $^{1}$H NMR spectrum of $FeC_{10}(HgO_2CCCl_3)_{10}$ (700 MHz, THF-$d_8$, r.t.).

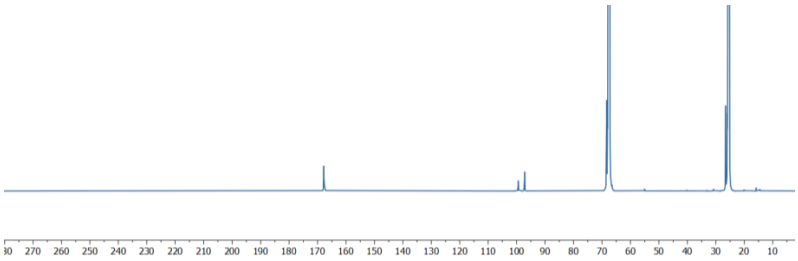

**Figure S33.** $^{13}$C NMR spectrum of $FeC_{10}(HgO_2CCCl_3)_{10}$ (176 MHz, THF-$d_8$, r.t.).

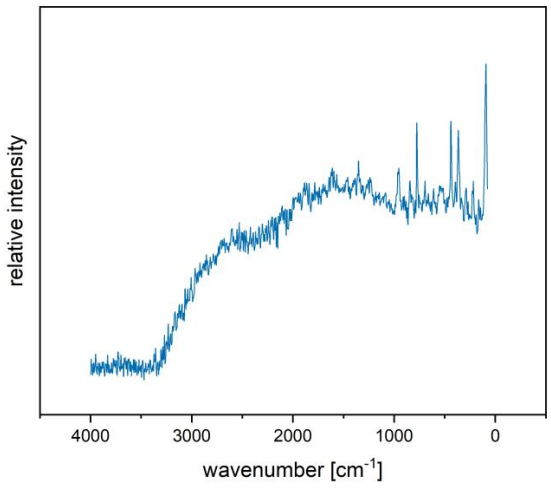


**Figure 34.** Raman spectrum (1064 nm) of $FeC_{10}(HgO_2CCCl_3)_{10}$

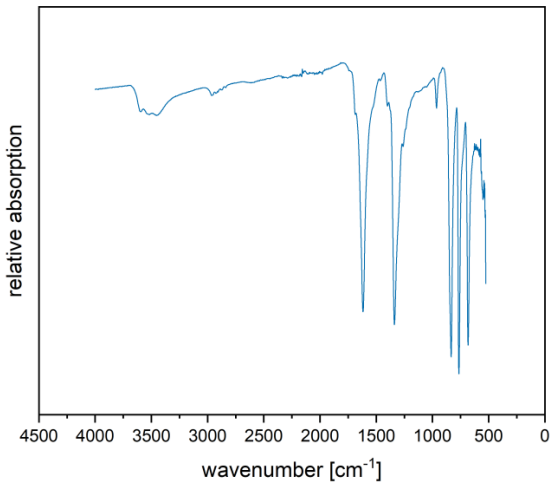


**Figure S35.** Infrared spectrum (ATR) of compound $FeC_{10}(HgO_2CCCl_3)_{10}$.

*Decakis(fluoridomercury)ferrocene*

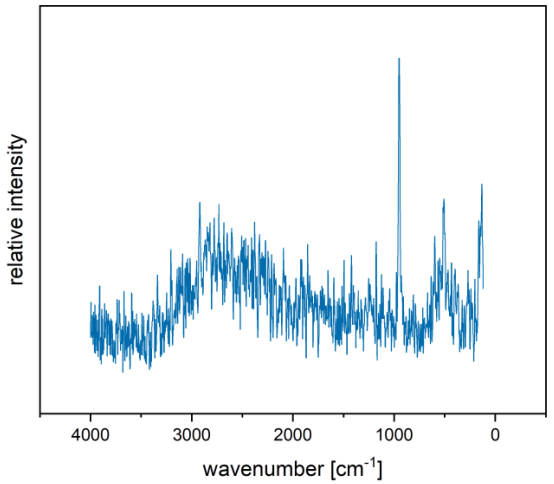


**Figure S36.** Raman spectrum (1064 nm) of $FeC_{10}(HgF)_{10}$.

*Decakis(chloridomercury)ferrocene*

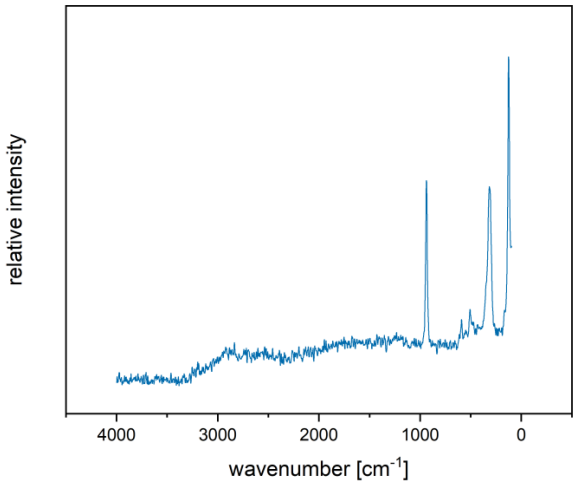


**Figure S37.** Raman spectrum (1064 nm) of $FeC_{10}(HgCl)_{10}$.

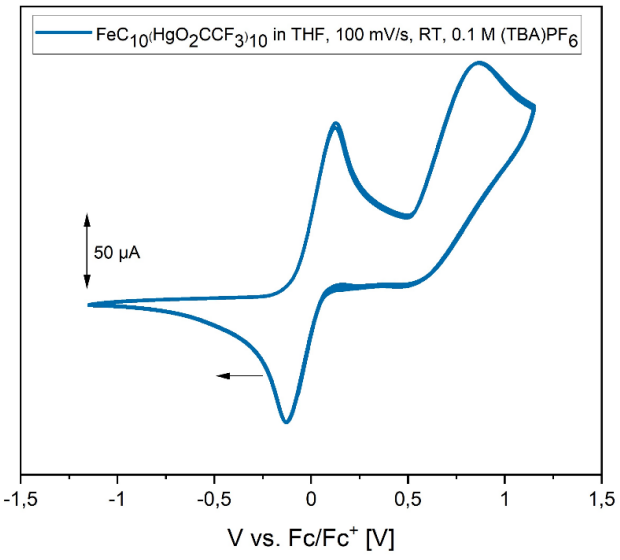


**Figure S38.** Cyclic voltammogram of $FeC_{10}(HgO_2CCF_3)_{10}$ referenced vs. $Cp_2Fe$.

## A.2 A Decacationic Ferrocene-Based Metallostar

SUPPORTING INFORMATION

# A Decacationic Ferrocene-Based Metallostar

Susanne M. Rupf, Amina L. Moshtaha, Moritz Malischewski*

# SUPPORTING INFORMATION

## Table of Contents

# SUPPORTING INFORMATION

## Experimental Procedures

### General Procedures

**CAUTION:** Mercury compounds are highly toxic. Therefore, the chemicals should be handled under a well-ventilated fume hood. Great care must be taken that organomercury compounds are not spilled on the skin. It is advisable to use multiple layers of impenetrable gloves and to remove the outer layer immediately if material is spilled on it. The face might be protected against splashes by using a face shield. Due to the hazardous effects of mercury on the environment, great care must be taken to prevent contamination of the wastewater with mercury. Moreover, $SbF_5$ and *a*HF are highly dangerous compounds with devastating effects on human tissue. They should only be handled in appropriate equipment by trained personnel. $SO_2$ and *a*HF are (toxic) gases at room temperature.

Commercially available chemicals were used as received, unless otherwise noted. $SbF_5$ was stored inside a glove box. Oxygen- and moisture-sensitive compounds were handled using Schlenk techniques and/or handled and stored in an argon-filled glovebox ($O_{2(g)}$ and $H_2O_{(g)}$ < 0.1 ppm). $SO_2$ was distilled from $CaH_2$ and stored in a stainless-steel cylinder. Reactions involving $SO_2$, *a*HF and $SbF_5$ were performed in PFA (tetrafluoroethene-perfluoroalkoxyvinyl-copolymer) tubes connected to stainless-steel valves. Instead of stirring, the mixtures were agitated with the help of the Mini-Vortex Mixer PV-1. $[FeC_{10}(HgO_2CCF_3)_{10}]$[1] and $[C_5F_5NH][SbF_6]$[2] were synthesized according to the literature procedure. Anhydrous MeCN and DCM were obtained from the solvent system FMBRAUN MB SPS-800. THT, MeCN and $C_5F_5N$ as well as deuterated solvents were stored in Young flasks under argon atmosphere over molar sieve (3 Å) which was dried beforehand at 250 °C under high vacuum. Solvents were degassed by three freeze-pump-thaw cycles.

$^1H$, $^{13}C$ and $^{19}F$ NMR spectra were recorded on a Bruker AVANCE III 700 spectrometer by using 6mm NMR glass tubes. All reported chemical shifts (δ) are referenced to the Ξ values given in IUPAC recommendations of 2008 using the $^2H$ signal of the deuterated solvent as internal reference.[3] All chemical shifts (δ) are given in parts per million (ppm) and the signals are specified according to the multiplicity (s = singlet, d = doublet, t = triplet, q = quartet, m = multiplet, br = broad) and the coupling constants *J* in Hz. The program MestRe Nova Version 14.0.1 was used to evaluate and plot the data.[4]

Infrared spectra were measured using a Thermo-Scientific Nicolet iS10 FTIR spectrometer with DuraSamplIR accessory in attenuated total reflection at room temperature or on a Bruker ALPHA FT-IR spectrometer inside a glovebox equipped with a diamond ATR attachment. Raman spectra were recorded on a Bruker MultiRAM II equipped with a low-temperature Ge detector (1064 nm, 30-80 mW, resolution 2 $cm^{-1}$). The software OriginPro 2017G was used to plot the data.[5]

Cyclic voltammetry was performed on an Interface 1010 B Potentiostat/Galvanostat/ZRA from Gamry Instruments. The investigations were carried out starting from 0 V going to the oxidation first and then to the reduction. The measurements were performed in anhydrous and oxygen free solvents under argon atmosphere without supporting electrolyte and platinum wires as working-, counter-, and quasi-reference electrodes. The voltammograms were internally referenced against $FeCp_2^{0/+}$. The software OriginPro 2017G was used to plot the data.[5]

X-Ray data were collected on a BRUKER D8 Venture system. Data were collected at 100(2) K using graphite-monochromated Mo $K_\alpha$ radiation ($\lambda_\alpha$ = 0.71073 Å) or a Cu $K_\alpha$ radiation (λ=1.54178). The strategy for the data collection was evaluated by using the Smart software. The data were collected by the standard "*ψ*-*ω* scan techniques" and were scaled and reduced using Saint+software. The structures were solved by using Olex2,[6] the structure was solved with the XT[7] structure solution program using Intrinsic Phasing and refined with the XL refinement package[8,9] using Least Squares minimization. If it is noted, bond length and angles were measured with Diamond Crystal and Molecular Structure Visualization Version 4.6.2.[10] Drawings were generated with POV-Ray.[11] Deposition numbers CCDC 2214089 ($[FeC_{10}(HgDMAP)_{10}][TFA]_{10}$), 2213962 ($[FeC_{10}(HgTHT)_{10}][SbF_6]_{10}$ · 24 MeCN) and 2213956 (**[**$FeCp_2(HgMeCN)_{10}][SbF_6]_{10}[MoF_6]$ · 2 $SO_2$ ·10 HF**)** contain the supplementary crystallographic data for this paper. These data are provided free of charge by the joint Cambridge Crystallographic Data Centre and Fachinformationszentrum Karlsruhe Access Structures service www.ccdc.cam.ac.uk/structures.

Elemental analysis was performed with Vario EL elemental analyser (Elementar, Germany). UV/vis spectra were recorded on a Varian Cary 50 Bio photo spectrometer (xenon lamp) by using Suprasil quartz cuvettes (d = 1 cm) equipped with a Schlenk valve cock. Observed spectra are consistent with those of ferrocene and ferrocenium salts.[12,13]

# SUPPORTING INFORMATION

**Syntheses**

*[$FeC_{10}Hg_{10}dmap_{10}$][TFA]$_{10}$ (**1**)*

$$[FeC_{10}(HgTFA)_{10}] \xrightarrow[\text{THF, 25 °C}]{\text{exc. dmap}} [FeC_{10}Hg_{10}dmap_{10}][TFA]_{10} \quad (\mathbf{1})$$

In a 100 mL round bottom flask $[FeC_{10}(HgTFA)_{10}]$ (580 mg, 0.175 mmol, 1.0 eq.) was dissolved in THF (25 mL). Then, dmap (370 mg, 3.03 mmol, 17 eq.) was added to the solution at room temperature, yielding an orange precipitate. The precipitate was filtered off, washed with THF (50 mL) and *n*-pentane (50 mL) and dried at high vacuum. The compound $[FeC_{10}(HgDMAP)_{10}][TFA]_{10}$ (425 mg, 0.093 mmol, 57%) was obtained as orange powder. Single crystals were obtained by diffusion of $[FeC_{10}(HgTFA)_{10}]$ and DMAP in tetrahydrofuran in a H-tube. **$^1$H NMR** (600 MHz, $CD_2Cl_2$, r.t.): *δ* [ppm] = 8.27 (m, 2H), 6.50 (m, 2H), 3.05 (s, 6H). **$^{13}$C{$^1$H} NMR** (101 MHz, $CD_2Cl_2$, r.t.): δ [ppm] = 161.4 (q, *J* = 34.3 Hz), 155.7, 148.8, 118.4 (q, *J* = 296.5 Hz), 106.9, 100.8, 39.6. **$^{19}$F NMR** (565 MHz, $CD_2Cl_2$, r.t.) δ [ppm] = −74.7 (s). **FT-IR** (ATR): $\tilde{\nu}$ [cm$^{-1}$] = 3094, 2931, 1790, 1621, 1549, 1446, 1396, 1235, 1196, 1174, 1122, 1072, 1023, 947, 813, 798, 718. **Raman** (1064 nm, r.t.): $\tilde{\nu}$ [cm$^{-1}$] = 3094, 2937, 2905, 2869, 2823, 1636, 1624, 1549, 1448, 1418, 1301, 1237, 1077, 951, 827, 765, 662, 595, 193, 100. **Elemental analysis:** m[%] = calculated: N: 6.41, C: 24.72, H: 1.38, found: N: 6.43, C: 24.76, H: 1.28.

*[($FeC_{10}Hg_{10}$(solv.)$_n$][$SbF_6$]$_{10}$ (**2**)*

$$[FeC_{10}(HgTFA)_{10}] \xrightarrow[\substack{\text{- HTFA}\\ SO_2,\ -25\ °C}]{10\ [HNC_5F_5][SbF_6]} [FeC_{10}Hg_{10}(NC_5F_5)_n][SbF_6]_{10} \xrightarrow[\substack{-\ n\ NC_5F_5\\ SO_2,\ -25\ °C}]{\text{solv.}} [FeC_{10}Hg_{10}(\text{solv.})_{10}][SbF_6]_{10} \quad (\mathbf{2})$$

**2a** – solv. = $C_5F_5N$: Pentafluoropyridinium hexafluoroantimonate (2.99 g, 7.38 mmol, 10 eq.) was filled in a 12 mm PFA tube under an atmosphere of argon. Sulfur dioxide was condensed at −196 °C into the reaction tube. Subsequently, the reaction mixture was brought to −10 °C and mechanically shaken until a colourless solution was obtained. The mixture was brought to −196 °C again, followed by addition of $FeC_{10}(HgTFA)_{10}$ (2.45 g, 0.738 mmol, 1.0 eq.). The mixture was warmed up to 0 °C until a deep red solution was obtained. Sulfur dioxide was evaporated under reduced pressure and the product (4.60 g, 0.738 mmol, quant.) was obtained as orange, amorphous solid. The compound was stored in a glovebox under argon atmosphere. **FT-IR** (ATR): $\tilde{\nu}$ [cm$^{-1}$] = 3345, 1778, 1668,1615, 1545, 1516, 1489, 1324, 1186, 1112, 1077, 998, 978, 660, 633, 555. **Raman** (1064 nm, r.t.): $\tilde{\nu}$ [cm$^{-1}$] = 939, 650, 639, 602, 522, 497, 458, 359, 279, 112.

$[FeC_{10}Hg_{10}(NC_5F_5)_n][SbF_6]_{10}$ was placed in a flame dried 20 mL Schlenk tube. Anhydrous donor solvent (solv., ca. 0.1 mL) was added yielding a red solution. The solvent was evaporated in an oil pump vacuum of $10^{-3}$ mbar to afford the product as pink, amorphous solid.

**2b** – solv. = THT: $[FeC_{10}Hg_{10}(NC_5F_5)_n][SbF_6]_{10}$ (100.0 mg, 0.016 mmol, 1.0 eq.), THT (ca. 1 mL, ), $[FeC_{10}Hg_{10}(THT)_{10}][SbF_6]_{10}$ (87.3 mg, 0.016 mmol, quant.). Single crystals were obtained, by slow cooling of **2b** dissolved in MeCN from r.t. to −35 °C. **$^1$H NMR** (600 MHz, MeCN-$d_3$, r.t.) δ [ppm] = 3.64 (m, 4H), 2.24 (m, 4H). **$^{13}$C NMR** (151 MHz, MeCN-$d_3$, r.t.) δ [ppm] = 111.8, 31.6. **$^{19}$F NMR** (565 MHz, MeCN-$d_3$, r.t.) δ [ppm] = −120.3 (m). **FT-IR** (ATR): $\tilde{\nu}$ [cm$^{-1}$] = 3607, 3535, 2955, 2869, 1629, 1491, 1435, 1275, 1260, 1194, 1143, 1077, 975, 957, 883, 811, 656, 635, 559, 518, 472. **Raman** (1064 nm, r.t.): $\tilde{\nu}$ [cm$^{-1}$] = strong fluorescence. **Elemental analysis:** m[%] = calculated : N: 0.00, C: 11.08, H: 1.49, S: 5.91, found: N: 0.00, C: 11.88, H: 1.66, S: 5.35.

**2c** – solv. = MeCN: $[FeC_{10}Hg_{10}(NC_5F_5)_n][SbF_6]_{10}$ (25.0 mg, 4.01 µmol, 1.0 eq.), MeCN (0.1 mL, ), $[FeC_{10}Hg_{10}(MeCN)_{10}][SbF_6]_{10}$ (19.9 mg, 4.01 µmol, quant.). **$^1$H NMR** (700 MHz, MeCN-$d_3$, r.t.) δ [ppm] = 1.96 (s). **$^{13}$C NMR** (176 MHz, MeCN-$d_3$, r.t.) δ [ppm] = 108.3 (s), 97.7 (s), 1.2 (q, *J* = 20.7 Hz). **$^{19}$F NMR** (565 MHz, MeCN-$d_3$, r.t.) δ [ppm] = −120.3 (m). **FT-IR** (ATR): $\tilde{\nu}$ [cm$^{-1}$] = 3015, 2947, 2331, 2305, 2247, 1416, 1368, 1215, 1162, 1032, 957, 795, 651, 638, 560. **Raman** (1064 nm, r.t.): $\tilde{\nu}$ [cm$^{-1}$] = strong fluorescence. **Elemental analysis:** m[%] = calculated : N: 2.83, C: 7.28, H: 0.61, found: N: 2.75, C: 7.45, H: 1.24.

# SUPPORTING INFORMATION

*[(FeC$_{10}$Hg$_{10}$(solv.)$_n$]$^{11+}$ (**3**)*

$$[FeC_{10}Hg_{10}(solv.)_n][SbF_6]_{10} \xrightarrow[-\,Ox]{Ox[An]} [FeC_{10}Hg_{10}(solv.)_n][SbF_6]_{10}[An] \qquad (\mathbf{3})$$

**Table S1.** Summary of oxidation attempts. Orange-red solution – Fe(II), green/blue solution – Fe(III).

| starting material | oxidant | solvent | observation |
|---|---|---|---|
| [(FeC$_{10}$Hg$_{10}$(NC$_5$F$_5$)$_n$]$^{11+}$ (**3a**) | $NOBF_4$ (8.6 eq.) | $SO_2$ | brown suspension |
| | $NO_2SbF_6$ (2.1 eq.) | $SO_2$ | green solution |
| [(FeC$_{10}$Hg$_{10}$(THT)$_{10}$]$^{11+}$ (**3b**) | $AgSbF_6$ | dcm | no reaction |
| | $NOBF_4$ (5.0 eq.) | $SO_2$ | green solution |
| | $NO_2SbF_6$ (1.0 eq.) | $SO_2$ | green solution |
| | $MoF_6$ (11.0 eq.) | $SO_2$ | green solution |
| [(FeC$_{10}$Hg$_{10}$(MeCN)$_n$]$^{11+}$ (**3c**) | $NOBF_4$ (2.7 eq.) | $SO_2$ | blue solution |
| | $NO_2SbF_6$ (1.8 eq.) | $SO_2$ | blue solution |
| | $MoF_6$ (12.0 eq.) | $SO_2$ | blue solution |

**3c** – solv. = MeCN: [FeC$_{10}$Hg$_{10}$(MeCN)$_{10}$][SbF$_6$]$_{10}$ (39.6 mg, 0.008 mmol, 1.0 eq.) was filled in an 8 mm PFA tube under an atmosphere of argon and dissolved in liquid $SO_2$ (1 mL). Then, $MoF_6$ (20.00 mg, 0.095 mmol, 11.9 eq.) was added at −196 °C. The reaction mixture was brought to −10 °C and mechanically shaken until a dark blue solution was obtained. All liquid components were evaporated under reduced pressure and the product (41.5 mg, 0.008 mmol, quant.) was obtained as blue solid and stored under argon. Single crystals were obtained by recrystallisation from HF/$SO_2$ at −74 °C. **FT-IR** (ATR): $\tilde{\nu}$ [cm$^{-1}$] = 2942, 2332, 2306, 2247, 1552, 1408, 1374, 1221, 1167, 1019, 957, 865, 653, 634, 557, 520. **Raman** (1064 nm, r.t.): $\tilde{\nu}$ [cm$^{-1}$] = 2949, 2339, 2991, 2248, 1369, 945, 644, 393, 364, 125.

## Crystallographic Data

**Table S2**. Crystallographic data.

| Compound | $[FeC_{10}(HgDMAP)_{10}][TFA]_{10}$ | $[FeC_{10}(HgTHT)_{10}][SbF_6]_{10}$ · 24 MeCN | $[FeCp_2(HgMeCN)_{10}][SbF_6]_{10}[MoF_6]$ · 2 $SO_2$ ·10 HF |
|---|---|---|---|
| **Empirical formula** | $FeC_{98}Hg_{10}N_{20}H_{100}O_{18}F_{27}$ | $C_{98}F_{60}FeH_{150}Hg_{10}N_{24}S_{10}Sb_{10}$ | $C_{30}F_{88}FeH_{42}Hg_{10}MoN_{10}O_{12}S_6Sb_{10}$ |
| **Formula weight** | 4420.72 | 6404.26 | 5974.28 |
| **Temperature/K** | 100 | 100.0 | 100 |
| **Crystal system** | monoclinic | monoclinic | triclinic |
| **Space group** | $P2_1/n$ | *C*2/*c* | *P*-1 |
| **a/Å** | 16.8907(4) | 18.7149(8) | 11.5091(7) |
| **b/Å** | 40.5278(10) | 36.9102(16) | 16.0047(12) |
| **c/Å** | 23.0130(5) | 32.7166(14) | 16.9690(11) |
| **α/°** | 90 | 90 | 78.893(3) |
| **β/°** | 109.0010(10) | 94.377(2) | 83.202(2) |
| **γ/°** | 90 | 90 | 80.190(3) |
| **Volume/Å³** | 14895.0(6) | 22533.8(17) | 3010.4(4) |
| **Z** | 4 | 4 | 1 |
| **$\rho_{calc}$/g·cm³** | 1.971 | 1.888 | 3.295 |
| **μ/mm⁻¹** | 19.530 | 8.197 | 15.392 |
| **F(000)** | 8164 | 11768.0 | 2654.0 |
| **Crystal size/mm³** | 0.5 × 0.44 × 0.39 | 0.5 × 0.38 × 0.33 | 0.26 × 0.18 × 0.15 |
| **Crystal shape** | block | block | block |
| **Radiation** | CuKα (λ=1.54178) | MoKα (λ = 0.71073) | MoKα (λ = 0.71073) |
| **2Θ range for data collection/°** | 4.61 to 134.364 | 3.966 to 50.328 | 4.18 to 56.594 |
| **Index ranges** | -20 ≤ h ≤ 20, -48 ≤ k ≤ 48, -27 ≤ l ≤ 27 | -22 ≤ h ≤ 22, -44 ≤ k ≤ 44, -39 ≤ l ≤ 39 | -15 ≤ h ≤ 15, -21 ≤ k ≤ 21, -22 ≤ l ≤ 22 |
| **Reflections collected** | 416111 | 325039 | 66569 |
| **Independent reflections** | 26601 [$R_{int}$ = 0.0781, $R_{sigma}$ = 0.0277] | 20131 [$R_{int}$ = 0.0376, $R_{sigma}$ = 0.0141] | 14855 [$R_{int}$ = 0.0291, $R_{sigma}$ = 0.0243] |
| **Data/restrains/parameters** | 26601/1/1710 | 20131/0/911 | 14855/0/660 |
| **Goodness-of-fit on F²** | 1.052 | 1.040 | 1.083 |
| **Final R indexes [I>=2σ(I)]** | $R_1$ = 0.0519, $wR_2$ = 0.1389 | $R_1$ = 0.0384, $wR_2$ = 0.1055 | $R_1$ = 0.0309, $wR_2$ = 0.0702 |
| **Final R indexes [all data]** | $R_1$ = 0.0569, $wR_2$ = 0.1439 | $R_1$ = 0.0426, $wR_2$ = 0.1095 | $R_1$ = 0.0344, $wR_2$ = 0.0717 |
| **Largest diff. peak/hole / e·Å³** | 3.38/-1.87 | 2.14/-1.87 | 2.75/-2.47 |

# SUPPORTING INFORMATION

In the crystal structure of $[FeC_{10}(HgTHT)_{10}][SbF_6]_{10} \cdot 24$ MeCN the iron atoms produce a hexagonal closed arrangement along the ac-plane with an AB-stacking pattern (Fig. S20). However, the iron atoms of layer B are not found within the trigonal voids similar to the Mg-type but displaced along the c-axis causing a number of surrounding iron atoms of ten instead twelve as expected for a Mg-type packing. Considering only the centers of gravity for all molecular entities, no simple packing arrangement is observed for the anionic units as they are not located neither within the tetrahedral nor in the octahedral voids. For the THT-structure the decacation is surrounded by 20 anions but due to disordering of the anions no ordered arrangement of Sb atoms is visible.

## References


[1] S. M. Rupf, G. Schröder, R. Sievers, M. Malischewski, *Chem. Eur. J.* **2021**, *27*, 5125–5129.
[2] S. L. Bell, R. D. Chambers, K. R. Musgrave, J. G. Thorpe, *J. Fluor. Chem.* **1971**, *1*, 51–57.
[3] R. K. Harris, E. D. Becker, S. M. C. de Menezes, P. Granger, R. E. Hoffmann, K. W. Zilm, *Pure Appl. Chem.* **2008**, *80*, 59.
[4] M. R. Willcott, *J. Am. Chem. Soc.* **2009**, *131*, 13180.
[5] *Origin(Pro), Version 2016*, OriginLab Corporation, Northhampton, Massachusetts, USA, **2016**.
[6] O. V. Dolomanov, L. J. Bourhis, R. J. Gildea, J. A. K. Howard, H. Puschmann, *J. Appl. Cryst.* **2009**, *42*, 339–341.
[7] G. M. Sheldrick, *Acta Cryst.* **2015**, *A71*, 3–8.
[8] G. M. Sheldrick, *SHELXL Version 2014/7, Program for Crystal Structure Solution and Refinement*, Göttingen, Germany, **2014**.
[9] G. M. Sheldrick, *Acta Cryst.* **2008**, *A64*, 112–122.
[10] K. Brandenburg, “Diamond: Crystal and Molecular Structure Visualization,” can be found under http://www.crystalimpact.com/diamond, **2017**.
[11] Persistence of Vision Pty. Ltd., **2004**.
[12] Y. S. Sohn, D. N. Hendrickson, H. B. Gray, *J. Am. Chem. Soc.* **1971**, *93*, 3603–3612.
[13] H. Ju, B. Ye, J. Gu, *Sensors* **2004**, *4*, 71–83.

## Appendix

### Spectra

*[FeC$_{10}$(HgDMAP)$_{10}$][TFA]$_{10}$ (**1a**):*

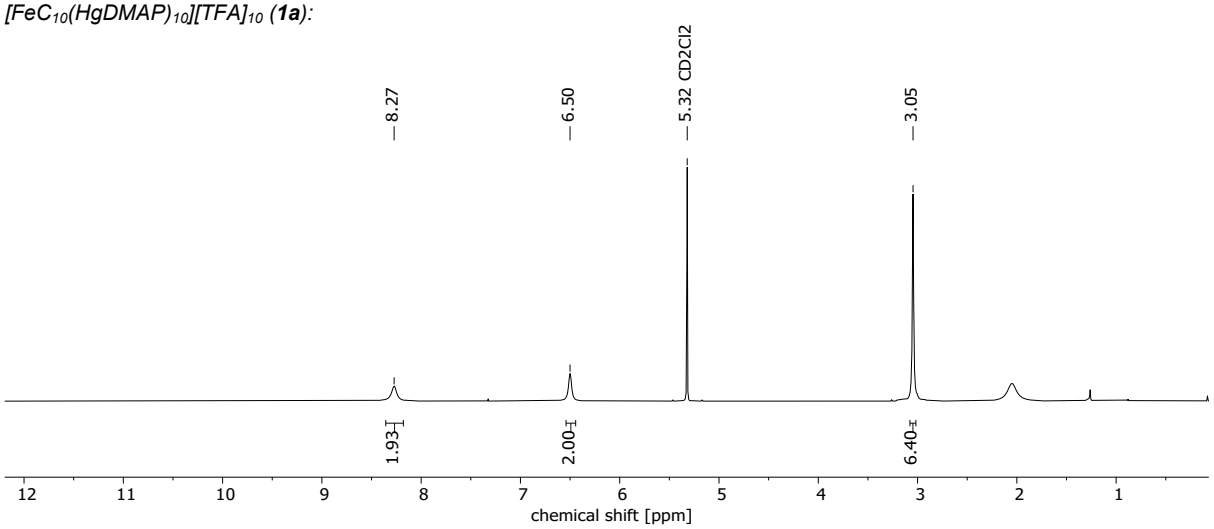


**Figure S1.** $^{1}$H NMR spectrum of [FeC$_{10}$(HgDMAP)$_{10}$][TFA]$_{10}$ (600 MHz, $CD_2Cl_2$, r.t.).

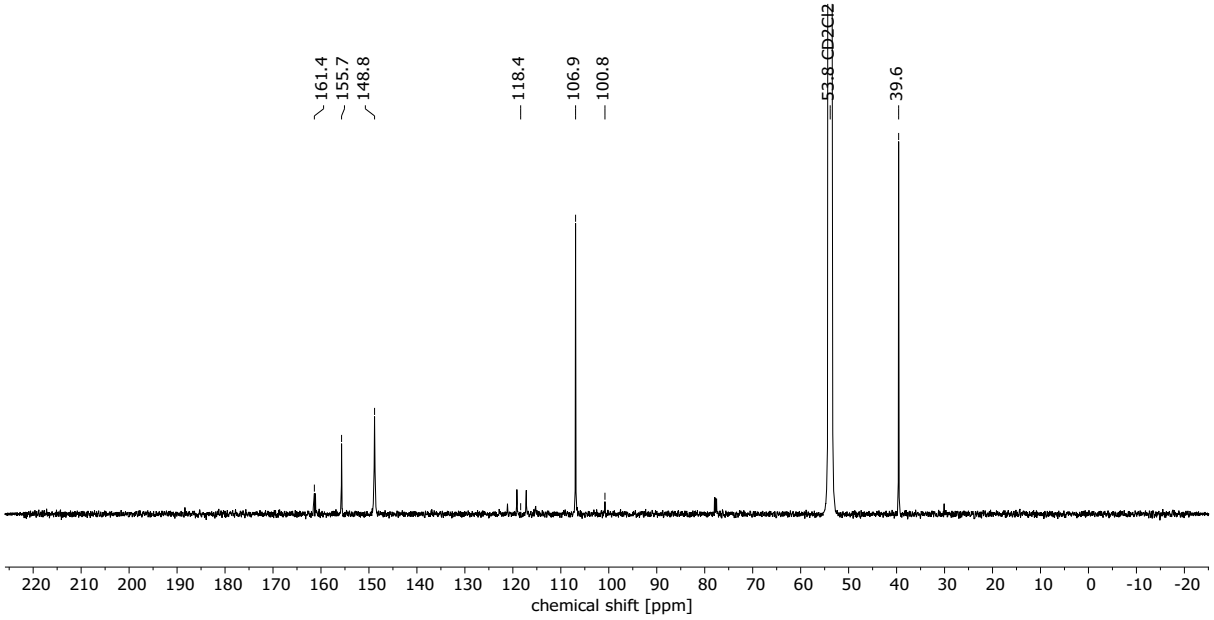


**Figure S2.** $^{13}$C NMR spectrum of [FeC$_{10}$(HgDMAP)$_{10}$][TFA]$_{10}$ (151 MHz, $CD_2Cl_2$, r.t.).

## SUPPORTING INFORMATION

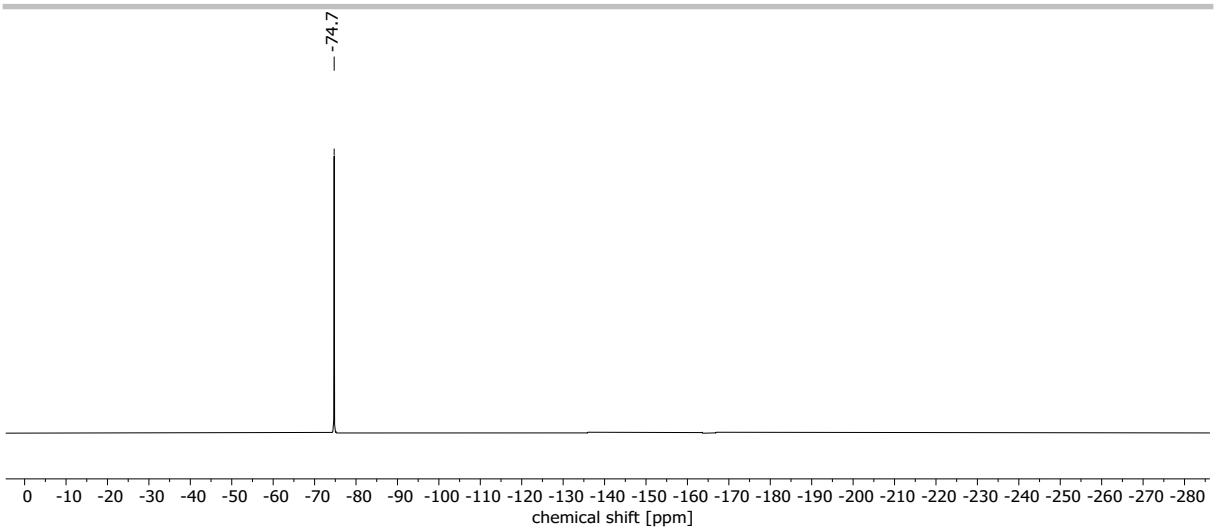


**Figure S3.** $^{19}F$ NMR spectrum of $[FeC_{10}(HgDMAP)_{10}][TFA]_{10}$ (565 MHz, $CD_2Cl_2$, r.t.).

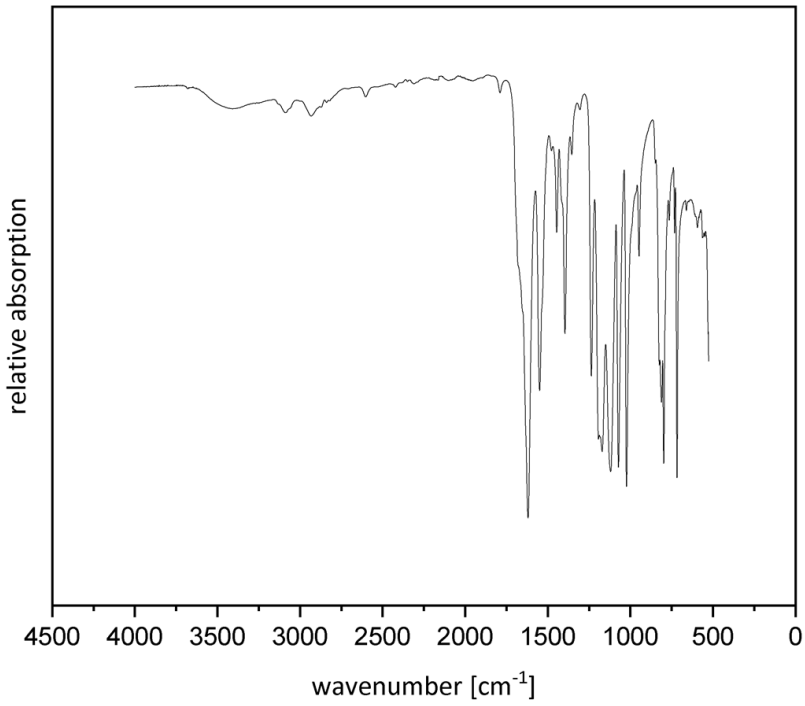


**Figure S4.** Infrared spectrum (ATR) of $[FeC_{10}(HgDMAP)_{10}][TFA]_{10}$.

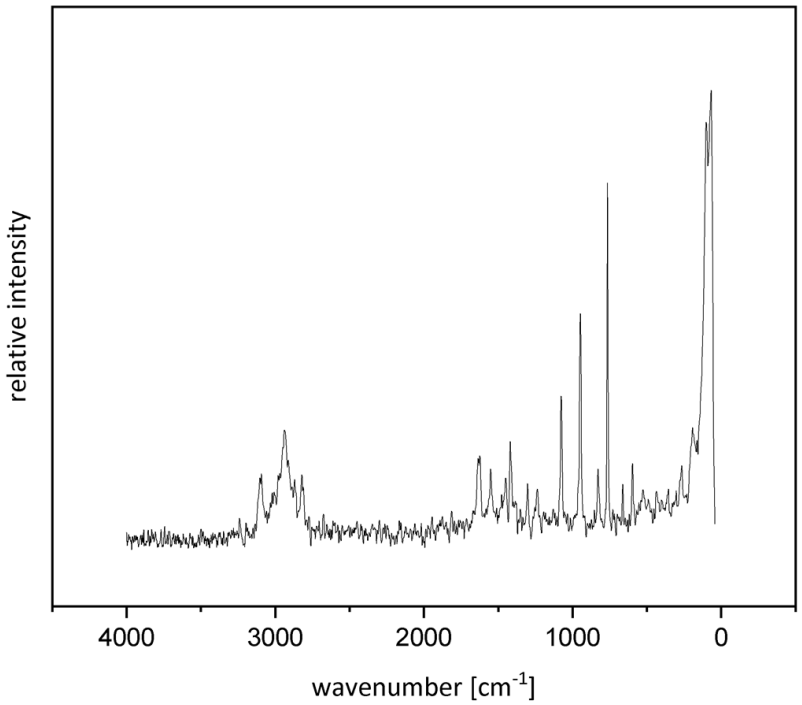


**Figure S5.** Raman spectrum (1064 nm, r.t.) of $[FeC_{10}(HgDMAP)_{10}][TFA]_{10}$.

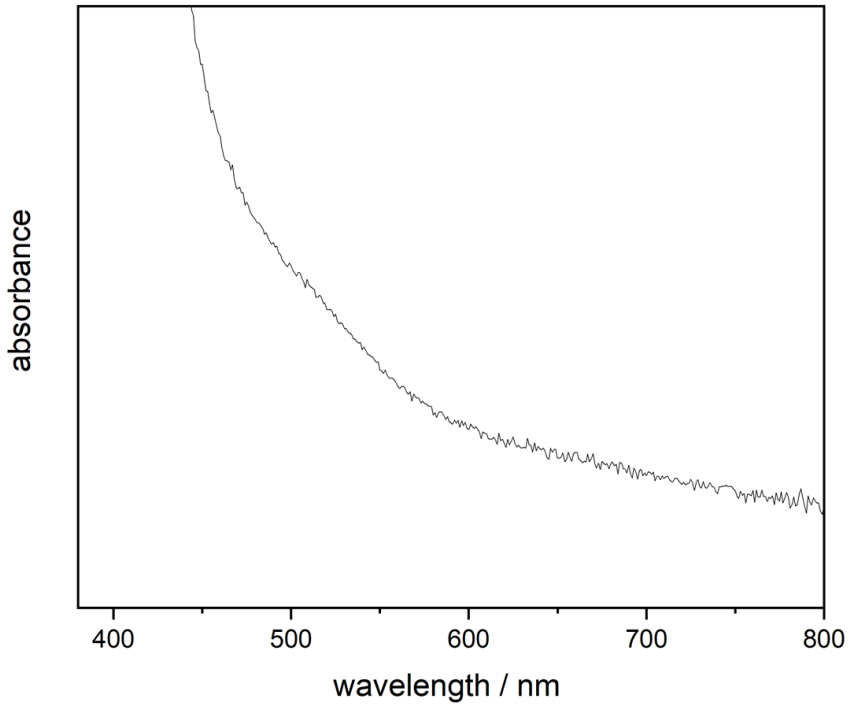


**Figure S6.** UV/Vis spectrum of $[FeC_{10}(HgDMAP)_{10}][TFA]_{10}$ in DCM.

## SUPPORTING INFORMATION

*$[FeC_{10}Hg_{10}(NC_5F_5)_n][SbF_6]_{10}$ (**2a**):*

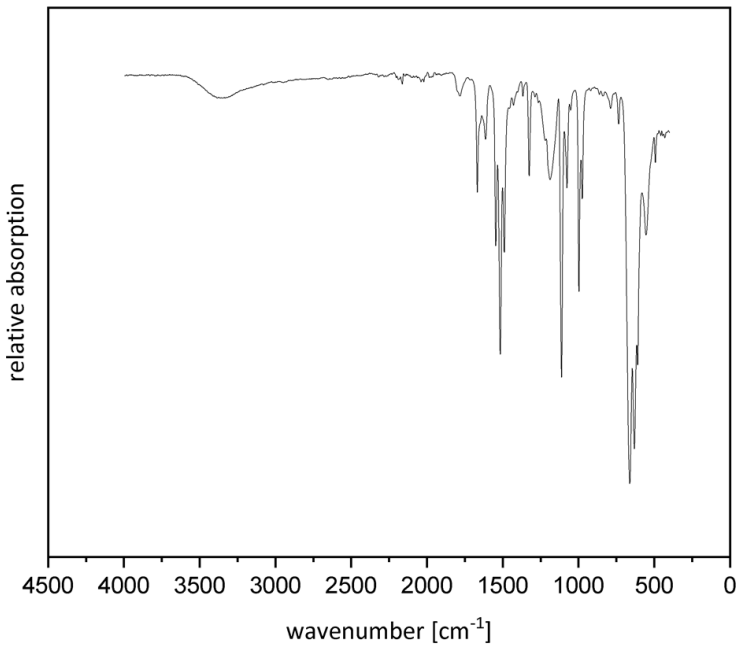


**Figure S7.** Infrared spectrum (ATR) of $[FeC_{10}Hg_{10}(NC_5F_5)_n][SbF_6]_{10}$.

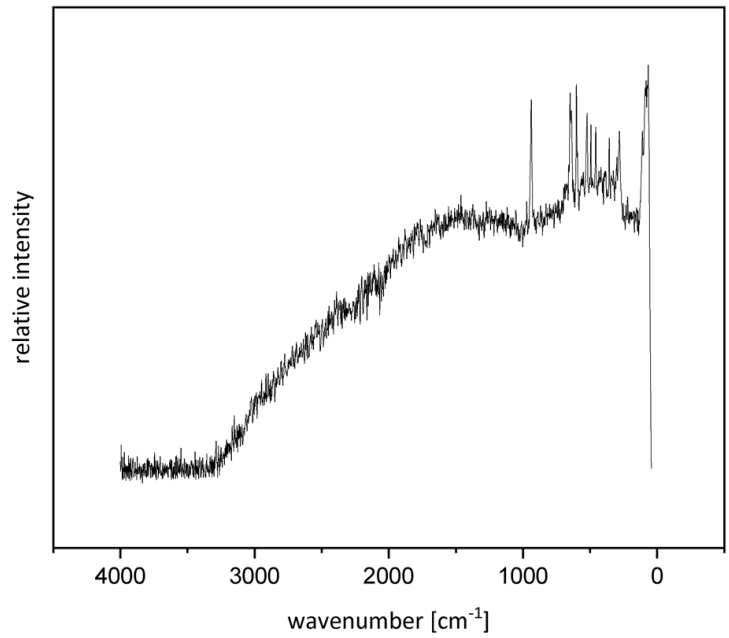


**Figure S8** Raman spectrum (1064 nm, r.t.) of $[FeC_{10}Hg_{10}(NC_5F_5)_n][SbF_6]_{10}$.

*$[FeC_{10}Hg_{10}(THT)_{10}][SbF_6]_{10}$ (**2b**):*

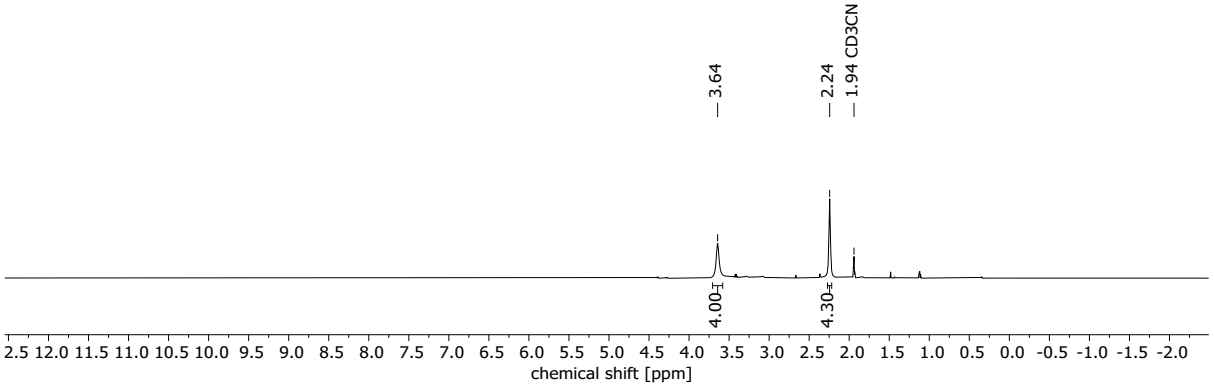


**Figure S9.** $^{1}H$ NMR spectrum of $[FeC_{10}Hg_{10}(THT)_{10}][SbF_6]_{10}$ (600 MHz, MeCN-$d_3$, r.t.).

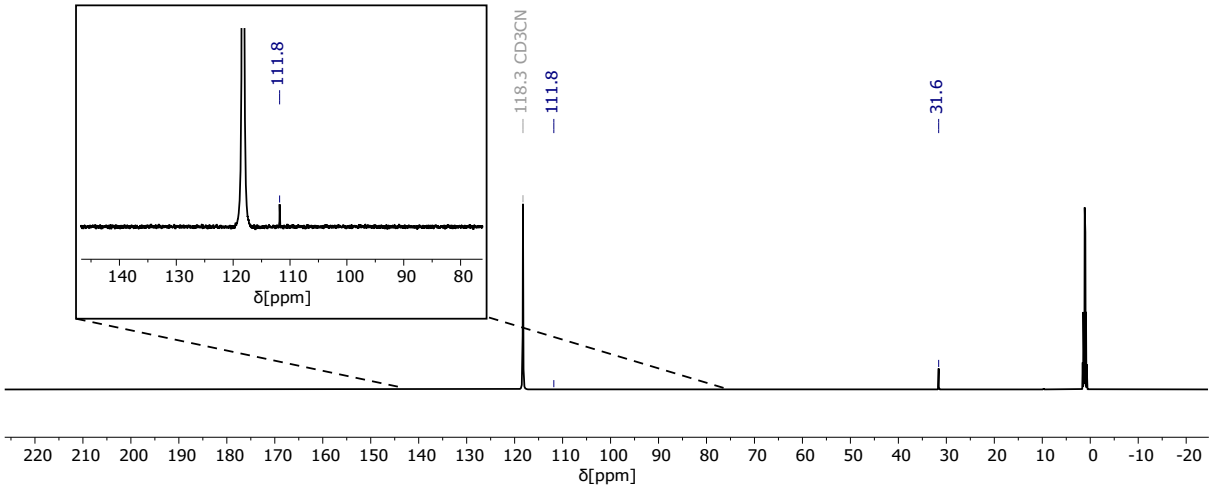


**Figure S10.** $^{13}C$ NMR spectrum of $[FeC_{10}Hg_{10}(THT)_{10}][SbF_6]_{10}$ (151 MHz, MeCN-$d_3$, r.t.).

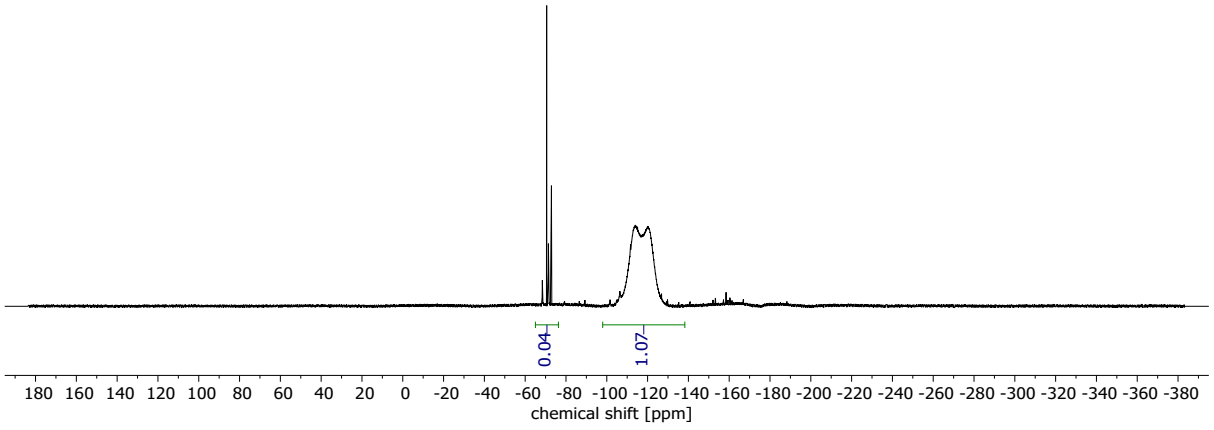


**Figure S11.** $^{19}F$ NMR spectrum of $[FeC_{10}Hg_{10}(THT)_{10}][SbF_6]_{10}$ (565 MHz, MeCN-$d_3$, r.t.).

## SUPPORTING INFORMATION

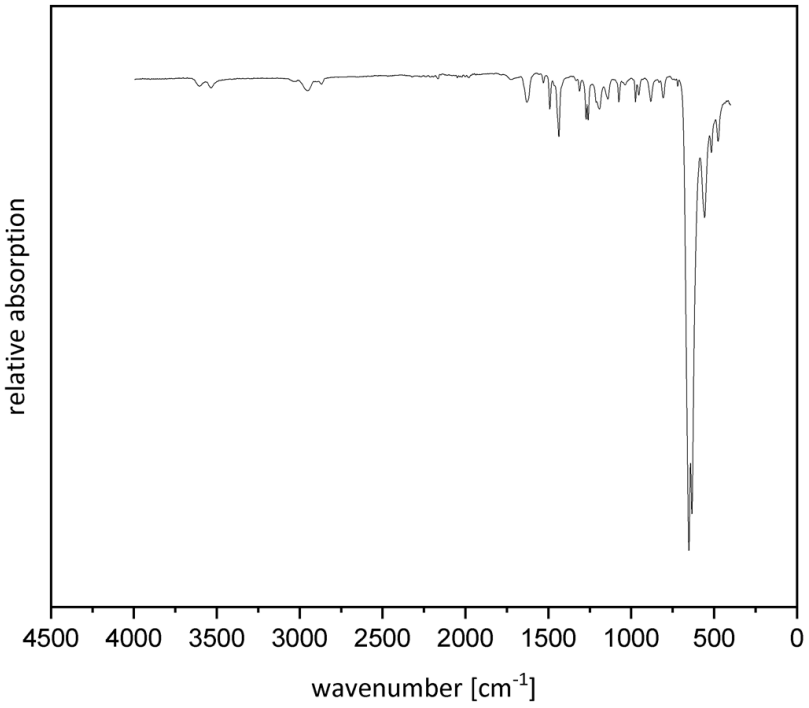


**Figure S12.** Infrared spectrum of $[FeC_{10}Hg_{10}(THT)_{10}][SbF_6]_{10}$ (ATR).

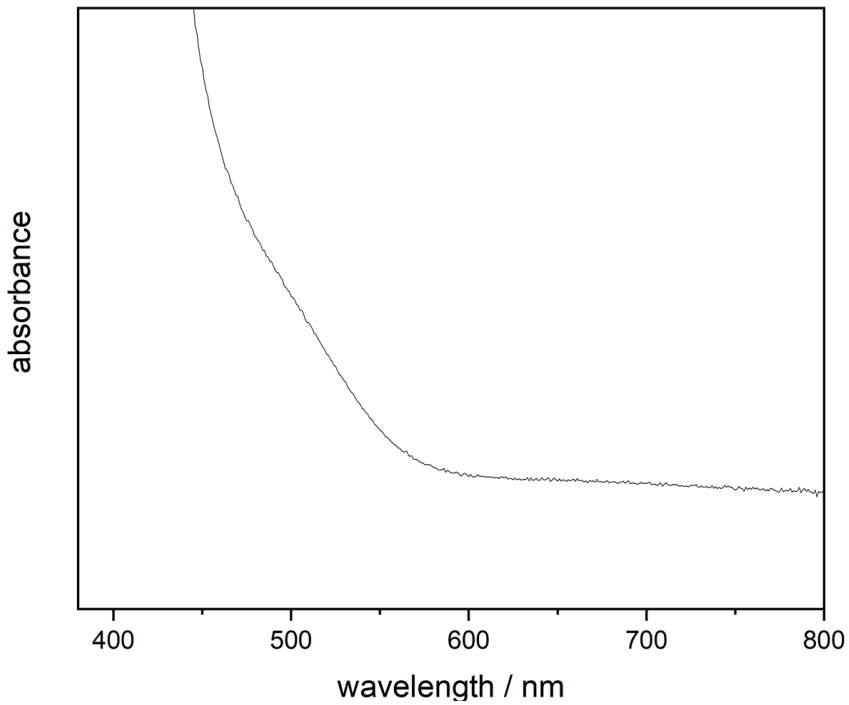


**Figure S13.** UV/Vis spectrum of of $[FeC_{10}Hg_{10}(THT)_{10}][SbF_6]_{10}$ in acetonitrile.

*$[FeC_{10}Hg_{10}(MeCN)_{10}][SbF_6]_{10}$ (**2c**):*

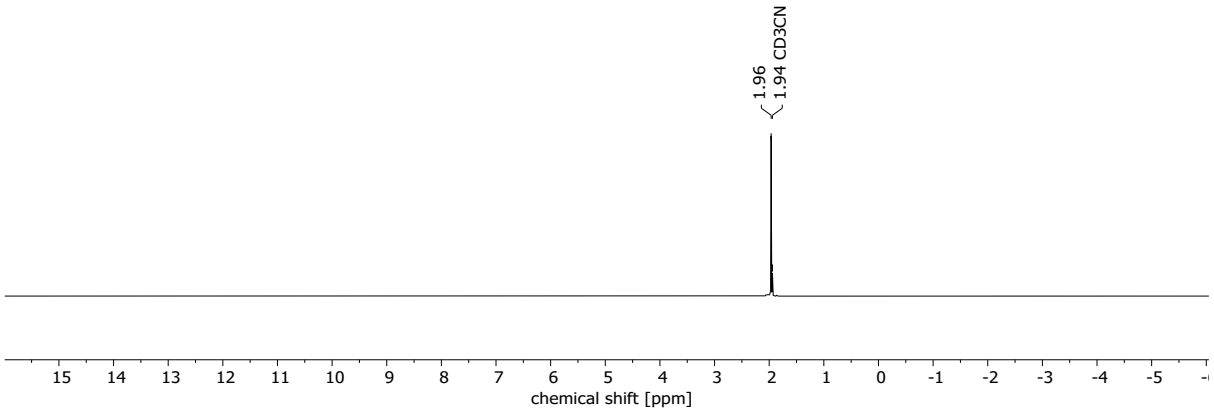


**Figure S14.** $^{1}H$ NMR spectrum of $[FeC_{10}Hg_{10}(MeCN)_{10}][SbF_6]_{10}$ (700 MHz, MeCN-$d_3$, r.t.).

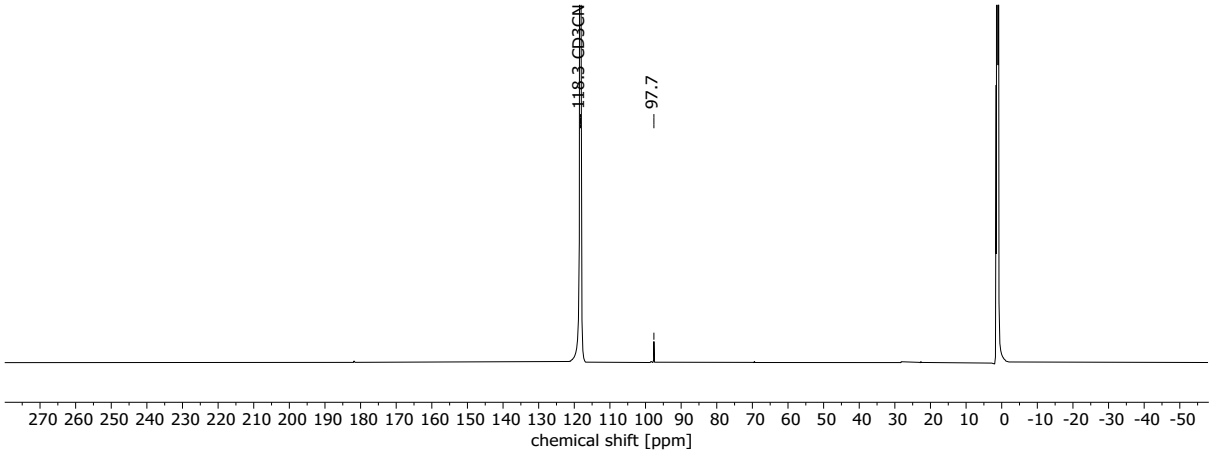


**Figure S15.** $^{13}C$ NMR spectrum of $[FeC_{10}Hg_{10}(MeCN)_{10}][SbF_6]_{10}$ (176 MHz, MeCN-$d_3$, r.t.).

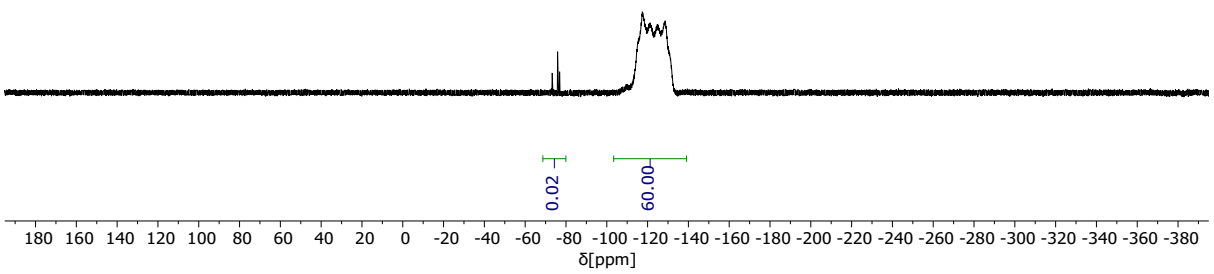


**Figure S16.** $^{19}F$ NMR spectrum of $[FeC_{10}Hg_{10}(MeCN)_{10}][SbF_6]_{10}$ (565 MHz, MeCN-$d_3$, r.t.).

## SUPPORTING INFORMATION

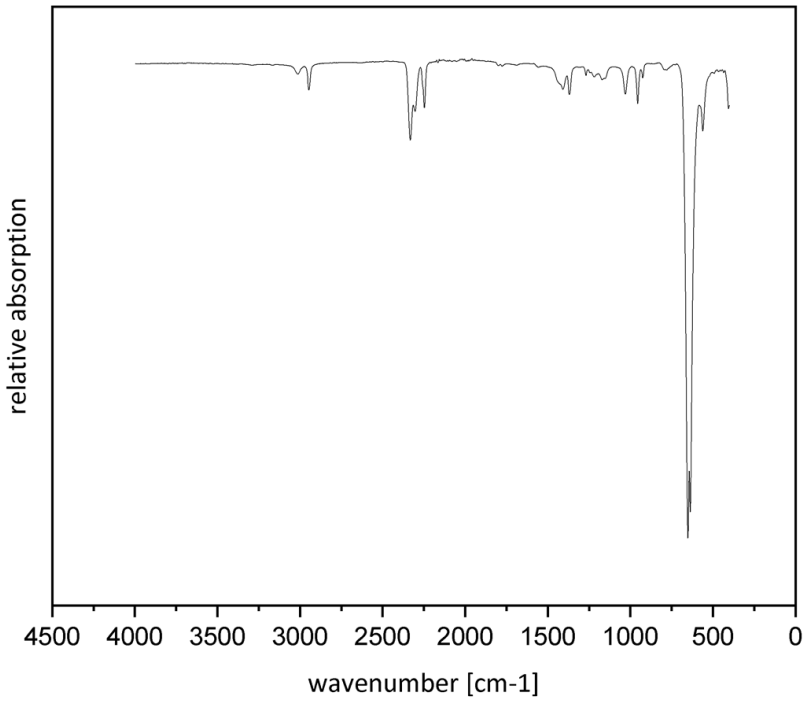


**Figure S17.** Infrared spectrum of $[FeC_{10}Hg_{10}(MeCN)_{10}][SbF_6]_{10}$ (ATR).

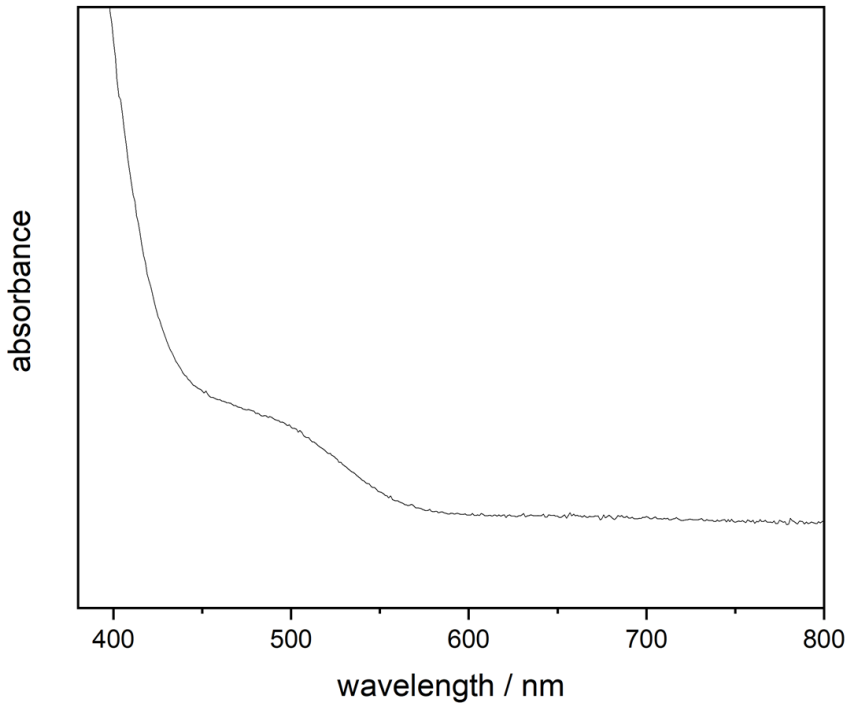


**Figure S18.** UV/vis spectrum of $[FeC_{10}Hg_{10}(MeCN)_{10}][SbF_6]_{10}$ in acetonitrile.

*$[FeC_{10}Hg_{10}(MeCN)_{10}][SbF_6]_{10}[MoF_6]$ (**3**):*

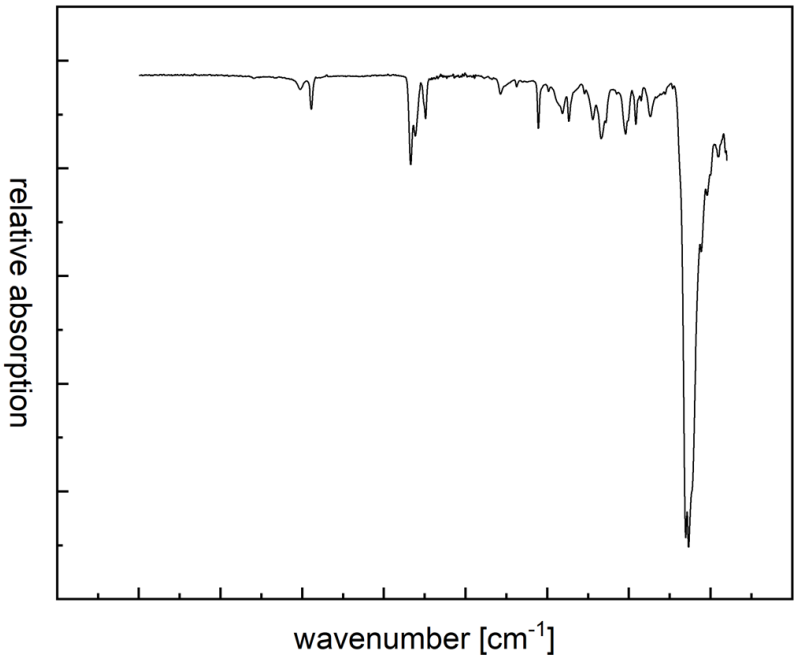


**Figure S19.** Infrared spectrum of $[FeC_{10}Hg_{10}(MeCN)_{10}][SbF_6]_{10}[MoF_6]$ (ATR).

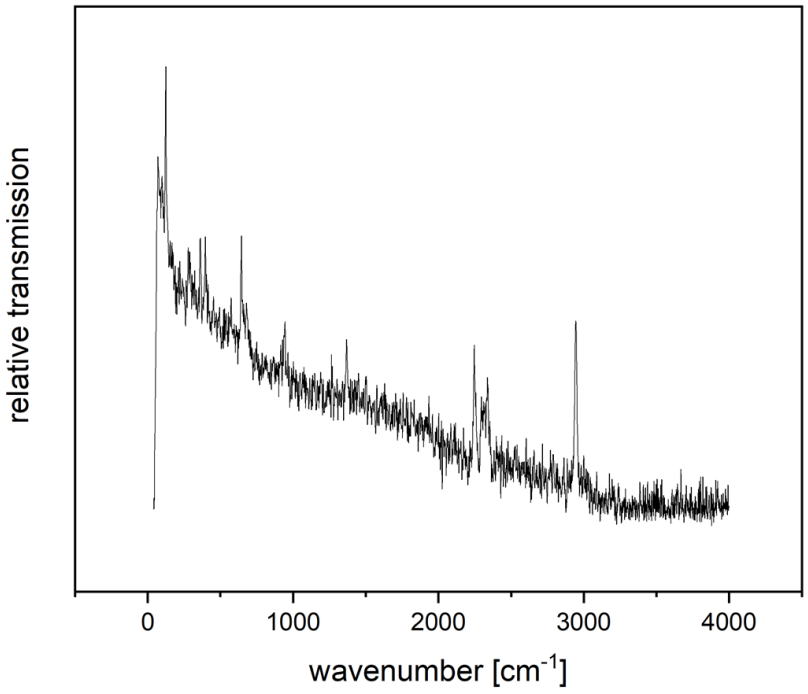


**Figure S20.** Raman spectrum (1064 nm, r.t.) of $[FeC_{10}Hg_{10}(MeCN)_{10}][SbF_6]_{10}[MoF_6]$.

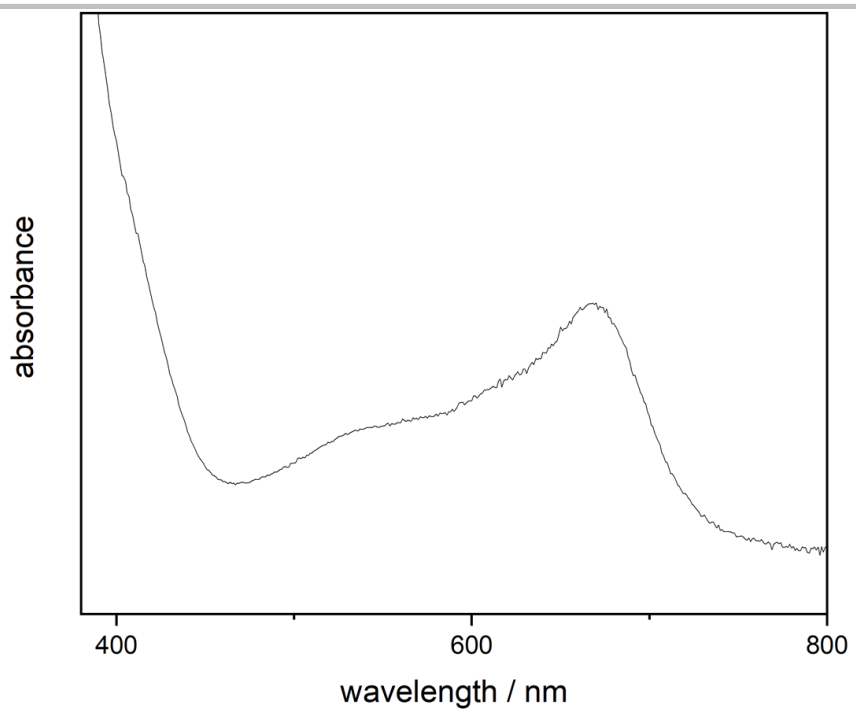


**Figure S21.** UV/vis spectrum of $[FeC_{10}Hg_{10}(MeCN)_{10}][SbF_6]_{10}[MoF_6]$ in acetonitrile. $\lambda_{max}$ = 668 nm.

*$[FeC_{10}Hg_{10}(C_5F_5N)_n][SbF_6]_{11}$:*

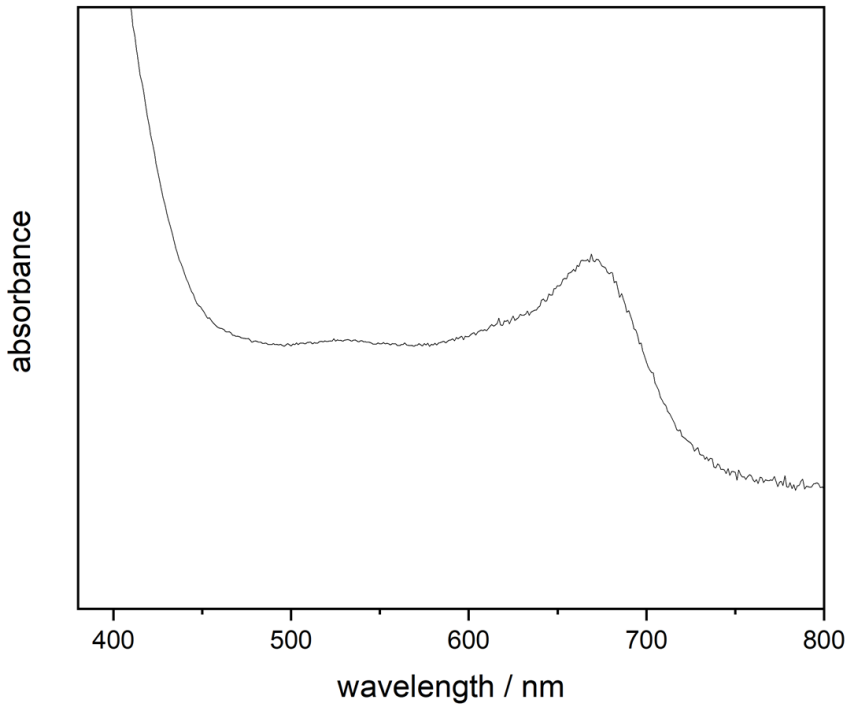


**Figure S22.** UV/vis spectrum of $[FeC_{10}Hg_{10}(C_5F_5N)_n][SbF_6]_{11}$ in acetonitrile synthesized by oxidation of $[FeC_{10}Hg_{10}(C_5F_5N)_n][SbF_6]_{10}$ with $NO_2SbF_6$. $\lambda_{max}$ = 669 nm.

*$[FeC_{10}Hg_{10}(THT)_{10}][SbF_6]_{11}$:*

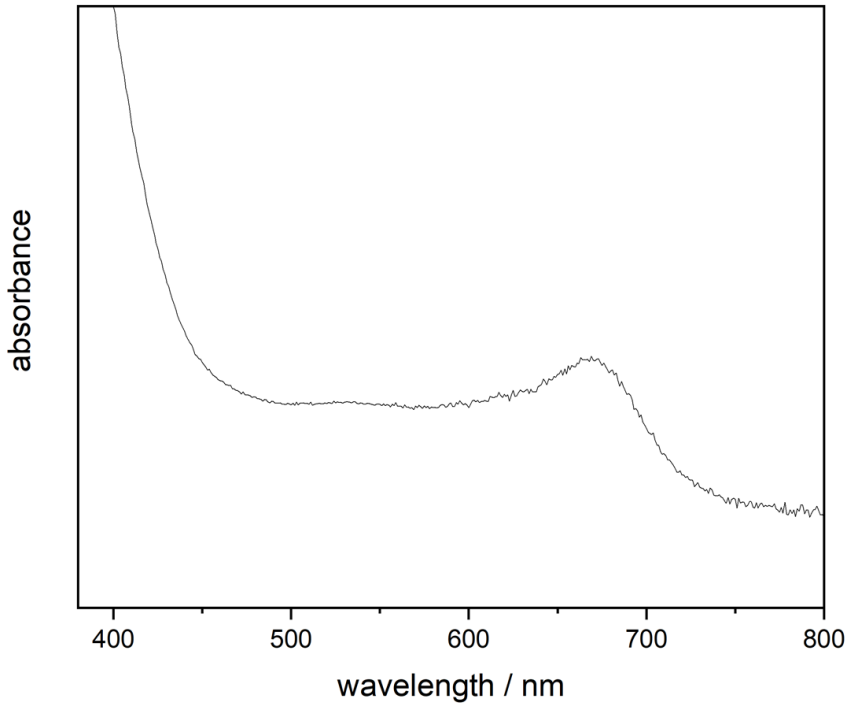


**Figure S23.** UV/vis spectrum of $[FeC_{10}Hg_{10}(THT)_{10}][SbF_6]_{11}$ in acetonitrile synthesized by oxidation of $[FeC_{10}Hg_{10}(THT)_{10}][SbF_6]_{10}$ with $NO_2SbF_6$. $\lambda_{max}$ = 673 nm.

**Cyclic voltammograms**

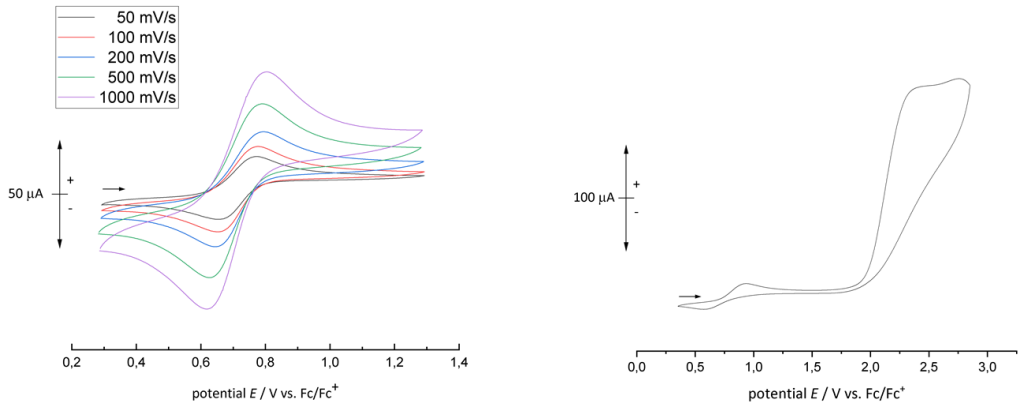


**Figure S24.** Cyclic voltammograms of $[FeC_{10}(HgMeCN)_{10}][SbF_6]_{10}$ in MeCN without supporting electrolyte at room temperature. First oxidation at different scan rates (left) and full cyclic voltammogram within the oxidation window of MeCN at 100 mV/s (right).

## SUPPORTING INFORMATION

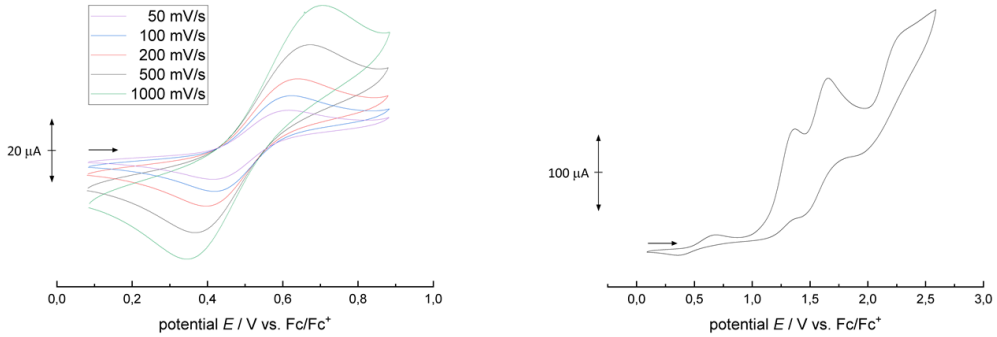


**Figure S25.** Cyclic voltammograms of $[FeC_{10}(HgTHT)_{10}][SbF_6]_{10}$ in MeCN without supporting electrolyte at room temperature. First oxidation at different scan rates (left) and full cyclic voltammogram within the oxidation window of MeCN at 100 mV/s (right).

### Crystal Packing

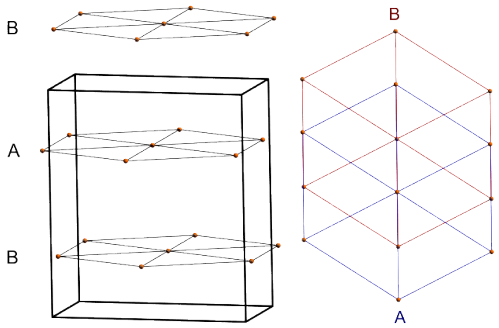


**Figure S26.** Packing of iron atoms in crystal structure of $[FeC_{10}(HgTHT)_{10}][SbF_6]_{10} \cdot 24$ MeCN.

## A.3 Preparation and One-Electron Oxidation of Decabromoferrocene

Supporting Information

# Preparation and One-Electron Oxidation of Decabromoferrocene

Susanne M. Rupf,[a] Irina S. Dimitrova,[a] Gabriel Schröder,[a] Moritz Malischewski[a*]

[a]Freie Universität Berlin, Fabeckstr. 34-36, 14195 Berlin Germany
E-Mail corresponding author: moritz.malischewski@fu-berlin.de

# 1 Cyclic voltammetry

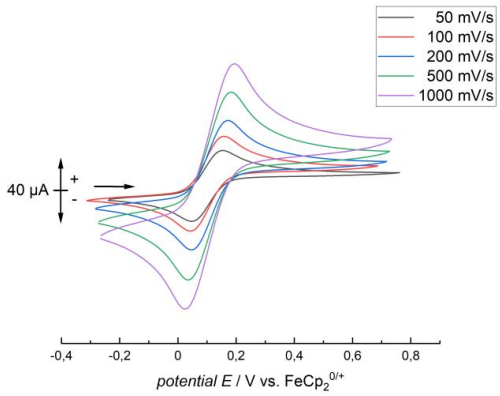


**Figure S1.** Cyclic voltammogram of $FeC_{10}BrH_9$ in dichloromethane at room temperature.

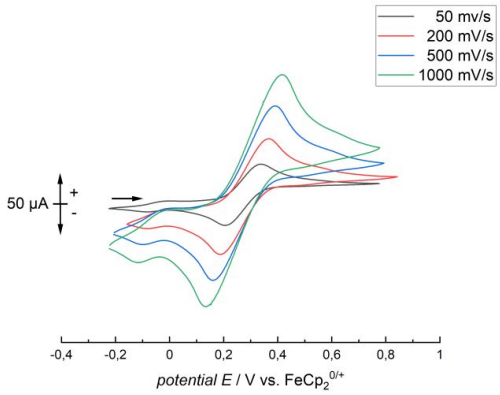


**Figure S2.** Cyclic voltammogram of 1,1'-$FeC_{10}Br_2H_8$ in dichloromethane at room temperature.

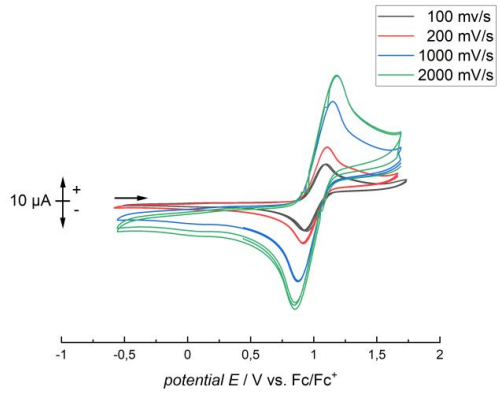


**Figure S3.** Cyclic voltammogram of $FeC_{10}Br_9H$ in dichloromethane at room temperature.

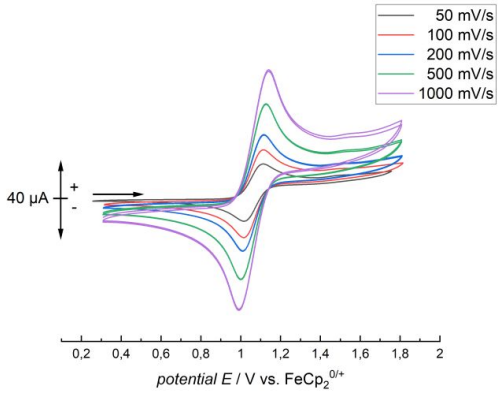


**Figure S4.** Cyclic voltammogram of $FeC_{10}Br_9HgBr$ in dichloromethane at room temperature.

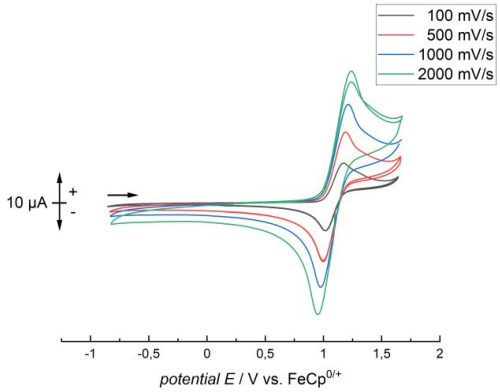


**Figure S5.** Cyclic voltammogram of $FeC_{10}Br_{10}$ in dichloromethane at room temperature.

# 2 Crystal Structure Determination

X-Ray data were collected on a BRUKER D8 Venture system. Data were collected at 100(2) K using graphite-monochromated Mo $K_\alpha$ radiation ($\lambda_\alpha$ = 0.71073 Å). The strategy for the data collection was evaluated by using the Smart software. The data were collected by the standard "ψ-ω scan techniques" and were scaled and reduced using Saint+software. The structures were solved by using Olex2,[1] the structure was solved with the XT[2] structure solution program using Intrinsic Phasing and refined with the XL refinement package[3,4] using Least Squares minimization. If it is noted, bond length and angles were measured with Diamond Crystal and Molecular Structure Visualization Version 4.6.2.[5] Drawings were generated with POV-Ray.[6] Deposition numbers CCDC 2162547 ($[C_{10}Br_{10}Fe][AsF_6]$, 2162548 ($[FeC_{10}Br_9HgBr][AsF_6]$), 2162554 $[FeC_{10}Br_9H]$, 2162561 $[FeC_{10}Br_{10}]$ contain the supplementary crystallographic data for this paper. These data are provided free of charge by the joint Cambridge Crystallographic Data Centre and Fachinformationszentrum Karlsruhe Access Structures service www.ccdc.cam.ac.uk/structures.

Table S1. Crystal data.

| **Compound** | **$FeC_{10}Br_9H$** | **$FeC_{10}Br_{10}$•dmso** |
|---|---|---|
| **Empirical formula** | $C_{10}HFeBr_9$ | $Br_{10}C_{10}Fe{\cdot}2(C_2H_6OS)$ |
| **Formula weight** | 896.15 | 1131.31 |
| **Temperature/K** | 100.0 | 100.0 |
| **Crystal system** | monoclinic | Monoclinic |
| **Space group** | C2/c | $P2_1/c$ |
| **a/Å** | 17.0944(18) | 11.0868 (5) Å |
| **b/Å** | 8.9490(9) | 10.4916 (5) Å |
| **c/Å** | 22.418(2) | 11.5971 (5) Å |
| **α/°** | 90 | 90 |
| **β/°** | 90.601(4) | 94.342 (2)° |
| **γ/°** | 90 | 90 |
| **Volume/Å³** | 3429.2(6) | 1345.08 (11) Å³ |
| **Z** | 8 | 2 |
| **$\rho_{calc}$/g•cm³** | 3.472 | 2.793 |
| **μ/mm⁻¹** | 21.837 | 15.58 |
| **F(000)** | 3216.0 | 1040 |
| **Crystal size/ in mm** | 0.25 × 0.11 × 0.10 | 0.297 × 0.214 × 0.180 |
| **Crystal shape** | block | Block |
| **Radiation** | MoKα (λ = 0.71073) | MoKα (λ = 0.71073) |
| **2Θ range for data collection/°** | 4.766 to 50.318 | 5.242 to 68.726° |
| **Index ranges** | -20 ≤ h ≤ 20, -10 ≤ k ≤ 10, -26 ≤ l ≤ 26 | -17 ≤ h ≤ 17, 0 ≤ k ≤ 16, 0 ≤ l ≤ 18 |
| **Reflections collected** | 32512 | 5604 |
| **Independent reflections** | 3078 [$R_{int}$ = 0.0700, $R_{sigma}$ = 0.0262] | 5604 [$R_{int}$ = 0.0570, $R_{sigma}$ = 0.0486] |
| **Data/restrains/parameters** | 3078/0/181 | 5600/0/135 |
| **Goodness-of-fit on $F^2$** | 1.072 | 1.062 |
| **Final R indexes [I>=2σ(I)]** | $R_1$ = 0.0471, $wR_2$ = 0.1159 | $R_1$ = 0.0393, $wR_2$ = 0.0895 |
| **Final R indexes [all data]** | $R_1$ = 0.0569, $wR_2$ = 0.1212 | $R_1$ = 0.0488, $wR_2$ = 0.0942 |
| **Largest diff. peak/hole / e•Å³** | 2.51/−1.08 | 3.59/−1.55 |

Table S2. Crystal data.

| **Compound** | **$[FeC_{10}Br_9HgBr][AsF_6]\cdot SO_2$** | **$[FeC_{10}Br_{10}][AsF_6]\cdot 2\ HF$** |
|---|---|---|
| **Empirical formula** | $AsBr_{10}C_{10}F_6FeHgO_2S$ | $AsBr_{10}C_{10}F_8Fe$ |
| **Formula weight** | 1428.62 | 1201.97 |
| **Temperature/K** | 100 | 100.0 |
| **Crystal system** | triclinic | monoclinic |
| **Space group** | P-1 | I2/m |
| **a/Å** | 7.6242(5) | 8.6070(5) |
| **b/Å** | 8.8334(8) | 11.5855(7) |
| **c/Å** | 20.9537(14) | 12.0858(9) |
| **α/°** | 92.335(4) | 90 |
| **β/°** | 97.309(2) | 90.126(3) |
| **γ/°** | 112.465(2) | 90 |
| **Volume/Å$^3$** | 1287.33(17) | 1205.15(14) |
| **Z** | 2 | 2 |
| **$\rho_{calc}$g/cm$^3$** | 3.686 | 3.312 |
| **μ/mm$^{-1}$** | 23.449 | 18.626 |
| **F(000)** | 1270.0 | 1082.0 |
| **Crystal size in mm** | 0.462 × 0.279 × 0.146 | 0.156 × 0.11 × 0.051 |
| **Crystal shape** | plate | block |
| **Radiation** | MoKα (λ = 0.71073) | MoKα (λ = 0.71073) |
| **2Θ range for data collection/°** | 3.938 to 51.524 | 4.87 to 51.372 |
| **Index ranges** | $-9 \le h \le 9, -10 \le k \le 10, -25 \le l \le 25$ | $-10 \le h \le 8, -14 \le k \le 11, -14 \le l \le 10$ |
| **Reflections collected** | 37371 | 2314 |
| **Independent reflections** | 4921 [$R_{int}$ = 0.0551, $R_{sigma}$ = 0.0327] | 1220 [$R_{int}$ = 0.0476, $R_{sigma}$ = 0.0403] |
| **Data/restraints/parameters** | 4921/0/292 | 1220/0/78 |
| **Goodness-of-fit on F$^2$** | 1.148 | 1.078 |
| **Final R indexes [I>=2σ (I)]** | $R_1$ = 0.0327, $wR_2$ = 0.0790 | $R_1$ = 0.0365, $wR_2$ = 0.0856 |
| **Final R indexes [all data]** | $R_1$ = 0.0366, $wR_2$ = 0.0811 | $R_1$ = 0.0490, $wR_2$ = 0.0896 |
| **Largest diff. peak/hole / e Å$^{-3}$** | 2.18/-2.11 | 2.89/−0.77 |

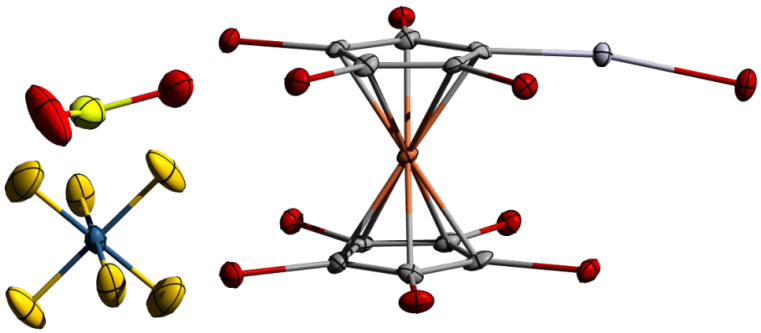

**Figure S6.** Asymmetric unit in the crystal structure of $[FeC_{10}Br_9HgBr][AsF_6]\cdot SO_2$. Ellipsoids with 50% probability level. Color code: light grey – mercury, dark red – bromine, orange – iron, turquoise – arsenic, light yellow – sulfur, dark yellow – fluorine, light red – oxygen, grey – carbon.

**Figure S7.** Asymmetric unit in the crystal structure of $FeC_{10}Br_{10}\cdot$dmso. Ellipsoids with 50% probability level. Hydrogen atoms are omitted for clarity. Color code: light dark red – bromine, orange – iron, yellow – sulfur, light red – oxygen, grey – carbon.

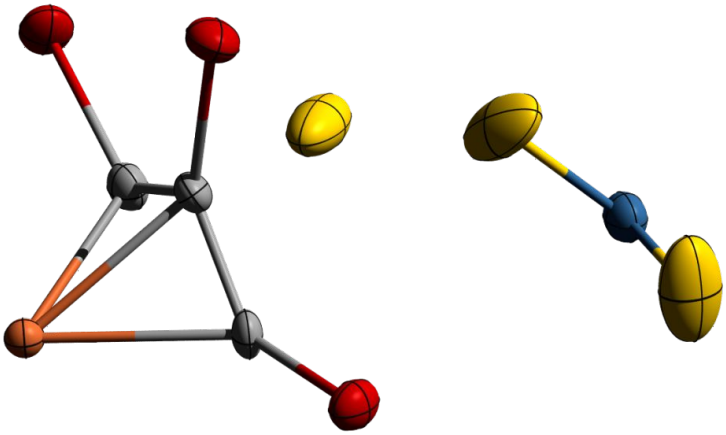

**Figure S8.** Asymmetric unit in the crystal structure of $[FeC_{10}Br_{10}][AsF_6]\cdot 2$ HF. Ellipsoids with 50% probability level. Color code: red – bromine, orange – iron, turquoise – arsenic, dark yellow – fluorine, grey – carbon.

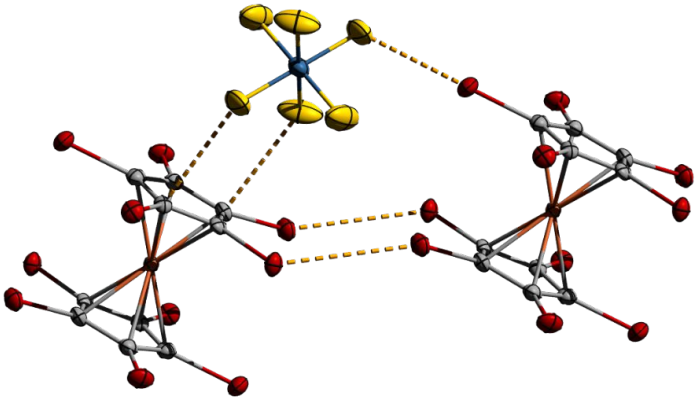

**Figure S9.** Non-covalent interactions in the crystal structure of $[FeC_{10}Br_{10}][AsF_6]\cdot 2\,HF$. Ellipsoids with 50% probability level. Color code: red – bromine, orange – iron, turquoise – arsenic, dark yellow – fluorine, grey – carbon, dashed – non-covalent interactions.

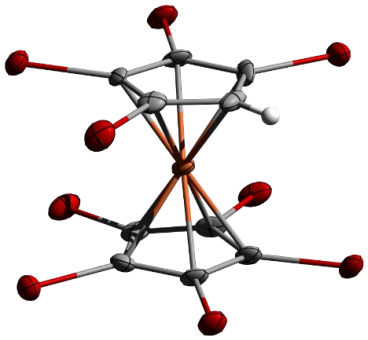

**Figure S10.** Asymmetric unit in the crystal structure of $FeC_{10}Br_9H$. Ellipsoids with 50% probability level. Color code: red – bromine, orange – iron, grey – carbon, white – hydrogen.

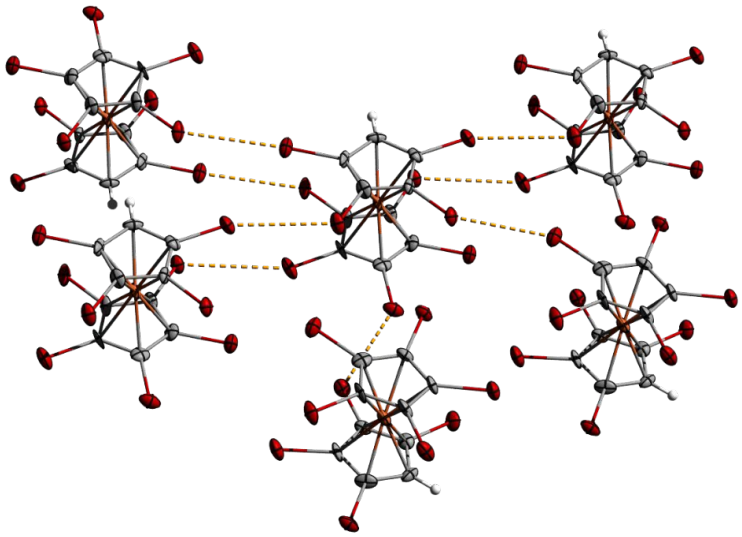

**Figure S11.** Non-covalent interactions in the crystal structure of $FeC_{10}Br_9H$. Ellipsoids with 50% probability level. Color code: red – bromine, orange – iron, grey – carbon, white – hydrogen, dashed – non-covalent interactions.

# 3 Spectra

## 3.1 $^{13}C$ NMR

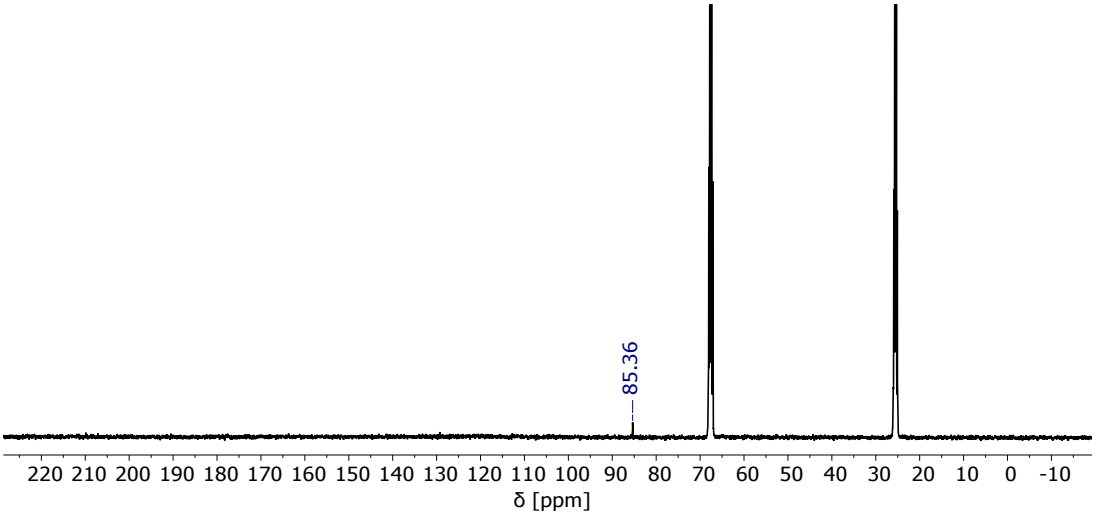


**Figure S12.** $^{13}C$ NMR ($d_8$-THF, RT, 176 MHz) spectrum of $FeC_{10}Br_{10}$.

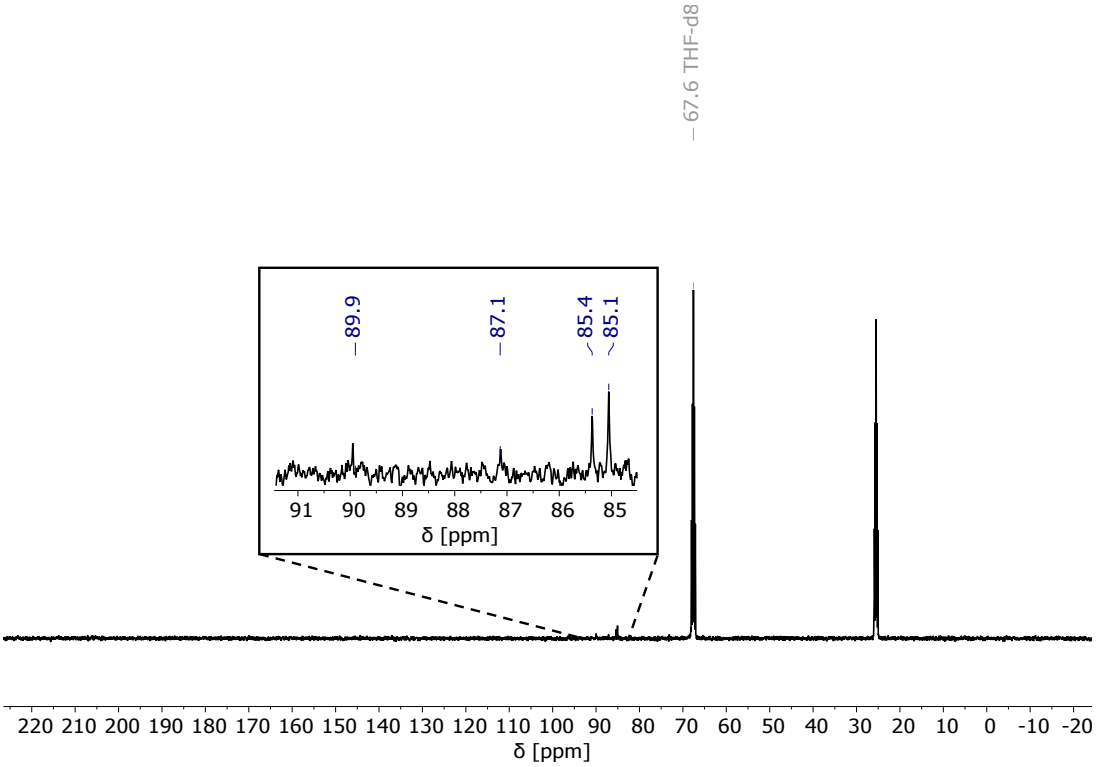


**Figure S13.** $^{13}C$ NMR ($d_8$-THF, RT, 176 MHz) spectrum of $FeC_{10}Br_9HgBr$.

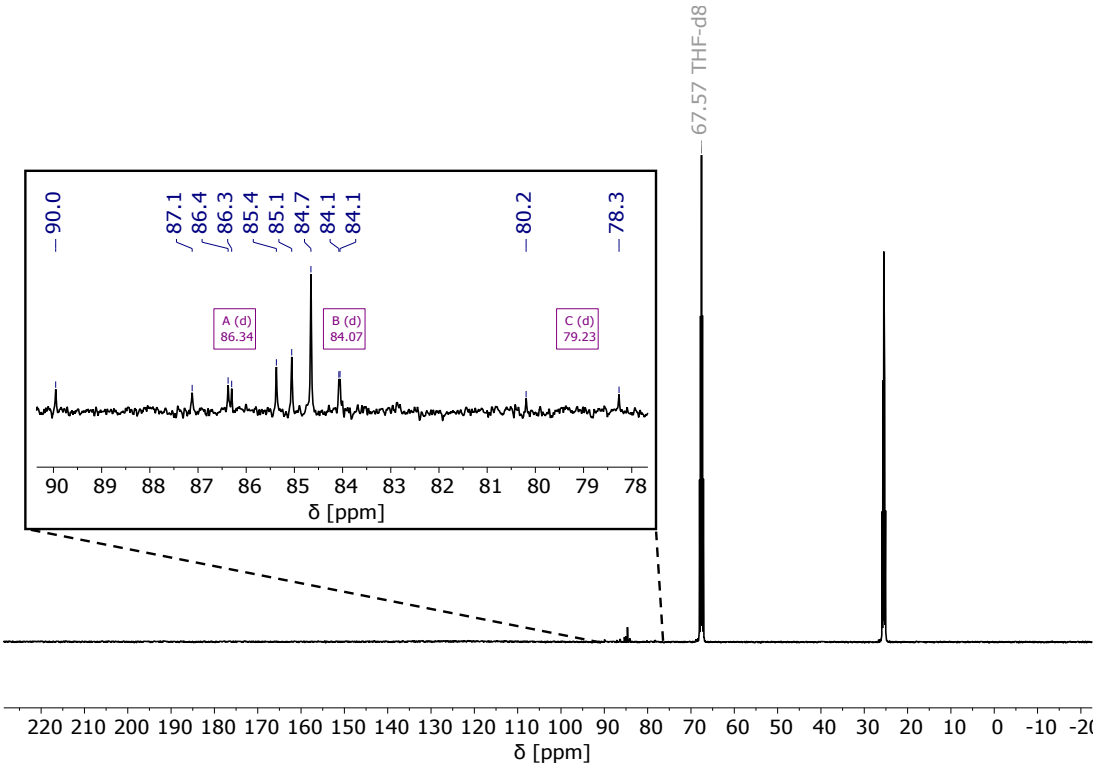


**Figure S14.** $^{13}C$ NMR ($d_8$-THF, RT, 176 MHz) spectrum of bromination products after reaction of $FeC_{10}(HgOAc)_{10}$ with $KBr_3$ containing $FeC_{10}Br_{10}$, $FeC_{10}Br_9HgBr$ and $FeC_{10}Br_9H$.

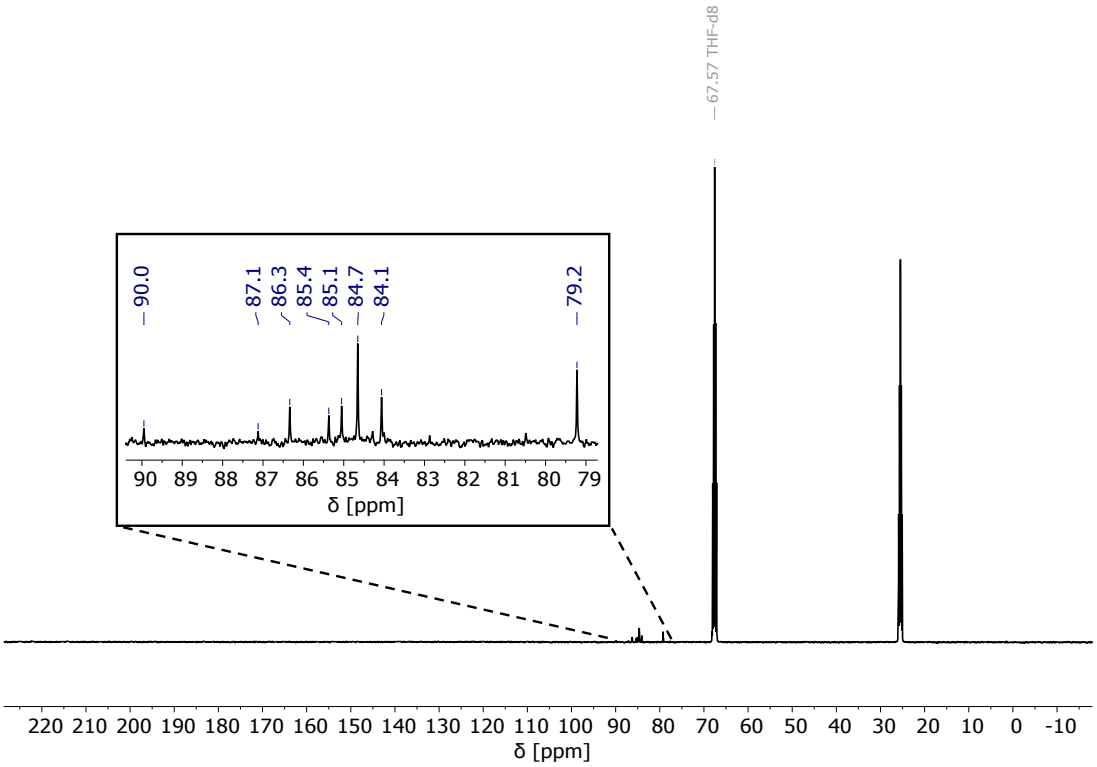


**Figure S15.** $^{13}C\{^{1}H\}$ NMR ($d_8$-THF, RT, 176 MHz) spectrum of bromination products after reaction of $FeC_{10}(HgOAc)_{10}$ with $KBr_3$ containing $FeC_{10}Br_{10}$, $FeC_{10}Br_9HgBr$ and $FeC_{10}Br_9H$.

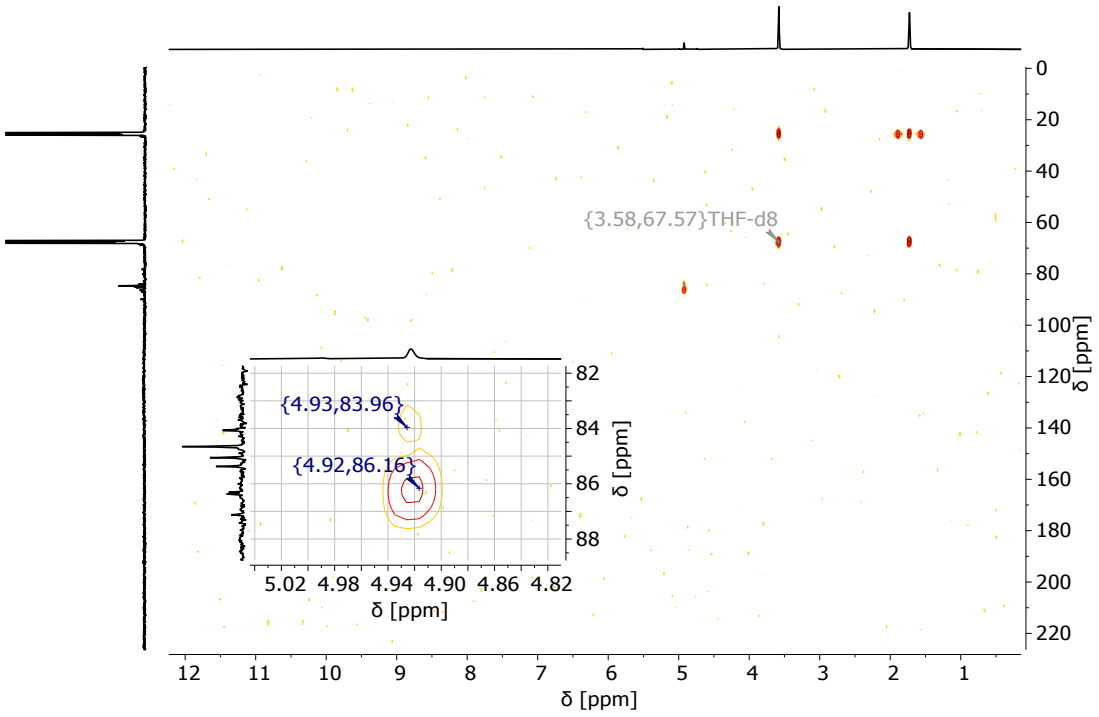


**Figure S16.** HMBC NMR spectrum of bromination products after reaction of $FeC_{10}(HgOAc)_{10}$ with $KBr_3$ containing $FeC_{10}Br_{10}$, $FeC_{10}Br_9HgBr$ and $FeC_{10}Br_9H$.

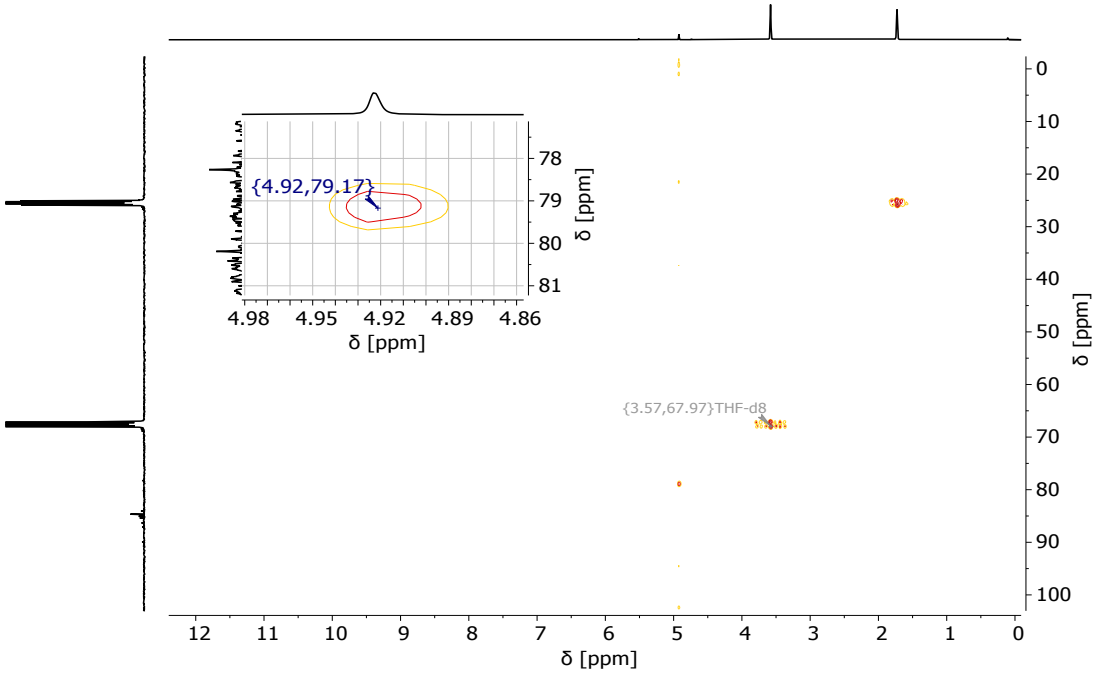


**Figure S17.** HMQC NMR spectrum of bromination products after reaction of $FeC_{10}(HgOAc)_{10}$ with $KBr_3$ containing $FeC_{10}Br_{10}$, $FeC_{10}Br_9HgBr$ and $FeC_{10}Br_9H$.

## 3.2 Infrared

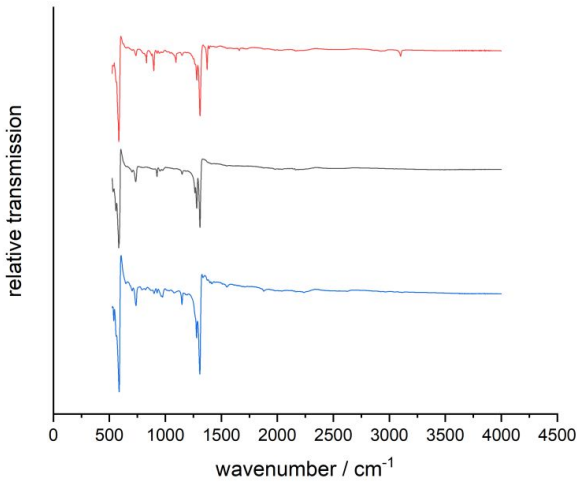


**Figure S18.** Infrared spectrum of bromination products after reaction of $FeC_{10}(HgOAc)_{10}$ with $KBr_3$ containing $FeC_{10}Br_{10}$, $FeC_{10}Br_9HgBr$ and $FeC_{10}Br_9H$ (red), pure $FeC_{10}Br_9HgBr$ (black) and pure $FeC_{10}Br_{10}$ (blue).

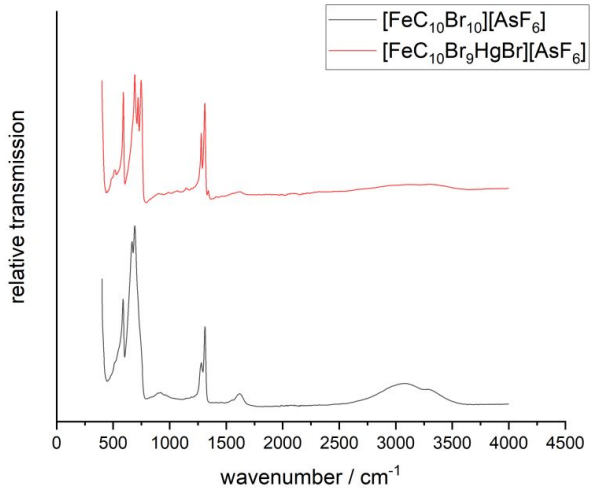


**Figure S19.** Infrared spectrum of $[FeC_{10}Br_{10}][AsF_6]$ (black), pure $[FeC_{10}Br_9HgBr][AsF_6]$ (red).

## 3.3 MS

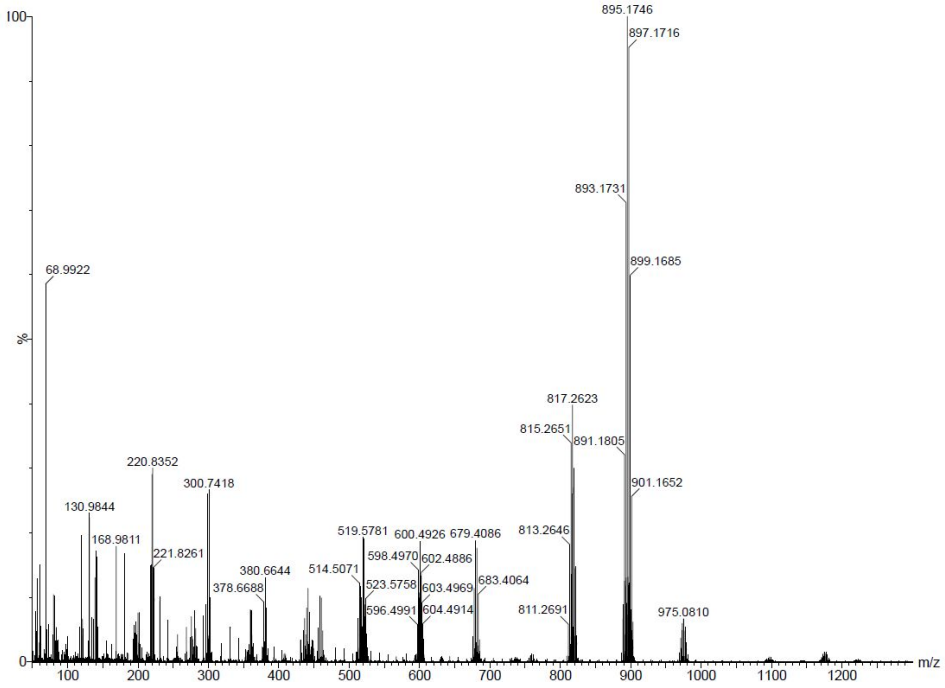


**Figure S20**. EI MS (+) of bromination products after reaction of $FeC_{10}(HgOAc)_{10}$ with $KBr_3$ containing $FeC_{10}Br_{10}$, $FeC_{10}Br_9HgBr$ and $FeC_{10}Br_9H$.

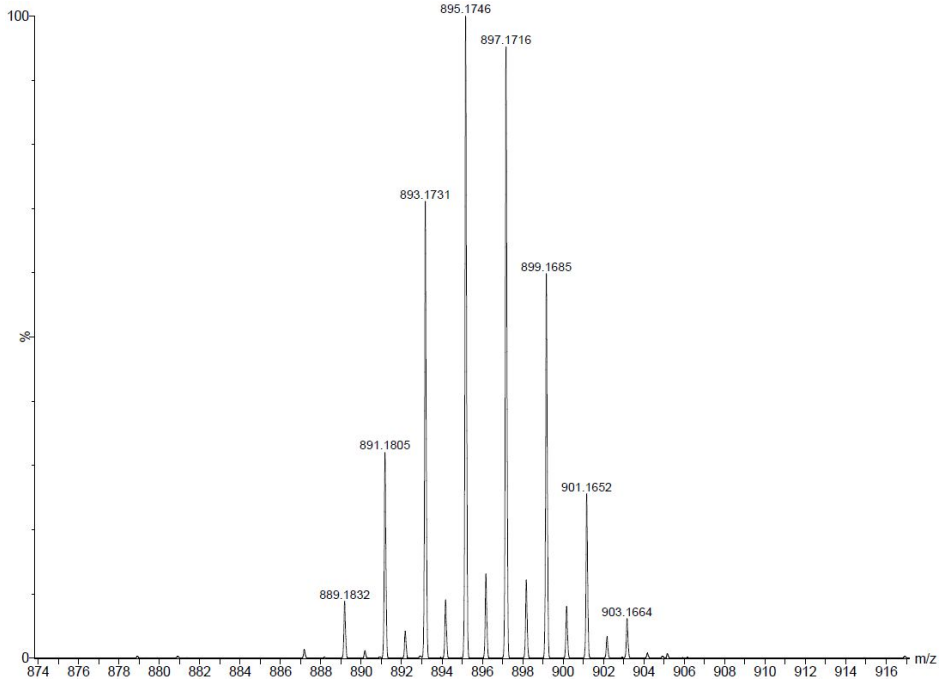


**Figure S21.** EI MS (+) of $FeC_{10}Br_9H$ (zoom).

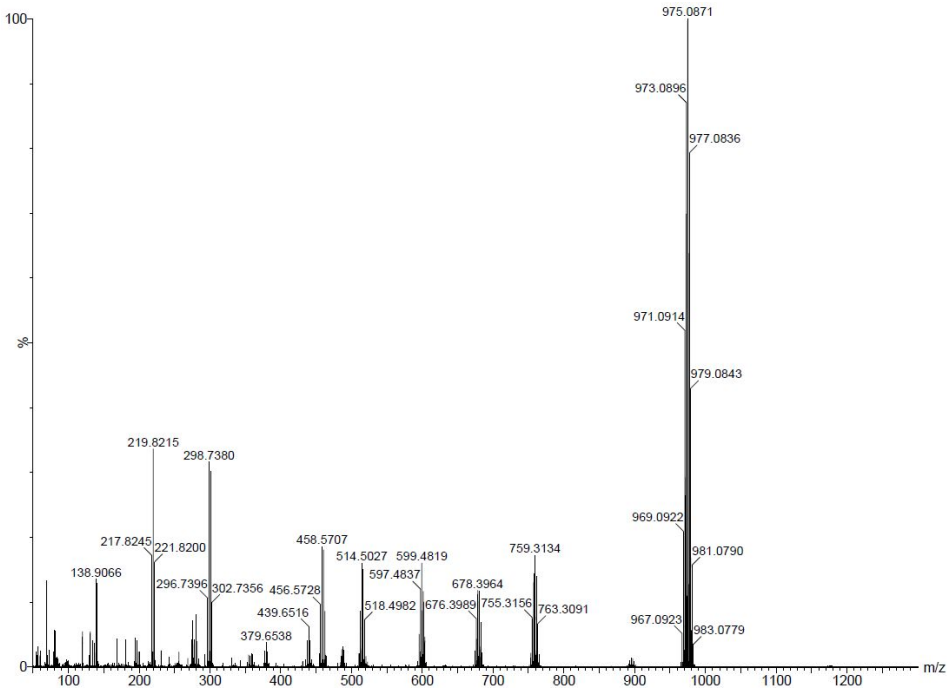


**Figure S22.** EI MS (+) of $FeC_{10}Br_{10}$.

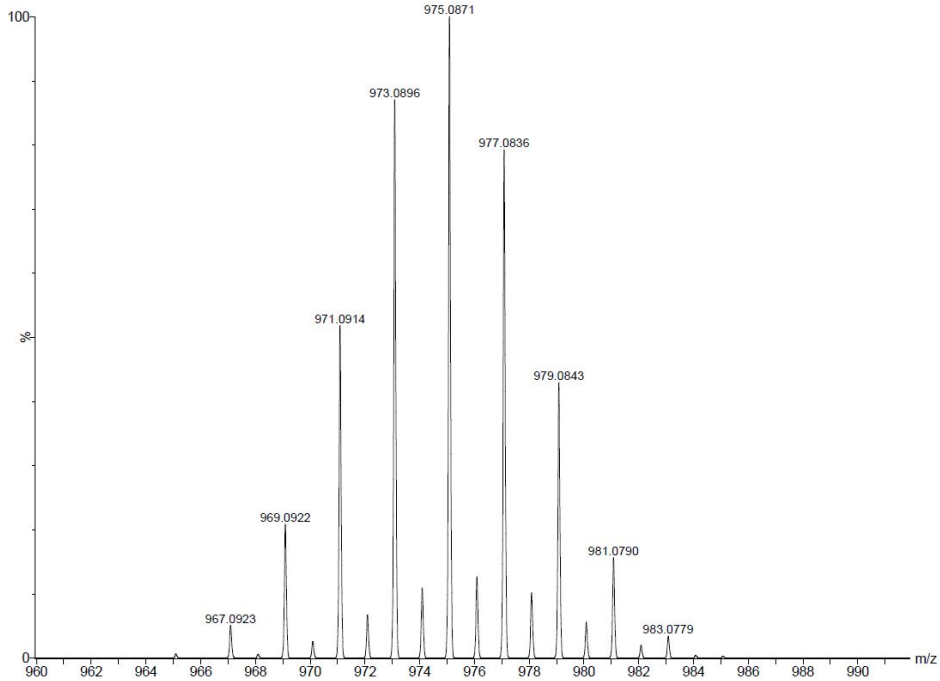


**Figure S23.** EI MS (+) of $FeC_{10}Br_{10}$ (zoom).

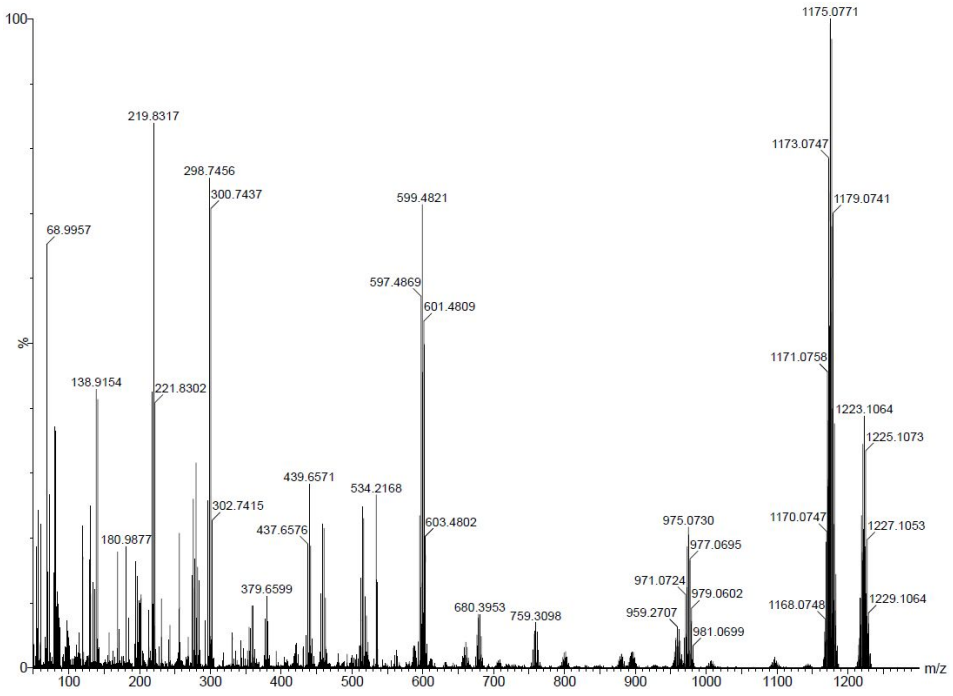


**Figure S24**. EI MS (+) of $FeC_{10}Br_9HgBr$.

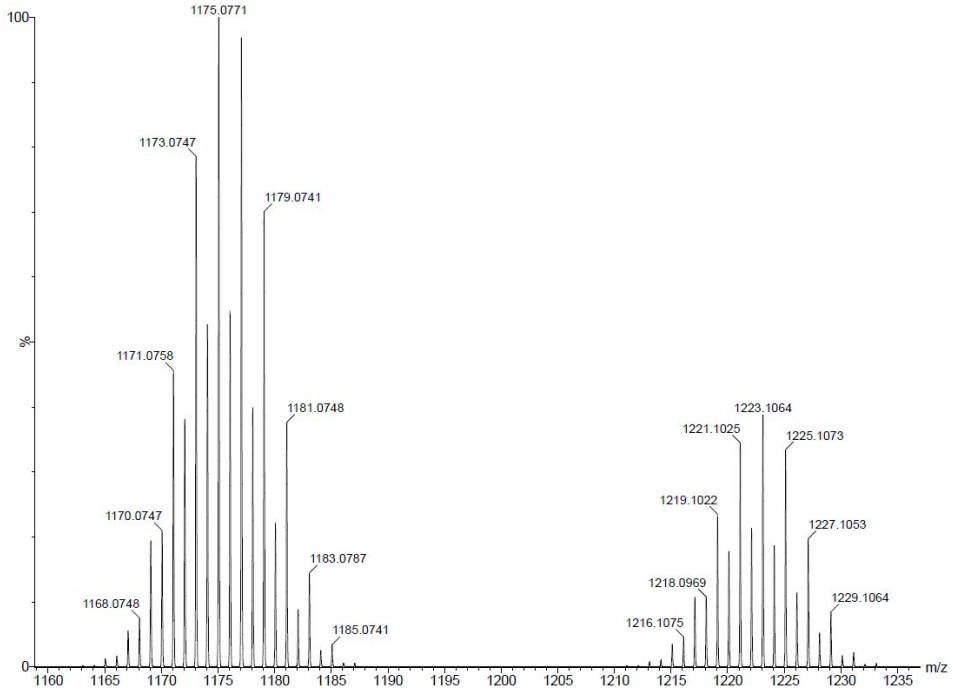


**Figure S25.** EI MS (+) of $FeC_{10}Br_9HgBr$ (zoom).

# 4 References

(1) Dolomanov, O. V.; Bourhis, L. J.; Gildea, R. J.; Howard, J. A. K.; Puschmann, H. OLEX2: A Complete Structure Solution, Refinement and Analysis Program. *J. Appl. Cryst.* **2009**, *42*, 339–341.

(2) Sheldrick, G. M. Crystal Structure Refinement with SHELXL. *Acta Cryst.* **2015**, *A71*, 3–8.

(3) Sheldrick, G. M. *SHELXL Version 2014/7, Program for Chrystal Structure Solution and Refinement*; Göttingen, Germany, 2014.

(4) Sheldrick, G. M. A Short History of SHELX. *Acta Cryst.* **2008**, *A64*, 112–122.

(5) Brandenburg, K. Diamond: Crystal and Molecular Structure Visualization http://www.crystalimpact.com/diamond.

(6) Persistence of Vision Pty. Ltd. Persistence of Vision Raytracer. Ltd., Persistence of Vision Pty. 2004.

## A.4 Persilylation of Ferrocene: The Ultimate Discipline in Sterically Overcrowded Metal Complexes

Supporting Information

# Persilylation of Ferrocene: The Ultimate Discipline in Sterically Overcrowded Metal Complexes

Susanne M. Rupf,[a] Robin Sievers,[a] Paulin S. Riemann,[a] Marc Reimann,[b] Prof. Dr. Martin Kaupp,[b] Dr. Carlo Fasting,[a] Dr. Moritz Malischewski[a*]

[a]Freie Universität Berlin, Fabeckstr. 34-36, 14195 Berlin Germany
[b]Technische Universität Berlin, Straße des 17. Juni 135, 10623 Berlin Germany

E-Mail corresponding author: moritz.malischewski@fu-berlin.de

# 1 General Considerations

Commercially available chemicals were used as received, unless otherwise noted. $[FeC_{10}Br_{10}]$[1,2] was prepared as described previously in literature. Dimethylchlorosilane was freshly distilled over $CaH_2$, degassed and stored in a flame dried Young flask. THF was freshly distilled over Na. *n*-Pentane was received from the solvent system FMBRAUN MB SPS-800. Both solvents were stored in Young flasks under argon atmosphere over molar sieve (3 Å) which was dried beforehand at 250 °C under high vacuum. The glass apparatuses were initially purged with *tert*-BuLi in addition to standard drying methods. $^t$BuLi is an extreme pyrophoric and toxic chemical. The recommended handling and quenching procedures should be strictly followed.[3] Mercury compounds are highly toxic and should only be handled with appropriate safety equipment.

$^1$H, $^{13}$C and $^{29}$Si NMR spectra were recorded on a Bruker AVANCE III 700 spectrometer by using 6mm NMR glass tubes. All reported chemical shifts (δ) are referenced to the Ξ values given in IUPAC recommendations of 2008 using the $^2$H signal of the deuterated solvent as internal reference.[4] All chemical shifts (δ) are given in parts per million (ppm) and the signals are specified according to the multiplicity (s = singlet, d = doublet, t = triplet, q = quartet, m = multiplet, br = broad) and the coupling constants J in Hz. The program MestRe Nova Version 14.0.1 was used to evaluate and plot the data.[5]

Mass spectrometry was performed on a Agilent 6210 ESI TOF (electrospray ionization time-of-flight spectrometer) of Aglient Technologies, Santa Clara, CA in negative mode. Flow rates were set to 10 µL·min$^{-1}$ or using a Varian MAT 711 spectrometer by electron impact ionization (EI) at the department of mass spectroscopy at the Freie Universität Berlin. The evaluation of the resulting data occurred by using Mmass 5.5.0.[6]

Infrared spectra were either measured using a Thermo-Scientific Nicolet iS10 FTIR spectrometer with DuraSamplIR accessory in attenuated total reflection at room temperature. The software OriginPro 2017G was used to plot the data.[7]

The UV/VIS spectra were recorded on a Varian Cary 50 Bio photospectrometer (xenon lamp) in Suprasil glass cuvettes (thickness of 1 cm).

# 2 Experimental Details

List of compounds:

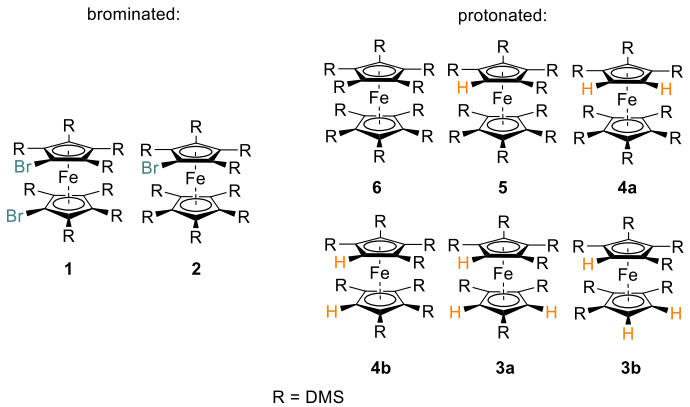


**Silylation – General Procedure via Grignard reaction.** In a dry 50 mL pressure tube magnesium (20 eq.) was placed in anhydrous and degassed THF (2 mL) under an argon atmosphere and was activated with some drops of 1,2-dibromethane. Then DMSCl (30 eq.) and decabromoferrocene (50 mg, 1.0 eq.) were suspended in anhydrous

and degassed THF (15 mL) were added subsequently dropwise and the reaction mixture was stirred for various reaction times at different temperatures:

Table S1. Varied reaction conditions in the reaction of decabromoferrocene with elemental Mg and DMSCl in THF. The corresponding ESI MS spectra are depicted in section 4.4.

| **Enrty** | 1 | 2 | 3 | 4 |
|---|---|---|---|---|
| **Time** | 16h | 2d | 2d | 16h |
| **Temperature** | 60°C | 60°C | room temperature | room temperature |

The suspension was quenched with $H_2O$ at 0°C and extracted with *n*-pentane. The organic layer was dried over $MgSO_4$, filtrated and the organic solvent was removed under reduced pressure to afford a red oil which was used for the mass experiments. The combined samples (using in total 2.3 g of decabromoferrocene) were prepurified with column chromatography [$SiO_2$, *n*-pentane]. The crude product (509 mg) was afforded as a red oil and was further purified by HPLC [RP-18, MeOH/$H_2O$ (98:2) then MeOH]. Several highly silylated ferrocenes could be isolated.

**4a**: 1,2,3,4,5-penta(dimethylsilyl)cyclopentadienyl-1,2,3-tri(dimethylsilyl)cyclopentadienyliron(II): pink solid, 55 mg, 4%. $^1$H NMR ($CDCl_3$, RT, 400 MHz): $\delta$ = 4.66 (hept, $J$ = 3.6 Hz, 7H, Si-H), 4.63 (s, 2H, Cp-H), 4.55 (hept, $J$ = 3.8 Hz, 1H, Si-H), 0.40 (d, $J$ = 3.9 Hz, 30H, Me), 0.38 (d, $J$ = 3.6 Hz, 6H, Me), 0.35 (d, $J$ = 3.8 Hz, 6H, Me), 0.17 (d, $J$ = 3.7 Hz, 6H, Me) ppm. $^{13}$C{$^1$H} NMR ($CDCl_3$, RT, 176 MHz): $\delta$ = 89.9 (s, Cp-C), 83.8 (s, Cp-C), 82.1 (s, Cp-C), 79.0 (s, Cp-C), 0.5 (s, Me), 0.2 (s, Me), -0.0 (s, Me), -1.4 (s, Me). ppm. $^{29}$Si NMR ($CDCl_3$, RT, 80 MHz) $\delta$ = -18.2, -22.2, -25.8 ppm. $\tilde{\nu}$ (cm$^{-1}$) = 2951 ($\nu_{C\text{-}H}$), 2902 ($\nu_{C\text{-}H}$), 2135 ($\nu_{Si\text{-}H}$), 1409, 1247, 1197, 1112, 1024, 992, 945, 867, 827, 778, 758. MS (ESI) cald for $[FeC_{10}DMS_8H_2]^+$: 650.2042. Found: 650.1946. EA: cald. 47.95 (C), 8.98 (H), 0.00 (N), 0.00 (S); found 47.63 (C), 8.90 (H), 0.01 (N), 0.00 (S).

**4b**: Bis(1,2,3,4-tetra(dimethylsilyl)cyclopentadienyl)iron(II): red solid, 80 mg, 5%. $^1$H NMR ($CDCl_3$, RT, 400 MHz): $\delta$ = 4.71 (hept, J = 3.9 Hz, 4H, Si-H), 4.66 (hept, J = 3.9 Hz, 4H, Si-H), 4.43 (s, 2H, Cp-H), 0.43 (m, 24H, Me), 0.32 (d, J = 3.8 Hz, 12H, Me), 0.12 (d, J = 3.6 Hz, 13H, Me).ppm. $^{13}$C{$^1$H} NMR ($CDCl_3$, RT, 176 MHz): $\delta$ = 86.6 (s, Cp-H), 85.4 (s, Cp-C), 82.9 (s, Cp-C), 0.4 (s, Me), 0.1 (s, Me), -0.4 (s, Me), -2.4 (s, Me) ppm. $^{29}$Si NMR ($CDCl_3$, RT, 80 MHz) $\delta$ = -18.0, -21.4 ppm. IR (ATR, RT): $\tilde{\nu}$ (cm$^{-1}$) = 2957 ($\nu_{C\text{-}H}$), 2924 ($\nu_{C\text{-}H}$), 2854 ($\nu_{C\text{-}H}$), 2176 ($\nu_{Si\text{-}H}$), 2141 ($\nu_{Si\text{-}H}$), 1253, 1202, 1113 ($\delta_{C\text{-}H}$), 1080 ($\delta_{C\text{-}H}$), 1023 ($\delta_{C\text{-}H}$), 947, 876, 823, 800, 759, 727, 698, 654, 678. MS (ESI) cald for $[FeC_{10}DMS_8H_2]^+$: 650.2042. Found: 650.1946. EA: cald. 47.95 (C), 8.98 (H), 0.00 (N), 0.00 (S); found 47.59 (C), 8.78 (H), 0.01 (N), 0.00 (S).

**3a**: 1,2,3,4-tetra(dimethylsilyl)cyclopentadienyl-1,2,4-tri(dimethylsilyl)cyclopentadienyliron(II): red solid, 45 mg, 3%. $^1$H NMR ($CDCl_3$, RT, 400 MHz): $\delta$ = 4.75 (m, 1H, Si-H), 4.66 – 4.57 (m, 6H, Si-H), 4.37 (s, 1H, Cp-H), 4.24 (s, 2H, Cp-H), 0.42 (d, $J$ = 3.3 Hz, 6H, Me), 0.37 (d, $J$ = 3.5 Hz, 6H, Me), 0.36 (d, $J$ = 3.8 Hz, 6H, Me), 0.33 (d, $J$ = 3.9 Hz, 6H, Me), 0.26 (d, $J$ = 3.6 Hz, 6H, Me), 0.24 (d, $J$ = 3.6 Hz, 6H, Me), 0.22 (d, $J$ = 3.6 Hz, 6H, Me) ppm. $^{13}$C{$^1$H} NMR ($CDCl_3$, RT, 176 MHz): $\delta$ = 89.3 (s, Cp-C), 85.4 (s, Cp-C), 84.4 (s, Cp-C), 81.4 (s, Cp-C), 81.1 (s, Cp-C), 78.2 (s, Cp-C), 74.5 (s, Cp-C), 0.0 (s, Me), 0.5 (s, Me), 0.8 (s, Me), 2.1 (s, Me), 2.3 (s, Me), 2.4 (s, Me) ppm. IR (ATR, RT): $\tilde{\nu}$ (cm$^{-1}$) = 2956 ($\nu_{C\text{-}H}$), 2905 ($\nu_{C\text{-}H}$), 2125 ($\nu_{Si\text{-}H}$), 1416, 1382, 1242, 1199, 1117, 1085, 1029, 987, 949, 929, 867, 830, 758, 729. MS (ESI) cald. for $[FeC_{10}DMS_7H_3]^+$: 592.1803. Found: 592.1711. EA: cald. 48.60 (C), 8.84 (H), 0.00 (N), 0.00 (S); found 48.84 (C), 8.79 (H), 0.00 (N), 0.00 (S).

**3b**: 1,2,3,4-tetra(dimethylsilyl)cyclopentadienyl-1,2,3-tri(dimethylsilyl)cyclopentadienyliron(II): red solid 11 mg, 1%. $^1$H NMR ($CDCl_3$, RT, 400 MHz): $\delta$ = 4.69 (m, 4H, Si-H), 4.66 (m, 2H, Si-H), 4.60 (m, 1H, Si-H), 4.54 (s, 2H, Cp-H), 4.41 (s, 1H, Cp-H), 0.45 (d, J = 3.8 Hz, 6H, Me), 0.43 (d, J = 3.2 Hz, 6H, Me), 0.42 (d, J = 3.3 Hz, 6H, Me), 0.38 (d, J = 3.8 Hz, 6H, Me), 0.36 (d, J = 3.9 Hz, 6H, Me), 0.21 – 0.19 (m, 12H, Me) ppm. $^{13}$C{$^1$H} NMR ($CDCl_3$, RT, 176 MHz): $\delta$ = 88.1 (s, Cp-C), 84.1 (s, Cp-C), 82.3 (s, Cp-C), 81.7 (s, Cp-C), 80.9 (s, Cp-C), 80.3 (s, Cp-C), 0.1 (s, Me), -0.2 (s, Me), -0.5 (s, Me), -0.7 (s, Me), -2.4 (s, Me), -2.5 (s, Me) ppm. $^{29}$Si NMR ($CDCl_3$, RT, 80 MHz) $\delta$ = −17.9, −18.1, −21.4, 25.5 ppm. IR (ATR, RT): $\tilde{\nu}$ (cm$^{-1}$) = 2957 (vC-H), 2925 (vC-H), 2856 ($\nu$C-H), 2140 ($\nu$Si-H), 1252, 1197, 1118 ($\delta$C-H), 1077 ($\delta$C-H), 1034 ($\delta$C-H), 951, 878, 827, 800, 799, 760, 737, 698,

660, 634. MS (ESI) cald. for $[FeC_{10}DMS_7H_3]^+$: 592.1803. Found: 592.1711. EA: cald. 48.60 (C), 8.84 (H), 0.00 (N), 0.00 (S); found 48.86 (C), 8.73 (H), 0.00 (N), 0.00 (S).

**Silylation – General Procedure via lithium-bromine exchange.** In a dry Schlenk tube decabromoferrocene (1 g, 1.03 mmol, 1.0 eq.) was placed in anhydrous and degassed *n*-pentane (50 mL) under an argon atmosphere. A solution of *tert*-BuLi (1.6 M in *n*-pentane, 25.8 mL, 41.2 mmol, 40 eq.) was added dropwise at −78 °C and the solution was stirred for 6 h at this temperature. DMSCl (0.690 mL, 61.8 mmol, 60 eq.) was added dropwise and stirred for 6 h at −50 °C. The reaction mixture was slowly warmed up to room temperature overnight. Then, the solvent was removed under reduced pressure and anhydrous *n*-pentane (50 mL) was added again. The resulting red suspension was cooled to (−78 °C) and a solution of *tert*-BuLi (1.6 M in *n*-pentane, 25:8 mL, 41:2 mmol, 40 eq.) was added dropwise at this temperature. The mixture was stirred for 6 h at this temperature. Afterwards, additional DMSCl (0.690 mL, 61.8 mmol, 60 eq.) was added dropwise and the mixture was allowed to warm up to room temperature overnight yielding a pink suspension. All volatile compounds were removed under reduced pressure. Then, saturated $NaHCO_3$ solution was added and extracted with *n*-pentane. The organic layer was dried over $MgSO_4$, filtrated and the organic solvent was removed under reduced pressure to afford a red oil that was pre-purified with column chromatography [$SiO_2$, *n*-pentane]. The crude product was afforded as a red oil and was further purified by HPLC [RP-18, MeOH/$H_2O$ (98:2) then MeOH]. Several highly silylated but still brominated ferrocenes could be isolated.

**1**: Bis(1-bromo-2,3,4,5-tetra(dimethylsilyl)cyclopentadienyl)iron(II): pink solid (130 mg, 16%). $^1$H NMR ($CDCl_3$, RT, 400 MHz): $\delta$ = 4.72 (hept, $J$ = 3.3, 2.8 Hz, 2H, Si-H), 4.64 (hept, $J$ = 4.0 Hz, 2H, Si-H), 0.76 (d, $J$ = 4.0 Hz, 6H, Me), 0.41 (d, $J$ = 4.0 Hz, 6H, Me), 0.39 (d, $J$ = 4.0 Hz, 6H, Me), 0.22 (d, $J$ = 3.9 Hz, 6H, Me) ppm. $^{13}$C{$^1$H} NMR ($CDCl_3$, RT, 176 MHz): $\delta$ = 99.4 (s, Cp-C), 87.7 (s, Cp-C), 85.0 (s, Cp-C), 0.5 (s, Me), 0.2 (s, Me), -0.0 (s, Me), -1.2 (s, Me) ppm. $^{29}$Si NMR ($CDCl_3$, RT, 80 MHz) $\delta$ = -17.4, -18.4 ppm. MS (EI) cald for $[FeC_{10}DMS_8Br_2]^+$: 808.0231. Found: 808.0328.

**2**: 1,2,3,4,5-penta(dimethylsilyl)cyclopentadienyl-1-bromo-2,3,4,5-tetra(dimethylsilyl)cyclopentadienyliron(II): purple solid (210 mg, 26%). $^1$H NMR ($CDCl_3$, RT, 400 MHz): $\delta$ = 4.74 (hept, $J$ = 3.9 Hz, 2H, Si-H), 4.60 (hept, $J$ = 3.7 Hz, 5H, Si-H), 4.51 (hept, $J$ = 3.8 Hz, 2H, Si-H), 0.39 (m, 60H, Me) ppm. $^{13}$C{$^1$H} NMR ($CDCl_3$, RT, 176 MHz): $\delta$ = 97.8 (s, Cp-C), 93.8 (s, Cp-C), 86.8 (s, Cp-C), 84.6 (s, Cp-C), 0.7 (s, Me), 0.4 (s, Me), -0.5 (s, Me) ppm. MS (EI) cald for $[FeC_{10}DMS_9Br]^+$: 788.1364. Found: 788.1330.

In a dry 50 mL Schlenk tube the mixture of partially brominated silylferrocenes (430 mg.) was placed in anhydrous and degassed tetrahydrofuran (5 mL) under an argon atmosphere. A solution of *tert*-BuLi (1.6 M in *n*-pentane, 25.8 mL, 41.2 mmol) was added dropwise at −78 °C. The dark red solution warmed up to at −20 °C over a period of 1 h. DMSCl (0.690 mL, 61.8 mmol) was added dropwise and the reaction mixture was slowly warmed up to room temperature overnight. After heating at 50 °C for 1 h, all volatile compounds were removed under reduced pressure. Then, saturated $NaHCO_3$ solution was added and extracted with *n*-pentane. The organic layer was dried over $MgSO_4$, filtrated and the organic solvent was removed under reduced pressure to afford a pink oil that was prepurified with column chromatography [$SiO_2$, *n*-pentane]. The crude product was afforded as a pink oil which was first recrystallized from THF or *n*-pentane (to yield $[FeC_{10}DMS_{10}]$ (**3**) as pink solid) and subsequently purified by HPLC [RP-18, 9:1 MeOH(98%) and THF]. Several highly silylated ferrocenes could be isolated.

**6**: Bis(1,2,3,4,5-penta(dimethylsilyl)cyclopentadienyl)iron(II): purple solid, 10 mg, 1%. $^1$H NMR ($CDCl_3$, RT, 400 MHz): $\delta$ = 4.64 (hept, $J$ = 4.0 Hz, 10H, Si-H), 0.76 (d, $J$ = 3.6 Hz, 30H, Me), 0.09 (d, $J$ = 3.7 Hz, 30H, Me) ppm. $^{13}$C{$^1$H} NMR ($CDCl_3$, RT, 176 MHz): δ = 93.21, 2.41, −0.18 ppm. $^{29}$Si NMR ($CDCl_3$, RT, 80 MHz) $\delta$ = -17.9 ppm. IR (ATR, RT): $\tilde{\nu}$ (cm$^{-1}$) = 2976 ($\nu_{C\text{-}H}$), 2908 ($\nu_{C\text{-}H}$), 2155 ($\nu_{Si\text{-}H}$), 1242, 1222, 914, 880, 831, 757, 697, 666. MS (ESI) cald for $[FeC_{10}DMS_{10}]^+$: 766.2520. Found: 766.2530. EA: cald. 46.94 (C), 9.19 (H), 0.00 (N), 0.00 (S); found 46.86 (C), 8.75 (H), 0.00 (N), 0.00 (S).

**5**: 1,2,3,4,5-penta(dimethylsilyl)cyclopentadienyl-1,2,3,4-tetra(dimethylsilyl)cyclopentadienyliron(II): purple solid, 41 mg, 6%. $^{1}$H NMR ($CDCl_3$, RT, 400 MHz): $\delta$ = 4.74 (hept, $J$ = 3.5 Hz, 2H, Si-H), 4.67 (hept, $J$ = 3.8 Hz, 5H, Si-H), 4.63 – 4.60 (m, 2H, Si-H), 4.59 (s, 1H, Cp-H), 0.39 (m, 42H, Me), 0.35 (d, $J$ = 3.7 Hz, 6H, Me), 0.16 (d, $J$ = 3.7 Hz, 6H, Me) ppm. $^{13}$C{$^{1}$H} NMR ($CDCl_3$, RT, 176 MHz): $\delta$ = 90.8 (s, Cp-C), 87.8 (s, Cp-C), 86.4 (s, Cp-C), 83.6 (s, Cp-C), 0.9 (s, Me), 0.8 (s, Me), 0.4 (s, Me), 0.1 (s, Me), -1.01 (s, Me) ppm. $^{29}$Si NMR ($CDCl_3$, RT, 80 MHz) $\delta$ = -17.4, -18.8 ppm. IR (ATR, RT): $\tilde{\nu}$ ($cm^{-1}$) = 2959 ($\nu_{C\text{-}H}$), 2906 ($\nu_{C\text{-}H}$), 2147 ($\nu_{Si\text{-}H}$), 1243, 1229, 1194, 1106 ($\delta_{C\text{-}H}$), 1069 ($\delta_{C\text{-}H}$), 1036 ($\delta_{C\text{-}H}$), 948, 870, 829, 757, 698, 758, 698, 663. MS (ESI) cald for $[FeC_{10}DMS_9H]^+$: 708.2281. Found: 708.2238. EA: cald. 47.41 (C), 9.09 (H), 0.00 (N), 0.00 (S); found 47.21 (C), 8.52 (H), 0.01 (N), 0.00 (S).

**Silylation of 1,1'-dimethyl ferrocene.** Mercury(II) butyrate (28.81 g, 76.7 mmol, 8,2 eq.) and 1,2-dichloroethane (200 mL) were placed in a 500 mL round bottom flask. 1,1'-dimethyl ferrocene (2 g, 9.34 mmol, 1.0 Eq.) was added and the suspension was stirred under reflux for 18 h. The orange solution allowed to cool down and filtered off, subsequently. Then, the solvent was removed under reduced pressure to afford a orange solid. Without further purification, deionized water (250 mL), bromine (30.00 g, 166.67 mmol, 17.7 eq.) and potassium bromide (34.00 g, 285.71 mmol, 30.6 eq.) were added. The suspension was stirred for four days at room temperature. Afterwards, the mixture was filtered off and the residue was washed with deionized water and methanol. The product, $[FeC_{10}Me_2Br_8]$, was extracted in DCM. The solvent was removed under reduced pressure and washed with (a few milliliters of) dichloromethane to yield a yellow solid (4.2 g, 53%).

$[FeC_{10}Me_2Br_8]$ (**7**): $^{1}$H NMR ($CDCl_3$, RT, 700 MHz): $\delta$ = 1.98 (s, Me-H) ppm. $^{13}$C{$^{1}$H} NMR ($CDCl_3$, RT, 176 MHz): $\delta$ = 85.3 (s, Cp-C), 84.1 (s, Cp-C), 82.3 (s, Cp-C), 9,8 (s, Me-C) ppm. IR (ATR, RT): $\tilde{\nu}$ ($cm^{-1}$) = 2964, 2874, 1520, 1497, 1370, 1345, 1262, 1218, 1093, 896, 754, 722, 589. MS (EI) cald for $[FeC_{10}Me_2Br_8]^+$: 845.3204. Found: 845.3196. EA: cald. 17.05 (C), 0.72 (H), 0.00 (N), 0.00 (S); found 16.91 (C), 0.43 (H), 0.01 (N), 0.00 (S).

In a dry 50 mL pressure tube magnesium (0.42 g, 18.26 mmol, 11 eq.) was placed in anhydrous and degassed THF (10 mL) under an argon atmosphere. Then DMSCl (5 mL, 45.03 mmol, 27 eq.) and $[FeC_{10}Me_2Br_8]$ (1.4 g, 1.65 mmol, 1.0 eq.) were suspended in anhydrous and degassed THF (15 mL) were added subsequently dropwise and the reaction mixture was stirred for 16 h at room temperature. Then, the solvent was evaporated under reduced pressure by using a cooling trap. The compound was extracted in anhydrous *n*-pentane and filtered off. The solvent was removed under reduced pressure to yield a pink oil which was washed with methanol. The residue was dried at high vacuum to afford the product as pink solid (0.99 g, 88%).

$[FeC_{10}Me_2DMS_8]$ (**8**): $^{1}$H NMR ($CDCl_3$, RT, 700 MHz): $\delta$ = 4.64 (m, Si-H, 2H), 4.58 (m, Si-H, 2H), 2.14 (s, $Me^{Cp}$, 3H), 0.53 (d, $J$ = 3.8 Hz, 6H), 0.36 (d, $J$ = 3.8 Hz, 6H), 0.33 (d, J = 3.8 Hz, 6H), 0.14 (d, $J$ = 3.7 Hz, 1H) ppm. $^{13}$C{$^{1}$H} NMR ($CDCl_3$, RT, 176 MHz): $\delta$ = 86.4 (Cp-C), 82.5 (Cp-C), 16.7 ($Me^{Cp}$), 0.5 (DMS), 0.1 (DMS), −0.6 (DMS), −0.8 (DMS) ppm. $^{29}$Si NMR ($CDCl_3$, RT, 80 MHz) $\delta$ = −19.3 ppm. IR (ATR, RT): $\tilde{\nu}$ ($cm^{-1}$) = 2957, 2903, 2153, 1384, 1334, 1245, 1220, 1022, 877, 827, 759, 676, 643. MS (EI) cald for $[FeC_{10}Me_2Br_8]^+$: 678.2355. Found: 678.2460. EA: cald. 49.51 (C), 9.20 (H), 0.00 (N), 0.00 (S); found 49.12 (C), 9.48 (H), 0.02 (N), 0.00 (S).

# 3 Crystal Structure Determination

X-Ray data were collected on a BRUKER D8 Venture system. Data were collected at 100(2) K using graphite-monochromated Mo $K_\alpha$ ($\lambda_\alpha$ = 0.71073 Å) or Cu $K_\alpha$ ($\lambda$ = 1.54178) radiation. The strategy for the data collection was evaluated by using the Smart software. The data were collected by the standard "ψ-ω scan techniques" and were scaled and reduced using Saint+software. The structures were solved by using Olex2,[8] the structure was solved with the XT[9] structure solution program using Intrinsic Phasing and refined with the XL refinement package[10,11] using Least Squares minimization. If it is noted, bond length and angles were measured with Diamond Crystal and Molecular Structure Visualization Version 4.6.2.[12] Drawings were generated with POV-Ray.[13] Deposition numbers CCDC 2248053 (**1**), 2248054 (**2**), 2248060 (**3a**), 2248059 (**3b**), 2248057 (**4a**), 2248058 (**4b**), 2248056 (**5**), 2248055 (**6**) contain the supplementary crystallographic data for this paper. These data are provided free of charge by the joint Cambridge Crystallographic Data Centre and Fachinformationszentrum Karlsruhe Access Structures service www.ccdc.cam.ac.uk/structures.

Table S2. Crystal data.

| **Compound** | **$FeC_{10}(DMS)_9Br$ (2)** | **$Fe(C_5(DMS)_4Br)_2$ (1)** |
|---|---|---|
| **Empirical formula** | $C_{28}H_{63}BrFeSi_9$ | $C_{26}H_{56}Br_2FeSi_8$ |
| **Formula weight** | 788.35 | 809.09 |
| **Temperature/K** | 100.0 | 100 |
| **Crystal system** | orthorhombic | tetragonal |
| **Space group** | Pnma | $P4_2/n$ |
| **a/Å** | 17.7129(9) | 36.0111(3) |
| **b/Å** | 18.7916(7) | 36.0111(3) |
| **c/Å** | 12.3172(6) | 12.1108(2) |
| **α/°** | 90 | 90 |
| **β/°** | 90 | 90 |
| **γ/°** | 90 | 90 |
| **Volume/Å³** | 4099.8(3) | 15705.3(4) |
| **Z** | 4 | 16 |
| **$\rho_{calc}$/g·cm³** | 1.277 | 1.369 |
| **μ/mm⁻¹** | 1.624 | 7.919 |
| **F(000)** | 1672.0 | 6720.0 |
| **Crystal size/mm³** | 0.22 × 0.22 × 0.18 | 0.23 × 0.23 × 0.22 |
| **Crystal shape** | Block | Block |
| **Radiation** | MoKα (λ = 0.71073) | CuKα (λ = 1.54178) |
| **2Θ range for data collection/°** | 4.028 to 56.602 | 5.488 to 136.552 |
| **Index ranges** | $-23 \le h \le 23$, $-25 \le k \le 24$, $-16 \le l \le 16$ | $-43 \le h \le 43$, $-42 \le k \le 43$, $-13 \le l \le 14$ |
| **Reflections collected** | 72426 | 83076 |
| **Independent reflections** | 5235 [$R_{int}$ = 0.0502, $R_{sigma}$ = 0.0194] | 14394 [$R_{int}$ = 0.0678, $R_{sigma}$ = 0.0438] |
| **Data/restrains/parameters** | 5235/0/238 | 14394/0/700 |
| **Goodness-of-fit on $F^2$** | 1.050 | 1.035 |
| **Final R indexes [I>=2σ(I)]** | $R_1$ = 0.0297, $wR_2$ = 0.0792 | $R_1$ = 0.0473, $wR_2$ = 0.1249 |
| **Final R indexes [all data]** | $R_1$ = 0.0357, $wR_2$ = 0.0823 | $R_1$ = 0.0536, $wR_2$ = 0.1295 |
| **Largest diff. peak/hole / e·Å³** | 0.53/−0.35 | 2.16/-1.39 |

Table S3. Crystal data.

| **Compound** | **$FeC_{10}(DMS)_{10}$ (6)** | **$FeC_{10}(DMS)_9H$ (5)** |
|---|---|---|
| **Empirical formula** | $C_{30}H_{70}FeSi_{10}$ | $C_{28}H_{64}FeSi_9$ |
| **Formula weight** | 767.61 | 709.45 |
| **Temperature/K** | 100.00 | 100 |
| **Crystal system** | monoclinic | triclinic |
| **Space group** | $P2_1/n$ | P-1 |
| **a/Å** | 11.9543(6) | 11.9336(7) |
| **b/Å** | 13.4426(7) | 18.9321(12) |
| **c/Å** | 13.3587(6) | 20.4215(13) |
| **α/°** | 90 | 63.840(2) |
| **β/°** | 93.029(2) | 77.549(2) |
| **γ/°** | 90 | 88.306(2) |
| **Volume/Å$^3$** | 2143.70(18) | 4032.5(4) |
| **Z** | 2 | 4 |
| **$\rho_{calc}$g/cm$^3$** | 1.189 | 1.169 |
| **μ/mm$^{-1}$** | 0.651 | 0.659 |
| **F(000)** | 832.0 | 1536.0 |
| **Crystal size/mm$^3$** | 0.11 × 0.08 × 0.07 | 0.1 × 0.1 × 0.1 |
| **Crystal shape** | block | block |
| **Radiation** | MoKα (λ = 0.71073) | MoKα (λ = 0.71073) |
| **2Θ range for data collection/°** | 4.456 to 52.736 | 3.982 to 56.564 |
| **Index ranges** | $-14 \le h \le 14$, $-16 \le k \le 16$, $-16 \le l \le 16$ | $-15 \le h \le 15$, $-25 \le k \le 25$, $-27 \le l \le 27$ |
| **Reflections collected** | 60684 | 133719 |
| **Independent reflections** | 4386 [$R_{int}$ = 0.0765, $R_{sigma}$ = 0.0284] | 19977 [$R_{int}$ = 0.0519, $R_{sigma}$ = 0.0320] |
| **Data/restraints/parameters** | 4386/0/255 | 19977/0/956 |
| **Goodness-of-fit on F$^2$** | 1.017 | 1.071 |
| **Final R indexes [I>=2σ (I)]** | $R_1$ = 0.0272, $wR_2$ = 0.0623 | $R_1$ = 0.0423, $wR_2$ = 0.1001 |
| **Final R indexes [all data]** | $R_1$ = 0.0339, $wR_2$ = 0.0656 | $R_1$ = 0.0534, $wR_2$ = 0.1055 |
| **Largest diff. peak/hole / e Å$^{-3}$** | 0.33/-0.23 | 0.75/-0.48 |

| Compound | $Fe(C_5(DMS)_5)(1,2,3\text{-}C_5(DMS)_3H_2)$ (4a) | $Fe(C_5(DMS)_4H)_2$ (4b) |
|---|---|---|
| **Empirical formula** | $C_{26}H_{58}FeSi_8$ | $C_{26}H_{58}FeSi_8$ |
| **Formula weight** | 651.29 | 651.29 |
| **Temperature/K** | 100.0 | 100.0 |
| **Crystal system** | monoclinic | monoclinic |
| **Space group** | Cc | $P2_1/n$ |
| **a/Å** | 18.8023(14) | 19.7412(7) |
| **b/Å** | 16.3214(13) | 20.9752(7) |
| **c/Å** | 11.9698(9) | 19.7446(7) |
| **α/°** | 90 | 90 |
| **β/°** | 94.187(3) | 112.4200(10) |
| **γ/°** | 90 | 90 |
| **Volume/Å$^3$** | 3663.5(5) | 7557.8(5) |
| **Z** | 4 | 8 |
| **$\rho_{calc}$g/cm$^3$** | 1.181 | 1.145 |
| **μ/mm$^{-1}$** | 0.688 | 0.667 |
| **F(000)** | 1408.0 | 2816.0 |
| **Crystal size/mm$^3$** | 0.18 × 0.14 × 0.12 | 0.27 × 0.23 × 0.11 |
| **Crystal shape** | block | block |
| **Radiation** | MoKα (λ = 0.71073) | MoKα (λ = 0.71073) |
| **2Θ range for data collection/°** | 4.344 to 50.754 | 3.71 to 50.804 |
| **Index ranges** | $-22 \le h \le 22$, $-19 \le k \le 19$, $-14 \le l \le 14$ | $-23 \le h \le 23$, $-19 \le k \le 25$, $-23 \le l \le 23$ |
| **Reflections collected** | 25907 | 85294 |
| **Independent reflections** | 6673 [$R_{int}$ = 0.0726, $R_{sigma}$ = 0.0641] | 13876 [$R_{int}$ = 0.0833, $R_{sigma}$ = 0.0585] |
| **Data/restraints/parameters** | 6673/2/332 | 13876/0/663 |
| **Goodness-of-fit on F$^2$** | 0.813 | 0.969 |
| **Final R indexes [I>=2σ (I)]** | $R_1$ = 0.0397, $wR_2$ = 0.1088 | $R_1$ = 0.0457, $wR_2$ = 0.1323 |
| **Final R indexes [all data]** | $R_1$ = 0.0450, $wR_2$ = 0.1154 | $R_1$ = 0.0778, $wR_2$ = 0.1580 |
| **Largest diff. peak/hole / e Å$^{-3}$** | 0.49/-0.36 | 0.52/-0.47 |

| **Compound** | **Fe($C_5$(DMS)$_4$H)(1,2,4-$C_5$(DMS)$_3H_2$) (3a)** | **Fe($C_5$(DMS)$_4$H)(1,2,3-$C_5$(DMS)$_3H_2$) (3b)** |
|---|---|---|
| **Empirical formula** | $C_{24}H_{52}FeSi_7$ | $C_{24}H_{52}FeSi_7$ |
| **Formula weight** | 593.13 | 593.13 |
| **Temperature/K** | 100.0 | 159.0 |
| **Crystal system** | triclinic | triclinic |
| **Space group** | P-1 | P-1 |
| **a/Å** | 9.6168(3) | 11.1775(6) |
| **b/Å** | 10.8650(4) | 12.2628(6) |
| **c/Å** | 17.6366(7) | 13.4623(7) |
| **α/°** | 78.884(2) | 79.414(2) |
| **β/°** | 81.1830(10) | 68.618(2) |
| **γ/°** | 65.9980(10) | 80.572(2) |
| **Volume/Å$^3$** | 1646.09(10) | 1679.52(15) |
| **Z** | 2 | 2 |
| **$\rho_{calc}$g/cm$^3$** | 1.197 | 1.173 |
| **μ/mm$^{-1}$** | 0.725 | 0.711 |
| **F(000)** | 640.0 | 640.0 |
| **Crystal size/mm$^3$** | 0.31 × 0.3 × 0.25 | 0.25 × 0.25 × 0.23 |
| **Crystal shape** | block | block |
| **Radiation** | MoKα (λ = 0.71073) | MoKα (λ = 0.71073) |
| **2Θ range for data collection/°** | 4.148 to 56.628 | 4.802 to 56.61 |
| **Index ranges** | $-12 \le h \le 12$, $-14 \le k \le 14$, $-23 \le l \le 23$ | $-14 \le h \le 14$, $-16 \le k \le 16$, $-17 \le l \le 17$ |
| **Reflections collected** | 106271 | 136233 |
| **Independent reflections** | 8170 [$R_{int}$ = 0.0555, $R_{sigma}$ = 0.0215] | 8332 [$R_{int}$ = 0.0577, $R_{sigma}$ = 0.0206] |
| **Data/restraints/parameters** | 8170/0/303 | 8332/0/303 |
| **Goodness-of-fit on F$^2$** | 1.023 | 1.041 |
| **Final R indexes [I>=2σ (I)]** | $R_1$ = 0.0332, $wR_2$ = 0.0871 | $R_1$ = 0.0330, $wR_2$ = 0.0873 |
| **Final R indexes [all data]** | $R_1$ = 0.0396, $wR_2$ = 0.0901 | $R_1$ = 0.0392, $wR_2$ = 0.0911 |
| **Largest diff. peak/hole / e Å$^{-3}$** | 0.65/-0.68 | 0.77/-0.65 |

| Compound | $FeC_{10}Me_2DMS_8$ (8) |
|---|---|
| **Empirical formula** | $C_{28}H_{62}FeSi_8$ |
| **Formula weight** | 679.34 |
| **Temperature/K** | 102.0 |
| **Crystal system** | orthorhombic |
| **Space group** | $P2_12_12$ |
| **a/Å** | 17.4074(6) |
| **b/Å** | 35.0636(12) |
| **c/Å** | 12.7379(4) |
| **α/°** | 90 |
| **β/°** | 90 |
| **γ/°** | 90 |
| **Volume/Å$^3$** | 7774.8(4) |
| **Z** | 8 |
| **$\rho_{calc}$g/cm$^3$** | 1.161 |
| **μ/mm$^{-1}$** | 0.651 |
| **F(000)** | 2944.0 |
| **Crystal size/mm$^3$** | 0.53 × 0.37 × 0.29 |
| **Crystal shape** | block |
| **Radiation** | MoKα (λ = 0.71073) |
| **2Θ range for data collection/°** | 3.952 to 56.664 |
| **Index ranges** | $-23 \leq h \leq 23$, $-46 \leq k \leq 46$, $-14 \leq l \leq 16$ |
| **Reflections collected** | 168102 |
| **Independent reflections** | 19338 [$R_{int}$ = 0.0397, $R_{sigma}$ = 0.0245] |
| **Data/restraints/parameters** | 19338/0/731 |
| **Goodness-of-fit on F$^2$** | 1.048 |
| **Final R indexes [I>=2σ (I)]** | $R_1$ = 0.0440, $wR_2$ = 0.1201 |
| **Final R indexes [all data]** | $R_1$ = 0.0459, $wR_2$ = 0.1214 |
| **Largest diff. peak/hole / e Å$^{-3}$** | 1.43/-0.70 |

# 4 Spectra

## 5.1 NMR spectra of brominated silylferrocenes

1,2,3,4,5-penta(dimethylsilyl)cyclopentadienyl-1-bromo-2,3,4,5-tetra(dimethylsilyl)-cyclopentadienyliron(II):

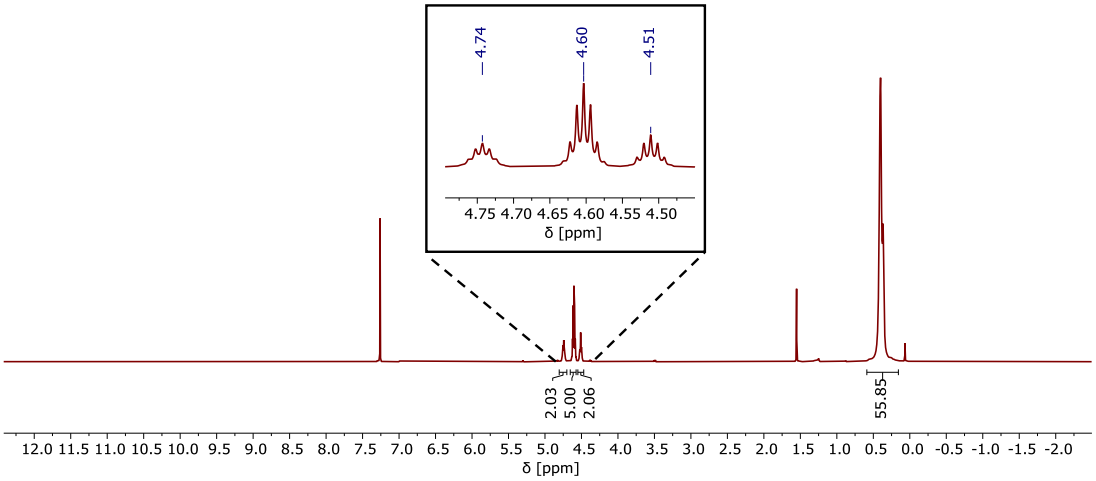


Figure S1. $^{1}H$ NMR spectrum ($CDCl_3$, RT, 400 MHz).

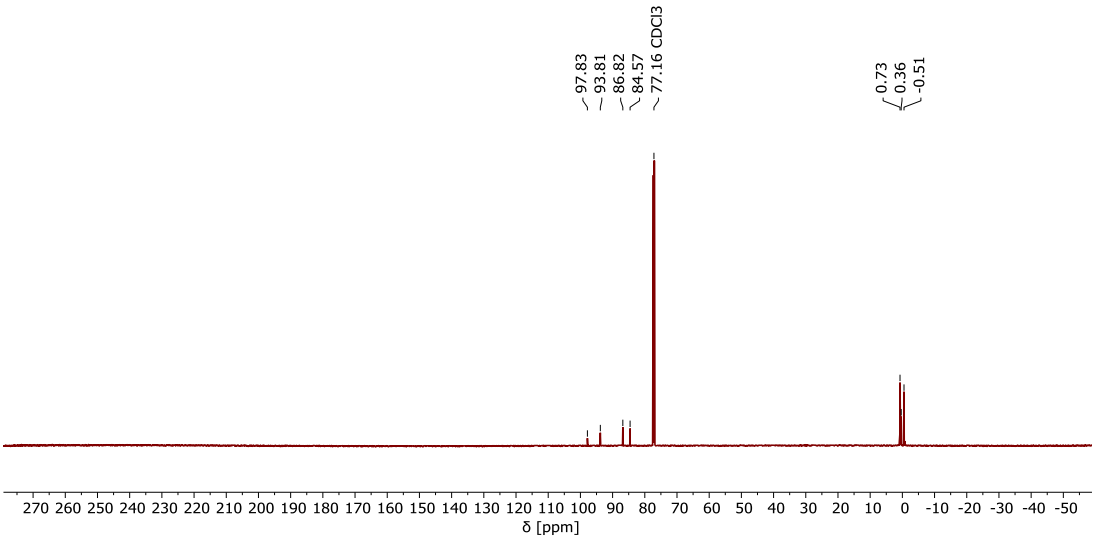


Figure S2. $^{13}C\{^{1}H\}$ NMR spectrum ($CDCl_3$, RT, 176 MHz).

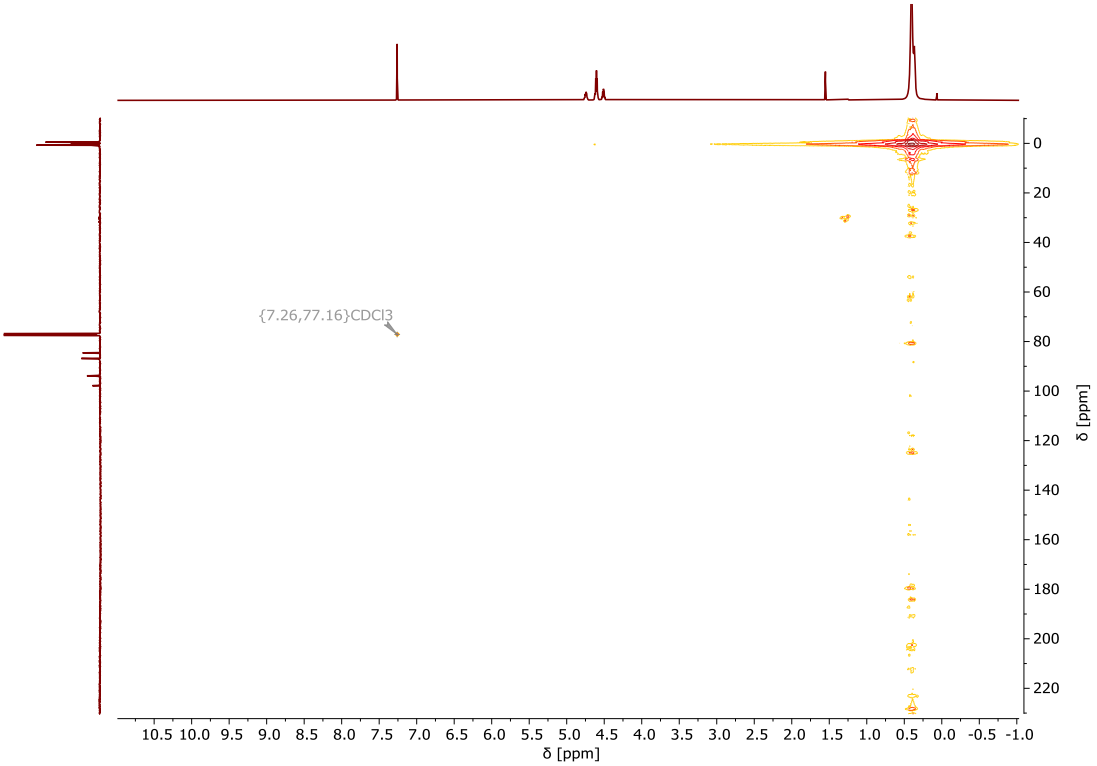


Figure S3. $^{1}H,^{13}C$ HMQC NMR spectrum.

Bis(1-bromo-2,3,4,5-tetra(dimethylsilyl)cyclopentadienyl)iron(II):

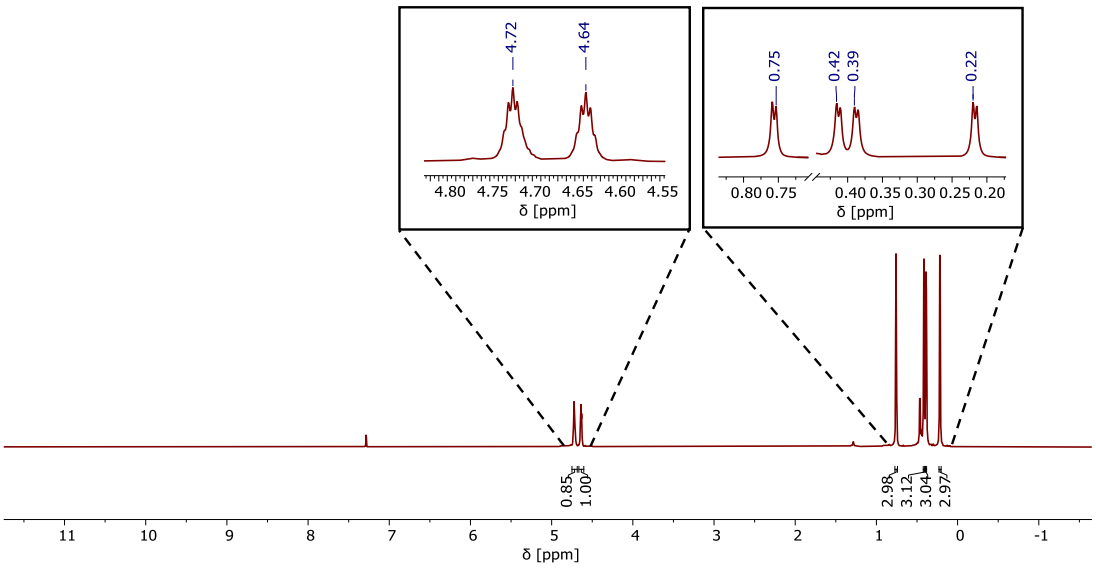


Figure S4. $^{1}H$ NMR spectrum ($CDCl_3$, RT, 400 MHz).

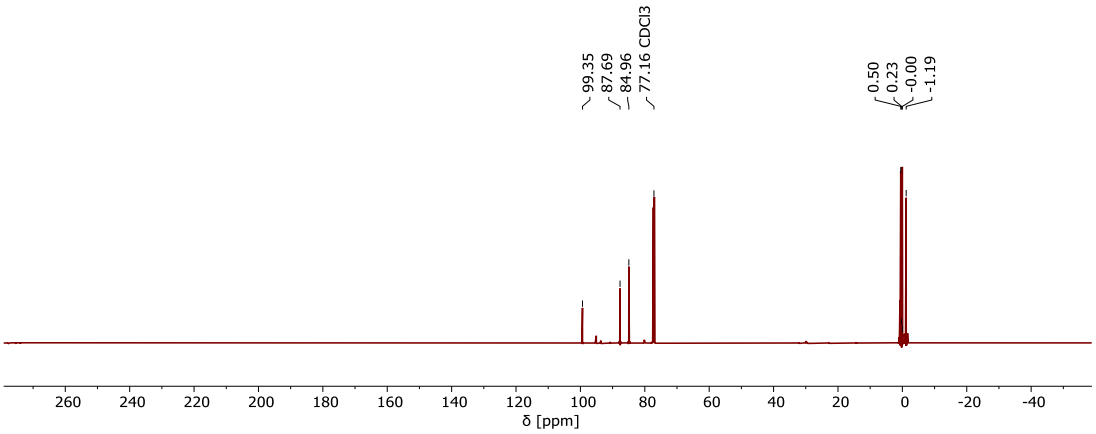


Figure S5. $^{13}C\{^{1}H\}$ NMR spectrum ($CDCl_3$, RT, 176 MHz).

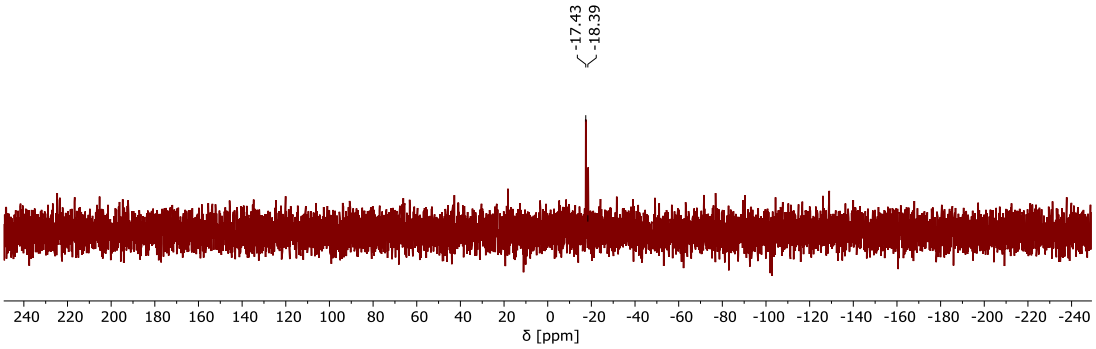


Figure S6. $^{29}Si$ DEPT spectrum ($CDCl_3$, RT, 80 MHz).

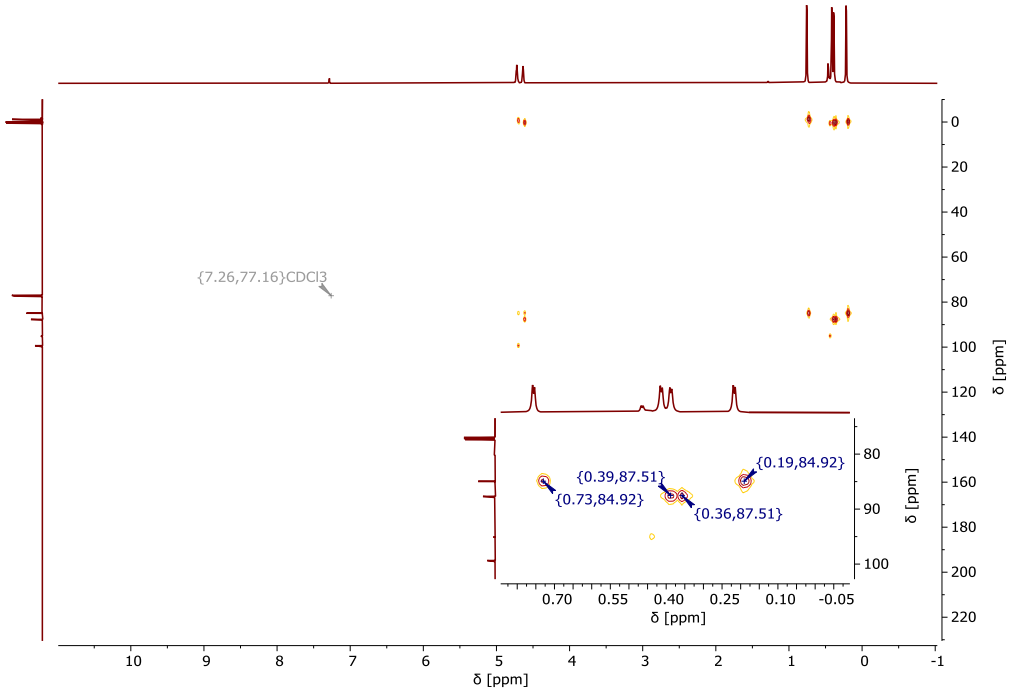


Figure S7. $^{1}H,^{13}C$ HMBC NMR spectrum.

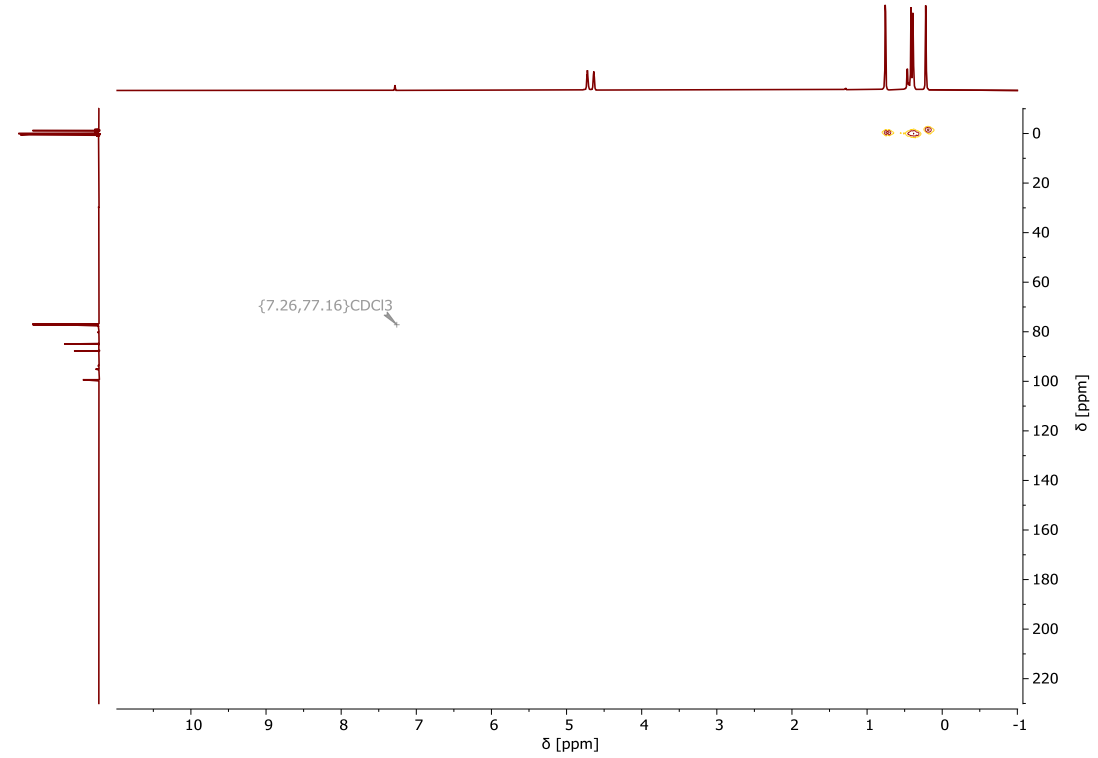


Figure S8. $^{1}H,^{13}C$ HMQC NMR spectrum.

## 5.2 NMR spectra of polysilylated ferrocenes

Bis(1,2,3,4,5-penta(dimethylsilyl)cyclopentadienyl)iron(II):

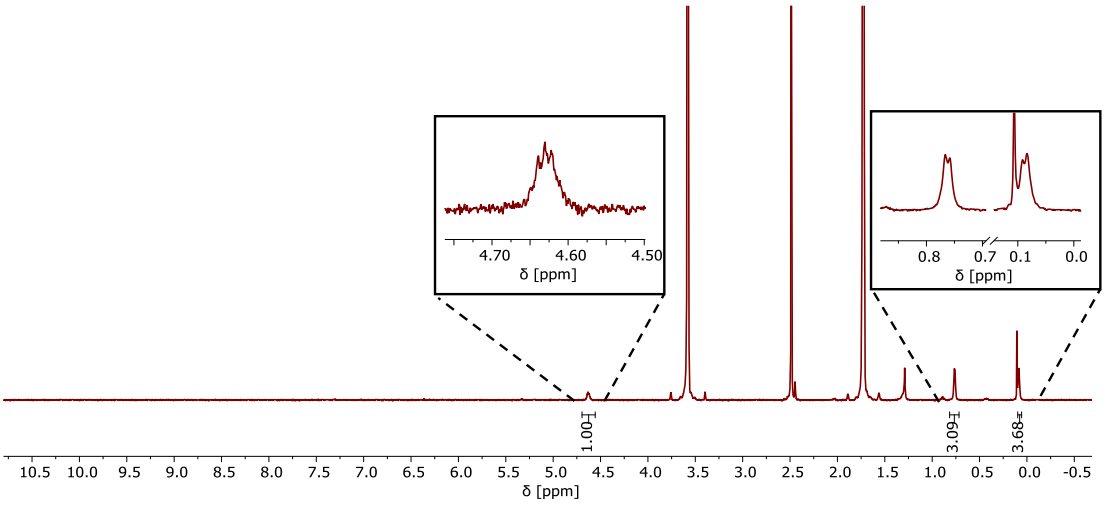


Figure S9. $^{1}H$ NMR spectrum (THF-$d_8$, RT, 400 MHz).

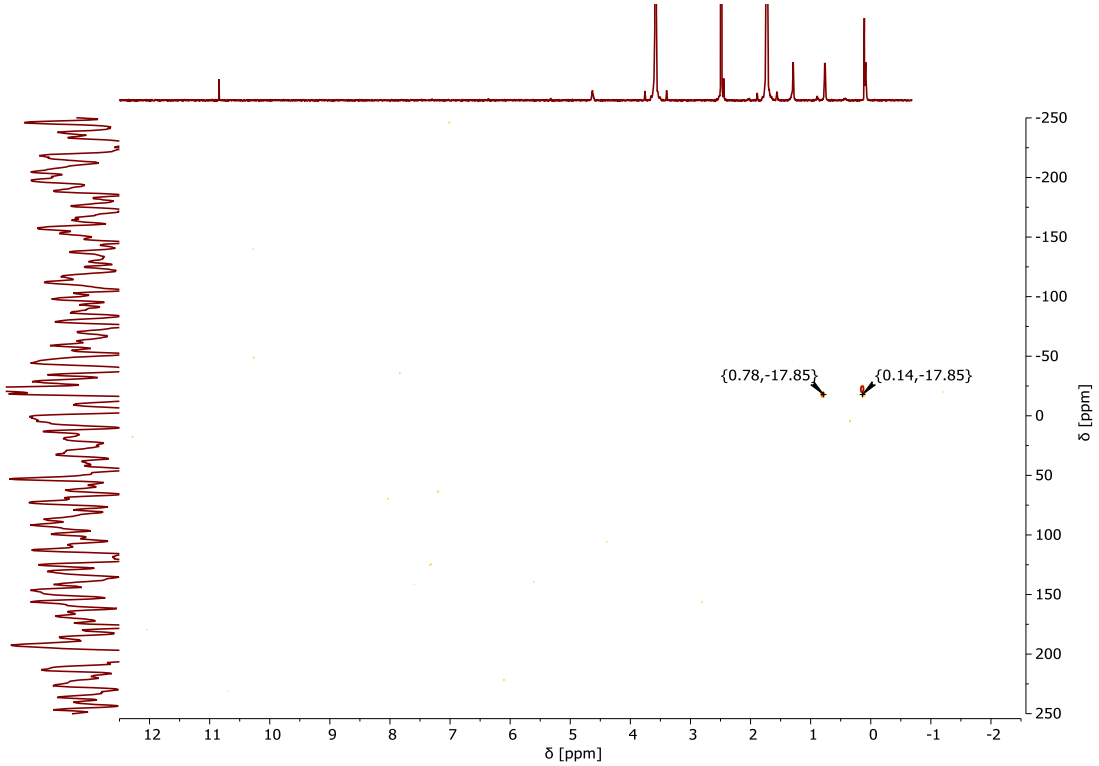


Figure S10. $^{1}H,^{29}Si$ HMBC NMR spectrum.

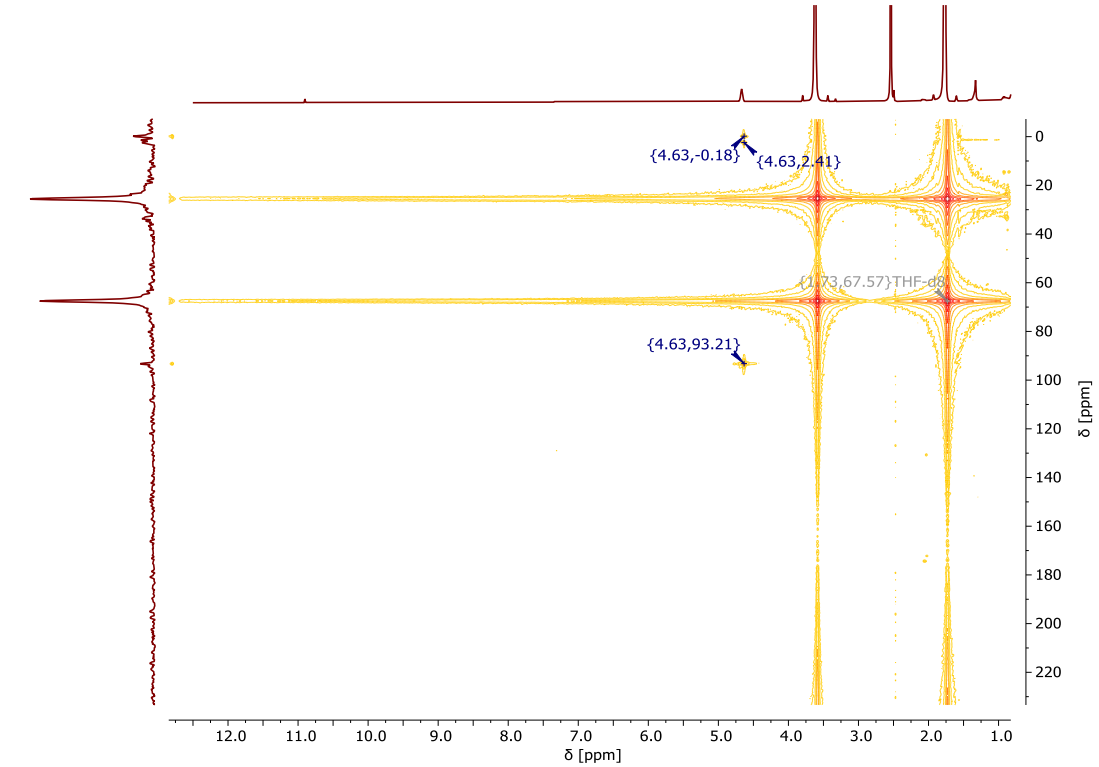


Figure S11. $^{1}H,^{13}C$ HMBC NMR spectrum.

1,2,3,4,5-penta(dimethylsilyl)cyclopentadienyl-1,2,3,4-tetra(dimethylsilyl)cyclopentadienyl-iron(II):

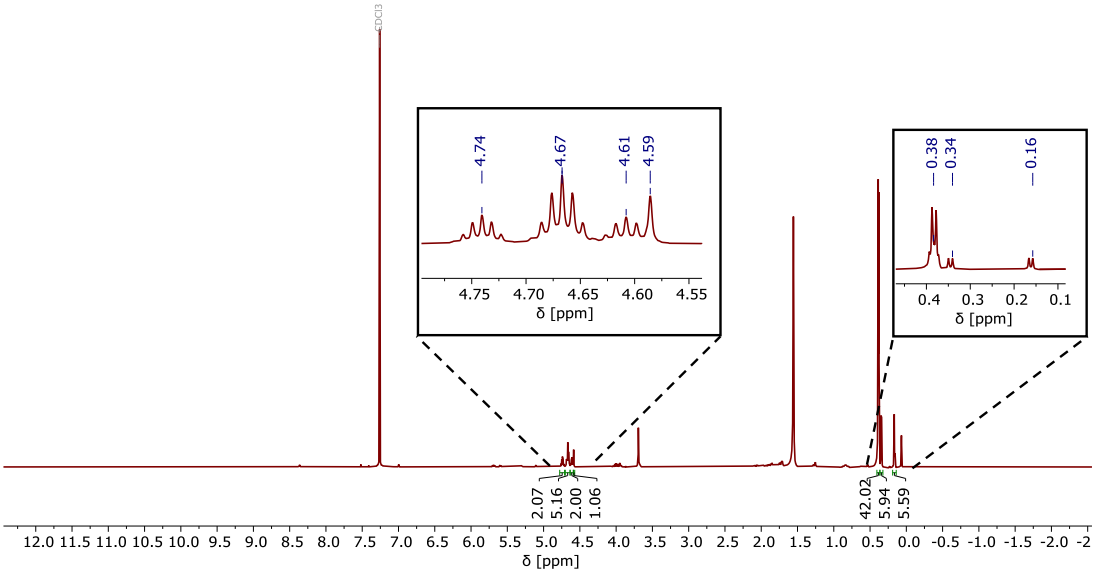


Figure S12. $^{1}H$ NMR spectrum (400 MHz, $CDCl_3$, RT).

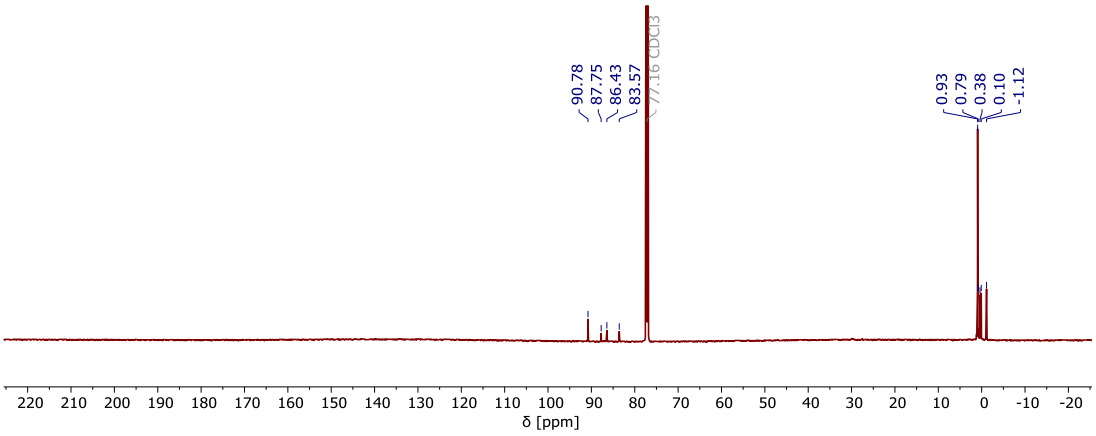


Figure 13. $^{13}C$ NMR spectrum (176 MHz, $CDCl_3$, RT).

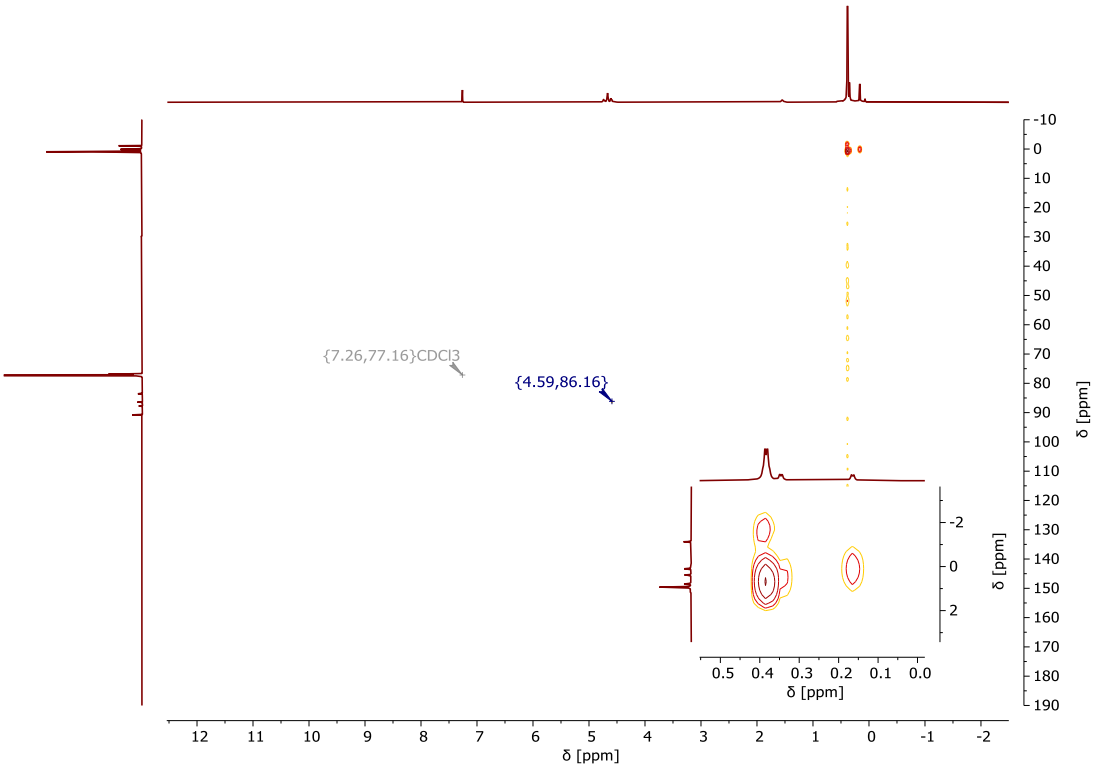


Figure 14. $^{1}H,^{13}C$ HMQC NMR spectrum.

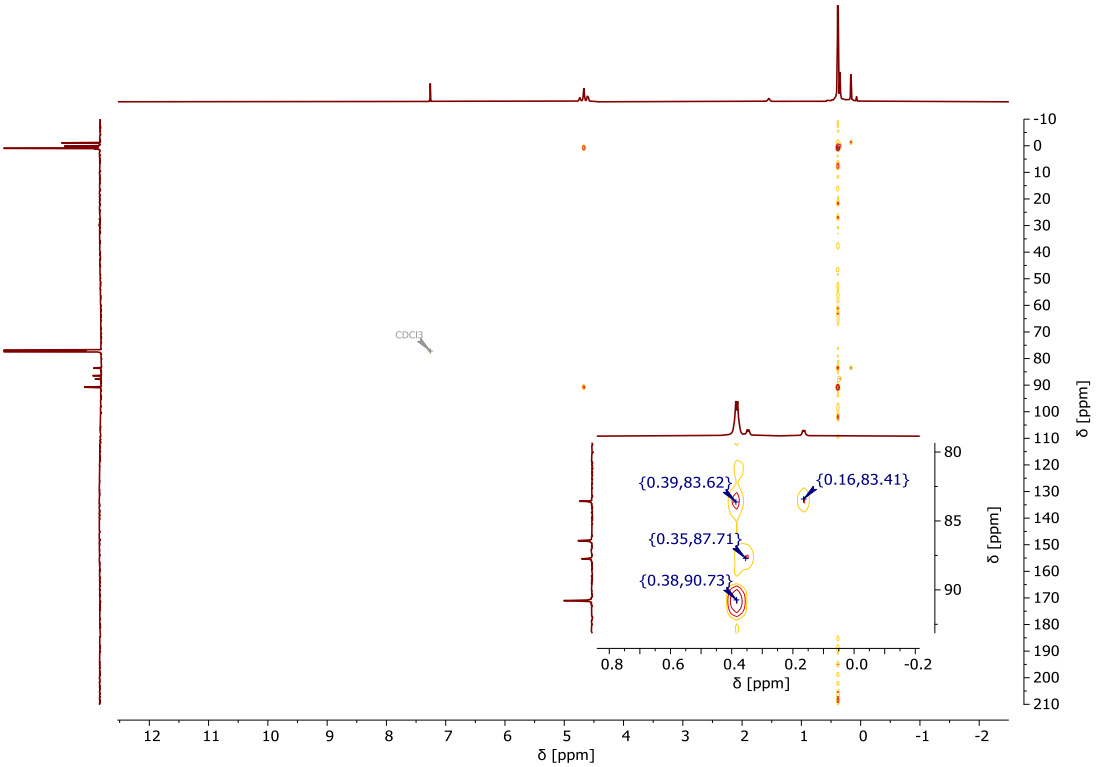


Figure 15. $^{1}H,^{13}C$ HMBC NMR spectrum.

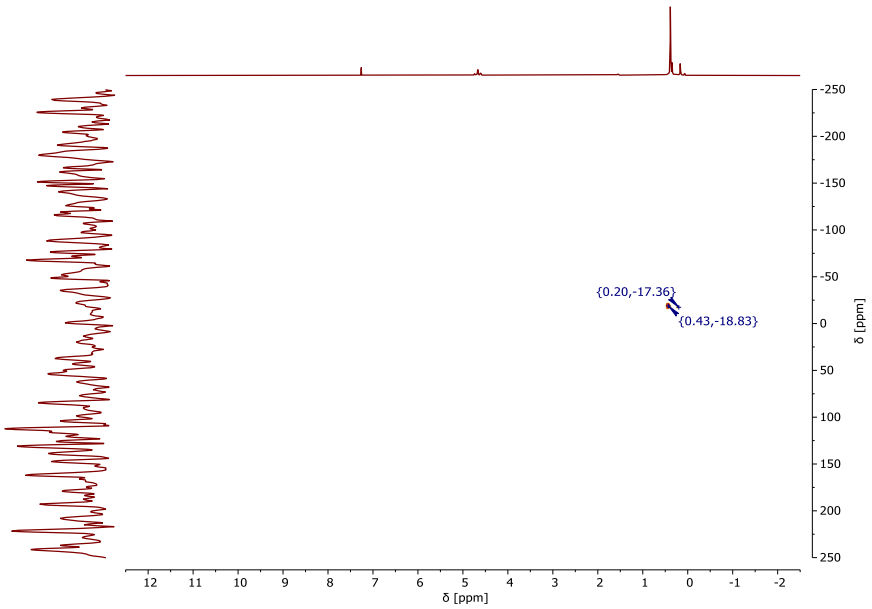


Figure 16. $^{1}H$, $^{29}Si$ HMBC NMR spectrum.

1,2,3,4,5-penta(dimethylsilyl)cyclopentadienyl-1,2,3-tri(dimethylsilyl)cyclopentadienyl-iron(II):

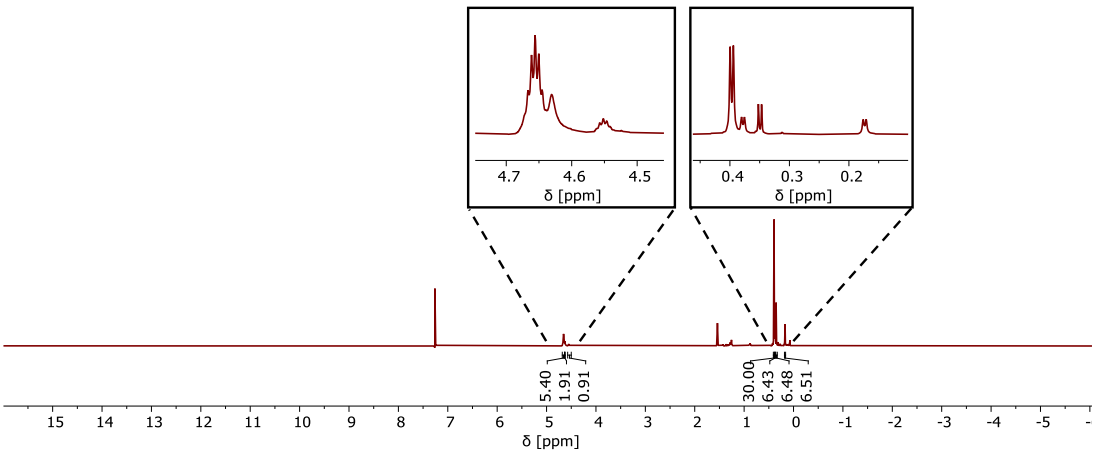


Figure S17. $^{1}H$ NMR spectrum (700 MHz, $CDCl_3$, RT).

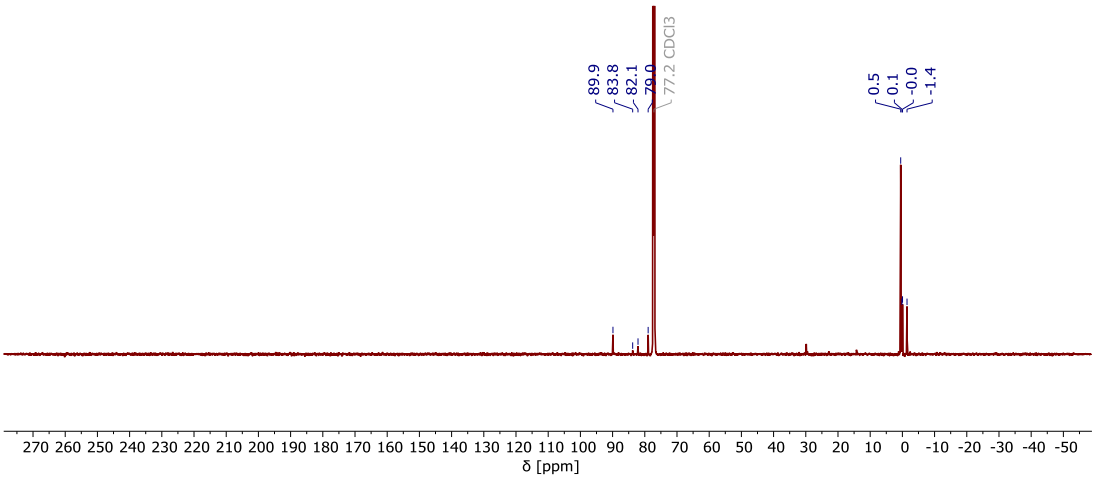


Figure S18. $^{13}C\{^{1}H\}$ NMR spectrum (176 MHz, $CDCl_3$, RT).

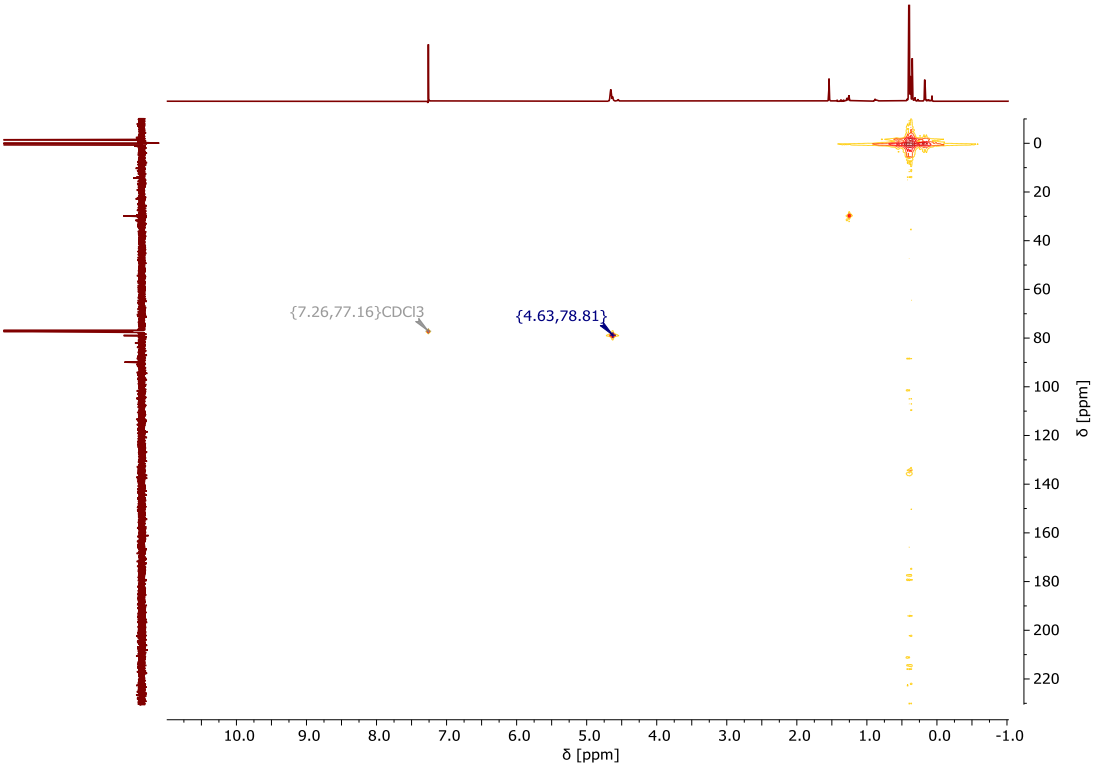


Figure S19. $^{1}H,^{13}C$ HMQC NMR spectrum.

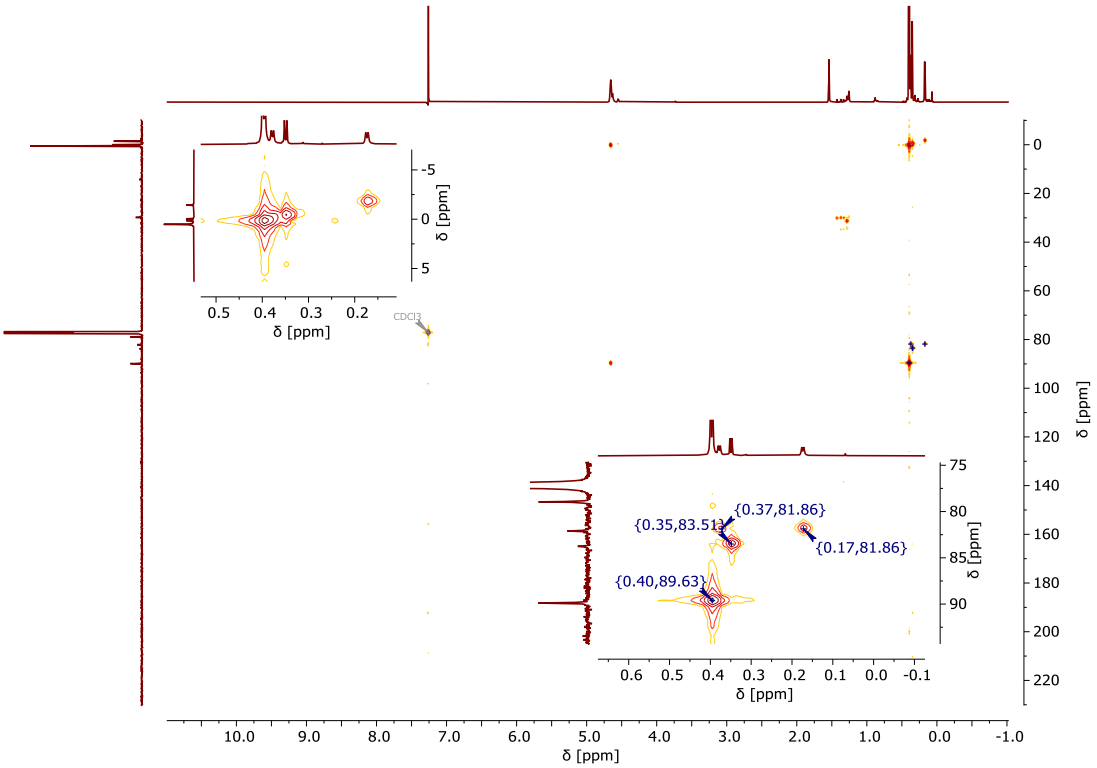


Figure S20. $^{1}H,^{13}C$ HMBC NMR spectrum.

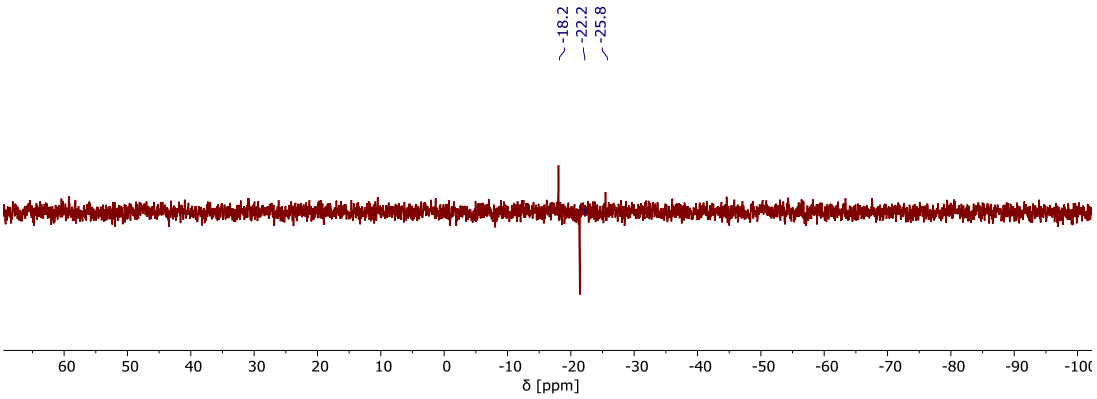


Figure S21. $^{29}Si$ DEPT spectrum ($CDCl_3$, RT, 80 MHz).

Bis(1,2,3,4-tetra(dimethylsilyl)cyclopentadienyl)iron(II):

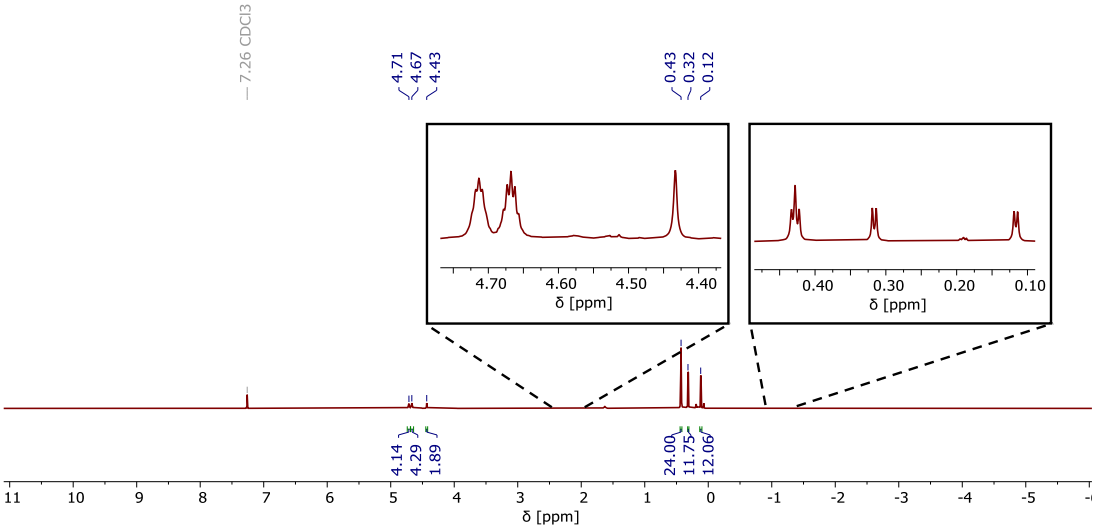


Figure S22. $^{1}H$ NMR spectrum (700 MHz, $CDCl_3$, RT).

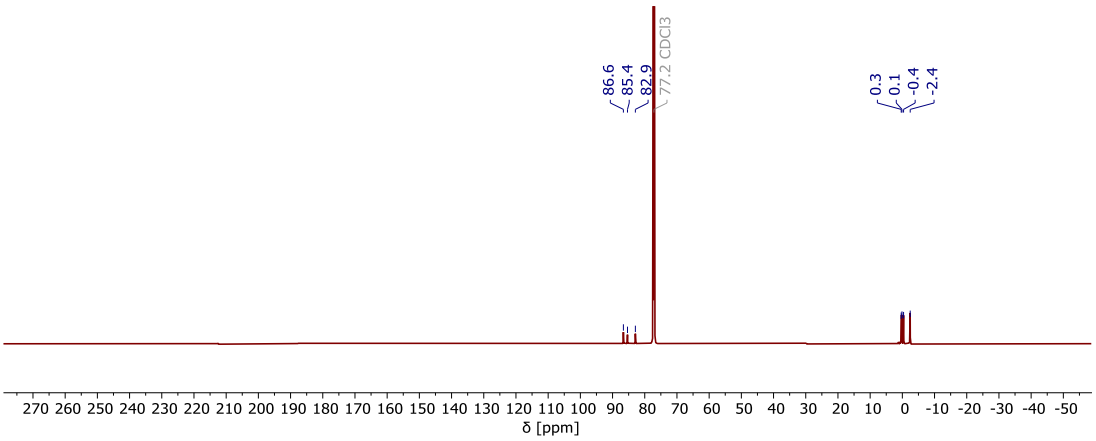


Figure S23. $^{13}C\{^{1}H\}$ NMR spectrum (176 MHz, $CDCl_3$, RT).

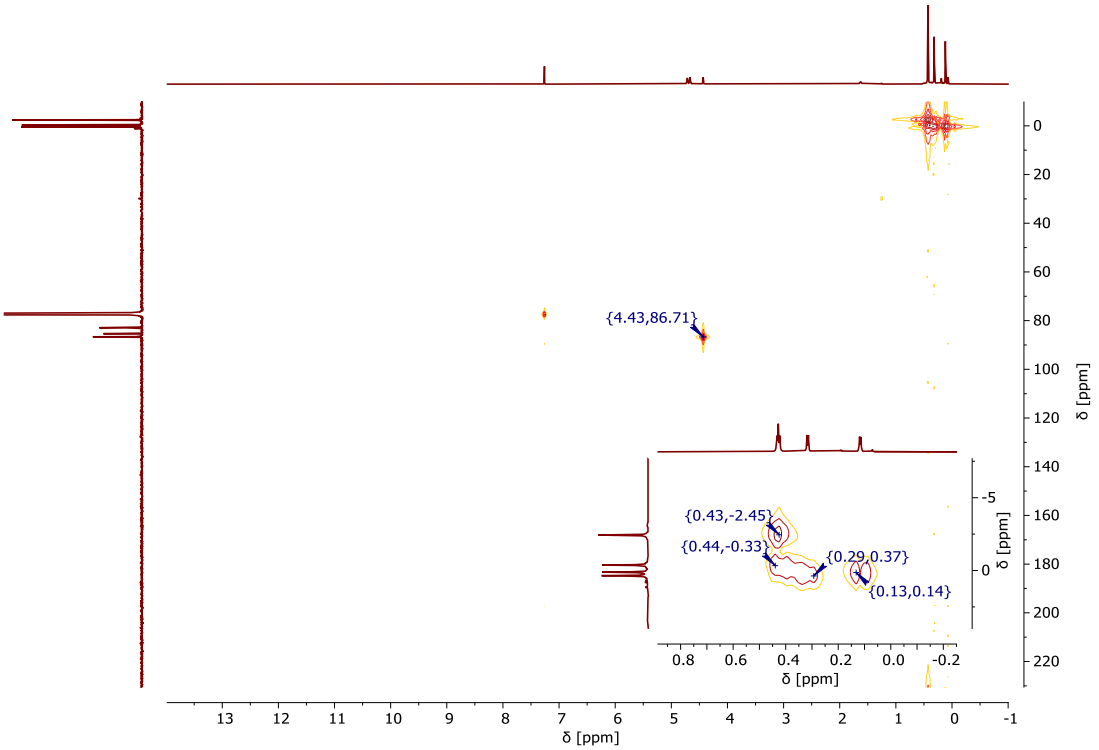


Figure S24. $^{1}H,^{13}C$ HMQC NMR spectrum.

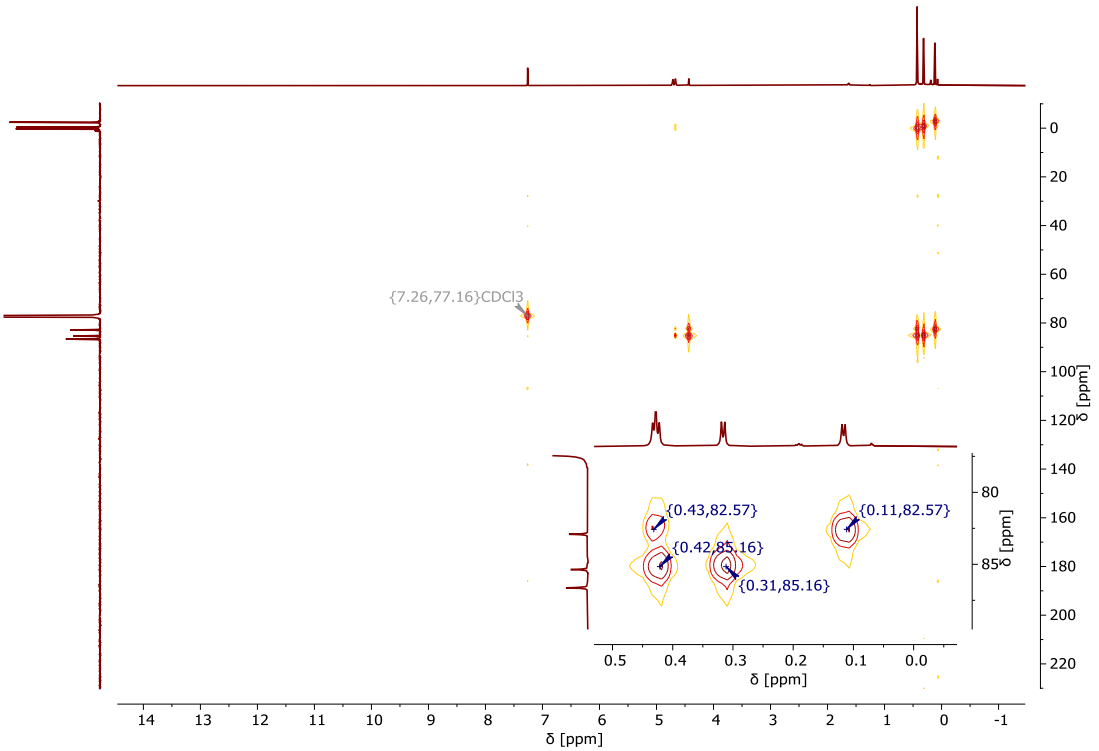


Figure S25. $^{1}H,^{13}C$ HMBC NMR spectrum.

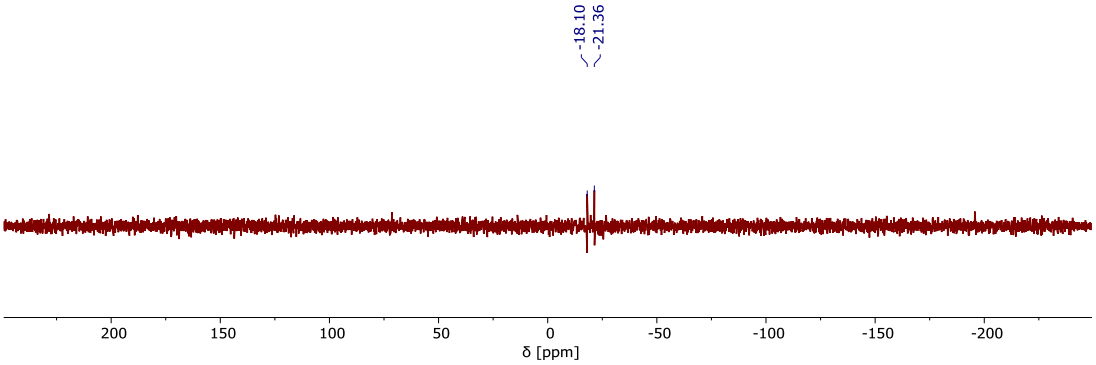


Figure S26. $^{29}$Si DEPT spectrum ($CDCl_3$, RT, 80 MHz).

1,2,3,4-tetra(dimethylsilyl)cyclopentadienyl-1,2,4-tri(dimethylsilyl)cyclopentadienyliron(II):

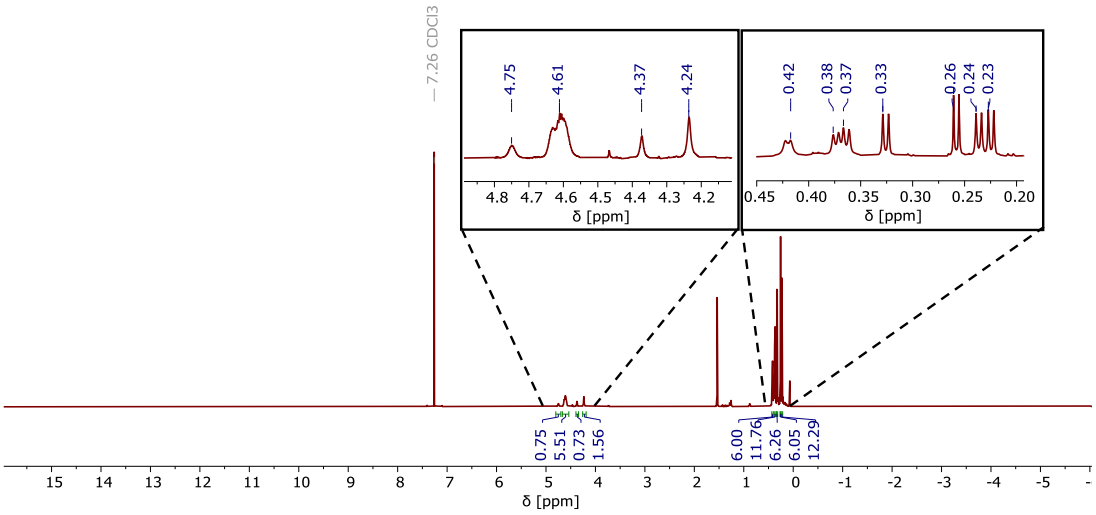


Figure S27. $^{1}$H NMR spectrum (700 MHz, $CDCl_3$, RT).

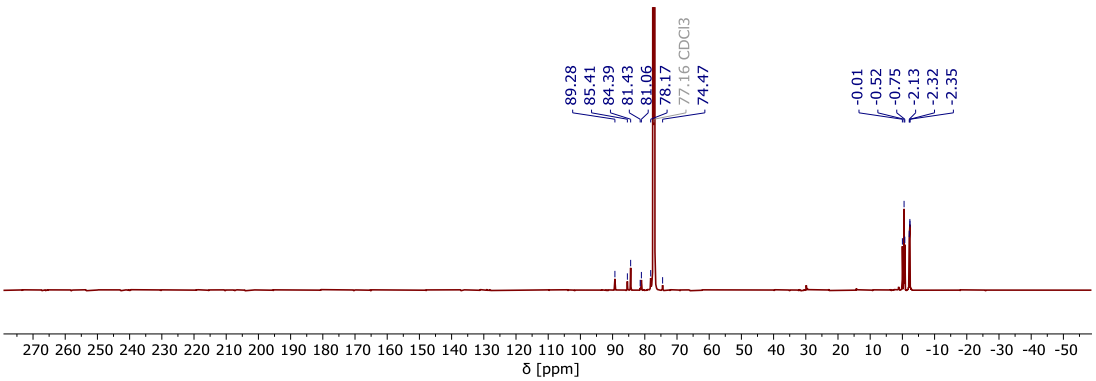


Figure S28. $^{13}$C{$^{1}$H} NMR spectrum (176 MHz, $CDCl_3$, RT).

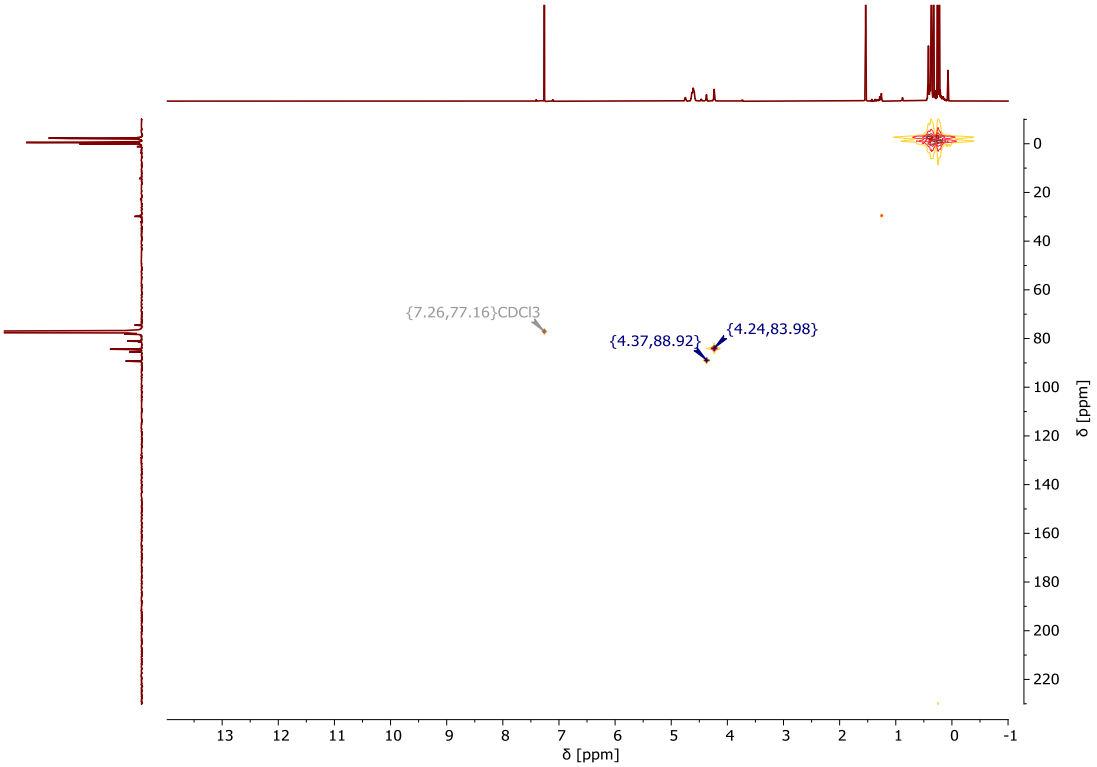


Figure S29. $^{1}H,^{13}C$ HMQC NMR spectrum.

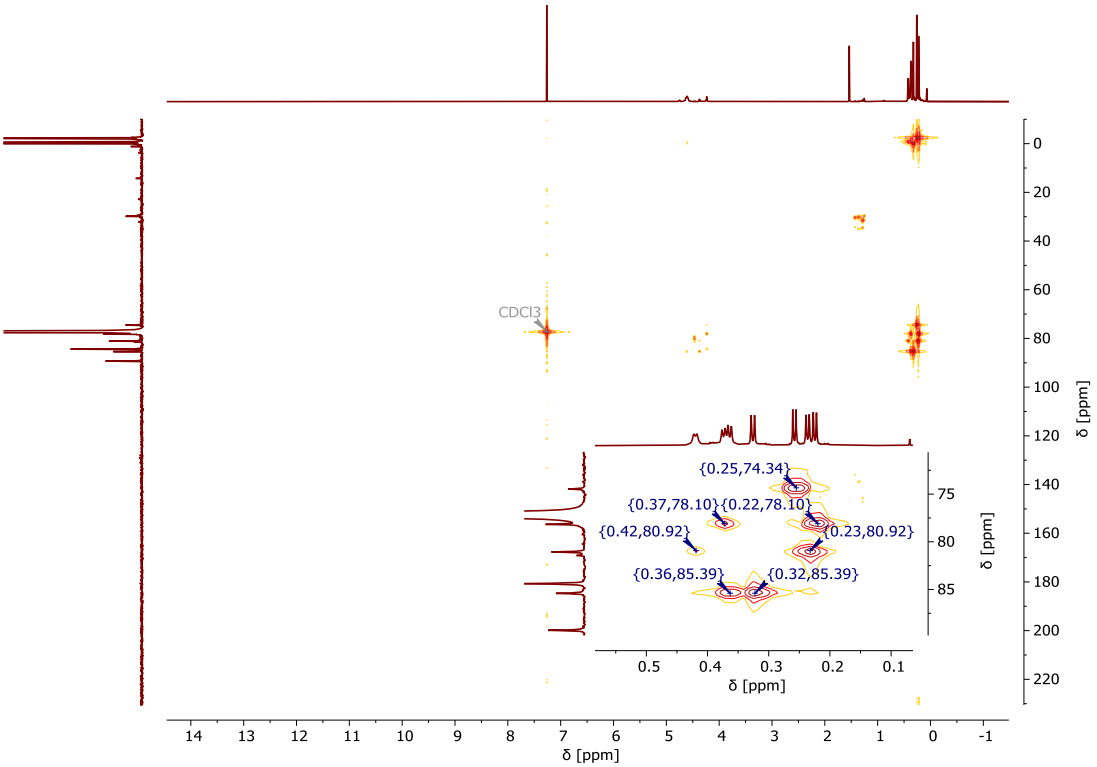


Figure S30. $^{1}H,^{13}C$ HMBC NMR spectrum.

1,2,3,4-tetra(dimethylsilyl)cyclopentadienyl-1,2,3-tri(dimethylsilyl)cyclopentadienyliron(II):

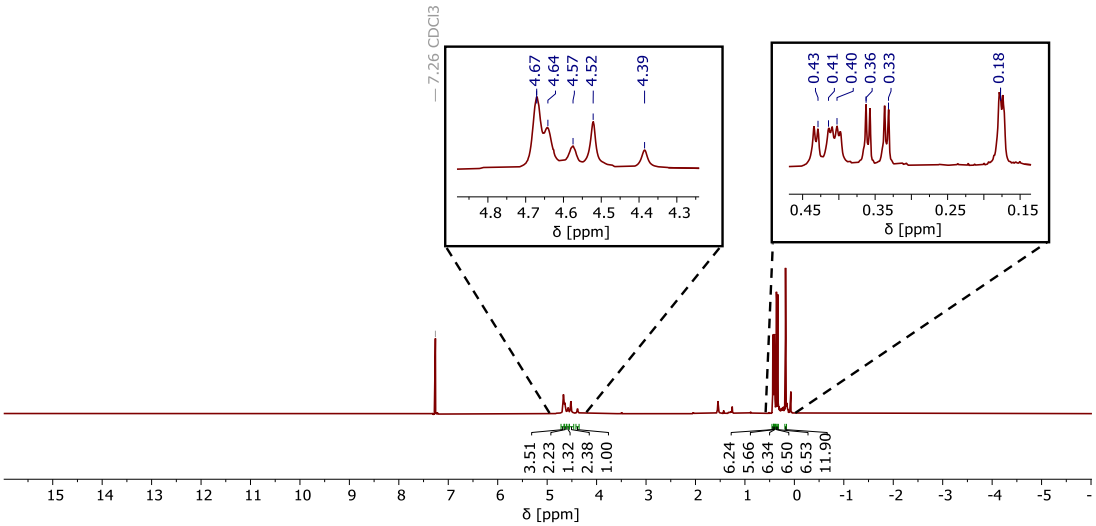


Figure S31. $^{1}H$ NMR spectrum (700 MHz, $CDCl_3$, RT).

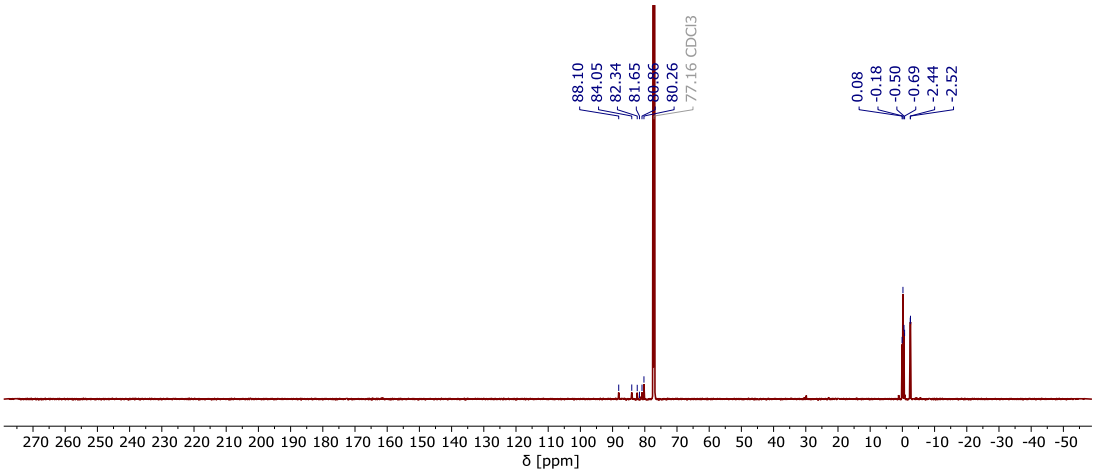


Figure S32. $^{13}C\{^{1}H\}$ NMR spectrum (700 MHz, $CDCl_3$, RT).

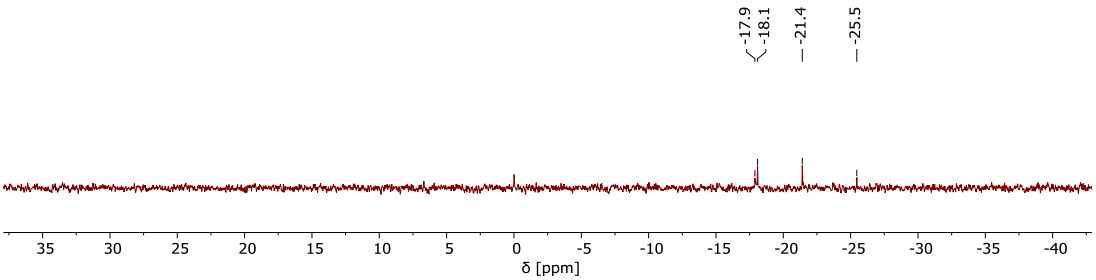


Figure S33. $^{29}Si\{^{1}H\}$ NMR spectrum (80 MHz, $CDCl_3$, RT).

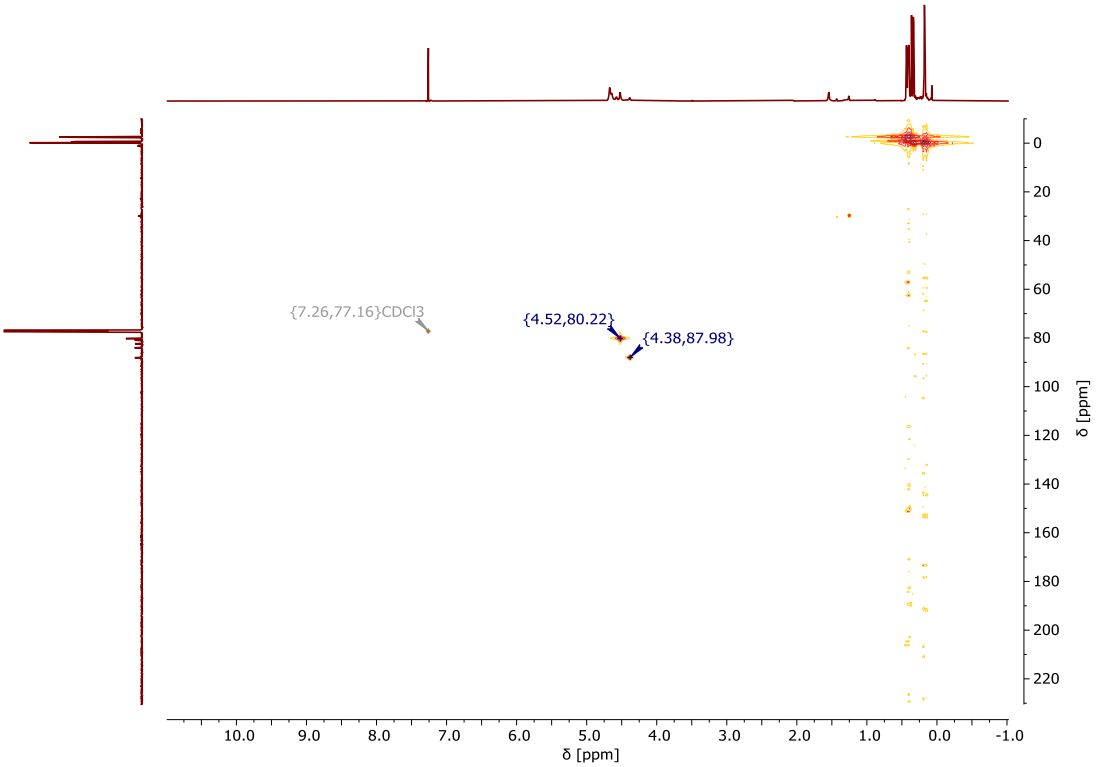


Figure S34. $^{13}C,^{1}H$ HMQC spectrum.

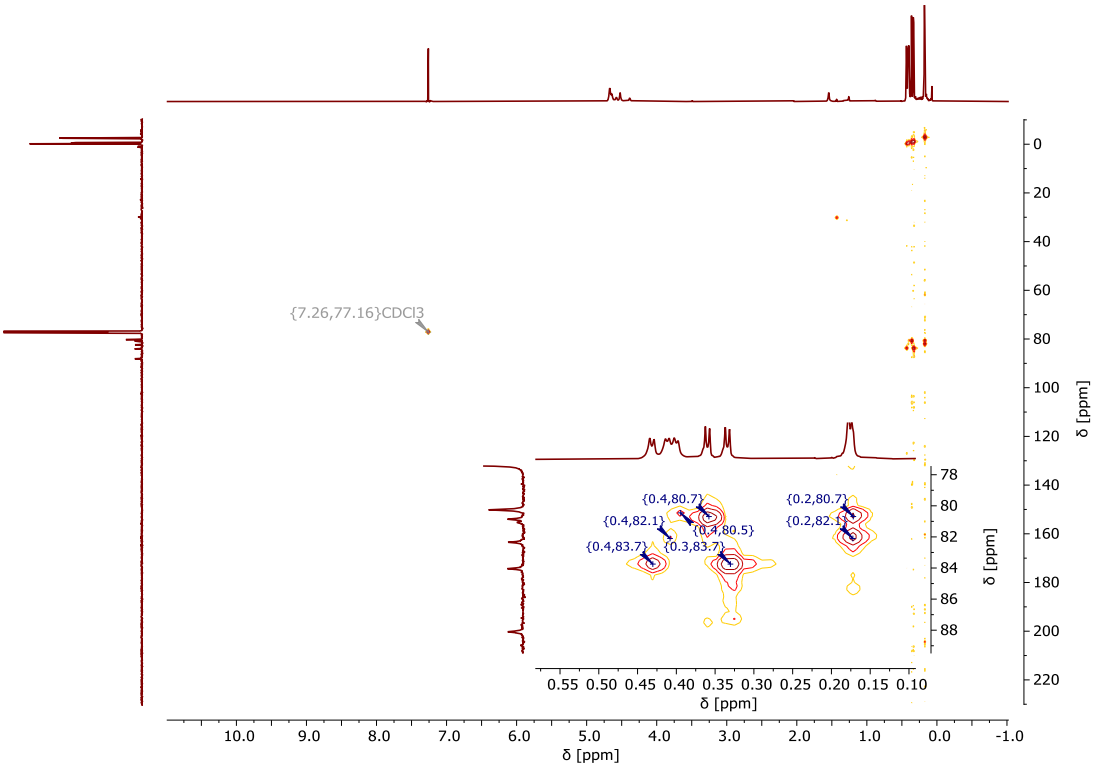


Figure S35. $^{13}C,^{1}H$ HMBC spectrum.

Bis(1-methyl-2,3,4,5-tetra-bromo-cyclopentadienyl)iron(II):

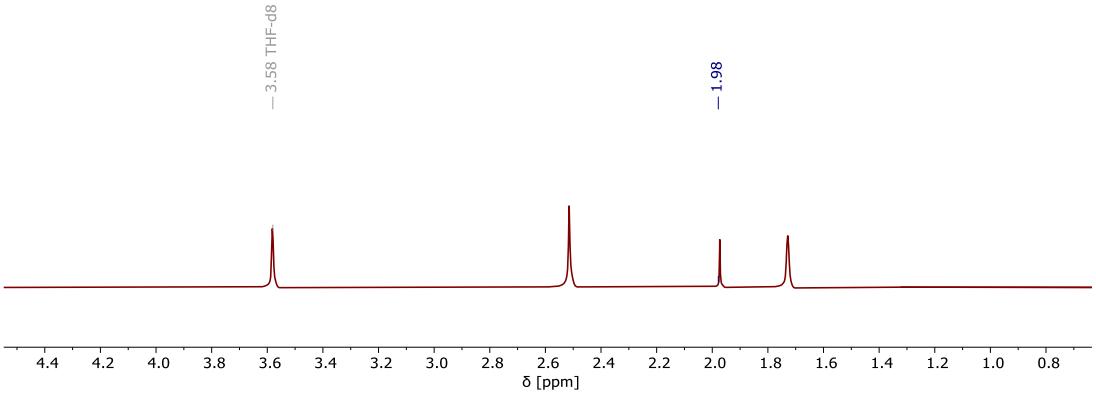


Figure S36. $^{1}H$ NMR spectrum (700 MHz, $CDCl_3$, RT).

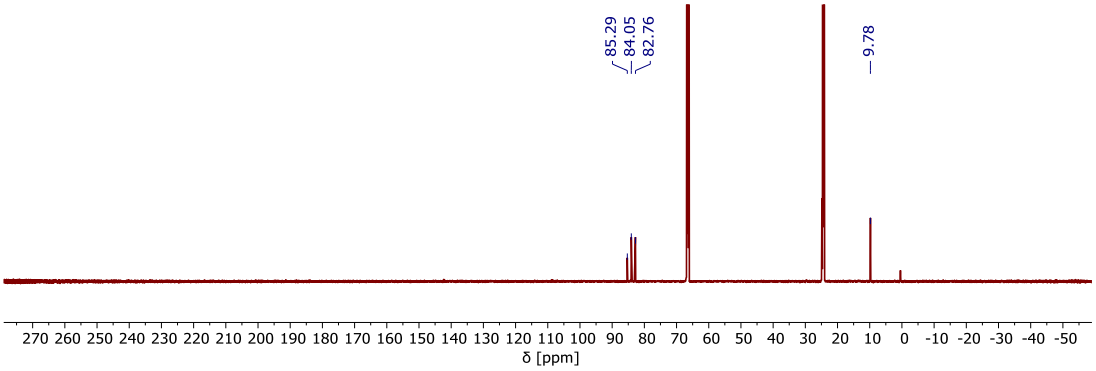


Figure S37. $^{13}C\{^{1}H\}$ NMR spectrum (700 MHz, $CDCl_3$, RT).

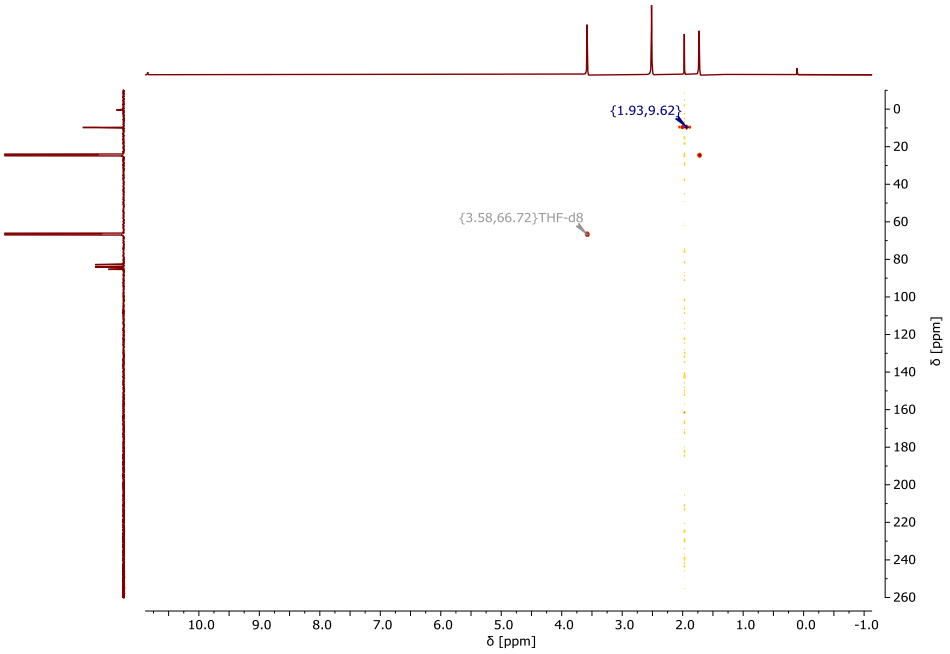


Figure S38. $^{13}C,^{1}H$ HMQC spectrum.

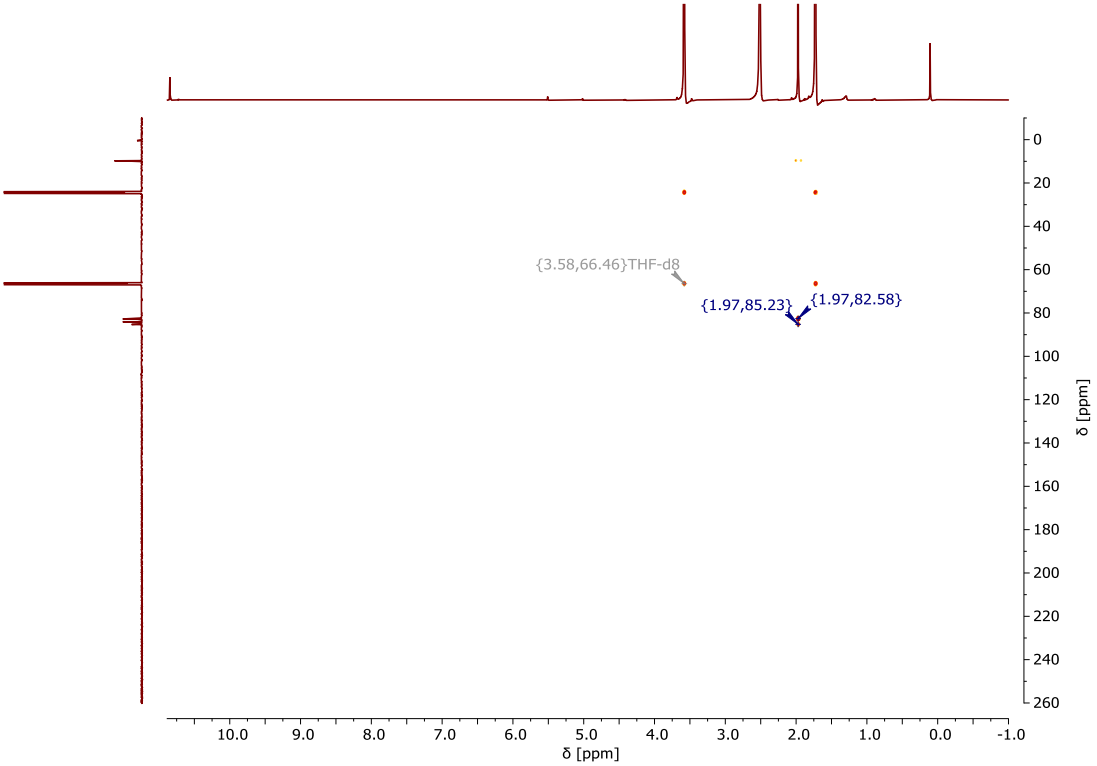


Figure S39. $^{13}C,^{1}H$ HMBC spectrum.

Bis(1-methyl-2,3,4,5-tetra-dimethylsilyl-cyclopentadienyl)iron(II):

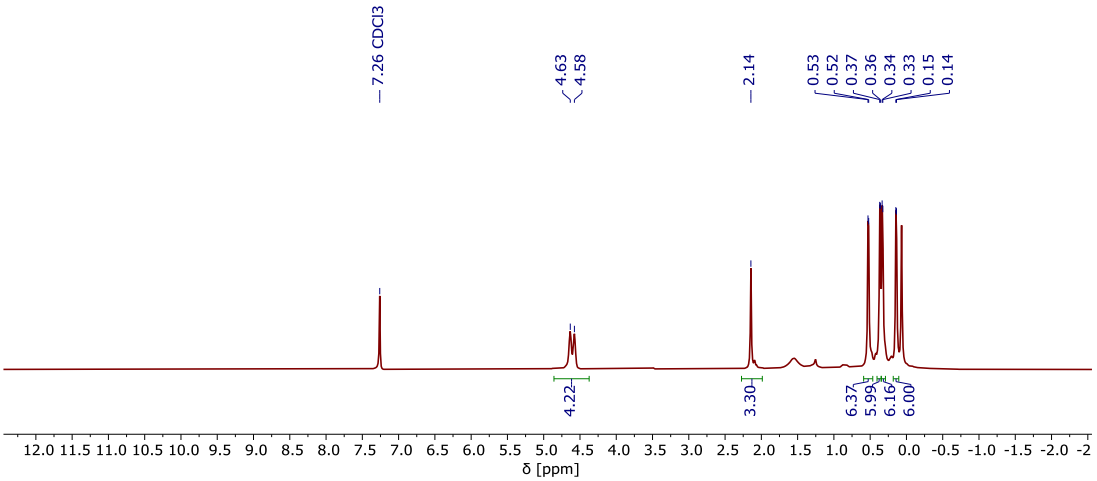


Figure S40. $^{1}H$ NMR spectrum (400 MHz, $CDCl_3$, RT).

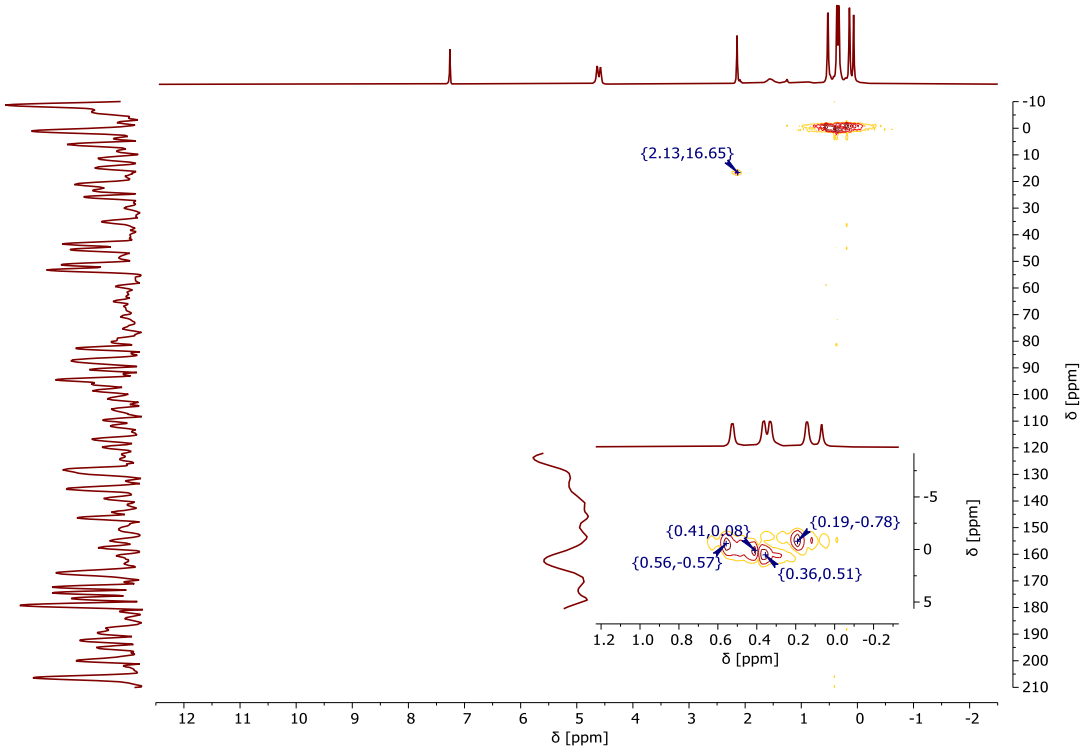


Figure S41. $^{13}C,^{1}H$ HMQC spectrum.

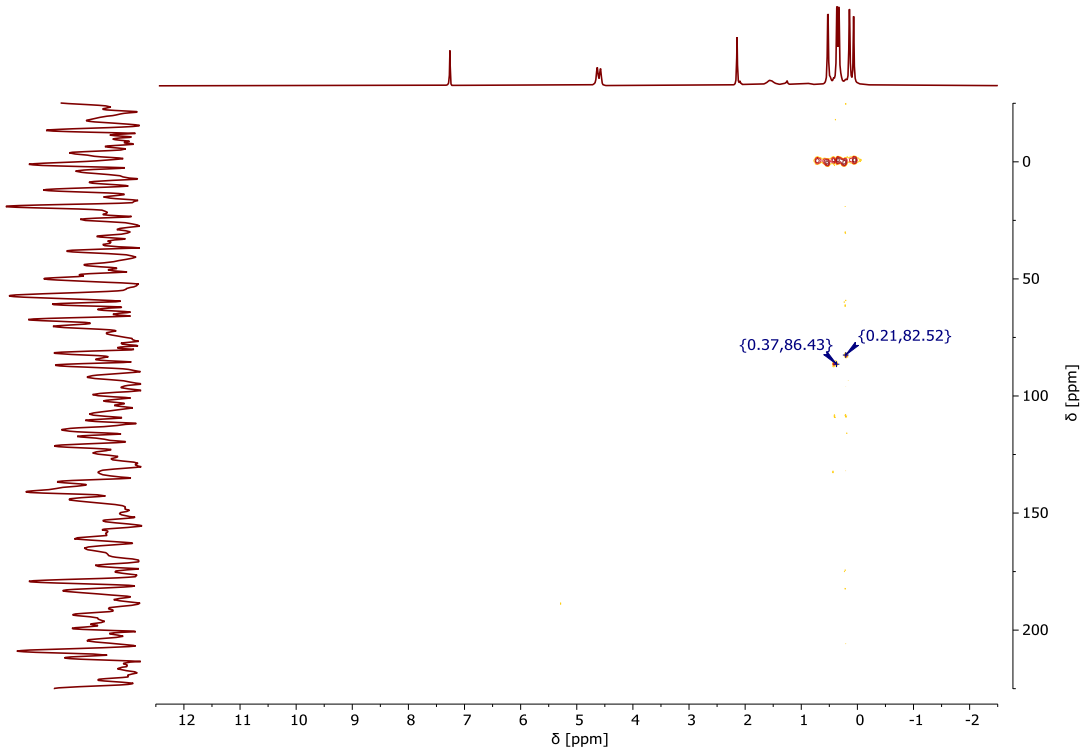


Figure S42. $^{13}C,^{1}H$ HMBC spectrum.

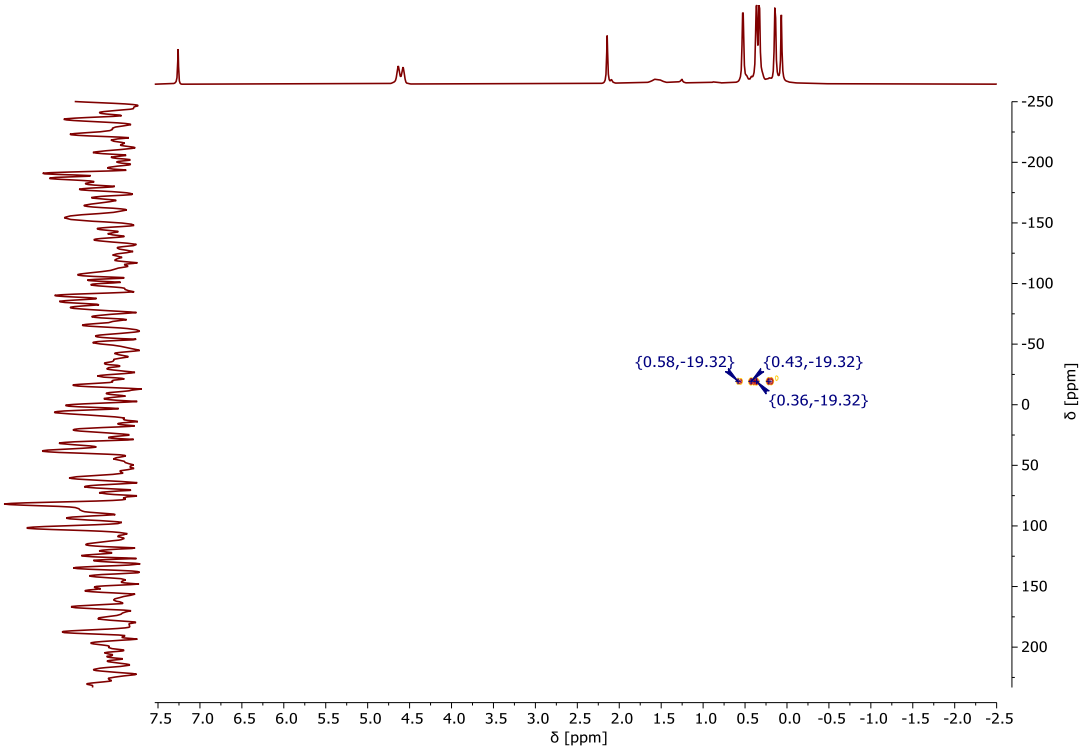


Figure S43. $^{1}H$, $^{29}Si$ HMBC NMR spectrum.

## 5.2 Infrared

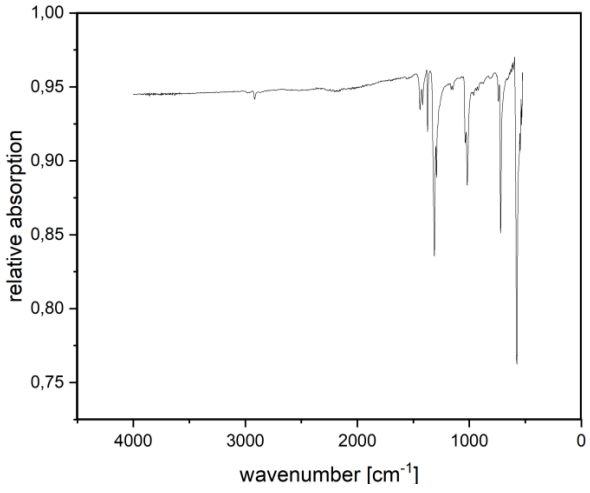


**Figure S44.** Infrared spectrum (ATR) of compound $[FeC_{10}Me_2Br_8]$ (**7**).

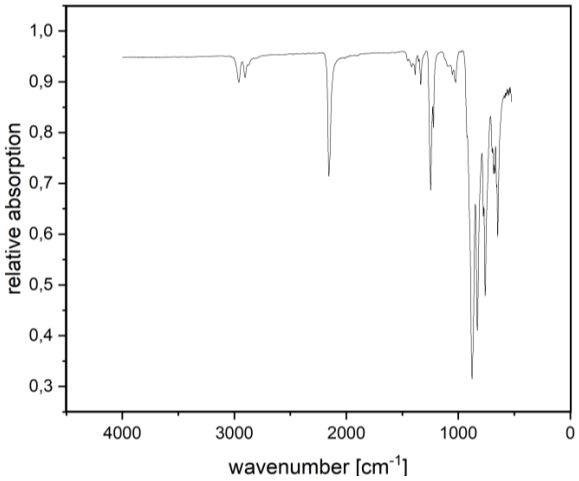


Figure S45. Infrared spectrum (ATR) of compound [$FeC_{10}Me_2DMS_8$] (**8**).

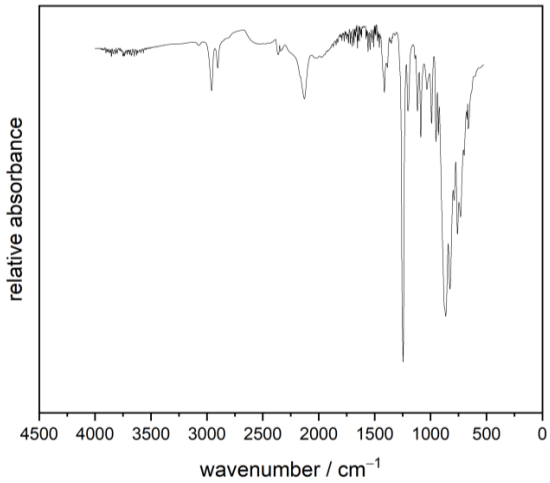


Figure S46. Infrared spectrum (ATR) of compound [$FeC_{10}DMS_7H_3$] (**3a**).

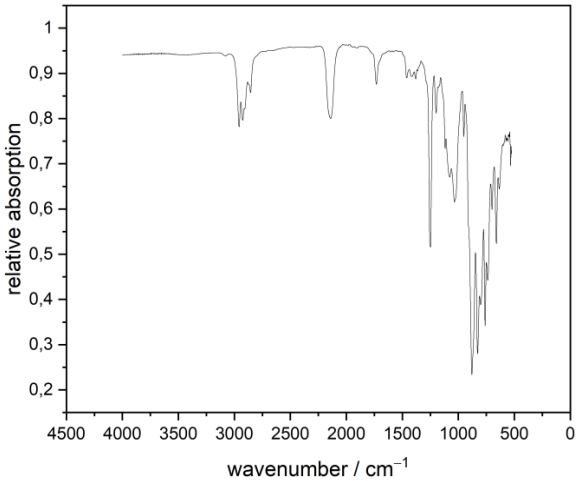


Figure S47. Infrared spectrum (ATR) of compound [$FeC_{10}DMS_7H_3$] (**3b**).

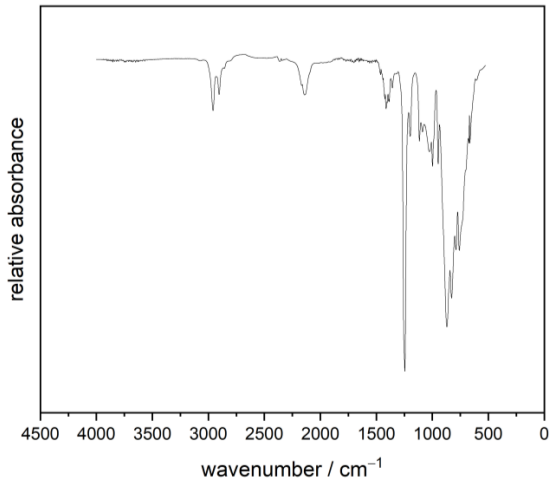


Figure S48. Infrared spectrum (ATR) of compound [$FeC_{10}DMS_8H_2$] (**4a**).

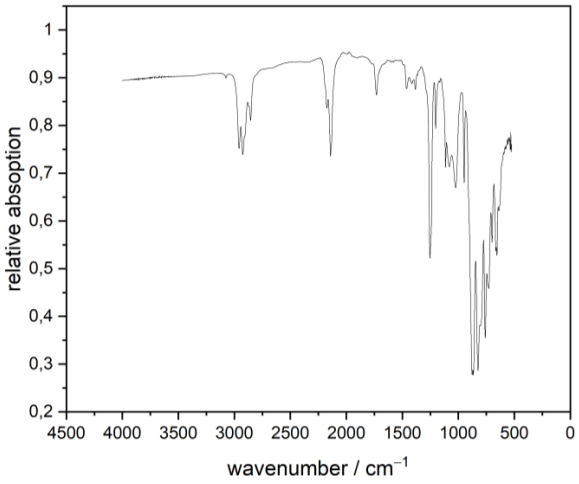


Figure S49. Infrared spectrum (ATR) of compound [$FeC_{10}DMS_8H_2$] (**4b**).

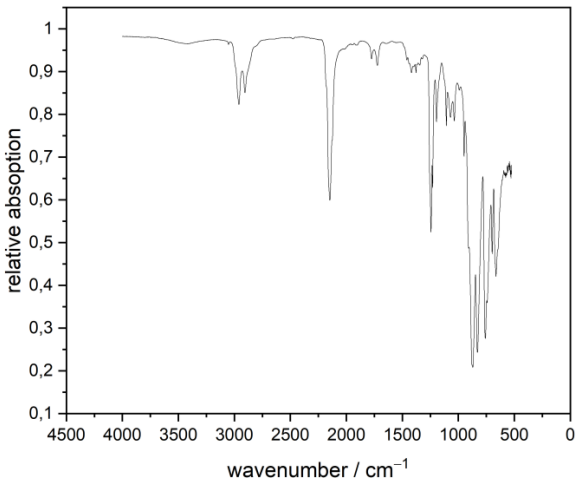


Figure S50. Infrared spectrum (ATR) of compound [$FeC_{10}DMS_9H$] (**5**).

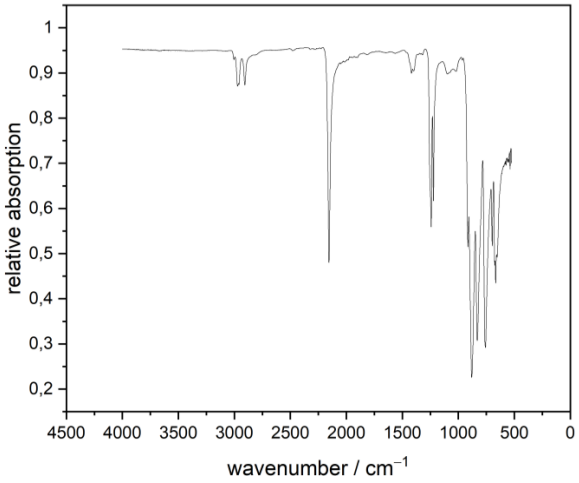


Figure S51. Infrared spectrum (ATR) of compound [$FeC_{10}DMS_{10}$] (**6**).

## 5.3 Cyclic voltammetry

Cyclic voltammetry was performed on a Interface 1010 B Potentiostat/Galvanostat/ZRA from Gamry Instruments. The investigations were carried out starting from 0 V going to the oxidation first and then to the reduction. The measurements were performed in anhydrous and oxygen free solvents under argon atmosphere using tetrabutylammonium hexafluorophosphate as the supporting electrolyte and platinum wires as working-, counter-, and quasi-reference electrodes. The voltammograms were internally referenced against $FeCp_2^{0/+}$. The software OriginPro 2017G was used to plot the data.[8] THF was distilled over Na and stored in Young flasks under argon atmosphere over molar sieve (3 Å) which was dried beforehand at 250 °C under high vacuum. The conducting salt was dried at 250 °C under high vacuum. The solvents were condensed on the conducting salt in the cyclic voltammetry cells via a vacuum line.

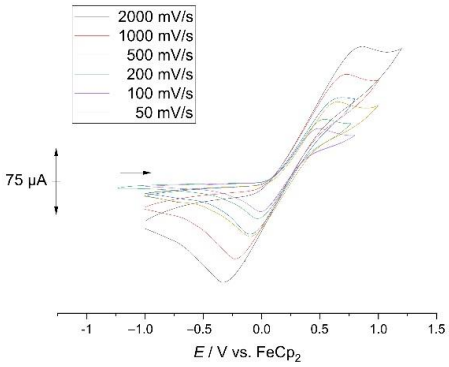


Figure S52. Cyclic voltammogram of compound [$FeC_{10}DMS_7H_3$] (**3b**) measured in tetrahydrofuran at 100 mV/s scan rate and [TBA][$PF_6$] as supporting electrolyte.

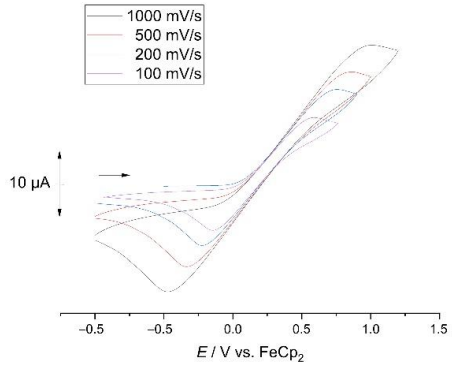


Figure S53. Cyclic voltammogram of compound [$FeC_{10}DMS_8H_2$] (**4b**) measured in tetrahydrofuran at 100 mV/s scan rate and [TBA][$PF_6$] as supporting electrolyte.

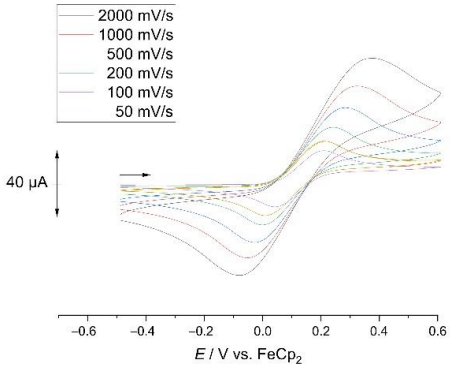


Figure S54. Cyclic voltammogram of compound [$FeC_{10}DMS_9H$] (**5**) measured in tetrahydrofuran at 100 mV/s scan rate and [TBA][$PF_6$] as supporting electrolyte.

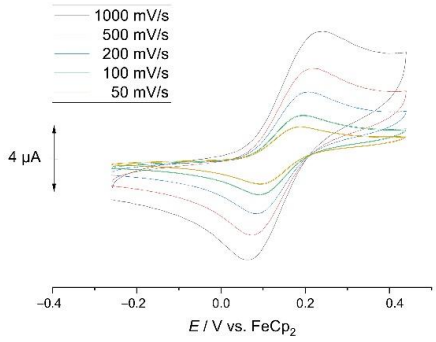


Figure S55. Cyclic voltammogram of compound [$FeC_{10}DMS_{10}$] (**6**) measured in tetrahydrofuran at 100 mV/s scan rate and [TBA][$PF_6$] as supporting electrolyte.

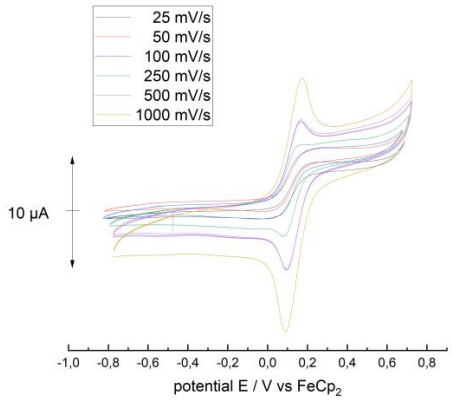


Figure S56. Cyclic voltammogram of compound [$FeC_{10}DMS_8Me_2$] (**8**) measured in tetrahydrofuran at 100 mV/s scan rate and [TBA][$PF_6$] as supporting electrolyte.

Table S4. Electrochemical data.

| **Compound** | $E_{pa}$ / **V** | $E_{pc}$ / **V** | $E_{1/2}$ / **V** | $\Delta E$ / **mV** |
|---|---|---|---|---|
| 6 (10x DMS) | 0.216 | 0.128 | 0.172 | 88 |
| 5 (9 x DMS) | 0.272 | 0.064 | 0.168 | 208 |
| 4b (8x DMS) | 0.407 | −0.067 | 0.170 | 474 |
| 3b (7x DMS) | 0.448 | −0.126 | 0.161 | 574 |
| 8 [$FeC_{10}DMS_8Me_2$] | 0.308 | −0.023 | 0.131 | 331 |

## 5.4 Mass Spectra

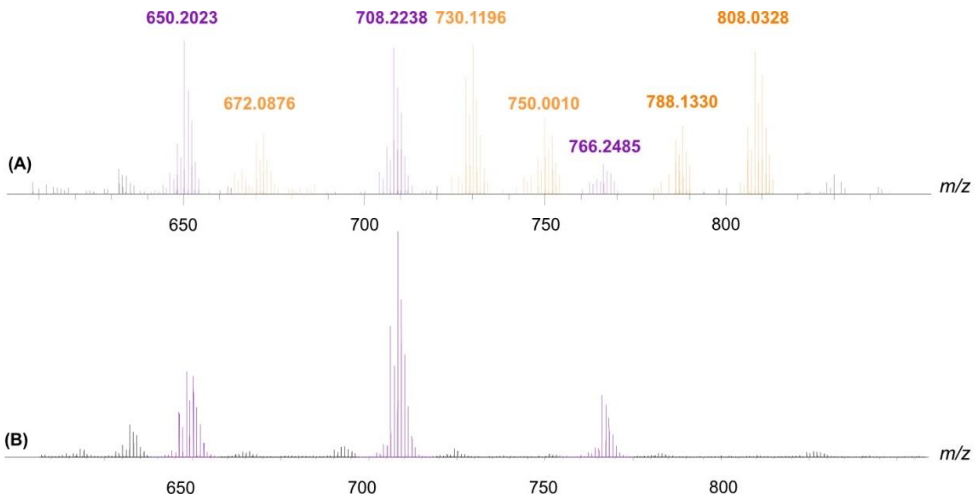


Figure S57. EI MS (+) after reaction of decabromoferrocene with $^t$BuLi and DMSCl in *n*-pentane (A) followed by reaction with $^t$BuLi and DMSCl in THF (B). Highlighted signals were assigned to purely silylated metallocenes (purple) or to partially brominated species (orange).

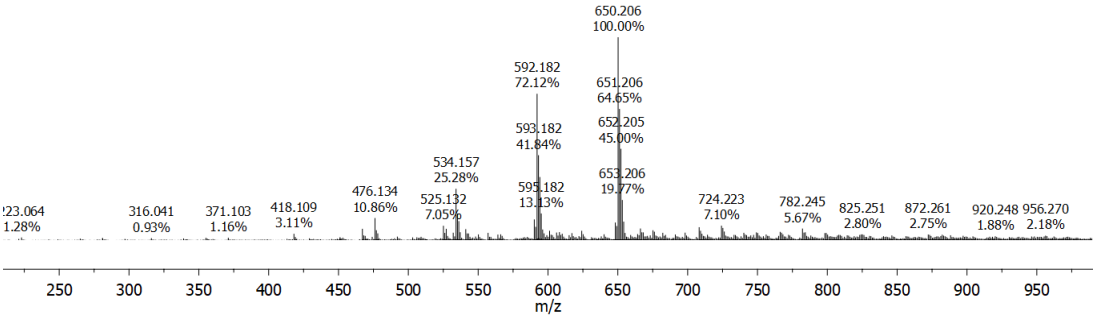


Figure S58. ESI MS (+) of entry 1 (Grignard).

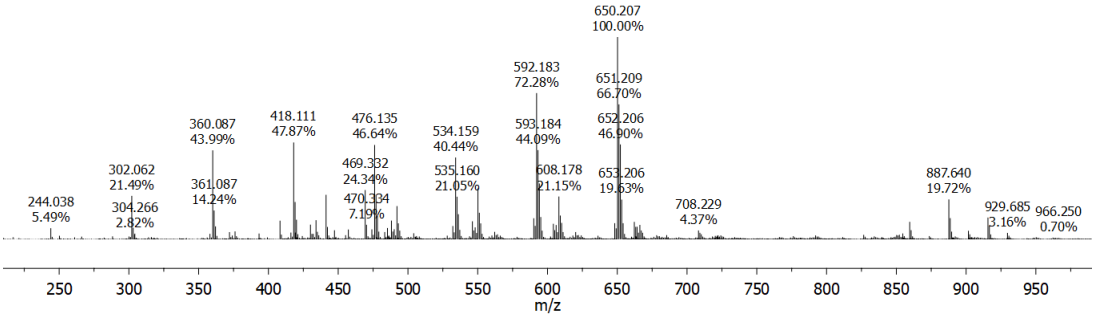


Figure S59. ESI MS (+) of entry 2 (Grignard).

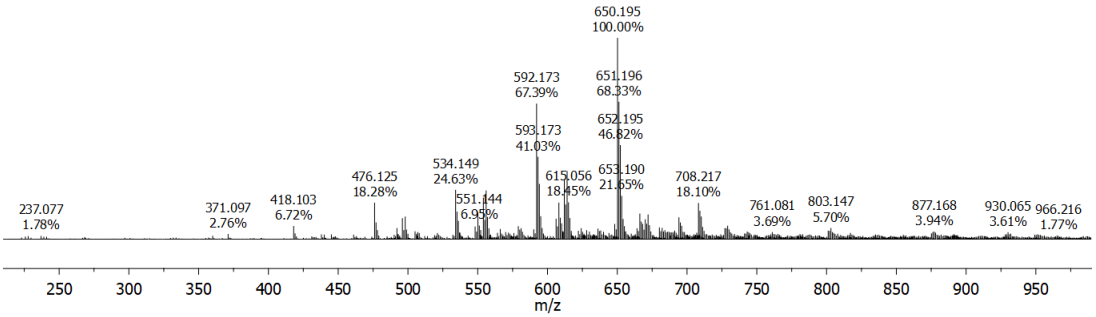


Figure S60. ESI MS (+) of entry 3 (Grignard).

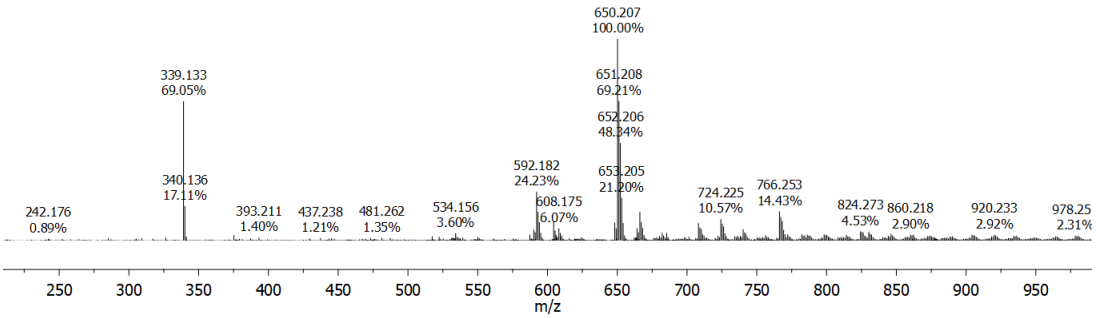


Figure S61. ESI MS (+) of entry 3 (Grignard).

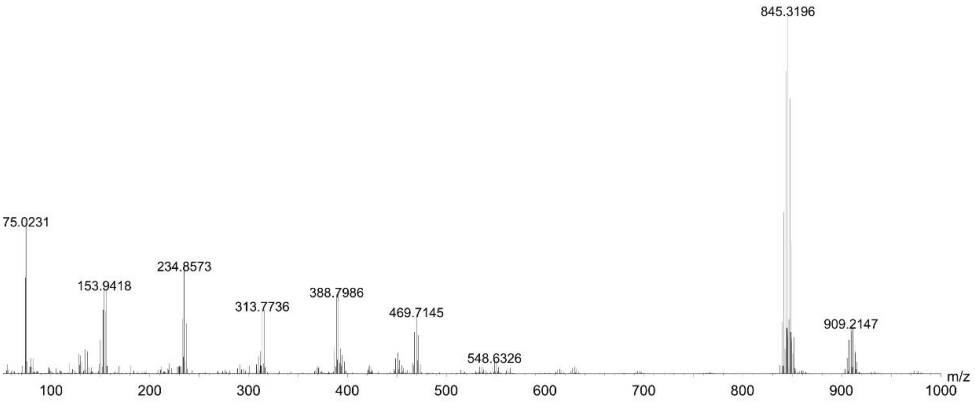


Figure S62. EI MS (+) spectrum of [$FeC_{10}Me_2Br_8$] (**7**).

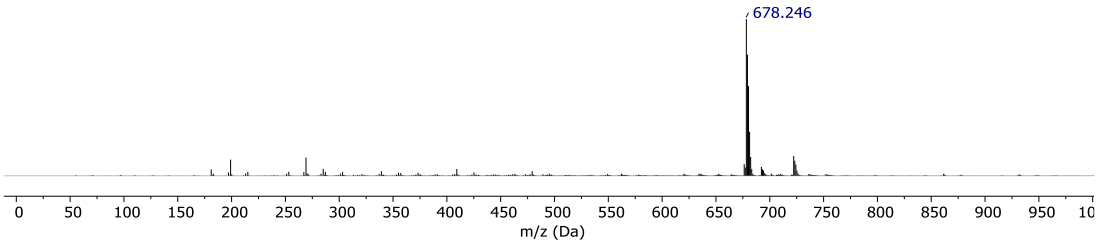


Figure S63. ESI MS (+) spectrum of [$FeC_{10}Me_2DMS_8$] (**8**).

## 5.5 UV/VIS

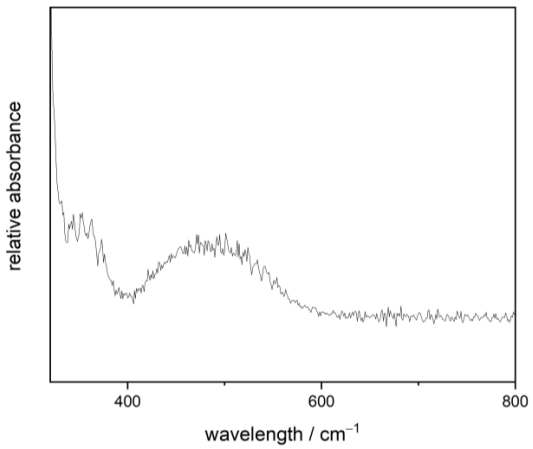


Figure S64. UV/VIS spectrum of [$FeC_{10}DMS_7H_3$] (**3a**) in *n*-pentane. $\lambda_{max}$ = 501 nm.

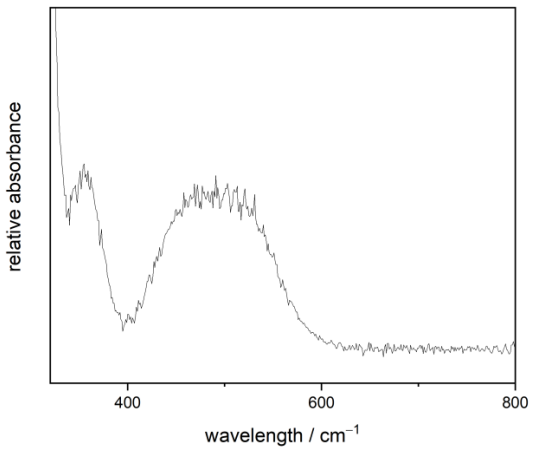


Figure S65. UV/VIS spectrum of [$FeC_{10}DMS_7H_3$] (**3b**) in *n*-pentane. $\lambda_{max}$ = 491 nm.

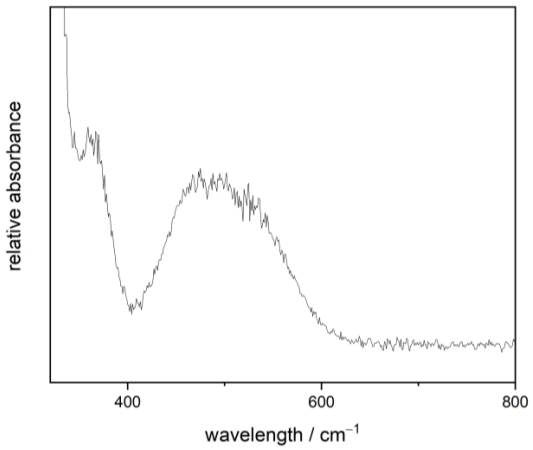


Figure S66. UV/VIS spectrum of [$FeC_{10}DMS_8H_2$] (**4a**) in *n*-pentane. $\lambda_{max}$ = 495 nm.

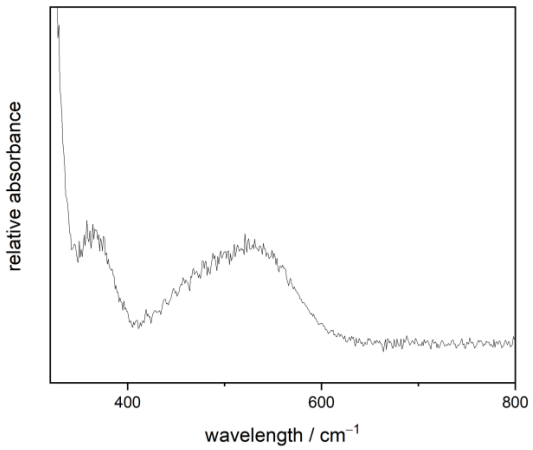


Figure S67. UV/VIS spectrum of [$FeC_{10}DMS_8H_2$] (**4b**) in *n*-pentane. $\lambda_{max}$ = 521 nm.

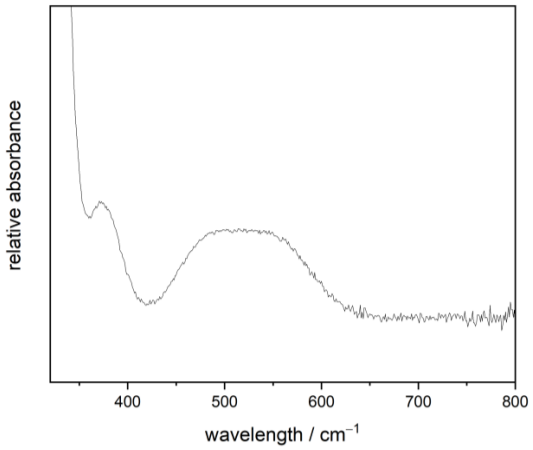


Figure S68. UV/VIS spectrum of [$FeC_{10}DMS_9H$] (**5**) in *n*-pentane. $\lambda_{max}$ = 524 nm.

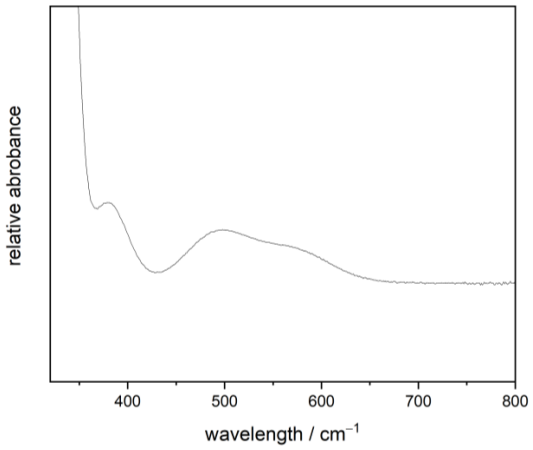


Figure S69. UV/VIS spectrum of [$FeC_{10}DMS_{10}$] (**6**) in *n*-pentane. $\lambda_{max}$ = 500 nm.

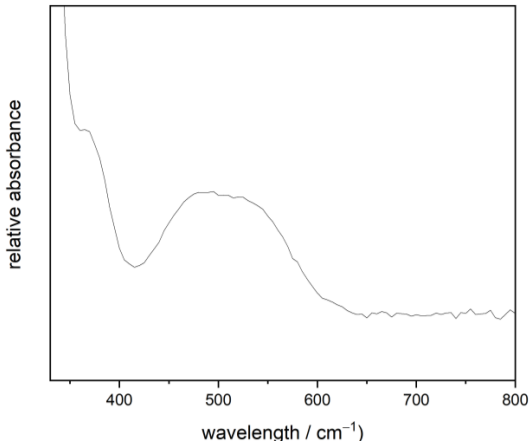


Figure S70. UV/VIS spectrum of [$FeC_{10}DMS_8Me_2$] (**8**) in *n*-pentane. $\lambda_{max}$ = 490 nm.

## 5.5 High Performance Chromatograms

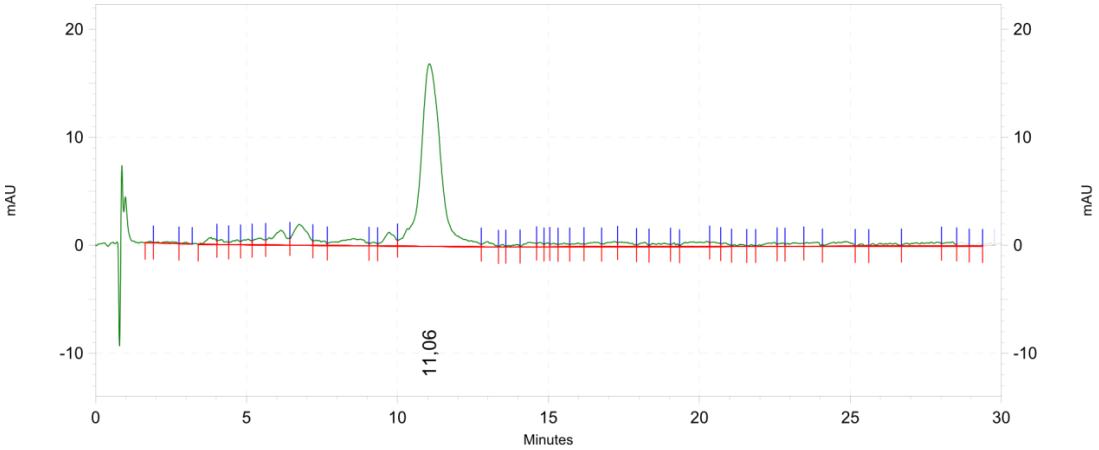


Figure S71. Chromatogram of [$FeC_{10}DMS_9Br$] (**2**). RP-18, MeOH(98%), room temperature.

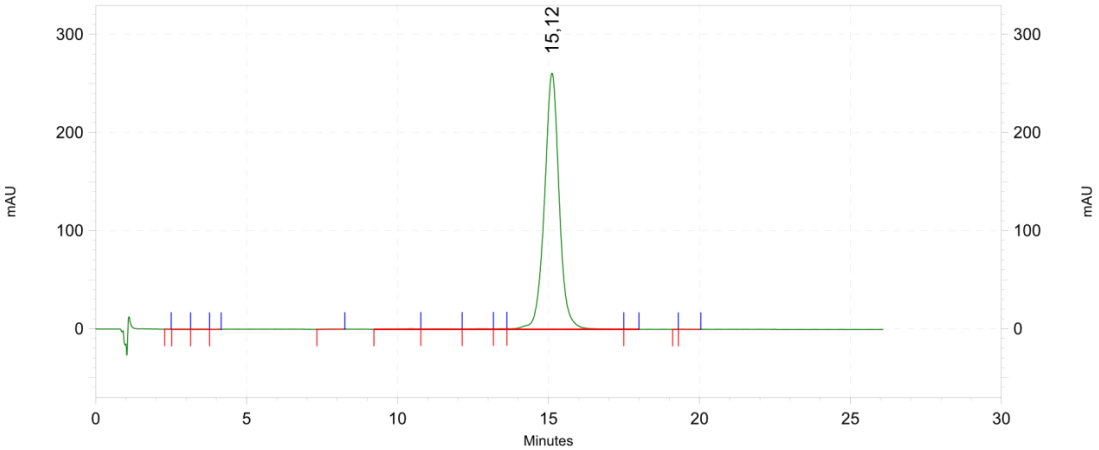


Figure S72. Chromatogram of [$FeC_{10}DMS_8Br_2$] (**1**). RP-18, MeOH(98%), room temperature.

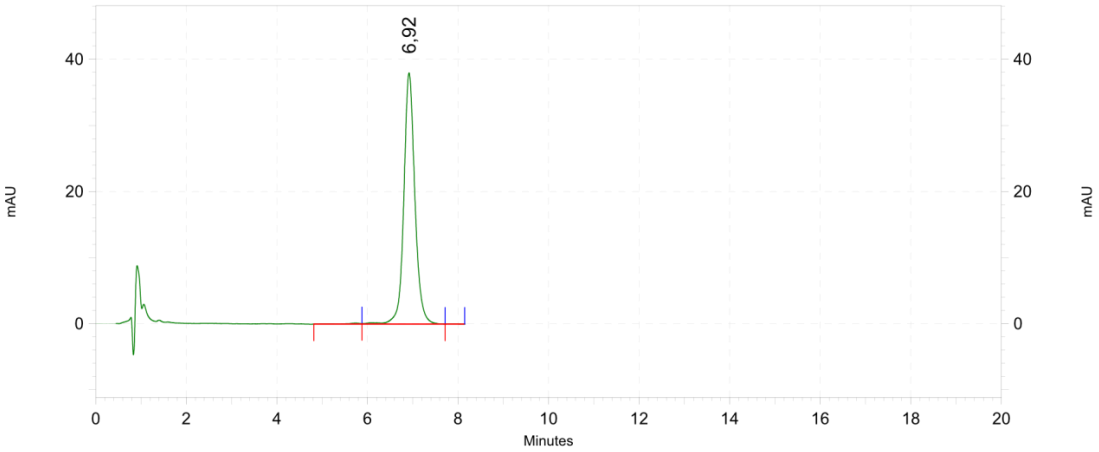


Figure S73. Chromatogram of [$FeC_{10}DMS_7H_3$] (**3a**). RP-18, MeOH(98%), room temperature.

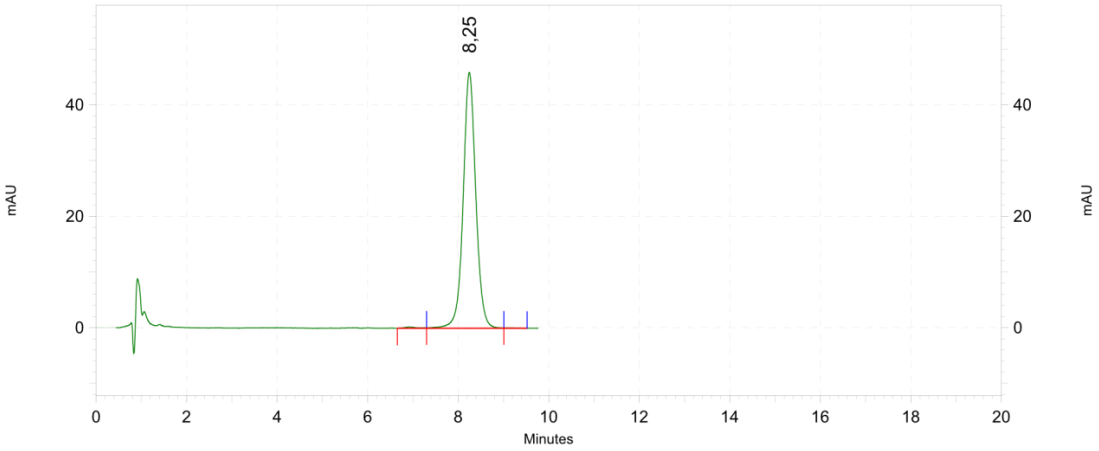


Figure S74. Chromatogram of [$FeC_{10}DMS_7H_3$] (**3b**). RP-18, MeOH(98%), room temperature.

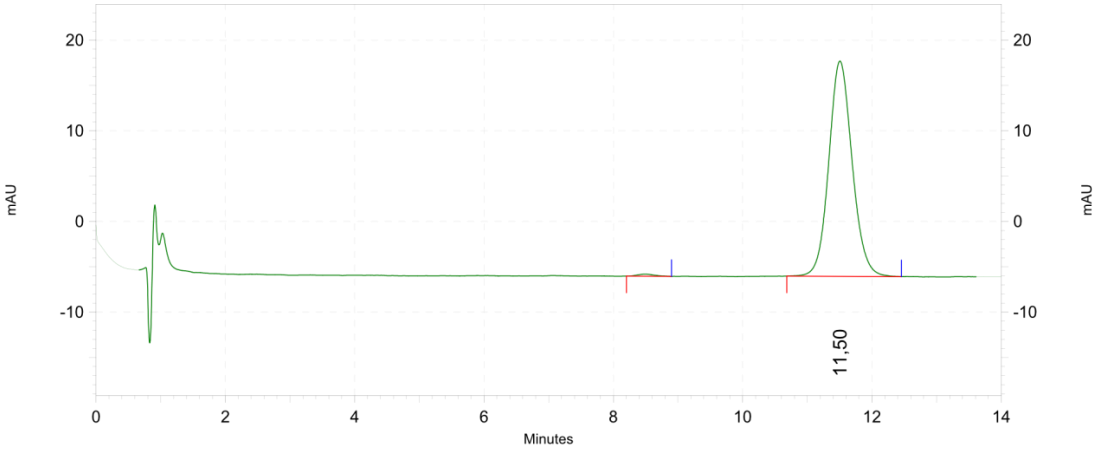


Figure S75. Chromatogram of [$FeC_{10}DMS_8H_2$] (**4a**). RP-18, MeOH(98%), room temperature.

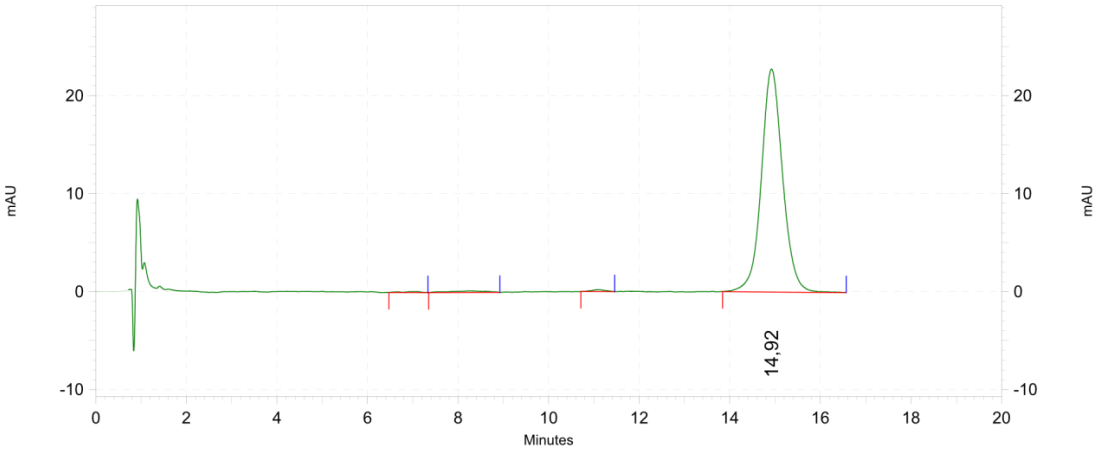


Figure S76. Chromatogram of [$FeC_{10}DMS_8H_2$] (**4b**). RP-18, MeOH(98%), room temperature.

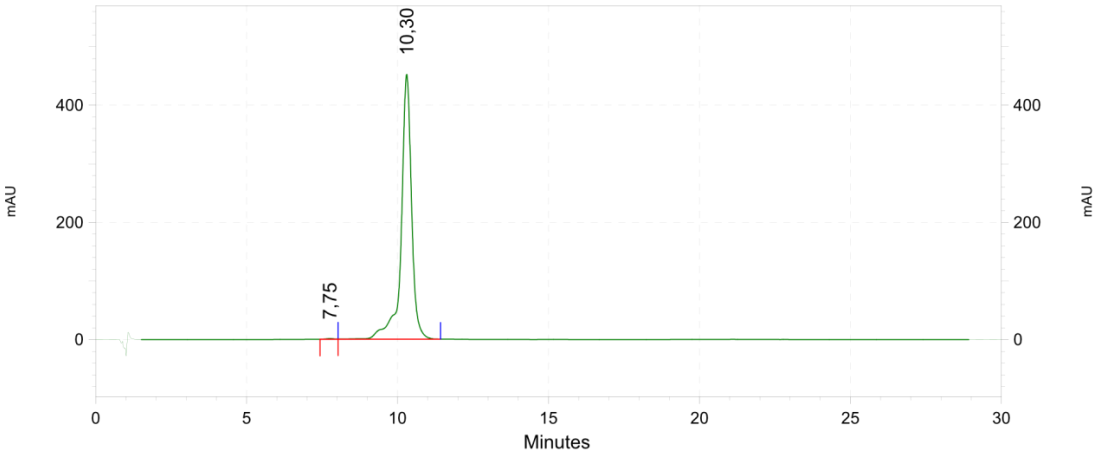


Figure S77. Chromatogram of [$FeC_{10}DMS_9H$] (**5**). RP-18, 9:1 MeOH(98%) and THF, room temperature.

# 5 Computational Details

All calculations were performed using the TURBOMOLE program code, Version 7.6.[14,15] Structures were optimized in the gas phase using the full molecular symmetry and the r$^2$SCAN-3c composite approach with the respective basis sets.[16] All structures were identified as minima of the potential energy surface by numerical frequency calculations.
All UV/vis spectra were calculated with time-dependent density functional theory using the ωB97X-D functional,[17] the def2-TZVPPD basis set[18] and in $C_1$ symmetry. For the species **6**, only a def2-TZVPP basis set was assigned to the DMS groups to improve numerical performance of the excitation energy calculations. For the calculation of UV/vis spectra, solvation effects for *n*-hexane were considered at the COSMO level,[19] using the FINE cavity ($cosmo_isorad),[20] a dielectric constant of 1.92 and a refractive index of 1.3855. The number of excitations was chosen in such a way that the highest excitation in each irreducible representation was above 7.0 eV.

The SCF was converged to energy changes below $10^{-9}$ Hartree and density matrix entry changes below $10^{-7}$. Every calculation used a non-standard grid (gridsize 3, radsize 8). All calculations employed the multipole-accelerated resolution of the identity (MARI-J) approximation[21] in combination with the appropriate auxiliary basis sets.[22] The calculations at the ωB97X-D level also employed semi-numerical exact exchange ($senex)[23] with a gridsize of 1 and de-aliasing. Atomic charges were computed using natural population analysis (NPA).[24]

Table S5. NPA charges and TDDFT results for the positions of the lowest-energy absorption bands (in nm) for [FeCp$_2$], [FeCp$_2$] with the elongated Fe-C distances of **6**, and for persilylated **6.** ωB97X-D/def2-TZVPP(D)/COSMO//r$^2$SCAN-3c data.

| | $q^{NPA}$(Fe) | band 1 | band 2 | band 3 |
|---|---|---|---|---|
| [FeCp$_2$] ($D_{5h}$) | 0.271 | 512 | 461 | 351 |
| [FeCp$_2$] ($D_{5d}$) | 0.276 | 525 | 468 | 355 |
| [FeCp$_2$] ($D_{5h}$) elongated | 0.298 | 654 | 557 | 405 |
| [FeCp$_2$] ($D_{5d}$) elongated | 0.302 | 667 | 563 | 408 |
| [Fe($C_5$DMS$_5$)$_2$] ($D_5$), **6** | 0.301 | 671 | 589 | 423 |
| [Fe($C_5$DMS$_5$)$_2$] ($S_{10}$), **6** | 0.303 | 683 | 595 | 426 |

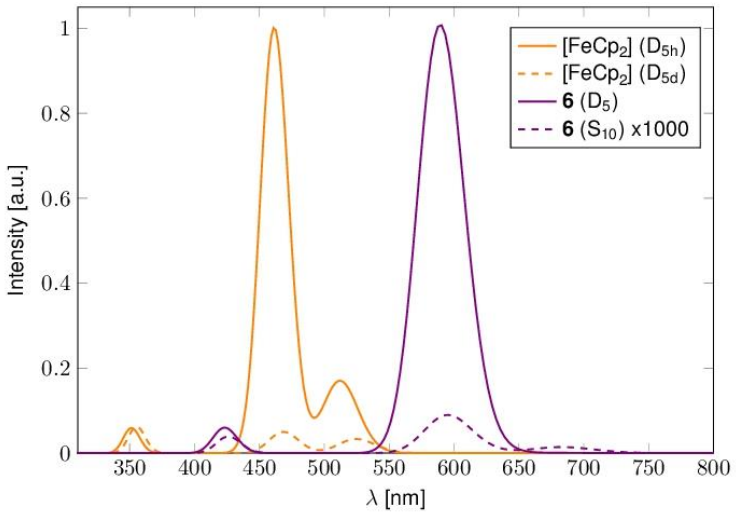


Figure S78. Excitation spectra obtained at TDDFT level (ωB97X-D/def2-TZVPP(D)/COSMO//r2SCAN-3c). Bands were modeled as Gaussians with a width at half maximum of 0.15 eV. The intensities are normalized to 1 for the most intense excitation of each species. The spectrum of the S10 symmetric species of **6** is enhanced by a factor of 1000.

Figure S79. Molecular structure of [$FeC_{10}DMS_{10}$] (**6**) in solid state. Left: asymmetric unit, center: conformer **A** ($D_5$), right: conformer **B** ($S_{10}$). hydrogen atoms are omitted for clarity. Color code: purple – silicon, orange – iron, gray – carbon.

# 6 References


(1) Rupf, S. M.; Dimitrova, I. S.; Schröder, G.; Malischewski, M. Preparation and One-Electron Oxidation of Decabromoferrocene. *Organometallics* **2022**, *41*, 1261–1267.

(2) Rupf, S. M.; Schröder, G.; Sievers, R.; Malischewski, M. Tenfold Metalation of Ferrocene: Synthesis, Structures, and Metallophilic Interactions in $FeC_{10}(HgX)_{10}$. *Chem. Eur. J.* **2021**, *27*, 5125–5129.

(3) Rathman, T. L.; Schwindeman, J. A. Preparation, Properties, and Safe Handling of Commercial Organolithiums: Alkyllithiums, Lithium sec-Organoamides, and Lithium Alkoxides. *Org. Process Res. Dev.* **2014**, *18*, 1192–1210.

(4) Harris, R. K.; Becker, E. D.; Menezes, S. M. C. de; Granger, P.; Hoffmann, R. E.; Zilm, K. W. Further Conventions for NMR Shielding and Chemical Shifts (IUPAC Recommendations 2008). *Pure Appl. Chem.* **2008**, *80*, 59.

(5) Willcott, M. R. MestRe Nova. *J. Am. Chem. Soc.* **2009**, *131*, 13180.

(6) T. H. J., N.; M., S. MMass as a Software Tool for the Annotation of Cyclic Peptide Tandem Mass Spectra. *PLoS One* **2012**, *7*, e44913.

(7) *Origin(Pro), Version 2016*; OriginLab Corporation: Northhampton, Massachusetts, USA, 2016.

(8) Dolomanov, O. V.; Bourhis, L. J.; Gildea, R. J.; Howard, J. A. K.; Puschmann, H. OLEX2: A Complete Structure Solution, Refinement and Analysis Program. *J. Appl. Cryst.* **2009**, *42*, 339–341.

(9) Sheldrick, G. M. Crystal Structure Refinement with SHELXL. *Acta Cryst.* **2015**, *A71*, 3–8.

(10) Sheldrick, G. M. *SHELXL Version 2014/7, Program for Crystal Structure Solution and Refinement*; Göttingen, Germany, 2014.

(11) Sheldrick, G. M. A Short History of SHELX. *Acta Cryst.* **2008**, *A64*, 112–122.

(12) Brandenburg, K. Diamond: Crystal and Molecular Structure Visualization http://www.crystalimpact.com/diamond.

(13) Persistence of Vision Pty. Ltd. Persistence of Vision Raytracer. Ltd., Persistence of Vision Pty. 2004.

(14) *TURBOMOLE Version 7.5 2020*, a Development of University of Karlsruhe and Forschungszentrum Karlsruhe GmbH, 1989-2007, TURBOMOLE GmbH, since 2007; TURBOMOLE GmbH. http://www.turbomole.com (accessed Mar 12, 2023).

(15) Balasubramani, S. G.; Chen, G. P.; Coriani, S.; Diedenhofen, M.; Frank, M. S.; Franzke, Y. J.; Furche, F.; Grotjahn, R.; Harding, M. E.; Hättig, C.; Hellweg, A.; Helmich-Paris, B.; Holzer, C.; Huniar, U.; Kaupp, M.; Khah, A. M.; Khani, S. K.; Müller, T.; Mack, F.; Nguyen, B. D.; Parker, S. M.; Perlt, E.; Rappoport,

D.; Reiter, K.; Roy, S.; Rückert, M.; Schmitz, G.; Sierka, M.; Tapavicza, E.; Tew, D. P.; van Wüllen, C.; Voora, V. K.; Weigend, F.; Wodyński, A.; Yu, J. M. *J. Chem. Phys.* **2020**, *152*, 184107.

(16) Grimme, S.; Hansen, A.; Ehlert, S.; Mewes, J.-M. r$^2$SCAN-3c: A "Swiss army knife" composite electronic-structure method. *J. Chem. Phys.* **2021**, *154*, 064103.

(17) Chai, J.-D.; Head-Gordon, M. Long-range corrected hybrid density functionals with damped atom–atom dispersion corrections. *Phys. Chem. Chem. Phys.* **2008**, *10*, 6615–6620.

(18) Wachters, A. J. H. Gaussian basis set for molecular wavefunctions containing third-row atoms. *J. Chem. Phys.* **1970**, *52*, 1033–1036.

(19) Klamt, A.; Schüürmann, G. COSMO. *J. Chem. Soc., Perkin Trans. 2* **1993**, *2*, 799–805.

(20) Klamt, A.; Diedenhofen, M. A refined cavity construction algorithm for the conductor-like screening model. *J. Comput. Chem.* **2018**, *39*, 1648–1655.

(21) Sierka, M.; Hogekamp, A.; Ahlrichs, R. Fast evaluation of the Coulomb potential for electron densities using multipole accelerated resolution of identity approximation. *J. Chem. Phys.* **2003**, *118*, 9136–9148.

(22) Weigend, F. Accurate Coulomb-fitting basis sets for H to Rn. *Phys. Chem. Chem. Phys.* **2006**, *8*, 1057–1065.

(23) Holzer, C. An improved seminumerical Coulomb and exchange algorithm for properties and excited states in modern density functional theory. *J. Chem. Phys.* **2020**, *153*, 184115.

(24) Reed, A. E.; Weinstock, R. B.; Weinhold, F. Natural population analysis. *J. Chem. Phys.* **1985**, *83*, 735.

## A.5 The [2+2] Cycloaddition Product of Perhalogenated Cyclopentadienyl Cations: Structural Characterization of Salts of the $[C_{10}Cl_{10}]^{2+}$ and $[C_{10}Br_{10}]^{2+}$ Dications

Supporting Information

# The [2+2] Cycloaddition Product of Perhalogenated Cyclopentadienyl Cations: Structural Characterization of Salts of the $[C_{10}Cl_{10}]^{2+}$ and $[C_{10}Br_{10}]^{2+}$ Dications

Susanne Margot Rupf, Patrick Pröhm and Moritz Malischewski

# Content

# 1 Experimental Part

## 1.1 General Procedures

Commercially available chemicals were used as received, unless otherwise noted. $AsF_5$ [1] and $C_5Br_6$ [2] were prepared as described previously in the literature. $SbF_5$ was stored inside a glove box. $SbF_5$ and $AsF_5$ are highly dangerous compounds with devastating effects on human tissue. They should only be handled in appropriate equipment by trained personnel. Attention: $AsF_5$, $SO_2$ and $SO_2ClF$ are (toxic) gases at room temperature. $C_5Cl_6$ was purchased from ABCR. Oxygen- and moisture-sensitive compounds were handled using Schlenk techniques and/or handled and stored in a argon-filled glovebox ($O_{2(g)}$ and $H_2O_{(g)} < 0.1$ ppm). $SO_2$ was distilled from $CaH_2$ and stored in a stainless-steel cylinder. $SO_2ClF$ was prepared according to literature methods[3] and stored in a stainless-steel cylinder. Reactions involving $SO_2ClF$, $AsF_5$ and $SbF_5$ were performed in PFA (tetrafluoroethene-perfluoroalkoxyvinyl-copolymer) tubes connected to stainless-steel valves. Instead of stirring, the mixtures were agitated with the help of the Mini-Vortex Mixer PV-1.

$^{13}C$ and $^{19}F$ NMR spectra were recorded on a JEOL 400 MHz ECS spectrometer by using sealed 5mm PFA tubes inside 6mm NMR glass tubes containing $d_6$-acetone as external lock standard. All reported chemical shifts ($\delta$) are referenced to the Ξ values given in IUPAC recommendations of 2008 using the $^2H$ signal of the deuterated solvent as internal reference.[4] All chemical shifts ($\delta$) are given in parts per million (ppm) and the signals are specified according to the multiplicity (s = singlet, d = doublet, t = triplet, m = multiplet, br = broad) and the coupling constants *J* in Hz.

X-Ray data were collected on a BRUKER D8 Venture system. Data were collected at 100(2) K using graphite-monochromated Mo $K_\alpha$ radiation ($\lambda_\alpha$ = 0.71073 Å). The strategy for the data collection was evaluated by using the Smart software. The data were collected by the standard "$\psi$-$\omega$ scan techniques" and were scaled and reduced using Saint+software. The structures were solved by using Olex2,[5] the structure was solved with the XT [6] structure solution program using Intrinsic Phasing and refined with the XL [7] refinement package using Least Squares minimization. If it is noted, bond length and angles were measured with Diamond Crystal and Molecular Structure Visualization Version 3.1. [8] Drawings were generated with Mercury.[9]

## 1.2 Synthesis

**$C_5Cl_6$:**

$C_5Cl_6$ (30 mg) was filled into a 8 mm PFA tube equipped with a stainless steel valve. $SO_2$ (0.5 mL) was condensed in at -196 °C. The $C_5Cl_6$ was dissolved at -20 °C. Afterwards, 0.4 mL of the solvent was evaporated under high vacuum. The mixture was slowly cooled to -78 °C in a freezer. The next day, colorless single crystals of $C_5Cl_6$ had formed.

**$^{13}C$ NMR** (100 MHz, $CH_2Cl_2$, ex. acetone-$d_6$, r.t.): $\delta$ = 131.49, 128.01, 88.66 ppm.

**$C_5Br_6$:**

KOH (220 g, 3.93 mol) was dissolved in 700 mL deionized water while stirring vigorously. Then bromine (30 mL, 0.59 mol) was added to the solution dropwise at 0 °C. Afterwards, the yellow solution was

warmed up to room temperature. After addition of freshly distilled cyclopentadiene (5 g, 0.08 mol) in 5 mL pentane a colorless precipitate had formed. The color changed from colorless to brown while stirring over night at room temperature. The brown precipitate was filtered off, washed with deionized water and dissolved in pentane. The solution was dried over $MgSO_4$, purified over active carbon and filtered. During the evaporation of the solvent at ambient pressure, brown crystals formed. The crystalline residue was washed with small amounts of pentane and recrystallized two times in methanol at reflux. After cooling down to room temperature $C_5Br_6$ was isolated as yellow crystalline solid in 47% yield (20 g, 0.04 mol). $C_5Br_6$ (50 mg) was dissolved in a mixture of dichloromethane (2 mL) and acetonitrile (0.5 mL). The mixture was slowly cooled to -78 °C in a freezer. After three months yellow single crystals of $C_5Br_6$ · MeCN had formed.

**$^{13}$C NMR** (100 MHz, $CD_2Cl_2$, r.t.): $\delta$ = 130.21, 122.97, 56.96 ppm.

**$[C_{10}Cl_{10}][Sb_3F_{16}]_2$:**

Inside a glovebox, antimony pentafluoride (1 g, 4.61 mmol) was filled into a 8 mm PFA tube equipped with a stainless steel valve. $SO_2ClF$ (1 mL) was condensed in at -196°C. After the antimony pentafluoride was dissolved at -20°C, the mixture was frozen again. Subsequently, $C_5Cl_6$ (0.1 g, 0.37 mmol) was added to the frozen solution. The mixture was brought to -20 °C, resulting in a green solution. The mixture was slowly cooled to -78 °C in a freezer. The next day, moisture-sensitive, thermally unstable yellow single crystals of $[C_{10}Cl_{10}][Sb_3F_{16}]_2$ · 2 $SO_2ClF$ had formed in the green solution.

**$^{13}$C NMR** (100 MHz, $SO_2$, ext. acetone-$d_6$, -60 °C): $\delta$ = 219.08, 158.23, 76.05 ppm.

**$^{19}$F NMR** (377 MHz, $SO_2$, ext. acetone-$d_6$, -60 °C): $\delta$ = -91.37 (br, 1F), -101.4 (br, 5F), -110.57 (br, 7F), 132.66 (br, 2F), -134.22 (br, 1F) ppm.

**$[C_{10}Br_{10}][As_2F_{11}]_2$:**

$C_5Br_6$ (40 mg, 0.07 mmol) was filled into a 8 mm PFA tube equipped with a stainless steel valve. $SO_2ClF$ (1 mL) was condensed in at -196°C. Subsequently, $AsF_5$ (25 mg, 0.15 mmol) was condensed to the frozen solution. The mixture was brought to -20 °C, resulting in a dark orange solution. The mixture was slowly cooled to -78 °C in a freezer. The next day, moisture-sensitive, thermally unstable orange single crystals of $[C_{10}Br_{10}][As_2F_{11}]_2$ · 4 $SO_2ClF$ had formed in the green solution.

**$^{13}$C NMR** (100 MHz, $SO_2$, ext. acetone-$d_6$, -60 °C): $\delta$ = 219.32, 155.29, 68.27 ppm.

**$^{19}$F NMR** (377 MHz, $SO_2$, ext. acetone-$d_6$, -60 °C): $\delta$ = -56.06 (br) ppm.

# 2 Appendix

## 2.1 Crystallographic data

***Table S1:*** *Crystallographic Data*

| **Compound** | **$[C_{10}Cl_{10}][Sb_3F_{16}]_2 \cdot 2\ SO_2ClF$** | **$[C_{10}Br_{10}][As_2F_{11}]_2 \cdot 4\ SO_2ClF$** |
|---|---|---|
| **Empirical formula** | $C_{10}Cl_{12}F_{34}O_4S_2Sb_6$ | $As_4Br_{10}C_{10}Cl_4F_{26}O_8S_4$ |
| **Formula weight** | 2050.12 | 2110.92 |
| **Temperature/K** | 102.37 | 100.09 |
| **Crystal system** | Monoclinic | triclinic |
| **Space group** | $P2_1/n$ | P-1 |
| **a/Å** | 9.8021(4) | 8.8126(5) |
| **b/Å** | 19.9917(8) | 11.9355(8) |
| **c/Å** | 12.0793(5) | 12.5355(8) |
| **α/°** | 90 | 68.761(2) |
| **β/°** | 97.4060(10) | 74.151(2) |
| **γ/°** | 90 | 75.960(2) |
| **Volume/Å³** | 2347.32(17) | 1166.97(13) |
| **Z** | 2 | 1 |
| **$\rho_{calc}$/g·cm³** | 2.901 | 3.004 |
| **μ/mm⁻¹** | 4.338 | 11.948 |
| **F(000)** | 1880.0 | 972.0 |
| **Crystal size/mm³** | 0.347 × 0.255 × 0.222 | 0.152 × 0.125 × 0.098 |
| **Crystal shape** | block | plate |
| **Radiation** | $MoK_\alpha$ (λ = 0.71073) | $MoK_\alpha$ (λ = 0.71073) |
| **2Θ range for data collection/°** | 4.66 to 56.692 | 4.868 to 52.886 |
| **Index ranges** | -11 ≤ h ≤ 13, -26 ≤ k ≤ 26, -16 ≤ l ≤ 16 | -11 ≤ h ≤ 11, -14 ≤ k ≤ 14, -15 ≤ l ≤ 15 |
| **Reflections collected** | 93745 | 80540 |
| **Independent reflections** | 5828 [$R_{int}$ = 0.0451, $R_{sigma}$ = 0.0157] | 4806 [$R_{int}$ = 0.0568, $R_{sigma}$ = 0.0198] |
| **Data/restrains/parameters** | 5828/0/326 | 4806/0/326 |
| **Goodness-of-fit on F²** | 1.131 | 0.987 |
| **Final R indexes [I>=2σ(I)]** | $R_1$ = 0.0173, $wR_2$ = 0.0408 | $R_1$ = 0.0283, $wR_2$ = 0.0601 |
| **Final R indexes [all data]** | $R_1$ = 0.0183, $wR_2$ = 0.0411 | $R_1$ = 0.0319, $wR_2$ = 0.0617 |
| **Largest diff. peak/hole / e·Å³** | 0.78/-0.78 | 1.34/-0.78 |

***Table S2:*** *Crystallographic Data*

| **Compound** | **$C_5Cl_6$** | **$C_5Br_6$ · MeCN** |
|---|---|---|
| **Empirical formula** | $C_5Cl_6$ | $C_7H_3Br_6N$ |
| **Formula weight** | 272.75 | 580.56 |
| **Temperature/K** | 100.0 | 103.68 |
| **Crystal system** | Triclinic | orthorhombic |
| **Space group** | P-1 | Pnma |
| **a/Å** | 8.2289(4) | 8.5108(5) |
| **b/Å** | 10.3003(5) | 7.1691(4) |
| **c/Å** | 12.5070(6) | 21.9711(11) |
| **α/°** | 97.189(2) | 90 |
| **β/°** | 107.491(2) | 90 |
| **γ/°** | 111.379(2) | 90 |
| **Volume/Å³** | 908.04(8) | 1340.56(13) |
| **Z** | 4 | 4 |
| **$\rho_{calc}$/g·cm³** | 1.995 | 2.877 |
| **μ/mm$^{-1}$** | 1.817 | 17.933 |
| **F(000)** | 528.0 | 1048.0 |
| **Crystal size/mm³** | 0.504 × 0.386 × 0.201 | 0.531 × 0.179 × 0.16 |
| **Crystal shape** | block | block |
| **Radiation** | $MoK_\alpha$ (λ = 0.71073) | $MoK_\alpha$ (λ = 0.71073) |
| **2Θ range for data collection/°** | 4.404 to 56.656 | 5.132 to 51.386 |
| **Index ranges** | -10 ≤ h ≤ 10, -13 ≤ k ≤ 13, -16 ≤ l ≤ 16 | -10 ≤ h ≤ 10, -8 ≤ k ≤ 8, -26 ≤ l ≤ 26 |
| **Reflections collected** | 31668 | 21875 |
| **Independent reflections** | 4500 [$R_{int}$ = 0.0275, $R_{sigma}$ = 0.0171] | 1385 [$R_{int}$ = 0.0661, $R_{sigma}$ = 0.0277] |
| **Data/restrains/parameters** | 4500/0/199 | 1385/0/84 |
| **Goodness-of-fit on F²** | 1.056 | 1.080 |
| **Final R indexes [I>=2σ(I)]** | $R_1$ = 0.0206, $wR_2$ = 0.0515 | $R_1$ = 0.0474, $wR_2$ = 0.1380 |
| **Final R indexes [all data]** | $R_1$ = 0.0244, $wR_2$ = 0.0541 | $R_1$ = 0.0491, $wR_2$ = 0.1392 |
| **Largest diff. peak/hole / e·Å³** | 0.50/-0.30 | 1.15/-1.61 |

The solid state structure of **1a** contains two independent $C_5Cl_6$ molecules in the asymmetric unit. The differences in bond distances and angles of both molecules are equal within ± 3σ. In structure of **1b · MeCN** the cyclopentadienyl ring is located in a crystallographic mirror plane. All atoms in this plane have a side occupation factor of 0.5 yielding an overall formula of $C_5Br_6$. In both compounds C1 is a saturated carbon atom. The C-C and C-X distances (X = Cl, Br) in these positions equals normal single bonds. The other C-C bond lengths (C2 to C5) exhibit a conjugated double bond system with distances of 1.34 and 1.48 Å. The halogen atoms attached to these carbon atoms contribute to the conjugated system. As a result, the C-Cl distances are decreased by 0.08 Å compared to the $C_{sp_3}$-X lengths in the crystal structure of **1a** and **1b**. Additionally, the crystal structure of **1a** shows short Cl···Cl contacts (3.334(3) to 3.493(3) Å) connecting each $C_5Cl_6$ unit in a polymeric structure. In the

structure of **1b · MeCN** the halogen bonds are replaced by solvent interactions (N-Br distance: 2.977(17) Å).

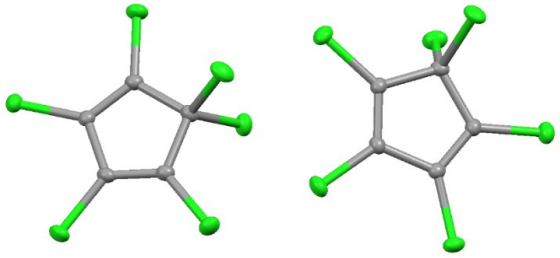

***Figure S1:*** *Ellipsoid (50% prob.) plot of compound $C_5Cl_6$. Color code: green – chlorine, grey – carbon.*

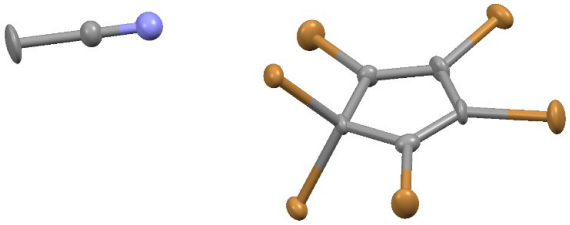

***Figure S2:*** *Ellipsoid (50% prob.) plot of compound $C_5Br_6$ · MeCN. Hydrogen atoms are omitted for clarity. Color code: blue – nitrogen, orange – bromine, grey – carbon.*

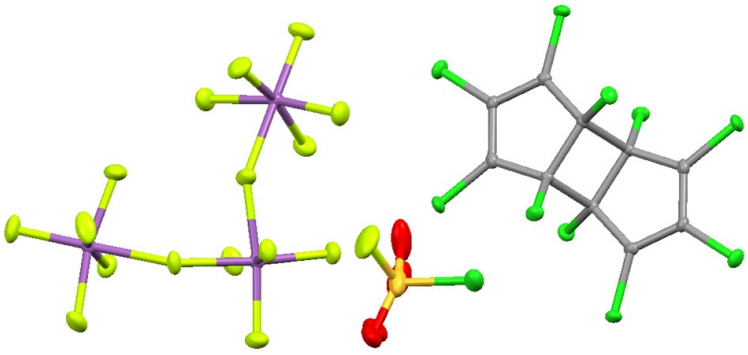

***Figure S3:*** *Ellipsoid (50% prob.) plot of compound $[C_{10}Cl_{10}][Sb_3F_{16}]_2$ · $SO_2ClF$. Color code: purple – antimony, green – chlorine, dark yellow – sulfur, yellow – fluorine, red – oxygen, grey – carbon.*

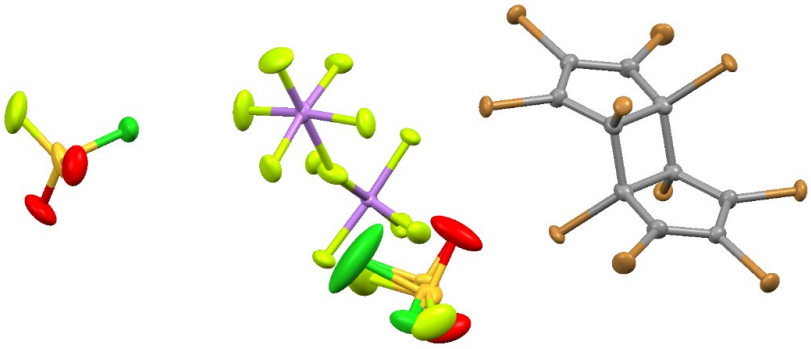

***Figure S4:*** *Ellipsoid (50% prob.) plot of compound* $[C_{10}Br_{10}][As_2F_{11}]_2 \cdot 2\ SO_2ClF$. *Color code: violet – arsenic, orange – bromine, green – chlorine, dark yellow – sulfur, yellow – fluorine, red – oxygen, grey – carbon.*

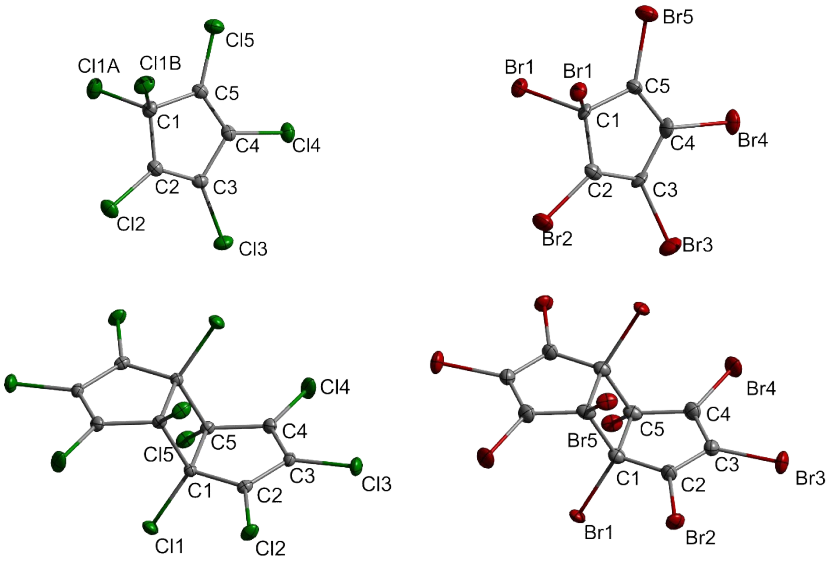


***Figure S5:*** *Ellipsoid (50% prob.) plot of compounds* ***1a***, ***1b*** $\cdot$ ***MeCN***, $[4a][Sb_3F_{16}]_2 \cdot SO_2ClF$ *(left) and* $[4b][As_2F_{11}]_2 \cdot 2\ SO_2ClF$ *(right). Counterions and solvent molecules are omitted for clarity. Color code: red – bromine, green – chlorine, grey – carbon.*

***Table S3:*** *Selected bond lengths of the compounds* ***1a***, ***1b***, $[4a][Sb_3F_{16}]_2$ *and* $[4b][As_2F_{11}]_2$ *[Å]*

| | $(C_{10}X_{10})^{2+}$ | | $C_5X_6$ | |
|---|---|---|---|---|
| | **X = Cl** | **X = Br** | **X = Cl** | **X = Br** |
| C1 – C2 | 1.507(3) | 1.501(7) | 1.511(3) | 1.509(15) |
| C2 – C3 | 1.386(3) | 1.386(6) | 1.336(2) | 1.311(15) |
| C3 – C4 | 1.394(3) | 1.392(8) | 1.475(2) | 1.470(16) |
| C4 – C5 | 1.507(3) | 1.511(6) | 1.334(3) | 1.365(15) |
| C5 – C1 | 1.566(3) | 1.568(7) | 1.507(2) | 1.505(14) |
| C1 – X1 | 1.740(2) | 1.908(4) | 1.781(2),1.780(2) | 1.950(6) |
| C2 – X2 | 1.643(2) | 1.803(6) | 1.696(1) | 1.856(10) |
| C3 – X3 | 1.678(2) | 1.833(5) | 1.698(2) | 1.875(11) |
| C4 – X4 | 1.634(2) | 1.797(4) | 1.697(1) | 1.840(11) |
| C5 – X5 | 1.739(2) | 1.912(5) | 1.699(2) | 1.838(11) |

## 2.2 NMR spectra

The samples of the dications were prepared in sealed 5 mm PFA tubes. The mother liquor was decanted off and the remaining single-crystals were dissolved in cold $SO_2$. The tubes were resealed in vacuum and stored in cold ethanol at -75°C. For the measurement, they were taken out, rapidly wiped off and placed inside a 6mm glass NMR tube containing acetone-$d_6$. Therefore, signals of acetone and ethanol can be observed in the $^{13}C$ NMR spectra.

**$[C_{10}Br_{10}][As_2F_{11}]_2$:**

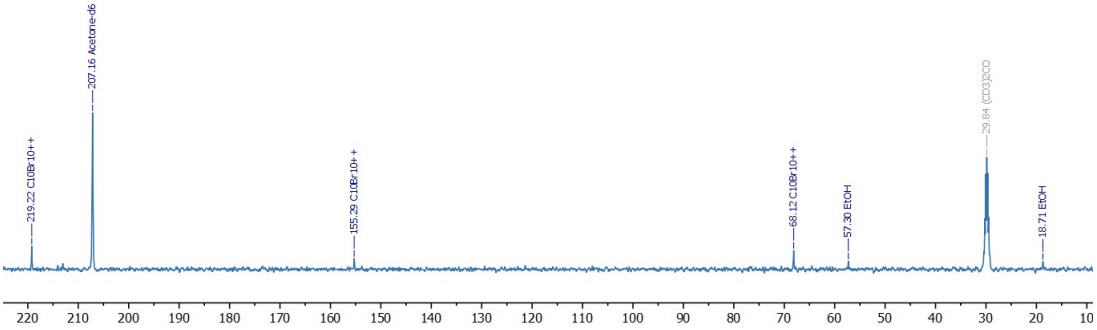


***Figure S6:*** *$^{13}C$ NMR spectrum (100 MHz, $SO_2$, ext. acetone-$d_6$, -60 °C).*

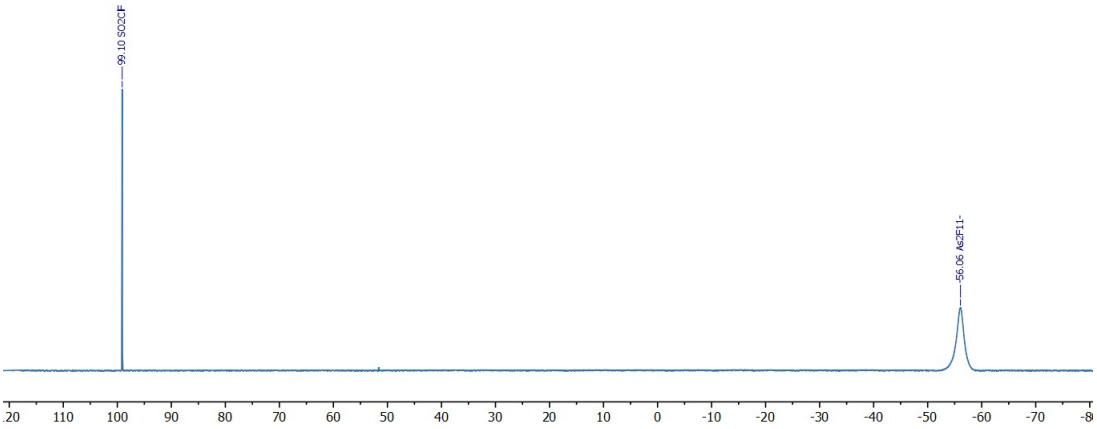


***Figure S7:*** *$^{19}F$ NMR spectrum (377 MHz, $SO_2$, ext. acetone-$d_6$, -60 °C).*

In case of $[C_{10}Br_{10}]^{2+}$ the NMR sample was warmed to -20°C as well (spectra below). The signals which we assigned to the dication vanish and new signals at 212 and 127 ppm appear as well as the formation of a brown oil was observed. The decomposition products are not identified yet.

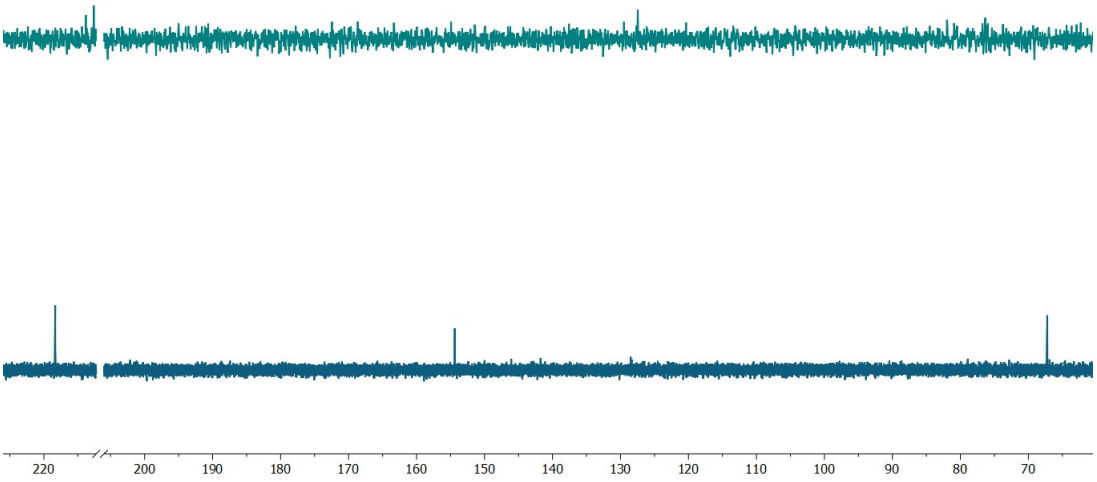


***Figure S8:*** *$^{13}$C NMR spectra (100 MHz, $SO_2$, ext. acetone-$d_6$) of $[C_{10}Br_{10}][As_2F_{11}]_2$ at first at -60°C (bottom) and afterwards at -20°C (top).*

**$[C_{10}Cl_{10}][Sb_3F_{16}]_2$:**

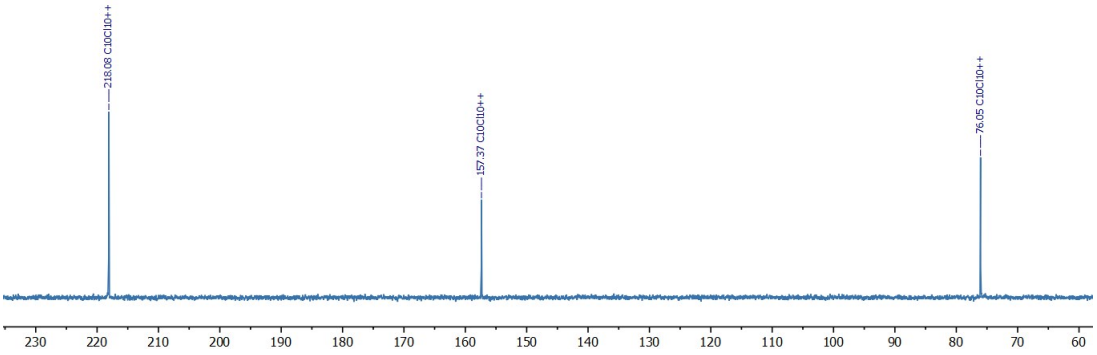


***Figure S9:*** *$^{13}$C NMR spectrum (100 MHz, $SO_2$, ext. acetone-$d_6$, -60 °C).*

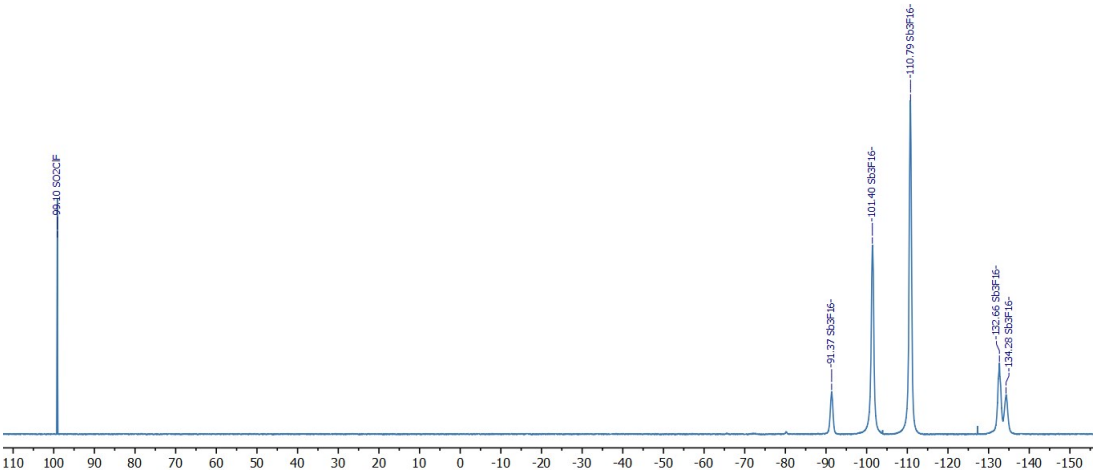


***Figure S10:*** *$^{19}$F NMR spectrum (377 MHz, $SO_2$, ext. acetone-$d_6$, -60 °C).*

**$C_5Br_6$:**

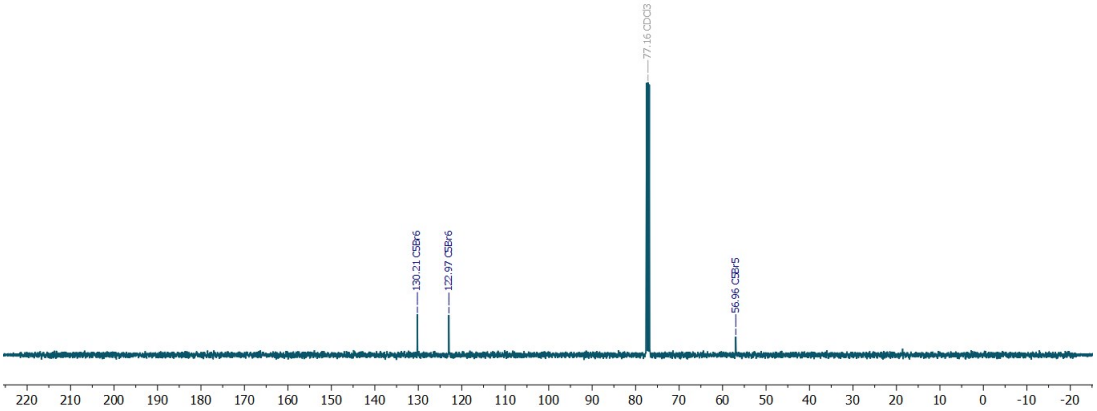


***Figure S11:*** *$^{13}$C NMR spectrum (100 MHz, $CDCl_3$, r.t.).*

**$C_5Cl_6$:**

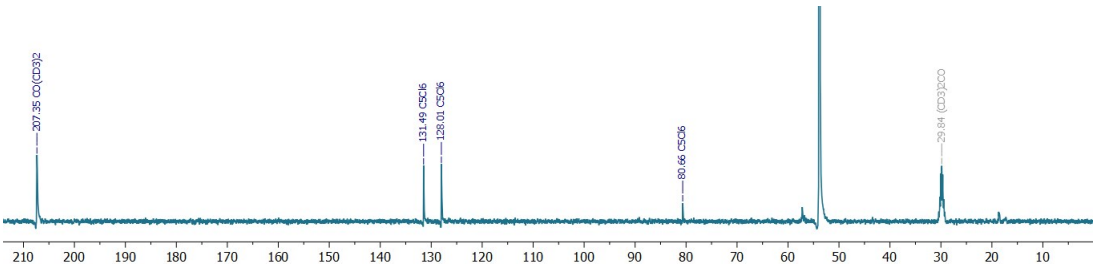


***Figure S12:*** *$^{13}$C NMR spectrum (100 MHz, $CH_2Cl_2$, ext. acetone-$d_6$, r.t.).*

# 3 Quantum-Chemical Calculations

Structure optimizations and frequency calculations were both performed using B3LYP/Def2TZVP with GD3BJ dispersion correction and MP2/cc-PVTZ with the Gaussian16 (Rev A.03) software.[10] Thermodynamic corrections were taken from these calculations (T = 213.15 K and p = 1 atm). The influence of the solvation was included by calculations using the Polarizable Continuum Model (PCM) using the integral equation formalism variant (IEFPCM). Dielectric constants of $\varepsilon_r$=2; 10 and 23 were used to simulate solvents of different polarity. NBO charges were calculated with NBO Version 3.1.[11] Results were visualized with Chemcraft.[12]

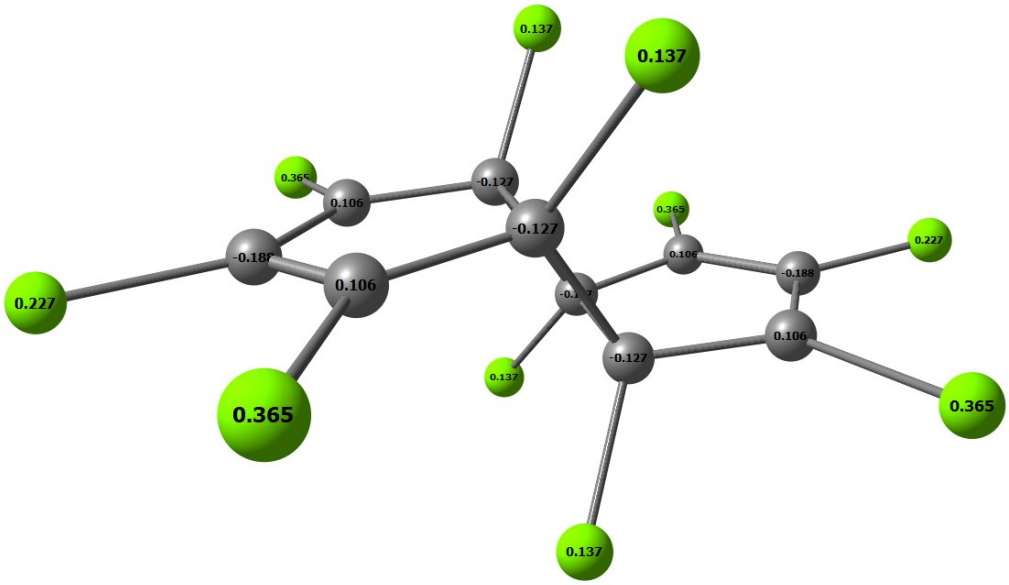


***Figure S13:*** *NBO charges of $C_{10}Cl_{10}^{2+}$ (B3LYP/Def2-TZVP)*

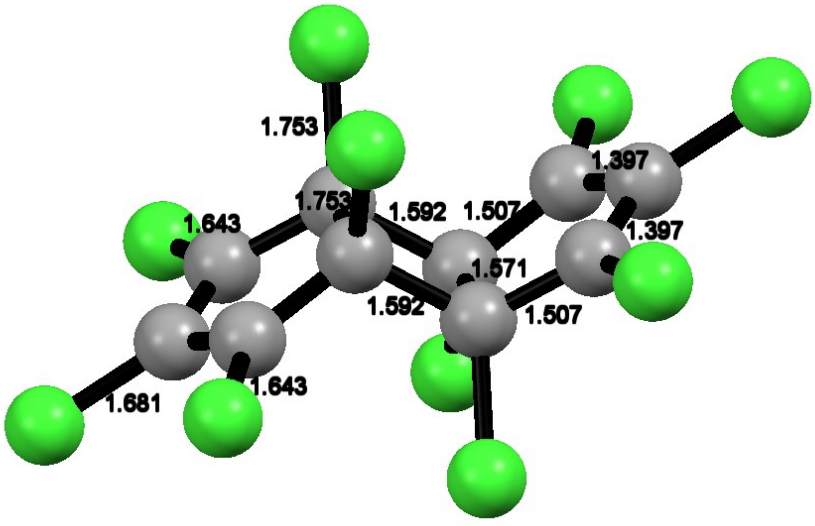


***Figure S14:*** *Optimized Structure of $C_{10}Cl_{10}^{2+}$ (B3LYP/Def2-TZVP) with C-Cl (left) and C-C (right) bond lengths*

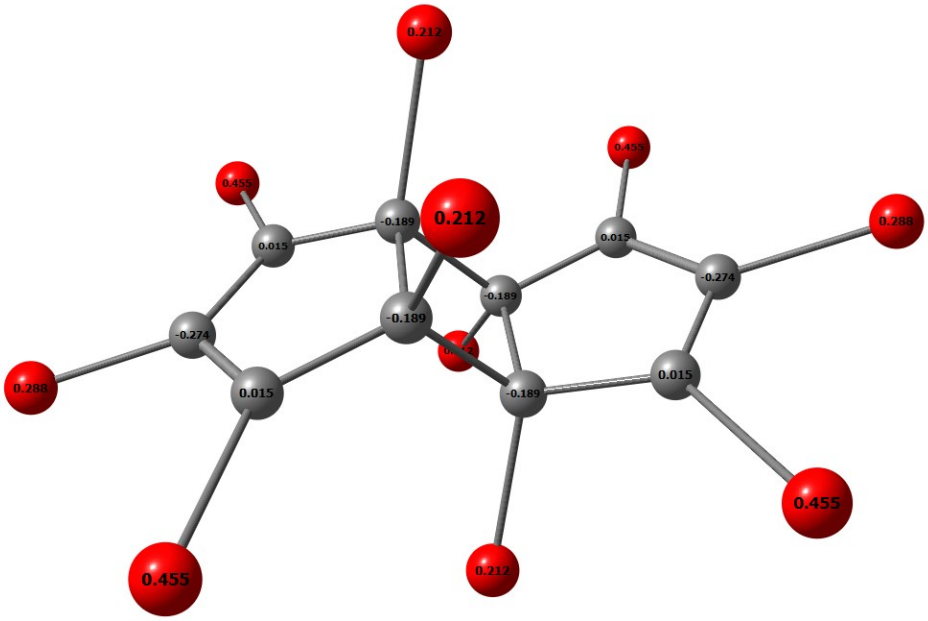


***Figure S15:*** NBO charges of $C_{10}Br_{10}^{2+}$ (B3LYP/Def2-TZVP)

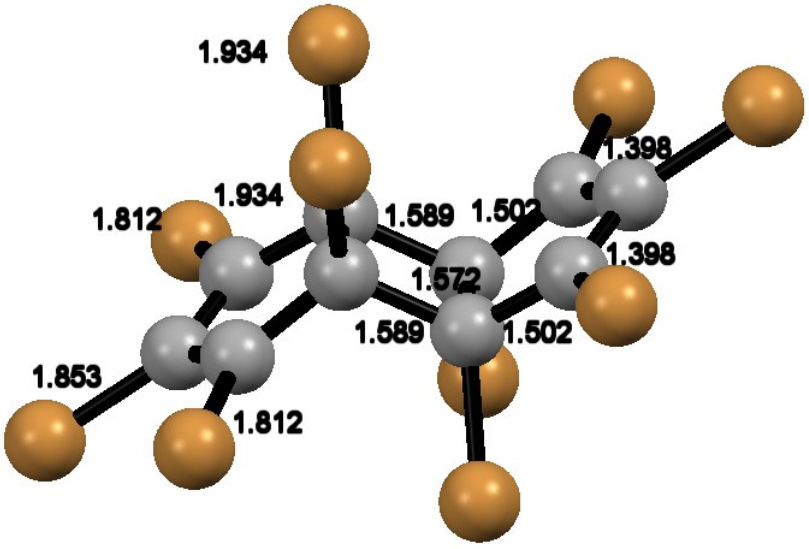


**Figure S16:** *Optimized Structure of $C_{10}Br_{10}^{2+}$ (B3LYP/Def2-TZVP) with C-Br (left) and C-C (right) bond lengths*

***Table S4:*** *Calculated energy differences ΔG in kJ/mol at 213.15 K. $\varepsilon_r$ is the dielectric constant, used for calculations with the polarizable Continuum Model (PCM) for solvent effects*

| | **B3LYP-GD3BJ/Def2-TZVP** | **MP2/cc-PVTZ** |
|---|---|---|
| $C_5Cl_5^+$ sing/trip **3a**/**2a** | + 32 / 0 | +15 / 0 |
| **2a** + **2a** → **4a** / **exo-5a** / **endo-5a** | +225/ + 317 / + 316 | +102 / +156 / +165 |
| With $\varepsilon_r$ = 2 | +108 / +195 /+201 | -13 / +37 / +41 |
| With $\varepsilon_r$ = 10 | +35 / +103 / +101 | -109 / -61 / -61 |
| With $\varepsilon_r$ = 23 | +5 / +89 / +90 | -123 / -75 / -76 |
| $C_5Br_5^+$ sing/trip **3b**/**2b** | +31 / 0 | |
| **2b** + **2b**→ **4b** / **exo-5b** / **endo-5b** | +202 / +296 / +292 | |
| With $\varepsilon_r$ = 2 | +89 / +185 / +177 | |
| With $\varepsilon_r$ = 10 | +7 / +97 / +92 | |
| With $\varepsilon_r$ = 23 | -6 / +81 / +78 | |

## Cartesian coordinates of the optimized structures:

### B3LYP-GD3BJ/Def2-TZVP - without solvent:

$C_5Cl_5^+$sing HF=-2491.3896934

Sum of electronic and thermal Free Energies= -2491.379865

| | | | |
|---|---|---|---|
| 17 | 0.000000000 | 2.780004000 | 0.940534000 |
| 17 | 0.000000000 | 0.000000000 | 2.798904000 |
| 17 | 0.000000000 | -2.780004000 | 0.940534000 |
| 17 | 0.000000000 | -1.675519000 | -2.332732000 |
| 17 | 0.000000000 | 1.675519000 | -2.332732000 |
| 6 | 0.000000000 | 1.199022000 | 0.343936000 |
| 6 | 0.000000000 | 0.000000000 | 1.160088000 |
| 6 | 0.000000000 | -1.199022000 | 0.343936000 |
| 6 | 0.000000000 | -0.774627000 | -0.944535000 |
| 6 | 0.000000000 | 0.774627000 | -0.944535000 |

$C_5Cl_5^+$trip HF=-2491.4023133

Sum of electronic and thermal Free Energies= -2491.392079

| | | | |
|---|---|---|---|
| 17 | 0.000000000 | 2.736995000 | 0.889192000 |
| 17 | 0.000000000 | 0.000000000 | 2.877852000 |
| 17 | 0.000000000 | -2.736995000 | 0.889192000 |
| 17 | 0.000000000 | -1.691740000 | -2.328101000 |
| 17 | 0.000000000 | 1.691740000 | -2.328101000 |
| 6 | 0.000000000 | 1.153176000 | 0.374730000 |
| 6 | 0.000000000 | 0.000000000 | 1.212764000 |
| 6 | 0.000000000 | -1.153176000 | 0.374730000 |
| 6 | 0.000000000 | -0.712754000 | -0.981161000 |

6 0.000000000 0.712754000 -0.981161000

$C_{10}Cl_{10}^{2+}$ HF=-4982.7402342

Sum of electronic and thermal Free Energies= -4982.698577

17 2.461574000 -2.686488000 -0.144544000
17 -0.027070000 -1.608036000 -2.071211000
17 -0.027113000 1.607997000 -2.071223000
17 0.027070000 -1.608034000 2.071213000
17 -2.461573000 -2.686488000 0.144543000
17 0.027113000 1.607999000 2.071223000
17 4.353903000 0.000019000 0.293611000
17 2.461557000 2.686504000 -0.144625000
17 -4.353902000 0.000018000 -0.293612000
17 -2.461558000 2.686504000 0.144623000
6 2.718033000 0.000010000 -0.093706000
6 1.926562000 1.137777000 -0.272077000
6 1.926568000 -1.137770000 -0.272039000
6 0.502636000 0.785458000 -0.616968000
6 0.502644000 -0.785467000 -0.616958000
6 -0.502644000 -0.785467000 0.616960000
6 -0.502636000 0.785458000 0.616969000
6 -1.926568000 -1.137770000 0.272040000
6 -2.718033000 0.000009000 0.093706000
6 -1.926562000 1.137777000 0.272077000

$C_{10}Cl_{10}^{2+}$exo HF=-4982.7042718

Sum of electronic and thermal Free Energies= -4982.663353

17 -2.948641000 -0.987564000 0.000000000
17 0.510191000 -3.372823000 1.700929000
17 0.510191000 -3.372823000 -1.700929000
17 -1.043138000 -0.732971000 2.761762000
17 -1.043138000 -0.732971000 -2.761762000
17 2.208442000 0.062291000 -1.564407000
17 2.208442000 0.062291000 1.564407000
17 0.113477000 2.379841000 2.672071000
17 0.113477000 2.379841000 -2.672071000
17 -0.599002000 4.153888000 0.000000000
6 0.178177000 -2.101751000 0.688776000
6 -0.376700000 -0.736567000 1.161009000
6 0.178177000 -2.101751000 -0.688776000
6 -0.376700000 -0.736567000 -1.161009000
6 -1.330957000 -0.793710000 0.000000000
6 0.656829000 0.391060000 0.798815000
6 0.656829000 0.391060000 -0.798815000
6 0.202293000 1.794886000 -1.137440000

| | | | |
|---|---|---|---|
| 6 | 0.202293000 | 1.794886000 | 1.137440000 |
| 6 | -0.076099000 | 2.554622000 | 0.000000000 |

$C_{10}Cl_{10}^{2+}$endo HF=-4982.7031388

Sum of electronic and thermal Free Energies= -4982.663620

| | | | |
|---|---|---|---|
| 17 | -1.651253000 | -2.769307000 | -0.219095000 |
| 17 | -1.668275000 | 2.759177000 | -0.228546000 |
| 17 | 0.149069000 | -1.540218000 | -2.535760000 |
| 17 | 0.144472000 | 1.536149000 | -2.538645000 |
| 17 | 2.026800000 | 2.691934000 | -0.012596000 |
| 17 | 3.823304000 | 0.010320000 | 0.743762000 |
| 17 | 2.043116000 | -2.682016000 | -0.012864000 |
| 17 | -0.703470000 | -1.706815000 | 2.708727000 |
| 17 | -0.715942000 | 1.711997000 | 2.703461000 |
| 17 | -3.544688000 | -0.011446000 | -0.581512000 |
| 6 | -0.807572000 | -0.684236000 | 1.397977000 |
| 6 | -0.812317000 | 0.684616000 | 1.395879000 |
| 6 | -1.019626000 | -1.166226000 | -0.059630000 |
| 6 | -1.953531000 | -0.006054000 | -0.295981000 |
| 6 | -1.026844000 | 1.160597000 | -0.063454000 |
| 6 | 0.239245000 | 0.795413000 | -0.945760000 |
| 6 | 0.243462000 | -0.796232000 | -0.944383000 |
| 6 | 1.560121000 | -1.134088000 | -0.297559000 |
| 6 | 1.553366000 | 1.141106000 | -0.297714000 |
| 6 | 2.298151000 | 0.005743000 | 0.034324000 |

**B3LYP-GD3BJ/Def2-TZVP with solvent model $\varepsilon_r$=2:**

$C_5Cl_5^+$trip HF=-2491.4391029

Sum of electronic and thermal Free Energies= -2491.429110

| | | | |
|---|---|---|---|
| 17 | 0.000000000 | 2.737489000 | 0.883976000 |
| 17 | 0.000000000 | 0.000000000 | 2.878598000 |
| 17 | 0.000000000 | -2.737489000 | 0.883976000 |
| 17 | 0.000000000 | -1.697106000 | -2.323490000 |
| 17 | 0.000000000 | 1.697106000 | -2.323490000 |
| 6 | 0.000000000 | 1.151950000 | 0.374520000 |
| 6 | 0.000000000 | 0.000000000 | 1.213241000 |
| 6 | 0.000000000 | -1.151950000 | 0.374520000 |
| 6 | 0.000000000 | -0.712407000 | -0.980530000 |
| 6 | 0.000000000 | 0.712407000 | -0.980530000 |

$C_{10}Cl_{10}^{2+}$ HF=-4982.8603122
Sum of electronic and thermal Free Energies= -4982.817201

| | | | |
|---|---|---|---|
| 17 | -2.459574000 | 2.684585000 | -0.120883000 |
| 17 | 0.018833000 | 1.622678000 | -2.060569000 |
| 17 | 0.019339000 | -1.603900000 | -2.074259000 |
| 17 | -0.018446000 | 1.603213000 | 2.076714000 |
| 17 | 2.452935000 | 2.686004000 | 0.133221000 |
| 17 | -0.018677000 | -1.622143000 | 2.064020000 |
| 17 | -4.357835000 | -0.004455000 | 0.273795000 |
| 17 | -2.454087000 | -2.685606000 | -0.132524000 |
| 17 | 4.353825000 | 0.004679000 | -0.291835000 |
| 17 | 2.463609000 | -2.684636000 | 0.132347000 |
| 6 | -2.718132000 | -0.001929000 | -0.098125000 |
| 6 | -1.924110000 | -1.137484000 | -0.268875000 |
| 6 | -1.928411000 | 1.136933000 | -0.263454000 |
| 6 | -0.502588000 | -0.783260000 | -0.616790000 |
| 6 | -0.504816000 | 0.787543000 | -0.611002000 |
| 6 | 0.503204000 | 0.782836000 | 0.619272000 |
| 6 | 0.505496000 | -0.788078000 | 0.614215000 |
| 6 | 1.923726000 | 1.137422000 | 0.267552000 |
| 6 | 2.716728000 | 0.001977000 | 0.091585000 |
| 6 | 1.929119000 | -1.137145000 | 0.265546000 |

$C_{10}Cl_{10}^{2+}$exo HF=-4982.8254363
Sum of electronic and thermal Free Energies= -4982.783801

| | | | |
|---|---|---|---|
| 17 | -0.922502000 | 0.041147000 | 2.954650000 |
| 17 | -3.354175000 | -1.749209000 | -0.459223000 |
| 17 | -3.383359000 | 1.671715000 | -0.550033000 |
| 17 | -0.699567000 | -2.741035000 | 1.098906000 |
| 17 | -0.765308000 | 2.780587000 | 0.994096000 |
| 17 | 0.088546000 | 1.567051000 | -2.212384000 |
| 17 | 0.010055000 | -1.554747000 | -2.201971000 |
| 17 | 2.365218000 | -2.675303000 | -0.152576000 |
| 17 | 2.352344000 | 2.670295000 | -0.045807000 |
| 17 | 4.160744000 | -0.009054000 | 0.543364000 |
| 6 | -2.103020000 | -0.704970000 | -0.147688000 |
| 6 | -0.728106000 | -1.153066000 | 0.401681000 |
| 6 | -2.114236000 | 0.669378000 | -0.179994000 |
| 6 | -0.751267000 | 1.166486000 | 0.362914000 |
| 6 | -0.774069000 | 0.021349000 | 1.336347000 |
| 6 | 0.380224000 | -0.795654000 | -0.656758000 |
| 6 | 0.383479000 | 0.800591000 | -0.656309000 |
| 6 | 1.784138000 | 1.134514000 | -0.189390000 |
| 6 | 1.789346000 | -1.138253000 | -0.228437000 |
| 6 | 2.552857000 | -0.004473000 | 0.045408000 |

$C_{10}Cl_{10}^{2+}$endo HF=-4982.8251481
Sum of electronic and thermal Free Energies= -4982.781793

| | | | |
|---|---|---|---|
| 17 | 1.646315000 | 2.764467000 | -0.237956000 |
| 17 | 1.644853000 | -2.765247000 | -0.238454000 |
| 17 | -0.149192000 | 1.530836000 | -2.553798000 |
| 17 | -0.151245000 | -1.529321000 | -2.554596000 |
| 17 | -2.053914000 | -2.685642000 | -0.065560000 |
| 17 | -3.759812000 | 0.000437000 | 0.873437000 |
| 17 | -2.053039000 | 2.686592000 | -0.064721000 |
| 17 | 0.721732000 | 1.708785000 | 2.696833000 |
| 17 | 0.720648000 | -1.709567000 | 2.696654000 |
| 17 | 3.546219000 | -0.001345000 | -0.516634000 |
| 6 | 0.800826000 | 0.684489000 | 1.386439000 |
| 6 | 0.800108000 | -0.685237000 | 1.386275000 |
| 6 | 1.012635000 | 1.163124000 | -0.070830000 |
| 6 | 1.947724000 | -0.000580000 | -0.283751000 |
| 6 | 1.011856000 | -1.163660000 | -0.071118000 |
| 6 | -0.249142000 | -0.793811000 | -0.960637000 |
| 6 | -0.248668000 | 0.794395000 | -0.960348000 |
| 6 | -1.559759000 | 1.136959000 | -0.303382000 |
| 6 | -1.560025000 | -1.136108000 | -0.303268000 |
| 6 | -2.274487000 | 0.000444000 | 0.080873000 |

**B3LYP-GD3BJ/Def2-TZVP with solvent model $\varepsilon_r$=10:**

$C_5Cl_5^{+}$trip HF=-2491.4687201
Sum of electronic and thermal Free Energies= -2491.458731

| | | | |
|---|---|---|---|
| 17 | 0.000000000 | 2.735835000 | 0.886897000 |
| 17 | 0.000000000 | 0.000000000 | 2.876846000 |
| 17 | 0.000000000 | -2.735835000 | 0.886897000 |
| 17 | 0.000000000 | -1.693209000 | -2.325297000 |
| 17 | 0.000000000 | 1.693209000 | -2.325297000 |
| 6 | 0.000000000 | 1.151334000 | 0.374077000 |
| 6 | 0.000000000 | 0.000000000 | 1.211487000 |
| 6 | 0.000000000 | -1.151334000 | 0.374077000 |
| 6 | 0.000000000 | -0.711818000 | -0.979887000 |
| 6 | 0.000000000 | 0.711818000 | -0.979887000 |

$C_{10}Cl_{10}^{2+}$ HF=-4982.9533426
Sum of electronic and thermal Free Energies= -4982.910637

| | | | |
|---|---|---|---|
| 17 | -2.452953000 | -2.684127000 | 0.126175000 |
| 17 | 0.024791000 | -1.613929000 | 2.066566000 |
| 17 | 0.024928000 | 1.607087000 | 2.070733000 |
| 17 | -0.025226000 | -1.606858000 | -2.070819000 |
| 17 | 2.449036000 | -2.684629000 | -0.129147000 |
| 17 | -0.024651000 | 1.614144000 | -2.066464000 |

| | | | |
|---|---|---|---|
| 17 | -4.353426000 | 0.002270000 | -0.276411000 |
| 17 | -2.448970000 | 2.684535000 | 0.128020000 |
| 17 | 4.353416000 | -0.002561000 | 0.276516000 |
| 17 | 2.452947000 | 2.684085000 | -0.125063000 |
| 6 | -2.713964000 | 0.000776000 | 0.102421000 |
| 6 | -1.922809000 | 1.136615000 | 0.270234000 |
| 6 | -1.925118000 | -1.136647000 | 0.269886000 |
| 6 | -0.501670000 | 0.784022000 | 0.617505000 |
| 6 | -0.502464000 | -0.785693000 | 0.615823000 |
| 6 | 0.501658000 | -0.783923000 | -0.617567000 |
| 6 | 0.502592000 | 0.785728000 | -0.615777000 |
| 6 | 1.922833000 | -1.136667000 | -0.270674000 |
| 6 | 2.714045000 | -0.000862000 | -0.102459000 |
| 6 | 1.925205000 | 1.136604000 | -0.269689000 |

$C_{10}Cl_{10}^{2+}$exo HF=-4982.9204234

Sum of electronic and thermal Free Energies= -4982.878125

| | | | |
|---|---|---|---|
| 17 | -0.893371000 | 0.000004000 | 2.953932000 |
| 17 | -3.375758000 | -1.701694000 | -0.493888000 |
| 17 | -3.375761000 | 1.701687000 | -0.493900000 |
| 17 | -0.735525000 | -2.764793000 | 1.040475000 |
| 17 | -0.735531000 | 2.764796000 | 1.040466000 |
| 17 | 0.041360000 | 1.560525000 | -2.207533000 |
| 17 | 0.041352000 | -1.560523000 | -2.207532000 |
| 17 | 2.359834000 | -2.671181000 | -0.099351000 |
| 17 | 2.359835000 | 2.671179000 | -0.099339000 |
| 17 | 4.159397000 | -0.000002000 | 0.534267000 |
| 6 | -2.106453000 | -0.685039000 | -0.157892000 |
| 6 | -0.738508000 | -1.159879000 | 0.383973000 |
| 6 | -2.106454000 | 0.685037000 | -0.157896000 |
| 6 | -0.738510000 | 1.159881000 | 0.383970000 |
| 6 | -0.759721000 | 0.000002000 | 1.341318000 |
| 6 | 0.381170000 | -0.798312000 | -0.657273000 |
| 6 | 0.381171000 | 0.798313000 | -0.657273000 |
| 6 | 1.786810000 | 1.136335000 | -0.212612000 |
| 6 | 1.786810000 | -1.136335000 | -0.212617000 |
| 6 | 2.550498000 | -0.000001000 | 0.038113000 |

$C_{10}Cl_{10}^{2+}$endo HF=-4982.9200142
Sum of electronic and thermal Free Energies= -4982.878870

| | | | |
|---|---|---|---|
| 17 | -1.610171000 | -2.780186000 | -0.278008000 |
| 17 | -1.670514000 | 2.744024000 | -0.280071000 |
| 17 | 0.251429000 | -1.533159000 | -2.531698000 |
| 17 | 0.211200000 | 1.538926000 | -2.530429000 |
| 17 | 2.026410000 | 2.707196000 | 0.024700000 |
| 17 | 3.800297000 | 0.042342000 | 0.871492000 |

| | | | |
|---|---|---|---|
| 17 | 2.087878000 | -2.661065000 | 0.023542000 |
| 17 | -0.816375000 | -1.709891000 | 2.690633000 |
| 17 | -0.886239000 | 1.691127000 | 2.690869000 |
| 17 | -3.515337000 | -0.040542000 | -0.664884000 |
| 6 | -0.847471000 | -0.693561000 | 1.372876000 |
| 6 | -0.870381000 | 0.674461000 | 1.373278000 |
| 6 | -0.995645000 | -1.173458000 | -0.089965000 |
| 6 | -1.935509000 | -0.021862000 | -0.344617000 |
| 6 | -1.023896000 | 1.150726000 | -0.090320000 |
| 6 | 0.270490000 | 0.797706000 | -0.934167000 |
| 6 | 0.289110000 | -0.791846000 | -0.934763000 |
| 6 | 1.591100000 | -1.119119000 | -0.252960000 |
| 6 | 1.564892000 | 1.154526000 | -0.252646000 |
| 6 | 2.301339000 | 0.025903000 | 0.107536000 |

**B3LYP-GD3BJ/Def2-TZVP with solvent model $\varepsilon_r$=23:**

$C_5Cl_5^+$trip HF=-2491.4730825

Sum of electronic and thermal Free Energies= -2491.463044

| | | | |
|---|---|---|---|
| 17 | 0.000000000 | 2.735724000 | 0.887247000 |
| 17 | 0.000000000 | 0.000000000 | 2.876693000 |
| 17 | 0.000000000 | -2.735724000 | 0.887247000 |
| 17 | 0.000000000 | -1.692158000 | -2.325646000 |
| 17 | 0.000000000 | 1.692158000 | -2.325646000 |
| 6 | 0.000000000 | 1.151263000 | 0.374130000 |
| 6 | 0.000000000 | 0.000000000 | 1.211265000 |
| 6 | 0.000000000 | -1.151263000 | 0.374130000 |
| 6 | 0.000000000 | -0.711682000 | -0.979613000 |
| 6 | 0.000000000 | 0.711682000 | -0.979613000 |

$C_{10}Cl_{10}^{2+}$ HF=-4982.967049

Sum of electronic and thermal Free Energies= -4982.924052

| | | | |
|---|---|---|---|
| 17 | -2.450970000 | -2.684756000 | 0.127777000 |
| 17 | 0.029038000 | -1.611820000 | 2.066897000 |
| 17 | 0.025352000 | 1.608078000 | 2.070507000 |
| 17 | -0.025546000 | -1.607956000 | -2.070512000 |
| 17 | 2.448971000 | -2.683688000 | -0.128722000 |
| 17 | -0.029036000 | 1.611913000 | -2.066745000 |
| 17 | -4.352438000 | 0.000836000 | -0.276004000 |
| 17 | -2.448867000 | 2.683656000 | 0.128077000 |
| 17 | 4.352497000 | -0.000992000 | 0.275773000 |

| | | | |
|---|---|---|---|
| 17 | 2.450906000 | 2.684757000 | -0.126993000 |
| 6 | -2.712981000 | -0.000184000 | 0.104083000 |
| 6 | -1.922644000 | 1.135861000 | 0.271097000 |
| 6 | -1.923963000 | -1.137105000 | 0.271913000 |
| 6 | -0.501408000 | 0.783985000 | 0.617962000 |
| 6 | -0.501341000 | -0.785554000 | 0.616593000 |
| 6 | 0.501406000 | -0.783938000 | -0.617925000 |
| 6 | 0.501427000 | 0.785524000 | -0.616482000 |
| 6 | 1.922685000 | -1.135893000 | -0.271418000 |
| 6 | 2.713079000 | 0.000151000 | -0.104228000 |
| 6 | 1.924003000 | 1.137075000 | -0.271749000 |

$C_{10}Cl_{10}^{2+}$exo HF=-4982.9346319

Sum of electronic and thermal Free Energies= -4982.892349

| | | | |
|---|---|---|---|
| 17 | -0.886014000 | 0.000000000 | 2.955235000 |
| 17 | -3.376213000 | -1.700969000 | -0.490497000 |
| 17 | -3.376214000 | 1.700966000 | -0.490498000 |
| 17 | -0.732055000 | -2.765037000 | 1.040357000 |
| 17 | -0.732058000 | 2.765037000 | 1.040357000 |
| 17 | 0.036268000 | 1.561900000 | -2.207619000 |
| 17 | 0.036268000 | -1.561899000 | -2.207619000 |
| 17 | 2.358478000 | -2.671203000 | -0.103213000 |
| 17 | 2.358476000 | 2.671205000 | -0.103212000 |
| 17 | 4.157694000 | 0.000001000 | 0.534667000 |
| 6 | -2.105809000 | -0.684614000 | -0.154866000 |
| 6 | -0.737563000 | -1.159531000 | 0.385398000 |
| 6 | -2.105809000 | 0.684614000 | -0.154866000 |
| 6 | -0.737564000 | 1.159531000 | 0.385398000 |
| 6 | -0.756185000 | 0.000000000 | 1.343793000 |
| 6 | 0.380242000 | -0.798202000 | -0.658466000 |
| 6 | 0.380242000 | 0.798202000 | -0.658466000 |
| 6 | 1.786664000 | 1.136135000 | -0.216758000 |
| 6 | 1.786664000 | -1.136135000 | -0.216759000 |
| 6 | 2.549334000 | 0.000001000 | 0.036380000 |

$C_{10}Cl_{10}^{2+}$endo HF=-4982.9338988
Sum of electronic and thermal Free Energies= -4982.891798

| | | | |
|---|---|---|---|
| 17 | -1.638303000 | -2.762973000 | -0.283690000 |
| 17 | -1.641512000 | 2.761019000 | -0.285257000 |
| 17 | 0.242215000 | -1.537422000 | -2.528929000 |
| 17 | 0.241321000 | 1.537007000 | -2.529306000 |
| 17 | 2.055068000 | 2.684646000 | 0.035444000 |
| 17 | 3.803434000 | 0.001995000 | 0.874120000 |
| 17 | 2.058220000 | -2.682647000 | 0.035292000 |

| | | | |
|---|---|---|---|
| 17 | -0.865127000 | -1.699757000 | 2.688660000 |
| 17 | -0.867932000 | 1.700289000 | 2.687781000 |
| 17 | -3.512107000 | -0.002196000 | -0.677590000 |
| 6 | -0.862885000 | -0.684052000 | 1.370414000 |
| 6 | -0.863892000 | 0.683894000 | 1.370068000 |
| 6 | -1.008114000 | -1.162510000 | -0.093163000 |
| 6 | -1.933679000 | -0.001170000 | -0.351347000 |
| 6 | -1.009491000 | 1.161393000 | -0.093796000 |
| 6 | 0.283289000 | 0.794882000 | -0.932738000 |
| 6 | 0.284124000 | -0.794915000 | -0.932557000 |
| 6 | 1.580638000 | -1.135946000 | -0.247274000 |
| 6 | 1.579324000 | 1.137393000 | -0.247236000 |
| 6 | 2.304066000 | 0.001141000 | 0.110808000 |

**B3LYP-GD3BJ/Def2-TZVP without solvent model:**

$C_5Br_5^+$sing HF=-13061.1724738

Sum of electronic and thermal Free Energies= -13061.170006

| | | | |
|---|---|---|---|
| 35 | -3.100449000 | -0.028385000 | 0.000000000 |
| 35 | -0.918052000 | -2.825187000 | 0.000000000 |
| 35 | 2.491126000 | -1.845519000 | 0.000000000 |
| 35 | 2.453969000 | 1.787336000 | 0.000000000 |
| 35 | -0.934792000 | 2.887120000 | 0.000000000 |
| 6 | -1.244274000 | 0.038856000 | 0.000000000 |
| 6 | -0.360969000 | -1.109386000 | 0.000000000 |
| 6 | 1.030035000 | -0.699173000 | 0.000000000 |
| 6 | 1.025604000 | 0.658952000 | 0.000000000 |
| 6 | -0.441748000 | 1.135388000 | 0.000000000 |

$C_5Br_5^+$trip HF=-13061.1846056

Sum of electronic and thermal Free Energies= -13061.181684

| | | | |
|---|---|---|---|
| 35 | -3.043417000 | 0.000006000 | 0.000000000 |
| 35 | -0.940604000 | -2.894661000 | 0.000000000 |
| 35 | 2.462291000 | -1.789061000 | 0.000000000 |
| 35 | 2.462317000 | 1.789031000 | 0.000000000 |
| 35 | -0.940552000 | 2.894682000 | 0.000000000 |
| 6 | -1.212321000 | 0.000017000 | 0.000000000 |
| 6 | -0.374568000 | -1.153102000 | 0.000000000 |
| 6 | 0.980925000 | -0.712695000 | 0.000000000 |
| 6 | 0.980932000 | 0.712684000 | 0.000000000 |
| 6 | -0.374556000 | 1.153104000 | 0.000000000 |

$C_{10}Br_{10}^{2+}$ HF=-26122.3146486
Sum of electronic and thermal Free Energies= -26122.286541

| | | | |
|---|---|---|---|
| 35 | -2.841237000 | -4.381696000 | -0.083774000 |
| 35 | 0.440877000 | -3.339976000 | -0.731297000 |
| 35 | -6.855612000 | -1.279170000 | 0.053696000 |
| 35 | -6.662813000 | 2.181100000 | 0.569869000 |
| 35 | -4.002665000 | -1.963610000 | 2.178057000 |
| 35 | 0.633674000 | 0.120328000 | -0.215366000 |
| 35 | -1.935053000 | 0.715075000 | 2.099833000 |
| 35 | -4.286802000 | -1.873891000 | -2.261405000 |
| 35 | -2.219296000 | 0.804870000 | -2.339607000 |
| 35 | -3.380730000 | 3.222884000 | -0.077700000 |
| 6 | -2.261559000 | -2.671045000 | 0.064005000 |
| 6 | -0.953913000 | -2.247511000 | -0.189432000 |
| 6 | -0.869087000 | -0.866898000 | 0.011218000 |
| 6 | -3.139979000 | -1.533213000 | 0.501082000 |
| 6 | -2.179685000 | -0.289104000 | 0.464727000 |
| 6 | -3.081952000 | 0.374417000 | -0.662635000 |
| 6 | -4.042239000 | -0.869702000 | -0.626302000 |
| 6 | -3.960385000 | 1.512227000 | -0.225512000 |
| 6 | -5.352845000 | -0.291931000 | -0.172792000 |
| 6 | -5.268023000 | 1.088672000 | 0.027927000 |

$C_{10}Br_{10}^{2+}$exo HF=-26122.2779017
Sum of electronic and thermal Free Energies= -26122.250623

| | | | |
|---|---|---|---|
| 35 | 4.336546000 | -0.000999000 | 0.653870000 |
| 35 | 2.493339000 | 2.820862000 | -0.117830000 |
| 35 | 2.493087000 | -2.821349000 | -0.123140000 |
| 35 | 0.050072000 | -1.663250000 | -2.342653000 |
| 35 | 0.053939000 | 1.664268000 | -2.342806000 |
| 35 | -0.748197000 | 2.914880000 | 1.137070000 |
| 35 | -0.745516000 | -2.913898000 | 1.139224000 |
| 35 | -3.497977000 | 1.779119000 | -0.575993000 |
| 35 | -3.498029000 | -1.780891000 | -0.571417000 |
| 35 | -1.042077000 | 0.001167000 | 3.111890000 |
| 6 | 2.571804000 | -0.000405000 | 0.081671000 |
| 6 | 1.815359000 | -1.139961000 | -0.196747000 |
| 6 | 1.815445000 | 1.139670000 | -0.194817000 |
| 6 | 0.411945000 | 0.801443000 | -0.636473000 |
| 6 | 0.411672000 | -0.800964000 | -0.636833000 |
| 6 | -0.800994000 | 0.000527000 | 1.332053000 |
| 6 | -0.729334000 | 1.161577000 | 0.380628000 |
| 6 | -2.084565000 | 0.688035000 | -0.183196000 |
| 6 | -0.728722000 | -1.161122000 | 0.381717000 |
| 6 | -2.084486000 | -0.688710000 | -0.181844000 |

$C_{10}Br_{10}^{2+}$endo HF=-26122.2791026
Sum of electronic and thermal Free Energies= -26122.252298

| | | | |
|---|---|---|---|
| 35 | -3.676287000 | -0.075590000 | -0.748656000 |
| 35 | -0.948296000 | 1.915308000 | 2.746997000 |
| 35 | -0.601364000 | -1.652560000 | 2.865973000 |
| 35 | 2.144688000 | -2.897399000 | -0.167488000 |
| 35 | 3.945687000 | -0.110075000 | 0.959216000 |
| 35 | 2.023031000 | 2.764312000 | 0.380954000 |
| 35 | 0.479305000 | 1.670051000 | -2.641957000 |
| 35 | 0.083932000 | -1.579591000 | -2.721791000 |
| 35 | -1.791274000 | 2.899926000 | -0.464160000 |
| 35 | -1.669163000 | -2.929808000 | -0.161065000 |
| 6 | 2.295126000 | -0.064372000 | 0.116917000 |
| 6 | 1.549916000 | 1.090353000 | -0.140477000 |
| 6 | 1.586716000 | -1.179760000 | -0.339612000 |
| 6 | 0.275929000 | -0.796372000 | -0.954371000 |
| 6 | 0.295635000 | 0.794211000 | -0.914316000 |
| 6 | -1.044543000 | 1.172549000 | -0.163244000 |
| 6 | -1.933856000 | -0.018730000 | -0.377790000 |
| 6 | -0.986530000 | -1.149277000 | -0.060635000 |
| 6 | -0.900463000 | 0.755738000 | 1.325948000 |
| 6 | -0.806881000 | -0.609262000 | 1.372056000 |

**B3LYP-GD3BJ/Def2-TZVP with solvent model $\varepsilon_r$=2:**

$C_5Br_5^+$trip HF=-13061.2192113

Sum of electronic and thermal Free Energies= -13061.215658

| | | | |
|---|---|---|---|
| 35 | -3.042226000 | 0.000003000 | 0.000000000 |
| 35 | -0.940436000 | -2.892942000 | 0.000000000 |
| 35 | 2.461440000 | -1.787838000 | 0.000000000 |
| 35 | 2.461465000 | 1.787809000 | 0.000000000 |
| 35 | -0.940381000 | 2.892965000 | 0.000000000 |
| 6 | -1.211709000 | 0.000016000 | 0.000000000 |
| 6 | -0.374269000 | -1.152245000 | 0.000000000 |
| 6 | 0.980407000 | -0.712267000 | 0.000000000 |
| 6 | 0.980413000 | 0.712256000 | 0.000000000 |
| 6 | -0.374257000 | 1.152247000 | 0.000000000 |

$C_{10}Br_{10}^{2+}$ HF=-26122.4280355
Sum of electronic and thermal Free Energies= -26122.397526

| | | | |
|---|---|---|---|
| 35 | -2.839336000 | -4.376420000 | -0.059313000 |
| 35 | 0.415617000 | -3.323251000 | -0.797890000 |
| 35 | -6.863586000 | -1.274994000 | 0.000505000 |
| 35 | -6.637787000 | 2.164470000 | 0.635757000 |
| 35 | -4.017836000 | -1.941598000 | 2.180312000 |

| | | | |
|---|---|---|---|
| 35 | 0.641643000 | 0.116110000 | -0.162413000 |
| 35 | -1.946724000 | 0.744455000 | 2.086916000 |
| 35 | -4.274858000 | -1.903220000 | -2.248375000 |
| 35 | -2.204165000 | 0.782867000 | -2.341660000 |
| 35 | -3.382708000 | 3.217625000 | -0.102132000 |
| 6 | -2.264964000 | -2.664812000 | 0.070361000 |
| 6 | -0.964355000 | -2.237913000 | -0.204597000 |
| 6 | -0.870069000 | -0.863314000 | 0.021765000 |
| 6 | -3.142819000 | -1.527075000 | 0.509223000 |
| 6 | -2.181918000 | -0.283958000 | 0.468488000 |
| 6 | -3.079073000 | 0.368264000 | -0.670499000 |
| 6 | -4.039916000 | -0.874863000 | -0.629836000 |
| 6 | -3.956966000 | 1.505959000 | -0.231664000 |
| 6 | -5.351842000 | -0.295562000 | -0.183314000 |
| 6 | -5.257664000 | 1.079056000 | 0.042958000 |

$C_{10}Br_{10}^{2+}$exo HF=-26122.3918002
Sum of electronic and thermal Free Energies= -26122.360983

| | | | |
|---|---|---|---|
| 35 | 4.313694000 | -0.006181000 | 0.695121000 |
| 35 | 2.491191000 | 2.817870000 | -0.107989000 |
| 35 | 2.487508000 | -2.819760000 | -0.146571000 |
| 35 | 0.020092000 | -1.646158000 | -2.347191000 |
| 35 | 0.076753000 | 1.658868000 | -2.350824000 |
| 35 | -0.752952000 | 2.913693000 | 1.132671000 |
| 35 | -0.729050000 | -2.909098000 | 1.143577000 |
| 35 | -3.499057000 | 1.768142000 | -0.600803000 |
| 35 | -3.498723000 | -1.785806000 | -0.555419000 |
| 35 | -0.998540000 | 0.004284000 | 3.110168000 |
| 6 | 2.564319000 | -0.002285000 | 0.083229000 |
| 6 | 1.810673000 | -1.139465000 | -0.204398000 |
| 6 | 1.810835000 | 1.139322000 | -0.186863000 |
| 6 | 0.410807000 | 0.803517000 | -0.638452000 |
| 6 | 0.407336000 | -0.797487000 | -0.642164000 |
| 6 | -0.790651000 | 0.003063000 | 1.329917000 |
| 6 | -0.732856000 | 1.162587000 | 0.375086000 |
| 6 | -2.086347000 | 0.684249000 | -0.185522000 |
| 6 | -0.726271000 | -1.158941000 | 0.383382000 |
| 6 | -2.085452000 | -0.690416000 | -0.172579000 |

$C_{10}Br_{10}^{2+}$endo HF=-26122.3939956
Sum of electronic and thermal Free Energies= -26122.363923

| | | | |
|---|---|---|---|
| 35 | -3.674687000 | -0.013084000 | -0.757517000 |
| 35 | -0.772522000 | 1.829288000 | 2.786625000 |
| 35 | -0.696072000 | -1.745795000 | 2.825028000 |
| 35 | 2.113691000 | -2.861792000 | 0.004887000 |
| 35 | 3.902664000 | -0.035300000 | 1.027203000 |
| 35 | 2.070758000 | 2.818430000 | 0.179936000 |

| | | | |
|---|---|---|---|
| 35 | 0.321157000 | 1.645377000 | -2.682983000 |
| 35 | 0.220059000 | -1.620382000 | -2.707737000 |
| 35 | -1.752572000 | 2.914136000 | -0.348038000 |
| 35 | -1.718505000 | -2.922961000 | -0.266483000 |
| 6 | 2.278404000 | -0.022137000 | 0.135411000 |
| 6 | 1.561115000 | 1.123775000 | -0.214573000 |
| 6 | 1.570753000 | -1.154635000 | -0.272569000 |
| 6 | 0.279592000 | -0.798180000 | -0.948113000 |
| 6 | 0.285745000 | 0.795480000 | -0.935961000 |
| 6 | -1.024993000 | 1.165070000 | -0.126493000 |
| 6 | -1.937242000 | -0.003819000 | -0.380076000 |
| 6 | -1.011746000 | -1.158017000 | -0.099088000 |
| 6 | -0.858913000 | 0.705198000 | 1.339885000 |
| 6 | -0.835377000 | -0.661005000 | 1.353154000 |

**B3LYP-GD3BJ/Def2-TZVP with solvent model $\varepsilon_r$=10**

$C_5Br_5^+$trip HF=-13061.2470708

Sum of electronic and thermal Free Energies= -13061.244543

| | | | |
|---|---|---|---|
| 35 | -3.041161000 | 0.000004000 | 0.000000000 |
| 35 | -0.940051000 | -2.892531000 | 0.000000000 |
| 35 | 2.460618000 | -1.787698000 | 0.000000000 |
| 35 | 2.460645000 | 1.787668000 | 0.000000000 |
| 35 | -0.939998000 | 2.892553000 | 0.000000000 |
| 6 | -1.210820000 | 0.000017000 | 0.000000000 |
| 6 | -0.374094000 | -1.151607000 | 0.000000000 |
| 6 | 0.979693000 | -0.711818000 | 0.000000000 |
| 6 | 0.979700000 | 0.711807000 | 0.000000000 |
| 6 | -0.374083000 | 1.151609000 | 0.000000000 |

$C_{10}Br_{10}^{2+}$ HF=-26122.5152669
Sum of electronic and thermal Free Energies= -26122.486282

| | | | |
|---|---|---|---|
| 35 | -2.851036000 | -4.370830000 | -0.087987000 |
| 35 | 0.429238000 | -3.333652000 | -0.745619000 |
| 35 | -6.846410000 | -1.286988000 | 0.047931000 |
| 35 | -6.651296000 | 2.174676000 | 0.584063000 |
| 35 | -4.010449000 | -1.955780000 | 2.176695000 |
| 35 | 0.624502000 | 0.128053000 | -0.209806000 |
| 35 | -1.939651000 | 0.726897000 | 2.092881000 |
| 35 | -4.282048000 | -1.885717000 | -2.254482000 |
| 35 | -2.211516000 | 0.797255000 | -2.338167000 |
| 35 | -3.370999000 | 3.212015000 | -0.073222000 |
| 6 | -2.264687000 | -2.666401000 | 0.066610000 |
| 6 | -0.960454000 | -2.241459000 | -0.188011000 |
| 6 | -0.871962000 | -0.864469000 | 0.015431000 |
| 6 | -3.142046000 | -1.529812000 | 0.504627000 |

| | | | |
|---|---|---|---|
| 6 | -2.181897000 | -0.287386000 | 0.466975000 |
| 6 | -3.079878000 | 0.371071000 | -0.666130000 |
| 6 | -4.039966000 | -0.871409000 | -0.628558000 |
| 6 | -3.957280000 | 1.507578000 | -0.227992000 |
| 6 | -5.349964000 | -0.294395000 | -0.177116000 |
| 6 | -5.261526000 | 1.082577000 | 0.026469000 |

$C_{10}Br_{10}^{2+}$exo HF=-26122.4805635
Sum of electronic and thermal Free Energies= -26122.452311

| | | | |
|---|---|---|---|
| 35 | 4.312610000 | -0.011205000 | 0.688321000 |
| 35 | 2.480730000 | 2.815804000 | -0.085310000 |
| 35 | 2.477805000 | -2.822530000 | -0.151740000 |
| 35 | 0.015368000 | -1.649144000 | -2.343915000 |
| 35 | 0.069390000 | 1.666469000 | -2.344287000 |
| 35 | -0.764652000 | 2.918606000 | 1.122397000 |
| 35 | -0.732592000 | -2.905965000 | 1.148325000 |
| 35 | -3.493477000 | 1.767505000 | -0.616295000 |
| 35 | -3.490171000 | -1.792959000 | -0.565466000 |
| 35 | -0.967688000 | 0.012762000 | 3.110378000 |
| 6 | 2.558644000 | -0.005386000 | 0.084690000 |
| 6 | 1.808118000 | -1.141210000 | -0.206755000 |
| 6 | 1.808506000 | 1.136959000 | -0.182029000 |
| 6 | 0.409780000 | 0.803911000 | -0.636913000 |
| 6 | 0.405771000 | -0.797518000 | -0.641471000 |
| 6 | -0.775847000 | 0.007192000 | 1.335706000 |
| 6 | -0.734701000 | 1.162745000 | 0.375821000 |
| 6 | -2.085023000 | 0.680249000 | -0.190246000 |
| 6 | -0.726276000 | -1.156222000 | 0.388070000 |
| 6 | -2.082987000 | -0.690065000 | -0.174908000 |

$C_{10}Br_{10}^{2+}$endo HF=-26122.4823529
Sum of electronic and thermal Free Energies= -26122.453957

| | | | |
|---|---|---|---|
| 35 | -3.674718000 | -0.003484000 | -0.737798000 |
| 35 | -0.771234000 | 1.807970000 | 2.795219000 |
| 35 | -0.725358000 | -1.774307000 | 2.808394000 |
| 35 | 2.074673000 | -2.850320000 | 0.085489000 |
| 35 | 3.925662000 | -0.019456000 | 0.984751000 |
| 35 | 2.060204000 | 2.828090000 | 0.163322000 |
| 35 | 0.312461000 | 1.640207000 | -2.688770000 |
| 35 | 0.253824000 | -1.629307000 | -2.700439000 |
| 35 | -1.735805000 | 2.916825000 | -0.333027000 |
| 35 | -1.728581000 | -2.915727000 | -0.295278000 |
| 6 | 2.289333000 | -0.011090000 | 0.115173000 |
| 6 | 1.564928000 | 1.130565000 | -0.228825000 |
| 6 | 1.568444000 | -1.145818000 | -0.257928000 |
| 6 | 0.281629000 | -0.796070000 | -0.944980000 |

| | | | |
|---|---|---|---|
| 6 | 0.285840000 | 0.795319000 | -0.938532000 |
| 6 | -1.018718000 | 1.162991000 | -0.120951000 |
| 6 | -1.937430000 | 0.000640000 | -0.374371000 |
| 6 | -1.013911000 | -1.157242000 | -0.108313000 |
| 6 | -0.851105000 | 0.692841000 | 1.342126000 |
| 6 | -0.838829000 | -0.672977000 | 1.347235000 |

**B3LYP-GD3BJ/Def2-TZVP with solvent model $\varepsilon_r$=23**

$C_5Br_5^+$trip HF=-13061.2511821
Sum of electronic and thermal Free Energies= -13061.248536

| | | | |
|---|---|---|---|
| 35 | -3.040986000 | 0.000004000 | 0.000000000 |
| 35 | -0.939779000 | -2.892442000 | 0.000000000 |
| 35 | 2.460254000 | -1.787717000 | 0.000000000 |
| 35 | 2.460281000 | 1.787687000 | 0.000000000 |
| 35 | -0.939727000 | 2.892465000 | 0.000000000 |
| 6 | -1.210633000 | 0.000017000 | 0.000000000 |
| 6 | -0.374024000 | -1.151477000 | 0.000000000 |
| 6 | 0.979533000 | -0.711709000 | 0.000000000 |
| 6 | 0.979540000 | 0.711697000 | 0.000000000 |
| 6 | -0.374013000 | 1.151479000 | 0.000000000 |

$C_{10}Br_{10}^{2+}$ HF=-26122.5279817
Sum of electronic and thermal Free Energies= -26122.499512

| | | | |
|---|---|---|---|
| 35 | -2.852723000 | -4.370673000 | -0.096715000 |
| 35 | 0.435573000 | -3.336899000 | -0.727453000 |
| 35 | -6.843181000 | -1.287680000 | 0.062542000 |
| 35 | -6.657479000 | 2.178024000 | 0.566098000 |
| 35 | -4.006215000 | -1.961652000 | 2.175921000 |
| 35 | 0.621235000 | 0.128855000 | -0.224191000 |
| 35 | -1.936273000 | 0.720618000 | 2.095122000 |
| 35 | -4.285623000 | -1.879402000 | -2.256739000 |
| 35 | -2.215755000 | 0.802880000 | -2.337506000 |
| 35 | -3.369194000 | 3.211834000 | -0.064674000 |
| 6 | -2.263946000 | -2.667659000 | 0.064915000 |
| 6 | -0.958451000 | -2.243439000 | -0.182822000 |
| 6 | -0.872169000 | -0.865313000 | 0.012932000 |
| 6 | -3.141205000 | -1.531231000 | 0.502649000 |
| 6 | -2.181448000 | -0.288715000 | 0.466039000 |
| 6 | -3.080738000 | 0.372433000 | -0.664234000 |
| 6 | -4.040487000 | -0.870093000 | -0.627643000 |
| 6 | -3.957995000 | 1.508841000 | -0.226440000 |
| 6 | -5.349772000 | -0.293507000 | -0.174529000 |
| 6 | -5.263479000 | 1.084605000 | 0.021321000 |

$C_{10}Br_{10}^{2+}$exo HF=-26122.4939119
Sum of electronic and thermal Free Energies= -26122.466199

| | | | |
|---|---|---|---|
| 35 | 4.313705000 | -0.011119000 | 0.683645000 |
| 35 | 2.477988000 | 2.815814000 | -0.082426000 |
| 35 | 2.475837000 | -2.822694000 | -0.146562000 |
| 35 | 0.018130000 | -1.652172000 | -2.342418000 |
| 35 | 0.063047000 | 1.668535000 | -2.341563000 |
| 35 | -0.766799000 | 2.919725000 | 1.120515000 |
| 35 | -0.737196000 | -2.907044000 | 1.147090000 |
| 35 | -3.491704000 | 1.769483000 | -0.620536000 |
| 35 | -3.488871000 | -1.792829000 | -0.574486000 |
| 35 | -0.953102000 | 0.013001000 | 3.111946000 |
| 6 | 2.557991000 | -0.005309000 | 0.085137000 |
| 6 | 1.807533000 | -1.141071000 | -0.205389000 |
| 6 | 1.808057000 | 1.136532000 | -0.182486000 |
| 6 | 0.408887000 | 0.803548000 | -0.636069000 |
| 6 | 0.405316000 | -0.797996000 | -0.640269000 |
| 6 | -0.772628000 | 0.006832000 | 1.338339000 |
| 6 | -0.735575000 | 1.162016000 | 0.377640000 |
| 6 | -2.085527000 | 0.679960000 | -0.190411000 |
| 6 | -0.728014000 | -1.156066000 | 0.389059000 |
| 6 | -2.083766000 | -0.689150000 | -0.176382000 |

$C_{10}Br_{10}^{2+}$endo HF=-26122.4953277
Sum of electronic and thermal Free Energies= -26122.467367

| | | | |
|---|---|---|---|
| 35 | -3.676733000 | 0.000445000 | -0.729313000 |
| 35 | -0.765473000 | 1.799482000 | 2.798327000 |
| 35 | -0.742915000 | -1.782967000 | 2.803798000 |
| 35 | 2.066224000 | -2.846219000 | 0.108181000 |
| 35 | 3.931335000 | -0.012397000 | 0.973872000 |
| 35 | 2.062036000 | 2.831875000 | 0.150442000 |
| 35 | 0.305233000 | 1.638819000 | -2.691040000 |
| 35 | 0.271560000 | -1.632302000 | -2.698176000 |
| 35 | -1.730945000 | 2.917948000 | -0.324725000 |
| 35 | -1.731582000 | -2.914627000 | -0.306199000 |
| 6 | 2.291420000 | -0.007207000 | 0.111508000 |
| 6 | 1.566448000 | 1.133022000 | -0.234791000 |
| 6 | 1.566913000 | -1.142837000 | -0.250618000 |
| 6 | 0.282358000 | -0.795623000 | -0.943589000 |
| 6 | 0.285579000 | 0.795311000 | -0.939752000 |
| 6 | -1.016666000 | 1.162083000 | -0.118359000 |
| 6 | -1.938331000 | 0.001761000 | -0.372416000 |
| 6 | -1.015648000 | -1.157597000 | -0.112371000 |
| 6 | -0.847561000 | 0.688295000 | 1.342740000 |
| 6 | -0.841942000 | -0.677614000 | 1.344976000 |

**MP2/cc-PVTZ (without solvent):**

$C_5Cl_5^+$sing MP2=-2488.3011085

Sum of electronic and thermal Free Energies= -2488.291834

| | | | |
|---|---|---|---|
| 17 | 0.863060000 | -2.674229000 | 0.000000000 |
| 17 | 2.937720000 | -0.000951000 | 0.000000000 |
| 17 | 0.863060000 | 2.676225000 | 0.000000000 |
| 17 | -2.325886000 | 1.749475000 | 0.000000000 |
| 17 | -2.326387000 | -1.750865000 | 0.000000000 |
| 6 | 0.401383000 | -1.105716000 | 0.000000000 |
| 6 | 1.254259000 | 0.000849000 | 0.000000000 |
| 6 | 0.403188000 | 1.106792000 | 0.000000000 |
| 6 | -1.045803000 | 0.674834000 | 0.000000000 |
| 6 | -1.045803000 | -0.675782000 | 0.000000000 |

$C_5Cl_5^+$trip MP2=-2488.3099986
Sum of electronic and thermal Free Energies= -2488.297552

| | | | |
|---|---|---|---|
| 17 | -0.887538000 | 2.731587000 | 0.000000000 |
| 17 | -2.872164000 | 0.000000000 | 0.000000000 |
| 17 | -0.887538000 | -2.731587000 | 0.000000000 |
| 17 | 2.323620000 | -1.688228000 | 0.000000000 |
| 17 | 2.323620000 | 1.688228000 | 0.000000000 |
| 6 | -0.375315000 | 1.155097000 | 0.000000000 |
| 6 | -1.214560000 | 0.000000000 | 0.000000000 |
| 6 | -0.375315000 | -1.155098000 | 0.000000000 |
| 6 | 0.982597000 | -0.713895000 | 0.000000000 |
| 6 | 0.982596000 | 0.713895000 | 0.000000000 |

$C_{10}Cl_{10}^{2+}$ MP2=-4976.5986755
Sum of electronic and thermal Free Energies= -4976.556388

| | | | |
|---|---|---|---|
| 17 | -2.435550000 | -2.680403000 | 0.189064000 |
| 17 | 0.076448000 | -1.604146000 | 2.061405000 |
| 17 | 0.076554000 | 1.604055000 | 2.061422000 |
| 17 | -0.076447000 | -1.604145000 | -2.061405000 |
| 17 | 2.435550000 | -2.680403000 | -0.189065000 |
| 17 | -0.076555000 | 1.604057000 | -2.061421000 |
| 17 | -4.318201000 | 0.000047000 | -0.304019000 |
| 17 | -2.435499000 | 2.680441000 | 0.189244000 |
| 17 | 4.318201000 | 0.000049000 | 0.304019000 |
| 17 | 2.435499000 | 2.680441000 | -0.189243000 |
| 6 | -2.697648000 | 0.000023000 | 0.098382000 |
| 6 | -1.900000000 | 1.135304000 | 0.296590000 |
| 6 | -1.900020000 | -1.135286000 | 0.296518000 |
| 6 | -0.482547000 | 0.782558000 | 0.632470000 |
| 6 | -0.482564000 | -0.782588000 | 0.632450000 |
| 6 | 0.482563000 | -0.782588000 | -0.632450000 |

| | | | |
|---|---|---|---|
| 6 | 0.482547000 | 0.782558000 | -0.632470000 |
| 6 | 1.900020000 | -1.135286000 | -0.296519000 |
| 6 | 2.697648000 | 0.000023000 | -0.098383000 |
| 6 | 1.899999000 | 1.135303000 | -0.296589000 |

$C_{10}Cl_{10}^{2+}$exo MP2=-4976.5772402
Sum of electronic and thermal Free Energies= -4976.535729

| | | | |
|---|---|---|---|
| 17 | -2.836111000 | -1.278728000 | 0.000000000 |
| 17 | 0.477407000 | -3.365475000 | 1.676175000 |
| 17 | 0.477407000 | -3.365475000 | -1.676175000 |
| 17 | -0.977377000 | -0.719785000 | 2.755992000 |
| 17 | -0.977377000 | -0.719785000 | -2.755992000 |
| 17 | 2.223439000 | 0.156444000 | -1.557152000 |
| 17 | 2.223439000 | 0.156444000 | 1.557152000 |
| 17 | 0.078454000 | 2.401447000 | 2.661059000 |
| 17 | 0.078454000 | 2.401447000 | -2.661059000 |
| 17 | -0.806291000 | 4.108349000 | 0.000000000 |
| 6 | 0.249900000 | -2.049890000 | 0.701083000 |
| 6 | -0.309789000 | -0.707487000 | 1.167826000 |
| 6 | 0.249900000 | -2.049890000 | -0.701083000 |
| 6 | -0.309789000 | -0.707487000 | -1.167826000 |
| 6 | -1.239558000 | -0.896729000 | 0.000000000 |
| 6 | 0.674342000 | 0.436379000 | 0.791812000 |
| 6 | 0.674342000 | 0.436379000 | -0.791812000 |
| 6 | 0.154920000 | 1.810575000 | -1.133911000 |
| 6 | 0.154920000 | 1.810575000 | 1.133911000 |
| 6 | -0.189947000 | 2.555405000 | 0.000000000 |

$C_{10}Cl_{10}^{2+}$endo MP2=-4976.5747062
Sum of electronic and thermal Free Energies= -4976.532167

| | | | |
|---|---|---|---|
| 17 | 1.562659000 | 2.764995000 | -0.406092000 |
| 17 | 1.589780000 | -2.748949000 | -0.418246000 |
| 17 | -0.418185000 | 1.533719000 | -2.541185000 |
| 17 | -0.409562000 | -1.531773000 | -2.543983000 |
| 17 | -2.017957000 | -2.690204000 | 0.146024000 |
| 17 | -3.697809000 | -0.016710000 | 1.157959000 |
| 17 | -2.045479000 | 2.673162000 | 0.144444000 |
| 17 | 1.071326000 | 1.681762000 | 2.588727000 |
| 17 | 1.090372000 | -1.683013000 | 2.581646000 |
| 17 | 3.492109000 | 0.017890000 | -0.621293000 |
| 6 | 0.888056000 | 0.699177000 | 1.263570000 |
| 6 | 0.895719000 | -0.696942000 | 1.260702000 |
| 6 | 0.944928000 | 1.175304000 | -0.189048000 |
| 6 | 1.881470000 | 0.009412000 | -0.373241000 |
| 6 | 0.956540000 | -1.166423000 | -0.193974000 |
| 6 | -0.355774000 | -0.789397000 | -0.964715000 |

| | | | |
|---|---|---|---|
| 6 | -0.362683000 | 0.788767000 | -0.963213000 |
| 6 | -1.593966000 | 1.127394000 | -0.175706000 |
| 6 | -1.582595000 | -1.140005000 | -0.175341000 |
| 6 | -2.287247000 | -0.009776000 | 0.261628000 |

---

**MP2/cc-PVTZ solvent model $\varepsilon_r$=2:**

$C_5Cl_5^+$trip MP2=-2488.3466052
Sum of electronic and thermal Free Energies= -2488.334168

| | | | |
|---|---|---|---|
| 17 | 0.882172000 | -2.731963000 | 0.000000000 |
| 17 | 2.872876000 | 0.000000000 | 0.000000000 |
| 17 | 0.882172000 | 2.731964000 | 0.000000000 |
| 17 | -2.318763000 | 1.694248000 | 0.000000000 |
| 17 | -2.318763000 | -1.694248000 | 0.000000000 |
| 6 | 0.375058000 | -1.153740000 | 0.000000000 |
| 6 | 1.214979000 | 0.000000000 | 0.000000000 |
| 6 | 0.375058000 | 1.153739000 | 0.000000000 |
| 6 | -0.982113000 | 0.713599000 | 0.000000000 |
| 6 | -0.982113000 | -0.713598000 | 0.000000000 |

$C_{10}Cl_{10}^{2+}$ MP2=-4976.7187775
Sum of electronic and thermal Free Energies= -4976.673239

| | | | |
|---|---|---|---|
| 17 | -0.074440000 | 2.440957000 | -2.681023000 |
| 17 | -2.064628000 | 0.033339000 | -1.597295000 |
| 17 | -2.064617000 | 0.032857000 | 1.597078000 |
| 17 | 2.064628000 | -0.033339000 | -1.597295000 |
| 17 | 0.074440000 | -2.440957000 | -2.681023000 |
| 17 | 2.064617000 | -0.032857000 | 1.597078000 |
| 17 | 0.599665000 | 4.271143000 | 0.000137000 |
| 17 | -0.074793000 | 2.440789000 | 2.681109000 |
| 17 | -0.599665000 | -4.271143000 | 0.000137000 |
| 17 | 0.074793000 | -2.440789000 | 2.681109000 |
| 6 | 0.074440000 | 2.685594000 | 0.000061000 |
| 6 | -0.190005000 | 1.910208000 | 1.135570000 |
| 6 | -0.189796000 | 1.910269000 | -1.135530000 |
| 6 | -0.605703000 | 0.515473000 | 0.782474000 |
| 6 | -0.605644000 | 0.515541000 | -0.782589000 |
| 6 | 0.605644000 | -0.515541000 | -0.782589000 |
| 6 | 0.605703000 | -0.515473000 | 0.782474000 |
| 6 | 0.189796000 | -1.910269000 | -1.135530000 |
| 6 | -0.074440000 | -2.685594000 | 0.000061000 |
| 6 | 0.190005000 | -1.910208000 | 1.135570000 |

$C_{10}Cl_{10}^{2+}$exo MP2=-4976.6979669
Sum of electronic and thermal Free Energies= -4976.654195

| | | | |
|---|---|---|---|
| 17 | -2.825140000 | -1.343139000 | 0.000000000 |
| 17 | 0.528115000 | -3.345788000 | 1.693835000 |
| 17 | 0.528115000 | -3.345788000 | -1.693835000 |
| 17 | -0.986055000 | -0.735547000 | 2.752279000 |
| 17 | -0.986055000 | -0.735547000 | -2.752279000 |
| 17 | 2.208977000 | 0.184622000 | -1.538408000 |
| 17 | 2.208977000 | 0.184622000 | 1.538408000 |
| 17 | 0.000827000 | 2.376506000 | 2.667622000 |
| 17 | 0.000827000 | 2.376506000 | -2.667622000 |
| 17 | -0.705119000 | 4.159401000 | 0.000000000 |
| 6 | 0.271795000 | -2.047819000 | 0.700623000 |
| 6 | -0.315585000 | -0.716405000 | 1.166813000 |
| 6 | 0.271795000 | -2.047819000 | -0.700623000 |
| 6 | -0.315585000 | -0.716405000 | -1.166813000 |
| 6 | -1.239141000 | -0.931127000 | 0.000000000 |
| 6 | 0.647150000 | 0.441722000 | 0.789944000 |
| 6 | 0.647150000 | 0.441722000 | -0.789944000 |
| 6 | 0.132594000 | 1.815296000 | -1.134039000 |
| 6 | 0.132594000 | 1.815296000 | 1.134039000 |
| 6 | -0.157597000 | 2.580636000 | 0.000000000 |

$C_{10}Cl_{10}^{2+}$endo MP2=-4976.6966016
Sum of electronic and thermal Free Energies= -4976.652572

| | | | |
|---|---|---|---|
| 17 | 1.549029000 | 2.766238000 | -0.415668000 |
| 17 | 1.572459000 | -2.751367000 | -0.424270000 |
| 17 | -0.419050000 | 1.525073000 | -2.555681000 |
| 17 | -0.414079000 | -1.525135000 | -2.556395000 |
| 17 | -1.971988000 | -2.690038000 | 0.171831000 |
| 17 | -3.693835000 | -0.014437000 | 1.143185000 |
| 17 | -2.002453000 | 2.672061000 | 0.170345000 |
| 17 | 1.039125000 | 1.696463000 | 2.572443000 |
| 17 | 1.058225000 | -1.695439000 | 2.566742000 |
| 17 | 3.501296000 | 0.017123000 | -0.560688000 |
| 6 | 0.872458000 | 0.700004000 | 1.256006000 |
| 6 | 0.879590000 | -0.695941000 | 1.253907000 |
| 6 | 0.942907000 | 1.173601000 | -0.196336000 |
| 6 | 1.885535000 | 0.008949000 | -0.356546000 |
| 6 | 0.953802000 | -1.164612000 | -0.200238000 |
| 6 | -0.351900000 | -0.786841000 | -0.976253000 |
| 6 | -0.358457000 | 0.786142000 | -0.975604000 |
| 6 | -1.584759000 | 1.125756000 | -0.182903000 |
| 6 | -1.573652000 | -1.138736000 | -0.181772000 |
| 6 | -2.285252000 | -0.009855000 | 0.242851000 |

**MP2/cc-PVTZ solvent model $\varepsilon_r$=10:**

$C_5Cl_5^+$trip MP2=-2488.3759556
Sum of electronic and thermal Free Energies= -2488.362671

| | | | |
|---|---|---|---|
| 17 | 0.884995000 | -2.730536000 | 0.000000000 |
| 17 | 2.871241000 | 0.000000000 | 0.000000000 |
| 17 | 0.884995000 | 2.730536000 | 0.000000000 |
| 17 | -2.320593000 | 1.690177000 | 0.000000000 |
| 17 | -2.320593000 | -1.690177000 | 0.000000000 |
| 6 | 0.374700000 | -1.153176000 | 0.000000000 |
| 6 | 1.213287000 | 0.000000000 | 0.000000000 |
| 6 | 0.374700000 | 1.153176000 | 0.000000000 |
| 6 | -0.981408000 | 0.712927000 | 0.000000000 |
| 6 | -0.981408000 | -0.712927000 | 0.000000000 |

$C_{10}Cl_{10}^{2+}$ MP2=-4976.810743
Sum of electronic and thermal Free Energies= -4976.766702

| | | | |
|---|---|---|---|
| 17 | -0.006645000 | 2.464537000 | -2.655515000 |
| 17 | -2.049163000 | 0.059819000 | -1.654013000 |
| 17 | -2.071795000 | -0.049659000 | 1.554649000 |
| 17 | 2.049163000 | -0.059819000 | -1.654013000 |
| 17 | 0.006645000 | -2.464537000 | -2.655515000 |
| 17 | 2.071795000 | 0.049659000 | 1.554649000 |
| 17 | 0.479603000 | 4.294004000 | 0.054895000 |
| 17 | -0.166940000 | 2.401242000 | 2.697419000 |
| 17 | -0.479603000 | -4.294004000 | 0.054895000 |
| 17 | 0.166940000 | -2.401242000 | 2.697419000 |
| 6 | 0.006645000 | 2.691349000 | 0.025201000 |
| 6 | -0.254464000 | 1.894688000 | 1.143745000 |
| 6 | -0.187495000 | 1.918065000 | -1.123627000 |
| 6 | -0.623699000 | 0.496436000 | 0.762991000 |
| 6 | -0.603128000 | 0.515281000 | -0.801040000 |
| 6 | 0.603128000 | -0.515281000 | -0.801040000 |
| 6 | 0.623699000 | -0.496436000 | 0.762991000 |
| 6 | 0.187495000 | -1.918065000 | -1.123627000 |
| 6 | -0.006645000 | -2.691349000 | 0.025201000 |
| 6 | 0.254464000 | -1.894688000 | 1.143745000 |

$C_{10}Cl_{10}^{2+}$exo MP2=-4976.791418
Sum of electronic and thermal Free Energies= -4976.748557

| | | | |
|---|---|---|---|
| 17 | -2.829703000 | -1.306050000 | 0.000000000 |
| 17 | 0.501607000 | -3.354892000 | 1.678522000 |
| 17 | 0.501607000 | -3.354892000 | -1.678522000 |
| 17 | -0.980756000 | -0.723457000 | 2.754050000 |
| 17 | -0.980756000 | -0.723457000 | -2.754050000 |
| 17 | 2.210411000 | 0.160324000 | -1.554075000 |
| 17 | 2.210411000 | 0.160324000 | 1.554075000 |

| | | | |
|---|---|---|---|
| 17 | 0.040135000 | 2.386243000 | 2.663451000 |
| 17 | 0.040135000 | 2.386243000 | -2.663451000 |
| 17 | -0.745749000 | 4.136302000 | 0.000000000 |
| 6 | 0.257359000 | -2.043974000 | 0.698962000 |
| 6 | -0.316025000 | -0.709453000 | 1.166467000 |
| 6 | 0.257359000 | -2.043974000 | -0.698962000 |
| 6 | -0.316025000 | -0.709453000 | -1.166467000 |
| 6 | -1.242802000 | -0.913869000 | 0.000000000 |
| 6 | 0.659135000 | 0.440062000 | 0.790410000 |
| 6 | 0.659135000 | 0.440062000 | -0.790410000 |
| 6 | 0.148858000 | 1.815835000 | -1.133108000 |
| 6 | 0.148858000 | 1.815835000 | 1.133108000 |
| 6 | -0.163319000 | 2.569982000 | 0.000000000 |

$C_{10}Cl_{10}^{2+}$endo MP2=-4976.7909901
Sum of electronic and thermal Free Energies= -4976.748572

| | | | |
|---|---|---|---|
| 17 | 2.272250000 | 2.159268000 | -0.780331000 |
| 17 | 0.732461000 | -3.077555000 | -0.020779000 |
| 17 | -0.190786000 | 1.434548000 | -2.633450000 |
| 17 | -0.661726000 | -1.597922000 | -2.441477000 |
| 17 | -2.762894000 | -2.074089000 | 0.073661000 |
| 17 | -3.542592000 | 0.952280000 | 1.170471000 |
| 17 | -1.175501000 | 3.045227000 | 0.152436000 |
| 17 | 1.637425000 | 1.642177000 | 2.341907000 |
| 17 | 0.560788000 | -1.511218000 | 2.781797000 |
| 17 | 3.343647000 | -1.021483000 | -0.548388000 |
| 6 | 1.102835000 | 0.609645000 | 1.160433000 |
| 6 | 0.670238000 | -0.704906000 | 1.339788000 |
| 6 | 1.241843000 | 0.857105000 | -0.342671000 |
| 6 | 1.804678000 | -0.537356000 | -0.342333000 |
| 6 | 0.583318000 | -1.363729000 | -0.032031000 |
| 6 | -0.558359000 | -0.753037000 | -0.919472000 |
| 6 | -0.165268000 | 0.767910000 | -1.019817000 |
| 6 | -1.215296000 | 1.439574000 | -0.181031000 |
| 6 | -1.867019000 | -0.730267000 | -0.193246000 |
| 6 | -2.200672000 | 0.553236000 | 0.258805000 |

**MP2/cc-PVTZ solvent model $\varepsilon_r$=23:**

$C_5Cl_5^+$trip MP2=-2488.3802615
Sum of electronic and thermal Free Energies= -2488.366842

| | | | |
|---|---|---|---|
| 17 | 0.000000000 | 2.730427000 | 0.885372000 |
| 17 | 0.000000000 | 0.000000000 | 2.871124000 |
| 17 | 0.000000000 | -2.730427000 | 0.885372000 |
| 17 | 0.000000000 | -1.689170000 | -2.320973000 |
| 17 | 0.000000000 | 1.689170000 | -2.320973000 |
| 6 | 0.000000000 | 1.153131000 | 0.374726000 |

| | | | |
|---|---|---|---|
| 6 | 0.000000000 | 0.000000000 | 1.213102000 |
| 6 | 0.000000000 | -1.153131000 | 0.374726000 |
| 6 | 0.000000000 | -0.712804000 | -0.981165000 |
| 6 | 0.000000000 | 0.712804000 | -0.981165000 |

$C_{10}Cl_{10}^{2+}$ MP2=-4976.824129
Sum of electronic and thermal Free Energies= -4976.780440

| | | | |
|---|---|---|---|
| 17 | -0.019405000 | 2.455218000 | -2.660658000 |
| 17 | -2.052086000 | 0.047687000 | -1.643158000 |
| 17 | -2.068899000 | -0.040453000 | 1.565687000 |
| 17 | 2.052086000 | -0.047687000 | -1.643158000 |
| 17 | 0.019405000 | -2.455218000 | -2.660658000 |
| 17 | 2.068899000 | 0.040453000 | 1.565687000 |
| 17 | 0.477962000 | 4.294219000 | 0.043710000 |
| 17 | -0.146961000 | 2.405235000 | 2.693673000 |
| 17 | -0.477962000 | -4.294219000 | 0.043710000 |
| 17 | 0.146961000 | -2.405235000 | 2.693673000 |
| 6 | 0.004984000 | 2.691184000 | 0.019825000 |
| 6 | -0.247252000 | 1.896531000 | 1.141649000 |
| 6 | -0.193983000 | 1.915109000 | -1.125808000 |
| 6 | -0.621776000 | 0.498112000 | 0.766825000 |
| 6 | -0.605305000 | 0.513026000 | -0.797039000 |
| 6 | 0.605305000 | -0.513026000 | -0.797039000 |
| 6 | 0.621776000 | -0.498112000 | 0.766825000 |
| 6 | 0.193983000 | -1.915109000 | -1.125808000 |
| 6 | -0.004984000 | -2.691184000 | 0.019825000 |
| 6 | 0.247252000 | -1.896531000 | 1.141649000 |

$C_{10}Cl_{10}^{2+}$ exo MP2=-4976.8052274
Sum of electronic and thermal Free Energies= -4976.762316

| | | | |
|---|---|---|---|
| 17 | -2.832695000 | -1.287951000 | 0.000000000 |
| 17 | 0.504414000 | -3.356437000 | 1.676066000 |
| 17 | 0.504414000 | -3.356437000 | -1.676066000 |
| 17 | -0.978589000 | -0.726819000 | 2.754379000 |
| 17 | -0.978589000 | -0.726819000 | -2.754379000 |
| 17 | 2.210918000 | 0.159981000 | -1.555415000 |
| 17 | 2.210918000 | 0.159981000 | 1.555415000 |
| 17 | 0.040470000 | 2.385955000 | 2.662810000 |
| 17 | 0.040470000 | 2.385955000 | -2.662810000 |
| 17 | -0.752930000 | 4.132075000 | 0.000000000 |
| 6 | 0.257035000 | -2.044535000 | 0.698321000 |
| 6 | -0.315517000 | -0.709958000 | 1.166096000 |
| 6 | 0.257035000 | -2.044535000 | -0.698321000 |
| 6 | -0.315517000 | -0.709958000 | -1.166096000 |
| 6 | -1.243685000 | -0.909074000 | 0.000000000 |
| 6 | 0.660160000 | 0.439576000 | 0.790604000 |

| | | | |
|---|---|---|---|
| 6 | 0.660160000 | 0.439576000 | -0.790604000 |
| 6 | 0.148606000 | 1.814830000 | -1.132807000 |
| 6 | 0.148606000 | 1.814830000 | 1.132807000 |
| 6 | -0.165812000 | 2.567507000 | 0.000000000 |

$C_{10}Cl_{10}^{2+}$endo MP2=-4976.8047703
Sum of electronic and thermal Free Energies= -4976.762677

| | | | |
|---|---|---|---|
| 17 | 2.275487000 | 2.154059000 | -0.799243000 |
| 17 | 0.722566000 | -3.073535000 | -0.000123000 |
| 17 | -0.210364000 | 1.443515000 | -2.627633000 |
| 17 | -0.638459000 | -1.598406000 | -2.446270000 |
| 17 | -2.773824000 | -2.077232000 | 0.038610000 |
| 17 | -3.543527000 | 0.935222000 | 1.174186000 |
| 17 | -1.160624000 | 3.032559000 | 0.189606000 |
| 17 | 1.657421000 | 1.650962000 | 2.329464000 |
| 17 | 0.546123000 | -1.486190000 | 2.790326000 |
| 17 | 3.339732000 | -1.031131000 | -0.549206000 |
| 6 | 1.110508000 | 0.617176000 | 1.155111000 |
| 6 | 0.665654000 | -0.692249000 | 1.342707000 |
| 6 | 1.244779000 | 0.856405000 | -0.349586000 |
| 6 | 1.803709000 | -0.539225000 | -0.341264000 |
| 6 | 0.579358000 | -1.359232000 | -0.024758000 |
| 6 | -0.557339000 | -0.753353000 | -0.922720000 |
| 6 | -0.166455000 | 0.767623000 | -1.017846000 |
| 6 | -1.211751000 | 1.432096000 | -0.167128000 |
| 6 | -1.871850000 | -0.734350000 | -0.208590000 |
| 6 | -2.201774000 | 0.544695000 | 0.258629000 |

# 4 References


1. D. R. Aris, C. Knapp, J. Passmore and X. Wang, *J. Fluorine Chem.*, 2005, **126**, 1368-1372.
2. J. Kovacs and C. S. Marvel, *J. Polym. Sci. Pol. Chem.*, 1967, **5**, 1279-1287.
3. V. P. Reddy, D. R. Bellew and G. K. S. Prakash, *J. Fluorine Chem.*, 1992, **56**, 195-197.
4. R. K. Harris, E. D. Becker, S. M. C. de Menezes, P. Granger, R. E. Hoffmann and K. W. Zilm, *Pure Appl. Chem.*, 2008, **80**, 59.
5. O. V. Dolomanov, L. J. Bourhis, R. J. Gildea, J. A. K. Howard and H. Puschmann, *J. Appl. Cryst.*, 2009, **42**, 339-341.
6. G. M. Sheldrick, *Acta Cryst.*, 2015, **C71**, 3-8.
7. G. Sheldrick, *Acta Cryst.*, 2008, **A64**, 112-122.
8. Diamond - Crystal and Molecular Structure Visualization Crystal Impact - Dr. H. Putz & Dr. K. Brandenburg GbR, Kreuzherrenstr. 102, 53227 Bonn, Germany http://www.crystalimpact.com/diamond
9. C. F. Macrae, P. R. Edgington, P. McCabe, E. Pidcock, G. P. Shields, R. Taylor, M. Towler and J. van de Streek, *J. Appl. Cryst.*, 2006, **39**, 453-457.
10. M. J. Frisch, G. W. Trucks, H. B. Schlegel, G. E. Scuseria, M. A. Robb, J. R. Cheeseman, G. Scalmani, V. Barone, G. A. Petersson, H. Nakatsuji, X. Li, M. Caricato, A. V. Marenich, J. Bloino, B. G. Janesko, R. Gomperts, B. Mennucci, H. P. Hratchian, J. V. Ortiz, A. F. Izmaylov, J. L.

Sonnenberg, D. Williams-Young, F. Ding, F. Lipparini, F. Egidi, J. Goings, B. Peng, A. Petrone, T. Henderson, D. Ranasinghe, V. G. Zakrzewski, J. Gao, N. Rega, G. Zheng, W. Liang, M. Hada, M. Ehara, K. Toyota, R. Fukuda, J. Hasegawa, M. Ishida, T. Nakajima, Y. Honda, O. Kitao, H. Nakai, T. Vreven, K. Throssell, J. A. Montgomery, J. E. P. Jr., F. Ogliaro, M. J. Bearpark, J. J. Heyd, E. N. Brothers, K. N. Kudin, V. N. Staroverov, T. A. Keith, R. Kobayashi, J. Normand, K. Raghavachari, A. P. Rendell, J. C. Burant, S. S. Iyengar, J. Tomasi, M. Cossi, J. M. Millam, M. Klene, C. Adamo, R. Cammi, J. W. Ochterski, R. L. Martin, K. Morokuma, O. Farkas, J. B. Foresman and D. J. Fox, Gaussian, Inc., Wallingford CT, 2016.

11. E. D. Glendening, A. E. Reed, J. E. Carpenter and F. Weinhold, NBO Version 3.1.
12. G. A. Zhurko, Chemcraft, http://www.chemcraftprog.com

## A.6 Structural Characterization and Reactivity of a Room Temperature-Stable, Antiaromatic Cyclopentadienyl Cation Salt

# Supporting Information

## Structural Characterization and Reactivity of a Room Temperature-Stable, Antiaromatic Cyclopentadienyl Cation Salt

*Yannick Schulte,[a] Christoph Wölper,[a], Susanne M. Rupf,[d] Moritz Malischewski,[d] Gebhard Haberhauer,[b]* and Stephan Schulz[a;c]**

*[a] Institute of Inorganic Chemistry, University of Duisburg-Essen, Universitätsstraße 5-7, D-45141 Essen, Germany*

*email: stephan.schulz@uni-due.de; https://www.uni-due.de/ak_schulz/index_en.php*

*[b] Institute of Organic Chemistry, University of Duisburg-Essen, Universitätsstraße 5-7, D-45141 Essen, Germany*

*email: gebhard.haberhauer@uni-due.de; https://www.uni-due.de/akhaberhauer/*

*[c] Institute of Inorganic Chemistry and Center for Nanointegration Duisburg-Essen (CENIDE), University of Duisburg-Essen, Carl-Benz-Straße 199, D-47057 Duisburg, Germany.*

*[d] Institute of Inorganic Chemistry, Freie Universität Berlin, Fabeckstr. 34-36, D-14195 Berlin, Germany*

*E-mail: moritz.malischewski@fu-berlin.de*

**Table of Contents**

## Experimental Section

**General Procedures.** All manipulations were performed using standard Schlenk and glovebox techniques under argon, which was dried by passing through preheated reduced BTS catalyst and molecular sieve columns. Toluene and *n*-hexane were dried with a MBraun solvent purification system, while benzene, THF, and deuterated benzene, and THF were distilled from Na/K alloy. Hexafluorobenzene was stirred with oleum for three days, washed with saturated $K_2CO_3$ solution (after careful phase separation), dried with $MgSO_4$, followed by molecular sieves (4 Å), and finally distilled from $SbF_5{\cdot}SO_2$. Decaline and deuterated DCM were dried over molecular sieves. All solvents except $SO_2$ were degassed and stored over activated molecular sieves (4 Å). $SO_2$ was stored over $P_2O_5$. $^1H$, $^{13}C$, and $^{19}F$ NMR spectra were referenced to internal $C_6D_5H$ ($^1H$: $\delta$ = 7.16 ppm; $^{13}C$: $\delta$ = 128.06 ppm), thf-$d_7$ ($^1H$: $\delta$ = 1.72 ppm; $^{13}C$: $\delta$ = 25.31 ppm), acetone-$d_6$ ($^1H$: $\delta$ = 2.05 ppm; $^{13}C$: $\delta$ = 53.84 ppm) and $CHDCl_2$ ($^1H$: $\delta$ = 5.32 ppm; $^{13}C$: $\delta$ = 53.84 ppm) and external $CFCl_3$ ($^{19}F$: $\delta$ = 0 ppm).

IR spectra were recorded in a glovebox using a BRUKER ALPHAT FT-IR spectrometer equipped with a single reflection ATR sampling module.

Microanalysis was not performed, because the analysis of a model compound (bromopentafluorobenzene calc.: C 29.18 %, H 0 %, N 0 %; found: C 1.94 %, H 0.25 %, N 0.157 %) showed that our equipment is not suitable for the analysis of highly fluorinated compounds.

Cyclovoltammetric studies in 1,2-difluorobenzene were performed in a glovebox using a Metrohm Autolab PGSTAT 204 potentiostat with a three-electrode setup consisting of a Pt disk (d = 1 mm) working electrode, Pt wire counter electrode, and an Ag wire pseudo-reference electrode, and ferrocene as internal standard. Positive feedback compensation was utilized to reduce the effects of solvent resistances. Cyclic voltammetry in $SO_2$ was performed on an Interface 1010 B Potentiostat/Galvanostat/ZRA from Gamry Instruments. The investigations were carried out starting from 0 V going to the oxidation first and then to the reduction. The measurements were performed in anhydrous and oxygen-free $SO_2$ under argon atmosphere using 0.1 M $TBASbF_6$ as supporting electrolyte and platinum wires as working-, counter-, and quasireference electrodes. $SO_2$ was distilled from $CaH_2$ and stored in a stainless-steel cylinder. Voltammograms were internally referenced against $FeCp_2^{0/+}$ using $Li_2B_{12}Cl_{12}$[1] as internal reference. The OriginPro 2017G software was used to plot the data.[2]

For EPR measurements, samples of **1** and **2** in $SO_2$ and toluene, respectively, were prepared in a glovebox in 50 µL capillaries (Hirschmann), sealed with critoseal. Continuous-wave (CW) X-band EPR spectra at room temperature (~9.43 GHz) were collected using a Bruker MS 5000 spectrometer. The spectra were obtained with 100 kHz field modulation frequency, 0.1 G modulation amplitude, and a scan time of 240 s. An effective time constant of 0.05 sec was applied digitally to the ~60 k point spectrum. The EPR data were processed and analysed in Matlab R2019b and simulated using the EasySpin package (v. 6.0.0-dev.30).[3]

Starting reagents were commercially available or freshly prepared.

### Synthetic Details

**Caution!**: Pentafluorophenyl copper and the complex of pentafluorophenylmagnesium bromide with diethyl ether have not, to the best of our knowledge, been reported to be explosive. However, a variation of the preparation described here, in which the complex of pentafluorophenylmagnesium bromide with diglyme was dried *in vacuo*, resulted in a vigorous

decomposition under pressure build-up which destroyed the apparatus. This happened only once although the preparation was carried out several times. Caution should be exercised because the exact cause of the decomposition is unknown. The following procedure avoids isolation of this complex.

**Bis(pentafluorophenyl)ethyne B:** 400 mmol (9.72 g) of magnesium turnings were suspended in diethyl ether (133 mL). At 0 °C 400 mmol (43.59 g, 29.9 mL) bromoethane was slowly added to this suspension. The resulting mixture was warmed to room temperature and stirred overnight. The light gray solution was cooled to 0 °C and 400 mmol (98.78 g, 50.65 mL) of bromopentafluorobenzene, 500 mmol (67.1 g, 71.4 mL) of diglyme (diethylene glycol dimethyl ether), and 400 mmol (57 g) of CuBr were slowly added in sequence. The resulting white semi-solid mass was dried *in vacuo* for 1 h and then re-suspended in 400 mL diglyme. 100 mmol (9.76 mL, 26.47 g) of tribromoethylene was added slowly at 0 °C. The suspension slowly turned brown upon stirring at 120 °C for 24 h. It was then diluted on air with 500 mL ethyl acetate, 100 mL saturated $NH_4Cl_{(aq)}$ solution, 40 mL acetic acid, and 200 mL $H_2O$. The aqueous phase was discarded, and the organic phase was washed five times with $H_2O$. It was then dried with $MgSO_4$, concentrated on a rotary evaporator, and stripped of any remaining volatiles at $10^{-3}$ mbar. A by-product (probably decafluorobiphenyl) was removed by sublimation at 60 °C/$10^{-3}$ mbar. The remaining crude product was crystallized from methanol at -30 °C.

**Yield** 14.4 g, 40.1 mmol, 40 %. **$^{19}$F NMR** (376 MHz, $C_6D_6$) δ -135.61 – -135.75 (m, 4F, *ortho*), -150.34 (t, 2F, $^3J_{FF}$ = 22.0 Hz, *para*), -161.29 – -161.47 (m, 4F, *meta*), ppm. Other analytical data are consistent with those reported in the literature.[1]

Comments: The protocol was adapted from a literature procedure.[4] In contrast to Webb and Gilman, we found a higher reaction temperature and the use of diglyme instead of THF more convenient due to the shorter reaction time. The aqueous workup prevents the formation of finely divided $Cu_2O$, which is otherwise difficult to remove by filtration.

**Tetrakis(pentafluorophenyl)cyclopentadienone C**: 40.1 mmol (14.4 g) of bis(pentafluorophenyl)ethyne and 42.1 mmol (14.4 g) of $Co_2(CO)_8$ were suspended in decaline (100 mL) and stirred until gas evolution has stopped (4 h). The solution was then stirred at 190 °C for 24 h to form a metal mirror. The flask was cooled to room temperature, the solution was diluted with 100 mL of ethyl acetate and 86.3 mmol (21.9 g) of $I_2$ was added. The suspension was stirred until dissolution of the metal mirror and complete cessation of gas evolution (15 min). The solution was diluted with ethyl acetate (500 mL) and washed with aqueous $NaHSO_3$ solution (200 mL, 30 %). The aqueous phase was discarded. The organic phase was dried with $MgSO_4$ and filtered over about 50 mL of active $Al_2O_3$. All volatiles were removed first on a rotary evaporator and then by distillation at up to 160 °C/$10^{-3}$ mbar. The product was then washed with 100 mL of *n*-hexane at -78 °C and recrystallized from $CHCl_3$ at -30 °C.

**Yield** 12.0 g, 16.1 mmol, 80 %. **$^{19}$F NMR** (376 MHz, $C_6D_6$) δ -137.57 – -137.82 (m, 8F, *ortho*), -145.76 (t, 2F, $^3J_{FF}$ = 21.6 Hz, *para*), 147.97 (t, 2F, $^3J_{FF}$ = 21.6 Hz, *para*), -157.96 – -158.17 (m, 4F, *meta*), -159.25 – -159.44 (m, 4F, *meta*) ppm. Other analytical data match those reported in the literature.[5]

Comments: Variations of this procedure omitting the oxidation step have been known for a long time,[6] but in our hands the main product of these reactions was a cobalt-containing complex of unknown structure. Oxidation of this complex with iodine yields the desired product.

**Pentakis(pentafluorophenyl)cyclopentadienol D**: 19.3 mmol (4.77 g, 2.41 mL) of bromopentafluorobenzene was slowly added at 0 °C to a solution of 19.3 mmol (6.44 mL) EtMgBr in diethyl ether (3 mol/L). All volatiles were removed under vacuum and the resulting colorless solid was redissolved in THF (10 mL). This solution was slowly added at –78 °C to a suspension of tetrakis(pentafluorophenyl)cyclopentadienone (16.1 mmol, 12.0 g) in THF (100 mL). The resulting mixture was gradually warmed to 25 °C within 4 h. Then 3 mL $HCl_{aq}$ (37 %), 100 mL diethyl ether, and 100 mL of water were added. The aqueous phase was discarded and the organic phase was washed with 100 mL of water. The solution was dried with $MgSO_4$ and all volatiles were removed under reduced pressure using a rotary evaporator. The product was purified by column chromatography (*n*-hexane/diethyl ether 20:1; $R_f$ = 0.30; colorless band with a blue fluorescence).

**Yield** 10.3 g, 11.3 mmol, 58 %. **Mp** 216 °C. **$^{19}$F NMR** (565 MHz, $CD_2Cl_2$) δ -134.96 (br s, 1F, $HOCC_6F_5$, *ortho*), -137.97 (br s, not integratable, $HOCCCC_6F_5$, *ortho*) -138.92 (m, 2F, $HOCCC_6F_5$, *ortho*), -139.53 (d, 2F, $^3J_{FF}$ = 21.7 Hz, $HOCCC_6F_5$, *ortho*), -144.02 (d, 2F, $^3J_{FF}$ = 21.3 Hz, $HOCC_6F_5$, *ortho*), -150.01(t, 2F, $^3J_{FF}$ = 20.8 Hz, $HOCCC_6F_5$ or $HOCCCC_6F_5$, *para*), -150.10 (t, 2F, $^3J_{FF}$ = 21.0 Hz, $HOCCC_6F_5$ or $HOCCCC_6F_5$, *para*), -152.60 (t, 1F, $^3J_{FF}$ = 21.2 Hz, $HOCC_6F_5$, *para*), -159.73 (td, 2F, $^3J_{FF}$ = 21.7 Hz, 7.7 Hz, $HOCCC_6F_5$, *meta*), -159.85 (td, 2F, $^3J_{FF}$ = 21.8 Hz, 7.7 Hz, $HOCCC_6F_5$, *meta*), -160.08 (td, 2F, $^3J_{FF}$ = 21.7 Hz, 7.7 Hz, $HOCCCC_6F_5$, *meta*), -160.45 (br t, 2F, $^3J_{FF}$ = 21.4 Hz, $HOCC_6F_5$, *meta*), -162.30 (br t, 2F, $^3J_{FF}$ = 20.9 Hz, $HOCC_6F_5$, *meta*). **$^1$H NMR** (400 MHz, $C_6D_6$) δ 3.40 (s, CpOH). **$^{13}$C{$^{19}$F} NMR** (151 MHz, $CD_2Cl_2$) δ 148.04 ($HOCC_6F_5$, *ortho*), 145.24 ($HOCCCC_6F_5$, *ortho*), 144.86 ($HOCC_6F_5$, *ortho*), 144.48 ($HOCCC_6F_5$, *ortho*), 144.35 ($HOCCC_6F_5$, *ortho*), 142.72 ($HOCCC_6F_5$ or $HOCCCC_6F_5$, *para*), 142.65 ($HOCCC_6F_5$ or $HOCCCC_6F_5$, *para*), 141.84, 141.83, 141.76 ($HOCC_6F_5$, *para*), 138.77 ($HOCC_6F_5$, *meta*), 138.26 ($HOCCCC_6F_5$, *meta*), 138.20 ($HOCCC_6F_5$, *meta*), 138.09 ($HOCC_6F_5$, *meta*), 137.86 ($HOCC_6F_5$, *meta*), 135.85 (HOCCC), 109.43 (HOCC), 106.76 ($HOCC_6F_5$ or $HOCCC_6F_5$, *ipso*), 106.36 ($HOCC_6F_5$ or $HOCCC_6F_5$, *ipso*), 90.36 (HOC). **ATR-IR** ν = 3601, 1646, 1514, 1484, 1341, 1305, 1118, 1088, 982, 912, 803, 731 $cm^{-1}$.

**Pentakis(pentafluorophenyl)cyclopentadienyl hexadecafluorotriantimonate 1**: Pentakis(pentafluorophenyl)cyclopentadienyl radical **2** (10 µmol, 8.6 mg) and $SbF_5{\cdot}SO_2$ (40 µmol, 11.2 mg) were suspended in 0.5 mL of hexafluorobenzene. 200 µmol (33.9 mg) of $XeF_2$ was added and the mixture was stirred for 30 min at 25 °C, resulting in the formation of a colorless gas, a deep blue solution, and a blue precipitate. The solution was decanted from the solid by using a glass syringe, sealed in a glass ampoule, and stored at 6 °C for three days.

The first run of this reaction gave the solvate $Cp(C_6F_5)_5Sb_3F_{16}{\cdot}2\ C_6F_5$ **1b**, all subsequent runs gave $Cp(C_6F_5)_5Sb_3F_{16}{\cdot}1.5\ C_6F_5$ **1a**. The yield varied from 8.6 mg to 15.1 mg (47-81 %) for solvate **1a** and was not determined for **1b**.

Alternative preparation: 10 µmol (9.1 mg) pentakis(pentafluorophenyl)cyclopentadienol **D** and 40 µmol (11.2 mg) $SbF_5{\cdot}SO_2$ were suspended in 0.5 mL hexafluorobenzene and stirred for 30 min at 25 °C, resulting in the formation of a deep blue solution and a blue precipitate. The solution

was decanted from the solid using a glass syringe, and further treated as above, yielding crystals with identical cell parameters and color.

*In situ* NMR spectroscopy: Pentakis(pentafluorophenyl)cyclopentadienol **D** (10 µmol, 9.1 mg) was dissolved in 0.5 mL of $SO_2$ at -78 °C in a Teflon-capped NMR tube, which also contained a capillary with acetone-$d_6$ and the first NMR spectrum was measured at -30 °C. The solution was again cooled to -78 °C, 50 µmol (14.0 mg) $SbF_5 \cdot SO_2$ were sublimed into the NMR tube, and the second NMR spectrum was measured at -30 °C.

Comments: The use of a glass syringe is necessary, because **1** reacts immediately with polypropylene syringes to form **2** and unidentified other products. An excess of $XeF_2$ is also necessary because $SbF_5 \cdot SO_2$ catalyzes the reaction of $XeF_2$ with hexafluorobenzene. For the second preparation, starting from **D**, the formation of hydroxide-containing counteranions $Sb_3(OH)_nF_{(16-n)}$ cannot be completely excluded. Crystals for sc-XRD were therefore obtained from the first reaction (oxidation of **2**).

**UV-Vis** (hexafluorobenzene): $\lambda_{max}$ (log ε) = 678 nm (4.68).

**Caution!** When $XeF_2$ and $SbF_5 \cdot SO_2$ are premixed and the solvent is added subsequently, a vigorous reaction with flame formation may occur even in the absence of air.

**Pentakis(pentafluorophenyl)cyclopentadienyl radical 2**: 1 mmol (912 mg) pentakis(pentafluorophenyl)cyclopentadienol and 20 mmol (5.33 g) $AlBr_3$ were suspended in 3 mL of benzene and 10 mmol (1.09 g, 746 µL) of bromoethane was slowly added at 0 °C. The red suspension was warmed to 25 °C, stirred for 30 min, and subsequently cooled to 0 °C. The suspension was filtered, and the filtrate was discarded. The solid was quenched with 200 mmol (3.6 g) ice and the mixture was kept at 25 °C until completely thawed. The solution was then removed by filtration and the solid was washed rapidly three times with 10 mL of water at 0 °C. All volatiles were removed under reduced pressure and the solid was sublimed at 150 °C/$10^{-3}$ mbar over 2 days. The sublimate was crystallized three times from 1 mL of toluene and again all volatiles were removed under vacuum.

**Yield** 484 mg, 541 µmol, 54 %. **Mp** 236 °C, evaporates undecomposed at approx. 300 °C. **ATR-IR** ν = 1647, 1517, 1487, 1383, 1344, 1312, 1138, 1104, 1079, 983, 919, 911, 836, 730, 654, 542 $cm^{-1}$. **UV-Vis** (hexafluorobenzene): $\lambda_{max}$ (log ε) = 546 nm (3.41).

Comments: The washing steps can be performed in a Büchner funnel without the need for an inert gas atmosphere, since crystalline **2** is stable under these conditions. The mother liquors and the liquid portion of the reaction mixture contain mainly pentakis(pentafluorophenyl)cyclopentadiene and can be used for the preparation of pyridinium pentakis(pentafluorophenyl)cyclopentadienide.

**Ferrocenium pentakis(pentafluorophenyl)cyclopentadienide 3a**: 5 µmol (4.5 mg) pentakis(pentafluorophenyl)cyclopentadienyl radical and 6 µmol (1.1 mg) ferrocene were dissolved in 0.3 mL 1,2-difluorobenzene. The product was crystallized by vapor phase diffusion with 3 mL *n*-hexane.

**Yield** 3.5 mg, 3.2 µmol, 65 %. **Mp** 232 °C. **$^{19}$F NMR** (565 MHz, thf-$d_8$) δ -142.96 (dd, 10F, $^3J_{FF}$ = 25.2 Hz, $^4J_{FF}$ = 8.3 Hz, *ortho*), -163.13 (t, 5F, $^3J_{FF}$ = 21.5 Hz, *para*), -166.38 – -166.51 (m, 10F, *meta*). **$^{13}$C NMR** (151 MHz, $CD_2Cl_2$) δ 145.1 (d, $^1J_{FC}$ = 243 Hz, *meta*), 139.2 (d, $^1J_{FC}$ = 243 Hz, *para*), 138.3zz (dt, $^1J_{FC}$ = 246 Hz, *ortho*, $^2J_{FC}$ = 14.5 Hz), 116.7 (t, $^2J_{FC}$ = 19.3 Hz, *ipso*), 108.5 ($C_5(C_6F_5)_5$). **ATR-IR** ν = 3111, 3075, 1514, 1471, 1418, 1282, 1267, 1098, 976, 915, 849, 759, 540 cm$^{-1}$.

**Tritylium pentakis(pentafluorophenyl)cyclopentadienide 3b:** 5 µmol (4.5 mg) of pentakis(pentafluorophenyl)cyclopentadienyl radical and 3 µmol (1.7 mg) of trityl$_2$·toluene were heated to 110 °C in 0.5 mL of toluene until all solids were dissolved (about 10 min). The solution was then slowly cooled to 25 °C and left undisturbed for 24 h, resulting in the formation of large yellow-green needles.

**Yield** 4.9 mg, 4.4 µmol, 87 %. **Mp** 227 °C. **$^{19}$F NMR** (565 MHz, $CD_2Cl_2$) δ -142.71 (dd, 10F, $^3J_{FF}$ = 25.6 Hz, $^4J_{FF}$ = 7.4 Hz, *ortho*), -161.53 (t, 5F, $^3J_{FF}$ = 21.5 Hz, *para*), -164.97 – -165.16 (m, 10F, *meta*). **$^1$H NMR** (400 MHz, $CD_2Cl_2$) δ 7.91 (br s). The signals in the $^{13}$C NMR spectrum were too broad to be well resolved. **ATR-IR** ν = 2945, 1574, 1516, 1479, 1350, 1290, 1181, 1099, 982, 916, 839, 764, 701, cm$^{-1}$.

**Decamethylaluminocenium pentakis(pentafluorophenyl)cyclopentadienide 3c:** 5 µmol (4.5 mg) of pentakis(pentafluorophenyl)cyclopentadienyl radical and 10 µmol (1.6 mg) of Cp*Al were heated to 110 °C in 0.5 mL of toluene until all reagents dissolved (about 10 min). This process was accompanied by the formation of a gray, finely dispersed solid (probably aluminum metal). The solution was then cooled to 25 °C. The grayish solid formed was isolated by centrifugation and extracted with 0.5 mL $CH_2Cl_2$. The extract was evaporated to dryness at 25 °C/10$^{-3}$ mbar.

The formation of single crystals was achieved by immersing the product in a small glass tube (5 mm diameter) containing 1 mL of benzene and heating the lower end of the solution to 80 °C, while keeping the upper end at 25 °C.

**Yield** 5.3 mg, 4.9 µmol, 89 % (before crystallization). **Mp** 230 °C. **$^{19}$F NMR** (565 MHz, $CD_2Cl_2$) δ -142.74 (dd, 10F, $^3J_{FF}$ = 25.5 Hz, $^4J_{FF}$ = 7.0 Hz, *ortho*), -161.57 (t, 5F, $^3J_{FF}$ = 21.0 Hz, *para*), -165.04 – -165.17 (m, 10F, *meta*). **$^1$H NMR** (600 MHz, $CD_2Cl_2$) δ 2.16. **$^{13}$C NMR** (151 MHz, $CD_2Cl_2$) δ 144.4 (d, $^1J_{FC}$ = 241 Hz, *meta*), 138.9 (d, $^1J_{FC}$ = 248 Hz, *para*), 137.8 (dt, $^1J_{FC}$ = 248 Hz, *ortho*, $^2J_{FC}$ = 14.0f Hz), 119.3 ($C_5Me_5$), 115.5 (t, $^2J_{FC}$ = 19.3 Hz, *ipso*), 107.9 ($C_5(C_6F_5)_5$) 10.4 ($C_5Me_5$). **ATR-IR** ν = 2952, 2914, 2867, 1514, 1481, 1098, 982, 916, 653, 623, 574, 538 cm$^{-1}$.

Comments: The unusual shape of the $^1$H NMR signal has been reported previously.[7]

**Pyridinium pentakis(pentafluorophenyl)cyclopentadienide 3d:** The combined mother liquors of **2**, including the soluble fraction of the reaction mixture, were washed with dilute hydrochloric acid (1 mol/L), dried with $MgSO_4$, and degassed by three freeze-thaw-pump cycles. 1 mmol (79.1 mg; 80.7 µL) of pyridine was added, initiating the formation of a colorless precipitate, which was removed by filtration, washed three times with 3 mL of benzene, and dried under reduced pressure.

**Yield** 302 mg, 314 µmol, 31 % (with respect to reagent **D**). **Mp** 218 °C. **$^{19}$F NMR** (565 MHz, thf-$d_8$) δ -143.02 (dd, 10F, $^3J_{FF}$ = 24.6 Hz, $^4J_{FF}$ = 7.7 Hz, *ortho*), -162.62 (t, 5F, $^3J_{FF}$ = 21.3 Hz, *para*), -166.03 – -166.22 (m, 10F, *meta*). **$^1$H NMR** (400 MHz, thf-$d_8$) δ 8.56 – 8.53 (m, 2H, *ortho*), 7.56 (tt, 1H, $^3J_{HH}$ = 7.6 Hz, $^4J_{HH}$ = 1.l9 Hz, *para*) 7.27 – 7.23 (m, 2H, *meta*). The signals in the $^{13}$C NMR spectrum were too broad to be well resolved. **ATR-IR** ν = 1516, 1474, 1099, 978, 915, 750, 691, 620, 538 cm$^{-1}$.

**Pentakis(pentafluorophenyl)cyclopentadienylcarboxylic acid 5:** 10 µmol (15.6 mg) of **1** was suspended in 0.5 mL of $C_6F_6$. The solution was degassed and 89 µmol (2 mL; 1.1 bar; 25 °C) of CO was added. The solution was stirred for 24 h, resulting in a color change from deep blue to pale yellow and the formation of brown solids. All volatiles were removed under vacuum. 1 mL of water and 1 mL of benzene were added to the solid residue. The phases were separated, the aqueous phase was discarded, and the organic phase was dried with $MgSO_4$. All volatiles were removed again under vacuum.

The product is a mixture of **5** and **6**, since **5** decomposes slowly to **6** under the conditions of the work-up and NMR measurement. Single crystals of **5** were obtained by vapor phase diffusion of *n*-hexane into a concentrated solution of **5** in hexafluorobenzene at 6 °C.

**Yield** 7 mg. **$^{19}$F NMR** (565 MHz, $C_6D_6$) δ -132.34 (br s, 1F, *ortho*), -135.05 (br s, 1F, *ortho*), -138.42 (d, 2F, $^3J_{FF}$ = 21.6 Hz, *ortho*), -139.28 – -139.48 (m, not integratable due to overlap and uneven baseline, *ortho*), -145.35 (t, 2F, $^3J_{FF}$ = 21.7 Hz, *para*), -146.33 (d, 2F, $^3J_{FF}$ = 21.7 Hz, *para*), -148.23 (d, 2F, $^3J_{FF}$ = 21.7 Hz, *para*), 158.0 – 158.41 (m, 9F, *meta*) 160.05 (td, 1H, $^3J_{FF}$ = 21.7 Hz, $^4J_{FF}$ = 6.1 Hz, *meta*).

Comment: Because **5** decomposes during column chromatography and on prolonged standing, only the $^{19}$F NMR spectrum and sc-XRD data are reported.

**Pentakis(pentafluorophenyl)cyclopentadiene 6:** 5 µmol of **3a**, **3b**, or **3c** are suspended in 1 mL of hydrochloric acid (1 mol/L). The suspension is extracted three times with 1 mL of dichloromethane (DCM). The combined extracts are dried with $MgSO_4$ and all volatiles are removed under reduced pressure (3 h to ensure the removal of ferrocene, Cp*H, and pyridine). The yield is almost quantitative.

If larger amounts of **6** are desired, the following procedure is advantageous: 0.5 mmol (456 mg) pentakis(pentafluorophenyl)cyclopentadienol and 10 mmol (2.67 g) $AlBr_3$ were suspended in 1.5 mL benzene and 5 mmol (0.55 g, 373 µL) bromoethane was slowly added at 0 °C. The red suspension was warmed to 25 °C and stirred for 30 min. The suspension was quenched with 100 mmol (1.8 g) ice and the mixture was kept at 25 °C until completely thawed. 0.5 mmol (93 mg) ferrocene and 1.5 mL hydrochloric acid (1 mol/L) were added and the suspension was stirred for 30 min. It was then diluted with 10 mL DCM and the phases were separated. The aqueous phase was discarded and the organic phase was dried with $MgSO_4$. All volatiles were removed under vacuum. The crude product was dissolved in 5 mL hot toluene and filtered while hot. 0.5 mmol (39.6 mg; 40.6 µL) pyridine was added to the filtrate and the solution was stored at 25 °C for 24 h. The separated solids were isolated by filtration and dissolved in a mixture of 1.5 mL

hydrochloric acid (1 mol /L) and 10 mL DCM. The aqueous phase was discarded and the organic phase was dried with $MgSO_4$. All volatiles were removed under vacuum.

**Yield** 309 mg, 345 mmol, 69 %. **Mp** 188 °C (dec.). **$^{19}$F NMR** (565 MHz, $C_6D_6$) δ -139.13 (d, 2F, $^3J_{FF}$ = 21.0 Hz, $HCCC_6F_5$, *ortho*), -140.00 (d, 4F, $^3J_{FF}$ = 21.2 Hz, $HCCCC_6F_5$, *ortho*) -140.62 (d, 2F, $^3J_{FF}$ = 23.0 Hz, $HCCC_6F_5$, *ortho*), -141.18 (d, 1F, $^3J_{FF}$ = 18.2 Hz, $HCC_6F_5$, *ortho*), -143.18 (d, 2F, $^3J_{FF}$ = 21.6 Hz, $HCC_6F_5$, *ortho*), -147.69 (t, 2F, $^3J_{FF}$ = 21.7 Hz, $HCCC_6F_5$ or $HCCCC_6F_5$, *para*), -148.14 (t, 2F, $^3J_{FF}$ = 21.3 Hz, $HCCC_6F_5$ or $HCCCC_6F_5$, *para*), -149.62 (t, 1F, $^3J_{FF}$ = 21.5 Hz, $HCC_6F_5$, *para*), -158.72 – 158.93 (m, 6F, *meta*), -159.18 – 159.42 (m, 3F, *meta*), -159.67 (td, 1F, $^3J_{FF}$ = 21.6 Hz, $^4J_{FF}$ = 8 Hz, $HCC_6F_5$, *meta*). **$^1$H NMR** (400 MHz, $C_6D_6$) δ 5.91 (s, CpH). **$^{13}$C{$^{19}$F} DEPT-135 NMR** (151 MHz, $C_6D_6$) δ 146.41 (d, $^3J_{HC}$ = 7.1 Hz $HCC_6F_5$, *ortho*), 145.94 (d, $^3J_{HC}$ = 5.7 Hz $HCC_6F_5$, *ortho*), 144.86 (s, $HCCC_6F_5$, *ortho*), 144.67 (s, $HCCCC_6F_5$, *ortho*), 144.31 (s, $HCCC_6F_5$, *ortho*), 142.47 (s, $HCCC_6F_5$ or $HCCCC_6F_5$, *para*), 142.31 (s, $HCCCC_6F_5$ or $HCCC_6F_5$, *para*), 142.08 (s, $HCC_6F_5$, *para*), 138.24 (s, $HCCC_6F_5$, *meta*), 138.21 (s, $HCC_6F_5$, *meta*), 138.18 (s, $HCCCC_6F_5$, *meta*), 138.17 (s, $HCCC_6F_5$, *meta*), 138.04 (s, $HCCCC_6F_5$, *meta*), 137.06 (s, $HCC_6F_5$, *meta*). **$^{13}$C{$^1$H} NMR** (151 MHz, $C_6D_6$) δ 146 – 136 (several multiplets) 107.84 – 106.83 (m, *ipso*), 53.56 (s, H*C*). **ATR-IR** ν = 1656, 1522, 1491, 1445, 1315, 1105, 1080, 982, 935, 916, 841, 735, 652, $cm^{-1}$.

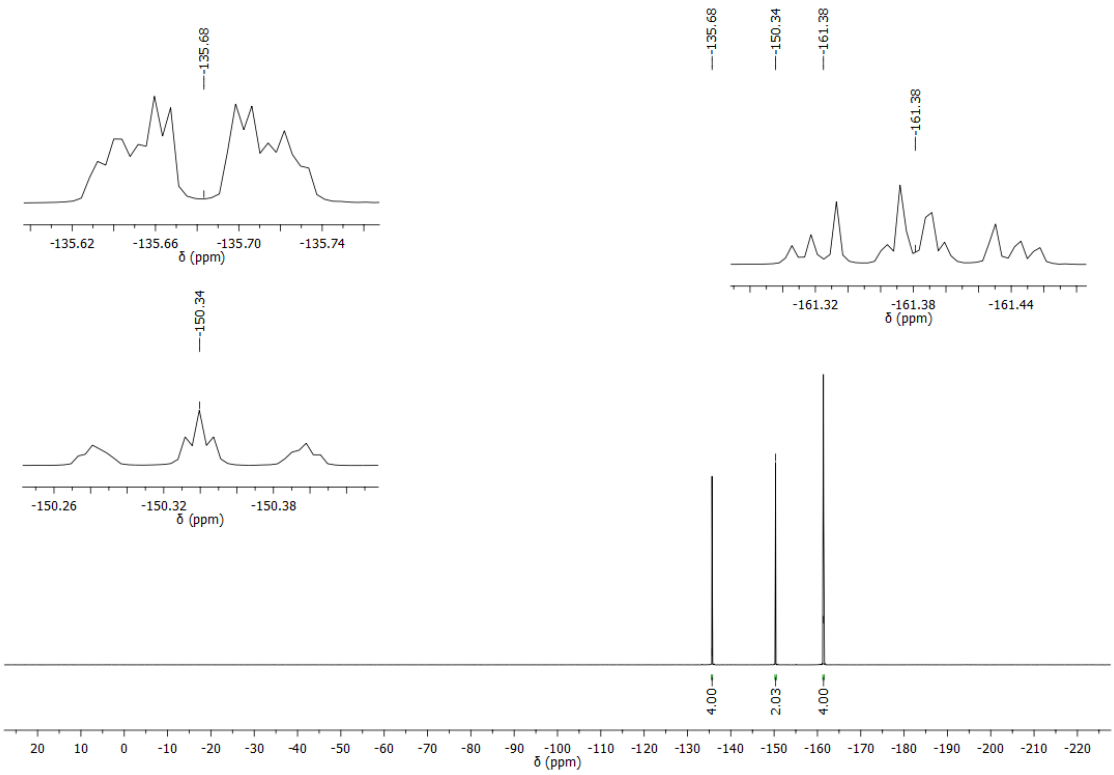


**Figure S1**. $^{19}F$ NMR spectrum of bis(pentafluorophenyl)ethyne **B** in $C_6D_6$ at 25 °C.

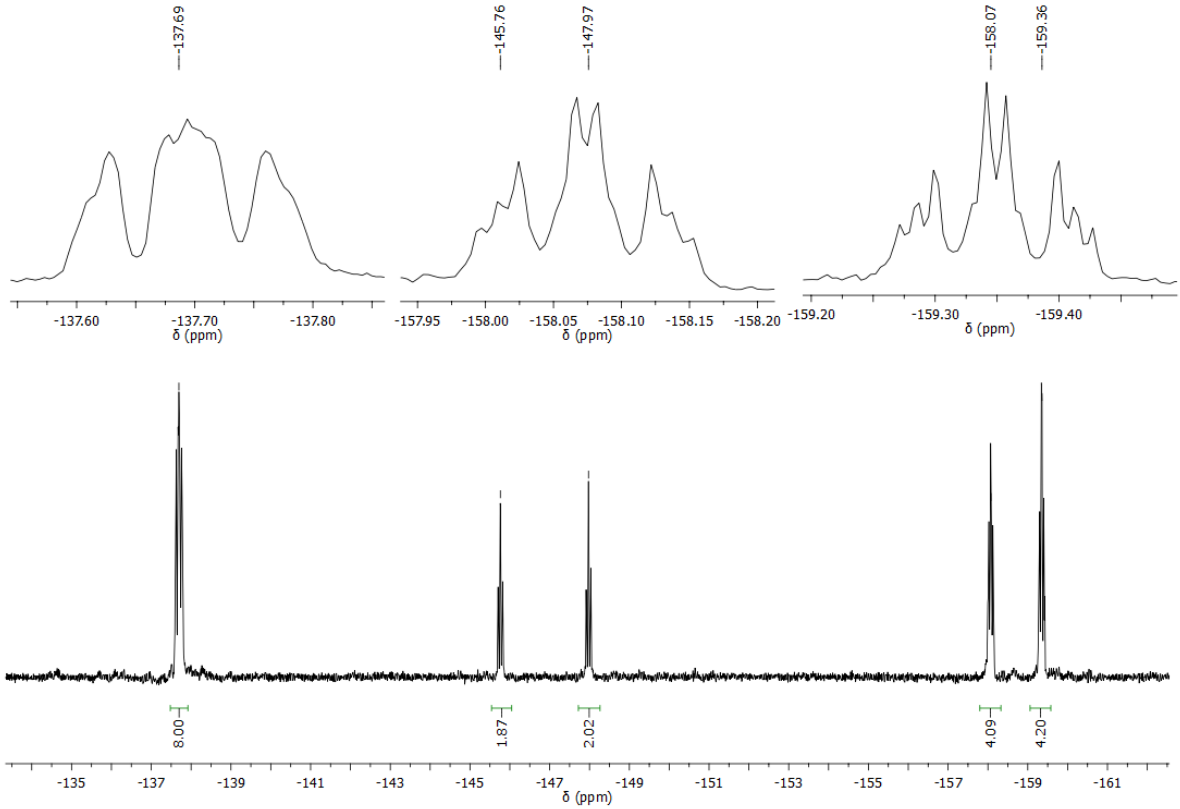


**Figure S2**. $^{19}F$ NMR spectrum of tetrakis(pentafluorophenyl)cyclopentadienone **C** in $C_6D_6$ at 25 °C.

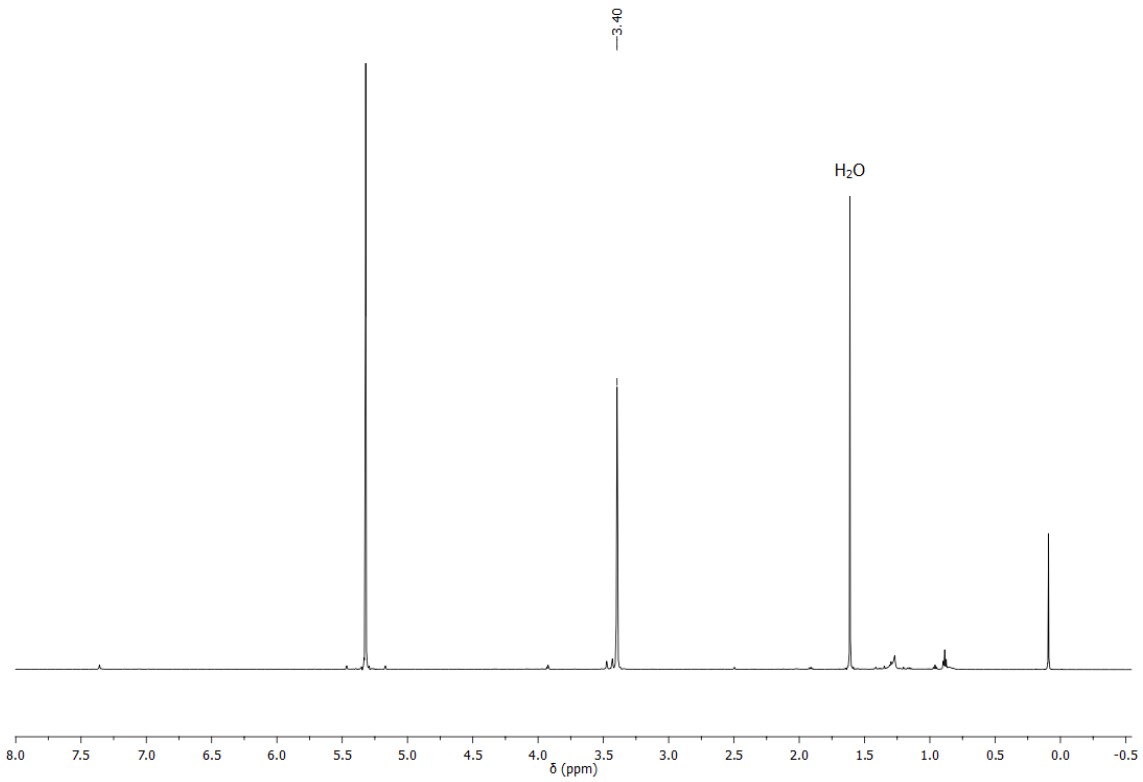


**Figure S3**. $^{1}$H NMR spectrum of pentakis(pentafluorophenyl)cyclopentadienol **D** in $CD_2Cl_2$ at 25 °C.

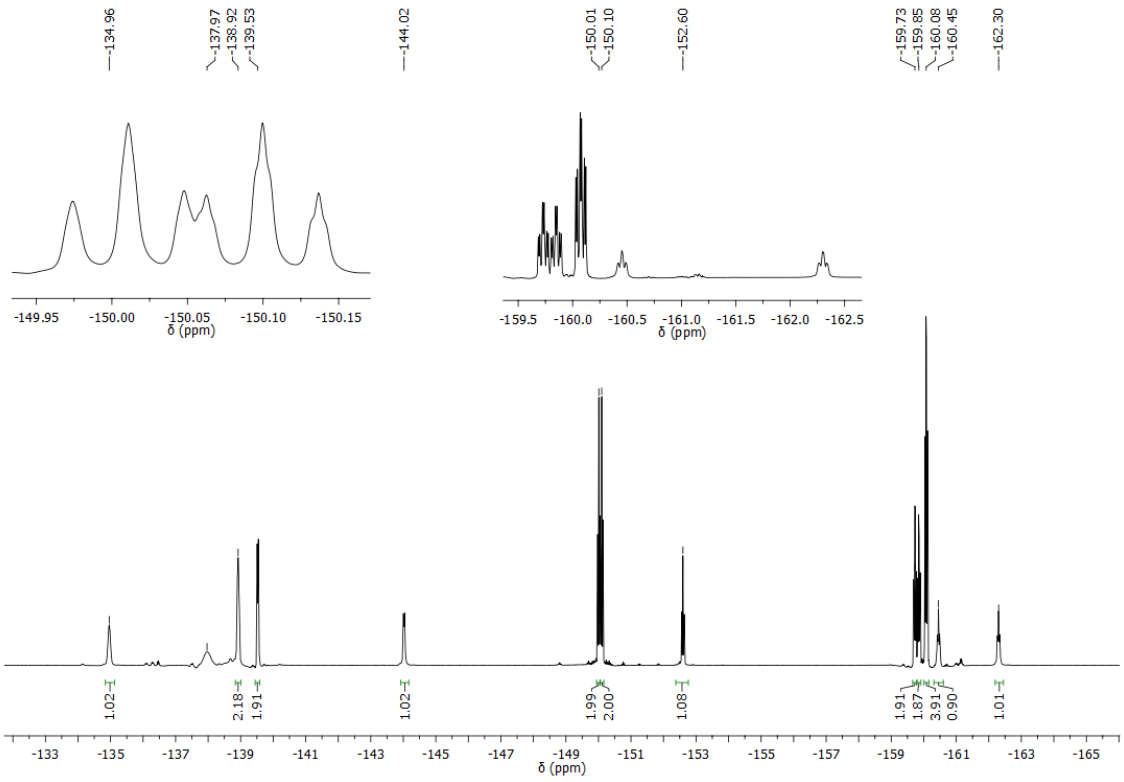


**Figure S4**. $^{19}F$ NMR spectrum of pentakis(pentafluorophenyl)cyclopentadienol **D** in $CD_2Cl_2$ at 25 °C.

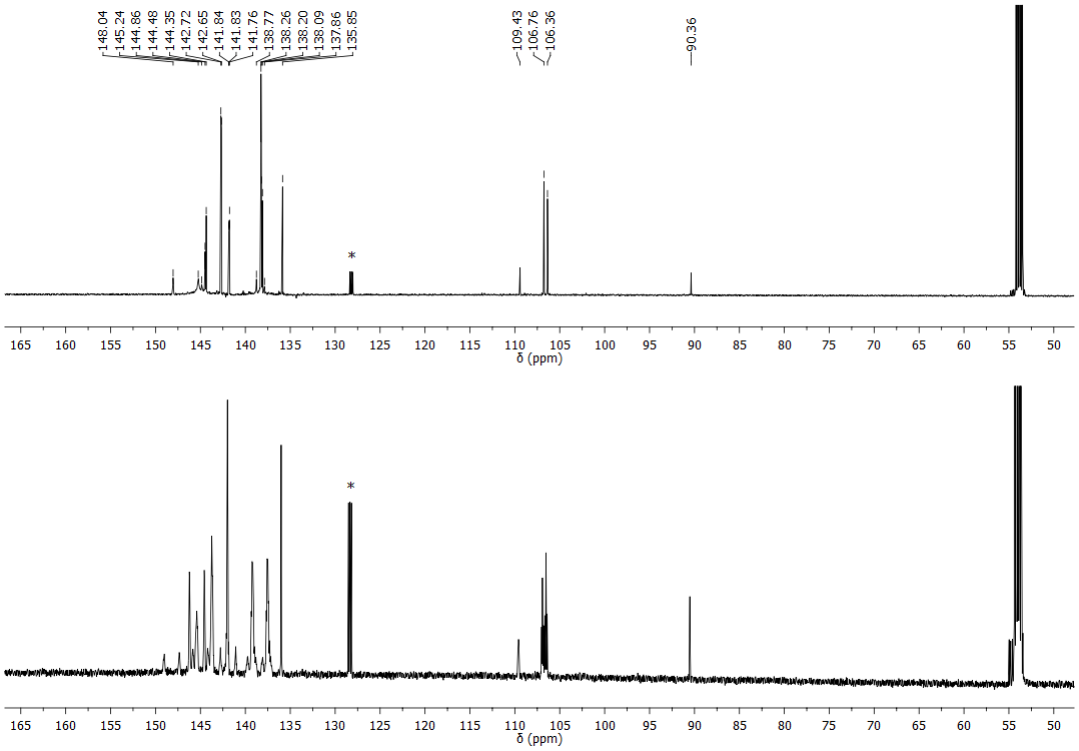


**Figure S5**. $^{13}C\{^{19}F\}$ NMR and $^{13}C\{^{1}H\}$ NMR spectrum of pentakis(pentafluorophenyl)cyclopentadienol **D** in $CD_2Cl_2$ at 25 °C (containing traces of $C_6D_6$ (*) from a previous measurement which was hindered by the low solubility in this solvent).

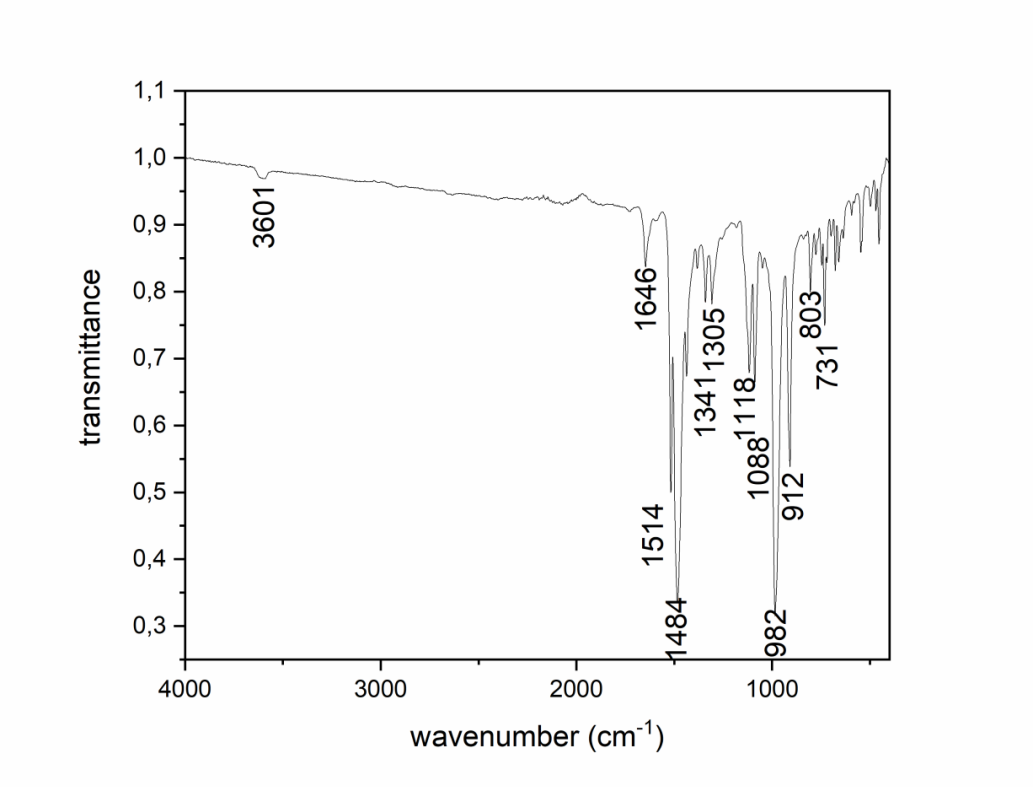


**Figure S6**. ATR-IR spectrum of pentakis(pentafluorophenyl)cyclopentadienol **D**.

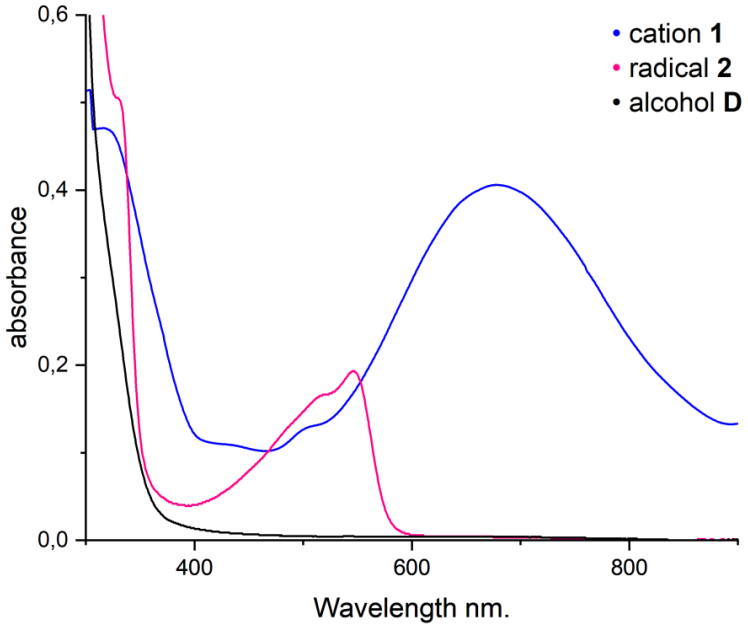

**Figure S7.** UV-vis spectra of cation **1**, radical **2**, and alcohol **D** (50 µmol/L in hexafluorobenzene). The solution of **1** contained an excess (250 µmol/L) of $SbF_5 \cdot SO_2$ to scavange traces of reducing agents or nucleophiles. Quantitative results for **1** may be imprecise because the concentration of **1** was not accurately known due to difficulties in the handling of its solution.

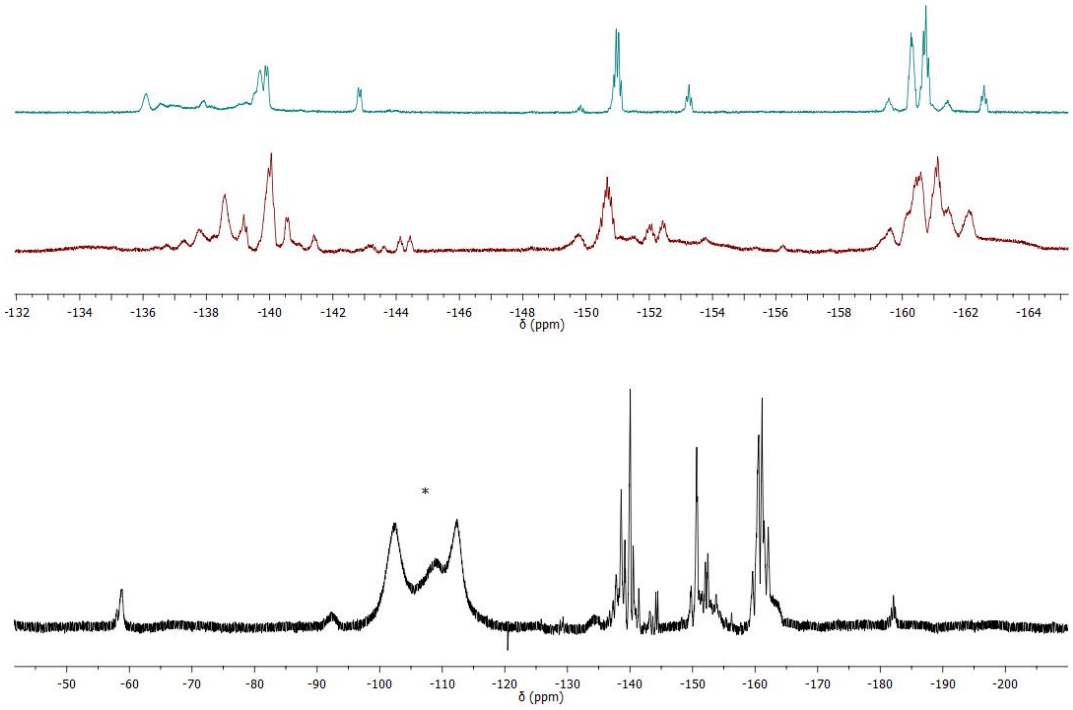


**Figure S8.** $^{19}F$ NMR spectra in liquid $SO_2$ at -30 °C of pentakis(pentafluorophenyl)cyclopentadienol **D** before (top, cyan) and after (middle, red and bottom, black) the addition of 5 equivalents of $SbF_5 \cdot SO_2$ using a glass capillary with acetone-$d_6$ as reference. The multiplet marked with an asterisk arises from $Sb_nF_mOH_o$ species.

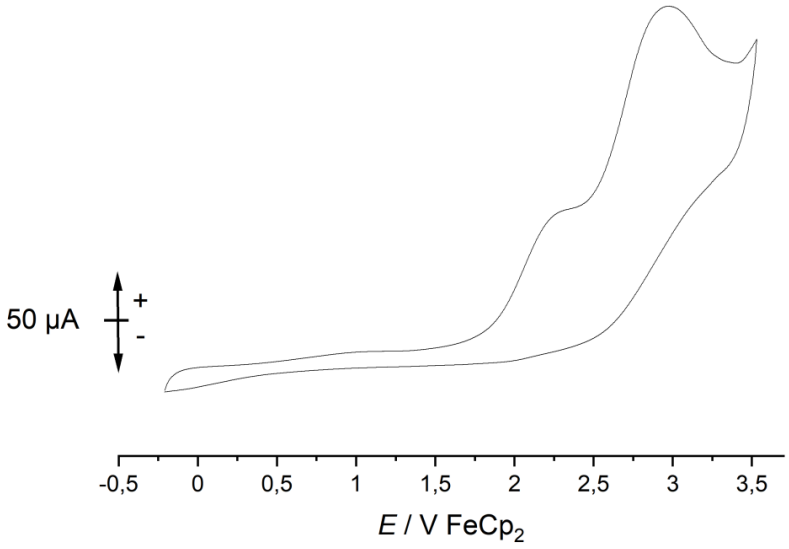


**Figure S9**. Cyclovoltammogram of the pentakis(pentafluorophenyl)cyclopentadienyl radical **2** at -20 °C in $SO_2$. We assign the first redox event at $E_{pa}$ = 2.30 V to its oxidation to cation **1** and the second redox event at $E_{pa}$ = 3.55 V to the subsequent oxidation of the aryl groups.

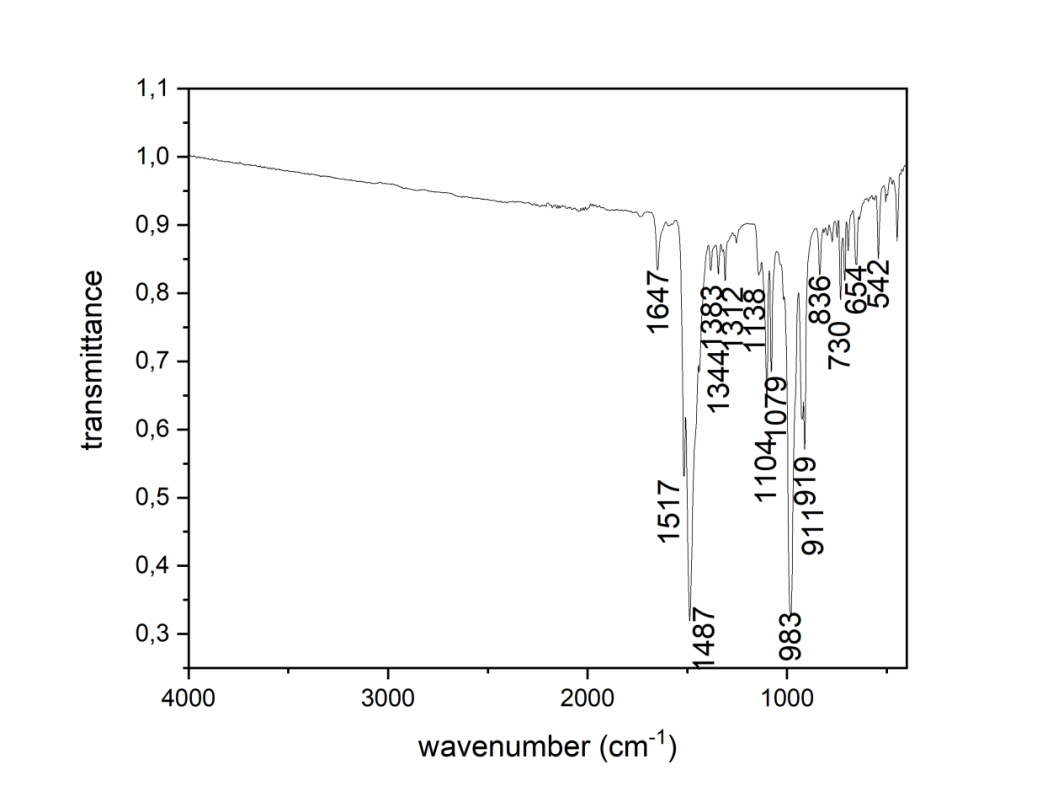


**Figure S10**. ATR-IR spectrum of the pentakis(pentafluorophenyl)cyclopentadienyl radical **2**.

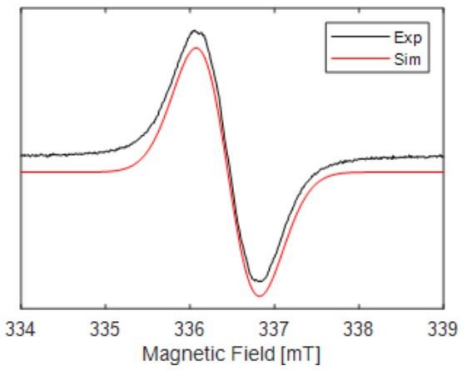


**Figure S11**. EPR spectrum of the pentakis(pentafluorophenyl)cyclopentadienyl radical **2**. For the simulation, a g value of 2.0033 and a linewidth (peak-to-peak) of 0.75 mT were used.

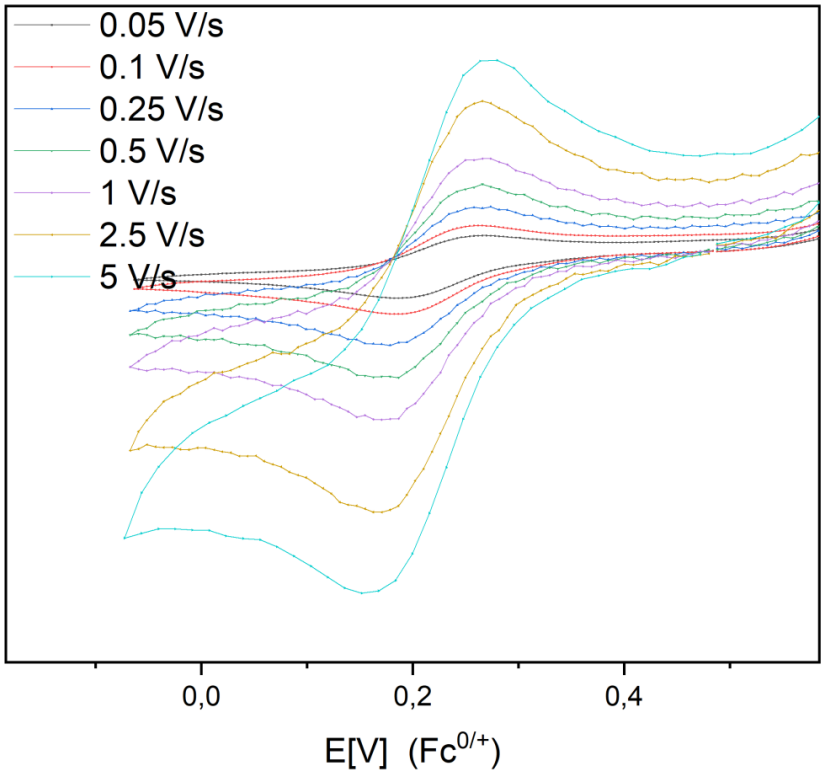


**Figure S12**. Cyclovoltammogramm of the pentakis(pentafluorophenyl)cyclopentadienyl radical **2** at 25 °C in 1,2-difluorobenzene. The reversible reduction to the corresponding anion **3** occurs at a half wave potential of $E_{1/2}$ = 0.48 V.

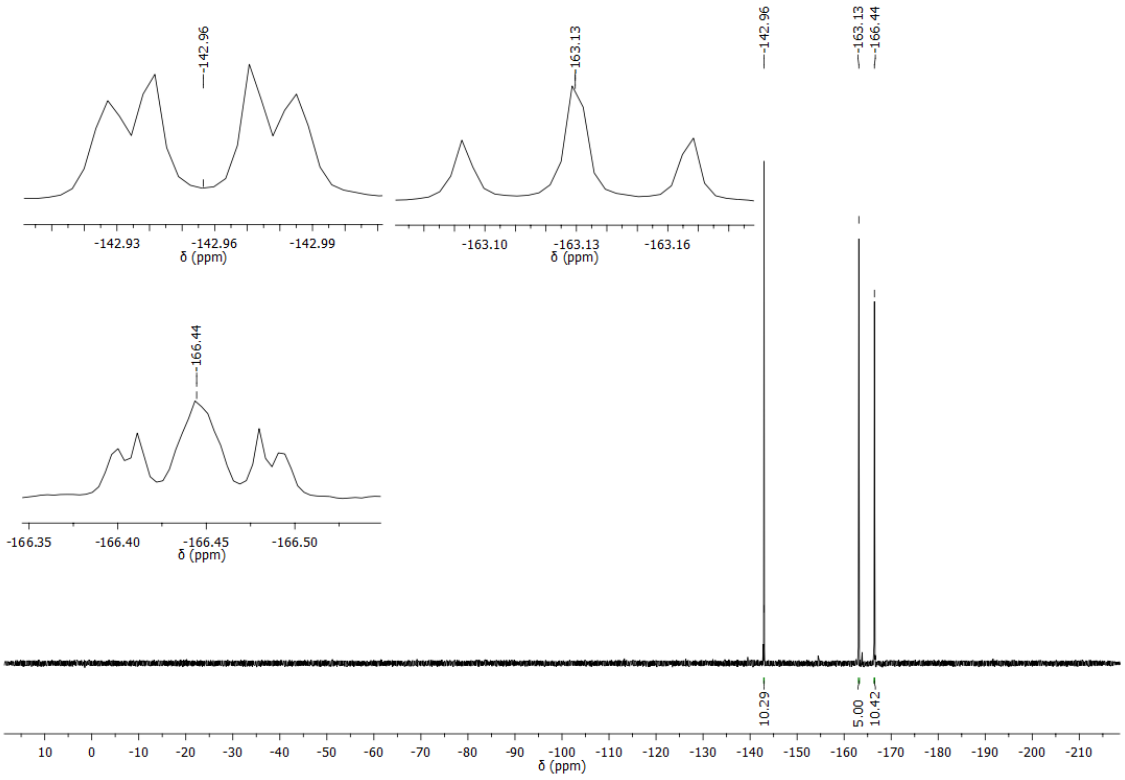


**Figure S13**. $^{19}$F NMR spectrum of ferrocenium pentakis(pentafluorophenyl)cyclopentadienide **3a** in THF-$d_8$ at 25 °C.

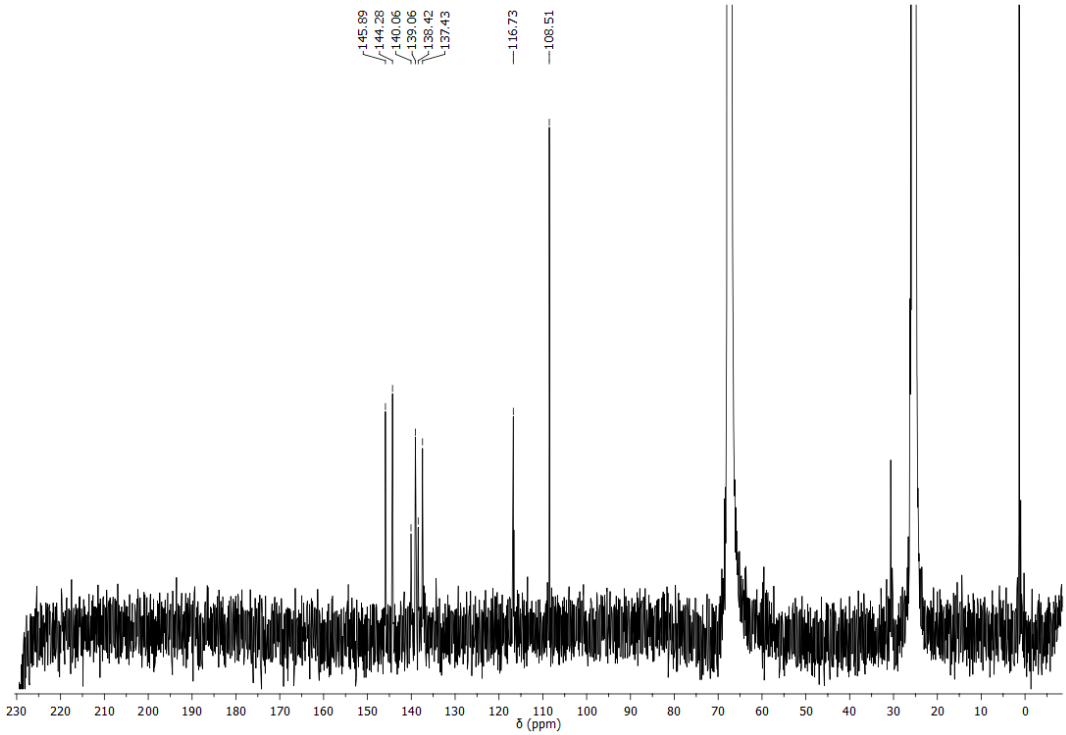


**Figure S14**. $^{13}C$ NMR spectrum of ferrocenium pentakis(pentafluorophenyl)cyclopentadienide **3a** in THF-$d_8$ at 25 °C.

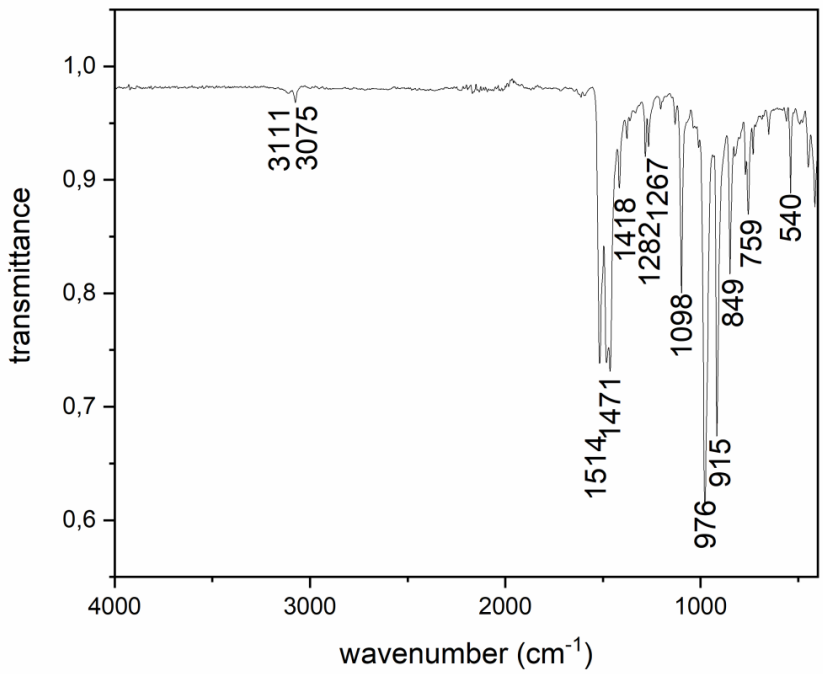


**Figure S15**. ATR-IR spectrum of ferrocenium pentakis(pentafluorophenyl)cyclopentadienide **3a**.

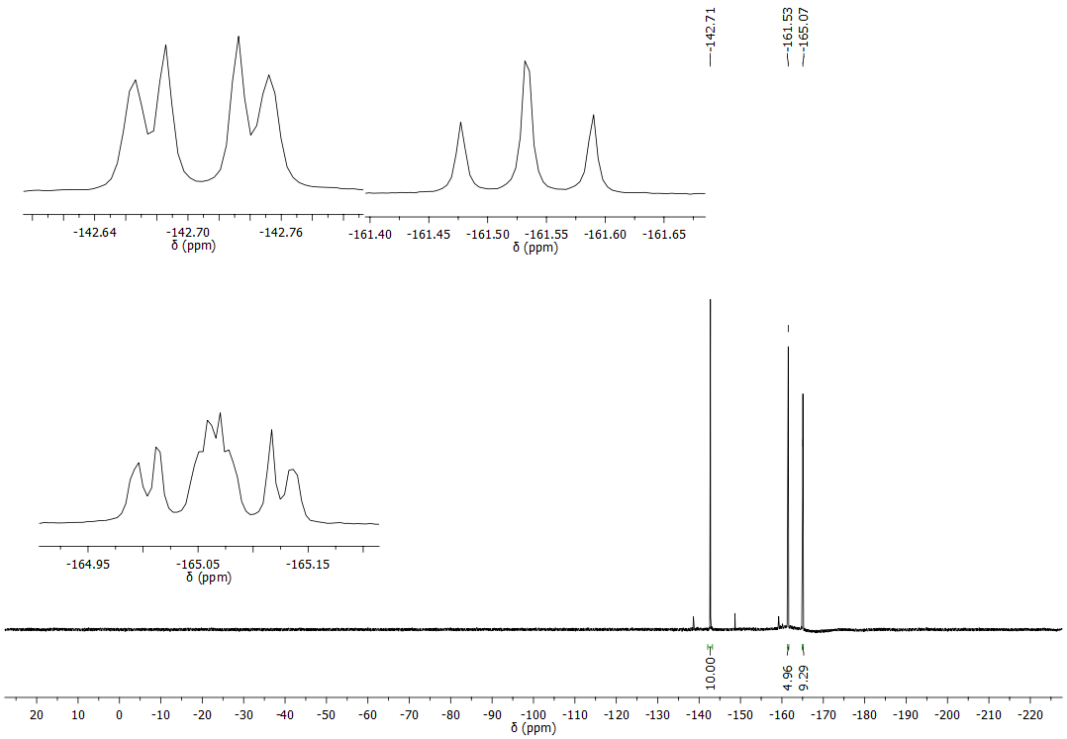


**Figure S16**. $^{19}F$ NMR spectrum of tritylium pentakis(pentafluorophenyl)cyclopentadienide **3b** in $CD_2Cl_2$ at 25 °C.

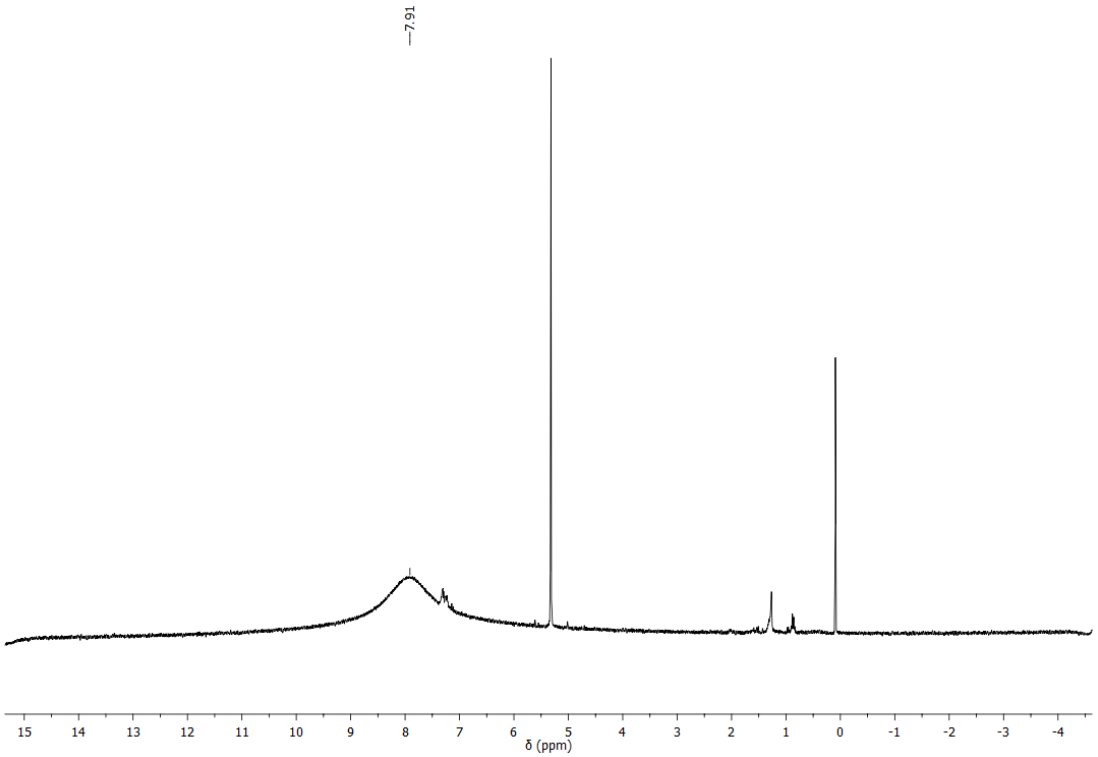


**Figure S17**. $^{1}H$ NMR spectrum of tritylium pentakis(pentafluorophenyl)cyclopentadienide **3b** in $CD_2Cl_2$ at 25 °C.

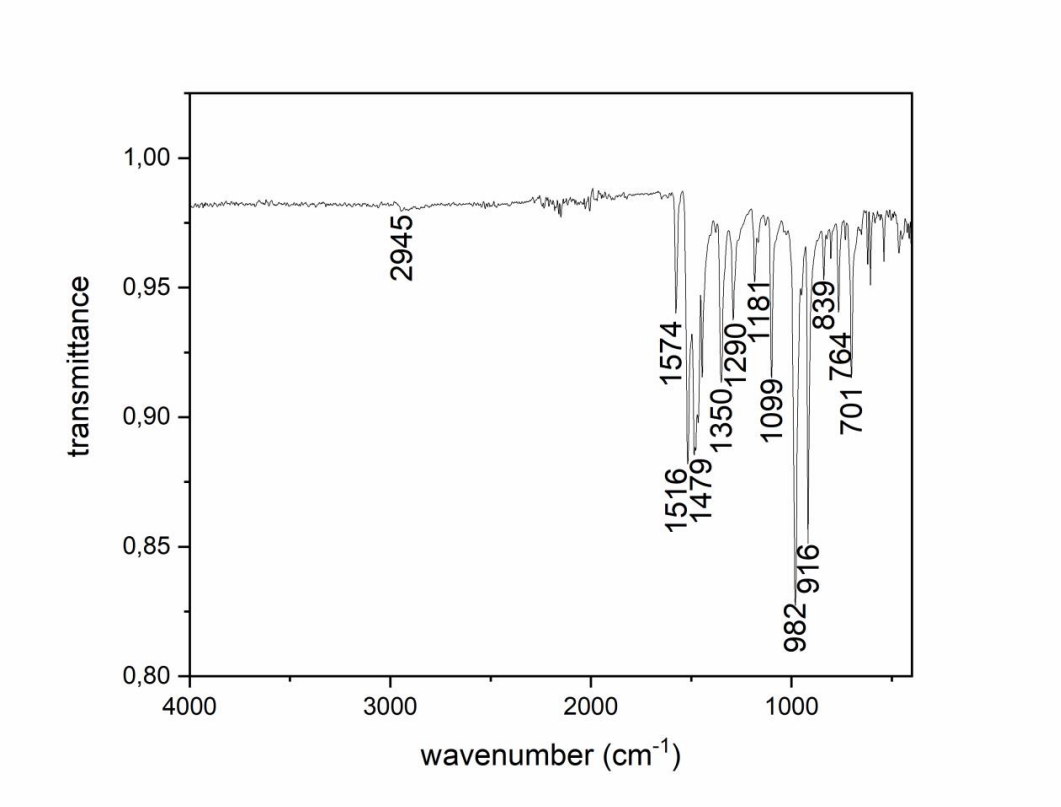


**Figure S18**. ATR-IR spectrum of tritylium pentakis(pentafluorophenyl)cyclopentadienide **3b**.

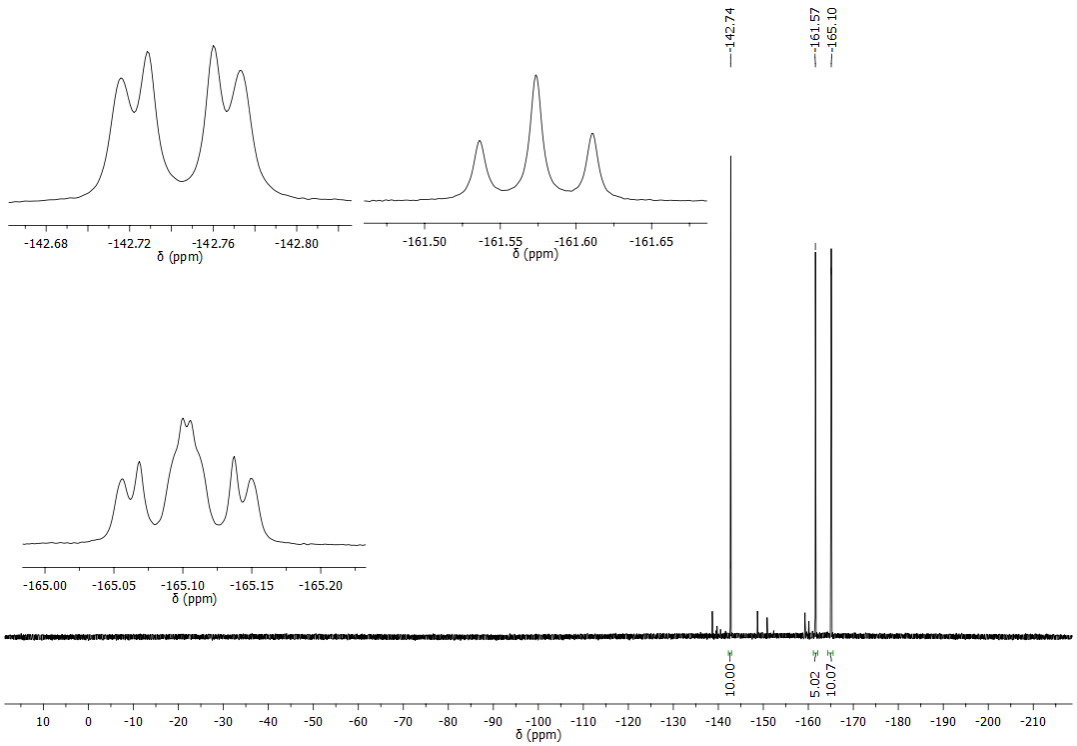


**Figure S19**. $^{19}F$ NMR spectrum of decamethylalumocenium pentakis(pentafluorophenyl)cyclopentadienide **3c** in $CD_2Cl_2$ at 25 °C.

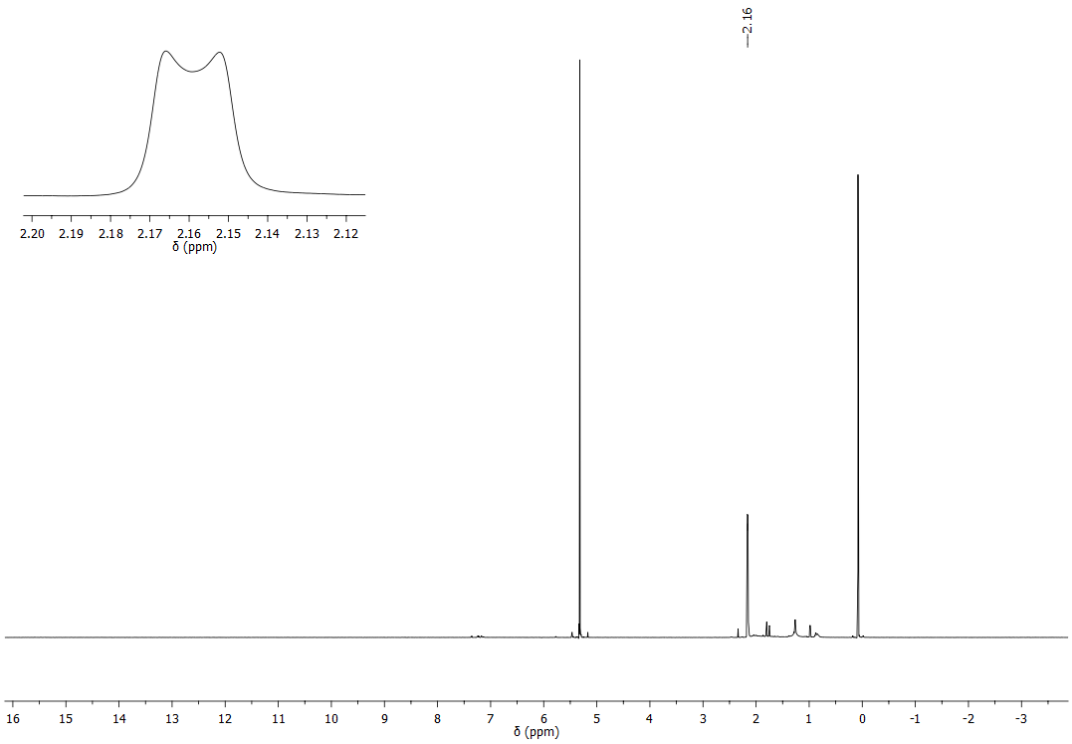


**Figure S20**. $^{1}H$ NMR spectrum of decamethylalumocenium pentakis(pentafluorophenyl)cyclopentadienide **3c** in $CD_2Cl_2$ at 25 °C.

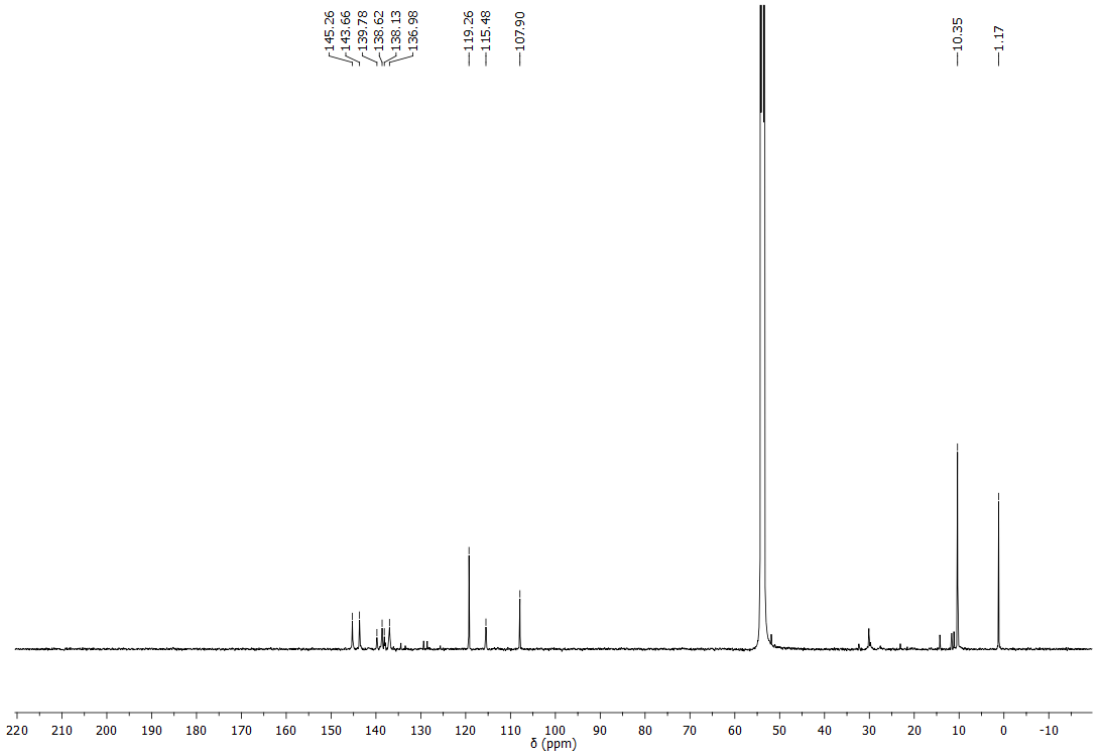


**Figure S21**. $^{13}C$ NMR spectrum of decamethylalumocenium pentakis(pentafluorophenyl)cyclopentadienide **3c** in $CD_2Cl_2$ at 25 °C.

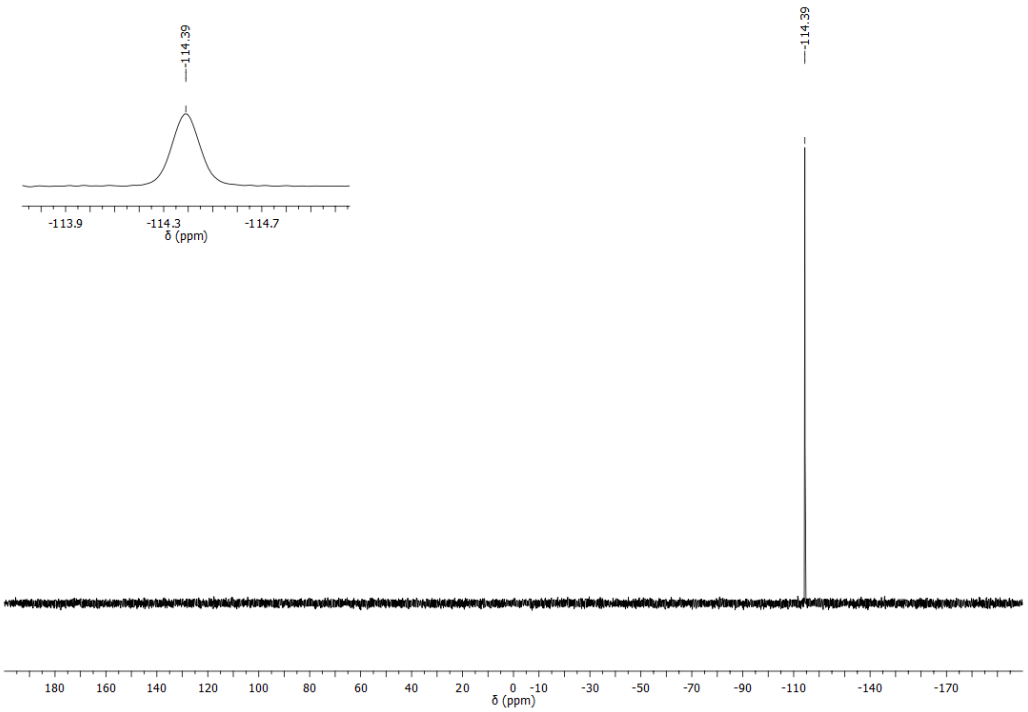


**Figure S22**. $^{27}Al$ NMR spectrum of decamethylalumocenium pentakis(pentafluorophenyl)cyclopentadienide **3c** in $CD_2Cl_2$ at 25 °C.

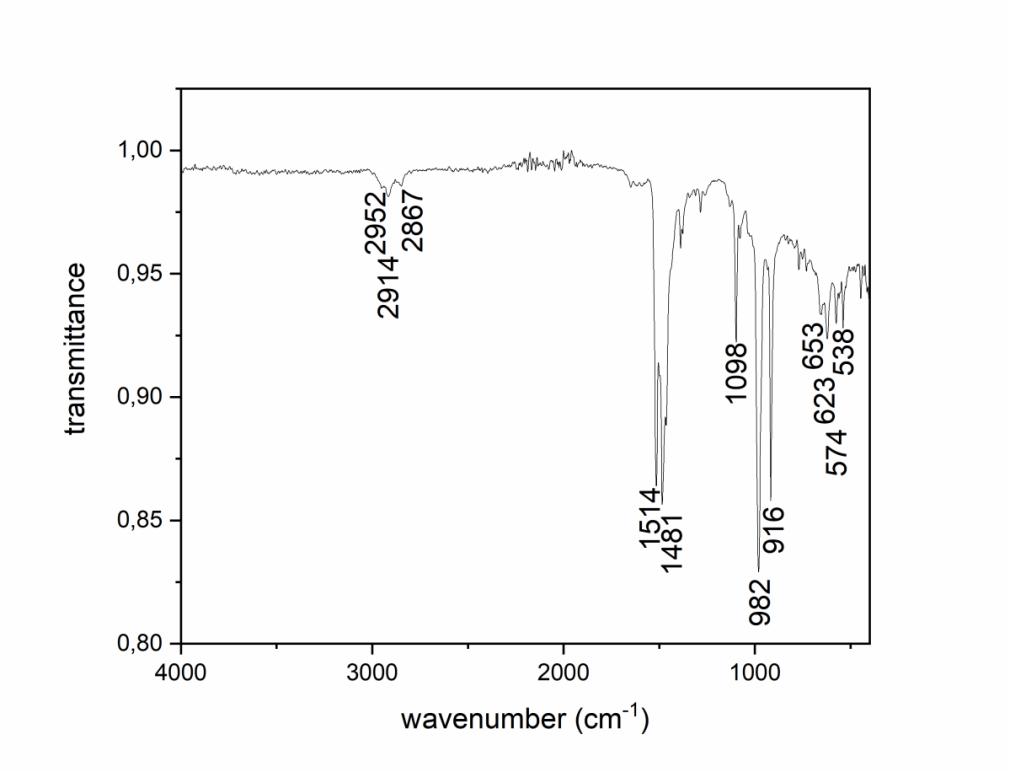


**Figure S23**. ATR-IR spectrum of decamethylalumocenium pentakis(pentafluorophenyl)cyclopentadienide **3c**.

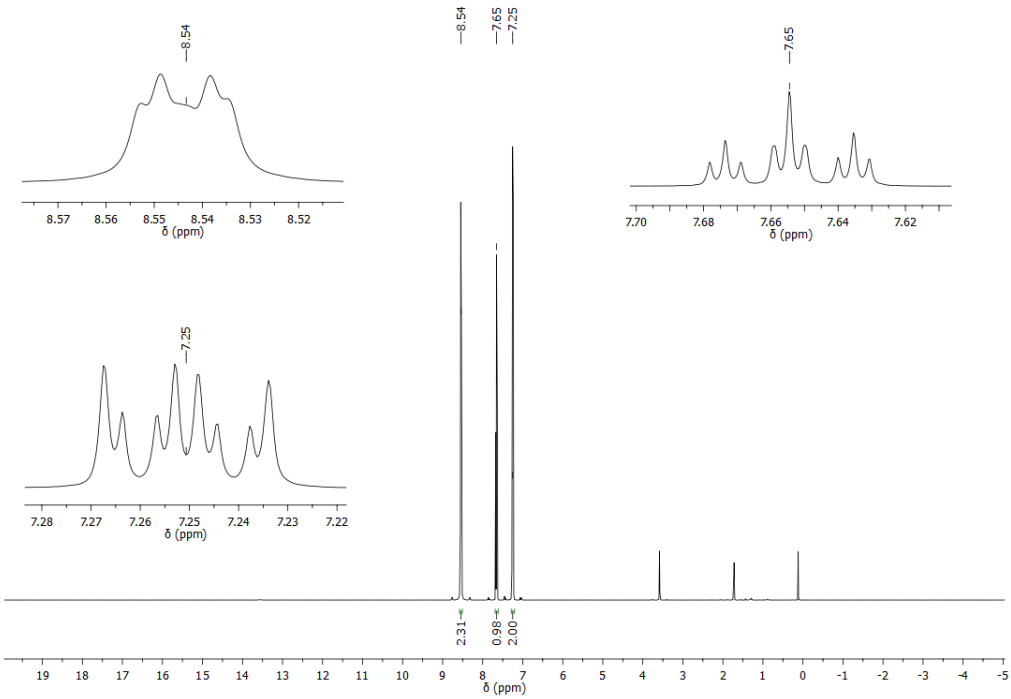


**Figure S24**. $^{1}$H NMR spectrum of pyridinium pentakis(pentafluorophenyl)cyclopentadienide **3d** in thf-$d_8$ at 25 °C.

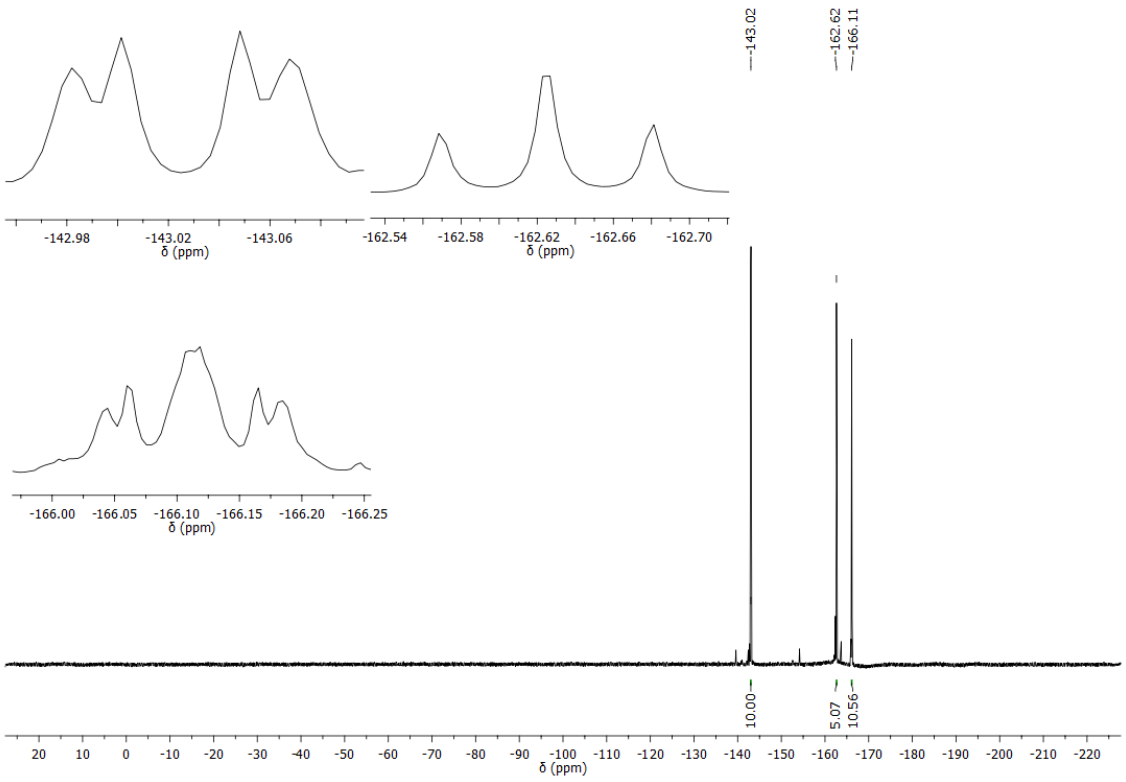


**Figure S25**. $^{19}$F NMR spectrum of pyridinium pentakis(pentafluorophenyl)cyclopentadienide **3d** in thf-$d_8$ at 25 °C.

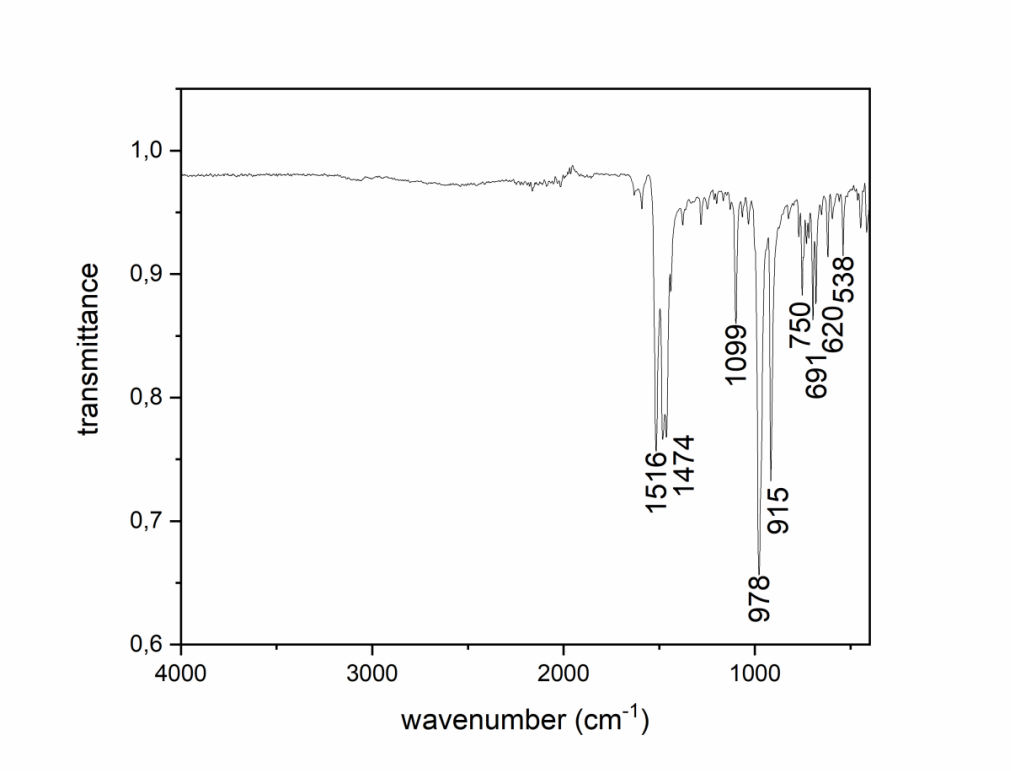


**Figure S26**. ATR-IR spectrum of pyridinium pentakis(pentafluorophenyl)cyclopentadienide **3d**.

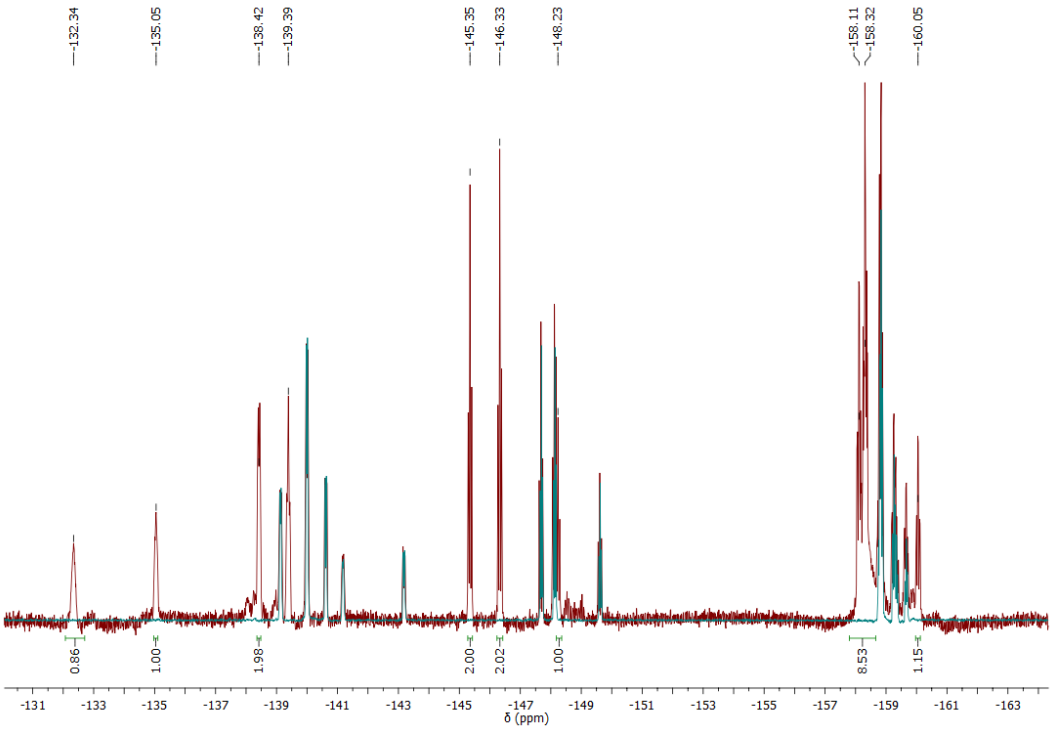


**Figure S27**. $^{19}$F NMR spectrum of pentakis(pentafluorophenyl)cyclopentadienyl carboxylic acid **5** and pentakis(pentafluorophenyl)cyclopentadiene **6** (red) and pure pentakis(pentafluorophenyl)cyclopentadiene **6** (cyan) in $C_6D_6$ at 25 °C.

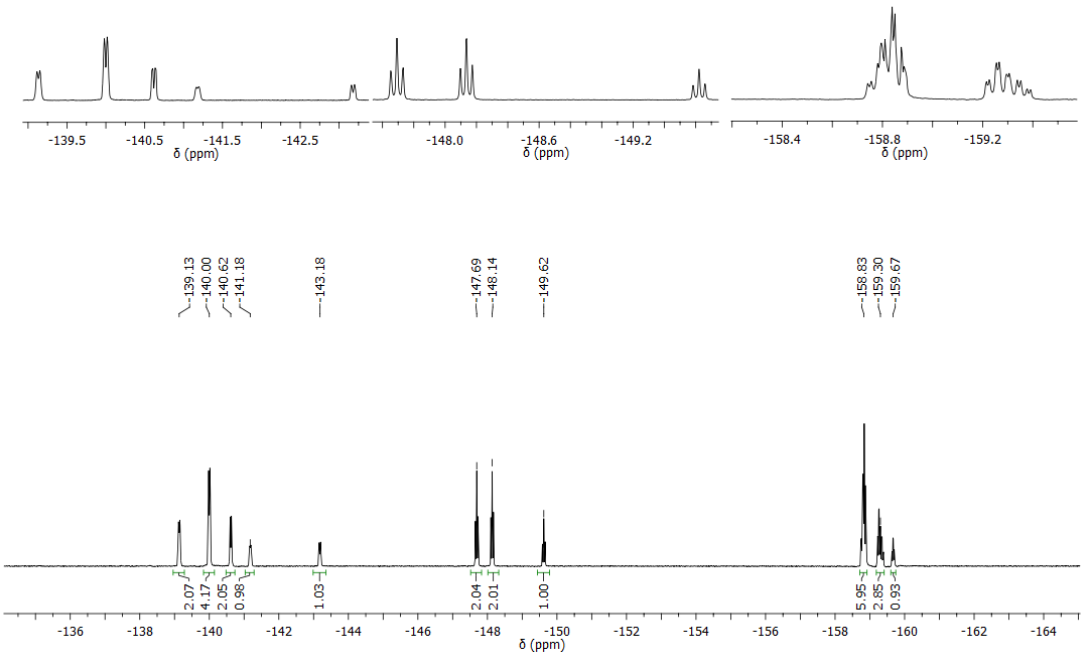


**Figure S28**. $^{19}F$ NMR spectrum of pentakis(pentafluorophenyl)cyclopentadiene **6** in $C_6D_6$ at 25 °C.

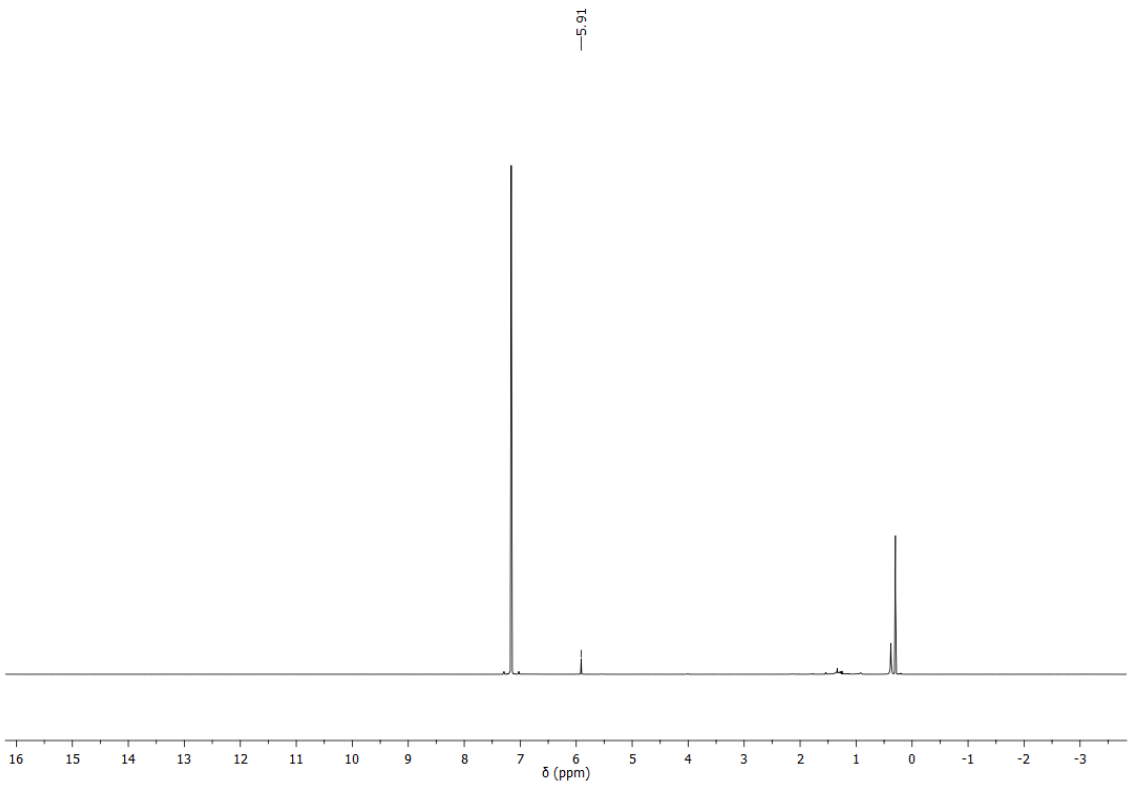


**Figure S29**. $^{1}$H NMR spectrum of pentakis(pentafluorophenyl)cyclopentadiene **6** in $C_6D_6$ at 25 °C.

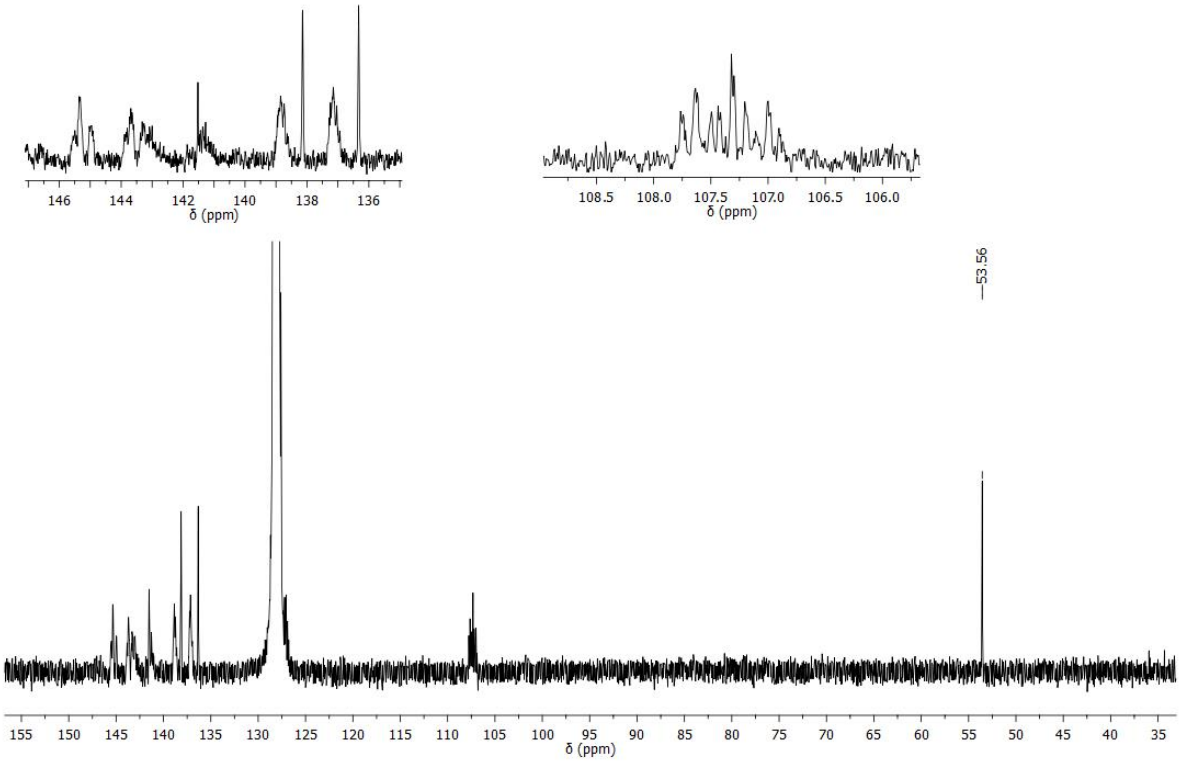


**Figure S30**. $^{13}C\{^{1}H\}$ NMR spectrum of pentakis(pentafluorophenyl)cyclopentadiene **6** in $C_6D_6$ at 25 °C.

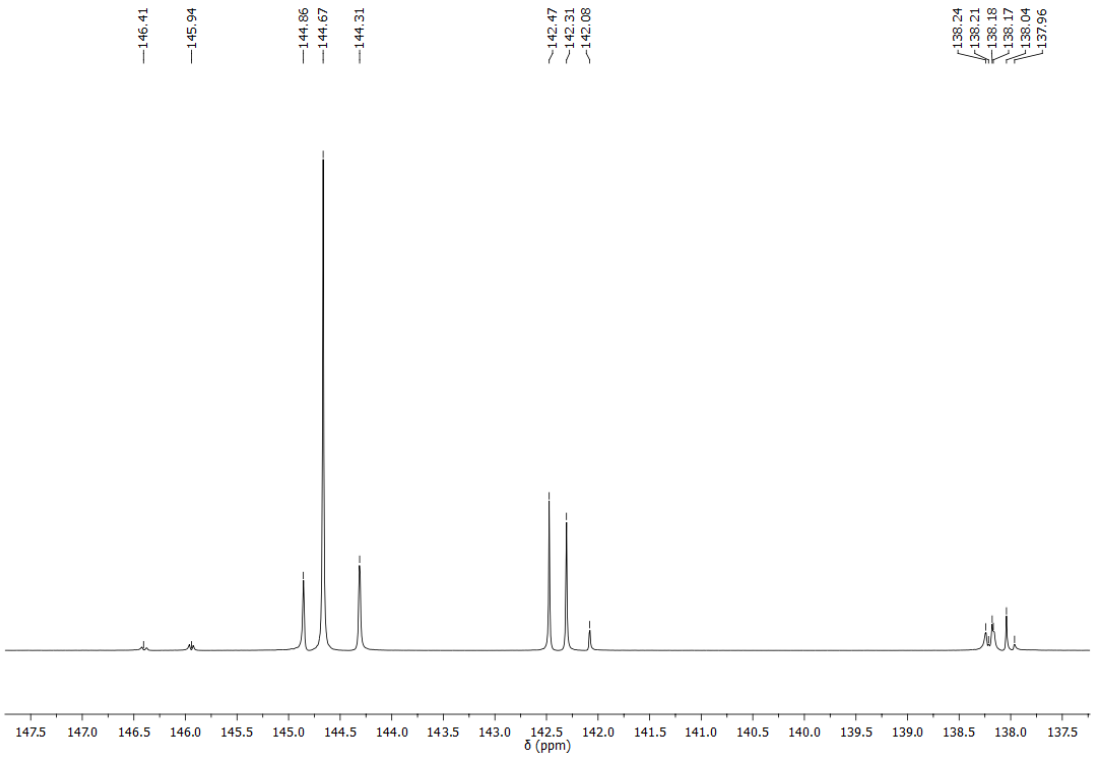


**Figure S31**. $^{13}C\{^{1}H\}$ DEPT-135 NMR spectrum of pentakis(pentafluorophenyl)cyclopentadiene **6** in $C_6D_6$ at 25 °C.

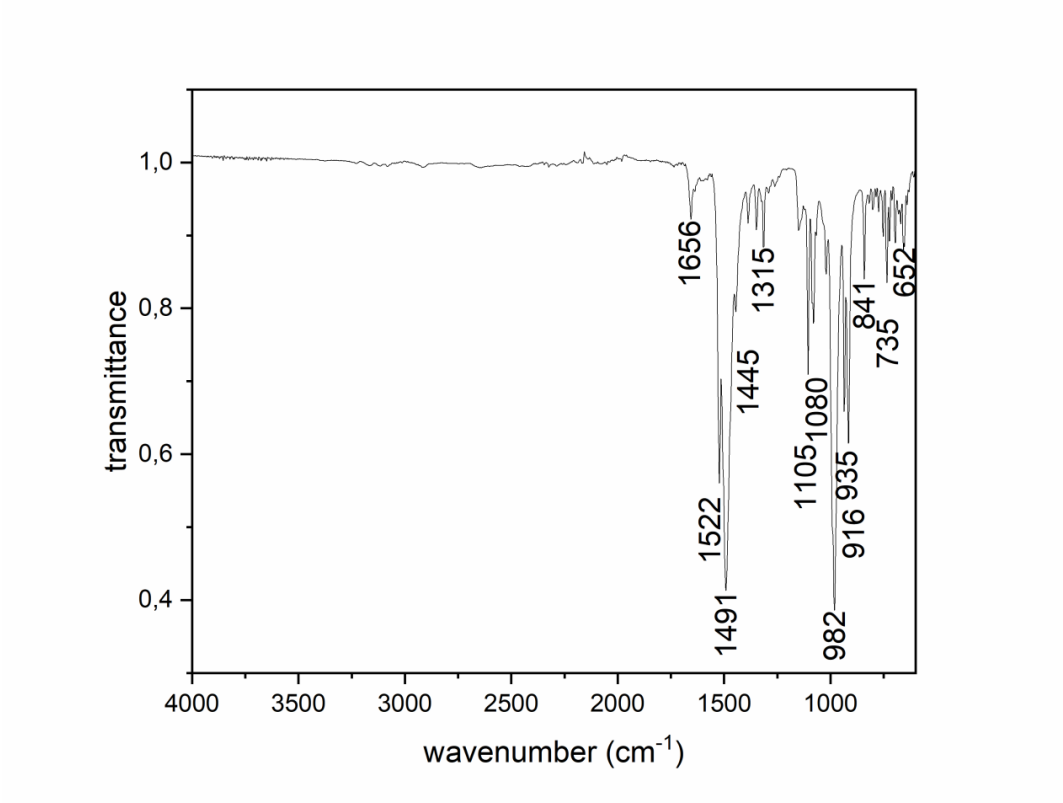


**Figure S32**. ATR-IR spectrum of pentakis(pentafluorophenyl)cyclopentadiene **6**.

**Single-crystal X-ray analyses**. Crystals were mounted on nylon loops in inert oil. Data of **1b** (ys_712m) were collected on a Bruker AXS D8 Kappa diffractometer with APEX2 detector (monochromated $Mo_{K\alpha}$ radiation, $\lambda$ = 0.71073 Å) at 100(2) K. Data of **B** (ys_584m), (**ys_586m), 1a** (ys_712am), **2a** (ys_631a_tw4)**, 2b** (ys_681m), **3a** (ys_679a), **3b** (ys_682am_sq), **3c** (ys_695cm), **5** (ys_719m_sq), and **6** (ys_705m) were collected on a Bruker AXS D8 Venture diffractometer with Photon II detector (monochromated $Cu_{K\alpha}$ radiation, $\lambda$ = 1.54178 Å, microfocus source) at 100(2) K. The structures were solved by Direct Methods (SHELXS-2013)[8] and refined anisotropically by full-matrix least-squares on $F^2$ (SHELXL-2017)[9,10]. Absorption corrections were performed semi-empirically from equivalent reflections on basis of multi-scans or numerical from indexed faces (**1b** (ys_712m)) (Bruker AXS APEX3). Hydrogen atoms were refined using a riding model or rigid methyl groups.

In **ys_586** a $-C_6F_5$ is disordered over two positions. The bond lengths and angles of the phenyl ring were restrained to be equal (SADI). SIMU and RIGU restraints were applied to the displacement parameters of the group. The displacement parameters of the carbon atoms were constrained to be equal for the alternate positions (EADP).

In **1a** (ys_712am) one solvent molecule is disordered over a center of inversion. The local symmetry was ignored in the refinement and the C–C bond lengths and angles of the solvent molecule were restrained to be equal as well as the F/F distances (SADI). RIGU restraints were applied to the displacement parameters of the solvent molecules' atoms.

The only available specimen of **1b** (ys_712m) was too large for the X-ray beam and we did not want to risk losing it by trying to cut it. Any attempts to obtain a more suitable one yielded the other polymorph. The uneven irradiation of the crystal led to distortions of the reflection intensities and consequently to problems with the absorption correction. Several methods and setting were tried but the residual electron density could not be reduced any further. Quantitative results should be carefully assessed. The solvent molecule is disordered over two positions. Its C–C bond lengths and C–C–C bond angles were restrained to be equal (SADI) as well as the F/F distances. All atoms of the molecule were restrained to lie on a common plane (FLAT).

The crystal of **2a** (ys_631a_tw4) was a non-merohedral twin and the model was refined against de-twinned HKLF4 data. Due to overlaps, the $R_{int}$ value is rather high.

One of the $SO_2$ molecules in **2b** (ys_681m) is disordered over two alternate sites. The bond lengths and angles of the $SO_2$ molecules were restrained to be equal (SADI), and RIGU restraints were applied to their displacement parameters. The residual electron density suggests that two of the $C_6F_5$ rings may be disordered, however a refinement failed due to the low occupancy.

**3a** (ys_679a) was refined as an inversion twin.

In **3b** (ys_682am_sq) a $C_6F_5$ is disordered over two positions. SIMU and RIGU restraints were applied to the displacement parameters of the corresponding atoms. Due to their close proximity F35 and F35' were refined with common displacement parameters (EADP). The structure also contains highly disordered solvent – possibly toluene. The final refinement was done with a solvent free dataset from a PLATON/SQUEEZE run. (For details see: A. L. Spek, *Acta Cryst. A46* **(1990)**, 194–201). Since the nature and amount of the solvent is not clear it was not included in the sum formula.

The quality of the diffraction data of **3c** (ys_695cm) was rather low (high *Rint*). To check the correct assignment of the Laue group the frames were integrated with a triclinic unit cell. This lead to an equally poor $R_{int}$. Considering the low quality of the data quantitative results should be carefully assessed.

The hydrogen atom of **5** (ys_719m_sq) was refined freely. The structure contains highly disordered solvent molecules: one hexafluoro benzene and two *n*-hexane disordered over special positions (2, -1 and 222). The final refinement was done with a solvent free data set from a PLATON/SQUEEZE run. (For details see: A. L. Spek, *Acta Cryst. A46* **(1990)**, 194–201). The molecules were included in the sum formula for completeness. The quality of the best specimen available was still rather poor and consequently results beyond the connectivity may be unreliable and should be carefully assessed.

CCDC-2246848 (ys_712a, **1a**), -2246849 (ys_712, **1b**), -2246850 (ys_631a_tw4, **2a**), -2246851 (ys_681, **2b**), -2246852 (ys_679a, **3a**), -2246853 (ys_682am_sq, **3b**), -2246854 (ys_695c, **3c**), -2246857 (ys_719m_sq, **5**), -2246858 (ys_705, **6**), -2246859 (ys_584, **B**), and -2246860 (ys_586 hexakis(pentafluorophenyl)benzene) contain the supplementary crystallographic data for this

paper. These data can be obtained free of charge from The Cambridge Crystallographic Data Centre via www.ccdc.cam.ac.uk/data_request/cif.

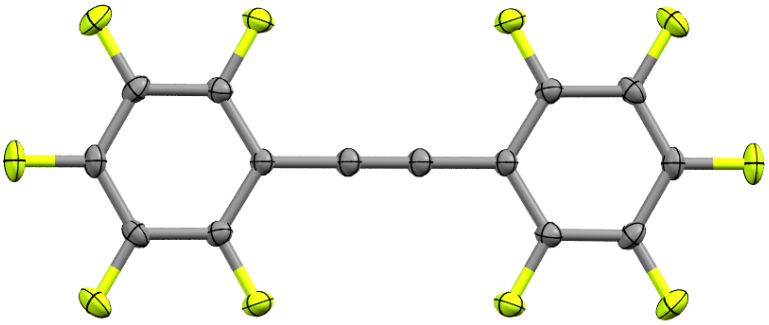

**Figure S33**. Molecular structure of bis(pentafluorophenyl)ethyne **B** in the solid state, crystallized from benzene. Ellipsoids are drawn at a probability level of 50%.

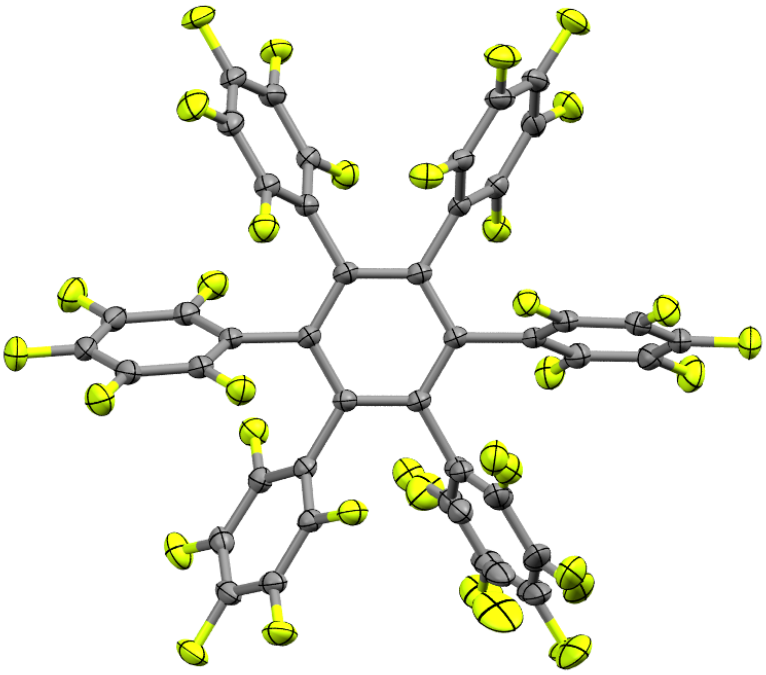

**Figure S34**. Molecular structure of hexakis(pentafluorophenyl)benzene in the solid state. Ellipsoids are drawn at a probability level of 50%. Hexakis(pentafluorophenyl)benzene (ys_586m) was obtained as a by-product in the synthesis of **C** and crystallized from toluene/DCM.

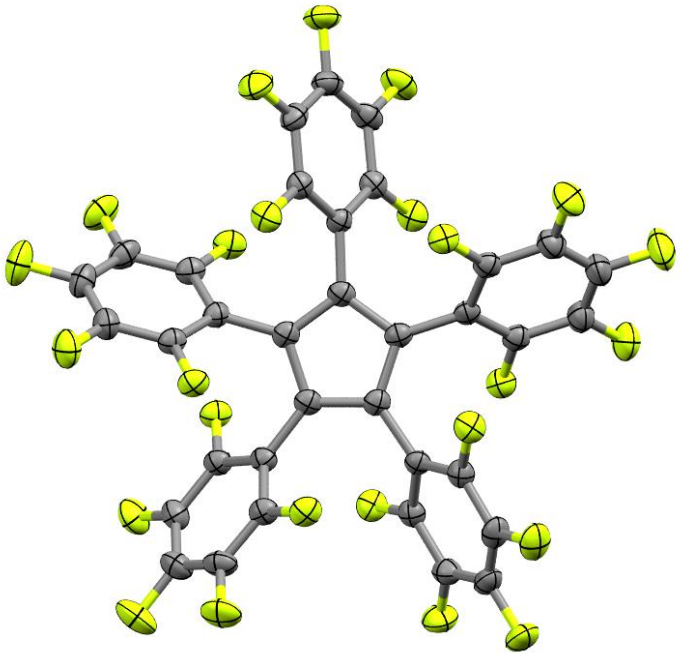

**Figure S35**. Molecular structure of pentakis(pentafluorophenyl)cyclopentadienyl radical **2** in the solid state, crystallized from benzene. Ellipsoids are drawn at a probability level of 50%.

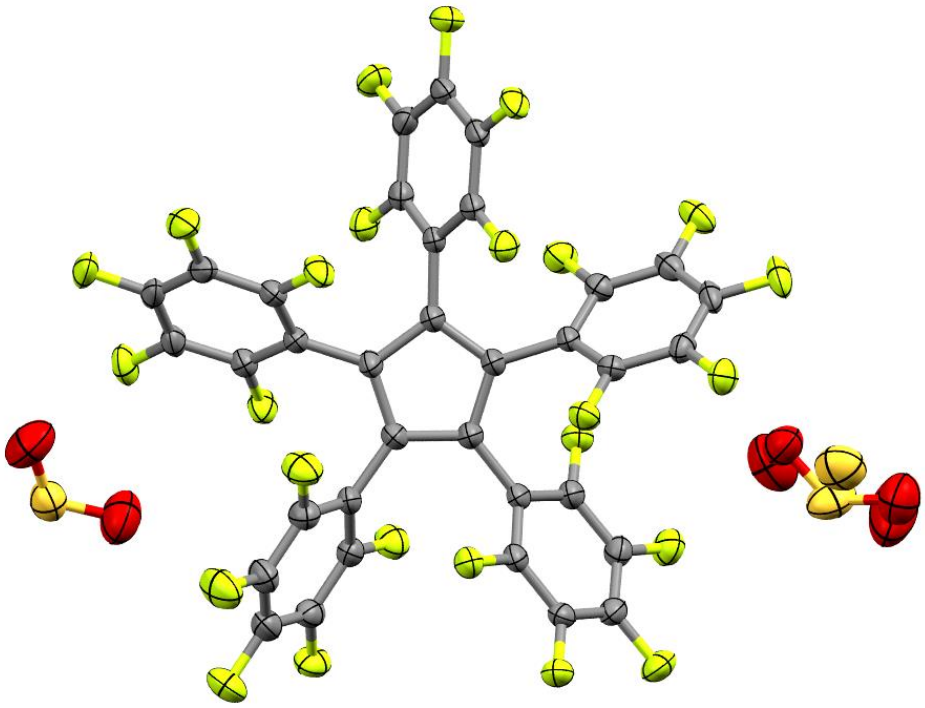

**Figure S36**. Molecular structure of pentakis(pentafluorophenyl)cyclopentadienyl radical **2** in the solid state, crystallized from $SO_2$. Ellipsoids are drawn at a probability level of 50%.

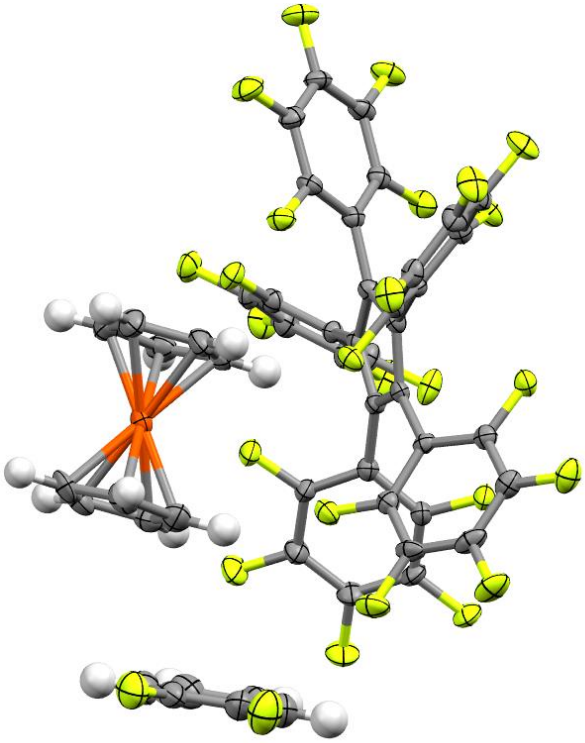

**Figure S37**. Molecular structure of ferrocenium pentakis(pentafluorophenyl)cyclopentadienide **3a** in the solid state, crystallized from 1,2-difluorobenzene/hexane. Ellipsoids are drawn at a probability level of 50%.

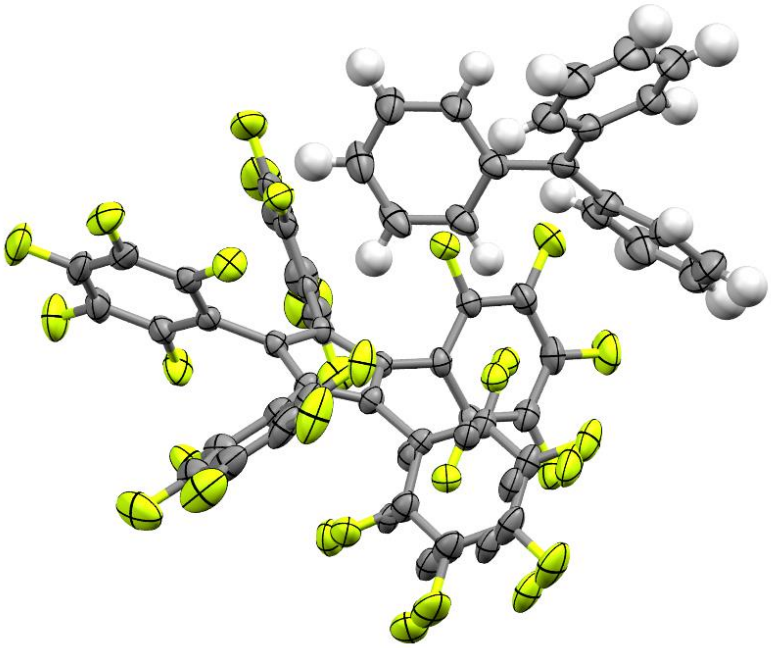

**Figure S38**. Molecular structure of tritylium pentakis(pentafluorophenyl)cyclopentadienide **3b** in the solid state, crystallized from toluene. Ellipsoids are drawn at a probability level of 50%.

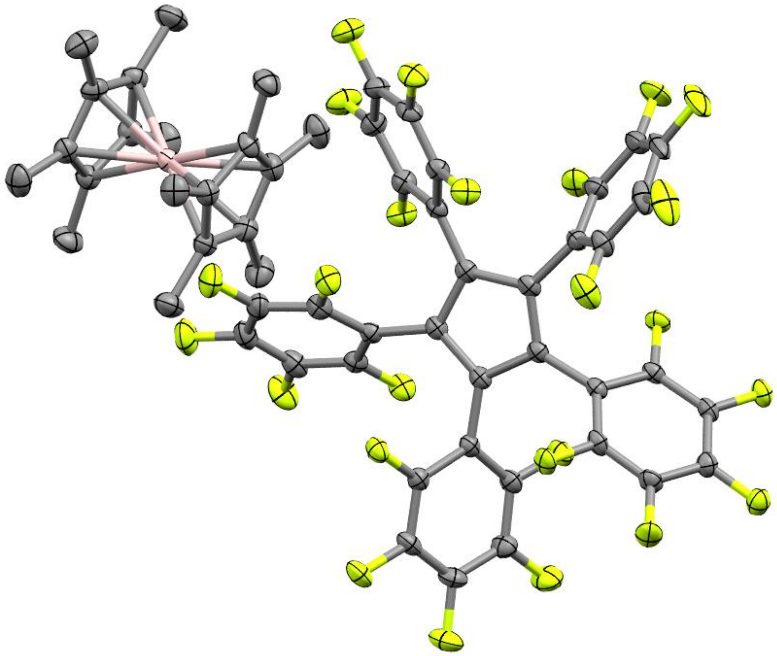

**Figure S39**. Molecular structure of tritylium pentakis(pentafluorophenyl)cyclopentadienide **3c** in the solid state, crystallized from benzene. Ellipsoids are drawn at a probability level of 50%. Hydrogen atoms are omitted for clarity.

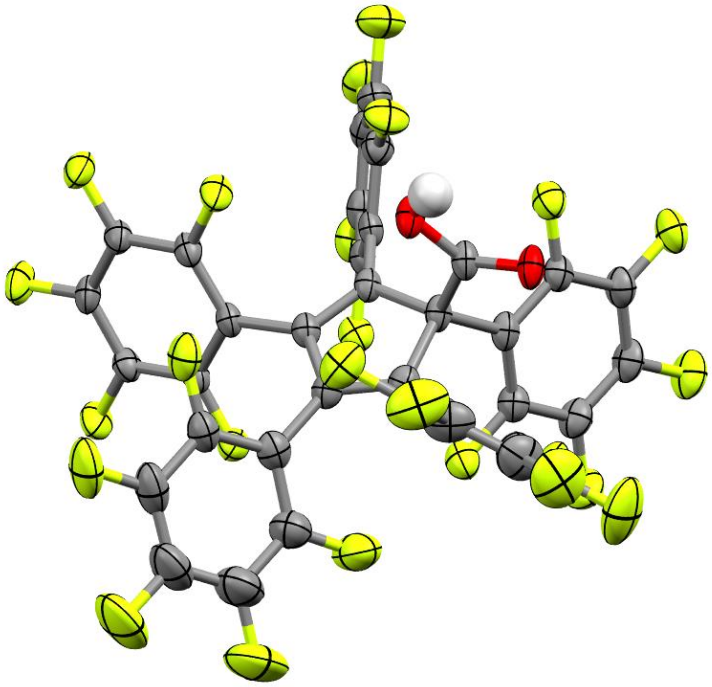

**Figure S40**. Molecular structure of pentakis(pentafluorophenyl)cyclopentadienylcarboxylic acid **5** in the solid state, crystallized from hexafluorobenzene/hexane. Ellipsoids are drawn at a probability level of 50%.

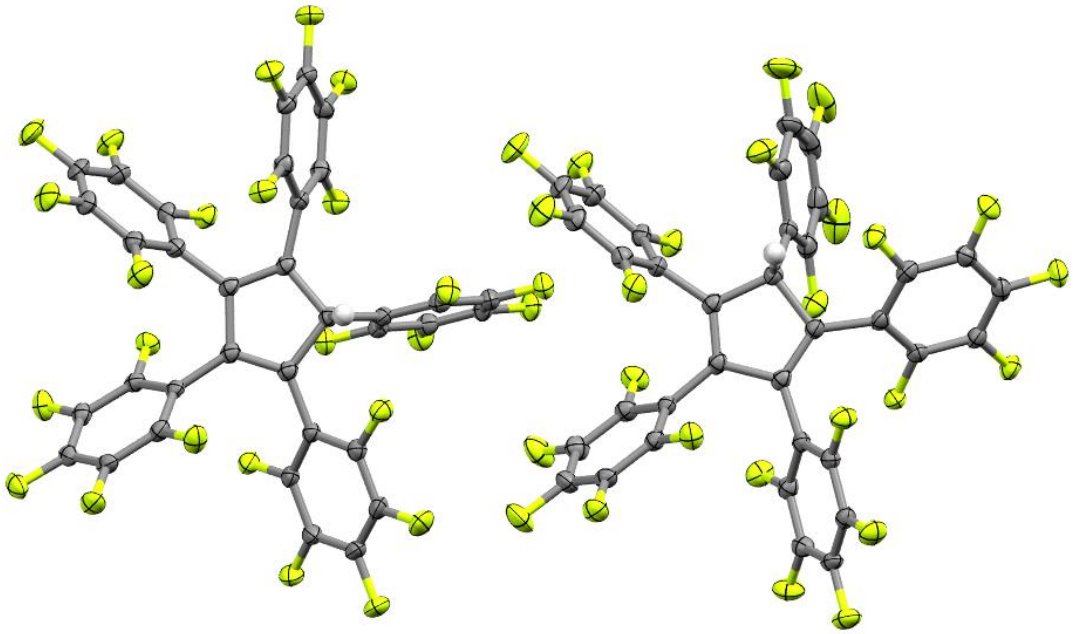

**Figure S41**. Asymmetric unit of pentakis(pentafluorophenyl)cyclopentadiene **6** in the solid state, featuring two independent molecules, crystallized from acetonitrile/hexane. Ellipsoids are drawn at a probability level of 50%.

**Table S1**. Bond lengths in the Cp ring and shortest distance of the Cp centroid to an adjacent hydrogen atom for **3a-c**.

| | **3a** | **3b** | **3c** |
|---|---|---|---|
| bond length (Å) of C1-C2 | 1.405(5) | 1.406(3) | 1.409(3) |
| bond length (Å) of C2-C3 | 1.408(5) | 1.409(3) | 1.420(3) |
| bond length (Å) of C3-C4 | 1.415(6) | 1.412(3) | 1.401(3) |
| bond length (Å) of C4-C5 | 1.411(5) | 1.409(3) | 1.414(3) |
| bond length (Å) of C5-C1 | 1.405(5) | 1.411(3) | 1.411(3) |
| | | | |
| distance (Å) between centroid(Cp)-H | 2.546 | 2.683 | 3.131 |

**Table S2**. Crystal and structure refinement data.

| Identification code | ys_584m | ys_586m | ys_631a_tw4 | ys_679am |
|---|---|---|---|---|
| Empirical formula | $C_{14}F_{10}$ | $C_{42}F_{30}$ | $C_{35}F_{25}$ | $C_{51}H_{14}F_{27}Fe$ |
| $M$ | 358.14 | 1074.42 | 895.35 | 1195.47 |
| Crystal size [mm] | 0.541 × 0.461 × 0.072 | 0.252 × 0.136 × 0.074 | 0.211 × 0.062 × 0.036 | 0.258 × 0.068 × 0.049 |
| $T$ [K] | 100(2) | 100(2) | 100(2) | 100(2) |
| Crystal system | monoclinic | orthorhombic | monoclinic | monoclinic |
| Space group | *C*2/*m* | *Pna*2$_1$ | *C*2/*c* | *Cc* |
| $a$ [Å] | 8.9583(11) | 12.8398(12) | 22.3002(17) | 10.7524(4) |
| $b$ [Å] | 7.6581(10) | 22.205(2) | 13.5353(11) | 20.8342(7) |
| $c$ [Å] | 9.2374(12) | 13.0139(11) | 11.4185(9) | 20.0712(7) |
| $\alpha$ [°] | 90 | 90 | 90 | 90 |
| $\beta$ [°] | 110.222(3) | 90 | 116.061(3) | 96.603(2) |
| $\gamma$ [°] | 90 | 90 | 90 | 90 |
| $V$ [Å$^3$] | 594.65(13) | 3710.3(6) | 3096.1(4) | 4466.5(3) |
| $Z$ | 2 | 4 | 4 | 4 |
| $D_{calc}$ [g·cm$^{-3}$] | 2.000 | 1.923 | 1.921 | 1.778 |
| $\mu$(Cu$K_\alpha$ [mm$^{-1}$]) | 2.098 | 2.018 | 2.015 | 4.123 |
| Transmissions | 0.75/0.44 | 0.75/0.58 | 0.75/0.47 | 0.75/0.53 |
| $F$(000) | 348 | 2088 | 1740 | 2356 |
| Index ranges | $-11 \le h \le 9$ | $-16 \le h \le 16$ | $-28 \le h \le 25$ | $-13 \le h \le 10$ |
| | $-9 \le k \le 9$ | $-22 \le k \le 28$ | $0 \le k \le 17$ | $-26 \le k \le 26$ |
| | $-11 \le l \le 11$ | $-16 \le l \le 16$ | $0 \le l \le 14$ | $-25 \le l \le 25$ |
| $\theta_{max}$ [°] | 79.642 | 80.740 | 80.306 | 81.190 |
| Reflections collected | 9187 | 80749 | 53232 | 65031 |
| Independent reflections | 699 | 7972 | 3359 | 8679 |
| $R_{int}$ | 0.0491 | 0.0462 | 0.1450 | 0.0976 |
| Refined parameters | 61 | 713 | 273 | 713 |
| $R_1$ [$I > 2\sigma(I)$] | 0.0398 | 0.0277 | 0.0619 | 0.0360 |
| $wR_2$ [all data] | 0.1368 | 0.0737 | 0.1543 | 0.0799 |

| | | | | |
|---|---|---|---|---|
| *x*(Flack) | – | 0.00(2) | – | 0.362(5) |
| GooF | 1.240 | 1.039 | 1.090 | 1.040 |
| $\Delta\rho_{final}$ (max/min) [e·Å$^{-3}$] | 0.262/-0.304 | 0.322/-0.152 | 0.320/-0.243 | 0.269/-0.393 |

**Table S2**. Crystal and structure refinement data (continuation).

| **Identification code** | **ys_681m** | **ys_682am_sq** | **ys_695cm** | **ys_705m** |
|---|---|---|---|---|
| Empirical formula | $C_{35}F_{25}O_4S_2$ | $C_{54}H_{15}F_{25}$ | $C_{55}H_{30}Al\ F_{25}$ | $C_{35}HF_{25}$ |
| $M$ | 1023.47 | 1138.66 | 1192.77 | 896.36 |
| Crystal size [mm] | 0.390 × 0.172 × 0.070 | 0.345 × 0.183 × 0.092 | 0.162 × 0.064 × 0.055 | 0.152 × 0.116 × 0.083 |
| $T$ [K] | 100(2) | 100(2) | 100(2) | 100(2) |
| Crystal system | triclinic | monoclinic | monoclinic | triclinic |
| Space group | $P$-1 | $P2_1/c$ | $P2_1/c$ | $P$-1 |
| $a$ [Å] | 11.1864(13) | 14.2425(7) | 15.6538(10) | 12.7006(9) |
| $b$ [Å] | 11.3372(10) | 20.3955(10) | 14.8935(9) | 13.3258(8) |
| $c$ [Å] | 16.478(3) | 20.0632(10) | 21.2611(14) | 18.1289(17) |
| $\alpha$ [°] | 106.938(9) | 90 | 90 | 91.743(6) |
| $\beta$ [°] | 91.037(10) | 99.626(3) | 101.546(4) | 95.967(6) |
| $\gamma$ [°] | 117.347(8) | 90 | 90 | 90.570(5) |
| $V$ [Å$^3$] | 1747.1(4) | 5746.0(5) | 4856.5(5) | 3049.9(4) |
| $Z$ | 2 | 4 | 4 | 4 |
| $D_{calc}$ [g·cm$^{-3}$] | 1.946 | 1.316 | 1.631 | 1.952 |
| $\mu$(Cu$K_\alpha$ [mm$^{-1}$]) | 3.063 | 1.205 | 1.617 | 2.046 |
| Transmissions | 0.75/0.51 | 0.75/0.54 | 0.75/0.59 | 0.75/0.63 |
| $F$(000) | 998 | 2256 | 2392 | 1744 |
| Index ranges | $-14 \le h \le 12$ | $-17 \le h \le 12$ | $-19 \le h \le 19$ | $-16 \le h \le 14$ |
| | $-14 \le k \le 14$ | $-26 \le k \le 25$ | $-18 \le k \le 18$ | $-17 \le k \le 17$ |
| | $-20 \le l \le 20$ | $-25 \le l \le 25$ | $-23 \le l \le 26$ | $-22 \le l \le 23$ |
| $\theta_{max}$ [°] | 75.114 | 81.806 | 80.572 | 81.119 |
| Reflections collected | 94339 | 134589 | 196985 | 169427 |
| Independent reflections | 7163 | 12546 | 10504 | 13260 |
| $R_{int}$ | 0.0509 | 0.0788 | 0.1482 | 0.0485 |
| Refined parameters | 623 | 806 | 740 | 1081 |
| $R_1$ [$I > 2\sigma(I)$] | 0.0550 | 0.0672 | 0.0540 | 0.0366 |
| $wR_2$ [all data] | 0.1684 | 0.1670 | 0.1485 | 0.0987 |
| GooF | 1.049 | 1.095 | 1.026 | 1.017 |

| | | | | |
|---|---|---|---|---|
| $\Delta\rho_{final}$ (max/min) [e·Å$^{-3}$] | 0.754/-0.480 | 0.446/-0.253 | 0.466/-0.392 | 0.533/-0.271 |

**Table S2**. Crystal and structure refinement data (continuation).

| Identification code | ys_712m | ys_712am | ys_719m_sq |
|---|---|---|---|
| Empirical formula | $C_{47}F_{53}Sb_3$ | $C_{44}F_{50}Sb_3$ | $C_{43.50}H_{11.50}F_{28}O_2$ |
| $M$ | 1936.72 | 1843.69 | 1098.03 |
| Crystal size [mm] | 1.008 × 0.255 × 0.212 | 0.213 × 0.138 × 0.073 | 0.380 × 0.125 × 0.100 |
| $T$ [K] | 100(2) | 100(2) | 100(2) |
| Crystal system | orthorhombic | monoclinic | orthorhombic |
| Space group | $Pna2_1$ | $P2_1/c$ | $Fddd$ |
| $a$ [Å] | 27.1610(13) | 23.1788(8) | 11.6321(6) |
| $b$ [Å] | 15.5739(8) | 10.9694(4) | 47.785(2) |
| $c$ [Å] | 13.0018(6) | 22.1030(8) | 60.097(3) |
| $\alpha$ [°] | 90 | 90 | 90 |
| $\beta$ [°] | 90 | 113.0712(15) | 90 |
| $\gamma$ [°] | 90 | 90 | 90 |
| $V$ [Å$^3$] | 5499.8(5) | 5170.4(3) | 33405(3) |
| $Z$ | 4 | 4 | 32 |
| $D_{calc}$ [g·cm$^{-3}$] | 2.339 | 2.369 | 1.747 |
| $\mu$(Cu$K_\alpha$ [mm$^{-1}$]) | 1.682 (Mo$K_\alpha$) | 14.417 | 1.769 |
| Transmissions | 0.27/0.16 | 0.49/0.12 | 0.75/0.57 |
| $F$(000) | 3648 | 3468 | 17296 |
| Index ranges | $-45 \le h \le 45$ | $-29 \le h \le 29$ | $-14 \le h \le 14$ |
| | $-26 \le k \le 26$ | $-13 \le k \le 14$ | $-60 \le k \le 61$ |
| | $-21 \le l \le 21$ | $-27 \le l \le 20$ | $-76 \le l \le 73$ |
| $\theta_{max}$ [°] | 36.455 | 80.949 | 81.008 |
| Reflections collected | 144720 | 139588 | 146520 |
| Independent reflections | 26619 | 11292 | 9180 |
| $R_{int}$ | 0.0421 | 0.0764 | 0.0654 |
| Refined parameters | 1039 | 928 | 573 |
| $R_1$ [$I > 2\sigma(I)$] | 0.0639 | 0.0417 | 0.0770 |
| $wR_2$ [all data] | 0.1681 | 0.1170 | 0.2211 |
| $x$(Flack) | 0.33(2) | – | – |
| GooF | 1.099 | 1.042 | 1.064 |

| | | | |
|---|---|---|---|
| $\Delta\rho_{final}$ (max/min) [e·Å$^{-3}$] | 5.049/-1.355 | 2.308/-1.889 | 0.484/-0.524 |

**Computational Details**

All calculations were performed by using the program packages Gaussian 16[11] and Amsterdam Density Functional (ADF)[12-13]. DFT geometry optimizations were carried out using B3LYP[14-16] and CAM-B3LYP[17] for closed-shell species and the corresponding unrestricted versions UB3LYP and UCAM-B3LYP for open-shell species. To consider the dispersion interaction in an appropriate way, the additional dispersion correction with Becke-Johnson damping (D3BJ)[18] was employed. As basis sets 6-31G(d), 6-311++G(d,p) and TZP were applied. Furthermore, the open-shell singlet states were calculated using UB3LYP-D3BJ/6-31G(d), UCAM-B3LYP-D3BJ/6-31G(d) and UB3LYP-D3BJ/6-311++G(d,p) and the "guess = mix" keyword. In all cases these calculations converged into the closed-shell states. To treat relativistic effects the zeroth order regular approximation (ZORA)[19] to the Dirac equation was used for the B3LYP-D3BJ/TZP calculations. Frequency calculations were carried out at each of the structures to verify the nature of the stationary point. It turned out that all structures have none.

A NICS-based scan was used as a magnetic criterion of aromaticity. Therefore, the NICS values were calculated using CAM-B3LYP/def2-TZVP//CAM-B3LYP-D3BJ/6-311++G(d,p) along a line perpendicular from the center of the ring plane to 5 Å, with a step size of 0.1 Å (Figure S43). Magnetic shieldings were calculated by employing the GIAO method[20].

The degree of (anti)aromaticity was further evaluated by using the harmonic oscillator model of aromaticity (HOMA)[21-22] index:

$$HOMA = 1 - \frac{\alpha}{n}\sum_{i}^{n}\left(R_{opt} - R_i\right)^2$$

In this equation, $R_{opt}$ corresponds to the optimal bond length taken as 1.388 Å for a CC bond. $R_i$ represents an individual bond length; n is the number of bonds taken up in the summation and α is an empirical constant (257.7 $Å^{-2}$).[22]

Single-point calculations were performed using the double hybrid method B2PLYP-D3BJ[23] and the TZ2P[24] basis set. Furthermore, the zeroth order regular approximation (ZORA)[19] to the Dirac

equation was employed. The geometrical data for these single point calculations stem from the B3LYP-D3BJ/TZP calculations as well as from the X-ray structure analyses.

**Table S3.** Energy (Δ*E*) and Gibbs energy (Δ*G*) of the triplet state of **1** and **1 SbF$_6$** relative to the singlet state. The values are given in kcal/mol.

| method | molecule | Δ*E* | Δ*G* |
|---|---|---|---|
| cam-B3LYP-D3BJ/6-31G(d) | **1** | -6.20 | -5.43 |
| cam-B3LYP-D3BJ/6-311++G(d,p) | **1** | -5.55 | -4.58 |
| B3LYP-D3BJ/6-31G* | **1** | -5.62 | -5.39 |
| B3LYP-D3BJ/TZP[a] | **1** | -4.96 | -5.45 |
| B3LYP-D3BJ/TZP[a] | **1 SbF$_6$** | -3.65 | -2.54 |
| B2PLYP-D3BJ/TZ2P//B3LYP-D3BJ/TZP[a] | **1** | -2.27 | -2.77 |
| B2PLYP-D3BJ/TZ2P//B3LYP-D3BJ/TZP[a] | **1 SbF$_6$** | -0.75 | +0.36 |

[a] The zeroth order regular approximation (ZORA) to the Dirac equation was used.

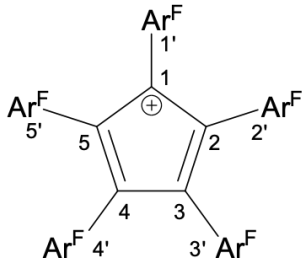


**1**

**Figure S42.** Assignment of atom labels.

**Table S4.** Bond distances [Å] in the singlet und triplet state of **1** and **1 $SbF_6$** calculated by means of B3LYP-D3BJ/TZP(ZORA).

| bond | **1** | | **1 $SbF_6$** | |
|---|---|---|---|---|
| | singlet | triplet | singlet | triplet |
| C1-C2 | 1.458 | 1.431 | 1.460 | 1.431 |
| C2-C3 | 1.366 | 1.431 | 1.365 | 1.429 |
| C3-C4 | 1.539 | 1.434 | 1.532 | 1.430 |
| C4-C5 | 1.371 | 1.434 | 1.354 | 1.432 |
| C5-C1 | 1.453 | 1.433 | 1.474 | 1.432 |
| C1-C1’ | 1.434 | 1.455 | 1.426 | 1.454 |
| C2-C2’ | 1.471 | 1.455 | 1.474 | 1.456 |
| C3-C3’ | 1.449 | 1.455 | 1.451 | 1.457 |
| C4-C4’ | 1.446 | 1.454 | 1.456 | 1.455 |
| C5-C5’ | 1.471 | 1.454 | 1.468 | 1.454 |

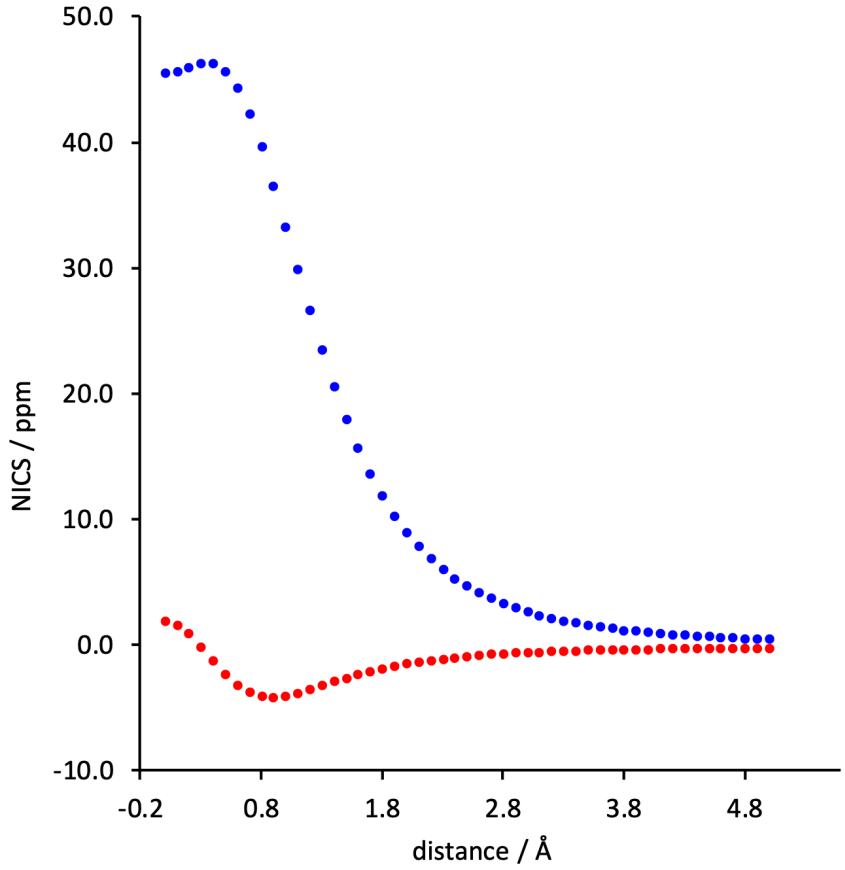


**Figure S43.** NICS scans of **1** calculated using CAM-B3LYP/def2-TZVP//CAM-B3LYP-D3BJ/6-311++G(d,p). Blue-colored curve refers to singlet state and red-colored curve refers to triplet state.

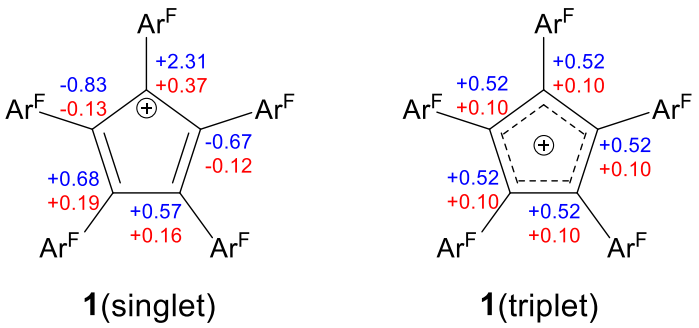

**Figure S44.** APT (atomic polar tensor) charges (blue; CAM-B3LYP-D3BJ/6-311++G(d,p)) and NBO (natural bond orbitals) charges (red; CAM-B3LYP/def2-TZVP//CAM-B3LYP-D3BJ/6-311++G(d,p)) of **1** in the singlet (left) und triplet (right).

**Calculated HIA and FIA of 1**

The structures of $Me_3SiH$, $Me_3SiF$, $Me_3Si^+$, $Cp(C_6F_5)_5^+$ (singlet), $Cp(C_6F_5)_5H$ and $Cp(C_6F_5)_5F$ were optimized using B3LYP-D3(BJ)/def2-TZVPP. To determine the hydride ion affinity (HIA) / fluoride ion affinity (FIA), energy differences were calculated for the reactions:

$Cp(C_6F_5)_5^+$ (singlet) + $Me_3SiH$ → $Cp(C_6F_5)_5H$ + $Me_3Si^+$

-3830.9595312 + (-409.9693680 ) → -3831.8835472 + (-409.0821314)

-4240.9288992 Hartree → -4240.9656786 Hartree

(1 Hartree = 2625 kJ/mol) The reaction is 96.5 kJ/mol exothermic.

The hydride affinity of $Cp(C_6F_5)_5^+$ (singlet) is 96.5 kJ/mol higher than that of $Me_3Si^+$.

$Cp(C_6F_5)_5^+$ (singlet) + $Me_3SiF$ → $Cp(C_6F_5)_5F$ + $Me_3Si^+$

-3830.9595312 + (-509.3337305) → -3931.1420727 + (-409.0821314)

-4340.2932617 Hartree → -4340.2242041 Hartree

The reaction is 181.3 kJ/mol endothermic.

The fluoride affinity of $Cp(C_6F_5)_5^+$ (singlet) is 181.3 kJ/mol higher than that of $Me_3Si^+$.

The $Me_3SiX$ (X = H, F)/$Me_3Si^+$ pair has been established in the literature as a reliable anchor point to calculate hydride and fluoride ion affinities of other Lewis acids. The fluoride affinity of the $Me_3Si^+$ cation has been calculated to be 952.5 kJ/mol (CCSD(T)/CBS).[32] The hydride affinity of $Me_3Si^+$ calculated with the same method is 924 kJ/mol.[32]

Since the hydride abstraction from $Me_3SiH$ is exothermic by kJ/mol, the hydride ion affinity of $Cp(C_6F_5)_5^+$ (singlet) is 1020.5 kJ/mol. Since the fluoride abstraction from $Me_3SiF$ is endothermic by 181.3 kJ/mol, the fluoride ion affinity of $Cp(C_6F_5)_5^+$ (singlet) is 771.2 kJ/mol .

**Examples for side reactions**

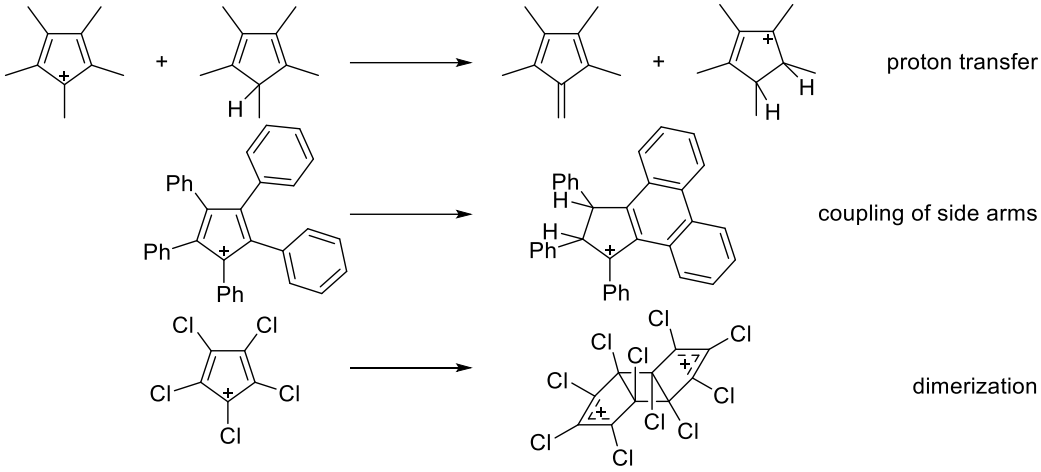


**Scheme S42**: Examples of side reactions that hindered the isolation of Cp cations.[25-31]

**References**


1. Boeré, R. T. *et al.* Oxidation of closo-$B_{12}Cl_{12}$- to the radical anion $B_{12}Cl_{12}$*- and to neutral $B_{12}Cl_{12}$. *Angew. Chem. Int. Ed. Engl.* **50**, 549–552 (2011).
2. *Origin(Pro), Version 2016*, OriginLab Corporation, Northhampton, Massachusetts, USA, (2016).
3. Stoll, S. & Schweiger, A. EasySpin, a comprehensive software package for spectral simulation and analysis in EPR. *J. Magnet. Res.* **178**, 42–55 (2006).
4. Webb, A. F. & Gilman, H. Reactions of some perhaloarenes with metals and metal halides. *J. Organomet. Chem.* **20**, 281–283 (1969).
5. Inés, B., Holle, S., Bock, D. & Alcarazo, M. Polyfluorinated Cyclopentadienones as Lewis Acids. *Synlett* **25**, 1539–1541 (2014).
6. Birchall, J. M., Bowden, F. L., Haszeldine, R. N. & Lever, A. B. P. Polyfluoroarenes. Part IX. Decafluorotolan: synthesis, properties, and use as an organometallic ligand. *J. Chem. Soc., A* 747 (1967).
7. Burns, C. T., Shapiro, P. J., Budzelaar, P. H. M., Willett, R. & Vij, A. Bis(permethylcyclopentadienyl)aluminum Compounds: Precursors to $[Cp^*_2Al]^+$ but Not to $Cp^*_3Al$. *Organometallics* **19**, 3361–3367; 10.1021/om000173x (2000).
8. Sheldrick, G. M. Phase annealing in SHELX-90: direct methods for larger structures. *Acta Cryst.* **46**, 467–473 (1990).
9. Sheldrick, G. M. SHELXL-2017, Program for the Refinement of Crystal Structures University of Göttingen, Göttingen (Germany) (2017). See also: Sheldrick, G. M. Crystal structure refinement with SHELXL, *Acta Cryst.,* **C71**, 3-8 (2015).
10. Hübschle, C. B., Sheldrick, G. M. & Dittrich, B. ShelXle: a Qt graphical user interface for SHELXL. *J. Appl. Cryst.* **44**, 1281–1284 (2011).
11. Frisch, M. J. *et al.* Gaussian 16, Revision A.03, Wallingford CT, (2016).
12. te Velde, G. *et al.* Chemistry with ADF. *J. Comput. Chem.* **22**, 931–967 (2001).
13. Baerends, E. J. *et al.* ADF 2020.1, SCM, Theoretical Chemistry, Vrije Universiteit, Amsterdam, The Netherlands, http://www.scm.com, **2020**.
14. Becke, A. D. Density-functional exchange-energy approximation with correct asymptotic behavior. *Phys. Rev. A* **38**, 3098–3100 (1988).
15. Lee, C., Yang, W. & Parr, R. G. Development of the Colle-Salvetti correlation-energy formula into a functional of the electron density. *Phys. Rev. B* **37,** 785–789 (1988).
16. Miehlich, B., Savin, A., Stoll, H. & Preuss, H. Results obtained with the correlation energy density functionals of becke and Lee, Yang and Parr. *Chem. Phys. Lett.* **157**, 200–206 (1989).
17. Yanai, T., Tew, D. P. & Handy, N. C. A new hybrid exchange–correlation functional using the Coulomb-attenuating method (CAM-B3LYP). *Chem. Phys. Lett.* **393**, 51–57 (2004).
18. Grimme, S., Ehrlich, S. & Goerigk, L. Effect of the damping function in dispersion corrected density functional theory. *J. Comp. Chem.* **32**, 1456–1465 (2011).

19. van Lenthe, E., Ehlers, A. & Baerends, E.-J. Geometry optimizations in the zero order regular approximation for relativistic effects. *J. Chem. Phys.* **110**, 8943–8953 (1999).
20. Wolinski, K., Hinton, J. F. & Pulay, P. Efficient implementation of the gauge-independent atomic orbital method for NMR chemical shift calculations. *J. Am. Chem. Soc.* **112**, 8251–8260 (1990).
21. Julg, A. & Franois, P. Recherches sur la géométrie de quelques hydrocarbures non-alternants: son influence sur les énergies de transition, une nouvelle définition de l'aromaticité. *Theoret. Chim. Acta* **8**, 249–259 (1967).
22. Krygowski, T. M. & Cyrański, M. Separation of the energetic and geometric contributions to the aromaticity of π-electron carbocyclics. *Tetrahedron* **52**, 1713–1722 (1996).
23. Grimme, S. Semiempirical hybrid density functional with perturbative second-order correlation. *J. Chem. Phys.* **124**, 34108 (2006).
24. van Lenthe, E. & Baerends, E. J. Optimized Slater-type basis sets for the elements 1-118. *J. Comput. Chem.* **24**, 1142–1156 (2003).
25. Otto, M. *et al.* The Stable Pentamethylcyclopentadienyl Cation Remains Unknown. *Angew. Chem. Int. Ed. Engl.* **41**, 2275 (2002).
26. Lambert, J. B., Lin, L. & Rassolov, V. The Stable Pentamethylcyclopentadienyl Cation. *Angew. Chem. Int. Ed. Engl.* **41,** 1429–1431 (2002).
27. Breslow, R. & Chang, H. W. The Rearrangement of the Pentaphenylcyclopentadienyl Cation. *J. Am. Chem. Soc.* **83**, 3727-3728 (1961).
28. Rupf, S. M., Pröhm, P. & Malischewski, M. The 2+2 cycloaddition product of perhalogenated cyclopentadienyl cations: structural characterization of salts of the C10Cl102+ and C10Br102+ dications. *Chem. Commun.* **56**, 9834-9837 (2020).
29. Jones, J. N., Cowley, A. H. & Macdonald, C. L. B. The crystal structure of the 'pentamethylcyclopentadienyl cation' is that of the pentamethylcyclopentenyl cation. *Chem. Commun.,* 1520–1521 (2002).
30. Müller, T. Comment on the X-Ray Structure of Pentamethylcyclopentadienyl Cation. *Angew. Chem. Int. Ed. Engl.* **41**, 2276-2278 (2002).
31. Lambert, J. B. Statement. *Angew. Chem. Int. Ed. Engl.* **41**, 2278 (2002).
32. Erdmann, P. Leitner, J. Schwarz & J. Greb, L. *ChemPhysChem* **21**, 987-994 (2020).